

Neutrinos and their interactions with matter

M. Sajjad Athar^{a,*}, A. Fatima^a, S. K. Singh^a

^a*Department of Physics, Aligarh Muslim University, Aligarh - 202002, India*

Abstract

We have presented a review of the properties of neutrinos and their interactions with matter. The different (anti)neutrino processes like the quasielastic scattering, inelastic production of mesons and hyperons, and the deep inelastic scattering from the free nucleons are discussed, and the results for the scattering cross sections are presented. The polarization observables for the leptons and hadrons produced in the final state, in the case of quasielastic scattering, are also studied. The importance of nuclear medium effects in the low, intermediate, and high energy regions, in the above processes along with the processes of the coherent neutrino-nucleus scattering, coherent meson production, and trident production, has been highlighted. In some cases, the results of the cross sections are also given and compared with the available experimental data as well as with the predictions in the different theoretical models. This study would be helpful in understanding the (anti)neutrino interaction cross section with matter in the few GeV energy region relevant to the next generation experiments like DUNE, Hyper-Kamiokande, and other experiments with accelerator and atmospheric neutrinos. We have emphasized the need of better theoretical models for some of these processes for studying the nuclear medium effects in nuclei.

Keywords: Neutrino-nucleon scattering, neutrino-nucleus scattering, nuclear medium effects, standard model, polarization, trident production, coherent production

Contents

1	Introduction	3
1.1	Experimental observations and properties of neutrinos	6
1.1.1	Detection of neutrinos	6
1.1.2	Sources of neutrinos and their fluxes	6
1.1.3	Masses, mixing and oscillation of neutrinos	9
1.1.4	Electromagnetic properties of neutrinos	11
1.2	Theoretical description of neutrinos and their interactions	13
1.2.1	Dirac neutrinos	13
1.2.2	Weyl neutrinos	14
1.2.3	Majorana neutrinos	15
1.3	Standard model of electroweak interactions	16
1.3.1	Introduction	16
1.3.2	SM of electroweak interaction of leptons	17
1.3.3	Higgs mechanism and generation of mass	20
1.3.4	Neutral current interactions and the weak mixing angle	22
1.3.5	Extension of the SM to the leptons, quarks and nucleons	22
1.3.6	Higher order effects in electroweak interactions	24
1.3.7	$\nu_l - e$ and $\bar{\nu}_l - e$ scattering	25
1.3.8	(Anti)neutrino-quark scattering	26
1.4	Resonance scattering of neutrinos: Glashow resonance	26
2	Neutrino scattering from nucleons	27
2.1	Quasielastic and elastic ν -scattering processes on nucleons	31
2.1.1	Introduction	31
2.1.2	Charged current quasielastic reactions and weak nucleon form factors	31
2.1.3	Neutral current elastic reactions and weak nucleon form factors	32

*Corresponding author

Email address: sajathar@gmail.com (M. Sajjad Athar)

2.1.4	Symmetry properties of the weak hadronic current	32
2.1.5	Parameterization of the weak form factors	35
2.1.6	Cross sections for charged current processes	39
2.2	Quasielastic hyperon production	40
2.2.1	Matrix element and form factors	40
2.2.2	Cross sections: Experimental results	41
2.3	Polarization of final hadrons and leptons	42
2.3.1	Polarization of the final hadron	42
2.3.2	Polarization of the final lepton	44
3	Inelastic ν-scattering processes from nucleons	47
3.1	Introduction	47
3.2	Kinematics	50
3.3	Structure of matrix elements	51
3.3.1	Nonresonant contribution	51
3.3.2	Meson - meson interaction	52
3.3.3	Baryon - meson interaction	53
3.3.4	Decuplet baryon - octet baryon - meson interaction	53
3.3.5	Resonance (R_J ; $J = \frac{1}{2}, \frac{3}{2}$) contribution	53
3.3.6	Charged current induced resonance excitation	54
3.3.7	Neutral current induced resonance excitation	59
3.3.8	Strong couplings of the resonances	60
3.4	Single pion production	61
3.4.1	Charged current (anti)neutrino induced processes	62
3.4.2	Neutral current (anti)neutrino induced processes	64
3.4.3	Results and discussion	65
3.5	Eta production	70
3.5.1	η production induced by photons	71
3.5.2	η production induced by (anti)neutrinos	74
3.6	Strange particle production	75
3.6.1	Charged current ν_l induced K^+/K^0 production	76
3.6.2	Charged current $\bar{\nu}_l$ induced K^-/\bar{K}^0 production	77
3.6.3	Associated particle production induced by photons	79
3.6.4	Associated particle production induced by (anti)neutrinos	81
3.6.5	Single pion production with hyperon ($Y\pi$)	85
3.6.6	Kaon production with Ξ hyperon	86
3.7	Two pion production	88
3.8	NC $\nu(\bar{\nu})$ induced single photon production off the nucleon target	88
4	Deep inelastic scattering	89
4.1	Introduction	89
4.2	DIS of electrons from nucleons	90
4.3	Parton model of DIS	92
4.4	ν -N scattering in the DIS region	94
4.5	Experimental results	96
4.6	QCD corrections	97
4.7	Results and discussion	100
5	Neutrino scattering from nuclei	103
5.1	Coherent elastic neutrino-nucleus scattering in the low energy region	103
5.2	Neutrino trident production	107
5.3	Exclusive reactions in ν -nucleus scattering in the low energy region	110
5.4	Inclusive quasielastic scattering in the low and intermediate energy regions	115
5.4.1	(Anti)neutrino-nucleus quasielastic scattering in Fermi gas models	118
5.4.2	Inclusive quasielastic scattering at low energy	123
5.4.3	Quasielastic (anti)neutrino scattering at intermediate energy with $\nu_e(\bar{\nu}_e)$ and $\nu_\mu(\bar{\nu}_\mu)$	125
5.4.4	MiniBooNE axial dipole mass anomaly and nuclear medium effects	130
5.4.5	Nuclear medium effects due to two particle-two hole excitations	130
5.4.6	Nuclear medium effects beyond the impulse approximation	132

5.4.7	$ \Delta S = 1$ quasielastic scattering in nuclei	133
5.4.8	Final state interaction	133
5.5	Inelastic scattering and pion production in the Δ dominance model	134
5.5.1	Final state interaction effect	137
5.6	A comparative discussion of results for quasielastic hyperon and delta production from nuclei leading to pions	138
5.7	Coherent production of mesons	141
5.7.1	Coherent pion production	142
5.7.2	Coherent kaon production	146
5.8	Deep inelastic $\nu_l/\bar{\nu}_l - A$ scattering	147
5.8.1	Introduction	147
5.8.2	Formalism	149
5.8.3	Fermi motion, binding and nucleon correlation effects	150
5.8.4	Mesonic contribution	154
5.8.5	Shadowing and antishadowing effects	156
5.8.6	Phenomenological approach to understand NME in DIS	156
5.8.7	Isoscalarity correction	158
5.8.8	Results and discussion	158
6	Quark-hadron duality in ν_l scattering	162
7	Monte Carlo event generators and some of the recent results from the accelerator experiments	167
8	Summary and outlook	168
A	Expression of the hadronic current $J_{\mu\nu}$	175
A.1	Expressions of $N(Q^2)$, $A^h(Q^2)$, $B^h(Q^2)$, and $C^h(Q^2)$	175
A.2	Expressions of $A^l(Q^2)$, $B^l(Q^2)$ and $C^l(Q^2)$	177
B	Cabibbo theory, $SU(3)$ symmetry and weak $N - Y$ transition form factors	178
C	Density parameters	180

1. Introduction

The idea of neutrino initially called “neutron”, as neutral, weakly interacting, spin $\frac{1}{2}$ particle which obeys exclusion principle, having mass of the same order of magnitude as that of the electron mass was proposed by Pauli [1], in 1930. This particle was hypothesized in order to explain the two outstanding problems in contemporary nuclear physics related with the observed continuous energy spectrum (violation of energy-momentum conservation) of electrons in β -decays of nuclei and the nuclear structure (anomalies in understanding the spin-statistics relation). Immediately after neutrinos were conjectured, the theoretical study of nuclear beta decay started with the works of Fermi [2, 3, 4] and Perrin [5], followed by the works of Henderson [6]. This may be considered to be the beginning of the study of neutrino interactions with electrons and nucleons. Fermi conceived the idea of “four fermion current-current type point interaction” with the strength of the interaction given by a coupling constant G_F to describe the β decay rates and the shape of the beta spectrum. He considered the interaction currents to be vector in nature following the analogy with the quantum electrodynamics (QED). The experimental analyses of the shape of the β -spectrum from the various nuclear beta decays showed that the neutrino mass has to be very much smaller than the electron mass. Bethe and Peierls [7] were the first who performed the theoretical calculations for the total scattering cross sections for $\bar{\nu} + p \rightarrow e^+ + n$ process using G_F as the strength of the interaction determined from nuclear beta decays. The calculated cross section was found to be too small (10^{-44} cm² for a 2.3 MeV neutrino beam) to be observed experimentally unless the neutrino flux and/or the mass of the detector material were increased by many orders of magnitude. This hindered any further progress in attempts to experimentally study the neutrino interactions with matter and supported Pauli’s apprehension that “I did a terrible thing, which no theorist should do, I postulated a particle that can not be detected”. After more than twenty five years of neutrino hypothesis and several experimental efforts, Reines and Cowan in 1956 [8, 9] were finally able to observe neutrinos at the Savannah River reactor, and sent a telegram to Pauli about their findings “We are happy to inform you that we have definitely detected neutrinos...”. Pauli publicly announced this discovery in 1956 to the participants at the CERN Symposium, and replied to their message that “Everything comes to him who knows how to wait”. Since then the progress in understanding the physics of neutrinos and the development in neutrino physics has been amazing and full of surprises. The neutrinos continue to challenge our expectations even today regarding the validity of some symmetry

principles and conservation laws in particle physics. A better understanding of these symmetry principles would be helpful in the fields of nuclear and particle physics as well as in the fields of cosmology and astrophysics [10].

The experimental study of β decays of various nuclei made considerable progress and helped in the formulation of the theory of weak interactions by extending the Fermi theory of beta decay. During the next forty years following the idea of neutrinos, extensive work on the nuclear beta decays and many other weak decays of muons, nucleons, hyperons, and mesons led to the phenomenological theory of weak interactions known as the $V - A$ (Vector-Axial Vector) theory [11, 12, 13]. This theory was formulated using the various properties of neutrinos determined experimentally like their mass, spin, helicity i.e. left (right) handed neutrinos (antineutrino) and the theoretical idea of the chiral (γ_5) invariance of neutrino interactions leading to the prediction of parity violation [14, 15], which was confirmed subsequently by Wu et al. [16] and later by other experiments. With the discovery of the τ lepton in 1975 and various hadrons with heavy quark contents like the charm (c), bottom (b), and top (t) quarks and analyses of their weak decays, the $V - A$ theory of weak interactions was reformulated in terms of the leptons and quarks using the concept of quark mixing proposed by Cabibbo [17] and extended by Kobayashi and Maskawa [18] described in terms of the Cabibbo-Kobayashi-Maskawa (CKM) matrix [19]. The experimental analyses of various weak interaction processes using the phenomenological $V - A$ theory were performed, which resulted in understanding the following properties of neutrinos and their interactions with matter:

- There are three flavors of (anti)neutrinos i.e. $\nu_e(\bar{\nu}_e)$, $\nu_\mu(\bar{\nu}_\mu)$, $\nu_\tau(\bar{\nu}_\tau)$ with limits on the masses so tiny that they can be considered to be massless. They are classified according to separate lepton flavor numbers for each flavor i i.e. $L_i (i = e, \mu, \tau)$ and assigned $L_i = +1(-1)$ for the individual neutrino and antineutrino flavors.
- The neutrinos and antineutrinos of each flavor are neutral, spin half fermions with helicity -1 ($+1$) popularly known as left (right)-handed fermions.
- Neutrinos interact with the charged leptons and quarks through the exchange of massive charged vector fields W_μ^\pm between the neutrino-charged lepton and quark-quark currents with the same strength for all the flavors. These currents transform as $V^\mu - A^\mu$ and are constructed as the charge carrying bilinear covariants from the lepton fields of the same flavor in the case of leptons and the quark fields in a CKM rotated flavor space in the case of quarks and carry linear momentum and energy. This is known as the phenomenological $V - A$ theory [11, 12, 13].
- In this theory, the neutrino interactions are such that:
 - The lepton flavor number (LFN) $L_i (i = e, \mu, \tau)$ is conserved separately for each flavor and there are no lepton flavor violating (LFV) currents.
 - The neutrinos of all flavors ($\nu_i; i = e, \mu, \tau$) interact with the leptons of the same flavor and quarks with the same strength for each flavor i.e. there exists lepton flavor universality (LFU).
 - Most of the weak processes involving neutrinos and hadrons are charge changing with the hadronic currents obeying $\Delta S = 0$ or $|\Delta S| = 1$ rule, where S is the strangeness quantum number. The strength of the couplings of $|\Delta S| = 1$ hadronic currents is suppressed as compared to the $\Delta S = 0$ hadronic currents by a factor of $\tan^2 \theta_C$, where $\theta_C = 13.1^\circ$ is the Cabibbo angle. However, neutral currents (NC) are highly suppressed in $|\Delta S| = 1$ sector leading to the principle of the absence of flavor changing neutral current (FCNC). There is no conclusive evidence of the existence of charge conserving NC in the $\Delta S = 0$ sector.

Therefore, the weak transitions like $\nu_l(\bar{\nu}_l) \rightarrow l^-(l^+); l = e, \mu, \tau$ occur with the same strength for each l . The weak transitions like $\nu_l(\bar{\nu}_l) \rightarrow \nu_l(\bar{\nu}_l)$ and $l^-(l^+) \rightarrow l^-(l^+)$, without involving any change of charge are highly suppressed and the transitions like $\nu_l(\bar{\nu}_l) \rightarrow l'^-(l'^+)$, $\nu_l(\bar{\nu}_l) \rightarrow \nu_{l'}(\bar{\nu}_{l'})$, where $l \neq l'$ with $l, l' = e$ or μ or τ , and have not been observed are not allowed in the $V^\mu - A^\mu$ theory.

The phenomenological $V - A$ theory of weak interaction successfully describes the neutrino interactions with matter specially at low energies. In the high energy region of neutrinos, the scattering cross section from the charged leptons and nucleons leads to divergences when calculated in higher orders of the perturbation theory and the theory is not renormalizable. Various attempts to find a renormalizable theory of weak interactions were not successful until a unified theory of weak and electromagnetic interactions of leptons was formulated by Weinberg [20] and Salam [21] and extended to the quark sector using GIM mechanism proposed by Glashow et al. [22]. This unified theory of electroweak interactions is known popularly as the standard model (SM).

The SM was formulated using various experimental results on the neutrino properties and their weak interactions obtained from the phenomenological $V - A$ theory as described above and the theoretical ideas inspired from the gauge field theory of electromagnetic interactions based on the local $U(1)$ symmetry group and its extension to the higher nonabelian local symmetry groups by Yang and Mills [23]. Such gauge field theories predict the existence of massless vector fields as the mediating field for generating the underlying interactions. The masses of the massless gauge fields are then generated using the idea of the spontaneously broken gauge theories by introducing the interacting scalar fields in the theory developed by Englert and Brout [24], and Higgs [25]. In the SM, the group structure of the higher local gauge symmetry

and the interacting scalar fields to break the symmetry spontaneously are chosen such that the four massless vector gauge fields appear by the requirement of the invariance under local gauge symmetry out of which masses are generated for the three vector fields and the fourth vector field remains massless. The three massive vector fields are identified as the fields mediating the weak interactions and the fourth massless field is identified as the vector field mediating the electromagnetic interactions thus providing a unified theory of electroweak interactions. The renormalizability of the theory was soon demonstrated by 't Hooft and Veltman [26], and Lee and Zinn-Justin [27]. The theory reproduces all the results obtained by the phenomenological $V - A$ theory and predicts various new physical processes which have been observed by the later experiments confirming the SM as a unified theory of electroweak interactions. For example, the prediction of:

- neutral weak currents ($\Delta Q = 0$) in the neutrino interactions with $\Delta S = 0$, which were first observed in neutrino experiments at CERN [28] and confirmed later in many other experiments [29, 30, 31].
- neutral weak currents in the electron sector leading to the parity violation in the polarized electron scattering, which were first observed in electron scattering experiments at SLAC [32] and confirmed later in many other experiments.
- charged (W^\pm) and neutral (Z^0) gauge bosons which were observed at CERN in UA1 and UA2 experiments [33, 34] with masses $M_{W^\pm} = 80.38$ GeV and $M_{Z^0} = 91.18$ GeV.
- scalar Higgs boson (H) and its decays which were experimentally confirmed in CMS [35] and ATLAS [36] experiments in 2012 with a mass of Higgs boson $M_H = 125.25$ GeV.

However, there are some experimental results which are not explained by the SM and need physics beyond the standard model (BSM). For example, the existence of:

- neutrino oscillations which imply
 - (i) mixing of neutrino flavors,
 - (ii) the neutrinos to be massive,
 - (iii) additional flavor of nonstandard neutrino i.e. sterile neutrino which has no interaction with ordinary matter.
- early indication of CP violation in neutrino interactions.
- FCNC like $K_L^0 \rightarrow \mu^+ \mu^-$, $K^+ \rightarrow \pi^+ \nu \bar{\nu}$, etc. [37, 38].

Furthermore, various experimental efforts are going on to observe rare processes that would require the existence of nonstandard interactions (NSI). For example, the possible observation of [39, 40, 41, 42, 43, 44]:

- neutrinoless double beta decay (NDBD), for which many experiments are being done implying neutrino to be its own antiparticle, known as the Majorana type of neutrino, requiring major changes in our understanding of neutrino interactions with matter.
- decays like $K^+ \rightarrow \pi^+ e^\mp \mu^\pm$, $K^- \rightarrow \pi^- e^\mp \mu^\pm$, $B^+ \rightarrow K^+ \mu^\pm \tau^\mp$, $B^+ \rightarrow K^+ \mu^\pm e^\mp$, etc., which involve both FCNC and LFV.
- LFV in purely leptonic processes with or without a photon like $\mu^- \rightarrow e^- \gamma$, $\mu^+ \rightarrow e^- e^+ e^+$, or $\mu \leftrightarrow e$ conversion in nuclei.
- lepton flavor universality violation (LFUV) in weak decays like $\pi^+ \rightarrow \mu^- e^+ e^+ \nu_e$ as well as in the heavy quark sector like $b \rightarrow s l \bar{l}$, $b \rightarrow c l \bar{\nu}_l$, etc.

In the last 90 years since the neutrino was postulated and speculations were made about its interactions by Pauli, enormous progress has been made in understanding the neutrino interactions with matter but it is still far from being understood satisfactorily. Most of the observed electroweak processes are explained with the SM but the observation of certain phenomena like the neutrino oscillation, CP violation and FCNC requires BSM physics and there are many theoretical studies being made presently to study the BSM physics [45]. However, in view of the space limitations, we focus in this review only on the standard model interaction of neutrinos with matter. In literature, there are quite a few recent review articles [46, 47, 48, 49, 50, 51, 52] dealing with various aspects of the neutrino interactions with matter in the Standard Model. The present review deliberates at length on the interaction of neutrinos with nucleons and nuclei in the low, intermediate, and high energy regions focussing on the nuclear medium effects. The importance of various nuclear medium effects (NME) like the Fermi motion, Pauli blocking, multinucleon correlation effects are discussed in various neutrino processes of quasielastic, inelastic, and deep inelastic scattering when the (anti)neutrino scattering takes place in nuclei like ^{12}C , ^{16}O , ^{40}Ar , ^{208}Pb , etc. relevant for the present and future $\nu(\bar{\nu})$ -nucleus scattering experiments. The importance of understanding the role of quark-hadron duality in describing the neutrino scattering from nucleons and nuclei in the shallow inelastic region has been emphasized.

In Section 1.1, we summarize the properties of neutrinos as we understand them today and describe various sources of neutrinos in the energy range of eV to EeV. In Section 1.2, a brief discussion about the theoretical description of neutrinos and their interaction is presented. In Section 1.3, the basic theory of the neutrino interactions with leptons and quarks in the framework of the SM is obtained. In Sections 2, 3, and 4, we describe the various processes of neutrino scattering from the nucleons viz. elastic, quasielastic, inelastic and deep inelastic scattering, respectively, and discuss NME in these processes in Section 5. In Section 6, we present in brief the concept of quark-hadron duality in the weak sector. The different neutrino event Monte Carlo generators are discussed in Section 7. Finally, we summarize the neutrino interaction physics presented in this review in Section 8.

1.1. Experimental observations and properties of neutrinos

1.1.1. Detection of neutrinos

The experimental attempts to make direct observation of neutrinos and antineutrinos started immediately after the formulation of the theory of beta decay, and the first attempt was made by Nahimas [53] as early as 1935 at the underground station Holborn in London, and later by Rodeback and Allen [54], Leipunski [55], Snell and Pleasonton [56], Jacobsen [57], Sherwin [58], and Crane and Halpern [59], which showed no conclusive evidence of the existence of neutrinos. The attempts took much longer time to succeed experimentally and the final success came when Reines and Cowan [8, 9] in 1956 at the Savannah River reactor reported the observation of antineutrinos from the reactor in the reaction

$$\bar{\nu}_e + p \rightarrow e^+ + n \quad (1.1)$$

by making a coincidence measurement of the photons from particle annihilation $e^+ + e^- \rightarrow \gamma + \gamma$ and a neutron capture $n + {}^{108}\text{Cd} \rightarrow {}^{109}\text{Cd} + \gamma$ reaction a few microseconds later [8, 60] induced by e^+ and n produced in reaction (1.1).

The original proposal of Pontecorvo [61] and Alvarez [62] to use ${}^{37}\text{Cl}$ as target to observe neutrinos from the reactors was followed by Davis [63, 64] who looked for $\nu_e + {}^{37}\text{Cl} \rightarrow e^- + {}^{37}\text{Ar}$ reaction at the Brookhaven reactor using 4000 L of liquid CCl_4 and tried to observe the ${}^{37}\text{Ar}$ produced in the reaction. No event was observed but a limit of $\bar{\sigma}(\bar{\nu} + {}^{37}\text{Cl} \rightarrow e^- + {}^{37}\text{Ar}) < 0.9 \times 10^{-45} \text{cm}^2$ was obtained while the theoretical prediction was $\approx 2.6 \times 10^{-45} \text{cm}^2$. This negative result was of importance as it showed that the neutrinos from the reactors do not produce electrons hinting that ν_e and $\bar{\nu}_e$ are different particles. In order to phenomenologically describe the situation, a new quantum number was proposed called the electron lepton number: L_e . The ν_e and e^- were assigned $L_e = +1$, and $\bar{\nu}_e$ and e^+ were assigned $L_e = -1$.

It was suggested by Markov [65], Pontecorvo [66], and Schwartz [67] to use proton accelerators to produce high energy neutrino beam from pion decays to perform experiments like:

$$\nu + n \longrightarrow \mu^- + p \quad \nu + n \longrightarrow e^- + p \quad (1.2)$$

$$\bar{\nu} + p \longrightarrow \mu^+ + n \quad \bar{\nu} + p \longrightarrow e^+ + n \quad (1.3)$$

to test whether the neutrinos from pion decays produce muons or electrons. Theoretical calculations for the above processes were done by Lee and Yang [68], Cabibbo and Gatto [69], and Yamaguchi [70] using the phenomenological $V - A$ theory. The experiments performed at the Brookhaven National Laboratory (BNL) by Danby et al. [71] and later at CERN by Bienlein et al. [72] observed that neutrinos from the pion decays, which were accompanied by muons, produce only muons in the above reactions (Eq. (1.2)) and never an electron/positron was observed. This confirmed that these neutrinos are different from the neutrinos produced in beta decay implying $\nu_\mu \neq \nu_e$. Consequently, for the muon family separate lepton number L_μ was defined. These lepton numbers were assumed to be conserved separately. The L_e and L_μ were combined to define a new quantum number, i.e., LFN, L_f ($f = e, \mu$).

In 1975 when τ -lepton was discovered [73] and its weak decays were observed the existence of a new flavor of neutrinos ν_τ was proposed, which was observed much later in the DONUT experiment [74, 75] in 2000 at the Fermilab. More observations of ν_τ induced events were later made in experiments with the accelerator and the atmospheric neutrinos by DONUT [75], OPERA [76, 77, 78], Super-Kamiokande [79], and IceCube [80] collaborations. Future experiments like DsTau [81], SHiP [82, 83] and DUNE [84, 85, 86] are planning to observe significantly large number of events induced by the ν_τ interactions.

1.1.2. Sources of neutrinos and their fluxes

The SM neutrinos are of three flavors viz. ν_e , ν_μ and ν_τ and the corresponding antineutrinos. Initially the experiments were performed with the reactor antineutrinos and the solar neutrinos and later with the development of accelerators, ν_μ and $\bar{\nu}_\mu$ beams were used. Today we know that there are various sources of neutrinos all around us and these sources may be broadly divided into two groups, one the natural sources and the other man made sources of (anti)neutrinos as shown in Fig. 1.1. The neutrinos produced from the natural sources are the ones coming from the sun's core, earth's core and mantle, etc. Neutrinos are always produced during the birth, collision, and the death of stars. Particularly huge flux of neutrinos is emitted during a supernovae explosion. There are neutrinos around us which are relics of the Big Bang,

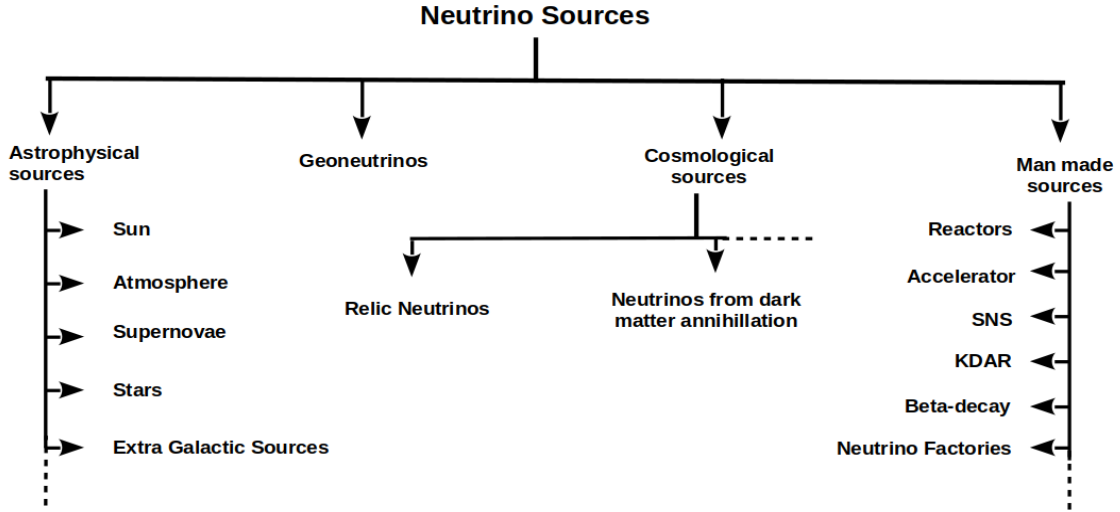
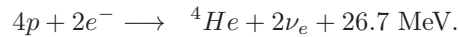


Figure 1.1: Different sources of neutrinos.

and were produced almost 13.7 billion years ago, soon after the birth of the Universe. There are many other sources of astrophysical neutrinos like the cosmogenic neutrinos, neutrinos being produced in the violent collisions of high energy protons with active galactic nuclei, etc. Besides the various natural sources, there are man made sources of neutrinos and antineutrinos being produced at the particle accelerators, nuclear reactors, spallation neutron source (SNS) facilities, etc. These neutrinos and antineutrinos from the various sources cover an energy span from μeV (10^{-6} eV) to EeV (10^{18} eV) as shown in Fig. 1.2 [87]. Recently, Vitagliano et al. [88] have also provided neutrino spectrum at earth obtained using different neutrino sources. The ν_τ and $\bar{\nu}_\tau$ from the atmospheric source come with a very small flux which have been recently observed in the Super-Kamiokande [89, 79] and the IceCube [80] experiments.

- **Natural neutrino sources**

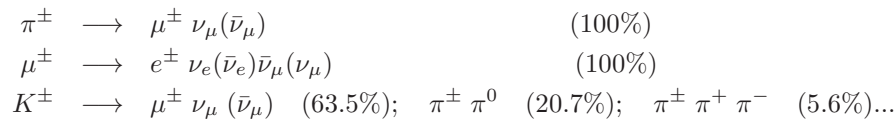
All the stars including the sun create their energy through nuclear fusion reactions that take place in the star's core [90]. The proton-proton chain reaction dominates in stars with mass of the order of the mass of the sun or smaller, while the Carbon-Nitrogen-Oxygen (CNO) cycle reaction dominates in the stars with mass greater than 1.3 times mass of the sun. The process like hydrogen fusion to helium takes place via a sequence of chain reactions that begins with the fusion of two protons to form deuterium nucleus along with the emission of e^+ and ν_e and the complete process may be written as



Corresponding to the luminosity of the sun as 3.9×10^{26} Watt, almost $7 \times 10^{10} \nu_e/\text{cm}^2/\text{sec}$ reach the earth's surface. Atmospheric neutrinos [91] are produced through the decay of secondary cosmic ray particles (π, K , etc.) produced in the interaction of primary cosmic rays (mainly protons) with the earth's atmosphere through the processes like:



The pions (kaons) subsequently give rise to (anti)neutrinos



The spectrum of these secondaries peaks in the GeV range, extends to high energy region with approximately a power-law spectrum and therefore the neutrino flux decreases rapidly with the increasing energy. Up to the energies of about 100 TeV, the neutrino flux is dominated by pion and kaon decays.

Supernova neutrinos [92] are produced during the death phase of a massive star. When the core collapse-supernovae burst out, a colossal amount of energy is carried out mainly by all the flavors of neutrinos and antineutrinos. The energy released in a supernova explosion is the difference in the binding energy of the parent star and a neutron star and such explosions give rise to about 10^{58} ν s and $\bar{\nu}$ s in a few tens of seconds of time, carrying out almost 99% of the gravitational binding energy of a dying star.

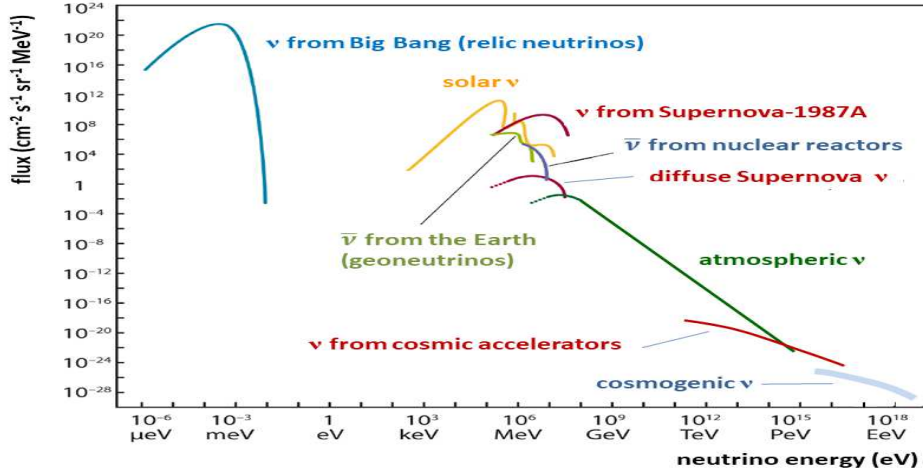


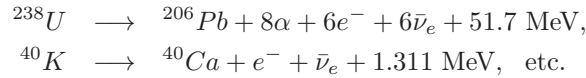
Figure 1.2: Particle fluxes of neutrinos from different sources on earth. The flux is given in units of neutrinos per square centimeter, second, steradian and MeV. The neutrinos from the sun are indeed neutrinos, while those from the earth's interior and from nuclear reactors are antineutrinos. All other sources contain about as many neutrinos as antineutrinos. The relic neutrinos from the Big Bang, the diffuse supernova neutrinos and, at highest energies, cosmogenic neutrinos have not been detected yet (courtesy C. Spiering) [87].

Active galactic nuclei (AGN) are considered to be one of the sources of very high energy neutrinos [93]. These AGN can accelerate protons up to about a maximum energy of $\sim 10^{20}$ eV and are surrounded by high intensity radiation fields, which act as the source of photo-hadron interactions and subsequently give rise to neutrinos.

Cosmogenic neutrinos are produced in the interaction of cosmic rays like the nucleons, whether they are free or bound in nuclei with the Lorentz boost factor $\Gamma \geq 10^{10}$ with the cosmic microwave background radiation and gives rise to photo-pion production, where the pions decay to give rise to neutrinos:

$$N + \gamma \rightarrow N' + \pi^\pm; \quad N, N' = p \text{ or } n.$$

The earth's interior radiates heat at the rate of about 47 TW. Some part of this heat loss is accounted for the heat generated upon the decay of radioactive isotopes like ^{40}K , ^{232}Th , ^{238}U , etc. in the earth's interior which produce antineutrinos through a series of decays including beta decays like



which constitute geoneutrinos [94]. It has been estimated that about $10^6 \bar{\nu}_e/\text{cm}^2$ reach the earth's surface from the decay of radioactive isotopes present in the earth's core. Recently, the information about spatial distribution of radionuclides has been studied and from this the size of the earth's core and mantle has been estimated.

The cosmic-neutrino background (CνB) or more commonly known as the relic neutrinos are the relics of the Big Bang and their origin is similar to the cosmic microwave background radiation observed by Penzias and Wilson in 1965. CνB are neutrinos which decoupled from matter when the universe was around one second old. It is estimated that these relic neutrinos have a temperature of about 1.95 K and an average density of around $330/\text{cm}^3$.

- **Man made sources: accelerator and reactor (anti)neutrinos**

Accelerator and reactor based neutrino and antineutrino sources have been crucial to understand the neutrino properties. Markov [65], Pontecorvo [66], and Schwartz [67], independently, proposed the idea of doing neutrino experiments with accelerators. They proposed the possibility of an experiment making use of a neutrino beam produced by pion decays at the proton accelerators. The more robust experiments with high energy neutrinos started with the development of synchrotron accelerators during 1960s, the AGS at Brookhaven and the PS at CERN operating at proton energies up to 30 GeV, and with this new window of studying neutrino interactions at the GeV scale opened. The first experiments with the accelerator neutrinos ran in 1962 at Brookhaven and CERN which showed ν_e and ν_μ are different particles [71]. The accelerator facilities are used to accelerate the protons to very high energies. These highly energetic protons are smashed into a target, the target can be any material, although it has to be able to withstand very high temperatures. When a proton traveling near the speed of light hits a target, it slows down and the proton's energy is used to produce a jet of hadrons. There are different kinds of particles in this jet, however, the most common are pions and kaons. The charged pions so produced are unstable

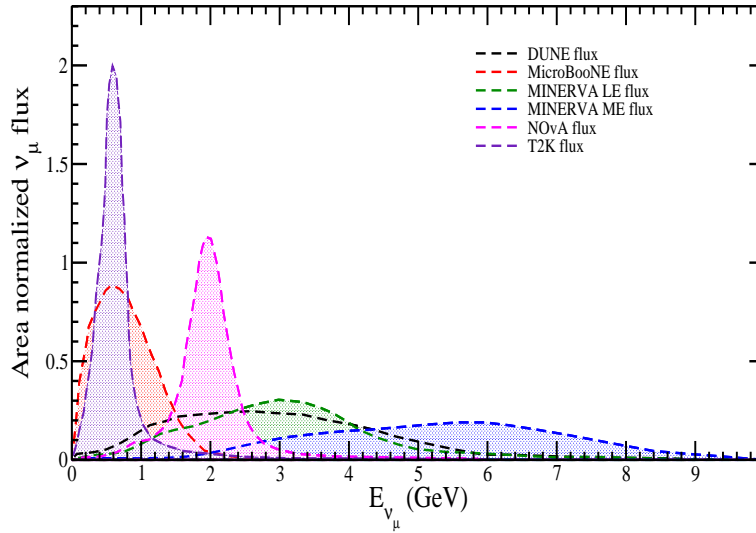


Figure 1.3: Neutrino flux as a function of neutrino energy for the accelerator neutrinos.

and decay essentially into muons and neutrinos. A meson, carrying electric charge, can be collimated using electric and magnetic fields known as magnetic horns. Thus, to get a neutrino beam in a certain direction, one points the pions/kaons in the direction of the detector. A properly designed horn system can enhance the neutrino flux. To estimate the neutrino flux with better accuracy, it is important to precisely measure the momentum and the angular spectra of the mesons. In 1965, at BNL a new method to determine the flux of neutrinos as a function of the protons on target (POT) was implemented which was later applied at CERN in 1967. Later accelerator neutrino experiments started at ANL. With the start of 1970s several accelerator neutrino experiments started to operate like the 350–400 GeV proton accelerator at Fermilab, the 70 GeV proton accelerator at Serpukhov, and in 1976, the 300 GeV super proton synchrotron (SPS) at CERN and since then the tradition of using accelerator neutrinos have gradually strengthened [95, 96].

In the beginning of 21st century, several neutrino experiments started coming up around the globe like MiniBooNE, K2K, CNGS, MicroBooNE, NOvA, etc. and have used accelerators to produce pions and kaons which were collimated to produce neutrinos. The next generation experiment DUNE@Fermilab would be using imaging type of liquid argon time projection chamber (LArTPC), and similarly T2HyperK in Japan would be important in addition to the current generation experiments to understand many of the neutrino properties. In Fig. 1.3, we show the neutrino spectra of some of the accelerator experiments.

The first antineutrino ($\bar{\nu}_e$) was observed at the nuclear reactor and since then many more studies using reactor antineutrinos have been performed. This is because the nuclear reactors are intense, pure and controllable sources of $\bar{\nu}_e$. The recent experiments like Daya Bay, RENO, Chooz, Double Chooz, etc. have resulted precise information about neutrino properties. The next generation experiment JUNO is expected to shed more light on the neutrino properties. There are four main radioisotopes viz. ^{235}U , ^{238}U , ^{239}Pu and ^{241}Pu , which are responsible for the production of almost 99% of $\bar{\nu}_e$ s, and in each fission reaction about six $\bar{\nu}_e$ s are produced. Therefore, typically for each 1 GW of thermal energy power about 6×10^{20} $\bar{\nu}_e$ s are released. These antineutrinos have a maximum energy of about 8 MeV as shown in Fig. 1.2.

1.1.3. Masses, mixing and oscillation of neutrinos

• Neutrino masses

Experimentally, the neutrino masses are measured for the different flavors of neutrinos in different ways [19]:

- (i) direct determination of m_{ν_e} by studying the end point energy spectrum of electrons produced in the beta decay of nuclei.
- (ii) m_{ν_e} determination by the e^- -capture reaction on nuclei.
- (ii) m_{ν_μ} determination from the pion decay.
- (iii) m_{ν_τ} determination from the tau decay.
- (iv) indirect determination of m_{ν_e} from astrophysics, cosmology and NDBD.

It was Fermi [3, 4] and Perrin [5] who first discussed the determination of the neutrino mass from the study of the end-point spectrum of beta decay. These works were followed by the work of Henderson [6] who studied the thorium

beta decay spectrum and concluded that the mass of neutrino must be much smaller than the electron mass. Hanna and Pontecorvo [97] in 1949, through the measurement of the beta-decay spectrum of tritium concluded that the mass of neutrino could not be larger than 500 eV. In 1972, Bergkvist [98] in his seminal work measured the energy spectrum of the electrons near threshold end point in tritium decay and concluded that $m_{\nu_e} < 60$ eV, which was almost a factor of ten smaller than the limit given by Hanna and Pontecorvo [97]. Later many other attempts have been made to determine the ν_e mass.

The present upper limits on the neutrino masses are [19]:

$$- \nu_e, \bar{\nu}_e: m_\nu \leq 1.1 \text{ eV}, \quad \nu_\mu, \bar{\nu}_\mu: m_\nu \leq 190 \text{ keV} \quad 90\% \text{ CL} \quad \nu_\tau, \bar{\nu}_\tau: m_\nu \leq 18.2 \text{ MeV} \quad 95\% \text{ CL}$$

• Neutrino mixing and oscillations

Pontecorvo [99] in 1957 proposed the idea of neutrino oscillation by stating that the physical state of neutrinos produced in weak interaction processes is a superposition of neutrino and antineutrino states with definite masses. This was developed in analogy with the neutral kaon regeneration phenomenon which was proposed by Gell-Mann and Pais [100], where K^0 and \bar{K}^0 could transform into each other via weak interaction with intermediate states of pions $K^0 \longleftrightarrow 2\pi \longleftrightarrow \bar{K}^0$, $K^0 \longleftrightarrow 3\pi \longleftrightarrow \bar{K}^0$, which implies that a beam that initially consists of $|K^0\rangle$ pure state, would have some component of $|\bar{K}^0\rangle$ after some time and they propagate as the superposition of the states, $|K_1\rangle$ and $|K_2\rangle$, having definite masses and decay widths. Later Maki, Nakagawa and Sakata [101] applied the idea of neutrino oscillation in flavor space in which neutrino oscillation between neutrinos of two flavor i.e. ν_e and ν_μ was proposed and was later extended to three flavors of neutrinos. In the three flavor neutrino oscillation, a neutrino created in a specific flavor eigenstate is a specific quantum superposition of all three mass eigenstates. As a consequence the three flavor of neutrinos, viz. ν_e, ν_μ, ν_τ , while propagating in space, travel as some admixture of three neutrino mass eigenstates viz. ν_i ($i = 1, 2, 3$) with masses m_i , where the strengths of the mixing of the mass eigenstates for the three neutrino flavors are different like ν_e has maximum contribution from ν_1 or ν_τ has maximum contribution from ν_3 mass eigenstate. The idea of neutrino mixing leading to neutrino oscillations requires the neutrino mass states to be nondegenerate and in the case of n flavor oscillation, $(n - 1)$ neutrino mass states have nonzero masses.

The physics of neutrino mass, mixing and oscillations can be demonstrated by a simple example of two flavor mixing of ν_e and ν_μ in analogy with the quark mixing [18]. A pure ν_e beam described by a wave function while traveling in space may develop a component of ν_μ in this beam and the mixture of the ν_μ wave function will describe the probability of finding ν_μ component in the ν_e beam after a time t . We assume that the flavor states ν_e and ν_μ participating in the weak interactions are mixture of the mass eigenstates ν_1 and ν_2 and the mixing is described by a unitary mixing matrix U such that:

$$\nu_{l=e,\mu} = \sum_{i=1,2} U_{li} \nu_i. \quad (1.4)$$

The unitarity of the U matrix requires that in 2-dimensional space it is described by one parameter which is generally chosen to be θ such that:

$$U = \begin{pmatrix} c_{12} & s_{12} \\ -s_{12} & c_{12} \end{pmatrix} \quad (1.5)$$

where $c_{12} = \cos\theta$ and $s_{12} = \sin\theta$. As pure beam of ν_e at $t = 0$ propagates, the mass eigenstates $|\nu_1\rangle$ and $|\nu_2\rangle$, occurring in Eq. (1.4), would evolve according to

$$|\nu_1(t)\rangle = \nu_1(0)e^{-iE_1 t}; \quad |\nu_2(t)\rangle = \nu_2(0)e^{-iE_2 t}, \quad (1.6)$$

where $E_1 = \sqrt{|\vec{p}|^2 + m_1^2} \approx |\vec{p}| + \frac{m_1^2}{2|\vec{p}|}$ and $E_2 = \sqrt{|\vec{p}|^2 + m_2^2} \approx |\vec{p}| + \frac{m_2^2}{2|\vec{p}|}$, with common momentum \vec{p} and energies E_1 and E_2 . m_1 and m_2 are the masses of ν_1 and ν_2 states, respectively. After a time t , the state $|\nu_e(t)\rangle$ will be a different admixture of $|\nu_1\rangle$ and $|\nu_2\rangle$. The probability of finding ν_μ in the beam of ν_e at a later time t is given by [10]:

$$P(\nu_e \rightarrow \nu_\mu) = \sin^2 2\theta \sin^2 \left(\frac{\Delta m^2}{4E} L \right) = \sin^2 2\theta \sin^2 \left(1.27 \frac{\Delta m^2}{E} L \frac{[\text{eV}^2][\text{km}]}{[\text{GeV}]} \right). \quad (1.7)$$

Thus, we see that for $P(\nu_e \rightarrow \nu_\mu) \neq 0$ we need $\Delta m^2 \neq 0$ and $\theta \neq 0$ i.e. we need the mass difference between the neutrino mass eigenstates to be nonzero implying that at least one of them is massive and the mixing angle θ to be nonzero. Thus, if the explanation of the solar neutrino flux deficit and other deficits observed in the atmospheric, reactor and accelerator neutrinos are explained to be due to the neutrino oscillations, the neutrinos should have nonzero mass and the neutrino flavors should mix. In the case of three flavor neutrino mixing, these flavor and mass eigenstates are related by a 3×3 unitary lepton mixing matrix [10]:

$$|\nu_\alpha\rangle = \sum_{i=1}^3 U_{\alpha i} |\nu_i\rangle \quad (\alpha = e, \mu, \tau), \quad (1.8)$$

where U is Pontecorvo-Maki-Nakagawa-Sakata (PMNS) mixing matrix [99, 101, 102]. The most popular parameterization of the PMNS matrix is given by [19]:

$$U = \begin{pmatrix} c_{13}c_{12} & c_{13}s_{12} & s_{13}e^{-i\delta_{CP}} \\ -c_{23}s_{12} - s_{13}s_{23}c_{12}e^{i\delta_{CP}} & c_{23}c_{12} - s_{13}s_{23}s_{12}e^{i\delta_{CP}} & c_{13}s_{23} \\ s_{23}s_{12} - s_{13}c_{23}c_{12}e^{i\delta_{CP}} & -s_{23}c_{12} - s_{13}c_{23}s_{12}e^{i\delta_{CP}} & c_{13}c_{23} \end{pmatrix} \quad (1.9)$$

where $c_{ij} = \cos \theta_{ij}$ and $s_{ij} = \sin \theta_{ij}$, and δ is the CP violating phase.

The general expression for the transition probability is given by [10]:

$$P_{\nu_\alpha \rightarrow \nu_\beta}(L, E) = 4 \sum_{i>j} \left(|U_{\alpha i}|^2 |U_{\alpha j}|^2 \right) \sin^2 \left(\frac{\Delta m_{ij}^2}{4E} L \right). \quad (1.10)$$

For the three flavors of neutrinos $i, j = 1, 2, 3$, with $i > j$, the mass squared difference terms are Δm_{32}^2 , Δm_{31}^2 , and Δm_{21}^2 . Since

$$\Delta m_{32}^2 = m_3^2 - m_2^2 = (m_3^2 - m_1^2) + (m_1^2 - m_2^2) = \Delta m_{31}^2 - \Delta m_{21}^2, \quad (1.11)$$

therefore, only two of the three Δm_{ij} 's are independent.

In deriving Eqs. (1.7) and (1.10) for the oscillation probability, a plane wave description of neutrino beam given in Eq. (1.6) has been assumed. However, to give a realistic description of the neutrino propagation, a wave packet description is used [103, 104]. If one considers the neutrino described by the wave packet, then the transition probability of $\nu_\alpha \rightarrow \nu_\beta$ is obtained as [103, 104]:

$$P_{\nu_\alpha \rightarrow \nu_\beta}(L, E) \approx \sum_{ij} \left\{ U_{\alpha i}^* U_{\beta i} U_{\alpha j}^* U_{\beta j} \exp \left[-i \frac{2\pi L}{L_{ij}^{osc}} \right] \right\} \\ \times \left\{ \left(\frac{1}{1 + y_{ij}^2} \right)^{\frac{1}{4}} \exp(-\lambda_{ij}) \exp \left(-\frac{i}{2} \tan^{-1}(y_{ij}) \right) \exp(i\lambda_{ij} y_{ij}) \right\} \quad (1.12)$$

where

$$\begin{aligned} \lambda_{ij} &= \frac{x_{ij}^2}{1 + y_{ij}^2}, & y_{ij} &= \frac{L}{L_{ij}^{dis}}, & x_{ij} &= \frac{L}{L_{ij}^{coh}}, \\ L_{ij}^{coh} &= \frac{L_{ij}^{osc}}{\pi \sigma_{wp}}, & L_{ij}^{dis} &= \frac{L_{ij}^{osc}}{2\pi \sigma_{wp}^2}, & L_{ij}^{osc} &= \frac{4\pi E}{\Delta m_{ij}^2}, \\ \sigma_{wp} &= \frac{\sigma_\nu}{E_i(p_\nu)}. \end{aligned} \quad (1.13)$$

E_i is the energy of the $|\nu_i\rangle$ eigenstate, and p_ν is the mean momentum. The first term in Eq. (1.12) is the plane wave neutrino oscillation probability, modified by a numerical factor depending upon σ_ν , the width of the wave packet in the momentum space, which is independent of the neutrino energy. The term with quartic correction to y_{ij} describes the dispersion effects and depends on the dispersion length L_{ij}^{dis} . The $\exp(-\lambda_{ij})$ term corresponds to the decoherence effect arising due to the fact that the different neutrino mass eigenstates propagate at different speeds. The term x_{ij} is related to the coherence length L_{ij}^{coh} . It may also be observed from Eq. (1.13) that $x_{ij} \propto \sigma_{wp}$ while $y_{ij} \propto \sigma_{wp}^2$, therefore, if the wave packet impact $\sigma_{wp} \ll 1$, the dispersion effect is expected to be more suppressed and negligible.

The various experimental efforts, with the the solar, reactor, atmospheric, and accelerator neutrinos made with the short and long baseline experiments are sensitive to the different parameters of the PMNS matrix which have been tabulated in Table-1.1.

1.1.4. Electromagnetic properties of neutrinos

Pauli in his neutrino proposal speculated that the magnetic moment of this particle should not be larger than $e \times 10^{-13} \text{cm}$ [1]. Very soon after the discovery of antineutrinos, in 1956, Reines and Cowan [105] gave an upper limit on the neutrino magnetic moment $\mu_{\bar{\nu}_e} = 10^{-9} \mu_B$ (μ_B is the Bohr magneton), based on the extent of nonobservation of scintillator pulses along the path of reactor antineutrinos in their experiment. Their studies motivated Bernstein and Lee [106] and many others to phenomenologically study neutrino magnetic moment.

$\nu(\bar{\nu})$ -Experiment	Dominant	Important
Solar	θ_{12}	$\Delta m_{21}^2, \theta_{13}$
Reactor LBL	Δm_{21}^2	θ_{12}, θ_{13}
Reactor MBL	$\theta_{13}, \Delta m_{31,32}^2 $	
Atmospheric		$\theta_{23}, \Delta m_{31,32}^2 , \theta_{13}, \delta_{CP}$
Accelerator LBL $\nu_\mu(\bar{\nu}_\mu)$ disappearance	$ \Delta m_{31,32}^2 , \theta_{23}$	
Accelerator LBL $\nu_e(\bar{\nu}_e)$ appearance	δ_{CP}	θ_{13}, θ_{23}

Table 1.1: Sensitivity of the (anti)neutrino sources to the oscillation parameters [19].

In general, the electroweak properties of a spin $\frac{1}{2}$ Dirac particle are described in terms of the two vector form factors called the electric and the magnetic form factors, which in the static limit define the charge and the magnetic moment, and the two axial-vector form factors called the axial-vector and the tensor form factors which in the static limit define the axial charge and the electric dipole moment, and that is related to the matrix element of the electromagnetic current between the initial and final neutrino mass states [10]:

$$\langle \psi(p') | J_\mu^{EM} | \psi(p) \rangle = \bar{u}(p') [F_Q(Q^2)\gamma_\mu - F_M(Q^2)i\sigma_{\mu\nu}q^\nu + F_E(Q^2)\sigma_{\mu\nu}q^\nu\gamma_5 + F_A(Q^2)(-Q^2\gamma_\mu - q_\mu q) \gamma_5] u(p),$$

where $q = p - p'$, $F_Q(Q^2)$, $F_M(Q^2)$, $F_E(Q^2)$ and $F_A(Q^2)$ are, respectively, charge, magnetic dipole, electric dipole and axial charge neutrino electromagnetic form factors.

If the neutrino is considered to be the Dirac neutrino with nonzero mass, it could have these form factors to be nonvanishing and experimental attempts can be made to study them. In this case, they have magnetic dipole moment like neutrons and can have electric dipole moment if CP is violated in the lepton sector. Since neutrinos participate in weak interaction which violates CP invariance, they may have an electric dipole moment. If the neutrinos are Majorana fermions then from CPT invariance, regardless of whether CP invariance is violated or not, $F_Q(Q^2) = F_M(Q^2) = F_E(Q^2) = 0$, and only the axial-vector form factor $F_A(Q^2)$ can be nonvanishing. Thus the electromagnetic properties of the (anti)neutrinos depend upon the type of (anti)neutrinos.

- (i) The SM calculations for the magnetic moment of a neutrino depends upon its mass m_ν and is therefore very small of the order $3 \times 10^{-19} \frac{m_\nu}{eV} \mu_B$. There are models where the neutrino magnetic moment is not proportional to the neutrino mass and give larger magnetic moments [107, 108]. Experimentally, the laboratory limits on the neutrino magnetic moments are obtained by performing the elastic $\nu_e - e$, $\bar{\nu}_e - e$ and $\nu_\mu - e$ scattering. The present upper limits on the neutrino magnetic moments are [19]:

$$-\mu_{\nu_e} < 0.28 \times 10^{-10} \mu_B; \quad \mu_{\nu_\mu} < 6.8 \times 10^{-10} \mu_B; \quad \mu_{\nu_\tau} < 3.9 \times 10^{-7} \mu_B \quad 90\% \text{ CL}$$

- (ii) The neutrinos are assumed to be electrically neutral, but there are attempts to measure the charge of the neutrino in β -decays by measuring the charge of the neutron Q_n and the total charge of the proton and electron i.e. $|Q_p + Q_e|$ in the decay $n \rightarrow p + e^- + \bar{\nu}_e$ [109, 110]. This gives a limit on $Q_{\bar{\nu}} < (0.5 \pm 2.9) \times 10^{-21} e$. The astrophysical limit derived from the SN1987A supernova observation is [111]:

$$Q_{\bar{\nu}} < 2 \times 10^{-15} e.$$

- (iii) The charge of neutrino is consistent with zero to a very high degree of precision but it may have a charge distribution like a neutron. Attempts to determine the charge radius have been made [112] for ν_e and ν_μ from $\nu_e e$ [113], $\bar{\nu}_e e$ [114] and $\nu_\mu e$ [115] scattering. Like hadrons, the mean square charge radius of a neutrino is deduced from the measurement of the vector form factor in the $\nu_e e$ and $\nu_\mu e$ elastic scattering using the relation

$$\langle r^2 \rangle = 6 \frac{d}{dQ^2} F(Q^2) \Big|_{Q^2=0}, \quad (1.14)$$

where $F(Q^2)$ is the charge form factor corresponding to the matrix element of the vector current. In the standard model, the value of $\langle r^2 \rangle$ is estimated to be of the order of 10^{-32} cm^2 [116]. In the case of neutral particles, the value of $\langle r^2 \rangle$ could be negative or positive and the following experimental limits [19, 117, 118] are obtained in the case of ν_e and ν_μ :

$$\begin{aligned} -5.3 \times 10^{-32} &< [\langle r^2 \rangle_{\nu_\mu}] < 1.3 \times 10^{-32} \text{ cm}^2, \\ -0.77 \times 10^{-32} &< [\langle r^2 \rangle_{\nu_\mu}] < 2.5 \times 10^{-32} \text{ cm}^2, \\ -5.0 \times 10^{-32} &< [\langle r^2 \rangle_{\nu_e}] < 10.2 \times 10^{-32} \text{ cm}^2. \end{aligned}$$

1.2. Theoretical description of neutrinos and their interactions

1.2.1. Dirac neutrinos

The Dirac theory of electrons formulated in 1928 [119] is conventionally used to describe the neutrinos. The Pauli's neutrinos proposed in 1930 [1] were assumed to have a tiny mass but the later developments in the phenomenological study of neutrino interactions through the nuclear β decays and the (anti)neutrino-nucleus scattering using the Fermi or the $V - A$ theory of weak interactions seem to be consistent with neutrinos being massless. This did not pose any problem in applying the Dirac theory of electrons to neutrinos as the theory can be extrapolated smoothly to the massless limit of the spin $\frac{1}{2}$ fermion of mass $m \rightarrow 0$. These neutrinos are called Dirac neutrinos, ν^D , and the wave function $\Psi_{\nu^D}(x)$ describing these neutrinos satisfies the Dirac equation [119]:

$$(i\gamma^\mu \partial_\mu - m) \Psi_{\nu^D}(x) = 0, \quad (1.15)$$

where γ^μ s ($\mu = 0, 1, 2, 3$) are four 4×4 matrices and satisfy the algebra:

$$\{\gamma^\mu, \gamma^\nu\} = 2g^{\mu\nu}, \quad g^{00} = 1, \quad g^{ij} = -\delta_{ij} \quad (i, j = 1, 2, 3), \quad \gamma^{\mu\dagger} = \gamma^0 \gamma^\mu \gamma^0. \quad (1.16)$$

These relations are independent of the representation used to parameterize the γ^μ matrices for which many representations exist. The most popular is the Pauli-Dirac representation in which

$$\gamma^0 = \begin{pmatrix} \mathbb{I} & 0 \\ 0 & -\mathbb{I} \end{pmatrix}, \quad \gamma^i = \begin{pmatrix} 0 & \sigma^i \\ -\sigma^i & 0 \end{pmatrix},$$

where σ^i being Pauli matrices. But there are parameterizations like the Weyl, and Majorana representations, which are also used to describe the neutrinos [10]. The wave function Ψ_{ν^D} in Eq. (1.15) is a four component spinor and is generally written as

$$\Psi_{\nu^D}(x) = \sum_{r,p} \frac{1}{\sqrt{2\omega_{\vec{p}}}} [a_r(p) u_r(\vec{p}) e^{-ip \cdot x} + b_r^\dagger(p) v_r(\vec{p}) e^{ip \cdot x}], \quad (1.17)$$

where $u_r(\vec{p})$ and $v_r(\vec{p})$ are the two component spinors which describe the two spin states of particles (neutrinos) and antiparticles (antineutrinos) corresponding to the spin states labeled by $|s \ s_z\rangle = |\frac{1}{2} \ \pm \frac{1}{2}\rangle$ and satisfy, in the momentum space, the equations

$$(\not{p} - m) u_r(\vec{p}) = 0; \quad (\not{p} + m) v_r(\vec{p}) = 0. \quad (1.18)$$

If the spin quantization axis is chosen in the direction of motion along the Z -axis, then the ν^D state $|\frac{1}{2} \ + \frac{1}{2}\rangle$ with its spin along the $+Z$ -axis is denoted by ν_+^D (right handed), while the ν^D state $|\frac{1}{2} \ - \frac{1}{2}\rangle$ has the spin opposite to Z -axis (left handed) is denoted by ν_-^D . Similarly, we have the two spin up and spin down states of the antineutrinos $\bar{\nu}_+^D$ and $\bar{\nu}_-^D$. It should be noted that under CPT transformation, a particle becomes an antiparticle with opposite spin, $\nu_-^D \rightarrow \bar{\nu}_+^D$ and $\nu_+^D \rightarrow \bar{\nu}_-^D$, with the same mass. Moreover, if the neutrinos have a mass then its speed is less than the speed of light and an observer can move faster than this speed. In this frame, an observer would see a right handed neutrino ν_+^D as the left handed ν_-^D but all other properties, if any, like the lepton number, etc., would be the same. In fact, ν_+^D and ν_-^D are the two spin states of the same particle neutrino. Similarly, $\bar{\nu}_+^D$ and $\bar{\nu}_-^D$ are the two spin states of the same antineutrino. There are, therefore, four states of a Dirac neutrino, described by Ψ_{ν^D} . The phenomenological study of the weak interaction processes involving (anti)neutrinos establishes that for each flavor of neutrinos [10]:

- (i) the neutrinos are left handed i.e. ν_-^D and the antineutrinos are right handed i.e. $\bar{\nu}_+^D$, which take part in the weak interactions.
- (ii) ν_-^D always produces a charged lepton l^- and $\bar{\nu}_+^D$ always produces a charged lepton l^+ in charged current (CC) interactions, which imply that ν_-^D and $\bar{\nu}_+^D$ are distinct particles.

To ensure that ν_-^D and $\bar{\nu}_+^D$ are distinct particles like l^- and l^+ and obey the selection rules of weak processes, it was proposed that

1. there exists a new quantum number called lepton number L_l for each flavor l and $(\nu_{l-}^D \ l^-)$ were assigned $L_l = +1$ while $(\bar{\nu}_{l+}^D \ l^+)$ were assigned $L_l = -1$.
2. The lepton number L_l is conserved for each flavor.

- (iii) While the charged leptons and their antiparticles like l^- and l^+ are different in their charge and lepton number, the corresponding neutrinos and antineutrinos being neutral are different only in their lepton number L_l and helicities. It should be noted that ν_{l+}^D and ν_{l-}^D have the same lepton number $L_l = +1$. Similarly, $\bar{\nu}_{l+}^D$ and $\bar{\nu}_{l-}^D$ also have the same lepton number $L_l = -1$.

1.2.2. Weyl neutrinos

In the limit of mass $m \rightarrow 0$, interesting features arise which become more intriguing in the case of neutrinos being neutral particles. In this limit, the Dirac equation becomes Weyl equation and the Weyl wave function Ψ_{ν^W} satisfies

$$i\gamma^\mu \partial_\mu \Psi_{\nu^W}(x) = 0. \quad (1.19)$$

This equation of motion for a spin $\frac{1}{2}$ particle with $m = 0$ was especially studied by Weyl in 1929 [120], a year after the Dirac equation [119], and is most easily solved using the Weyl representation for the γ matrices [120].

However, we discuss its solution using the chirality operator which is defined as $\gamma^5 = i\gamma^0\gamma^1\gamma^2\gamma^3 = \begin{pmatrix} 0 & \mathbb{I} \\ \mathbb{I} & 0 \end{pmatrix}$ for the following reason. Using the 4-dimensional representation of spin $\vec{\Sigma} = \begin{pmatrix} \vec{\sigma} & 0 \\ 0 & \vec{\sigma} \end{pmatrix} = \gamma^5\gamma^0\vec{\gamma}$, the helicity operator $\vec{\Sigma} \cdot \hat{p}$ is written as $\vec{\Sigma} \cdot \hat{p} = \gamma^5\gamma_0\vec{\gamma} \cdot \hat{p}$. In the case of $m \rightarrow 0$, the Weyl equation is written, in momentum space, as

$$\not{p} \Psi_{\nu^W}(p) = 0. \quad (1.20)$$

Now, consider the equation

$$\vec{\Sigma} \cdot \vec{p} \Psi_{\nu^W}(p) = \gamma^5\gamma_0\vec{\gamma} \cdot \vec{p} \Psi_{\nu^W}(p). \quad (1.21)$$

Using $p_0 = |\vec{p}|$ and Eq. (1.20) in the case of $m = 0$, we get

$$\vec{\Sigma} \cdot \hat{p} \Psi_{\nu^W}(p) = \gamma^5 \Psi_{\nu^W}(p). \quad (1.22)$$

Thus, in the case of $m = 0$, γ^5 is the helicity operator $\vec{\Sigma} \cdot \hat{p}$, which is also called the chirality operator. Since $\vec{\Sigma} \cdot \hat{p} \vec{\Sigma} \cdot \hat{p} \equiv (\gamma^5)^2 = 1$, γ^5 has two eigenvalues ± 1 corresponding to helicity $+1$ and -1 , also called the right handed (R) and left handed (L) helicity states of the massless neutrinos. The eigen functions corresponding to the eigenvalues $+1$ and -1 are, respectively, Ψ_R^W and Ψ_L^W , which satisfy

$$\vec{\Sigma} \cdot \hat{p} \Psi_R^W(p) = \gamma_5 \Psi_R^W(p) = (+1) \Psi_R^W(p), \quad \vec{\Sigma} \cdot \hat{p} \Psi_L^W(p) = \gamma_5 \Psi_L^W(p) = (-1) \Psi_L^W(p). \quad (1.23)$$

It should be noted that in $m \rightarrow 0$, ν_R^W and ν_L^W are two distinct particles and not the two spin states of one particle as in the case of the Dirac neutrinos ν_+^D and ν_-^D (in the case of $m \neq 0$) because there exists no frame in which ν_R^W would appear as ν_L^W due to the Weyl neutrinos moving with the speed of light. In principle, while ν_+^D and ν_-^D have the same lepton number, ν_R^W and ν_L^W could have different lepton numbers. If neutrinos exist in ν_L^W state, then they cannot exist in ν_R^W state. Consequently, the antineutrinos will exist in $\bar{\nu}_R^W$ state and not in $\bar{\nu}_L^W$ state. Thus, the Weyl (anti)neutrinos have only two states unlike the Dirac (anti)neutrinos which have four states. If physical neutrinos observed in nuclear β decays or other weak processes are ν_L^W (or ν_R^W), the massless Weyl neutrinos imply maximal violation of the left-right symmetry i.e., parity violation. This is the reason that the Weyl equation was disfavored during 1930–1957. After the parity violation was proposed and observed experimentally [16], the two component theory of neutrinos with chiral invariance was proposed by Lee and Yang [121], Landau [122], and Salam [123]. If the two states ν_L^W and ν_R^W are independent, in the case of $m = 0$, then we can write a neutrino state ν^W as

$$\Psi^W = \Psi_L^W + \Psi_R^W. \quad (1.24)$$

Using Eqs. (1.23) and (1.24), we obtain

$$\Psi_L^W = \frac{\mathbb{I} - \gamma_5}{2} \Psi^W, \quad \Psi_R^W = \frac{\mathbb{I} + \gamma_5}{2} \Psi^W, \quad (1.25)$$

as the left-handed and right-handed Weyl neutrinos. Conversely, if ν^W exists either in ν_L^W or in ν_R^W state, it has to be massless as the mass term in the Lagrangian given by

$$\mathcal{L}_{mass}^W = -m \bar{\Psi}^W \Psi^W = -m (\bar{\Psi}_L^W \Psi_R^W + \bar{\Psi}_R^W \Psi_L^W) \quad (1.26)$$

vanishes.

The $V - A$ theory of weak interaction was formulated using the two component neutrinos by Sudarshan and Marshak [11], and Feynman and Gell-Mann [12] using left handed neutrinos ν_L^W . The antineutrino in the Weyl theory are obtained in a similar manner by performing a CPT transformation such that

$$\nu_R^W \xrightarrow{CPT} \bar{\nu}_L^W, \quad \nu_L^W \xrightarrow{CPT} \bar{\nu}_R^W. \quad (1.27)$$

The relation between the Dirac and Weyl neutrinos can be expressed as

- (i) Four component Dirac spinor is equivalent to two two-component Weyl spinors.
- (ii) While Dirac neutrinos could have nonvanishing mass (m) and can be extrapolated to $m \rightarrow 0$, Weyl neutrinos are necessarily massless.
- (iii) $\nu_{+(-)}^D \xrightarrow{m \rightarrow 0} \nu_{R(L)}^W; \bar{\nu}_{+(-)}^D \xrightarrow{m \rightarrow 0} \bar{\nu}_{R(L)}^W$.

1.2.3. Majorana neutrinos

While the phenomenology of the weak interaction processes was consistent with the massless neutrinos, the experimental attempts to measure their masses were continuing relentlessly. Theoretically also the mass of ν_e ($\bar{\nu}_e$) was being inferred from the experimental observations made in astrophysics and cosmology. The improvements in the experimental limits of the neutrino masses of various flavors are reported periodically and a nonzero mass for neutrino is not ruled out. However, the observation of neutrino oscillations involving all the three flavors of neutrinos ν_e , ν_μ and ν_τ in the experiments with solar, reactor, atmospheric, and accelerator neutrinos, confirmed that the neutrinos (at least two flavors) have masses even though very small. This rules out the neutrinos being Weyl neutrinos. However, the neutrinos being neutral particles could be still described by a two component neutrino, if they are their own antiparticles. Such a possibility was studied by Majorana in his celebrated paper on “The symmetry of the theory of electrons and positrons” [124]. These neutrinos are called Majorana neutrinos ν^M . If the Majorana neutrino is its own antiparticle, then its wave function described by $\Psi_{\nu^M}(x)$ satisfies the equation

$$\Psi_{\nu^M}(x) = \Psi_{\nu^M}^*(x) \quad (1.28)$$

implying that $\Psi_{\nu^M}(x)$ is real. But the wave function of the neutrinos written in Eq. (1.15) or Eq. (1.28) is complex due to some of the coefficients γ^μ being complex. If a representation could be found in which all the γ^μ 's are imaginary such that the coefficients $(i\gamma_\mu\partial^\mu - m)$ are real, then the solutions $\Psi_\nu(x)$ and Eq. (1.28) would be satisfied. This was done by Majorana by using Majorana representation of the gamma matrices, in which $\tilde{\gamma}_\mu$'s are defined as:

$$\tilde{\gamma}^0 = \begin{pmatrix} 0 & \sigma_2 \\ \sigma_2 & 0 \end{pmatrix}, \quad \tilde{\gamma}^1 = \begin{pmatrix} i\sigma_3 & 0 \\ 0 & i\sigma_3 \end{pmatrix}, \quad \tilde{\gamma}^2 = \begin{pmatrix} 0 & -\sigma_2 \\ \sigma_2 & 0 \end{pmatrix}, \quad \tilde{\gamma}^3 = \begin{pmatrix} -i\sigma_1 & 0 \\ 0 & -i\sigma_1 \end{pmatrix},$$

$\tilde{\gamma}^5 = i\tilde{\gamma}^0\tilde{\gamma}^1\tilde{\gamma}^2\tilde{\gamma}^3 = \begin{pmatrix} \sigma_2 & 0 \\ 0 & -\sigma_2 \end{pmatrix}$, and all of them are purely imaginary. This Majorana representation $\tilde{\gamma}^\mu$ of gamma matrices satisfy the algebra given in Eq. (1.16). However, Eq. (1.28) is not covariant i.e. if this equation is satisfied in Majorana representation in one Lorentz frame, it will not be satisfied in another Lorentz frame as the Lorentz transformation of spinors depend on $\tilde{\gamma}^\mu$ matrices which change in another frame. For making this equation valid in other frames a conjugate field $\Psi_\nu^c(x)$ is defined as

$$\Psi_\nu^c(x) = C\gamma^0\Psi_\nu^*(x), \quad (1.29)$$

where C is chosen such that $\Psi_\nu(x)$ and Ψ_ν^c satisfy

$$\Psi_\nu^c(x) = \Psi_\nu^{c*}(x). \quad (1.30)$$

The matrix C is a unitary matrix, which satisfies $CC^\dagger = C^\dagger C = \mathbb{I}_{4 \times 4}$, $C^T = C^\dagger = -C$, and $C^2 = -\mathbb{I}_{4 \times 4}$ and depends upon the representation used for defining the γ^μ matrices. Obviously in Majorana representation $C = C^M = -i\tilde{\gamma}^0$ such that Eq. (1.30) is recovered. In Pauli-Dirac representation, $C = C^D = i\gamma^2\gamma^0$ with γ^2 and γ^0 being the Pauli-Dirac gamma matrices.

Eq. (1.30) implies that in Eq. (1.15) $u_r(\vec{p})$ and $v_r(\vec{p})$ satisfy [125]

$$C\gamma^0 v_r^*(\vec{p}) = v_r(\vec{p}) \quad C\gamma^0 u_r^*(\vec{p}) = u_r(\vec{p}). \quad (1.31)$$

The Majorana neutrino is, therefore, described by a wave function $\Psi_{\nu^M}(x)$ given by

$$\Psi_{\nu^M}(x) = \Psi_\nu^c(x) \quad (1.32)$$

and $\Psi_{\nu^M}(x)$ can be defined in any representation provided C and $\Psi_\nu^*(x)$ are chosen in the same representation. The field theory of Majorana particles is obtained by treating $\Psi_{\nu^M}(x)$ as fields and formulating its quantization as discussed in Refs. [124, 126, 127].

Eq. (1.29) relating the neutrino wave functions in various representation ensures that the wave function of neutrino has the required covariance properties under the Lorentz transformation in any given representation. The Majorana neutrinos could have mass like the Dirac neutrinos or could be massless like the Weyl neutrinos. In the case of Majorana neutrinos with mass, the Lagrangian would contain a term like $m\bar{\Psi}_\nu^C(x)\Psi_\nu(x)$ or $m\bar{\Psi}_\nu^C(x)\Psi_\nu^C(x)$ or $m\bar{\Psi}_\nu(x)\Psi_\nu^C(x)$. The mechanism for generation of mass or a field theoretic description of Majorana neutrinos and its properties under C , CP and CPT transformations is beyond the scope of this article. However, some interesting features appear due to the neutrinos being neutral Majorana particles which we mention in the following:

- (i) If neutrinos are their own antiparticles i.e. $\nu^M = \bar{\nu}^M$ then there are only two neutrino states with spin states $|\frac{1}{2}, +\frac{1}{2}\rangle$ and $|\frac{1}{2}, -\frac{1}{2}\rangle$, even in the case of massive Majorana neutrinos. In the case of massless Majorana neutrinos, the two spin states become helicity states and describe the two independent particles.
- (ii) The familiar picture of neutrino and antineutrino interactions conceived in the Dirac's neutrino picture is replaced by the spin dependent interaction of neutrinos in which a left-handed Majorana neutrinos ν_L^M produces a l^- and a right-handed Majorana neutrinos ν_R^M produces a l^+ through the weak CC interactions.

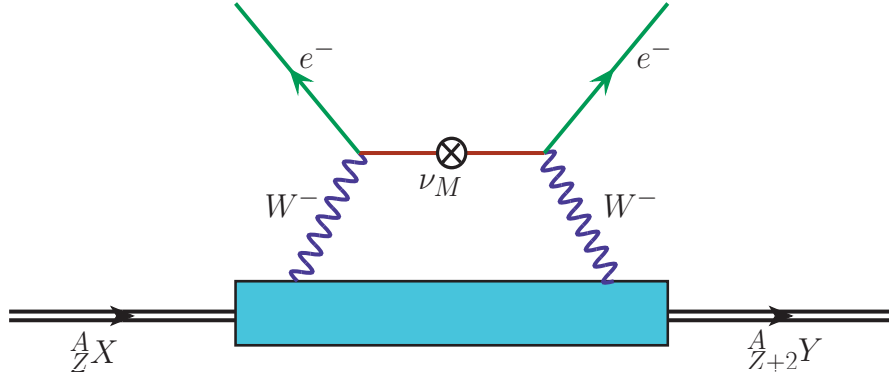


Figure 1.4: Feynman diagram of the transition $dd \rightarrow uue^-e^-$, which induced NDBD.

(iii) The concept of lepton number (L_l) and its conservation is irrelevant in the case of Majorana neutrinos.

(iv) Under the CPT transformations $\nu^M(s)$ and $\nu^M(-s)$ are related

$$CPT |\nu^M(s)\rangle = \eta^s |\nu^M(-s)\rangle. \quad (1.33)$$

(v) The CPT properties of the Majorana neutrino ensure that they do not have vector current interaction implying that the charge and magnetic moment of Majorana neutrinos vanish [125].

(vi) It is a challenging task to discriminate between the Dirac and Majorana neutrinos specially if the neutrinos are completely relativistic or ultrarelativistic. This is because, in this case, all the three types of neutrinos (antineutrinos) are left (right) handed particles distinguished by their helicities $-1(+1)$, notwithstanding the fact that in the case of Dirac and Weyl neutrinos (antineutrinos) they are also distinguished by an additional quantum number, i.e., lepton number.

There is extensive discussion of various processes, in which there is a possibility to distinguish between the Dirac and the Majorana neutrinos [128, 129]. However, the most distinct process which establishes the existence of Majorana neutrinos is the process of NDBD of nuclei in which the $\bar{\nu}_e$ produced in the process $n \rightarrow p + e^- + \bar{\nu}_e$ is absorbed by another neutron i.e. $n + \bar{\nu}_e (= \nu_e) \rightarrow e^- + p$ such that $n + n \rightarrow p + p + e^- + e^-$ in the nucleus leading to ${}^A_Z X \rightarrow {}^A_{Z+2} Y + e^- + e^-$ as shown in Fig. 1.4. These processes were discussed by Racah [130] and Furry [131, 132] soon after Majorana's theory. In Fig. 1.4, \otimes denotes the neutrino interaction in the Majorana mass term, which changes the helicity of the neutrino. Such an interaction requires the Majorana neutrino to have mass or the presence of right handed currents. Various theoretical models have been used to calculate NDBD using BSM physics. Experimentally, there are enormous efforts being made to observe such nuclear decays in various experiments being done around the world, for example, EXO-200, KamLAND-Zen, NEMO-3, CUORE, ELEGANT-IV, GERDA, etc. For a review, see Ref. [133].

In this work, we focus on the neutrino interactions with matter using the SM. The SM is presented briefly in the following Section.

1.3. Standard model of electroweak interactions

1.3.1. Introduction

The SM was formulated by Weinberg [20] and Salam [21] as the theory of the electroweak interaction of leptons. It was extended to the quark sector using the Glashow, Illiopolis and Maiani [22] scheme of quark mixing proposed earlier by Cabibbo [17]. The formulation of SM makes use of the experimental results on the properties and interactions of neutrinos obtained from the phenomenological $V - A$ theory of weak interactions and the theoretical ideas from the local gauge field theories based on the invariance under continuous symmetry, to generate the interactions. Such gauge field theories require the existence of massless vector bosons known as Nambu-Goldstone bosons, which mediate the interaction between the matter fields describing the physical particles in field theories. This mechanism of generating interactions works in the case of electromagnetic interactions where the invariance of the Lagrangian describing the charged leptons $l (= e, \mu, \tau)$ under the local gauge $U(1)$ symmetry, generates a massless vector field $A^\mu(x)$, which is identified as the electromagnetic field and mediates the electromagnetic interaction between the charged particles. However, this mechanism is not sufficient to generate CC weak interactions, which are mediated by the two massive vector fields $W^{\mu+}(x)$ and $W^{\mu-}(x)$. Consequently, a symmetry group higher than $U(1)$, which can generate more than one vector field and includes a mechanism to generate masses of the vector fields is needed. In the SM proposed by Weinberg [20] and

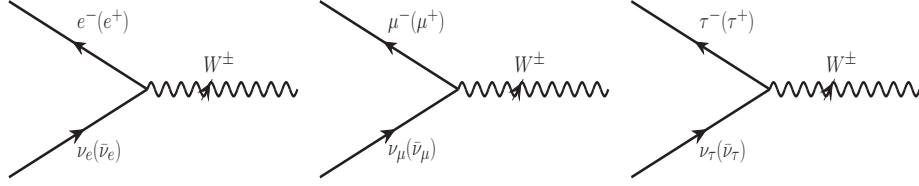


Figure 1.5: Feynman diagrams for $\nu_l l^- W^+$ ($l = e, \mu, \tau$) and $\bar{\nu}_l l^+ W^-$ ($l = e, \mu, \tau$) vertices.

Salam [21], a higher group $SU(2)_{I_W} \times U(1)_{Y_W}$ (where I_W and Y_W are the isospin and hypercharge operators in weak interactions defined in analogy with the strong interactions), is considered, which requires the existence of four massless vector fields, when the invariance under this symmetry is imposed on the Lagrangian. The masses of three of these vector fields leaving one field massless are generated using the mechanism of spontaneous breaking of symmetry proposed by Englert and Brout [24], and Higgs [25] by introducing a doublet of interacting scalar fields $\phi^+(x)$ and $\phi^0(x)$ in the theory. The two out of the three massive fields are identified as $W^{\mu+}(x)$ and $W^{\mu-}(x)$ fields, mediating the CC weak interactions and the third massive field is the neutral vector field Z^μ , which is new and is predicted to mediate NC interactions in the weak sector. The massless field $A^\mu(x)$ is identified as the electromagnetic field. The SM was shown later, to be renormalizable by 't Hooft and Veltman [26], and Lee and Zinn-Justin [27].

For a review of the local gauge field theories based on the continuous symmetries, implying the existence of massless Nambu-Goldstone bosons and the phenomenon of Higgs mechanism to generate the masses of the Nambu-Goldstone bosons and the renormalizability of the SM, the reader is referred to a general text on quantum field theory [134].

1.3.2. SM of electroweak interaction of leptons

The essential results about the neutrino properties and their interactions obtained from the phenomenological $V - A$ theory used in formulating the SM are summarized as:

- (i) the (anti)neutrinos are considered to be neutral, massless, left-handed spin $\frac{1}{2}$ particles with helicity $(+1) - 1$, which exist in three flavors i.e. $\nu_l = \nu_e, \nu_\mu, \nu_\tau$.
- (ii) the (anti)neutrino of each flavor l are assigned a lepton number $L_l = (-1) + 1$, which is conserved in weak interactions.
- (iii) the neutrinos of flavor $l (= e, \mu, \tau)$ interact with other leptons through the interaction of leptonic currents $l^\mu(x)$, which has $V - A$ structure defined as

$$l^\mu(x) = \sum_{l=e,\mu,\tau} \bar{\Psi}_l(x) \gamma_\mu (1 - \gamma_5) \Psi_{\nu_l}(x) \quad (1.34)$$

and interact with $W_\mu^+(x)$ to produce charged leptons of the same flavor. In the lowest order, the interaction Lagrangian for describing the $\nu_l l W$ vertex is given by:

$$L_{\text{WI}}^{\text{int}} = \frac{g}{2\sqrt{2}} (l^\mu(x) W_\mu^+(x) + h.c.), \quad (1.35)$$

where $\frac{g}{2\sqrt{2}}$ is the strength of the $\nu_l l W$ interaction. As a consequence of the $V - A$ structure of the leptonic currents, the left handed neutrino ($\nu_L = \frac{1}{2}(1 - \gamma_5)\Psi_\nu$) interacts only with the left handed component of the electron ($e_L = \frac{1}{2}(1 - \gamma_5)\Psi_e$) and $\bar{\Psi}_{e_R} \gamma_\mu (1 - \gamma_5) \Psi_{\nu_{e_L}} = 0$. Therefore, only ν_L and e_L participate in the weak interaction. Moreover, ν_L and e_L always interact in pairs of (ν_L, e_L) . The Feynman diagrams describing the various vertices $\nu_l l^- W^+$ and $\bar{\nu}_l l^+ W^-$ ($l = e, \mu, \tau$) are represented in Fig. 1.5.

- (iv) The physical processes like $\mu^- \rightarrow e^- \bar{\nu}_e \nu_\mu$ and $\nu_\mu e^- \rightarrow \nu_e \mu^-$ (shown in Fig. 1.6), etc., take place in the second order such that at low energies, the effective interaction is given by the phenomenological $V - A$ interaction Lagrangian with the strength G_F by

$$\frac{G_F}{\sqrt{2}} = \frac{g^2}{8M_W^2}. \quad (1.36)$$

- (v) On the other hand, in the theory of electromagnetic interaction described by QED, the interaction Lagrangian for the interaction of the charged leptons l with the electromagnetic field $A_\mu(x)$ is given by:

$$\mathcal{L}_{\text{int}} = -eQ_{|l|} A_\mu(x) \bar{\Psi}_l(x) \gamma^\mu \Psi_l(x), \quad (1.37)$$

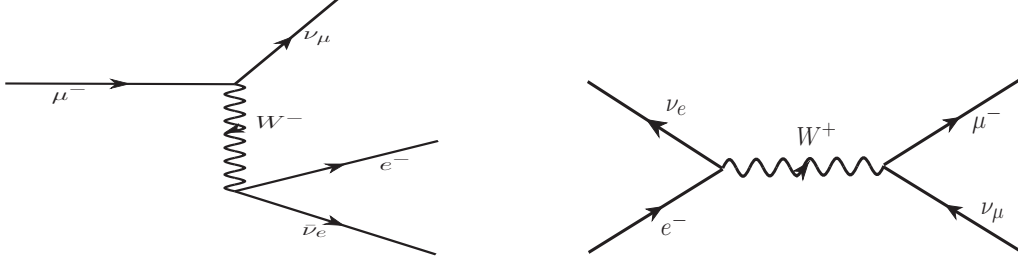


Figure 1.6: Second order Feynman diagram for the processes $\mu^- \rightarrow e^- \bar{\nu}_e \nu_\mu$ (left) and $\nu_\mu e^- \rightarrow \nu_e \mu^-$ (right).

where $Q_{|l|}$ is the electronic charge of the lepton in units of $|e|$. It may be noticed that the interaction Lagrangian for the electromagnetic interactions of the charged leptons l involve both the left (l_L) as well as the right (l_R) handed components of the lepton, as:

$$\Psi_l(x) = \Psi_{lL}(x) + \Psi_{lR}(x) \quad (1.38)$$

Therefore, while the weak interaction Lagrangian involves only the left handed component of leptons i.e. ν_{lL} and l_L , the electromagnetic interaction Lagrangian involves both the left handed as well as the right handed components of the charged lepton fields $\Psi_{lL}(x)$ and $\Psi_{lR}(x)$.

In the SM of Weinberg and Salam, the local gauge symmetry group is chosen to be $SU(2)_{I_W} \times U(1)_{Y_W}$. Since the left handed component of the neutrinos and the corresponding leptons i.e. ν_L and l_L ($l = e, \mu, \tau$) interact in pairs, they are assigned to a doublet under $SU(2)_{I_W}$ corresponding to the $|\frac{1}{2} \quad +\frac{1}{2}\rangle$ and $|\frac{1}{2} \quad -\frac{1}{2}\rangle$ states of I_W and I_{3W} . Accordingly, the right handed components ν_{lR} , l_R are assigned to singlet $|0 \quad 0\rangle$ under $SU(2)_{I_W}$. The weak hypercharge Y_W is assigned so that the charge of the leptons ν_l and l are reproduced using the weak interaction analogue of the Gell-Mann Nishijima relation in strong interactions and the relation $Y_W = 2(Q - I_{3W})$ is used in this case. In Table-1.2, we tabulate the weak isospin and weak hypercharge of all the left and right handed leptons in the upper panel where we also show these assignments for the scalar particles and quarks in the middle and lower panels for further use in Sections 1.3.3 and 1.3.5.

In the following, we summarize the main steps in formulating the SM for leptons and for simplicity consider the case of ν_e and e^- which can be generalized to other flavors of leptons. We introduce the notation $\Psi_L(x)$ and $\Psi_R(x)$ to represent the doublet state of the left handed component of leptons (ν_L, e_L) and the singlet state of the right handed component of the leptons ν_R and e_R as:

$$\Psi_L = \begin{pmatrix} \Psi_{\nu_e} \\ \Psi_e \end{pmatrix}_L = \begin{pmatrix} \nu_L \\ e_L \end{pmatrix}, \quad \Psi_{e_R} = e_R, \quad \Psi_{\nu_R} = \nu_R \quad (1.39)$$

where $\Psi_L = \frac{1}{2}(1 - \gamma_5)\Psi$, with $\Psi = \begin{pmatrix} \Psi_{\nu_e} \\ \Psi_e \end{pmatrix}$, $\Psi_{e_R} = \frac{1}{2}(1 + \gamma_5)\Psi_e$ and $\Psi_{\nu_R} = \frac{1}{2}(1 + \gamma_5)\Psi_{\nu_e}$.

A Lagrangian for the free massless leptons ν_L , e_L and e_R is written as

$$\mathcal{L} = \sum_{j=L, e_R, \nu_R} \bar{\Psi}_j \not{\partial} \Psi_j(x) \quad (1.40)$$

with $\not{\partial} = \gamma^\mu \frac{\partial}{\partial x^\mu}$. The Lagrangian is invariant under the transformations of the global symmetry group $SU(2)_{I_W} \times U(1)_{Y_W}$ generated by the gauge transformations $U = U_1 U_2$, where $U_1 = e^{i\vec{\alpha} \cdot \frac{\vec{\tau}}{2}}$, $U_2 = e^{i\beta I}$, and $\vec{\alpha}(\alpha_1, \alpha_2, \alpha_3)$ and β are the parameters describing the transformation of U_1 and U_2 , respectively, and $\tau_1 = \begin{pmatrix} 0 & 1 \\ 1 & 0 \end{pmatrix}$, $\tau_2 = \begin{pmatrix} 0 & -i \\ i & 0 \end{pmatrix}$ and $\tau_3 = \begin{pmatrix} 1 & 0 \\ 0 & -1 \end{pmatrix}$ are the Pauli matrices, I is the unit matrix. A mass term like $m\bar{\Psi}_j \Psi_j$ ($= \bar{\Psi}_{jL} \Psi_{jR} + \bar{\Psi}_{jR} \Psi_{jL}$) is not included as it is not invariant under global $SU(2)_{I_W} \times U(1)_{Y_W}$. However, when the transformations are made local by replacing $\vec{\alpha} \rightarrow \vec{\alpha}(x)$ and $\beta \rightarrow \beta(x)$ then the Lagrangian given in Eq. (1.40) is not invariant under the local gauge group generated by the local gauge transformations $U_1(x)U_2(x)$ due to the presence of the derivation term $\frac{\partial}{\partial x^\mu}$ in the Lagrangian. In order to restore the invariance of the Lagrangian under local transformation, the Lagrangian is rewritten in terms of the covariant derivative $\frac{D}{Dx^\mu}$ instead of the ordinary derivative $\frac{\partial}{\partial x^\mu}$ by introducing the matrix valued gauge fields $W^\mu = \sum_i \frac{\tau_i}{2} \cdot W^{\mu i}$ corresponding to $U_1(x)$ and the field B^μ corresponding to $U_2(x)$ transformation of $SU(2)_{I_W}$ and $U(1)_{Y_W}$ and defining the covariant derivative $\frac{D}{Dx^\mu}$ as

$$\frac{D}{Dx^\mu} = \frac{\partial}{\partial x^\mu} + ig \frac{\vec{\tau} \cdot \vec{W}^\mu}{2} + i \frac{g'}{2} Y_W B^\mu(x), \quad (1.41)$$

g and g' being the coupling constant corresponding to $SU(2)_{I_W}$ and $U(1)_{Y_W}$ gauge fields. A factor of $\frac{1}{2}$ is introduced with the $B^\mu(x)$ field in analogy with the $\vec{W}^\mu(x)$. Requiring that the new gauge vector field W^μ and B^μ transform under

$U_1(x)$ and $U_2(x)$ as:

$$\vec{W}^\mu(x) \rightarrow \vec{W}'^\mu(x) = \vec{W}^\mu(x) - \vec{\alpha} \times \vec{W}^\mu - \frac{i}{g} \partial_\mu \vec{\alpha}, \quad B^\mu(x) \rightarrow B'^\mu(x) = B^\mu(x) - \frac{i}{g'} \partial_\mu \beta(x) \quad (1.42)$$

ensures that under the local gauge transformation

$$\Psi(x) \rightarrow \Psi'(x) = U\Psi(x), \quad D\Psi(x) \rightarrow (D\Psi)'(x) = U(D\Psi(x)) \quad (1.43)$$

making the redefined Lagrangian invariant under the local gauge transformations $U(x)$. It can be shown using Eq. (1.41), that

$$[D^\mu, D^\nu] = \frac{g}{2} \vec{\tau} \cdot \vec{G}^{\mu\nu}(x) + \frac{g'}{2} Y_W B^{\mu\nu}(x), \quad (1.44)$$

where $B^{\mu\nu}$ and $\vec{G}^{\mu\nu}$ being the field tensors for $B^\mu(x)$ and $\vec{W}^\mu(x)$ fields given by:

$$B^{\mu\nu} = \partial^\mu B^\nu(x) - \partial^\nu B^\mu(x), \quad \vec{G}^{\mu\nu}(x) = \partial^\mu \vec{W}^\nu(x) - \partial^\nu \vec{W}^\mu(x) + g \vec{W}^\mu(x) \times \vec{W}^\nu(x), \quad (1.45)$$

and are used to define the kinetic energy of the vector B^μ and \vec{W}^μ fields.

Consequently, the free particle Lagrangian is redefined as

$$\mathcal{L} = \sum_{j=L, e_R, \nu_R} \bar{\Psi}_j(x) \not{D} \Psi_j. \quad (1.46)$$

Writing the expressions for $D^\mu \Psi_L$, $D^\mu \Psi_{e_R}$ and $D^\mu \Psi_{\nu_R}$, using the values of Y_W for Ψ_L , Ψ_{e_R} and Ψ_{ν_R} given in Table.1.2, we obtain

$$D^\mu \Psi_L(x) = \left(\partial^\mu + \frac{ig}{2} \vec{\tau} \cdot \vec{W}^\mu(x) - \frac{ig'}{2} B^\mu(x) \right) \Psi_L, \quad D^\mu \Psi_{e_R}(x) = (\partial^\mu - ig' B^\mu(x)) \Psi_{e_R}, \quad D^\mu \Psi_{\nu_R} = \partial^\mu \Psi_{\nu_R} \quad (1.47)$$

The Lagrangian in Eq. (1.46) is expanded over j and is written as

$$\begin{aligned} \mathcal{L} &= \mathcal{L}_0 + \mathcal{L}_{int}, & \text{with} \\ \mathcal{L}_0 &= i\bar{\Psi}_L \not{D} \Psi_L + i\bar{\Psi}_{e_R} \not{D} \Psi_{e_R} + i\bar{\Psi}_{\nu_R} \not{D} \Psi_{\nu_R}, & \text{and} \\ \mathcal{L}_{int} &= -\frac{g}{2\sqrt{2}} \left(\bar{\nu}_e \gamma^\mu (1 - \gamma_5) e W_\mu^+ + \bar{e} \gamma^\mu (1 - \gamma_5) \nu_e W_\mu^- \right) - \frac{\sqrt{g^2 + g'^2}}{2} \bar{\nu}_L \gamma^\mu \nu_L Z_\mu \\ &\quad + \frac{gg'}{\sqrt{g^2 + g'^2}} \bar{e} \gamma^\mu e A_\mu + \frac{1}{\sqrt{g^2 + g'^2}} \left[-g'^2 \bar{e}_R \gamma^\mu e_R + \frac{g^2 - g'^2}{2} \bar{e}_L \gamma^\mu e_L \right] Z_\mu, \end{aligned} \quad (1.48)$$

where

$$W_\mu^\pm = \frac{W_\mu^1 \mp iW_\mu^2}{\sqrt{2}}, \quad Z_\mu = \frac{gW_\mu^3 - g'B_\mu}{\sqrt{g^2 + g'^2}} \quad \text{and} \quad A_\mu = \frac{g'W_\mu^3 + gB_\mu}{\sqrt{g^2 + g'^2}}. \quad (1.49)$$

We can observe from \mathcal{L} that

- (i) no terms like $W_i^\mu W_{i\mu}$ and $B^\mu B_\mu$ (or equivalently like $A^\mu A_\mu$, $Z^\mu Z_\mu$ or $W^{\pm\mu} W_\mu^\mp$) appear in \mathcal{L} , implying that all the fields $W^{+\mu}$, $W^{-\mu}$, Z^μ and A^μ are massless.
- (ii) \mathcal{L}_{int} correctly reproduces

1. CC weak interaction of ν_e and e with strength $\frac{g}{2\sqrt{2}}$ given by

$$\mathcal{L}_{int}^{CC} = -\frac{g}{2\sqrt{2}} \bar{\Psi}_{\nu_e} \gamma^\mu (1 - \gamma_5) \Psi_e W_\mu^+ + h.c. \quad (1.50)$$

2. the electromagnetic interaction of electrons with the electromagnetic coupling given by

$$\mathcal{L}_{int}^{EM} = \frac{gg'}{\sqrt{g^2 + g'^2}} \bar{\Psi}_e \gamma^\mu \Psi_e A_\mu. \quad (1.51)$$

- (iii) \mathcal{L}_{int} predicts

Quantum numbers→ Particles↓	I_W	I_{W3}	Y_W	Q
$\nu_{eL}, \nu_{\mu L}, \nu_{\tau L}$	$\frac{1}{2}$	$+\frac{1}{2}$	-1	0
e_L, μ_L, τ_L	$\frac{1}{2}$	$-\frac{1}{2}$	-1	-1
e_R, μ_R, τ_R	0	0	-2	-1
ϕ^+	$\frac{1}{2}$	$+\frac{1}{2}$	1	+1
ϕ^0	$\frac{1}{2}$	$-\frac{1}{2}$	1	0
u_L, c_L, t_L	$\frac{1}{2}$	$+\frac{1}{2}$	$\frac{1}{3}$	$+\frac{2}{3}$
d_L', s_L', b_L'	$\frac{1}{2}$	$-\frac{1}{2}$	$\frac{1}{3}$	$-\frac{1}{3}$
u_R, c_R, t_R	0	0	$\frac{4}{3}$	$+\frac{2}{3}$
d_R', s_R', b_R'	0	0	$-\frac{2}{3}$	$-\frac{1}{3}$

Table 1.2: Weak isospin(I_W), its third component(I_{W3}), weak-hypercharge($Y = 2(Q - I_3)$), charge($Q(|e|)$) of the leptons, scalar mesons and quarks in the SM model.

1. NC interaction of neutrinos is given by:

$$\mathcal{L}_{NC}^\nu = -\frac{\sqrt{g^2 + g'^2}}{4} \bar{\Psi}_\nu \gamma_\mu (1 - \gamma_5) \Psi_\nu Z^\mu, \quad \text{with strength } \frac{\sqrt{g^2 + g'^2}}{2}. \quad (1.52)$$

2. NC interaction of electrons is given by:

$$\mathcal{L}_{NC}^e = -\frac{Z^\mu}{\sqrt{g^2 + g'^2}} \left[\frac{g^2 - g'^2}{4} \bar{\Psi}_e \gamma_\mu (1 - \gamma_5) \Psi_e - \frac{g'^2}{2} \bar{\Psi}_e \gamma_\mu (1 + \gamma_5) \Psi_e \right]. \quad (1.53)$$

- (iv) The SM therefore describes the electroweak interaction of leptons in terms of the two parameters g and g' . Comparing \mathcal{L}_{int}^{CC} and \mathcal{L}_{int}^{EM} given in Eqs. (1.50) and (1.51), respectively, with the $V - A$ theory of weak interactions and QED of the charged leptons, we see that g and g' are related with the strength of Fermi interaction G_F and the electromagnetic coupling e through the relations

$$\frac{G_F}{\sqrt{2}} = \frac{g^2}{8M_W^2}, \quad \frac{1}{e^2} = \frac{1}{g^2} + \frac{1}{g'^2}, \quad (1.54)$$

where M_W is the mass of $W^{\mu(\pm)}$ vector fields.

- (v) The Lagrangian obtained using the local gauge field theory, thus, predicts the electromagnetic and weak interactions mediated by four vector gauge fields, $W^{\mu+}(x)$, $W^{\mu-}(x)$, $Z^\mu(x)$ and $A^\mu(x)$, all being massless as there are no mass terms like $M_V^2 V_i^\mu V_{i\mu}$ ($V_i = W^+, W^-, Z, A$) for any of the fields. While the model can describe the electromagnetic interaction, it can not describe the weak interaction which is mediated by massive vector fields $W^{\mu\pm}$. Therefore, the model in this form is inconsistent with the phenomenological $V - A$ theory of weak interactions unless a mechanism is devised to generate the masses of these fields. This is done using the Higgs mechanism.

Since all the fields W_+^μ , W_-^μ , Z^μ , and A^μ are massless, the kinetic energy terms are added by hand to redefine the free Lagrangian \mathcal{L}_0 as

$$\mathcal{L}_0 \rightarrow \mathcal{L}_0 - \frac{1}{4} B^\mu B_\mu - \frac{1}{4} G^{\mu\nu} G_{\mu\nu}$$

in analogy with the kinetic energy term for massless electromagnetic field A^μ in QED.

1.3.3. Higgs mechanism and generation of mass

The phenomenon of spontaneous breaking of continuous symmetry in field theory proposed by Englert and Brout [24] and Higgs [25], generally called the Higgs mechanism was used by Weinberg [20] and Salam [21] to generate the mass of the gauge vector bosons. In this phenomenon, strongly interacting doublet of scalar fields $\phi(x)$ are introduced in the Lagrangian. The vacuum state of this Lagrangian breaks the symmetry while the Lagrangian respects the symmetry. Hence, the name spontaneous breaking of symmetry instead of the explicit breaking of symmetry in field theory is given to this phenomenon. In local gauge field theories the invariance of the Lagrangian generates massless vector gauge fields corresponding to each generator of the symmetry. In the SM, the spontaneous breaking of symmetry based on $SU(2)_{I_W} \times U(1)_{Y_W}$, is realized by introducing interacting scalar fields $\phi(x)$ which transform as doublet under $SU(2)_{I_W}$ i.e.

$$\phi(x) = \begin{pmatrix} \phi^+(x) \\ \phi^0(x) \end{pmatrix} = \frac{1}{\sqrt{2}} \begin{pmatrix} \phi_1(x) + i\phi_2(x) \\ \phi_3(x) + i\phi_4(x) \end{pmatrix} \quad (1.55)$$

with fields $\phi^+(x)$ and $\phi^0(x)$ having $I = \frac{1}{2}$ and $I_3 = \pm\frac{1}{2}$ and are assigned $Y_W = +1$ to reproduce their charges as shown in Table-1.2 (middle panel). The interaction Lagrangian for the scalar fields ϕ is written in a locally gauge invariant way under the $SU(2)_{I_W} \times U(1)_{Y_W}$ transformation using the covariant derivative D^μ given by:

$$D^\mu \phi = (\partial_\mu + ig\vec{\tau} \cdot \vec{W}^\mu + i\frac{g'}{2}Y_W B^\mu)\phi \quad (1.56)$$

and is written as:

$$\mathcal{L}_\phi = D^\mu \phi^\dagger D_\mu \phi - V(\phi^* \phi) \quad (1.57)$$

where the potential $V(\phi^* \phi)$ is given by:

$$V(\phi^* \phi) = -\mu^2 \phi^*(x)\phi(x) + \lambda(\phi^* \phi)^2 \quad (1.58)$$

and has minimum value given by the condition:

$$\frac{\partial V}{\partial \phi^*} = \phi(x)(-\mu^2 + 2\lambda\phi^* \phi) = 0 \quad (1.59)$$

which implies that for $\mu^2 < 0$, the minimum occurs at $\phi(x) = 0$, but for $\mu^2 > 0$, there is minima at $\phi^\dagger(x)\phi(x) = \frac{\mu^2}{2\lambda}$. While $\phi(x) = 0$ is a trivial ground state, $\phi^\dagger(x)\phi(x) = \frac{\mu^2}{2\lambda}$ implies an infinitely degenerate value to $\phi(x)$ since it is a complex field given by $\phi(x) = e^{i\theta}\phi(x)$, θ being arbitrary.

The $SU(2)_{I_W} \times U(1)_{Y_W}$ symmetry is spontaneously broken in the SM by choosing:

$$\phi_1(x) = \phi_2(x) = \phi_4(x) = 0, \quad \phi_3(x) \neq 0$$

such that vacuum expectation value (VEV) of $\phi(x)$ is given by:

$$\langle 0 | \phi(x) | 0 \rangle = \begin{pmatrix} 0 \\ \frac{v}{\sqrt{2}} \end{pmatrix}, \quad v = \frac{1}{\sqrt{2}} \langle 0 | \phi_3(x) | 0 \rangle \quad (1.60)$$

This choice of ground state ensures that the ground state $\phi_0(x)$ remains invariant under the symmetry group transformations of $U(1)_Q$, where $Q = \frac{1}{2}\tau_3 + \frac{Y}{2}$ is the generator of the group because $Q|\phi_0\rangle = 0$. This means that $SU(2)_{I_W} \times U(1)_{Y_W}$ is spontaneously broken to $U(1)_Q$, keeping the gauge fields corresponding to $U(1)_Q$ symmetry i.e. the electromagnetic field massless, while generating the mass corresponding to other three generators τ^+ , τ^- and $\frac{1}{2}(\tau_3 - Y)$. The Lagrangian for the Higgs field $\phi(x)$, invariant under the local gauge group $SU(2)_{I_W} \times U(1)_{I_W}$, written in terms of the covariant derivative $D^\mu \phi$ given in Eq. (1.56) is written explicitly using the value of Y_W for ϕ from Table-1.2 (middle panel) as

$$\mathcal{L}_\phi = \left(\partial^\mu + i\frac{g}{2}\vec{\tau} \cdot \vec{W}^\mu + i\frac{g'}{2}B^\mu \right) \phi^*(x) \left(\partial_\mu + i\frac{g}{2}\vec{\tau} \cdot \vec{W}_\mu + i\frac{g'}{2}B_\mu \right) \phi(x) - V(\phi^*(x)\phi(x)) \quad (1.61)$$

Expanding the field $\phi(x)$ around its VEV $\langle \phi(x) \rangle_0$ given in Eq. (1.60), and writing

$$\phi(x) = \frac{1}{\sqrt{2}} \begin{pmatrix} 0 \\ v + H(x) \end{pmatrix}, \quad (1.62)$$

we write

$$\begin{aligned} \mathcal{L}_\phi &= \frac{1}{2} \partial^\mu H(x) \partial_\mu H(x) + \frac{v^2 g^2}{8} (|W_\mu^+|^2 + |W_\mu^-|^2) + \frac{g^2}{8} (H^2 + 2Hv) (|W_\mu^+|^2 + |W_\mu^-|^2) + \left(\frac{g^2 + g'^2}{4} \right) \left(\frac{H^2 + 2Hv + v^2}{2} \right) \\ &\times Z_\mu Z^\mu + \left[\frac{g^2 g'^2}{4(g^2 + g'^2)} (H^2 + 2Hv) - \frac{g^2 g'^2}{4(g^2 + g'^2)} (H^2 + 2Hv) \right] A_\mu A^\mu - V(\phi^*(x)\phi(x)). \end{aligned} \quad (1.63)$$

The above Lagrangian predicts the masses of the vector gauge bosons $W^{+\mu}$, $W^{-\mu}$, Z^μ , where $Z_\mu = \frac{gW_\mu^3 - g'B_\mu}{\sqrt{g^2 + g'^2}}$ and $A_\mu = \frac{g'W_\mu^3 + gB_\mu}{\sqrt{g^2 + g'^2}}$ to obtain

$$M_{W^+} = M_{W^-} = \frac{vg}{2}; \quad M_Z = \frac{v\sqrt{g^2 + g'^2}}{2}; \quad M_A = 0, \quad (1.64)$$

and mass of the Higgs scalar $H(x)$ is predicted by expanding $V(\phi^*(x)\phi(x))$ using Eq. (1.62) to obtain:

$$M_H = \sqrt{2\lambda}v. \quad (1.65)$$

We see that the mass of Z^μ and W^μ vector fields are related by

$$\frac{M_Z}{M_W} = \sqrt{\left(1 + \frac{g'^2}{g^2}\right)} \geq 1 \quad (1.66)$$

and the absolute values of M_W and M_Z are determined by g , g' , and v .

1.3.4. Neutral current interactions and the weak mixing angle

It has been shown by Eqs. (1.50) and (1.51) that the SM reproduces CC weak and electromagnetic interactions of leptons mediated by $W^{\mu\pm}$ vector bosons with mass $M_W = \frac{vq}{2}$ and the massless electromagnetic vector field \vec{A}^μ , as well as predicts NC weak interactions for the neutrinos and electrons which are mediated by the neutral vector boson Z^μ with mass $M_Z = M_W \sqrt{1 + \frac{g'^2}{g^2}}$, as shown by Eq. (1.66). The strength of the NC weak interaction is alternatively defined in terms of a weak mixing angle θ_W defined as

$$\tan \theta_W = \frac{g'}{g} \quad \text{such that}$$

$$M_W = M_Z \cos \theta_W; \quad e = g \sin \theta_W = g' \cos \theta_W \quad (1.67)$$

$$Z^\mu = \cos \theta_W W_3^\mu - \sin \theta_W B^\mu; \quad A^\mu = \sin \theta_W W_3^\mu + \cos \theta_W B^\mu. \quad (1.68)$$

The weak mixing angle θ_W mixes the neutral gauge vector bosons W_3^μ and B^μ corresponding to the $SU(2)_{I_W}$ and $U(1)_{Y_W}$ gauge bosons to produce the physical gauge vector fields Z^μ and A^μ responsible for the weak NC and the electromagnetic current carrying vector fields. In terms of the weak mixing angle, the Lagrangians for the weak CC and NC as well as the electromagnetic interactions written in Eq. (1.48) are rewritten as:

$$\mathcal{L}_{CC} = -\frac{g}{2\sqrt{2}} [\bar{\nu}_e \gamma^\mu (1 - \gamma_5) e W_\mu^+ + h.c.], \quad (1.69)$$

$$\mathcal{L}_{NC} = -\frac{g}{2 \cos \theta_W} [\bar{\nu}_e \gamma^\mu (g_V^{\nu_e} - g_A^{\nu_e} \gamma_5) \nu_e + \bar{e} \gamma^\mu (g_V^e - g_A^e \gamma_5) e] Z_\mu, \quad (1.70)$$

$$\mathcal{L}_{EM} = -|e| \bar{e} \gamma^\mu e A_\mu, \quad (1.71)$$

where

$$g_V^e = 2 \sin^2 \theta_W - \frac{1}{2}, \quad g_V^{\nu_e} = \frac{1}{2}, \quad g_A^e = -\frac{1}{2}, \quad g_A^{\nu_e} = \frac{1}{2}. \quad (1.72)$$

1.3.5. Extension of the SM to the leptons, quarks and nucleons

The extension of the SM to the leptons of other flavors is straightforward. The left and right handed components of (ν_μ, μ^-) and (ν_τ, τ^-) are assigned to the $SU(2)_{I_W} \times U(1)_{Y_W}$ representations in same way as done for the (ν_e, e^-) leptons and shown in Table-1.2 and interaction can be generated following the procedure in Section 1.3.2 with implicit assumption of LFU and the interactions for all the flavors of leptons can be written as:

$$\mathcal{L}_{CC} = -\frac{g}{2\sqrt{2}} \sum_{l=e,\mu,\tau} [\bar{\nu}_l \gamma^\mu (1 - \gamma_5) l W_\mu^+ + h.c.], \quad (1.73)$$

$$\mathcal{L}_{NC} = -\frac{g}{2 \cos \theta_W} \sum_{l=e,\mu,\tau} [\bar{\nu}_l \gamma^\mu (g_V^{\nu_l} - g_A^{\nu_l} \gamma_5) \nu_l + \bar{l} \gamma^\mu (g_V^l - g_A^l \gamma_5) l] Z_\mu, \quad (1.74)$$

with $g_V^e, g_A^e, g_V^{\nu_e}$, and $g_A^{\nu_e}$ given in Eq. (1.72), and have the same values for all the lepton flavors l .

However, the formalism presented in Section 1.3.2 can be reformulated in terms of the weak isospin ($\vec{\tau}_f$) and the charge operators Q_f for the fermions f instead of the weak hypercharge. The weak CC and NC currents are written using $SU(2)_{I_Y}$ doublets, $\Psi_{fL} = \frac{1-\gamma_5}{2} \Psi_f$ and $\Psi_{fR} = \frac{1+\gamma_5}{2} \Psi_f$ for a fermion f , so that they can be applied to a lepton and quark in a unified way.

It is straightforward to see that the weak CC interaction Lagrangian is given by:

$$\mathcal{L}_{CC} = -\frac{g}{2\sqrt{2}} \sum_{f=e,\mu,\tau} \bar{\Psi}_{fL} \gamma^\mu (1 - \gamma_5) \Psi_{fL} W_\mu^+ + h.c. \quad (1.75)$$

The weak NC Lagrangian using Eq. (1.74) is written as:

$$\mathcal{L}_{NC} = - \sum_{f=e,\mu,\tau} \left[\bar{\Psi}_{fL} \left(g \frac{\tau_3^f}{2} W^3 + g' \frac{Y_L^f}{2} \not{B} \right) \Psi_{fL} + \bar{\Psi}_{fR} g' \frac{Y_R^f}{2} \not{B} \Psi_{fR} \right] \quad (1.76)$$

where τ_3^f is isospin operator and Y_L^f and Y_R^f are the hypercharges of the left- and right- handed fermions in Table-1.2. Since, $\tau_3 \Psi_{fR} = 0$ as Ψ_{fR} is isosinglet, the two terms in Eq. (1.76) are combined to write:

$$\mathcal{L}_{NC} = - \sum_{f=e,\mu,\tau} \sum_{i=L,R} \bar{\Psi}_{fi} \left(g \frac{\tau_3^{fi}}{2} W^3 + g' \frac{Y^{fi}}{2} \not{B} \right) \Psi_{fi}. \quad (1.77)$$

States \rightarrow Couplings \downarrow	ν_l	l	u,c,t	d', s', b'
$2g_V$	1	$-1 + 4 \sin^2 \theta_W$	$1 - \frac{8}{3} \sin^2 \theta_W$	$-1 + \frac{4}{3} \sin^2 \theta_W$
$2g_A$	1	-1	1	-1

Table 1.3: Couplings of the leptons and quarks to Z_μ field.

Using Eq. (1.68) to express $W^{3\mu}$ and B^μ in terms of Z^μ and A^μ and $\Psi^{f_i} = 2Q^{f_i} - \tau_3^{f_i}$, \mathcal{L}_{NC} can be expressed as:

$$\mathcal{L}_{NC} = -\frac{g}{2 \cos \theta_W} \sum_{f=e,\mu,\tau} \sum_{i=L,R} \bar{\Psi}_{f_i} \gamma^\mu (\tau_3^{f_i} - 2Q^{f_i} \sin^2 \theta_W) \Psi_{f_i} Z_\mu. \quad (1.78)$$

After further expanding over $i = L, R$ and using $\tau_3^{f_R} \Psi_{f_R} = 0$, for $f = e, \mu, \tau$ the following expression is obtained

$$\begin{aligned} \mathcal{L}_{NC} &= -\frac{g}{2 \cos \theta_W} \sum_{f=e,\mu,\tau} \bar{\Psi}_f \gamma^\mu (g_V^f - g_A^f \gamma_5) \Psi_f, \quad \text{with} \\ g_V^f &= \frac{1}{2} \tau_3^f - 2Q^f \sin^2 \theta_W, \quad g_A^f = \frac{1}{2} \tau_3^f \end{aligned} \quad (1.79)$$

After operating τ_3^f and Q^f on leptons, in Table-1.2, $\mathcal{L}_{NC}^{\text{lepton}}$ is obtained as stated in Eq. (1.78).

In this form, it can be used to generate the weak CC and NC interactions of quarks which are classified under $SU(2)_{I_W} \times U(1)_{Y_W}$ as shown in Table-1.2 (lower panel) for their left handed and right handed components and arranged in three flavors of doublets as:

$$q_L = \begin{pmatrix} u \\ d' \end{pmatrix}_L, \begin{pmatrix} c \\ s' \end{pmatrix}_L, \begin{pmatrix} t \\ b' \end{pmatrix}_L \quad (1.80)$$

and singlet as $q_R = u_R, d'_R, c_R, s'_R, t_R, b'_R$, where

$$\begin{pmatrix} d'_R \\ s'_R \\ b'_R \end{pmatrix} = U \begin{pmatrix} d_R \\ s_R \\ b_R \end{pmatrix} \quad (1.81)$$

and U being the CKM matrix [19]. The $\mathcal{L}_{CC,NC}^{\text{quarks}}$ are then written as:

$$\mathcal{L}_{CC} = -\frac{g}{2\sqrt{2}} \sum_q \bar{\Psi}_q \gamma^\mu (1 - \gamma_5) \tau^+ \Psi_q W_\mu^+ + h.c. \quad (1.82)$$

$$\mathcal{L}_{NC} = -\frac{g}{2 \cos \theta_W} \sum_q \bar{\Psi}_q \gamma^\mu (g_V^q - g_A^q \gamma_5) \Psi_q \quad (1.83)$$

where g_V^q and g_A^q are given by Eq. (1.79), and the explicit values of g_V^q and g_A^q for each quark are shown in the Table-1.3.

The weak interaction Lagrangian for the nucleons is evaluated in a straightforward manner assuming the quark structure of the protons and neutrons as composed of antisymmetrized uud and udd quarks and using the isospin structure of CC and NC currents. Since the weak CC currents are charge raising and charge lowering components, they can be written in a straightforward way for the nucleons as:

$$\mathcal{L}_{CC}^N = -\frac{g}{2\sqrt{2}} J_{CC}^\mu W_\mu^+ + h.c., \quad \text{with} \quad J_{CC}^\mu = \bar{\Psi}_N \gamma^\mu (1 - \gamma_5) \tau^+ \Psi_N, \quad (1.84)$$

where $\Psi_N = \begin{pmatrix} u \\ d' \end{pmatrix}$ is the quark isodoublet after implementing GIM mechanism, with $d' = V_{ud} d + V_{us} s$.

In the case of NC

$$\mathcal{L}_{NC}^N = -\frac{g}{2 \cos \theta_W} J_{NC}^\mu Z_\mu, \quad \text{where} \quad J_{NC}^\mu = V_{NC}^\mu - A_{NC}^\mu. \quad (1.85)$$

The expressions for V_{NC}^μ and A_{NC}^μ can be written in a straightforward manner using the isospin structure of these currents given in Eq. (1.79) as [135]:

$$V_{NC}^\mu = V^{\mu 3} - \left(2 \sin^2 \theta_W J_{EM}^\mu + \frac{1}{2} V_S^\mu \right); \quad A_{NC}^\mu = A^{\mu 3} + \frac{1}{2} A_S^\mu, \quad (1.86)$$

$$\begin{aligned} \text{with} \quad V^{\mu 3} &= \bar{\Psi}_N \gamma^\mu \frac{\tau_3}{2} \Psi_N, & A^{\mu 3} &= \bar{\Psi}_N \gamma^\mu \gamma_5 \frac{\tau_3}{2} \Psi_N & J_{EM}^\mu &= e_N \bar{\Psi}_N \gamma^\mu \Psi_N \\ V_S^\mu &= \bar{s} \gamma^\mu s & A_S^\mu &= \bar{s} \gamma^\mu \gamma_5 s, \end{aligned} \quad (1.87)$$

S. No.	Quantity	SM prediction	Experimental value
1	Mass of the W^\pm boson	80.361 ± 0.006 GeV	80.376 ± 0.033 GeV
2	Mass of the Z^0 boson	91.1882 ± 0.002 GeV	91.1876 ± 0.0021 GeV
3	W^\pm total decay width, Γ_W	2.090 ± 0.001 GeV	2.046 ± 0.049 GeV
4	Z^0 total decay width, Γ_Z	2.4942 ± 0.0009 GeV	2.4955 ± 0.0023 GeV
5	Mass of Higgs boson	125.30 ± 0.13 GeV	125.30 ± 0.13 GeV
6	Vector coupling $g_V^{\nu_e}$	-0.0398 ± 0.0001	-0.040 ± 0.015
7	Axial-vector coupling $g_A^{\nu_e}$	-0.5064	-0.507 ± 0.014
8	Weak charge of electron	-0.0476 ± 0.0002	-0.0403 ± 0.0053
9	$\sin^2 \theta_W$	0.23121 ± 0.00004	0.2299 ± 0.0043

Table 1.4: Predictions of the SM and the experimentally observed values [19].

where $\Psi_N = \begin{pmatrix} u \\ d \end{pmatrix}$ is the isodoublet of nonstrange quarks with charge e_N , and s is an isoscalar, which represents the strange quark contribution.

The triumphs of the SM are many, like the predictions of the existence of W , Z bosons, and Higgs boson as well as the prediction of NC in the neutrino and electron sectors. The model also predicts various relations between the weak decays of the charm, bottom and top quarks. The agreement between the SM values and the experimentally observed results for many observables are unprecedented, and in Table 1.4, some of the experimentally observed values and their SM predictions that will be used later in this article, have been tabulated.

1.3.6. Higher order effects in electroweak interactions

The theoretical calculations of the various electroweak observables from which the parameters shown in Table 1.4 are extracted, are done including the corrections due to the higher order loop effects beyond the lowest order nonvanishing contributions in the Born approximation, using the standard model of the electroweak interactions in order to compare them with the very high precision experimental results for these parameters obtained in various experiments [19]. The physical processes studied in these experiments involve the interactions of leptons and quarks, and therefore, are also subject to the corrections due to the higher order loop effects in QCD, in addition to the higher order loop effects in the electroweak interactions. The corrections due to the higher order effects generally fall in the following categories and have been discussed extensively in the literature [19, 136, 137, 138, 139]:

(i) QED and QCD corrections

There are two types of these corrections. The first type of corrections arise due to the vacuum polarization effects of the QED and QCD vacuum. In the case of QED, the one loop, two loops, and higher loop corrections in the photon propagator due to the fermion-antifermion pairs in the intermediate state lead to the renormalization of the electromagnetic coupling α , and make it energy dependent. Similarly, in the case of QCD, the renormalization of the gluon propagator due to the higher order loop effects arising due to the quark-antiquark pairs and higher order self interactions of the gluons in the intermediate states make the strong coupling α_s energy dependent making it smaller at higher energies leading to the asymptotic freedom of QCD. Since most of the electroweak measurements are made at higher energies corresponding to the weak gauge boson (W/Z) mass, except the low energy process of muon decay, a value of $\alpha_s(M_Z) = 0.1185 \pm 0.0016$ is used in fitting the electroweak observables. Using this value of $\alpha_s(M_Z)$, the QED and QCD vacuum polarization effects change the value of electromagnetic coupling α from its value of $\alpha^{-1}(m_e) = 133.472 \pm 0.007$ to $\alpha^{-1}(M_Z) = 127.952 \pm 0.009$. These changes due to the vacuum polarization effects in the value of $\alpha(M_Z)$ and $\alpha_s(M_Z)$ affect the extraction of various parameters (shown in Table 1.4) from the electroweak observables like the weak decay widths of heavy leptons (μ and τ), and gauge bosons W and Z , as well as the asymmetries observed in the electron scattering experiments.

The second type of the higher order corrections arise due to the photons (gluons) appearing in the one, two, and higher loop diagrams. These corrections are generally gauge invariant and finite but energy dependent. Therefore, depending upon the individual physical processes and the energy involved in these processes, these effects are, in general, different for every process and need to be calculated accordingly.

(ii) Electroweak corrections

The corrections due to the higher order loop effects calculated in the standard model of the electroweak interactions arise due to the vacuum polarization effects of W and Z propagator due to the virtual γZ , ZZ , and WW pairs as well as the fermion-antifermion pairs ($q\bar{q}$) in the one loop, two loop, and higher loop diagrams. In addition to the vacuum polarization effects on the gauge boson propagators, the contribution due to the vertex corrections, box diagrams involving virtual W and Z bosons and the contribution due to the virtual $q\bar{q}$ loops in the intermediate

Process	α	β	γ
$\nu_{l'} e^- \rightarrow \nu_{l'} e^-$	$(g_V^e + g_A^e)^2$	$(g_V^e - g_A^e)^2$	$(g_A^e)^2 - (g_V^e)^2$
$\bar{\nu}_{l'} e^- \rightarrow \bar{\nu}_{l'} e^-$	$(g_V^e - g_A^e)^2$	$(g_V^e + g_A^e)^2$	$(g_A^e)^2 - (g_V^e)^2$
$\nu_e e^- \rightarrow \nu_e e^-$	$(g_V' + g_A')^2$	$(g_V' - g_A')^2$	$g_A'^2 - g_V'^2$
$\bar{\nu}_e e^- \rightarrow \bar{\nu}_e e^-$	$(g_V' - g_A')^2$	$(g_V' + g_A')^2$	$g_A'^2 - g_V'^2$

Table 1.5: Values of α , β and γ for $\nu_{l'} e^-$, $\bar{\nu}_{l'} e^-$, $\nu_e e^-$ and $\bar{\nu}_e e^-$ scattering, where $l' = \mu, \tau$.

state are important. These corrections at the one loop level have been calculated for most of the weak processes of the weak decays and parity violating asymmetries. The two loop and higher order loop contributions have also been calculated for some weak processes.

(iii) Mixed QCD-electroweak corrections

The higher order loop corrections due to the mixed QCD-electroweak interactions, where $q\bar{q}$ pairs are not involved, are calculated upto order $\alpha\alpha_s$ and $\alpha\alpha_s^2$. The corrections due to the higher order loop diagrams involving $q\bar{q}$ pairs of the order of $\alpha\alpha_s m_t^2$, $\alpha\alpha_s^2 m_t^2$, $\alpha\alpha_s^3 m_t^2$, $\alpha^2\alpha_s m_t^4$, etc., where m_t is the top quark mass, are calculated in some processes.

The combined corrections because of the higher loop diagrams arising due to the QED, QCD, electroweak, and mixed QCD-electroweak interactions outlined above have been calculated for all the electroweak processes and their influence on extracting various parameters like G_F , M_W , M_Z , $\sin^2 \theta_W$, etc. have been discussed in the literature. For some recent reviews, see Refs. [19, 136, 137, 138, 139].

In the following sections, we illustrate some simple examples of the neutrino scattering from the electrons and quarks in the nonvanishing lowest order perturbation theory using the standard model.

1.3.7. $\nu_l - e$ and $\bar{\nu}_l - e$ scattering

First let us consider the process

$$\nu_e(\vec{k}, E_{\nu_e}) + e^-(\vec{p}, E_e) \longrightarrow \nu_e(\vec{k}', E_{\nu_e}') + e^-(\vec{p}', E_e') \quad (1.88)$$

which is mediated by the neutral (Z^0) as well as the charged (W^\pm) current interactions and using the Lagrangian given in Eqs. (1.69) and (1.70) one may write the invariant matrix element for CC interaction as:

$$\mathcal{M}^{CC} = \frac{G_F}{\sqrt{2}} \left[\bar{u}(\vec{p}') \gamma_\mu (1 - \gamma_5) u(\vec{k}) \right] \cdot \left[\bar{u}(\vec{k}') \gamma^\mu (1 - \gamma_5) u(\vec{p}) \right], \quad (1.89)$$

and for NC interaction as:

$$\mathcal{M}_{NC} = \frac{G_F}{\sqrt{2}} \left[\bar{u}(\vec{k}') \gamma_\mu (1 - \gamma_5) u(\vec{k}) \right] \cdot \left[\bar{u}(\vec{p}') \gamma^\mu (g_V^e - g_A^e \gamma_5) u(\vec{p}) \right], \quad (1.90)$$

where the value of g_V^e and g_A^e are given in Table-1.3.

Using the Fierz transformation, the total contribution for CC and NC induced reactions may be written as:

$$\mathcal{M}_{CC} + \mathcal{M}_{NC} = \frac{G_F}{\sqrt{2}} \left[\bar{u}(\vec{k}') \gamma_\mu (1 - \gamma_5) u(\vec{k}) \right] \cdot \left[\bar{u}(\vec{p}') \gamma^\mu (g_V' - g_A' \gamma_5) u(\vec{p}) \right], \quad (1.91)$$

where $g_V' = g_V^e + 1$, $g_A' = g_A^e + 1$.

The matrix element square $|\mathcal{M}|^2$ averaged over the initial spin state and summed over the final spin state is given by

$$\overline{\sum_i \sum_f |\mathcal{M}|^2} = 16 G_F^2 \left[\alpha (k' \cdot p')(k \cdot p) + \beta (k' \cdot p)(k \cdot p') - \gamma m_e^2 (k \cdot k') \right], \quad (1.92)$$

where the values of α , β and γ are given in Table 1.5.

The expression for the differential cross section in CM frame is obtained as [10]:

$$\left. \frac{d\sigma}{d\Omega} \right|_{CM} = \frac{1}{4\pi^2 s} G_F^2 \left[\alpha \left(\frac{s - m_e^2}{2} \right)^2 + \beta \left(\frac{u - m_e^2}{2} \right)^2 + \gamma \frac{m_e^2}{2} t \right], \quad (1.93)$$

where the values of α , β and γ are given in Table 1.5, and s, t, u are the Mandelstam variables. The $\nu_{l'} e^-$ and $\bar{\nu}_{l'} e^-$ ($l' = \mu, \tau$) scattering take place via. NC only, and the corresponding values of α , β and γ are tabulated in Table 1.5.

In the massless limit of electron, the differential and total scattering cross sections for CC induced $\nu_e e^-$ scattering process are obtained as

$$\left. \frac{d\sigma}{d\Omega} \right|_{CC} (\nu_e e^-) = \frac{G_F^2 s}{4\pi^2} \quad \text{and} \quad \sigma|_{CC} (\nu_e e^-) = \frac{G_F^2 s}{3\pi}. \quad (1.94)$$

Similarly, for $\bar{\nu}_e e^-$ scattering, the differential and total scattering cross sections for CC induced process are obtained as

$$\left. \frac{d\sigma}{d\Omega} \right|_{CC} (\bar{\nu}_e e^-) = \frac{G_F^2 s}{16\pi^2} (1 - \cos \theta_{CM})^2 \quad \text{and} \quad \sigma|_{CC} (\bar{\nu}_e e^-) = \frac{G_F^2 s}{3\pi}, \quad (1.95)$$

where θ_{CM} is the angle between the incoming $\bar{\nu}_e$ and the outgoing electron.

1.3.8. (Anti)neutrino-quark scattering

For (anti)neutrino-quark scattering like the processes

$$\nu_l + d \longrightarrow l^- + u, \quad \bar{\nu}_l + u \longrightarrow l^+ + d, \quad (1.96)$$

which can take place only through CC channel, the general expression for the differential scattering cross section is similarly obtained with the values of g_V and g_A for the quarks defined in Table 1.3.

In the massless lepton limit, the differential scattering cross sections are given by

$$\frac{d\sigma}{d\Omega} (\nu_l + d \rightarrow l^- + u) = \frac{G_F^2 s}{4\pi^2}, \quad \text{and} \quad \frac{d\sigma}{d\Omega} (\bar{\nu}_l + u \rightarrow l^+ + d) = \frac{G_F^2 s}{16\pi^2} (1 + \cos \theta_{CM})^2. \quad (1.97)$$

For $\bar{\nu}_l \bar{d} \rightarrow l^+ \bar{u}$ and $\nu_l \bar{u} \rightarrow l^- \bar{d}$ processes, the differential scattering cross sections are given by

$$\frac{d\sigma}{d\Omega} (\bar{\nu}_l + \bar{d} \rightarrow l^+ + \bar{u}) = \frac{G_F^2 s}{4\pi^2}, \quad \text{and} \quad \frac{d\sigma}{d\Omega} (\nu_l + \bar{u} \rightarrow l^- + \bar{d}) = \frac{G_F^2 s}{16\pi^2} (1 + \cos \theta_{CM})^2. \quad (1.98)$$

1.4. Resonance scattering of neutrinos: Glashow resonance

In the early days of the development of the theory of weak processes mediated by the intermediate vector bosons (W), Glashow [140] considered the reaction

$$\bar{\nu} + e^- \rightarrow \bar{\nu} + \mu^- \quad (1.99)$$

and speculated about the resonance scattering of $\bar{\nu}$ through the process $\bar{\nu} + e^- \rightarrow W^- \rightarrow \bar{\nu} + \mu^-$ which would radically enhance the cross section for the reaction shown in Eq. (1.99). This would happen for an antineutrino ($\bar{\nu}$) scattering from the electron at rest. This resonance is commonly known as the Glashow resonance [140]. In the SM of the electroweak interactions, the weak processes are mediated by the charged W^\pm and neutral Z^0 bosons, respectively. Consequently, the resonance scattering is predicted to occur at an antineutrino energy $E_{\bar{\nu}_e} \approx \frac{M_W^2}{2m_e} = 6.3$ PeV, where M_W is the mass of the vector boson. Such antineutrino energies are too high to be produced in the terrestrial accelerators but can be produced in the case of astrophysical sources of neutrinos. The astrophysical neutrinos are produced as decay products of the unstable mesons and baryons created in various cosmic reactions involving very high energy pp and γp collisions in space. The flavor composition of the very high energy astrophysical neutrinos and antineutrinos and their energy distribution has been recently studied by many authors like Barger et al. [141], Biehl et al. [142], Loewy et al. [143], Bhattacharya et al. [144], in the context of the observation of these (anti)neutrinos in the PeV energy region recently by the IceCube Collaboration [145].

It has been shown that the resonant cross section for $\bar{\nu}_e + e^- \rightarrow W^-$ production assuming a Breit-Wigner form for the W^- resonance is given by [141]:

$$\sigma_{\text{res}}(s) = \frac{(s \Gamma_W^2)}{(s - M_W^2)^2 + (M_W \Gamma_W)^2} \sigma_{\text{res}}^{\text{peak}} \quad (1.100)$$

where $s = (k + p)^2$ and Γ_W is the W 's full width at half maximum (2.1 GeV).

$\sigma_{\text{res}}^{\text{peak}}$ is the cross section of W -resonance given by

$$\sigma_{\text{res}}^{\text{peak}} = \frac{24\pi}{M_W^2} B(W^- \rightarrow \bar{\nu}_e + e^-) = 5.02 \times 10^{-31} \text{cm}^2, \quad (1.101)$$

where $B(W^- \rightarrow \bar{\nu}_e + e^-)$ is the branching ratio for the $W^- \rightarrow \bar{\nu}_e + e^-$ mode. Since the process $\bar{\nu}_e + e^- \rightarrow W^- \rightarrow \text{hadrons}$ is more frequent because the branching ratio for the $W^- \rightarrow \text{hadrons}$ is 67%, it is the more likely mode for the

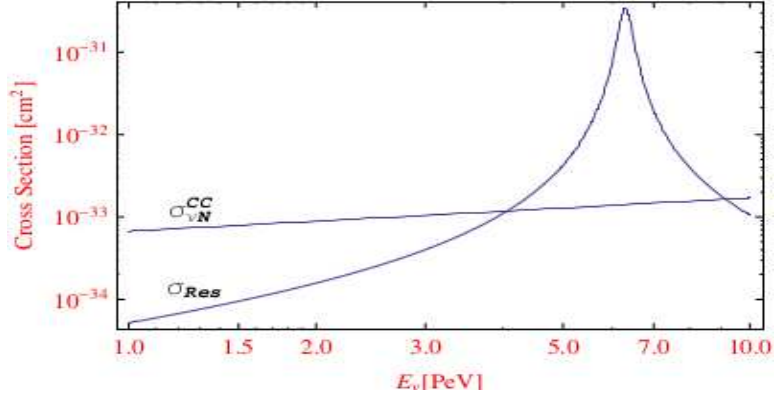


Figure 1.7: Cross sections for the resonant process $\bar{\nu}_e + e^- \rightarrow W^- \rightarrow \text{hadrons}$, and the nonresonant (NR) process $\nu_e + N \rightarrow e^- + \text{hadrons}$ in the 1 - 10 PeV region. The figure has been taken from Ref. [141].

detection of W^- , the Glashow resonance. Moreover, the hadron production through the $\bar{\nu}_e + e^- \rightarrow W^- \rightarrow \text{hadrons}$ is considerably larger than the hadron production in the neutrino-nucleon scattering through the $\nu_e + N \rightarrow e^- + \text{hadrons}$ process in the energy region of Glashow resonance as shown in Fig. 1.7.

The resonance production peak is affected by the Doppler effect of the moving electrons in the case of $\bar{\nu}_e$ scattering from atomic electrons in atoms leading to the broadening of the peak shown in Fig. 1.7 but the effect is shown to be small [143]. While the cross section at the peak energy of $E_{\bar{\nu}_e} = 6.3$ PeV for the resonance production of hadrons is more than 300 times larger than CC neutrino nucleon cross section, the production of e^- events, i.e. the rate of resonance events also depends upon the $\bar{\nu}_e$ content in the neutrino flux arriving at the detector which is affected by the flavor oscillations of the antineutrinos. In general the $\bar{\nu}_e$ content in the neutrino flux is smaller than the $\bar{\nu}_\mu$ content, but it is enhanced by the $\bar{\nu}_\mu \rightarrow \bar{\nu}_e$ oscillations during their propagation from the source to the detector. An experimental observation of resonant e^- events by the W^- resonance production and a theoretical study of the flavor decomposition of the antineutrino flux generated in the various neutrino producing reactions from the high energy pp and γp reactions in space including the effect of flavor oscillations of neutrinos, will provide important information about the source and production mechanism of very high energy neutrinos in the PeV energy region.

A recent report of the IceCube neutrino observatory [145] has claimed to observe one event of a cascade of high energy particle shower with a visible energy of 6.05 ± 0.72 PeV detected from the Cherenkov radiation of the shower particles, which is claimed to be due to the Glashow resonance. After correcting the visible energy for shower particles which do not radiate, the neutrino energy is inferred to be 6.3 PeV consistent with the prediction of the SM. The IceCube Generation-2 experiment [146] planned for future would improve the statistics and enable to measure the high energy antineutrino flux which would give information about the different mechanism for producing high energy astrophysical neutrinos in the PeV region and enrich our knowledge of the neutrino astronomy.

2. Neutrino scattering from nucleons

Neutrino experiments are done in the wide range of energy starting from a few MeV to TeV region using solar, reactor, atmospheric, and accelerator (anti)neutrinos. The present goal of the experimenters is to measure with better precision the various neutrino oscillation parameters, like the mixing angles, the mass-squared-difference of the neutrino mass eigenstates, CP violating phase δ in the lepton sector as well as to determine the mass hierarchy of the neutrino mass eigenstates. These parameters are sensitive to the neutrinos of different energy range which are obtained from accelerator, atmospheric, reactor and solar neutrino and/or (anti)neutrinos sources as mentioned in Section-1.1.3 and summarized in Table-1.1. Almost all the current generation (anti)neutrino experiments are using moderate to heavy nuclear targets. These experiments are measuring (anti)neutrino events which are convolution of energy dependent (anti)neutrino flux and the energy dependent neutrino-nucleus cross section where NME play very important role. In the precision era of neutrino physics, to achieve an accuracy of a few percent (2–3%) in the systematics, a good understanding of the neutrino-nucleon and neutrino-nucleus cross sections is highly desirable both experimentally as well as theoretically, which has been highlighted by various review articles [50, 51, 52, 47]. Apart from being significant to the determination of neutrino oscillation parameters, the neutrino-nucleon and neutrino-nucleus cross sections are important in their own right as they provide information about the axial-vector response of the nucleons bound inside the nucleus, which is not accessible via. photon or electron induced reactions, and recently it has been suggested [147] to perform neutrino experiments using hydrogen and deuterium targets. In this section, we focus on the neutrino-nucleon reactions and take up the neutrino-nucleus reactions in Section 5.

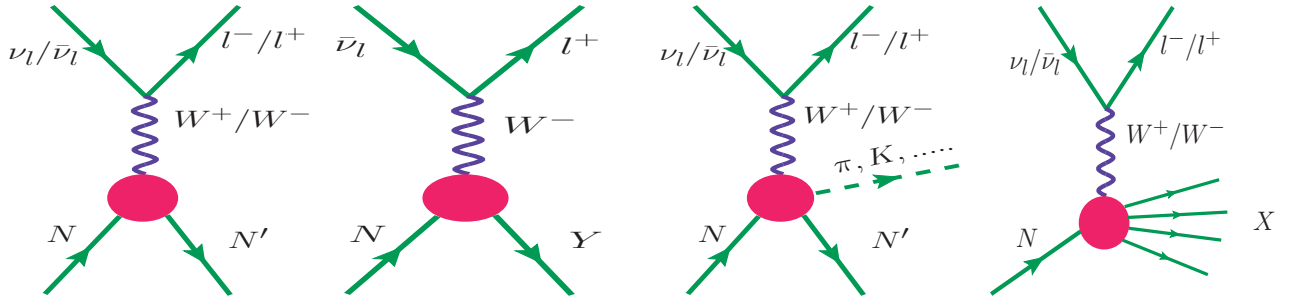


Figure 2.1: (Left to right) Feynman diagram depicting the $\Delta S = 0$ QE process, $\Delta S = 1$ QE process, IE process, and the DIS process in CC induced reactions. Similar processes for $\nu_l(\bar{\nu}_l) \rightarrow \nu_l(\bar{\nu}_l)$ reactions are also induced by NC through the Z exchange.

The (anti)neutrino interaction with a nucleon target starts with the elastic and quasielastic (QE) scattering processes. With the increase in available neutrino energy, the inelastic (IE) reactions in which new particles like 1π , multiple pions, 1η , $1K$, $Y\pi$, and YK ($Y = \Lambda, \Sigma, \Xi$), etc. are created as well as the deep inelastic scattering (DIS) become possible which are diagrammatically shown in Fig. 2.1 and described below [10]:

- **Elastic and quasielastic scattering:** Neutrinos and antineutrinos of all flavors interact with a nucleon through CC as well as NC interactions,

$$\nu_\ell/\bar{\nu}_\ell + N \longrightarrow \ell^-/\ell^+ + N', \quad (\text{CC}) \quad (2.1)$$

$$\text{and} \quad \nu_\ell/\bar{\nu}_\ell + N \longrightarrow \nu_\ell/\bar{\nu}_\ell + N, \quad (\text{NC}) \quad (2.2)$$

in the $\Delta S = 0$ sector, and

$$\bar{\nu}_\ell + N \longrightarrow \ell^+ + Y, \quad (\text{CC}), \quad (2.3)$$

in the $\Delta S = 1$ sector; where $N, N' = n, p$ and $Y = \Lambda, \Sigma^{-,0}$.

It may be noticed that in the strangeness sector, single hyperon (like $\Lambda, \Sigma^{-,0}$, etc.) produced in the final states, are possible only in the antineutrino induced reactions while it is prohibited in neutrino channel due to the $\Delta S = \Delta Q$ and FCNC rules.

S. No.	CC induced $\nu(\bar{\nu})$ reactions	NC induced $\nu(\bar{\nu})$ reactions
1.	$\nu_\ell(\bar{\nu}_\ell) + N \longrightarrow \ell^-(\ell^+) + N' + \pi$	$\nu_\ell(\bar{\nu}_\ell) + N \longrightarrow \nu_\ell(\bar{\nu}_\ell) + N' + \pi$
2.	$\nu_\ell(\bar{\nu}_\ell) + N \longrightarrow \ell^-(\ell^+) + N' + n\pi$	$\nu_\ell(\bar{\nu}_\ell) + N \longrightarrow \nu_\ell(\bar{\nu}_\ell) + N' + n\pi$
3.	$\nu_\ell(\bar{\nu}_\ell) + N \longrightarrow \ell^-(\ell^+) + N' + \eta$	$\nu_\ell(\bar{\nu}_\ell) + N \longrightarrow \nu_\ell(\bar{\nu}_\ell) + N' + \eta$
4.	$\nu_\ell(\bar{\nu}_\ell) + N \longrightarrow \ell^-(\ell^+) + Y + K$	$\nu_\ell(\bar{\nu}_\ell) + N \longrightarrow \nu_\ell(\bar{\nu}_\ell) + Y + K$
5.	$\nu_\ell(\bar{\nu}_\ell) + N \longrightarrow \ell^-(\ell^+) + N' + K(\bar{K})$	
6.	$\bar{\nu}_\ell + N \longrightarrow \ell^+ + Y + \pi$	

Table 2.1: CC and NC induced IE processes. Here N, N' represent proton and neutron, $Y = \Lambda, \Sigma$ represents the hyperons, $K = K^+, K^0$ represents the kaons, $\bar{K} = K^-, \bar{K}^0$ represents the antikaons and $\ell = e, \mu, \tau$ represents the leptons.

- **Inelastic scattering:** The IE processes like the single and multiple mesons are produced in the CC and NC reactions subject to the absence of FCNC. A list of such reactions is given in Table 2.1.
- **Deep inelastic scattering:** The DIS processes induced by the CC and NC interactions are represented by the reactions

$$\nu_\ell/\bar{\nu}_\ell + N \longrightarrow \ell^-/\ell^+ + X, \quad \nu_\ell/\bar{\nu}_\ell + N \longrightarrow \nu_\ell/\bar{\nu}_\ell + X. \quad (2.4)$$

where X is jet of hadrons in the final state.

In the region of intermediate and high energies relevant to the atmospheric and accelerator neutrinos, the inclusive reactions discussed above become important in various regions of energy as shown in Fig. 2.2, where the total scattering cross section per nucleon per unit energy of the incoming (anti)neutrino is presented as a function of the (anti)neutrino energy. The individual contributions to the QE, IE, and DIS cross sections as well as the sum of all the processes are shown and compared with the available experimental data starting from the Gargamelle collaboration in 1973 to

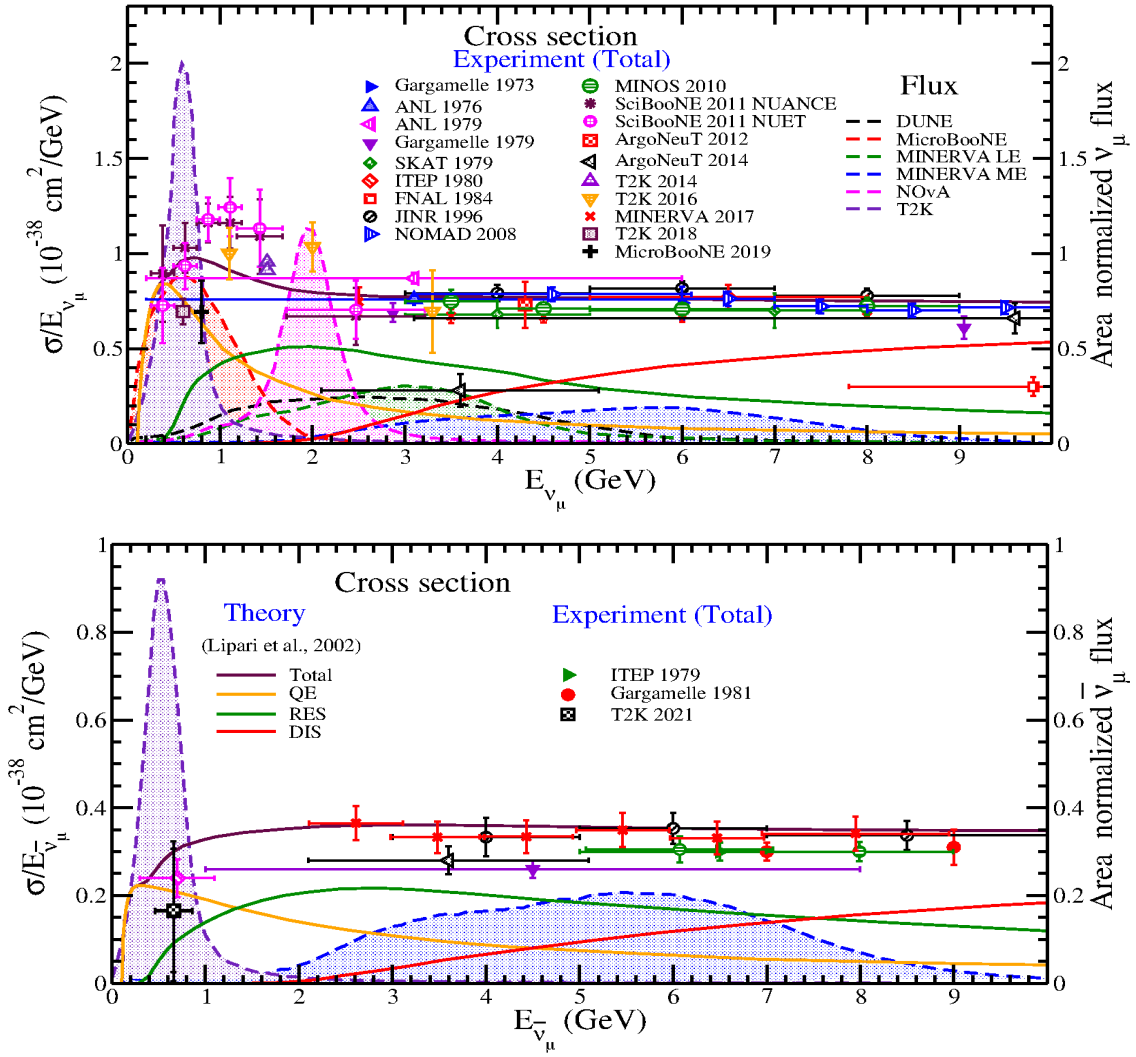


Figure 2.2: $\frac{\sigma}{E_{\nu\mu}}$ vs $E_{\nu\mu}$ (top panel) and $\frac{\sigma}{E_{\bar{\nu}\mu}}$ vs $E_{\bar{\nu}\mu}$ (bottom panel) for an isoscalar target. The data are the experimental points for the inclusive cross section (σ) in various nuclear targets. The theoretical result for $\frac{\sigma}{E_{\nu\mu}(\bar{\nu}\mu)}$ (solid line) has the contribution from total cross section (maroon line), QE scattering (orange line), resonance production (green line), and DIS (red line) provided by the NUANCE generator (Casper, 2002) and compiled by Lipari et al. The various neutrino fluxes which are being used in the T2K, MINERvA low energy ($< E_{\nu\mu} >= 3$ GeV), medium energy ($< E_{\nu\mu} >= 6$ GeV), NOvA, MicroBooNE experiments along with the proposed DUNE experiment at the Fermilab are shown to highlight the importance of the understanding of the cross section in the few GeV energy region. These neutrino fluxes are normalized to unit area.

MicroBooNE collaboration in 2019, extracted from the interaction of accelerator and atmospheric (anti)neutrinos with free nucleons as well as with nuclear targets. Also, in the same plot, we have shown the area normalized flux for present and future neutrino experiments like MicroBooNE, T2K, MINERvA, NOvA, and DUNE. It is evident from the figure that in the few GeV energy region all the three processes, viz., QE, IE, and DIS, have contributions to the neutrino and antineutrino induced processes. The different neutrino experiments have their flux peaked at different average energies for the corresponding experiment.

In the high energy region of neutrinos of the order of TeV and PeV, Bustamante and Connolly [148] have studied the energy dependence of the neutrino-nucleon cross section measured in the IceCube experiment and concluded that the results are compatible with predictions based on nucleon structure extracted from scattering experiments at lower energies and disfavor extreme deviations that could result from new physics in the TeV–PeV range. This has been further discussed in Ref. [149]. Experimentally, the IceCube collaboration [150] has measured the neutrino-nucleon cross section between 60TeV and 10PeV energy range and found the results to be compatible with the SM predictions.

While the QE and elastic scattering processes are kinematically well defined, the kinematic region defining the IE scattering and the onset of DIS is not free from ambiguities. We discuss $\Delta S = 0$ QE scattering of (anti)neutrinos with the free nucleon in Section 2.1 and the antineutrino induced $|\Delta S| = 1$ QE scattering in Section 2.2. The IE scattering processes start with the single pion production which is dominated by the Δ resonance. But the NR production of single

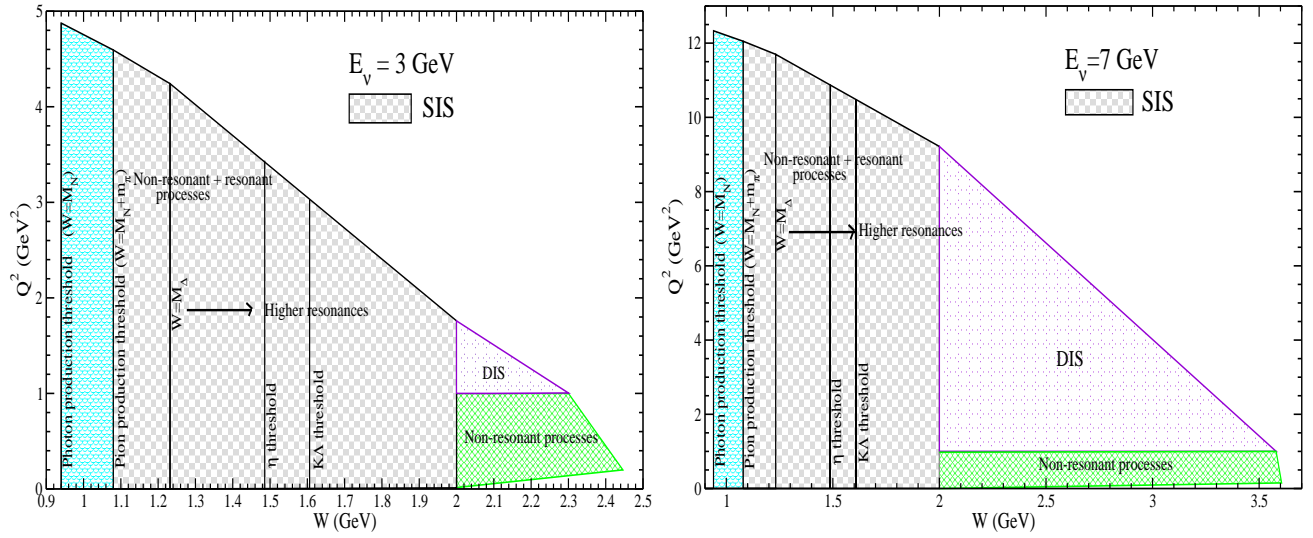


Figure 2.3: Q^2, W plane depicting neutrino-nucleon scattering at two representative laboratory neutrino energies, where $Q^2 \geq 0$ is the negative of the four momentum transfer squared $q^2 (\leq 0)$ and W is the center of mass (CM) energy.

pion starts earlier at the threshold of pion production corresponding to $W = 1.08$ GeV, where W is the CM energy of the final pion-nucleon system. In recent years, some authors have advocated to consider the onset of IE processes much earlier in energy with the production of single photon at $M < W < M + m_\pi$ [151], where M (m_π) is the nucleon (pion) mass. Traditionally, the kinematic region of the IE scattering is considered to be from $W = 1.08$ GeV to the onset of DIS for which $W = 2$ GeV is generally taken but a precise value is not defined. The kinematic region of the IE scattering above $W = 1.08$ GeV with moderate $Q^2 \leq 1$ GeV² is quite intriguing and is called the shallow inelastic scattering (SIS) region. Recently the need to understand the IE processes has been highlighted in many workshops and conferences like NuINT, NUSTEC, etc. A recent compilation of articles by several experimenters, theorists and phenomenologists have highlighted the development in the area of neutrino interactions in the intermediate and high energy regions [51]. The present accelerator experiments like NOvA, and MINERvA (low energy beam) and the future experiment like DUNE have average energies of about 3 GeV. For example at DUNE, it is expected that more than 50% events would come from the SIS plus DIS regions. Moreover, the atmospheric neutrino studies in the next generation Hyper-Kamiokande experiment will also have significant contributions from the SIS and DIS regions. With the increase in Q^2 , one approaches the onset of DIS. Therefore, it becomes essential to understand the dynamics of this kinematic region which is presently neither well understood theoretically nor experimentally [52, 152, 153]. Most of the present neutrino event generators use the prescription of Bodek et al. [154, 155, 156] to take care of the transition region using parton distribution functions empirically extrapolated from the DIS region to lower W and Q^2 . To understand the significance of the IE region in Fig. 2.3, we have shown different (Q^2, W) regions at the two representative incident neutrino energies of 3 GeV and 7 GeV. It may be observed that above the pion production threshold $W \approx 1.08$ GeV the excitation of the $\Delta(1232)$ resonance dominates, but at higher W the hadron dynamics results from a nontrivial interplay of overlapping baryon resonances, NR amplitudes and their interference.

In most of the neutrino event generators, the Rein-Sehgal approach [157] has been used to describe the pion production, associated particle production, etc., which considers nucleon-resonance transition form factors obtained using a constituent quark model. Some modifications in this approach have been recently done by updating the resonance properties like resonance masses, decay widths and branching ratios but interferences are neglected. Recently this model has been updated by Kabirnezhad [158, 159] by considering NR part of the amplitude and the empirical inputs for the vector part of the transition current. To understand weak pion production off the nucleon, several authors [160, 161, 162, 163, 164] have used approximate chiral symmetry of quantum chromodynamics (QCD) to construct the transition amplitude in the region of small energy and momentum transfers. Though the single pion production is dominated by the $\Delta(1232)$ resonance, there are other resonances like $N^*(1440)$, $N^*(1520)$, $N^*(1535)$, $N^*(1650)$, etc. which contribute in $n\pi^+$ ($p\pi^-$) and $p\pi^0$ ($n\pi^0$) channels for (anti)neutrino induced interaction. Furthermore, there are additional contributions from the NR amplitudes as well as their interferences with the resonance counterpart [165, 166] and these will be discussed in Section 3.4. Similarly in the case of single kaon production due to the absence of $S = 1$ baryonic resonances it is possible to obtain model independent predictions for the scattering cross sections using chiral perturbation theory which has been done by our group [162], while for the antikaon production there is additional contribution from the $\Sigma^*(1385)$ resonance, which has been studied by us [167]. Some of the results are presented for the scattering cross section for the (anti)neutrino scattering off nucleon leading to (anti)kaon production in Sections 3.6.1 and 3.6.2. In the case of eta production, it is

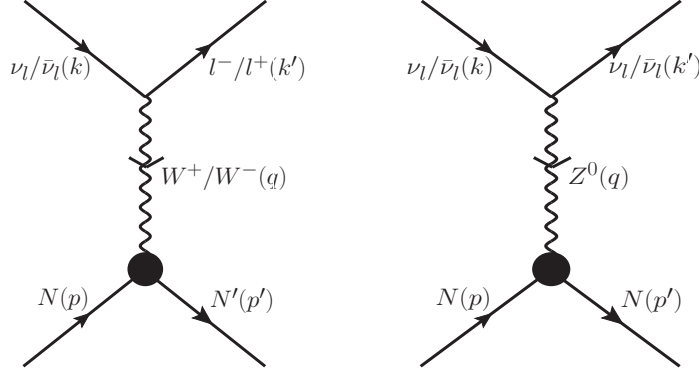


Figure 2.4: QE (left panel) and elastic (right panel) ν -scattering processes on the nucleons ($N = n, p$ and $N' = p, n$) target.

well known from πN scattering, that it is dominated by $N^*(1535)$ resonance besides very small contributions from the higher resonances like $N^*(1650)$ and $N^*(1710)$, and the NR terms. We have discussed first the eta production induced by the real photons off the nucleon targets in Section 3.5.1 and compared the results with the MAMI data [168, 169] and then extended the formalism to the weak sector in Section 3.5.2. Similarly for the associated particle production, our group [170] has studied associated particle production induced by photons off proton target and compared the results with the CLAS data [171] and extended this study to include the (anti)neutrino induced associated particle production off nucleon target. These are discussed in Sections 3.6.3 and 3.6.4. We also discuss in brief $Y\pi$ production following the works of Benitez Galan et al. [172], ΞK production following the works of Alam et al. [173] and two pion production [161, 174] in Sections 3.6.5, 3.6.6 and 3.7, respectively. Finally, in Section 4, we discuss DIS of (anti)neutrinos with free nucleon, where a jet of hadron is produced in the final state.

2.1. Quasielastic and elastic ν -scattering processes on nucleons

2.1.1. Introduction

Neutrinos and antineutrinos interact with the free nucleons via the CC as well as NC induced weak processes like:

$$\nu_l(k) + n(p) \rightarrow l^-(k') + p(p'), \quad \bar{\nu}_l(k) + p(p) \rightarrow l^+(k') + n(p') \quad (\text{CC}) \quad (2.5)$$

$$\left. \begin{aligned} \nu_l(k) + n(p) &\rightarrow \nu_l(k') + n(p'), & \nu_l(k) + p(p) &\rightarrow \nu_l(k') + p(p') \\ \bar{\nu}_l(k) + n(p) &\rightarrow \bar{\nu}_l(k') + n(p'), & \bar{\nu}_l(k) + p(p) &\rightarrow \bar{\nu}_l(k') + p(p') \end{aligned} \right\} \quad (\text{NC}) \quad (2.6)$$

In the above processes, k and k' are, respectively, the four momenta of the (anti)neutrino and the corresponding charged/neutral lepton and p and p' are four momenta of the incoming and outgoing nucleons. Feynman diagrams corresponding to reactions given in Eqs. (2.5) and (2.6) are shown in Fig. 2.4.

2.1.2. Charged current quasielastic reactions and weak nucleon form factors

The general expression for the differential scattering cross section for reactions given in Eqs. (2.5) and (2.6) is written as,

$$d\sigma = \frac{(2\pi)^4 \delta^4(k + p - p' - k')}{4(k \cdot p)} \frac{d\vec{k}'}{(2\pi)^3 2E_l'} \frac{d\vec{p}'}{(2\pi)^3 2E'} \bar{\Sigma} \Sigma |\mathcal{M}|^2, \quad (2.7)$$

which results in the expression of the double differential cross section $\sigma_{free}(E_l', \Omega_l')$ on the free nucleon target in the laboratory frame as

$$\sigma_{free}(E_l', \Omega_l') \equiv \left(\frac{d^2\sigma}{dE_l' d\Omega_l'} \right)_{\nu/\bar{\nu}-N} = \frac{|\vec{k}'|}{64\pi^2 E_\nu E E'} \bar{\Sigma} \Sigma |\mathcal{M}|^2 \delta[q_0 + E - E'], \quad (2.8)$$

where $q_0 (= E_\nu - E_l')$ is the energy transferred to the hadronic system; E_ν , E_l' are the energies of the incoming neutrino and outgoing lepton, E ($= M$) and E' ($= M + q_0$), respectively, are the energies of the incoming and outgoing nucleons in the laboratory frame, \mathcal{M} is the invariant matrix element and for Eq. (2.5) is given by

$$\mathcal{M} = \frac{G_F}{\sqrt{2}} l^\mu J_\mu. \quad (2.9)$$

In the above expression G_F is the Fermi coupling constant, and the leptonic weak current is given by

$$l^\mu = \bar{u}(\vec{k}')\gamma^\mu(1 \mp \gamma_5)u(\vec{k}), \quad (2.10)$$

and $-(+)$ represents the neutrino (antineutrino) induced QE scattering processes. The hadronic current (J_μ) for CC induced interaction is given by

$$J_\mu^{CC} = \bar{u}(\vec{p}') \mathcal{O}_\mu^{CC} u(\vec{p}), \quad (2.11)$$

where $\mathcal{O}_\mu^{CC} = V_\mu^{CC} - A_\mu^{CC}$ is CC weak hadronic vertex, and the matrix elements of the vector (V_μ^{CC}) and the axial-vector (A_μ^{CC}) currents are given by [175, 176]:

$$\langle N'(\vec{p}') | V_\mu^{CC} | N(\vec{p}) \rangle = \cos \theta_C \bar{u}(\vec{p}') \left[\gamma_\mu f_1(Q^2) + i\sigma_{\mu\nu} \frac{q^\nu}{(M + M')} f_2(Q^2) + \frac{2q_\mu}{(M + M')} f_3(Q^2) \right] u(\vec{p}), \quad (2.12)$$

$$\langle N'(\vec{p}') | A_\mu^{CC} | N(\vec{p}) \rangle = \cos \theta_C \bar{u}(\vec{p}') \left[\gamma_\mu \gamma_5 g_1(Q^2) + i\sigma_{\mu\nu} \frac{q^\nu}{(M + M')} \gamma_5 g_2(Q^2) + \frac{2q_\mu}{(M + M')} \gamma_5 g_3(Q^2) \right] u(\vec{p}). \quad (2.13)$$

In the above expression, $N, N' = n, p$; θ_C is the Cabibbo angle, $Q^2 = -q^2 = -(k - k')^2$ is the four momentum transfer squared. M and M' are the masses of the initial and the final nucleons, respectively. $f_1(Q^2)$, $f_2(Q^2)$ and $f_3(Q^2)$ are the vector, weak magnetic and induced scalar form factors and $g_1(Q^2)$, $g_2(Q^2)$ and $g_3(Q^2)$ are the axial-vector, induced tensor (or weak electric) and induced pseudoscalar form factors, respectively.

Using the leptonic and hadronic currents given in Eqs. (2.10) and (2.11) in Eq. (2.9), the matrix element squared is obtained as:

$$|\mathcal{M}|^2 = \frac{G_F^2}{2} L^{\mu\nu} J_{\mu\nu}, \quad (2.14)$$

where the leptonic tensor $L^{\mu\nu}$ is calculated to be

$$L^{\mu\nu} = 8 \left[k^\mu k'^\nu + k'^\mu k^\nu - g^{\mu\nu} k \cdot k' \pm i\epsilon^{\mu\nu\alpha\beta} k'_\alpha k_\beta \right], \quad (2.15)$$

$+(-)$ is for the neutrino (antineutrino) induced processes.

The hadronic tensor $J_{\mu\nu}$ given in Eq. (2.14), is obtained using Eq. (2.11) averaged over the initial spin state of the nucleon and summed over the final spin state as:

$$J_{\mu\nu} = \overline{\sum} \sum J_\mu^{CC\dagger} J_\nu^{CC} = \frac{1}{2} \text{Tr} \left[(\not{p}' + M) \mathcal{O}_\mu (\not{p} + M) \tilde{\mathcal{O}}_\nu \right], \quad (2.16)$$

where $\tilde{\mathcal{O}}_\nu = \gamma^0 \mathcal{O}_\nu^\dagger \gamma^0$. The expression for $J_{\mu\nu}$ is given in Appendix A.

The differential scattering cross section $\frac{d\sigma}{dQ^2}$ for CC and NC induced processes, in the laboratory frame is then obtained as

$$\frac{d\sigma}{dQ^2} = \frac{G_F^2}{8\pi M^2 E_\nu^2} N(Q^2), \quad (2.17)$$

where $N(Q^2) = J_{\mu\nu} L^{\mu\nu}$ and the expression for $N(Q^2)$ is given in Appendix A.1.

2.1.3. Neutral current elastic reactions and weak nucleon form factors

We define the hadronic current for the weak NC induced processes on the proton and neutron targets, given in Eq. (2.6), in terms of NC form factors $\tilde{f}_i^{p,n}(Q^2)$ and $\tilde{g}_i^{p,n}(Q^2)$ ($i = 1, 2, 3$) for the protons and neutrons, respectively, as

$$\begin{aligned} J_\mu^{NC}|_i &= \bar{u}(\vec{p}') \mathcal{O}_\mu^{NC} u(\vec{p}) = \bar{u}(\vec{p}') \left[\gamma_\mu \tilde{f}_1^i(Q^2) + \frac{i\sigma_{\mu\nu} q^\nu \tilde{f}_2^i(Q^2)}{2M} + \frac{q_\mu}{M} \gamma_5 \tilde{f}_3^i(Q^2) \right. \\ &\quad \left. + \gamma_\mu \gamma_5 \tilde{g}_1^i(Q^2) + \frac{(p_\mu + p'_\mu)}{M} \gamma_5 \tilde{g}_2^i(Q^2) + \frac{q_\mu \gamma_5 \tilde{g}_3^i(Q^2)}{M} \right] u(\vec{p}), \end{aligned} \quad (2.18)$$

with $i = p, n$. Here the nomenclature of the form factors is the same as in the case of CC QE process (Eqs. (2.12) and (2.13)) and the parameterizations for $\tilde{f}_i(Q^2)$ and $\tilde{g}_i(Q^2)$ are given in Section 2.1.5.

2.1.4. Symmetry properties of the weak hadronic current

The weak hadronic current J_μ has the vector V_μ and the axial-vector A_μ terms constructed using the bilinear covariants associated with the nucleon fields as well as the four momenta of the incoming and outgoing nucleons. These bilinear covariants have certain definite properties under discrete transformation like C, P and T as well as the internal symmetries like the isospin and unitary symmetry [10, 176]. These symmetry properties are exploited in writing the matrix elements of these currents between the initial and final states of spin 0, $\frac{1}{2}$, and $\frac{3}{2}$ particles. We discuss below these symmetry properties and their role in writing the general structure of the matrix elements.

(i) **Isospin properties of the weak hadronic current**

The weak hadronic currents between the neutron and proton states involve a change of charge $\Delta Q = \pm 1$ in the case of $n \rightarrow p$ and $p \rightarrow n$ transitions. Since $Q = I_3 + \frac{B}{2}$ for the nonstrange baryons, therefore $\Delta Q = \pm 1$ implies $\Delta I_3 = \pm 1$ using baryon number conservation. Since protons and neutrons are assigned to a doublet, therefore, they can be written as a two component isospinor under the group of isospin transformation, i.e.

$$u = \begin{pmatrix} u_p \\ u_n \end{pmatrix}. \quad (2.19)$$

The isospin group of transformations is generated by the three 2×2 Pauli matrices τ_i ($i = 1 - 3$), which along with the vector currents constitute the isovector part of the hadronic current. By defining the isospin raising and lowering operators $\tau^\pm = \frac{\tau_1 \pm i\tau_2}{2}$, we can write

$$\bar{u}_p V_\mu^{CC} u_n = \bar{u} V_\mu^{CC} \tau^+ u = \bar{u} V_\mu^{CC+} u, \quad \bar{u}_n V_\mu^{CC} u_p = \bar{u} V_\mu^{CC} \tau^- u = \bar{u} V_\mu^{CC-} u. \quad (2.20)$$

It may be observed from the above relations that the charged weak vector currents are purely isovector in nature. Similarly, for the electromagnetic vector current, the hadronic current is given by

$$J_{\mu(p,n)}^{em}(p, p') = \bar{u}(\vec{p}'_{p,n}) V_\mu^{em} u(\vec{p}_{p,n}), \quad (2.21)$$

with

$$V_\mu^{em}(p, n) = \left[\gamma_\mu F_1^{p,n}(Q^2) + i\sigma_{\mu\nu} \frac{q^\nu}{(2M)} F_2^{p,n}(Q^2) \right], \quad (2.22)$$

where $q = p' - p$ with $Q^2 = -q^2$. $F_1^{p,n}(Q^2)$ and $F_2^{p,n}(Q^2)$ are, respectively, the Dirac and Pauli form factors of the nucleon. In terms of the Pauli matrices, the hadronic currents for the electromagnetic induced interactions are written as

$$\bar{u}_p V_\mu^{em} u_p = \bar{u} V_\mu^{em} \frac{\mathbb{I} + \tau_3}{2} u, \quad \bar{u}_n V_\mu^{em} u_n = \bar{u} V_\mu^{em} \frac{\mathbb{I} - \tau_3}{2} u, \quad (2.23)$$

implying the isoscalar and isovector current matrix elements as

$$\bar{u} \mathbb{I} V_\mu^{em} u = \bar{u}_p V_\mu^{em} u_p + \bar{u}_n V_\mu^{em} u_n, \quad \bar{u} \tau_3 V_\mu^{em} u = \bar{u}_p V_\mu^{em} u_p - \bar{u}_n V_\mu^{em} u_n. \quad (2.24)$$

If we parameterize the matrix element of the isoscalar (with form factors $F_{1,2}^S(Q^2)$) and isovector (with form factors $F_{1,2}^V(Q^2)$) components as

$$\bar{u} \mathbb{I} V_\mu^{em} u = \bar{u} \left[F_1^S(Q^2) \gamma_\mu + i F_2^S(Q^2) \frac{\sigma_{\mu\nu} q^\nu}{2M} \right] u, \quad \bar{u} \tau_3 V_\mu^{em} u = \bar{u} \left[F_1^V(Q^2) \gamma_\mu + i \frac{\sigma_{\mu\nu} q^\nu}{2M} F_2^V(Q^2) \right] \tau_3 u, \quad (2.25)$$

and the electromagnetic matrix element of protons and neutrons given in Eq. (2.21) with V_μ^{em} given in Eq. (2.22), then we can write:

$$F_{1,2}^S(Q^2) = F_{1,2}^p(Q^2) + F_{1,2}^n(Q^2), \quad F_{1,2}^V(Q^2) = F_{1,2}^p(Q^2) - F_{1,2}^n(Q^2). \quad (2.26)$$

The above expression shows that the electromagnetic current transforms as the sum of the isoscalar and isovector currents.

(ii) **T invariance**

Time reversal invariance holds if

$$\mathcal{M}' = \mathcal{M}^*, \quad (2.27)$$

where \mathcal{M}' represents the time reversed matrix element and \mathcal{M}^* represents the Hermitian conjugate of the unreversed matrix element. Under time-reversal invariance (T invariance), the initial and final state particles are interchanged as well as their spin and angular momenta are reversed.

Taking all the bilinear covariants used with the form factors in the vector and the axial-vector currents individually, we obtain the transformation of the vector and axial-vector form factors under T invariance as [10]:

$$\begin{aligned} \bar{u}_p u_n &\xrightarrow{T} \bar{u}_n u_p, & \bar{u}_p \gamma_5 u_n &\xrightarrow{T} \bar{u}_n \gamma_5 u_p, \\ \bar{u}_p \gamma^\mu u_n &\xrightarrow{T} \bar{u}_n \gamma_\mu u_p, & \bar{u}_p \gamma^\mu \gamma_5 u_n &\xrightarrow{T} \bar{u}_n \gamma_\mu \gamma_5 u_p, \\ \bar{u}_p \sigma^{\mu\nu} u_n &\xrightarrow{T} -\bar{u}_n \sigma_{\mu\nu} u_p, & \bar{u}_p \sigma^{\mu\nu} \gamma_5 u_n &\xrightarrow{T} \bar{u}_n \sigma_{\mu\nu} \gamma_5 u_p. \end{aligned}$$

The hadronic current J_μ is defined in Eq. (2.11) with V_μ and A_μ defined in Eqs. (2.12) and (2.13), respectively. The time reversed current J'_μ is obtained as [10]:

$$\begin{aligned} J'_\mu &= \cos\theta_C \bar{u}_n \left[f_1(Q^2)\gamma_\mu + i\sigma_{\mu\nu}\frac{q^\nu}{M+M'}f_2(Q^2) + \frac{2q_\mu}{M+M'}f_3(Q^2) \right. \\ &\quad \left. - g_1(Q^2)\gamma_\mu\gamma_5 - i\sigma_{\mu\nu}\frac{q^\nu}{M+M'}\gamma_5g_2(Q^2) - \frac{2q_\mu}{M+M'}\gamma_5g_3(Q^2) \right] u_p. \end{aligned} \quad (2.28)$$

Hermitian conjugate of Eq. (2.11) is written as

$$\begin{aligned} J_\mu^* &= \cos\theta_C \bar{u}_p \left[f_1^*(Q^2)\gamma_\mu + i\sigma_{\mu\nu}\frac{q^\nu}{M+M'}f_2^*(Q^2) + \frac{2q_\mu}{M+M'}f_3^*(Q^2) - g_1^*(Q^2)\gamma_\mu\gamma_5 \right. \\ &\quad \left. - i\sigma_{\mu\nu}\frac{q^\nu}{M+M'}\gamma_5g_2^*(Q^2) - \frac{2q_\mu}{M+M'}\gamma_5g_3^*(Q^2) \right] u_n. \end{aligned} \quad (2.29)$$

Comparing Eqs. (2.28) and (2.29), we find that $f_i(Q^2) = f_i^*(Q^2)$ and $g_i(Q^2) = g_i^*(Q^2)$ which implies that if time reversal invariance holds, the form factors must be real.

(iii) Conserved vector current hypothesis

The hypothesis of the conserved vector current (CVC) was proposed by Gershtein and Zeldovich [177] and Feynman and Gell-Mann [12]. They made an important observation in the study of the nuclear β decays in Fermi transition driven by the vector currents, with no change in parity. They observed that the strength of the weak vector coupling (weak charge) for the muon and neutron decays are the same, just like in the case of the electromagnetic interactions where the strength of the electromagnetic coupling i.e. e , remains the same for the electrons and protons. Since the equality of the charge coupling, also known as the universality of the electromagnetic interactions follows from the conservation of the electromagnetic current, therefore, it was suggested that the weak vector current is also conserved i.e. $\partial_\mu V^\mu(x) = 0$, which leads to the equality of the weak coupling for the leptons and hadrons.

In fact, they proposed a stronger hypothesis of the isotriplet of the vector currents which goes beyond the hypothesis of CVC and predicts the form factors $f_{1,2}(Q^2)$ describing the matrix elements of the weak vector current in terms of the electromagnetic form factors of hadrons. According to the isotriplet hypothesis, the weak vector currents V_μ^+ , V_μ^- and the isovector part of the electromagnetic current V_μ^{em} are assumed to form an isotriplet under the isospin symmetry such that f_1 and f_2 are given in terms of the isovector electromagnetic form factors i.e.

$$f_1(Q^2) = F_1^V(Q^2) = F_1^p(Q^2) - F_1^n(Q^2), \quad f_2(Q^2) = F_2^V(Q^2) = F_2^p(Q^2) - F_2^n(Q^2). \quad (2.30)$$

The CVC hypothesis, i.e. $\partial_\mu V^\mu(x) = 0$ implies $f_3(Q^2) = 0$. It should be noted that while the isotriplet current hypothesis implies CVC due to the isospin symmetry, the vice versa is not true. In the literature, the term CVC is mostly used meaning both the isotriplet hypothesis of weak vector currents V_μ^+ and V_μ^- and the CVC hypothesis.

(iv) Partial conservation of axial-vector current

In contrast to the vector current which is conserved, the axial-vector current is not conserved. To see this explicitly, consider the matrix element of the axial-vector current between one pion state and vacuum which enters in the πl_2 decay of pion i.e. $\langle 0 | A^\mu(x) | \pi^- \rangle = i f_\pi q^\mu e^{-iq \cdot x}$, where q is the four momentum of the pion. Taking its divergence leads to

$$\langle 0 | \partial_\mu A^\mu(x) | \pi^-(q) \rangle = (-i) i f_\pi q_\mu q^\mu e^{-iq \cdot x} = f_\pi m_\pi^2 e^{-iq \cdot x}, \quad (2.31)$$

as $q^2 = m_\pi^2$. If the axial-vector current A^μ is divergenceless then either $m_\pi = 0$ or $f_\pi = 0$, implying the pion to be massless or it does not decay. Since $m_\pi \neq 0$, conservation of axial-vector current implies $f_\pi = 0$, which is also not true. Therefore, the axial-vector current is not conserved. However, since the pion is the lightest hadron, we can work in the limit of $m_\pi \rightarrow 0$, and say that the axial-vector current is conserved in the limit

$$\lim_{m_\pi \rightarrow 0} \partial_\mu A^\mu(x) = 0, \quad (2.32)$$

which is termed as the partial conservation of axial-vector current (PCAC). The hypothesis of PCAC has been very useful in calculating many processes in the weak interaction physics and deriving relations between various processes in the limit of $m_\pi \rightarrow 0$. However, the real predictive power of PCAC lies in making further assumptions about the divergence of the axial-vector field $\partial_\mu A^\mu(x)$ and identifying with the pion field $\phi_\pi(x)$ that establishes a connection between the weak and strong interaction physics and assuming that the transition amplitudes derived in the $m_\pi \rightarrow 0$ limit can be smoothly extrapolated to the physical mass of the pion. The success of PCAC in various applications of calculating the physical processes is based on the following assumptions:

- (i) The divergence of the axial-vector field is a pseudoscalar field and the pion is also described by a pseudoscalar field. If it is assumed that both are related then the physical pion field is described by the divergence of the axial-vector current, i.e. $\partial_\mu A^\mu(x) \propto \phi_\pi(x)$, such that $\partial_\mu A^\mu(x) = e_\pi \phi_\pi(x)$. This assumption makes it possible to relate the weak interaction processes induced by A^μ to the pion physics in the strong interaction processes through the matrix element of its derivative i.e. $\partial_\mu A^\mu$.
- (ii) Taking the limit $m_\pi \rightarrow 0$ (corresponding to the conserved axial-vector current) in the processes involving pions and nucleons, makes it easier to evaluate the transition amplitude in many weak processes. If further assumption is made that these amplitudes vary smoothly with q^2 and do not change much over the range of q^2 involved in the processes, then the amplitudes evaluated at $q^2 = 0$ can be extrapolated to the physical limit of $q^2 = m_\pi^2$, i.e. $f(0) \rightarrow f(m_\pi^2)$, where $f(q^2)$ is the pion form factor. This is called the soft pion limit widely used in the weak interaction physics. However, there remains an ambiguity whether to take the limit as $m_\pi^2 \rightarrow 0$ or $m_\pi \rightarrow 0$ [178, 179]. For more discussion see Ref. [10].

(v) **G-parity and second class currents**

G-parity is a multiplicative quantum number, first used to classify the multipion states in pp and πp collisions [180, 181, 182, 183] and later used by Weinberg [184] to classify the weak hadronic currents. It is defined as the product of C, the charge conjugation operation and a rotation by 180° about the Y-axis in the isospin space i.e.

$$G = C e^{i\pi I_Y}. \quad (2.33)$$

Since strong interactions are invariant under C and isospin, they are also invariant under G-parity. The G-parity is a very useful concept in the study of pion production in $N\bar{N}$ collisions. Since the weak currents involve bilinear covariants formed out of the nucleon fields $\bar{\psi}(p')$ and $\psi(p)$, their transformations can be well defined under G-parity. The weak vector and axial-vector currents between a neutron and a proton are defined in Eqs. (2.12) and (2.13). Since the currents belong to the triplet representation of the isospin, therefore, all the terms have similar transformation under the rotation $e^{i\pi I_Y}$. It is their transformation under C-parity which defines their relative transformation under G-parity. Under C-parity, the bilinear terms in Eqs. (2.12) and (2.13) transforms as:

$$\bar{u}_p u_n \xrightarrow{C} -\bar{u}_n u_p \quad (\text{assumed with } f_3) \quad (2.34)$$

$$\bar{u}_p \gamma_5 u_n \xrightarrow{C} -\bar{u}_p \gamma_5 u_n \quad (\text{assumed with } g_3) \quad (2.35)$$

$$\bar{u}_p \gamma_\mu \gamma_5 u_n \xrightarrow{C} -\bar{u}_p \gamma_\mu \gamma_5 u_p \quad (\text{assumed with } g_1) \quad (2.36)$$

while

$$\bar{u}_p \gamma^\mu u_n \xrightarrow{C} \bar{u}_n \gamma^\mu u_p \quad (\text{assumed with } f_1) \quad (2.37)$$

$$\bar{u}_p \sigma^{\mu\nu} u_n \xrightarrow{C} \bar{u}_n \sigma^{\mu\nu} u_p \quad (\text{assumed with } f_2) \quad (2.38)$$

$$\bar{u}_p \sigma^{\mu\nu} \gamma_5 u_n \xrightarrow{C} \bar{u}_n \sigma^{\mu\nu} \gamma_5 u_p \quad (\text{assumed with } g_2) \quad (2.39)$$

What is observed from Eqs. (2.34)–(2.39) is that the bilinear terms associated with f_2 transforms the same way as f_1 does, while f_3 transforms in opposite way. Similarly, g_3 transforms the same way as g_1 does while g_2 transforms in a different way. It was Weinberg [184] who first used the G-parity to classify the weak currents. He called the currents associated with f_1 , f_2 , g_1 and g_3 which are invariant under G-parity as the first class currents, and the currents associated with f_3 and g_2 which violate G-parity as the second class currents (SCC). Consequently, if G invariance is valid in the weak interactions then the currents with form factors $f_1(Q^2)$, $f_2(Q^2)$, $g_1(Q^2)$ and $g_3(Q^2)$ should exist and $f_3(Q^2) = g_2(Q^2) = 0$. It should be noted that $f_3(Q^2) = 0$ is also predicted as a consequence of CVC hypothesis.

2.1.5. Parameterization of the weak form factors

(i) **Vector form factors**

In the case of CC interactions, the hadronic current contains two isovector form factors $f_{1,2}(Q^2)$ of the nucleons, which can be related to the isovector combination of the Dirac ($F_{1,2}^p(Q^2)$) and Pauli ($F_{1,2}^n(Q^2)$) form factors of the proton and the neutron using the relation

$$f_{1,2}(Q^2) = F_{1,2}^p(Q^2) - F_{1,2}^n(Q^2). \quad (2.40)$$

The Dirac ($F_1(Q^2)$) and Pauli ($F_2(Q^2)$) form factors are, in turn, expressed in terms of the experimentally determined

Sachs' electric ($G_E^{p,n}(Q^2)$) and magnetic ($G_M^{p,n}(Q^2)$) form factors of the nucleon as:

$$F_1^{p,n}(Q^2) = \left(1 + \frac{Q^2}{4M^2}\right)^{-1} \left[G_E^{p,n}(Q^2) + \frac{Q^2}{4M^2} G_M^{p,n}(Q^2) \right], \quad (2.41)$$

$$F_2^{p,n}(Q^2) = \left(1 + \frac{Q^2}{4M^2}\right)^{-1} [G_M^{p,n}(Q^2) - G_E^{p,n}(Q^2)]. \quad (2.42)$$

Initially, it was observed from the experimental data of the electromagnetic scattering that the Sachs' form factors may have a dipole form. However, with the development of electron beam accelerator experiments, it was observed that the Sachs' form factors deviate from the dipole form. Galster et al. [185] parameterized the deviated Sachs' form factors as

$$\begin{aligned} G_E^p(Q^2) &= G_D(Q^2) & G_M^p(Q^2) &= (1 + \mu_p)G_D(Q^2) \\ G_M^n(Q^2) &= \mu_n G_D(Q^2) & G_E^n(Q^2) &= -\left(\frac{Q^2}{4M^2}\right)\mu_n G_D(Q^2)\xi_n \\ \xi_n &= \frac{1}{\left(1 - \lambda_n \frac{Q^2}{4M^2}\right)}, & G_D(Q^2) &= \frac{1}{\left(1 + \frac{Q^2}{M_V^2}\right)^2}, \end{aligned}$$

with $\mu_p = 1.7927\mu_N$, $\mu_n = -1.913\mu_N$, $M_V = 0.84$ GeV and $\lambda_n = 5.6$.

Recently for $G_E^{p,n}(Q^2)$ and $G_M^{p,n}(Q^2)$, various parameterizations are available in the literature like BBBA05 parameterized by Bradford et al. [186], BBA03 parameterized by Budd et al. [187], Alberico et al. [188], Bosted [189], modified Galster parameterization given by Platchkov et al. [190], Kelly [191], and modified Kelly parameterization given by Punjabi et al. [192]. We have used, in our numerical calculations, the parameterization given by Bradford et al. [186].

The vector form factors for NC induced processes are obtained as

$$\tilde{f}_{1,2}^p(Q^2) = \left(\frac{1}{2} - 2\sin^2\theta_W\right) F_{1,2}^p(Q^2) - \frac{1}{2}F_{1,2}^n(Q^2) - \frac{1}{2}F_{1,2}^s(Q^2), \quad (2.43)$$

$$\tilde{f}_{1,2}^n(Q^2) = \left(\frac{1}{2} - 2\sin^2\theta_W\right) F_{1,2}^n(Q^2) - \frac{1}{2}F_{1,2}^p(Q^2) - \frac{1}{2}F_{1,2}^s(Q^2), \quad (2.44)$$

where θ_W is the Weinberg angle, and $F_1^s(Q^2)$ and $F_2^s(Q^2)$ are the strangeness vector form factors, which are discussed later in this section.

(ii) Axial-vector form factor

The isovector axial-vector form factor is parameterized as

$$g_1(Q^2) = g_A(0) \left(1 + \frac{Q^2}{M_A^2}\right)^{-2}, \quad (2.45)$$

where $g_A(0)$ is determined experimentally from the β decay of neutron. M_A is known as the axial-dipole mass and is obtained from the QE neutrino and antineutrino scattering as well as from the pion electroproduction data (Fig. 2.5). The dipole parameterization is extensively used in the analysis of various experiments in the QE (anti)neutrino scattering. However, a new parameterization based on Z -expansion has been recently proposed in literature [193, 194]. Theoretically $g_1(Q^2)$ is also calculated in various models of lattice gauge theory [193, 195, 196, 197, 198].

The numerical value of M_A to be used in the calculations of neutrino-nucleon cross section has been a subject of intense discussion in the neutrino physics community in recent years and a wide range of the values of M_A has been discussed in the literature [47, 48, 49]. The old data available on (anti)neutrino scattering on hydrogen and deuterium targets [199, 200, 201] reanalyzed by Bodek et al. [202] gives a value of $M_A = 1.014 \pm 0.014$ GeV, while the analysis of the same data by Meyer et al. [194] gives a value in the range of 1.02-1.17 GeV depending upon which, data of ANL [199], BNL [200] and FNAL [201] experiments are considered. Bernard et al. [203] had earlier reanalyzed the data of the neutrino and antineutrino scattering on the hydrogen and deuterium targets as well as the electroproduction data and got the best χ^2 fit for M_A as:

$$M_A = 1.026 \pm 0.021 \text{ GeV}.$$

Since then high statistics data on QE neutrino-nucleus scattering have been obtained and analyzed from neutrino and antineutrino scattering on the nuclear targets both at the low and intermediate energies. The data from

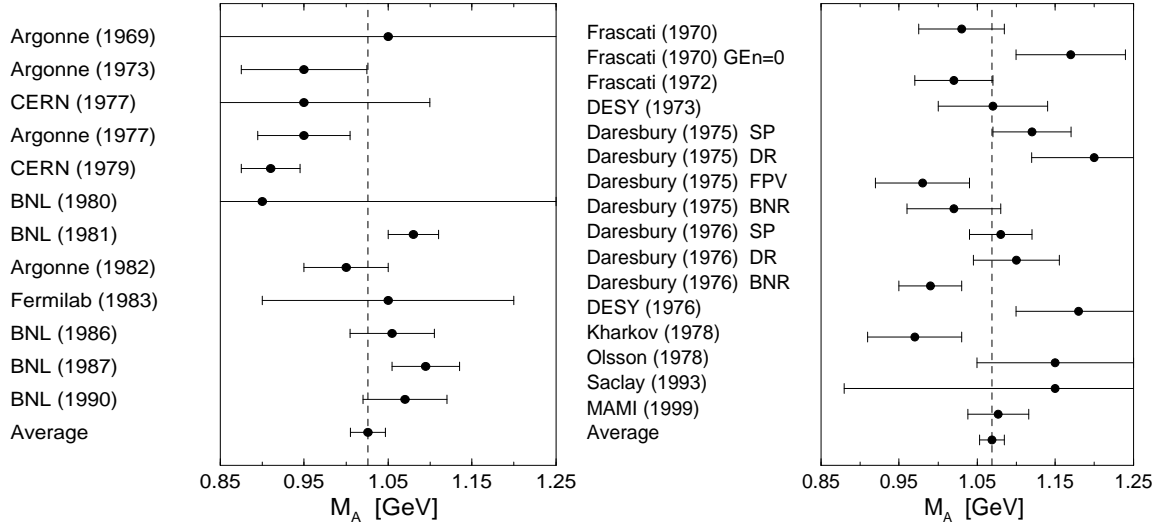


Figure 2.5: Axial mass M_A extractions from (quasi)elastic neutrino and antineutrino scattering experiments on hydrogen and deuterium targets (left) and from the charged pion electroproduction experiments (right). The weighted average from the left panel is $M_A = 1.026 \pm 0.021$ GeV and from the right panel is $M_A = 1.069 \pm 0.016$ GeV.

Experiment	M_A (GeV)	Experiment	M_A (GeV)
MINERvA [205, 206]	0.99	SciBooNE [214]	1.21 ± 0.22
NOMAD [204]	$1.05 \pm 0.02 \pm 0.06$	K2K-SciBar [212]	1.144 ± 0.077
MiniBooNE [207, 208, 209]	1.23 ± 0.20	K2K-SciFi [212]	1.20 ± 0.12
MINOS [210, 211]	$1.19(Q^2 > 0)$ $1.26(Q^2 > 0.3 \text{ GeV}^2)$	World Average	1.026 ± 0.021 [203] 1.014 ± 0.014 [202]

Table 2.2: Recent measurements of the axial dipole mass(M_A).

NOMAD [204] and MINERvA [205, 206] favor a lower value of M_A around 1.03 GeV, while the data from MiniBooNE [207, 208, 209], MINOS [210, 211], K2K [212], T2K [213] and SciBooNE [214, 215] favor a higher value of M_A which lies in the range of 1.2–1.35 GeV. The suggested values of M_A from these experiments have been tabulated in Table-2.2. Since the data from NOMAD [204] and MINERvA [205] collaborations are at relatively higher energies than the data from the other experiments, the higher value of M_A could be the manifestation of NME in the region of low energies of few hundred MeV. This has been discussed in recent literature. Alternatively it could be an indication of an energy dependent M_A . Such a possibility and the energy dependence of M_A has recently been discussed by Kuzmin et al. [216, 217].

In the case of NC induced reactions, the axial-vector form factor for the nucleon is given by:

$$\tilde{g}_1^{p,n}(Q^2) = \pm \frac{1}{2}g_1(Q^2) - \frac{1}{2}F_A^s(Q^2), \quad (2.46)$$

where $g_1(Q^2)$ is given in Eq. (2.45) with $M_A = 1.026$ GeV and $F_A^s(Q^2)$ is the strangeness axial-vector form factor.

(iii) Pseudoscalar form factor

In CC sector where PCAC is assumed, the pseudoscalar form factor $g_3(Q^2)$ is dominated by the pion pole dominance of the divergence of the axial-vector current (PDDAC) and is given using the Goldberger-Treiman relation [218] as

$$g_3(Q^2) = \frac{2M^2 g_1(Q^2)}{m_\pi^2 + Q^2}. \quad (2.47)$$

However, in the literature, there are various other versions of the pseudoscalar form factor like the one in Ref. [219]:

$$g_3(Q^2) = \frac{M}{Q^2} \left[\left(\frac{2m_\pi^2 f_\pi}{m_\pi^2 + Q^2} \right) \left(\frac{M g_A(0)}{f_\pi} + \frac{g_{\pi NN}(0) \Delta Q^2}{m_\pi^2} \right) + 2M g_1(Q^2) \right], \quad (2.48)$$

where $g_{\pi NN}(0) = 13.21$, $f_\pi = 92.42$ MeV and $\Delta = 1 + \frac{M g_A(0)}{f_\pi g_{\pi NN}(0)}$.

Pseudoscalar form factor is also calculated in the chiral perturbation theory and is given by [219, 220]

$$g_3(0) = \frac{2Mg_{\pi NN}(0)f_\pi}{m_\pi^2 + Q^2} + \frac{g_A(0)M^2r_A^2}{3}, \quad (2.49)$$

where axial radius $r_A = \frac{2\sqrt{3}}{M_A}$.

The contribution of the pseudoscalar form factor to the cross section in the QE reactions is proportional to the square of the lepton mass and hence, it vanishes in the case of NC interactions.

(iv) **Second class current form factors**

In Section 2.1.4(v), we have discussed G-parity and the classification of the first and the SCC. Here, we discuss the parameterization of the form factor associated with the SCC. In the $\Delta S = 0$ sector, the violation of G-parity due to the difference in the masses of u and d quarks or the intrinsic charge symmetry violation of the strong interaction, is very small, and the form factors $f_3(Q^2)$ and $g_2(Q^2)$ are expected to be very small. Moreover, in the vector sector, the hypothesis of CVC predicts $f_3(Q^2) = 0$. However, in the axial-vector sector there is no such constraint on the form factor $g_2(Q^2)$ and it could be nonvanishing albeit small. It is because of this reason that most of the experiments in $\Delta S = 0$ sector are analyzed for the search of SCC assuming $f_3(Q^2) = 0$ with a nonvanishing $g_2(Q^2)$ which is found to be quite small. Generally, the form factor $g_2(Q^2)$, in analogy with $g_1(Q^2)$, is parameterized as

$$g_2(Q^2) = g_2(0) \left[1 + \frac{Q^2}{M_2^2} \right]^{-2}, \quad (2.50)$$

where for simplicity $M_2 = M_A$.

This form factor $g_2(Q^2)$ may also give information about the time reversal invariance (TRI). If TRI is assumed, then $g_2(Q^2)$ must be real while in the absence of TRI the form factor $g_2(Q^2)$ can be taken as imaginary. We have explored the possibility of both real and imaginary $g_2(Q^2)$, and discussed the effect of TRI. In the numerical calculations, we have taken the real and imaginary values of $g_2(0)$ in the range -3 to 3 , which have been guided phenomenologically by the works of Fearing et al. [221], and Berman and Veltman [222], and discussed recently in Refs. [176, 223]. However, the experimental limits of $g_2(0)$ obtained from the muon capture and high precision β decays are too stringent and lie between $10^{-3} - 10^{-2}$ [224].

(v) **Strangeness form factors**

(a) **Strangeness vector form factors**

The strangeness vector form factors $F_1^s(Q^2)$ and $F_2^s(Q^2)$ may be redefined in terms of the strangeness Sachs' electric and magnetic form factors as:

$$G_E^s(Q^2) = F_1^s(Q^2) - \tau F_2^s(Q^2), \quad G_M^s(Q^2) = F_1^s(Q^2) + F_2^s(Q^2), \quad (2.51)$$

where $\tau = \frac{Q^2}{4M^2}$. At $Q^2 = 0$, the Sachs' electric form factor gives the net strangeness of the nucleon, i.e. $G_E^s(0) = 0$. At low momentum transfer, the electric form factor is expressed in terms of ρ^s , i.e.

$$\rho^s = \frac{dG_E^s(Q^2)}{dQ^2} = -\frac{1}{6}\langle r_s^2 \rangle, \quad (2.52)$$

where $\langle r_s^2 \rangle$ is the strangeness radius. Similarly, at $Q^2 = 0$, $G_M^s(Q^2) = \mu^s$, the strangeness magnetic moment. Therefore, these two parameters ρ^s and μ^s determine NC form factors $F_1^s(Q^2)$ and $F_2^s(Q^2)$ in the low Q^2 region. The Q^2 dependence of $G_E^s(Q^2)$ and $G_M^s(Q^2)$ is parameterized as:

$$G_E^s = \frac{\rho^s \tau}{\left(1 + \frac{Q^2}{\Lambda_E^2}\right)}, \quad G_M^s = \frac{\mu^s}{\left(1 + \frac{Q^2}{\Lambda_M^2}\right)}, \quad (2.53)$$

where the best fits for ρ^s and μ^s assuming $\Lambda_{E,M}^s$ to be very large, are given as [225]:

$$\rho^s = 0.13 \pm 0.21 \quad \text{and} \quad \mu^s = 0.035 \pm 0.053.$$

(a) **Strangeness axial-vector form factor**

The strangeness axial-vector form factor $g_1^s(Q^2)$ is taken to be of the dipole form:

$$g_1^s(Q^2) = \frac{\Delta s}{\left(1 + \frac{Q^2}{M_A^2}\right)^2}, \quad (2.54)$$

where $\Delta s = 0.08$ is the strange quark contribution to the nucleon spin [208, 226].

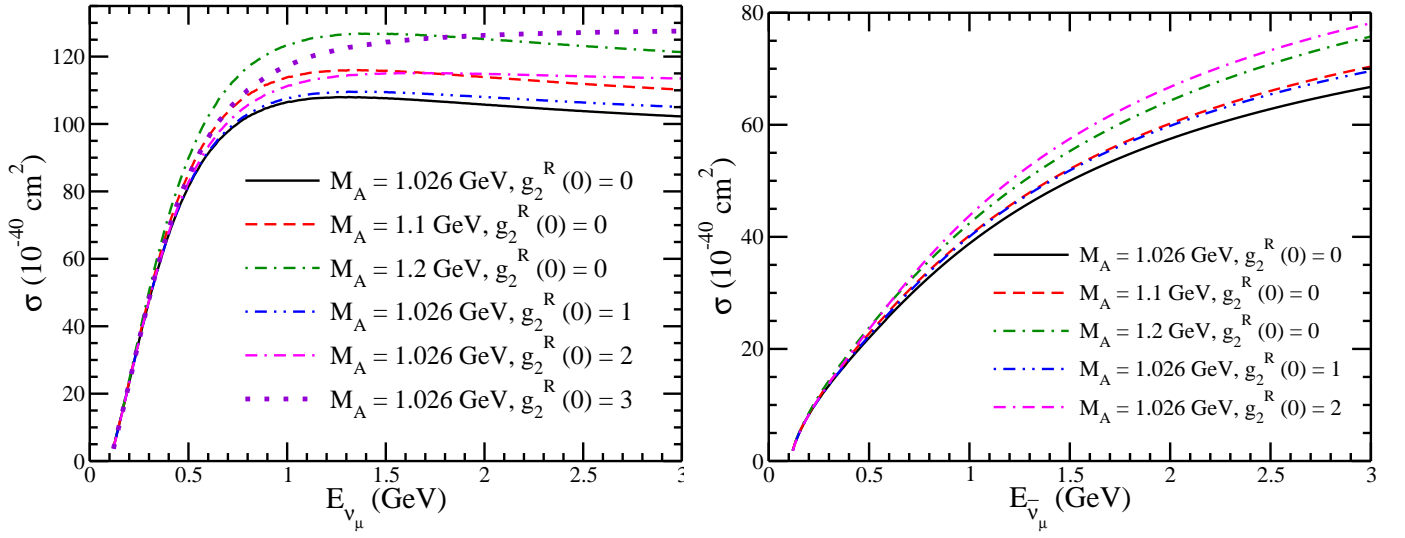


Figure 2.6: σ vs $E_{\nu\mu}(\bar{\nu}\mu)$ for the process $\nu_\mu + n \rightarrow \mu^- + p$ (left panel) and $\bar{\nu}_\mu + p \rightarrow \mu^+ + n$ (right panel) for the different combinations of M_A , and $g_2^R(0)$ viz. $M_A = 1.026$ GeV and $g_2^R(0) = 0$ (solid line), $M_A = 1.1$ GeV and $g_2^R(0) = 0$ (dashed line), $M_A = 1.2$ GeV and $g_2^R(0) = 0$ (dashed-dotted line), $M_A = 1.026$ GeV and $g_2^R(0) = 1$ (double-dotted-dashed line), $M_A = 1.026$ GeV and $g_2^R(0) = 2$ (double-dashed-dotted line) and $M_A = 1.026$ GeV and $g_2^R(0) = 3$ (dotted line) [176].

2.1.6. Cross sections for charged current processes

The differential scattering cross section for the QE (anti)neutrino scattering from the free nucleons is then calculated using Eq. (2.17) and the total cross section is obtained by integrating $\frac{d\sigma}{dQ^2}$ over Q^2 . These results have been discussed in detail in Refs. [176, 227]. It has been observed that

- (i) in the case (anti)neutrino induced $\Delta S = 0$ QE scattering processes, the total as well as the differential cross sections are almost insensitive to the change in the parameterization of the vector form factors, i.e., by taking into account the various parameterizations for the Sachs' electric and magnetic form factors [176].
- (ii) in the case of (anti)neutrino scattering from the free nucleon the effect of pseudoscalar form factor is almost negligible in the case of $\nu_l, \bar{\nu}_l$; ($l = e, \mu$) induced reactions [176]. However, in the case of $\nu_\tau, \bar{\nu}_\tau$ scattering [227], it has been observed that there is some dependence of the pseudoscalar form factor on the differential cross section for neutrino induced reactions. Moreover, in the case of $\bar{\nu}_\tau$ induced reactions, the different choice of the pseudoscalar form factors leads to a variation of about 50% in $\frac{d\sigma}{dQ^2}$ in the threshold region which increases with the increase in antineutrino energy.
- (iii) the cross section for CCQE reactions increases with increase in the value of M_A , for example, an increase (decrease) in the value of M_A by 10% increases (decreases) σ by about 15% at $E_\nu = 1$ GeV, which becomes 10% at $E_\nu = 2$ GeV in the case of ν_μ induced CCQE reactions while in the case of $\bar{\nu}_\mu$, the variation with change in M_A is about 10% at $E_\nu = 1$ GeV, which becomes 6% at $E_\nu = 2$ GeV, as may be observed from Fig. 2.6. Similar observations have been made in the case of $\nu_\tau, \bar{\nu}_\tau$ induced reactions [227].
- (iv) the presence of SCC form factor $g_2(Q^2)$ increases the cross sections for both neutrino and antineutrino induced processes.

Since the cross section for CCQE processes is sensitive to both M_A and $g_2(Q^2)$, therefore, the dependence of the total scattering cross section on M_A is shown in Fig. 2.6 by varying M_A in the range 1.026–1.2 GeV, with or without the presence of SCC by varying $g_2^R(0)$ in the range 0–3, using the BBBA05 [186] parameterization of the Sachs' electric and magnetic form factors. It may be observed from the figure that:

- (a) in the absence of SCC ($g_2^R(0) = 0$) [176], the cross section for both neutrino and antineutrino induced reactions increases with increase in the value of M_A as discussed above.
- (b) for the process $\nu_\mu + n \rightarrow \mu^- + p$, the results obtained by taking $M_A = 1.1$ GeV and $g_2^R(0) = 0$ are comparable to the results obtained with $M_A = 1.026$ GeV and $g_2^R(0) = 2$, whereas the results obtained by taking $M_A = 1.2$ GeV and $g_2^R(0) = 0$ are comparable to the results obtained using $M_A = 1.026$ GeV and $g_2^R(0) = 3$.
- (c) for the process $\bar{\nu}_\mu + p \rightarrow \mu^+ + n$, the results obtained by taking $M_A = 1.1$ GeV and $g_2^R(0) = 0$ are comparable to the results obtained with $M_A = 1.026$ GeV and $g_2^R(0) = 1$, whereas the results obtained by taking $M_A = 1.2$ GeV

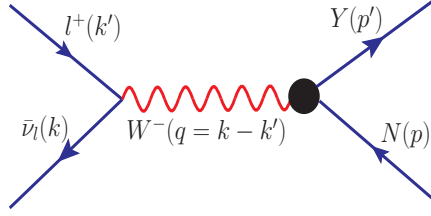


Figure 2.7: Feynman diagram for the process $\bar{\nu}_l(k) + N(p) \rightarrow l^+(k') + Y(p')$, where $N(= p, n)$ and $Y(= \Lambda, \Sigma^0, \Sigma^-)$ represent the initial nucleon and the final hyperon, respectively.

and $g_2^R(0) = 0$ are slightly lower than the results obtained using $M_A = 1.026$ GeV and $g_2^R(0) = 2$. Thus, a higher value of $\sigma(E_{\bar{\nu}_\mu})$ may be obtained by either taking a nonzero value of $g_2(0)$ or increasing the value of M_A .

- (d) The cross section measurements may give information only about the nonzero value of $g_2(0)$ irrespective of the nature of the SCC current i.e. with or without time reversal invariance. However, one may obtain the nature of the SCC by measuring the polarization observables which gives different results with the real and imaginary values of $g_2(0)$, corresponding to the SCC with or without time reversal invariance, and this has been discussed by us in brief in Section 2.3. For more discussion, readers are referred to Fatima et al. [176, 227].

2.2. Quasielastic hyperon production

The following processes are induced when an antineutrino interacts with a nucleon to produce a hyperon and an antilepton (Fig. 2.7):

$$\bar{\nu}_l(k) + p(p) \rightarrow l^+(k') + \Lambda/\Sigma^0(p'), \quad (2.55)$$

$$\bar{\nu}_l(k) + n(p) \rightarrow l^+(k') + \Sigma^-(p'); \quad l = e, \mu, \tau, \quad (2.56)$$

where the quantities in the brackets represent the four momenta of the particles.

2.2.1. Matrix element and form factors

The transition matrix element for the processes presented in Eqs. (2.55) and (2.56) is written as

$$\mathcal{M} = \frac{G_F}{\sqrt{2}} l^\mu J_\mu. \quad (2.57)$$

The leptonic current (l^μ) is given in Eq. (2.10). The hadronic current (J_μ) for the QE hyperon production can be written in analogy with the antineutrino-nucleon scattering except that the mass of the final nucleon is replaced by the mass of the hyperon and the electroweak form factors of the nucleons are replaced by the $N - Y$ transition form factors. The general expression for J_μ is given in Eq. (2.11) and the matrix elements of the vector (V_μ) and the axial-vector (A_μ) currents between a hyperon $Y(= \Lambda, \Sigma^0$ and $\Sigma^-)$ and a nucleon $N = n, p$ are written as:

$$\langle Y(\vec{p}') | V_\mu | N(\vec{p}) \rangle = \sin \theta_c \bar{u}(\vec{p}') \left[\gamma_\mu f_1^{NY}(Q^2) + i \sigma_{\mu\nu} \frac{q^\nu}{M + M'} f_2^{NY}(Q^2) + \frac{2 q_\mu}{M + M'} f_3^{NY}(Q^2) \right] u(\vec{p}), \quad (2.58)$$

$$\langle Y(\vec{p}') | A_\mu | N(\vec{p}) \rangle = \sin \theta_c \bar{u}(\vec{p}') \left[\gamma_\mu \gamma_5 g_1^{NY}(Q^2) + i \sigma_{\mu\nu} \frac{q^\nu}{M + M'} \gamma_5 g_2^{NY}(Q^2) + \frac{2 q_\mu}{M + M'} \gamma_5 g_3^{NY}(Q^2) \right] u(\vec{p}), \quad (2.59)$$

where M and M' are the masses of the nucleon and hyperon, respectively. $f_1^{NY}(Q^2)$, $f_2^{NY}(Q^2)$ and $f_3^{NY}(Q^2)$ are the vector, weak magnetic and induced scalar $N - Y$ transition form factors and $g_1^{NY}(Q^2)$, $g_2^{NY}(Q^2)$ and $g_3^{NY}(Q^2)$ are the axial-vector, induced tensor (or weak electric) and induced pseudoscalar form factors, respectively.

The transition matrix element squared is obtained as

$$\overline{\sum \sum} |\mathcal{M}|^2 = \frac{G_F^2}{2} J_{\mu\nu} L^{\mu\nu}, \quad (2.60)$$

where $J_{\mu\nu}$ and $L^{\mu\nu}$ are obtained in a similar way, as mentioned in Section 2.1.2.

The weak transition form factors $f_i(Q^2)$ and $g_i(Q^2)$; $i = 1 - 3$ are determined using Cabibbo theory of $V - A$ interaction extended to the strange sector with the application of $SU(3)$ symmetry. The details are given in Appendix-B.

The expressions for the vector form factors in terms of the electromagnetic form factors $F_{1,2}^p(Q^2)$ and $F_{1,2}^n(Q^2)$ for the various processes given in Eqs. (2.55) and (2.56), are given as [10, 176]:

$$f_{1,2}^{p\Lambda}(Q^2) = -\sqrt{\frac{3}{2}} F_{1,2}^p(Q^2), \quad f_{1,2}^{n\Sigma^-}(Q^2) = -[F_{1,2}^p(Q^2) + 2F_{1,2}^n(Q^2)], \quad f_{1,2}^{p\Sigma^0}(Q^2) = -\frac{1}{\sqrt{2}} [F_{1,2}^p(Q^2) + 2F_{1,2}^n(Q^2)]. \quad (2.61)$$

The axial-vector form factors $g_i^{NY}(Q^2)$ ($i = 1, 2, 3$) are expressed in terms of the two functions $F_i^A(Q^2)$ and $D_i^A(Q^2)$ corresponding to the antisymmetric and symmetric couplings of the two octets. But we express the form factors $g_i^{NY}(Q^2)$ in terms of $g_i(Q^2)$ and $x_i(Q^2)$, which are defined as [10, 176]:

$$g_i(Q^2) = F_i^A(Q^2) + D_i^A(Q^2) = g_i^{np}(Q^2), \quad x_i(Q^2) = \frac{F_i^A(Q^2)}{F_i^A(Q^2) + D_i^A(Q^2)}; \quad i = 1 - 3 \quad (2.62)$$

and the expressions for the axial-vector transition form factors for the various processes given in Eqs. (2.55) and (2.56) are given as [10, 176]:

$$g_{1,2}^{p\Lambda}(Q^2) = -\frac{1}{\sqrt{6}}(1 + 2x_{1,2})g_{A,2}^{np}(Q^2), \quad g_{1,2}^{n\Sigma^-}(Q^2) = (1 - 2x_{1,2})g_{A,2}^{np}(Q^2), \quad g_{1,2}^{p\Sigma^0}(Q^2) = \frac{1}{\sqrt{2}}(1 - 2x_{1,2})g_{A,2}^{np}(Q^2). \quad (2.63)$$

In the following we describe the explicit forms of the axial-vector form factors used for calculating the numerical results.

- (a) Axial vector form factor $g_1^{NY}(Q^2)$:

We note from Eq. (2.62), that $g_1(Q^2)$ is the axial-vector form factor for $n \rightarrow p$ transition and is defined in Eq. (2.45). The parameter $x_1(Q^2)$ occurring in Eq. (2.63) for $g_1^{NY}(Q^2)$ ($Y = \Lambda, \Sigma^0, \Sigma^-$) is determined at low Q^2 from the analysis of semileptonic hyperon decay and is found to be $x_1(Q^2 \approx 0) = 0.364$. There is no experimental information about the Q^2 dependence of $x_1(Q^2)$, therefore, we assume it to be constant i.e. $x_1(Q^2) \approx x_1(0) = 0.364$ for convenience.

- (b) Second class current form factor $g_2^{NY}(Q^2)$:

The expression for $g_2(Q^2)$ for the hyperons $\Lambda, \Sigma^-, \Sigma^0$ are given in Eq. (2.63) in terms of $g_2^{np}(Q^2)$ and $x_2(Q^2)$, where $g_2^{np}(Q^2)$ is parameterized in Eq. (2.50). There is some information on $g_2^{np}(Q^2)$ from neutrino and antineutrino scattering off the nucleons. It is shown that the value of $g_2^{np}(0)$ is correlated with the value of M_2 used in the analysis. There exists theoretical calculations for the $g_2^{R(np)}(0)$ and $g_2^{R(NY)}(0)$ for $Y = \Lambda, \Sigma^-, \Sigma^0$. In the literature, various values of $g_2^I(0)$ for the nucleons and hyperons have been used, which are in the range 1–10 [221, 222, 228]. However, there is no information about $x_2(Q^2)$. To see the dependence of $g_2^R(0)$ and $g_2^I(0)$ on the differential and the total scattering cross sections, we have varied $g_2^R(0)$ and $g_2^I(0)$ in the range of 0–3 and use $M_2 = M_A$ [176]. For the Q^2 dependence of the form factor $g_2^{NY}(Q^2)$, we use the $SU(3)$ symmetric expressions for $g_2^{np}(Q^2)$ taken to be of the dipole form given in Eq. (2.50) for the various transitions given in Eq. (2.63), treating $x_2(Q^2)$ to be constant and assuming $x_2 = x_1$ [176].

- (c) The induced pseudoscalar form factor $g_3^{NY}(Q^2)$:

In general, the contribution of $g_3^{NY}(Q^2)$ to the (anti)neutrino scattering cross sections is proportional to m_l^2 , where m_l is the mass of the corresponding charged lepton, and is small in e^\pm and μ^\pm productions but is significant in the processes involving τ^\pm leptons. For $g_3^{NY}(Q^2)$, Nambu [229] has given a generalized parameterization using PCAC and Goldberger-Treiman (GT) relation for the $\Delta S = 1$ currents

$$g_3^{NY}(Q^2) = \frac{(M + M')^2}{2(m_K^2 + Q^2)} g_1^{NY}(Q^2), \quad (2.64)$$

where m_K is the mass of kaon and $g_1^{NY}(Q^2)$ is given in Eq. (2.63), for $Y = \Lambda, \Sigma^-, \Sigma^0$.

Another parameterization for the pseudoscalar form factor in the case of $\Delta S = 1$ processes is given by Marshak et al. [230]:

$$g_3^{NY}(Q^2) = \frac{(M + M')^2}{2Q^2} \frac{g_1^{NY}(Q^2)(m_K^2 + Q^2) - m_K^2 g_1^{NY}(0)}{m_K^2 + Q^2}. \quad (2.65)$$

2.2.2. Cross sections: Experimental results

The results for the hyperon production cross sections from the free nucleons given in Eqs. (2.55) and (2.56) as a function of antineutrino energies are presented in Fig. 2.8. These results are presented for Λ, Σ^- and Σ^0 production cross sections at the two values of M_A viz. $M_A = 1.026$ GeV and 1.2 GeV. In this region, there is very little dependence of M_A on the cross section for Σ^- and Σ^0 productions, while in the case of Λ production, the cross section increases with energy

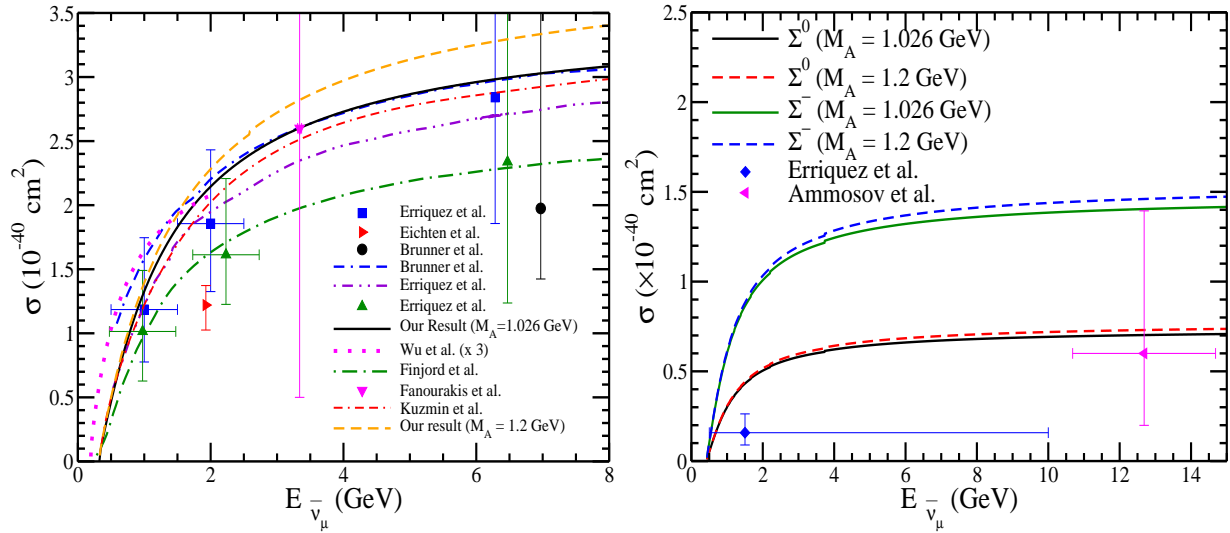


Figure 2.8: σ vs. $E_{\bar{\nu}_\mu}$ for the Λ production (left panel), Σ^0 and Σ^- production (right panel) cross sections [223]. Solid (dashed) line represents the result using $M_A = 1.026$ (1.2) GeV. Experimental results for the process $\bar{\nu}_\mu p \rightarrow \mu^+ \Lambda$ (triangle right [231], triangle up [232], square [233], triangle down ($\sigma = 2.6^{+5.9}_{-2.1} \times 10^{-40} \text{cm}^2$) [234], circle [237]) and for the process $\bar{\nu}_\mu p \rightarrow \mu^+ \Sigma^0$ (diamond [232]) are shown with error bars. Theoretical curves are of Kuzmin and Naumov [240] (double dashed-dotted line), Brunner et al. [237] (dashed line), Erriquez et al. [233] (dashed-double dotted line) obtained using Cabibbo theory with axial-vector dipole mass as 1 GeV, 1.1 GeV and 1 GeV, respectively, while the results of Wu et al. [238] (dotted line) and Finjord and Ravndal [239] (dashed dotted line) are obtained using quark model.

and the increase is about 5% at $E_{\bar{\nu}_\mu} = 1$ GeV. In the case of free nucleon, the cross sections for $\bar{\nu}_\mu + n \rightarrow \mu^+ + \Sigma^-$ and $\bar{\nu}_\mu + p \rightarrow \mu^+ + \Sigma^0$ are related by an isospin relation i.e. $\sigma(\bar{\nu}_\mu p \rightarrow \mu^+ \Sigma^0) = \frac{1}{2} \sigma(\bar{\nu}_\mu n \rightarrow \mu^+ \Sigma^-)$, while no Σ^+ is produced off the free nucleon target due to $\Delta S \neq \Delta Q$ rule. A comparison is made with available experimental results from CERN [231, 232, 233], BNL [234], FNAL [235, 236] and SKAT [237] experiments as well as with the theoretical calculations performed by Wu et al. [238] and Finjord and Ravndal [239] using quark model and the calculations performed by Erriquez et al. [233], Brunner et al. [237] and Kuzmin and Naumov [240] based on the prediction using Cabibbo theory. A reasonable agreement with the experimental results can be seen.

2.3. Polarization of final hadrons and leptons

In the case of elastic e^-p scattering, the polarized electron beam and the polarized proton target have played an important role in determining the vector form factors. In the weak sector, the vector form factors are expressed in terms of the electromagnetic form factors of the nucleons. In the axial-vector sector, the information on the form factors is obtained from the semileptonic decays of nucleons and hyperons at low Q^2 , one may also obtain information about these form factors by measuring the polarization of the final hadron. In the case of the QE scattering, experimentally, it is difficult to study the polarization of the final nucleon as one requires the double polarization measurement. However, in the case of the QE hyperon production, it is easier to study the polarization observables as the produced hyperon decays into pions which gives information about the polarization of the final hyperon. The calculations for the polarization observables of the final hadrons and leptons produced in the $\Delta S = 0$ and $|\Delta S| = 1$ QE scattering of (anti)neutrinos with free nucleons have been done earlier [241, 242] and summarized by Llewellyn Smith [175] but recently these calculations have been done by Bilenky et al. [243, 244], Graczyk and Kowal [245, 246, 247], Tomalak [248], Thorpe et al. [249] and our group [176, 223, 227, 250, 251, 252, 253, 254] in the SM. In Refs. [176, 223, 251, 252], we have calculated the polarization observables of the proton, neutron, Λ , and Σ^- produced in the $\bar{\nu}_\mu$ induced QE processes. In Refs. [227, 253], we have studied the τ^\pm polarization in the processes $\nu_\tau(\bar{\nu}_\tau) + N \rightarrow \tau^\pm + N$ and $\bar{\nu}_\tau + N \rightarrow \tau^+ + \Lambda(\Sigma)$.

2.3.1. Polarization of the final hadron

The polarization 4-vector ξ^τ of the hadron produced in the final state in reactions (2.5), (2.55), and (2.56) is written as [10, 255]:

$$\xi^\tau = \frac{\text{Tr}[\gamma^\tau \gamma_5 \rho_f(p')]}{\text{Tr}[\rho_f(p')]}, \quad (2.66)$$

where the spin density matrix $\rho_f(p')$ corresponding to the final hadron of momentum p' is given by

$$\rho_f(p') = L^{\alpha\beta} \text{Tr}[\Lambda(p') \mathcal{O}_\alpha \Lambda(p) \tilde{\mathcal{O}}_\beta \Lambda(p')], \quad (2.67)$$

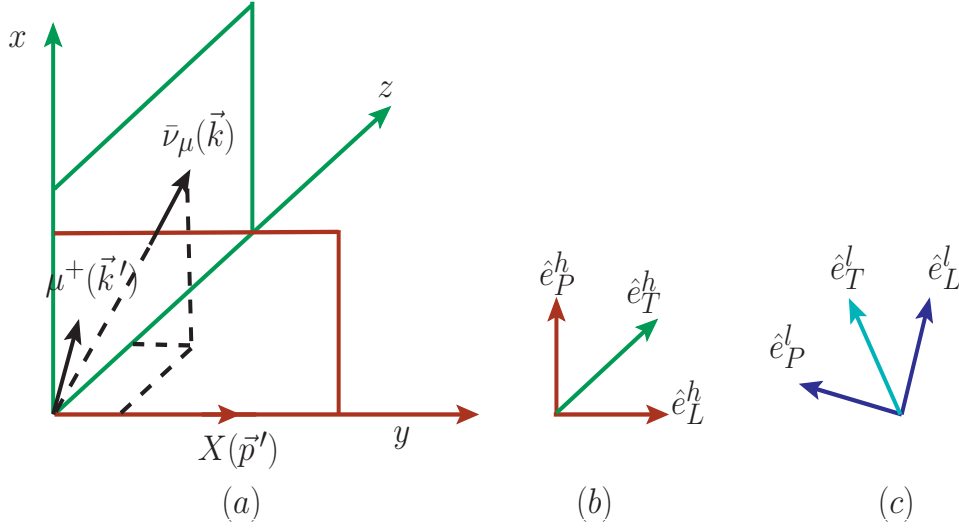


Figure 2.9: (a) Momentum and polarization directions of the final baryon and the lepton. $\hat{e}_L^{h,l}$, $\hat{e}_P^{h,l}$ and $\hat{e}_T^{h,l}$ represent the orthogonal unit vectors corresponding to the longitudinal, perpendicular and transverse directions with respect to the momentum of the final hadron in (b) and the final lepton in (c).

where $\Lambda(p') = \not{p}' + M'$ is the projection operator for spin $\frac{1}{2}$ fermions with momentum p' .

Using the following relations:

$$\Lambda(p')\gamma^\tau\gamma_5\Lambda(p') = 2M' \left(g^{\tau\sigma} - \frac{p'^\tau p'^\sigma}{M'^2} \right) \Lambda(p')\gamma_\sigma\gamma_5, \quad \Lambda(p')\Lambda(p') = 2M'\Lambda(p'), \quad (2.68)$$

where M' corresponds to the mass of the final hadron. ξ^τ defined in Eq. (2.66) may be rewritten as [10, 255]:

$$\xi^\tau = \left(g^{\tau\sigma} - \frac{p'^\tau p'^\sigma}{M'^2} \right) \frac{L^{\alpha\beta} \text{Tr} \left[\gamma_\sigma \gamma_5 \Lambda(p') \mathcal{O}_\alpha \Lambda(p) \tilde{\mathcal{O}}_\beta \right]}{L^{\alpha\beta} \text{Tr} \left[\Lambda(p') \mathcal{O}_\alpha \Lambda(p) \tilde{\mathcal{O}}_\beta \right]}. \quad (2.69)$$

Note that in Eq. (2.69), ξ^τ is manifestly orthogonal to p'^τ , *i.e.* $p' \cdot \xi = 0$. Moreover, the denominator is directly related to the differential scattering cross section given in Eq. (2.17). With $J^{\alpha\beta}$ and $L_{\alpha\beta}$ given in Eqs. (2.16) and (2.15), respectively, an expression for ξ^τ is obtained in terms of the 4-momenta of the particles. Here, we have considered two cases:

Case I: When time reversal invariance is assumed.

The polarization vector ξ^τ defined in Eq. (2.69) is evaluated in the laboratory frame, *i.e.* when the initial nucleon is at rest, $\vec{p} = 0$, and the momentum directions are depicted in Fig. 2.9(a). If the time reversal invariance is assumed then all the form factors defined in Eqs. (2.12), (2.13), (2.58), and (2.59) are real and ξ^τ is expressed as

$$\vec{\xi} = \frac{[A^h(Q^2)\vec{k} + B^h(Q^2)\vec{p}']}{N(Q^2)}, \quad (2.70)$$

where the expressions of $A^h(Q^2)$, $B^h(Q^2)$ and $N(Q^2)$ are given in Appendix-A.1, and are taken in the limit $f_3(Q^2) = 0$ and $g_2(0) = g_2^R(0)$ to ensure the time reversal invariance.

From Eq. (2.70), it follows that the polarization vector lies in the plane of reaction and there is no component of polarization in a direction perpendicular to the reaction plane. This is a consequence of time reversal invariance which makes the transverse component of polarization, perpendicular to the reaction plane, to vanish. We now expand $\vec{\xi}$ along the orthogonal directions, \hat{e}_L^h , \hat{e}_P^h and \hat{e}_T^h in the reaction plane corresponding to the longitudinal, perpendicular and transverse directions, defined as

$$\hat{e}_L^h = \frac{\vec{p}'}{|\vec{p}'|}, \quad \hat{e}_P^h = \hat{e}_L^h \times \hat{e}_T^h, \quad \text{where} \quad \hat{e}_T^h = \frac{\vec{p}' \times \vec{k}}{|\vec{p}' \times \vec{k}|}, \quad (2.71)$$

and have depicted in Fig. 2.9(b). We then write $\vec{\xi}$ as:

$$\vec{\xi} = \xi_L \hat{e}_L^h + \xi_P \hat{e}_P^h, \quad (2.72)$$

such that the longitudinal and perpendicular components of $\vec{\xi}$ in the laboratory frame are given by

$$\xi_L(Q^2) = \vec{\xi} \cdot \hat{e}_L^h, \quad \xi_P(Q^2) = \vec{\xi} \cdot \hat{e}_P^h. \quad (2.73)$$

From Eq. (2.73), the longitudinal $P_L^h(Q^2)$ and perpendicular $P_P^h(Q^2)$ components of the $\vec{\xi}$ defined in the rest frame of the final hadron are given by

$$P_L^h(Q^2) = \frac{M'}{E'} \xi_L(Q^2), \quad P_P^h(Q^2) = \xi_P(Q^2), \quad (2.74)$$

where $\frac{M'}{E'}$ is the Lorentz boost factor along \vec{p}' . With the help of Eqs. (2.70), (2.71), (2.73) and (2.74), the longitudinal $P_L^h(Q^2)$ and perpendicular $P_P^h(Q^2)$ components of polarization are calculated to be [10, 176]:

$$P_L^h(Q^2) = \frac{M'}{E'} \frac{A^h(Q^2) \vec{k} \cdot \vec{p}' + B^h(Q^2) |\vec{p}'|^2}{N(Q^2) |\vec{p}'|}, \quad (2.75)$$

$$P_P^h(Q^2) = \frac{A^h(Q^2) [(\vec{k} \cdot \vec{p}')^2 - |\vec{k}|^2 |\vec{p}'|^2]}{N(Q^2) |\vec{p}'| |\vec{p}' \times \vec{k}|}. \quad (2.76)$$

Case II: When time reversal violation is assumed.

In the absence of time reversal invariance, $\vec{\xi}$ is calculated as [10, 176]

$$\vec{\xi} = \frac{A^h(Q^2) \vec{k} + B^h(Q^2) \vec{p}' + C^h(Q^2) M(\vec{k} \times \vec{p}')}{N(Q^2)}, \quad (2.77)$$

where the expressions of $C^h(Q^2)$ is given in Appendix-A.1.

The $\vec{\xi}$ may be written in terms of the longitudinal, perpendicular and transverse components as

$$\vec{\xi} = \xi_L \hat{e}_L^h + \xi_P \hat{e}_P^h + \xi_T \hat{e}_T^h, \quad (2.78)$$

where the unit vectors are defined in Eq. (2.71). The longitudinal and perpendicular components are given in Eqs. (2.75) and (2.76), respectively. The transverse component of polarization in the rest frame of the final hadron is given as

$$P_T(Q^2) = \xi_T(Q^2) = \vec{\xi} \cdot \hat{e}_T. \quad (2.79)$$

Using Eqs. (2.71) and (2.78) in Eq. (2.79), we obtain [10, 176]

$$P_T^h(Q^2) = \frac{C^h(Q^2) M[(\vec{k} \cdot \vec{p}')^2 - |\vec{k}|^2 |\vec{p}'|^2]}{N(Q^2) |\vec{p}' \times \vec{k}|}. \quad (2.80)$$

If the T invariance is assumed then all the vector and the axial-vector form factors are real and the expression for $C^h(Q^2)$ vanishes which implies that the transverse component of the polarization perpendicular to the production plane, $P_T^h(Q^2)$ vanishes.

Using Eqs. (2.75), (2.76) and (2.80), the polarization components of the Λ produced in the reaction $\bar{\nu}_\mu + p \rightarrow \mu^+ + \Lambda$ are calculated, where the expressions of $A^h(Q^2)$, $B^h(Q^2)$, and $C^h(Q^2)$ are given in Appendix A.1. To see the dependence of $g_2^R(0)$ on the polarization observables, in Fig. 2.10, the results of $P_L(Q^2)$ and $P_P(Q^2)$ are presented as a function of Q^2 using $g_2^R(0) = 0, \pm 1$ and ± 3 at $E_{\bar{\nu}_\mu} = 1$ GeV. It may be observed that $P_L(Q^2)$ shows large variation as we change $|g_2^R(0)|$ from 0 to 3. For example, in the peak region of Q^2 , the difference is about 50% as $|g_2^R(0)|$ is changed from 0 to 3. In the case of $P_P(Q^2)$, Q^2 dependence is quite strong and similar to $P_L(Q^2)$.

To see the dependence of $g_2^I(0)$ on the polarization observables, in Fig. 2.11, the results are presented for $P_L(Q^2)$, $P_P(Q^2)$ and $P_T(Q^2)$ as a function of Q^2 using $g_2^I(0) = 0, 1$ and 3 at $E_{\bar{\nu}_\mu} = 1$ GeV. It may be deduced that while $P_L(Q^2)$ is less sensitive to $g_2^I(0)$ at low antineutrino energies, $P_P(Q^2)$ is sensitive to $g_2^I(0)$ at $E_{\bar{\nu}_\mu} = 1$ GeV. Moreover, $P_T(Q^2)$ shows 40% variations at $Q^2 = 0.4$ GeV², $E_{\bar{\nu}_\mu} = 1$ GeV, when $g_2^I(0)$ is varied from 0 to 3.

2.3.2. Polarization of the final lepton

In the case of final lepton polarization in CC reactions, the polarization 4-vector (ζ^τ) in reactions (2.5), (2.55), and (2.56) is written as [10, 176]:

$$\zeta^\tau = \frac{\text{Tr}[\gamma^\tau \gamma_5 \rho_f(k')]}{\text{Tr}[\rho_f(k')]}, \quad (2.81)$$

and the spin density matrix for the final lepton $\rho_f(k')$ is given by

$$\rho_f(k') = J^{\alpha\beta} \text{Tr}[\Lambda(k') \gamma_\alpha (1 + \gamma_5) \Lambda(k) \tilde{\gamma}_\beta (1 + \tilde{\gamma}_5) \Lambda(k')], \quad (2.82)$$

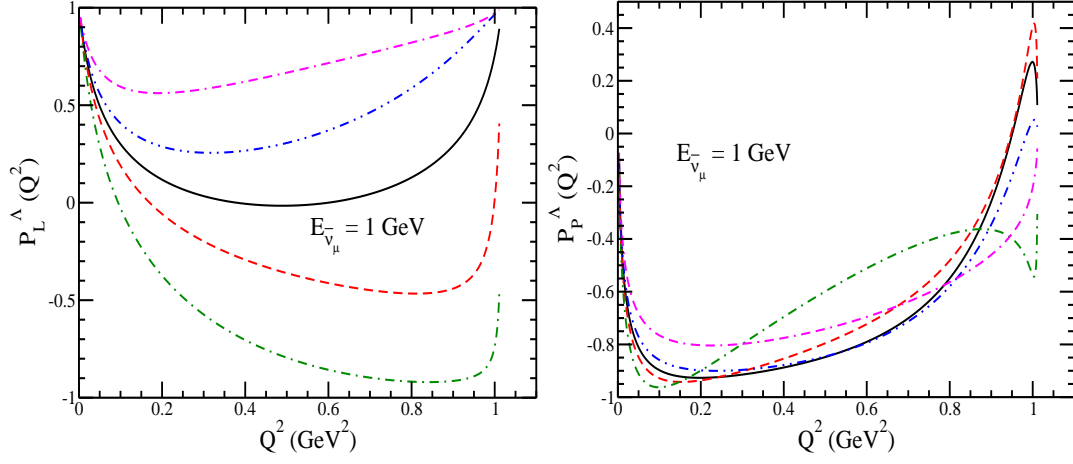


Figure 2.10: $P_L(Q^2)$ vs. Q^2 (left panel) and $P_P(Q^2)$ vs. Q^2 (right panel) for the process $\bar{\nu}_\mu + p \rightarrow \mu^+ + \Lambda$ at the incoming antineutrino energy, $E_{\bar{\nu}_\mu} = 1$ GeV for the polarized Λ in the final state, at the different values of $g_2^R(0)$ viz. $g_2^R(0) = 0$ (solid line), 1 (dashed line), 3 (dashed-dotted line), -1 (double-dotted-dashed line) and -3 (double-dashed-dotted line) [176].

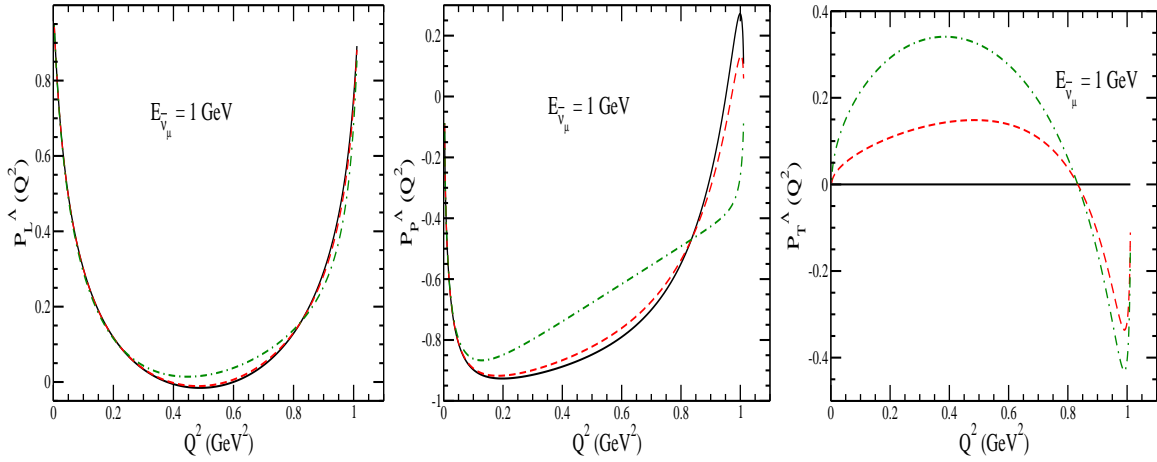


Figure 2.11: $P_L(Q^2)$ vs. Q^2 (left panel), $P_P(Q^2)$ vs. Q^2 (middle panel) and $P_T(Q^2)$ vs. Q^2 (right panel) for the process $\bar{\nu}_\mu + p \rightarrow \mu^+ + \Lambda$ at the incoming antineutrino energy $E_{\bar{\nu}_\mu} = 1$ GeV for the polarized Λ in the final state, at the different values of $g_2^I(0)$ viz. $g_2^I(0) = 0$ (solid line), 1 (dashed line) and 3 (dashed-dotted line) [176].

with $\tilde{\gamma}_\alpha = \gamma^0 \gamma_\alpha^\dagger \gamma^0$ and $\tilde{\gamma}_5 = \gamma^0 \gamma_5^\dagger \gamma^0$.

Using Eq. (2.68), ζ^τ defined in Eq. (2.81) may also be rewritten as [10, 176]

$$\zeta^\tau = \left(g^{\tau\sigma} - \frac{k'^\tau k'^\sigma}{m_l^2} \right) \frac{J^{\alpha\beta} \text{Tr} [\gamma_\sigma \gamma_5 \Lambda(k') \gamma_\alpha (1 + \gamma_5) \Lambda(k) \tilde{\gamma}_\beta (1 + \tilde{\gamma}_5)]}{J^{\alpha\beta} \text{Tr} [\Lambda(k') \gamma_\alpha (1 + \gamma_5) \Lambda(k) \tilde{\gamma}_\beta (1 + \tilde{\gamma}_5)]}, \quad (2.83)$$

where m_l is the charged lepton mass.

With $J^{\alpha\beta}$ and $L_{\alpha\beta}$ given in Eqs. (2.16) and (2.15), respectively, an expression for ζ^τ is obtained. In the laboratory frame where the initial nucleon is at rest, the polarization vector $\vec{\zeta}$ is calculated to be a function of 3-momenta of incoming antineutrino (\vec{k}) and outgoing lepton (\vec{k}'), and is given as [10, 176]

$$\vec{\zeta} = \frac{[A^l(Q^2)\vec{k} + B^l(Q^2)\vec{k}' + C^l(Q^2)M(\vec{k} \times \vec{k}')] }{N(Q^2)}, \quad (2.84)$$

where the expressions of $A^l(Q^2)$, $B^l(Q^2)$ and $C^l(Q^2)$ are given in Appendix-A.2.

One may expand $\vec{\zeta}$ along the orthogonal directions, \hat{e}_L^l , \hat{e}_P^l and \hat{e}_T^l in the reaction plane corresponding to the longitudinal, perpendicular and transverse directions, defined as

$$\hat{e}_L^l = \frac{\vec{k}'}{|\vec{k}'|}, \quad \hat{e}_P^l = \hat{e}_L^l \times \hat{e}_T^l, \quad \text{where} \quad \hat{e}_T^l = \frac{\vec{k} \times \vec{k}'}{|\vec{k} \times \vec{k}'|}, \quad (2.85)$$

and depicted in Fig. 2.9(c). We then write $\vec{\zeta}$ as:

$$\vec{\zeta} = \zeta_L \hat{e}_L^l + \zeta_P \hat{e}_P^l + \zeta_T \hat{e}_T^l, \quad (2.86)$$

such that the longitudinal, perpendicular and transverse components of the $\vec{\zeta}$ in the laboratory frame are given by

$$\zeta_L(Q^2) = \vec{\zeta} \cdot \hat{e}_L^l, \quad \zeta_P(Q^2) = \vec{\zeta} \cdot \hat{e}_P^l, \quad \zeta_T(Q^2) = \vec{\zeta} \cdot \hat{e}_T^l. \quad (2.87)$$

From Eq. (2.87), $P_L^l(Q^2)$, $P_P^l(Q^2)$ and $P_T^l(Q^2)$ defined in the rest frame of the final lepton are given by

$$P_L^l(Q^2) = \frac{m_l}{E_{k'}} \zeta_L(Q^2), \quad P_P^l(Q^2) = \zeta_P(Q^2), \quad P_T^l(Q^2) = \zeta_T(Q^2), \quad (2.88)$$

where $\frac{m_l}{E_{k'}}$ is the Lorentz boost factor along \vec{k}' . Using Eqs. (2.84), (2.85) and (2.87) in Eq. (2.88), $P_L^l(Q^2)$, $P_P^l(Q^2)$ and $P_T^l(Q^2)$ are calculated to be [10, 176]

$$P_L^l(Q^2) = \frac{m_l}{E_{k'}} \frac{A^l(Q^2)\vec{k} \cdot \vec{k}' + B^l(Q^2)|\vec{k}'|^2}{N(Q^2) |\vec{k}'|}, \quad (2.89)$$

$$P_P^l(Q^2) = \frac{A^l(Q^2)[|\vec{k}|^2 |\vec{k}'|^2 - (\vec{k} \cdot \vec{k}')^2]}{N(Q^2) |\vec{k}'| |\vec{k} \times \vec{k}'|}, \quad (2.90)$$

$$P_T^l(Q^2) = \frac{C^l(Q^2)M[(\vec{k} \cdot \vec{k}')^2 - |\vec{k}|^2 |\vec{k}'|^2]}{N(Q^2) |\vec{k} \times \vec{k}'|}. \quad (2.91)$$

Using Eqs. (2.17), (2.89), and (2.90) the differential scattering cross section as well as the polarization observables of the final lepton produced in the (anti)neutrino induced processes are calculated. It has been observed that

- (i) in the case of $\bar{\nu}_\mu$ induced processes, the outgoing μ^+ is almost longitudinally polarized because of the small mass of μ^+ while the perpendicular and transverse polarizations show some effect at lower $\bar{\nu}_\mu$ energy but become almost negligible at $E_{\bar{\nu}_\mu} = 1$ GeV [176]. However for the $\nu_\tau(\bar{\nu}_\tau)$ induced processes, the effect of polarization observables of the τ^\pm is significant [227, 253] and is shown in Figs. 2.12 and 2.13 for nucleon and Λ productions, respectively.
- (ii) The effect of the second class current form factor $g_2^R(0)$ on the total cross section and average polarizations is studied by integrating the expressions of $\frac{d\sigma}{dQ^2}$, $P_L^l(Q^2)$, and $P_P^l(Q^2)$ over Q^2 . In Fig. 2.12, the results for σ , $P_L(E_{\nu_\tau}(\bar{\nu}_\tau))$ and $P_P(E_{\nu_\tau}(\bar{\nu}_\tau))$ are presented as a function of (anti)neutrino energies by taking $g_2^R(0) = 0$ and ± 1 . It may be observed from the figure that in the case of σ , for both the processes $\nu_\tau + n \rightarrow \tau^- + p$ and $\bar{\nu}_\tau + p \rightarrow \tau^+ + n$, the results obtained with $g_2^R(0) = -1$ are slightly lower (1–2%) than the results obtained with $g_2^R(0) = 0$ in the range of $E_{\nu_\tau, \bar{\nu}_\tau}$ from threshold up to 10 GeV, while the results obtained with $g_2^R(0) = +1$, are higher from the results obtained with $g_2^R(0) = 0$ and the difference decreases with the increase in energy. For example, at $E_{\nu_\tau(\bar{\nu}_\tau)} = 5$ GeV, the results obtained with $g_2^R(0) = +1$ are higher by about 18 (30)% from the results of $g_2^R(0) = 0$, while at 10 GeV, this difference becomes 10 (12)% for the (anti)neutrino induced processes.

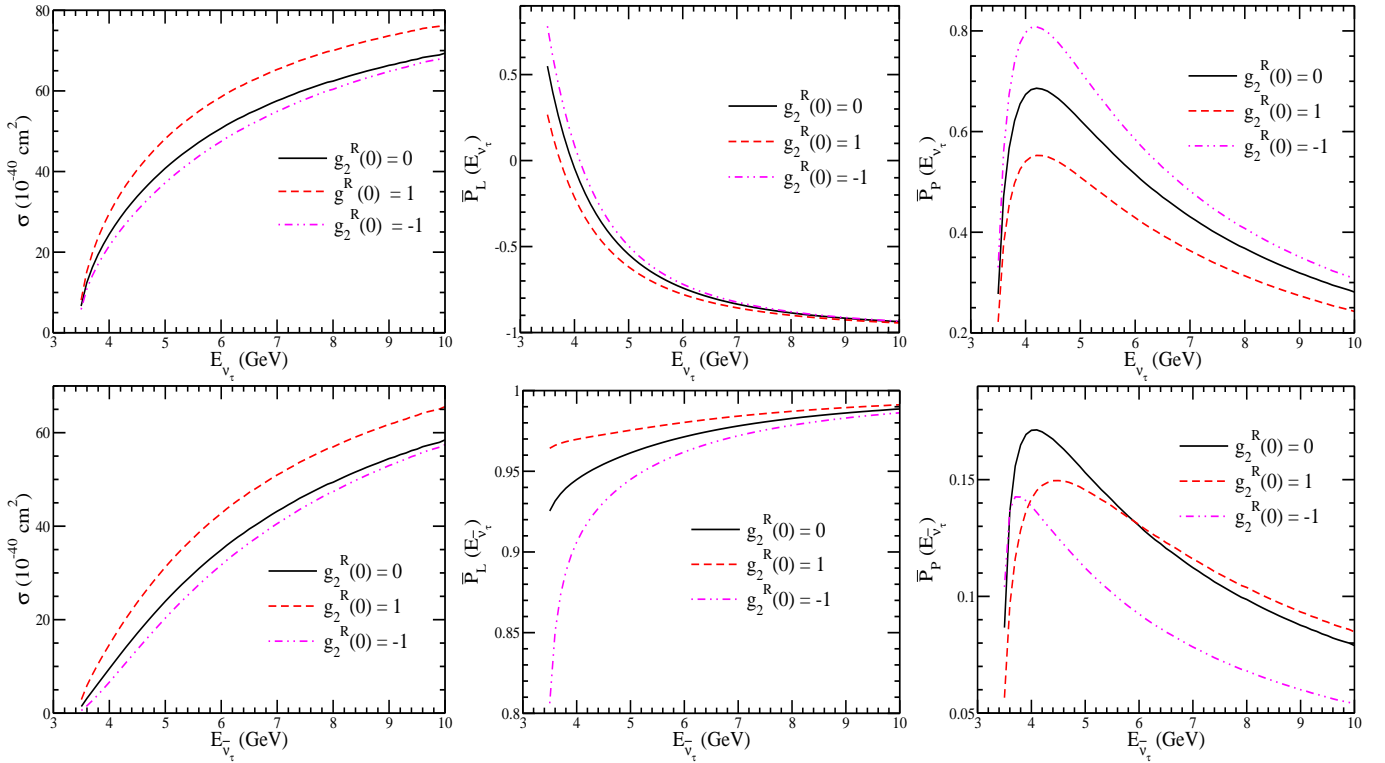


Figure 2.12: (Top panel) left to right: σ vs E_{ν_τ} , $\bar{P}_L(E_{\nu_\tau})$ vs E_{ν_τ} , and $\bar{P}_P(E_{\nu_\tau})$ vs E_{ν_τ} for the $\nu_\tau + n \rightarrow \tau^- + p$ process. (Bottom panel) left to right: σ vs $E_{\bar{\nu}_\tau}$, $\bar{P}_L(E_{\bar{\nu}_\tau})$ vs $E_{\bar{\nu}_\tau}$, and $\bar{P}_P(E_{\bar{\nu}_\tau})$ vs $E_{\bar{\nu}_\tau}$ for the $\bar{\nu}_\tau + p \rightarrow \tau^+ + n$ process. The calculations have been performed using electric and magnetic Sachs' form factors parameterized by Bradford et al. [186] with $M_A = 1.026$ GeV, and with the different values of $g_2^R(0)$ viz. $g_2^R(0) = 0$ (solid line), 1 (dashed line) and -1 (double-dotted-dashed line) used in Eq. (2.50) [227].

- (iii) In the case of $P_L(E_{\nu_\tau, \bar{\nu}_\tau})$, there is a slight variation due to the change in the value of $g_2^R(0)$ for neutrino induced process, while for the antineutrino induced process, this difference is large at lower antineutrino energies which gradually becomes smaller with the increase in energy.
- (iv) For $P_P(E_{\nu_\tau, \bar{\nu}_\tau})$, the results for both the neutrino as well as antineutrino induced processes show dependence on the choice of $g_2^R(0)$, while the nature of dependence is different. In the case of ν_τ induced reaction, in the peak region, the results are $\sim 20\%$ smaller for $g_2^R(0) = +1$ from the results obtained with $g_2^R(0) = 0$, while using $g_2^R(0) = -1$ the results are 18% higher than the results obtained using $g_2^R(0) = 0$. However, in the case of $\bar{\nu}_\tau$ induced processes, the results obtained with $g_2^R(0) = \pm 1$ are lower than the results obtained with $g_2^R(0) = 0$ in the region of threshold up to $E_{\bar{\nu}_\tau} = 6$ GeV.

To study the effect of M_A variation in the range 0.9–1.3 GeV on the differential cross section and polarization observables, in Fig. 2.13, the results for $\frac{d\sigma}{dQ^2}$, $P_L(Q^2)$ and $P_P(Q^2)$ as a function of Q^2 for $\bar{\nu}_\tau + p \rightarrow \tau^+ + \Lambda$ at $E_{\bar{\nu}_\tau} = 4$ GeV, 5 GeV and 10 GeV are presented. It has been found that at low $\bar{\nu}_\tau$ energies, there is some dependence of the differential cross section as well as the polarization observables on the choice of M_A . With the increase in $\bar{\nu}_\tau$ energy, this dependence on the variation in M_A decreases, especially for $\frac{d\sigma}{dQ^2}$ and to some extent for $P_L(Q^2)$ but not for $P_P(Q^2)$ distribution. Moreover, it is important to point out that in the case of $\bar{\nu}_\tau + p \rightarrow \tau^+ + \Lambda$ reaction, with the increase in M_A , $\frac{d\sigma}{dQ^2}$ decreases (0.9 GeV to 1.1 GeV), but with the further increase in M_A (1.1 GeV to 1.3 GeV), $\frac{d\sigma}{dQ^2}$ increases, which is not generally the case in $\nu_l + n \rightarrow l^- + p$; ($l = e, \mu, \tau$) scattering. Furthermore, in the case of $\bar{\nu}_l + p \rightarrow l^+ + n$, it has been shown that with the increase in M_A , $\frac{d\sigma}{dQ^2}$ decreases (from 0.9 GeV to 1.1 GeV) and with further increase in $M_A = 1.2$ GeV, $\frac{d\sigma}{dQ^2}$ increases [227]. A similar trend is observed in the case of Λ production induced by $\bar{\nu}_\mu$ [251], as in the case of $\bar{\nu}_\tau$ induced CCQE reaction [227] with $\Delta S = 0$ currents. It may be pointed out that with the increase in antineutrino energy, the polarization observables show a significant dependence on the axial dipole mass.

3. Inelastic ν –scattering processes from nucleons

3.1. Introduction

With the increase in energy of the neutrinos, the IE processes start to appear in which new particles are produced. The production of a single pion is the simplest IE process which starts at a threshold energy of $E_\nu \sim 135$ MeV in the reactions

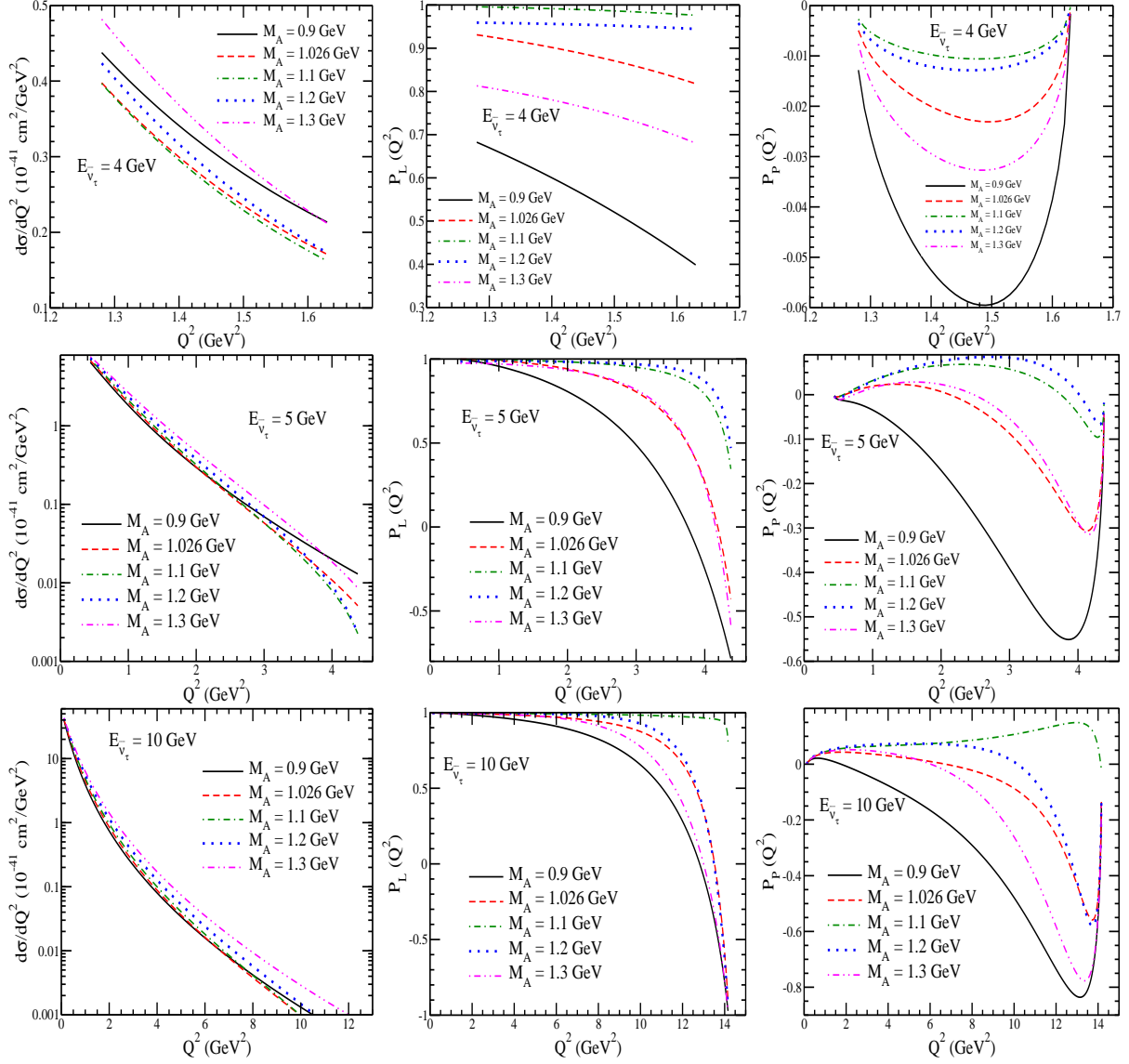


Figure 2.13: $\frac{d\sigma}{dQ^2}$ (left panel), $P_L(Q^2)$ (middle panel) and $P_P(Q^2)$ (right panel) versus Q^2 for the process $\bar{\nu}_\tau + p \rightarrow \tau^+ + \Lambda$ at $E_{\bar{\nu}_\tau} = 4$ GeV (upper panel), 5 GeV (middle panel) and 10 GeV (lower panel). The calculations have been performed using the electric and magnetic Sachs' form factors parameterized by Bradford et al. [186] and for the axial form factor (Eq. (2.63)), the different values of M_A have been used viz. $M_A = 0.9$ GeV (solid line), 1.026 GeV (dashed line), 1.1 GeV (dashed-dotted line), 1.2 GeV (dotted line) and 1.3 GeV (double-dotted-dashed line) [253].

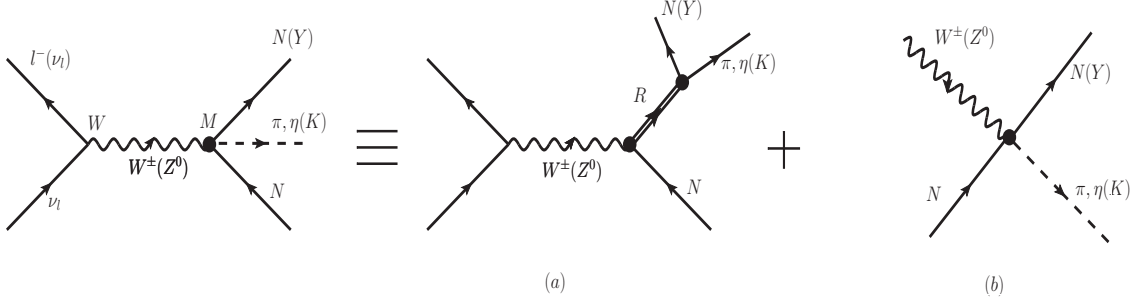


Figure 3.1: Generic Feynman diagrams representing CC and NC induced IE processes given in Table-2.1. In Fig. (a), R is the resonance excited by the (anti)neutrino interactions induced by $W^\pm(Z^0)$, which subsequently decays to a baryon and a meson and Fig. (b) shows the NR terms.

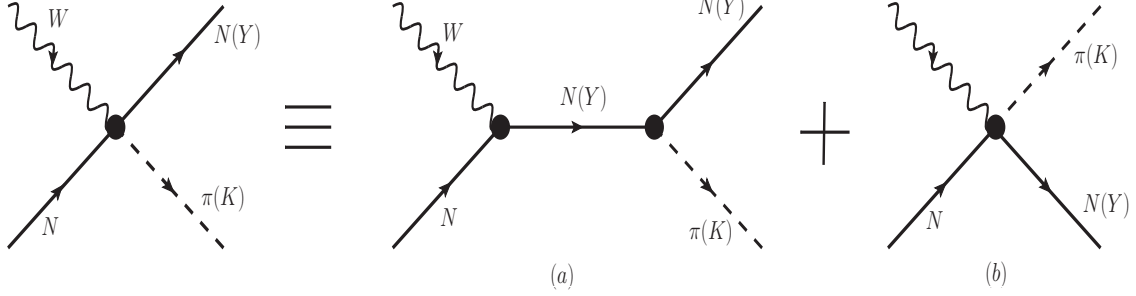


Figure 3.2: Generic Feynman diagrams representing the NR background terms contributing to the IE processes, where Fig. (a) shows the meson and baryon pole terms and Fig. (b) shows the contact diagram.

induced by the weak NC interactions of ν_e, ν_μ, ν_τ and their antiparticles $\bar{\nu}_e, \bar{\nu}_\mu, \bar{\nu}_\tau$. In case of the IE processes induced by the weak CC in which pions are accompanied by the corresponding charged leptons e^\mp, μ^\mp, τ^\mp , the threshold energies are $E_\nu \sim 150$ MeV, 280 MeV and 3.8 GeV, respectively. With the further increase in energy, various particles with masses higher than the pion mass like $\eta, K, \rho, \omega, \Lambda$, etc. are produced, subject to the selection rules satisfied by the weak charge and NC. Specifically, we focus in this section, on the reactions given in Table 2.1, which are induced by the CC and NC weak interaction processes.

Some of the IE processes listed in Table 2.1, specially in the $\Delta S = 0$ sector have been studied for many years in the reactions induced by photons and electrons where the contribution comes from the electromagnetic vector current only. The contribution of the weak vector current in the neutrino scattering processes are determined in the $\Delta S = 0$ sector using isospin symmetry which are extended to the $\Delta S = 1$ sector assuming $SU(3)$ symmetry. Therefore, the experimental and theoretical studies of IE production of various mesons like π, K, η , etc. induced by photons and electrons play very important role in the study of the weak IE production of various mesons induced by (anti)neutrinos as listed in Table 2.1. The contribution of the axial-vector current to the weak IE processes induced by (anti)neutrinos is determined in terms of the axial-vector transition form factors calculated using the generalized form of PCAC and the GT relation. However, all the transition form factors in the axial-vector sector in the case of nucleon-resonance transitions are not determined in this way and a phenomenological approach is used following the seminal work of Adler [256].

The study of the IE processes in the EM interactions induced by photons and electrons shows that the reactions receives contribution from the resonance excitations as well as from the nonresonant Born diagrams. These contributions are diagrammatically shown in Figs. 3.1 and 3.2. While the dominant contribution comes from the resonant diagrams specially from the Δ resonance in the case of pion production, and $S_{11}(1535)$ resonance in the case of η production, the contribution from the nonresonant diagrams is quite important in almost the entire range of energy and not only in the threshold region. This perception of the dynamics of these IE reactions is also expected to be valid in the weak IE reactions induced by (anti)neutrinos which are shown in Figs. 3.1 and 3.2. In Fig. 3.1, R is the resonance excited by the (anti)neutrino interactions induced by $W^\pm(Z^0)$ intermediate vector bosons and decays into nucleons and mesons. In Fig. 3.2, the interaction vertex includes the contribution of all the NR diagrams to the IE processes in s, t and u channels and the contact diagrams.

The weak IE processes induced by (anti)neutrinos play very important role in modeling the (anti)neutrino-nucleon cross sections to be used in formulating the neutrino event generators in simulating the neutrino oscillation experiments in the few GeV energy region. Moreover, the weak IE reactions on the nucleon targets also help to probe some aspects of hadronic structure in the axial-vector sector in conjunction with the hadronic structure being probed by the electromagnetic current in the vector sector using photons and electrons.

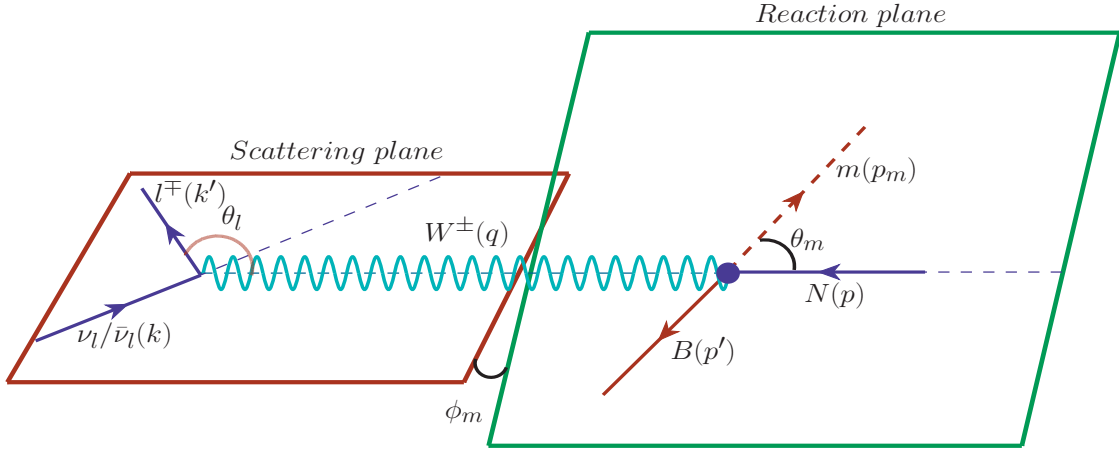


Figure 3.3: (Anti)neutrino scattering and reaction planes, depicting the hadronic plane in CM frame and scattering plane in the laboratory frame. The kinematical variables used in the calculation of the different IE scattering processes are defined in the figure.

In the following sections, we first describe the general kinematics of the IE reactions with the single meson production in Section 3.2. In Sections 3.4, 3.5.2, 3.6.1, and 3.6.4 we discuss the single pion, single eta, single kaon, and associated production of kaons, respectively. In Sections 3.6.5, 3.6.6, and 3.7, we discuss briefly $Y\pi$, ΞK and 2π productions, respectively.

3.2. Kinematics

The general expression for the differential scattering cross section of the IE processes discussed in Table-2.1 and written in general as

$$\nu_l/\bar{\nu}_l(k) + N(p) \longrightarrow l^\mp(k') + B(p') + m(p_m) \quad (3.1)$$

in the laboratory frame is given by

$$d\sigma = \frac{1}{4ME_\nu(2\pi)^5} \frac{d\vec{k}'}{(2E_l)} \frac{d\vec{p}'}{(2E_B)} \frac{d\vec{p}_m}{(2E_m)} \delta^4(k + p - k' - p' - p_m) \overline{\sum} \sum |\mathcal{M}|^2, \quad (3.2)$$

where in Eq. (3.1), $m(=\pi, \eta, K, \text{etc.})$ is a meson produced with a baryon ($B = N, Y, \text{etc.}$) in the final state. $k(k')$ is the four momentum of the incoming (outgoing) lepton having energy $E_\nu(E_l)$; p is the four momentum of the incoming nucleon which is at rest, E_B and p' are respectively the energy and four momentum of the outgoing baryon, and the meson four momentum is p_m with energy E_m , and M is the nucleon mass. The different kinematical variables used in the numerical calculations of the scattering cross section are depicted in Fig. 3.3, where the scattering plane is in the laboratory frame while the reaction plane is in the center of mass frame. $\overline{\sum} \sum |\mathcal{M}|^2$ is the square of the transition amplitude averaged (summed) over the spins of the initial (final) states and the transition matrix element is written in terms of the leptonic and the hadronic currents as

$$\mathcal{M} = \frac{G_F}{\sqrt{2}} l_\mu j^\mu, \quad (3.3)$$

where the leptonic current l_μ , and the constant G_F are defined after Eq. (2.10). $j_{CC(NC)}^\mu$ is the hadronic current for $W^i + N \longrightarrow B + \text{meson}$ interaction for CC ($W^i \equiv W^\pm$; $i = \pm$) and NC ($W^0 = Z^0$) induced processes.

Integrating over the three momentum of the outgoing baryon, the expression for the differential scattering cross section given in Eq. (3.1) becomes

$$\frac{d\sigma}{dE_m d\Omega_m} = \frac{1}{32(2\pi)^5} \int d\Omega_l dE_l \delta(E_\nu + M - E_l - E_B - E_\pi) \frac{|\vec{k}'||\vec{p}_m|}{E_\nu M E_B} \overline{\sum} \sum |\mathcal{M}|^2, \quad (3.4)$$

which after integration over dE_m becomes

$$\frac{d^4\sigma}{dE_l d\cos\theta_l d\cos\theta_m d\phi_m} = \frac{|\vec{k}'||\vec{p}_m|^2}{32(2\pi)^4 E_\nu M} \frac{G_F^2 L_{\mu\nu} J^{\mu\nu}}{4} \frac{1}{(E_\nu + M - E_l)|\vec{p}_m|^2 - E_m(\vec{p}_m \cdot \vec{q})}, \quad (3.5)$$

$L_{\mu\nu}$ is given in Eq. (2.15) and $J^{\mu\nu} = \sum j^\mu j^{\nu\dagger}$, where the hadronic current (j^μ) receives contribution from the nonresonant background (NRB) terms as well as from the resonance excitations and their decay into a particular meson-baryon final

state. The different IE channels receive contribution from the different background terms as well as from the different resonance excitations. In the next section, we present the structure of the hadronic currents for the background and the resonance terms in general. Moreover, for the different IE channels, the specific couplings and the contribution from the different terms are discussed in the respective sections. Specifically, the hadronic current for an IE scattering process is written as

$$j^\mu = j_{NR}^\mu + j_{R_{\frac{1}{2}}}^\mu + j_{R_{\frac{3}{2}}}^\mu, \quad (3.6)$$

where j_{NR}^μ , $j_{R_{\frac{1}{2}}}^\mu$, and $j_{R_{\frac{3}{2}}}^\mu$, respectively, represent the contribution of the hadronic current from the NRB terms, spin $\frac{1}{2}$ resonance, and spin $\frac{3}{2}$ resonance excitations.

3.3. Structure of matrix elements

As already discussed in the previous section, in the following we discuss the NRB contribution in Section 3.3.1 and the resonance excitation and their subsequent decay to different meson-baryon final state are discussed in Section 3.3.5.

3.3.1. Nonresonant contribution

The nonresonant (NR) contributions for the pion production have been calculated using a microscopic model based on the $SU(2)$ chiral Lagrangians. We have used $SU(2)$ nonlinear σ model involving pions and nucleons and the corresponding vector and axial-vector currents generated by the chiral symmetry transformations to determine the structure of the chiral NR terms [10]. It has been observed that the NR contributions are particularly important in the meson production threshold region, for values of $W \simeq M + m_m$, with m_m being the mass of the produced meson. To include the strange meson production, this model is extended to the $SU(3)$ chiral Lagrangians. The basic parameters of the model are the meson decay constant f_m , the Cabibbo's angle, the proton and neutron magnetic moments, and the asymmetric and symmetric axial-vector coupling constants for the two baryon octets, D and F , respectively, that are obtained from the analysis of the semileptonic decays of neutron and hyperons.

The Lagrangian for QCD is written as

$$\mathcal{L}_{QCD} = \bar{q}(i\not{D} - m_q)q - \frac{1}{4}G_{\mu\nu}^\alpha G^{\alpha\mu\nu}, \quad (3.7)$$

where $q = \begin{pmatrix} u \\ d \\ s \end{pmatrix}$ denotes the quark field, $G_{\mu\nu}^\alpha$ is the gluon field-strength tensor with α as a color index and D_μ is defined as

$$D_\mu = \partial_\mu + ig\frac{\lambda^\alpha}{2}G_{\mu\alpha}, \quad (3.8)$$

where g is the quark-gluon coupling strength and $G_{\mu\alpha}$ is the vector gluon field. The Lagrangian written in Eq. (3.7) does not preserve chiral symmetry in its present form, however, in the limit when quark masses are assumed to be zero, the QCD Lagrangian preserves chiral symmetry. Today it is well established that all the quarks have nonzero mass although the current quark masses for u, d, s are small as compared to the nucleon mass. Thus, in the case of strong interactions, chiral symmetry is a symmetry of the Lagrangian in the limit of $m_u, m_d, m_s \rightarrow 0$. The consequence of the symmetries of the Lagrangian leads to the conserved currents. The vector current is conserved in nature due to the isospin symmetry. Similarly, the axial-vector current is conserved in the presence of the chiral symmetry. In case, the chiral symmetry based on $SU(2) \times SU(2)$ is broken spontaneously, it leads to the existence of massless Goldstone bosons, which are identified as the pions in the limit $m_u, m_d \rightarrow 0$ and as the octet of pseudoscalar mesons in the case of chiral symmetry based on $SU(3) \times SU(3)$ symmetry in the limit $m_u, m_d, m_s \rightarrow 0$. The local gauge symmetry of QCD leads to the construction of the chiral effective theory of the Goldstone bosons as well as their interaction with the baryons.

In order to get the Lagrangian, which describes the dynamics of these pseudoscalar mesons, we need continuous fields which are described in terms of these Goldstone modes. The elements of $SU(3)$ pseudoscalar meson fields are written in terms of a unitary matrix [10]

$$U(\Theta) = \exp\left(-i\Theta_k \frac{\lambda_k}{2}\right), \quad (3.9)$$

where Θ_k ; ($k = 1 - 8$) are the real set of parameters and λ_k are the traceless, Hermitian 3×3 Gell-Mann matrices.

Each Goldstone boson corresponds to the x -dependent Cartesian component of the fields $\phi_k(x)$, which in turn, are expressed in terms of the physical fields as [10]:

$$\Phi(x) = \sum_{k=1}^8 \phi_k(x) \lambda_k = \begin{pmatrix} \pi^0 + \frac{1}{\sqrt{3}}\eta & \sqrt{2}\pi^+ & \sqrt{2}K^+ \\ \sqrt{2}\pi^- & -\pi^0 + \frac{1}{\sqrt{3}}\eta & \sqrt{2}K^0 \\ \sqrt{2}K^- & \sqrt{2}\bar{K}^0 & -\frac{2}{\sqrt{3}}\eta \end{pmatrix}. \quad (3.10)$$

For the baryons, we follow the same procedure as we do for the mesons. However, unlike the pseudoscalar mesons where the fields are real, in the case of baryon fields, represented by a B matrix, each entry is a complex-field and the general representation is given by [10]:

$$B(x) = \sum_{k=1}^8 \frac{1}{\sqrt{2}} b_k(x) \lambda_k = \begin{pmatrix} \frac{1}{\sqrt{2}} \Sigma^0 + \frac{1}{\sqrt{6}} \Lambda & \Sigma^+ & p \\ \Sigma^- & -\frac{1}{\sqrt{2}} \Sigma^0 + \frac{1}{\sqrt{6}} \Lambda & n \\ \Xi^- & \Xi^0 & -\frac{2}{\sqrt{6}} \Lambda \end{pmatrix}. \quad (3.11)$$

After getting the representation of the pseudoscalar meson fields octet $\Phi(x)$ in Eq. (3.10) and baryon fields octet $B(x)$ in Eq. (3.11), we now discuss the construction of the Lagrangian for meson-meson, baryon-meson interactions and their interaction with the external fields.

3.3.2. Meson - meson interaction

The lowest-order $SU(3)$ chiral Lagrangian describing the pseudoscalar mesons in the presence of an external current is obtained as [257, 258]:

$$\mathcal{L}_M = \frac{f_\pi^2}{4} \text{Tr}[D_\mu U (D^\mu U)^\dagger]. \quad (3.12)$$

The covariant derivatives $D^\mu U$ and $D^\mu U^\dagger$ appearing in Eq. (3.12) are expressed in terms of the partial derivatives as

$$D^\mu U \equiv \partial^\mu U - i r^\mu U + i U l^\mu, \quad D^\mu U^\dagger \equiv \partial^\mu U^\dagger + i U^\dagger r^\mu - i l^\mu U^\dagger, \quad (3.13)$$

where U is the $SU(3)$ unitary matrix given as

$$U(x) = \exp \left(i \frac{\Phi(x)}{f_m} \right), \quad (3.14)$$

where $\Phi(x)$ is given in Eq. (3.10). r_μ and l_μ , respectively, represent the right and left handed currents, defined in terms of the vector (v_μ) and axial-vector (a_μ) fields as

$$l_\mu = \frac{1}{2}(v_\mu - a_\mu), \quad r_\mu = \frac{1}{2}(v_\mu + a_\mu). \quad (3.15)$$

The vector and axial-vector fields are different for the interaction of the different gauge bosons with the meson fields.

In the case of electromagnetic interactions, the left and right handed currents are identical and are expressed as

$$l_\mu = r_\mu = -e \hat{Q} A_\mu, \quad (3.16)$$

where e is the strength of the electromagnetic interaction, A_μ represents the photon field and $\hat{Q} = \begin{pmatrix} 2/3 & 0 & 0 \\ 0 & -1/3 & 0 \\ 0 & 0 & -1/3 \end{pmatrix}$ represents the charge of the u , d , and s quarks. In the case of CC induced processes, the left and right handed currents are expressed as

$$l_\mu = -\frac{g}{2}(W_\mu^+ T_+ + W_\mu^- T_-), \quad r_\mu = 0, \quad (3.17)$$

where $g = \frac{e}{\sin \theta_W}$, θ_W is the Weinberg angle, W_μ^\pm represents the W-boson field and T_\pm is defined as

$$T_+ = \begin{pmatrix} 0 & V_{ud} & V_{us} \\ 0 & 0 & 0 \\ 0 & 0 & 0 \end{pmatrix}, \quad \text{and} \quad T_- = \begin{pmatrix} 0 & 0 & 0 \\ V_{ud} & 0 & 0 \\ V_{us} & 0 & 0 \end{pmatrix}, \quad (3.18)$$

with $V_{ud} = \cos \theta_C$ and $V_{us} = \sin \theta_C$ being the elements of the Cabibbo-Kobayashi-Maskawa matrix and θ_C being the Cabibbo angle.

The left and right handed currents for NC induced processes are expressed as

$$l_\mu = \left(-\frac{g}{\cos \theta_W} + e \tan \theta_W \right) Z_\mu \frac{\lambda_3}{2}, \quad r_\mu = g \tan \theta_W \sin \theta_W Z_\mu \frac{\lambda_3}{2}, \quad (3.19)$$

where Z_μ represents the Z-boson field and λ_3 is the third component of the Gell-Mann matrices.

3.3.3. Baryon - meson interaction

To incorporate baryons in the theory, we have to take care of their masses, which do not vanish in the chiral limit [259]. However, if we take nucleons as massive matter fields which couples to external currents and the pseudoscalar mesons, we have to then expand the Lagrangian according to their increasing number of momenta. Here, we shall present in brief the extension of the formalism to incorporate the heavy matter fields.

The lowest-order chiral Lagrangian for the baryon octet in the presence of an external current, may be written in terms of the $SU(3)$ matrix B as [257, 258],

$$\mathcal{L}_{MB} = \text{Tr} [\bar{B} (i\not{D} - M) B] - \frac{D}{2} \text{Tr} (\bar{B} \gamma^\mu \gamma_5 \{u_\mu, B\}) - \frac{F}{2} \text{Tr} (\bar{B} \gamma^\mu \gamma_5 [u_\mu, B]), \quad (3.20)$$

where M denotes the mass of the baryon octet, $D = 0.804$ and $F = 0.463$ are the symmetric and antisymmetric axial-vector coupling constants for the baryon octet, the matrix B is given in Eq. (3.11) and the Lorentz vector u^μ is given by [258]:

$$u^\mu = i [u^\dagger (\partial^\mu - ir^\mu) u - u (\partial^\mu - il^\mu) u^\dagger]. \quad (3.21)$$

In the case of meson-baryon interactions, the unitary matrix for the pseudoscalar field is expressed as

$$u = \sqrt{U} \equiv \exp \left(i \frac{\Phi(x)}{2f_m} \right), \quad (3.22)$$

and the covariant derivative D_μ on the baryon fields B is given by

$$D_\mu B = \partial_\mu B + [\Gamma_\mu, B], \quad \text{with} \quad \Gamma^\mu = \frac{1}{2} [u^\dagger (\partial^\mu - ir^\mu) u + u (\partial^\mu - il^\mu) u^\dagger], \quad (3.23)$$

which is known as the chiral connection.

3.3.4. Decuplet baryon - octet baryon - meson interaction

A systematic way of obtaining the relationships ($SU(3)$ factors) between the weak vertices for all the allowed transitions and that for the $n \rightarrow \Delta^+$ is to use the lowest order Lagrangian that couples the decuplet baryons with the octet baryons and mesons in the presence of an external current [260, 261] and that has been used in Refs. [163, 167, 173]. Its form is

$$\mathcal{L}_{DBM} = \mathcal{C} \left(\epsilon^{abc} \bar{T}_{ade}^\mu (u_\mu)_b^d B_c^e + \epsilon^{abc} \bar{B}_c^e (u_\mu)_b^d T_{aed}^\mu \right), \quad (3.24)$$

where B is given by Eq. (3.11), u_μ is given in Eq. (3.21), and T_{aed}^μ is the $SU(3)$ representation of the Rarita-Schwinger fields for the decuplet baryons. This representation is completely symmetric, which in the present notation is given by a $3 \times 3 \times 3$ array of matrices

$$T_{abc} = \begin{pmatrix} \Delta^{++} & \frac{1}{\sqrt{3}} \Delta^+ & \frac{1}{\sqrt{3}} \Sigma^{*+} \\ \frac{1}{\sqrt{3}} \Delta^+ & \frac{1}{\sqrt{3}} \Delta^0 & \frac{1}{\sqrt{6}} \Sigma^{*0} \\ \frac{1}{\sqrt{3}} \Sigma^{*+} & \frac{1}{\sqrt{6}} \Sigma^{*0} & \frac{1}{\sqrt{3}} \Xi^{*0} \end{pmatrix} \begin{pmatrix} \frac{1}{\sqrt{3}} \Delta^+ & \frac{1}{\sqrt{3}} \Delta^0 & \frac{1}{\sqrt{6}} \Sigma^{*0} \\ \frac{1}{\sqrt{3}} \Delta^0 & \Delta^- & \frac{1}{\sqrt{3}} \Sigma^{*-} \\ \frac{1}{\sqrt{6}} \Sigma^{*0} & \frac{1}{\sqrt{3}} \Sigma^{*-} & \frac{1}{\sqrt{3}} \Xi^{*-} \end{pmatrix} \begin{pmatrix} \frac{1}{\sqrt{3}} \Sigma^{*+} & \frac{1}{\sqrt{6}} \Sigma^{*0} & \frac{1}{\sqrt{3}} \Xi^{*0} \\ \frac{1}{\sqrt{6}} \Sigma^{*0} & \frac{1}{\sqrt{3}} \Sigma^{*-} & \frac{1}{\sqrt{3}} \Xi^{*-} \\ \frac{1}{\sqrt{3}} \Xi^{*0} & \frac{1}{\sqrt{3}} \Xi^{*-} & \Omega^- \end{pmatrix}. \quad (3.25)$$

in the three flavor indices (u, d, s), and an implicit sum over flavor indices ($a, b, \dots = 1, 2, 3$) is understood in Eq. (3.24). It is worth relating the T_{abc} representation to the physical states as:

$$\begin{aligned} T_{111} &= \Delta^{++}; & T_{112} &= \frac{\Delta^+}{\sqrt{3}}; & T_{122} &= \frac{\Delta^0}{\sqrt{3}}; & T_{222} &= \Delta^-; & T_{113} &= \frac{\Sigma^{*+}}{\sqrt{3}}; & T_{123} &= \frac{\Sigma^{*0}}{\sqrt{6}} \\ T_{223} &= \frac{\Sigma^{*-}}{\sqrt{3}}; & T_{133} &= \frac{\Xi^{*0}}{\sqrt{3}}; & T_{233} &= \frac{\Xi^{*-}}{\sqrt{3}}; & T_{333} &= \Omega^-. \end{aligned} \quad (3.26)$$

The hadronic current for the NRB terms contributing to the different IE scattering processes are obtained using the chiral Lagrangians of the nonlinear sigma model discussed in this section.

3.3.5. Resonance (R_J ; $J = \frac{1}{2}, \frac{3}{2}$) contribution

Besides the NRB contribution to the IE scattering processes, there are several resonances with spin $\frac{1}{2}, \frac{3}{2}, \frac{5}{2}$, etc., which contribute to these processes. In Table-3.1, we have tabulated the properties of those resonances which have been considered in this work and these will be separately discussed for each process of present interest. It may be noticed from the table that considered resonances are spin $\frac{1}{2}$ and spin $\frac{3}{2}$ resonant states with positive or negative parity. We discuss in brief the structure of the transition current for these resonant states. The nucleon and delta resonances which are excited in the IE reactions are characterized by their mass, parity, spin and isospin and are represented by the symbol $R_{IJ}(M_R)$ (Table-3.1), where R is the name of the resonance given on the basis of its orbital angular momentum i.e. $L = 0, 1, 2$ and named S, P, D , etc., showing its parity, M_R is the mass while I and J specify their isospin and spin quantum numbers.

Resonance	M_R	Γ	$I(J^P)$	Branching Ratios(in %)				
	(GeV)	(GeV)		$N\pi$	$N\eta$	$K\Lambda$	$K\Sigma$	$\pi\pi N$
$P_{11}(1440)$	1.370 ± 0.01	0.175 ± 0.015	$1/2(1/2^+)$	65	< 1	-	-	34
$S_{11}(1535)$	1.510 ± 0.01	0.130 ± 0.020	$1/2(1/2^-)$	42	42	-	-	8
$S_{31}(1620)$	1.600 ± 0.01	0.120 ± 0.020	$3/2(1/2^-)$	30	-	-	-	67
$S_{11}(1650)$	1.655 ± 0.015	0.135 ± 0.035	$1/2(1/2^+)$	60	25	10	-	22
$P_{11}(1710)$	1.700 ± 0.02	0.120 ± 0.040	$1/2(1/2^+)$	10	30	15	< 1	-
$P_{11}(1880)$	1.860 ± 0.04	0.230 ± 0.050	$1/2(1/2^+)$	6	30	20	17	55
$S_{11}(1895)$	1.910 ± 0.02	0.110 ± 0.030	$1/2(1/2^-)$	10	25	18	13	-
$P_{33}(1232)$	1.210 ± 0.001	0.100 ± 0.002	$3/2(3/2^+)$	99.4	-	-	-	-
$D_{13}(1520)$	1.510 ± 0.005	$0.110 \pm_{0.005}^{0.010}$	$1/2(3/2^-)$	60	-	-	-	30
$D_{33}(1700)$	1.665 ± 0.025	0.250 ± 0.05	$3/2(3/2^-)$	15	-	-	-	32
$P_{13}(1720)$	1.675 ± 0.015	$0.250 \pm_{0.150}^{0.100}$	$1/2(3/2^+)$	11	3	4.5	-	70
$P_{13}(1900)$	1.920 ± 0.02	0.150 ± 0.05	$1/2(3/2^+)$	10	8	11	5	60

Table 3.1: Properties of the spin 1/2 and 3/2 resonances available in the PDG [19], with Breit-Wigner mass M_R , the total decay width Γ , isospin I , spin J , parity P , and the central value of the branching ratio into different meson-baryon like $N\pi$, $N\eta$, $K\Lambda$, $K\Sigma$ and $\pi\pi N$.

3.3.6. Charged current induced resonance excitation

The basic (anti)neutrino induced CC reactions on the nucleon target for the IE processes through the resonance excitations are

$$\nu_l(k) + N(p) \longrightarrow l^-(k') + R(p_R) \longrightarrow l^-(k') + m(p_m) + B(p'), \quad (3.27)$$

$$\bar{\nu}_l(k) + N(p) \longrightarrow l^+(k') + R(p_R) \longrightarrow l^+(k') + m(p_m) + B(p'). \quad (3.28)$$

In the following, we will first discuss the excitation of spin $\frac{1}{2}$ resonances and their subsequent decay to meson-baryon final state, followed by the discussion of spin $\frac{3}{2}$ resonances.

A. Spin $\frac{1}{2}$ resonances

The hadronic current for nucleon to spin $\frac{1}{2}$ resonance state is given by

$$j_{\frac{1}{2}}^\mu = \bar{u}(p') \Gamma_{\frac{1}{2}}^\mu u(p), \quad (3.29)$$

where $u(p)$ and $\bar{u}(p')$ are respectively the Dirac spinor and adjoint Dirac spinor for spin $\frac{1}{2}$ particles and $\Gamma_{\frac{1}{2}}^\mu$ is the vertex function, given by

$$\Gamma_{\frac{1}{2}}^{\mu\pm} = [V_{\frac{1}{2}}^\mu - A_{\frac{1}{2}}^\mu] \cdot \begin{pmatrix} \mathbb{I}_4 \\ \gamma_5 \end{pmatrix} \quad (3.30)$$

where upper (lower) sign stands for a positive (negative) parity resonance, $V_{\frac{1}{2}}^\mu$ and $A_{\frac{1}{2}}^\mu$, respectively, represent the vector and axial-vector currents, which are parameterized in terms of the vector ($f_{1,2}(Q^2)$) and the axial-vector ($g_{1,3}(Q^2)$) form factors, assuming the absence of SCC, and are written as,

$$V_{\frac{1}{2}}^\mu = \frac{f_1^{CC}(Q^2)}{(2M)^2} (Q^2 \gamma^\mu + \not{q} q^\mu) + \frac{f_2^{CC}(Q^2)}{2M} i \sigma^{\mu\alpha} q_\alpha, \quad (3.31)$$

$$A_{\frac{1}{2}}^\mu = \left[g_1^{CC}(Q^2) \gamma^\mu + \frac{g_3^{CC}(Q^2)}{M} q^\mu \right] \gamma_5, \quad (3.32)$$

where $f_i^{CC}(Q^2)$ ($i = 1, 2$) are the isovector transition form factors which in turn are expressed in terms of the charged ($f_i^{R+}(Q^2)$) and neutral ($f_i^{R0}(Q^2)$) electromagnetic transition form factors as:

$$f_i^{CC}(Q^2) = f_i^{R+}(Q^2) - f_i^{R0}(Q^2), \quad i = 1, 2 \quad (3.33)$$

for isospin $\frac{1}{2}$ resonant states like $P_{11}(1440)$, $S_{11}(1535)$, etc., and as

$$f_i^{CC}(Q^2) = -f_i^R(Q^2), \quad i = 1, 2 \quad (3.34)$$

where $R = R^+$ for the proton target and $R = R^0$ for the neutron target, for isospin $\frac{3}{2}$ resonant states like $S_{31}(1620)$. The electromagnetic form factors are extracted from the meson electroproduction data, especially from the pion electroproduction data.

N^*	Amplitude	$\mathcal{A}_\alpha(0)$	a_1	b_1
$S_{11}(1535)$	$A_{\frac{1}{2}}$	95.0	0.5	0.51
	$S_{\frac{1}{2}}$	-2.0	23.9	0.81
$S_{11}(1650)$	$A_{\frac{1}{2}}$	33.3	1.45	0.62
	$S_{\frac{1}{2}}$	-3.5	2.88	0.76
$P_{11}(1710)$	$A_{\frac{1}{2}}$	50.0	1.4	0.95
	$S_{\frac{1}{2}}$	27.4	0.18	0.88
$P_{13}(1720)$	$A_{\frac{1}{2}}$	100.0	1.89	1.55
	$A_{\frac{3}{2}}$	30.0	1.83	1.0
	$S_{\frac{1}{2}}$	-53.0	2.46	1.55

Table 3.2: Parameterization of the transition form factors for the spin $\frac{1}{2}$ and $\frac{3}{2}$ resonances on proton target. $\mathcal{A}_\alpha(0)$ is given in units of $10^{-3} \text{ GeV}^{-\frac{1}{2}}$ and the coefficients a_1 , and b_1 in units of GeV^{-2} , and GeV^{-2} , respectively.

The electromagnetic transition form factors $f_i^{R+,R0}(Q^2)$ are derived from the helicity amplitudes $A_{\frac{1}{2}}$ and $S_{\frac{1}{2}}$ extracted from the real and/or virtual photon scattering experiments. In order to determine the helicity amplitudes $A_{1/2}$ and $S_{1/2}$, one assumes the interaction of a nucleon with a virtual/real photon to produce a spin 1/2 resonance. The helicity amplitudes for the process $\gamma N \rightarrow R_{1/2}$ are expressed in terms of the polarization of the photon and the spins of the incoming nucleon and the outgoing spin 1/2 resonance, where the spin of the resonance is fixed in the positive Z-direction, i.e. $J_z^R = +1/2$. The expressions for $A_{1/2}$ and $S_{1/2}$ are defined as [165]:

$$A_{1/2}^N = \sqrt{\frac{2\pi\alpha}{K_R}} \langle R, J_z^R = +1/2 | \epsilon_\mu^+ V^\mu | N, J_z^N = -1/2 \rangle e^{i\phi}, \quad (3.35)$$

$$S_{1/2}^N = -\sqrt{\frac{2\pi\alpha}{K_R}} \frac{|\vec{q}|}{\sqrt{Q^2}} \langle R, J_z^R = +1/2 | \epsilon_\mu^0 V^\mu | N, J_z^N = +1/2 \rangle e^{i\phi}, \quad (3.36)$$

where ϕ is the phase factor, which relates the amplitude for the production of the resonances and the nucleons in the final state, $K_R = (M_R^2 - M^2)/2M_R$ is the momentum of the real photon measured in the resonance rest frame and $|\vec{q}|$ is the momentum of the virtual photon measured in the laboratory frame given as

$$|\vec{q}| = \sqrt{\frac{(M_R^2 - M^2 - Q^2)^2}{(2M_R)^2} + Q^2}. \quad (3.37)$$

The expressions for V^μ is given in Eq. (3.31) and ϵ_μ represents the photon polarization vector. The transverse polarized photon vector ϵ_μ^\pm is defined as

$$\epsilon_\mu^\pm = \mp \frac{1}{\sqrt{2}} (0, 1, \pm i, 0), \quad (3.38)$$

and for the longitudinal polarization of the photon ϵ_μ^0 is defined as

$$\epsilon_\mu^0 = \frac{1}{\sqrt{Q^2}} (|\vec{q}|, 0, 0, q^0). \quad (3.39)$$

From Eqs. (3.35), (3.36), (3.38) and (3.39), one may observe that for the spin 1/2 resonances, $A_{1/2}$ represents the interaction of the transverse polarized photons with the $NR_{1/2}$ vertex whereas $S_{1/2}$ represents the interaction of the longitudinally polarized photons with the $NR_{1/2}$ vertex.

The explicit relations between the form factors $f_i^{R+,R0}(Q^2)$ and the helicity amplitudes $A_{\frac{1}{2}}^{p,n}(Q^2)$ and $S_{\frac{1}{2}}^{p,n}(Q^2)$, for $\phi = 0$, are given by [165]:

$$\begin{aligned} A_{\frac{1}{2}}^{p,n} &= \sqrt{\frac{2\pi\alpha}{M} \frac{(M_R \mp M)^2 + Q^2}{M_R^2 - M^2}} \left[\frac{Q^2}{4M^2} f_1^{R+,R0} + \frac{M_R \pm M}{2M} f_2^{R+,R0} \right], \\ S_{\frac{1}{2}}^{p,n} &= \mp \sqrt{\frac{\pi\alpha}{M} \frac{(M \pm M_R)^2 + Q^2}{M_R^2 - M^2}} \frac{(M_R \mp M)^2 + Q^2}{4M_R M} \left[\frac{M_R \pm M}{2M} f_1^{R+,R0} - f_2^{R+,R0} \right], \end{aligned} \quad (3.40)$$

where the upper sign represents the positive parity state and the lower sign denotes the negative parity state. M_R is the mass of corresponding resonance and $f_{1,2}^{R+,R0}(Q^2)$ are the electromagnetic transition form factors. The

N^*	Amplitude	$\mathcal{A}_\alpha(0)$	a_1	b_1
$S_{11}(1535)$	$A_{\frac{1}{2}}$	-78.0	1.75	1.75
	$S_{\frac{1}{2}}$	32.5	0.4	1.0
$S_{11}(1650)$	$A_{\frac{1}{2}}$	26.0	0.1	2.5
	$S_{\frac{1}{2}}$	3.8	0.4	0.71
$P_{11}(1710)$	$A_{\frac{1}{2}}$	-45.0	-0.02	0.95
	$S_{\frac{1}{2}}$	-31.5	0.35	0.85
$P_{13}(1720)$	$A_{\frac{1}{2}}$	-2.9	12.7	1.55
	$A_{\frac{3}{2}}$	-31.0	3.0	1.55
	$S_{\frac{1}{2}}$	0.0	0.0	0.0

Table 3.3: Parameterization of the transition form factors for the spin $\frac{1}{2}$ and $\frac{3}{2}$ resonances on neutron target. $\mathcal{A}_\alpha(0)$ is given in units of $10^{-3} \text{ GeV}^{-\frac{1}{2}}$ and the coefficients a_1 , and b_1 in units of GeV^{-2} , and GeV^{-2} , respectively.

Resonance	$g_{RN\pi}$	$g_{RN\eta}$	$g_{RK\Lambda}$	$g_{RK\Sigma}$
$P_{11}(1440)$	0.38	-	-	-
$S_{11}(1535)$	0.10195	-0.3696	-	-
$S_{31}(1620)$	0.18	-	-	-
$S_{11}(1650)$	0.0915	0.1481	0.09766	-
$P_{11}(1710)$	0.04182	0.15675	-0.2386	-
$P_{11}(1880)$	0.0277	0.137	-0.2218	0.1276
$S_{11}(1895)$	0.0261	0.0961	0.0758	0.05587
$P_{33}(1232)$	2.14	-	-	-
$D_{13}(1520)$	1.6	-	-	-
$D_{33}(1700)$	1.288	-	-	-
$P_{13}(1720)$	0.1165	0.2248	0.35	-
$P_{13}(1900)$	0.068	0.149	-0.091	0.1023

Table 3.4: Strong coupling constants g_{RMB} for the different resonances considered in the present work.

vector form factors $f_i^{R+,R0}(Q^2)$ are related with the helicity amplitudes (Eq. (3.40)) for which the Q^2 dependence is parameterized as [262]:

$$\mathcal{A}_\alpha(Q^2) = \mathcal{A}_\alpha(0)(1 + a_1 Q^2) e^{-b_1 Q^2}, \quad (3.41)$$

where $\mathcal{A}_\alpha(Q^2)$ are the helicity amplitudes; $A_{\frac{1}{2}}(Q^2)$ and $S_{\frac{1}{2}}(Q^2)$ and parameters $\mathcal{A}_\alpha(0)$ are generally determined by a fit to the photoproduction data of the corresponding resonance. While the parameters a_1 and b_1 in the case of proton target for each amplitude are obtained from the electroproduction data available at different Q^2 . While for the neutron target, these parameters are determined using the data available for the inverse pion photoproduction ($\pi^- p \rightarrow \gamma n$) process [263]. Not all the resonances quoted in Table 3.1 are well understood by the photo- and electro- production data. The MAID group [262] has parameterized the values of these parameters for the resonances which have been experimentally studied in the photo- and electro- production processes and the values of these parameters for the proton and neutron targets are taken from Ref. [262] for $P_{11}(1440)$, $D_{13}(1520)$, $S_{31}(1620)$, and $D_{33}(1700)$ resonances. However, for some resonances, like $S_{11}(1535)$, $S_{11}(1650)$, and $P_{13}(1720)$, there are latest experimental data for the photo- and electro- production processes as well as for the helicity amplitudes, therefore, we have refitted the values of $\mathcal{A}_\alpha(0)$, a_1 and b_1 , to explain the latest data, and the refitted values for these resonances are given in Tables 3.2 and 3.3, respectively, for proton and neutron targets. Moreover, for the resonances which are not parameterized by the MAID group, we have taken the value of $\mathcal{A}_\alpha(0)$ from PDG [19] and fitted the values of a_1 and b_1 to the available data. For example, in the case of $P_{11}(1710)$ resonance, we have fitted the Q^2 dependence to explain the pion electroproduction data from the CLAS collaboration given in Ref. [264].

The axial-vector current consists of two form factors viz. $g_1^{CC}(Q^2)$ and $g_3^{CC}(Q^2)$, which are determined assuming the PCAC hypothesis and PDDAC through the off diagonal GT relation for $N \rightarrow R$ transition. This assumption allows us to relate the axial-vector form factor at $Q^2 = 0$ to the pion-nucleon scattering (see Ref. [10]), which is also well understood experimentally, and leads to the following relation

$$g_1^{CC}(0) = 2g_{RN\pi}, \quad (3.42)$$

for the isospin $\frac{1}{2}$ resonances, and

$$g_1^{CC}(0) = -\sqrt{\frac{2}{3}}g_{RN\pi}, \quad (3.43)$$

for the isospin $\frac{3}{2}$ resonances, with $g_{RN\pi}$ being the coupling strength for $R_{\frac{1}{2}} \rightarrow N\pi$ decay, which has been determined by the partial decay width of the resonance. Since no information about the Q^2 dependence of the axial-vector form factor is known experimentally, therefore, a dipole form is assumed as in the case of $N \rightarrow N'$ or $N \rightarrow Y$ transitions:

$$g_1^{CC}(Q^2) = \frac{g_1^{CC}(0)}{\left(1 + \frac{Q^2}{M_A^2}\right)^2}, \quad (3.44)$$

with $M_A = 1.026$ GeV, and the pseudoscalar form factor $g_3^{CC}(Q^2)$ is given by

$$g_3^{CC}(Q^2) = \frac{(MM_R \pm M^2)}{m_\pi^2 + Q^2} g_1^{CC}(Q^2), \quad (3.45)$$

where $+$ ($-$) sign is for positive (negative) parity resonances.

The most general form of the hadronic currents for the s-channel (direct resonance pole diagram) and u-channel (cross resonance pole diagram) processes where a positive (negative) parity resonance state $R^{\frac{1}{2}\pm}$ is produced and decays to a meson and baryon in the final state, are written as

$$j^\mu|_{sR}^{\frac{1}{2}\pm} = i a \mathcal{C}^{\mathcal{R}} \bar{u}(p') \not{p}_m \Gamma_s \frac{\not{p} + \not{q} + M_R}{(p+q)^2 - M_R^2 + iM_R\Gamma_R} \Gamma_{\frac{1}{2}\pm}^\mu u(p), \quad (3.46)$$

$$j^\mu|_{uR}^{\frac{1}{2}\pm} = i a \mathcal{C}^{\mathcal{R}} \bar{u}(p') \Gamma_{\frac{1}{2}\pm}^\mu \frac{\not{p}' - \not{q} + M_R}{(p'-q)^2 - M_R^2 + iM_R\Gamma_R} \not{p}_m \Gamma_s u(p), \quad (3.47)$$

where $\Gamma_s = \gamma_5$ (\mathbb{I}_4) stands for the positive (negative) parity resonances, $a = \cos\theta_c$ ($\sin\theta_c$) for CC $\Delta S = 0$ ($\Delta S = 1$) process and $a = 1$ for NC process. M_R and Γ_R are, respectively, the masses and total decay width of these resonances and are given in Table 3.1. $\mathcal{C}^{\mathcal{R}}$ is a constant which includes the coupling strength tabulated in Table 3.4, and the isospin factor involve in $\mathcal{R} \rightarrow MB$ transition.

B. Spin $\frac{3}{2}$ resonances

The general structure for the hadronic current for spin three-half resonance excitation is determined by the following equation [175]

$$J_\mu^{\frac{3}{2}} = \bar{\psi}^\nu(p') \Gamma_{\nu\mu}^{\frac{3}{2}} u(p), \quad (3.48)$$

where $u(p)$ is the Dirac spinor for nucleon, $\psi^\mu(p)$ is the Rarita-Schwinger spinor for spin three-half particle and $\Gamma_{\nu\mu}^{\frac{3}{2}}$ is the weak $WNR_{\frac{3}{2}}$ vertex, given as

$$\Gamma_{\nu\mu}^{\frac{3}{2}\pm} = \left[V_{\nu\mu}^{\frac{3}{2}} - A_{\nu\mu}^{\frac{3}{2}} \right] \cdot \left(\gamma_5 \right), \quad (3.49)$$

where upper (lower) sign stands for a positive (negative) parity resonance, and $V_{\frac{3}{2}}^{\frac{3}{2}}$ ($A_{\frac{3}{2}}^{\frac{3}{2}}$) is the vector (axial-vector) current for spin three-half resonances. The vector and the axial-vector part of the currents are given by

$$V_{\nu\mu}^{\frac{3}{2}} = \left[\frac{C_3^V}{M} (g_{\mu\nu} \not{q} - q_\nu \gamma_\mu) + \frac{C_4^V}{M^2} (g_{\mu\nu} q \cdot p' - q_\nu p'_\mu) + \frac{C_5^V}{M^2} (g_{\mu\nu} q \cdot p - q_\nu p_\mu) + g_{\mu\nu} C_6^V \right], \quad (3.50)$$

$$A_{\nu\mu}^{\frac{3}{2}} = - \left[\frac{C_3^A}{M} (g_{\mu\nu} \not{q} - q_\nu \gamma_\mu) + \frac{C_4^A}{M^2} (g_{\mu\nu} q \cdot p' - q_\nu p'_\mu) + C_5^A g_{\mu\nu} + \frac{C_6^A}{M^2} q_\nu q_\mu \right] \gamma_5, \quad (3.51)$$

where C_i^V and C_i^A are the vector and axial-vector CC transition form factors which are functions of Q^2 . The CVC hypothesis leads to $C_6^V(Q^2) = 0$.

The isovector C_i^V ; ($i = 3, 4, 5$) form factors for the resonance which have $J = \frac{3}{2}$, $I = \frac{1}{2}$, like $D_{13}(1520)$, $P_{13}(1720)$, etc., are written in terms of the electromagnetic charged ($C_i^{R+}(Q^2)$) and neutral ($C_i^{R0}(Q^2)$) transition form factors through a simple relation [265] as

$$C_i^V = C_i^{R+} - C_i^{R0}; \quad i = 3, 4, 5, \quad (3.52)$$

while for the resonance with $J = \frac{3}{2}$ and $I = \frac{3}{2}$ like $P_{33}(1232)$, $D_{33}(1700)$, etc., the isovector form factors C_i^V ; ($i = 3, 4, 5$) are expressed as

$$C_i^V = -C_i^N; \quad i = 3, 4, 5, \quad (3.53)$$

with $N = R0$ ($R+$) stands for the neutral (charged) electromagnetic form factor.

In the case of spin 3/2 resonances, along with i.e. $J_z^R = +1/2$, $J_z^R = +3/2$ also contributes in the positive Z-direction. Again it is our choice to take J_z^R in the positive Z-direction, one may obtain the expressions for the helicity amplitudes by fixing J_z^R in the negative Z-direction. The expressions for $A_{1/2}$ and $S_{1/2}$ in terms of the matrix element of V^μ are given in Eqs. (3.35) and (3.36) with V^μ defined in Eq. (3.50). The expression for $A_{3/2}$ is given below:

$$A_{3/2}^N = \sqrt{\frac{2\pi\alpha}{K_R}} \langle R, J_z^R = +3/2 | \epsilon_\mu^+ V^\mu | N, J_z^N = +1/2 \rangle e^{i\phi}. \quad (3.54)$$

The relations between the vector form factors $C_i^{R+,R0}(Q^2)$ and helicity amplitudes are given as [266]:

$$A_{\frac{3}{2}}^{p,n} = \sqrt{\frac{\pi\alpha}{M} \frac{(M_R \mp M)^2 + Q^2}{M_R^2 - M^2}} \left[\frac{C_3^{R+,R0}}{M} (M \pm M_R) \pm \frac{C_4^{R+,R0}}{M^2} \frac{M_R^2 - M^2 - Q^2}{2} \pm \frac{C_5^{R+,R0}}{M^2} \frac{M_R^2 - M^2 + Q^2}{2} \right], \quad (3.55)$$

$$A_{\frac{1}{2}}^{p,n} = \sqrt{\frac{\pi\alpha}{3M} \frac{(M_R \mp M)^2 + Q^2}{M_R^2 - M^2}} \left[\frac{C_3^{R+,R0}}{M} \frac{M^2 + MM_R + Q^2}{M_R} - \frac{C_4^{R+,R0}}{M^2} \frac{M_R^2 - M^2 - Q^2}{2} - \frac{C_5^{R+,R0}}{M^2} \frac{M_R^2 - M^2 + Q^2}{2} \right], \quad (3.56)$$

$$S_{\frac{1}{2}}^{p,n} = \pm \sqrt{\frac{\pi\alpha}{6M} \frac{(M_R \mp M)^2 + Q^2}{M_R^2 - M^2}} \frac{\sqrt{Q^4 + 2Q^2(M_R^2 + M^2) + (M_R^2 - M^2)^2}}{M_R^2} \times \left[\frac{C_3^{R+,R0}}{M} M_R + \frac{C_4^{R+,R0}}{M^2} M_R^2 + \frac{C_5^{R+,R0}}{M^2} \frac{M_R^2 + M^2 + Q^2}{2} \right], \quad (3.57)$$

where upper (lower) signs stand for the positive (negative) parity resonances, $A_{\frac{3}{2}}(Q^2)$, $A_{\frac{1}{2}}(Q^2)$, and $S_{\frac{1}{2}}(Q^2)$ are the amplitudes corresponding to the transverse and longitudinal polarizations, respectively, and are parameterized as a function of Q^2 using Eq. (3.41). Once the parameters a_1 and b_1 are fixed for $A_{\frac{3}{2}}(Q^2)$, $A_{\frac{1}{2}}(Q^2)$, and $S_{\frac{1}{2}}(Q^2)$ amplitudes, one gets the form factors $C_i^{R+,R0}(Q^2)$.

For the $\Delta(1232)$ resonance, the three vector form factors C_i^V , $i = 3, 4, 5$ are given in terms of the isovector electromagnetic form factors for $p \rightarrow \Delta^+$ transition and the parameterization of which are taken from the Ref. [267],

$$\begin{aligned} C_3^V(Q^2) &= \frac{2.13}{(1 + Q^2/M_V^2)^2} \times \frac{1}{1 + \frac{Q^2}{4M_V^2}}, & C_4^V(Q^2) &= \frac{-1.51}{(1 + Q^2/M_V^2)^2} \times \frac{1}{1 + \frac{Q^2}{4M_V^2}}, \\ C_5^V(Q^2) &= \frac{0.48}{(1 + Q^2/M_V^2)^2} \times \frac{1}{1 + \frac{Q^2}{0.776M_V^2}}. \end{aligned} \quad (3.58)$$

with the vector dipole mass taken as $M_V = 0.84$ GeV.

The axial-vector form factors are determined from the early analysis of weak pion production data at ANL [268] and BNL [269] by Schreiner and von Hippel [270] using Adler's model, which are consistent with the hypothesis of PCAC and generalized GT relation. These considerations give $C_6^A(Q^2)$ in terms of $C_5^A(Q^2)$:

$$C_6^A(Q^2) = C_5^A(Q^2) \frac{M^2}{Q^2 + m_\pi^2}. \quad (3.59)$$

The Q^2 dependence of C_5^A is parameterized by Schreiner and von Hippel [270] and is given by

$$C_5^A(Q^2) = \frac{C_5^A(0) \left(1 + \frac{aQ^2}{b + Q^2}\right)}{(1 + Q^2/M_{A\Delta}^2)^2}, \quad (3.60)$$

with a and b determined from the experiments and found to be $a = -1.21$ and $b = 2 \text{ GeV}^2$ [268, 271]. $M_{A\Delta}$ is the axial dipole mass, and $C_5^A(0)$ is given in terms of $g_{\Delta N\pi}$ as

$$C_5^A(0) = f_\pi \frac{g_{\Delta N\pi}}{2\sqrt{3}M}, \quad (3.61)$$

with $g_{\Delta N\pi}$ being the $\Delta N\pi$ coupling strength for $\Delta \rightarrow N\pi$ decay.

The Q^2 dependence of $C_3^A(Q^2)$ and $C_4^A(Q^2)$ are obtained in the Adler's model as [256, 270]

$$C_4^A(Q^2) = -\frac{1}{4}C_5^A(Q^2); \quad C_3^A(Q^2) = 0. \quad (3.62)$$

The form factors $C_i^A(Q^2)$, ($i = 3, 4, 5, 6$) corresponding to the axial current have not been studied in the case of higher resonances. The earlier calculations have used PCAC to determine $C_5^A(Q^2)$ and $C_6^A(Q^2)$ and taken other form factors to be zero. In view of this, we have also taken a simple model for the determination of the axial form factors based on PCAC and GT relation and use the relation between $C_5^A(Q^2)$ and $C_6^A(Q^2)$ given in Eq. (3.59) to write $C_6^A(Q^2)$ in terms of $C_5^A(Q^2)$ as

$$C_6^A(Q^2) = C_5^A(Q^2) \frac{M^2}{Q^2 + m_\pi^2}. \quad (3.63)$$

For $C_5^A(Q^2)$, a dipole form has been assumed

$$C_5^A(Q^2) = \frac{C_5^A(0)}{(1 + Q^2/M_A^2)^2}, \quad (3.64)$$

with $C_5^A(0) = -2g_{RN\pi} (\sqrt{\frac{2}{3}}g_{RN\pi})$ for isospin $\frac{1}{2}$ ($\frac{3}{2}$) resonances, $g_{RN\pi}$ is the coupling for $R \rightarrow N\pi$ decay for each resonance R . M_A^R is taken as 1.026 GeV. $C_3^A(Q^2)$ as well as $C_4^A(Q^2)$ are taken as zero.

One may write the most general form of the hadronic current for the s-channel (direct resonance pole diagram) and the u-channel (cross resonance pole diagram) processes where a positive (negative) parity resonance state $R^{\frac{3}{2}\pm}$ is produced and decays to a meson and a baryon in the final state as

$$j^\mu|_R^{\frac{3}{2}\pm} = i a \mathcal{C}^{\mathcal{R}} \frac{p_m^\alpha \Gamma_s}{p_R^2 - M_R^2 + i M_R \Gamma_R} \bar{u}(p') P_{\alpha\beta}^{3/2}(p_R) \Gamma_{\frac{3}{2}\pm}^{\beta\mu}(p, q) u(p), \quad p_R = p + q, \quad (3.65)$$

$$j^\mu|_{CR}^{\frac{3}{2}\pm} = i a \mathcal{C}^{\mathcal{R}} \frac{p_m^\beta}{p_R^2 - M_R^2 + i M_R \Gamma_R} \bar{u}(\bar{p}') \hat{\Gamma}_{\frac{3}{2}\pm}^{\mu\alpha}(p', -q) P_{\alpha\beta}^{3/2}(p_R) \Gamma_s u(p), \quad p_R = p' - q, \quad (3.66)$$

where $\Gamma_s = \mathbb{I}_4$ (γ_5) stands for positive (negative) parity resonances, with \mathbb{I}_4 being the 4×4 identity matrix. $\hat{\Gamma}_{\frac{3}{2}\pm}^{\mu\alpha}(p', -q) = \gamma_0 \Gamma^{\mu\alpha\frac{1}{2}}(p', -q) \gamma_0$, $a = \cos \theta_c$ ($\sin \theta_c$) for CC $\Delta S = 0$ ($\Delta S = 1$) process and $a = 1$ for NC process. M_R and Γ_R are, respectively, the masses and total decay width of these resonances and are given in Table 3.1. The constant $\mathcal{C}^{\mathcal{R}}$ includes the coupling strength, isospin factor involve in $\mathcal{R} \rightarrow MB$ transition, etc., and has been tabulated in different sections for the corresponding IE processes. These resonances are generally off-shell and their off-shell effects are also taken into account. $P_{\alpha\beta}^{3/2}$ is spin three-half projection operator and is given by

$$P_{\alpha\beta}^{3/2}(p') = -(p' + M_R) \left(g_{\alpha\beta} - \frac{2}{3} \frac{p'_\alpha p'_\beta}{M_R^2} + \frac{1}{3} \frac{p'_\alpha \gamma_\beta - p'_\beta \gamma_\alpha}{M_R} - \frac{1}{3} \gamma_\alpha \gamma_\beta \right). \quad (3.67)$$

The structure of the matrix element for the hadronic current is given in Eqs. (3.65)–(3.66) for positive and negative parity resonances, respectively, and the weak vertex for positive and negative parity states are given in Eq. (3.49). The vector and axial-vector pieces are written in Eqs. (3.50) and (3.51), respectively, with corresponding form factors, C_i^V and C_i^A , defined for each resonances.

3.3.7. Neutral current induced resonance excitation

In this section, we present in brief the structure of resonance terms that may contribute to the hadronic current of (anti)neutrino induced NC processes. The basic NC (anti)neutrino induced reactions for meson production through resonance excitations are the following:

$$\nu_l(k) + N(p) \rightarrow \nu_l(k') + \mathcal{R}(p_R) \rightarrow \nu_l(k') + B(p') + m(p_m), \quad (3.68)$$

$$\bar{\nu}_l(k) + N(p) \rightarrow \bar{\nu}_l(k') + \mathcal{R}(p_R) \rightarrow \bar{\nu}_l(k') + B(p') + m(p_m), \quad (3.69)$$

where \mathcal{R} stands for the resonances (\mathcal{R}) which contribute to the meson production. We will discuss separately the contribution of spin $\frac{1}{2}$ and $\frac{3}{2}$ resonances to NC induced single meson production.

A. Spin $\frac{1}{2}$ resonances

For NC process producing a spin $\frac{1}{2}$ resonance in the intermediate state, the hadronic current is given by Eq. (3.29). $\Gamma_{\frac{1}{2}}^\mu$ is the vertex function which for positive and negative parity states is given in Eq. (3.30). The vector and axial-vector parts of the current are written in terms of vector and axial-vector form factors and have the same form as given in Eqs. (3.31) and (3.32), but with a modified form factor and a different expression for charged (f_i^{R+}) and neutral (f_i^{R0}) resonance states with the replacement of $f_{1,2}^{CC}$ by $\tilde{f}_{1,2}^{R+,R0}$, corresponding to isospin $\frac{1}{2}$ resonance.

In the case of isospin $\frac{1}{2}$ resonances, the explicit expressions for the vector and axial-vector form factors are written as

$$\tilde{f}_i^p(Q^2) = \left(\frac{1}{2} - 2\sin^2\theta_W\right) f_i^{R+}(Q^2) - \frac{1}{2} f_i^{R0}(Q^2), \quad \tilde{g}_1^p(Q^2) = \frac{1}{2} g_1^{CC}(Q^2), \quad (3.70)$$

for the positive charged state and

$$\tilde{f}_i^n(Q^2) = \left(\frac{1}{2} - 2\sin^2\theta_W\right) f_i^{R0}(Q^2) - \frac{1}{2} f_i^{R+}(Q^2), \quad \tilde{g}_1^n(Q^2) = -\frac{1}{2} g_1^{CC}(Q^2), \quad (3.71)$$

for the neutral state. While for the case of isospin $\frac{3}{2}$ resonances, these form factors \tilde{f}_i^p and \tilde{f}_i^n are given as:

$$\tilde{f}_i^p(Q^2) = (1 - 2\sin^2\theta_W) f_i^{R+}(Q^2), \quad \tilde{g}_1^p(Q^2) = -g_1^{CC}(Q^2), \quad (3.72)$$

for the positive charged state and

$$\tilde{f}_i^n(Q^2) = (1 - 2\sin^2\theta_W) F_i^{R0}(Q^2), \quad \tilde{g}_1^n(Q^2) = -g_1^{CC}(Q^2), \quad (3.73)$$

for the neutral state.

B. Spin $\frac{3}{2}$ resonances

The general structure for the hadronic current $J_\mu^{\frac{3}{2}}$ for NC induced spin $\frac{3}{2}$ resonance in the intermediate state is given by Eq. (3.48), for which $\Gamma_{\nu\mu}^{\frac{3}{2}+,-}$ is given by Eq. (3.49) for positive and negative parity states. The vector and axial-vector parts of the current are given by Eqs. (3.50) and (3.51) with the corresponding NC form factors (\tilde{C}_i^V) ($i = 3, 4, 5$) and (\tilde{C}_i^A) ($i = 4, 5, 6$) which in the SM are given in terms of C_i^V and C_i^A .

The NC form factors \tilde{C}_i^V and \tilde{C}_i^A ($i = 3, 4, 5$) for the case of isospin $\frac{1}{2}$ resonances, are given by:

$$(\tilde{C}_i^V) \xrightarrow{\text{for p}} \left(\frac{1}{2} - 2\sin^2\theta_W\right) C_i^{R+} - \frac{1}{2} C_i^{R0}, \quad (\tilde{C}_i^V) \xrightarrow{\text{for n}} \left(\frac{1}{2} - 2\sin^2\theta_W\right) C_i^{R0} - \frac{1}{2} C_i^{R+}, \quad (\tilde{C}_i^A) \xrightarrow{\text{for p,n}} \pm \frac{1}{2} \tilde{C}_i^A, \quad (3.74)$$

while for the isospin $\frac{3}{2}$ resonances, NC form factors for the proton and neutron targets, are given as:

$$(\tilde{C}_i^V) \xrightarrow{\text{for p}} (1 - 2\sin^2\theta_W) C_i^{R+}, \quad (\tilde{C}_i^V) \xrightarrow{\text{for n}} (1 - 2\sin^2\theta_W) C_i^{R0}, \quad (\tilde{C}_i^A) \xrightarrow{\text{for p,n}} -\tilde{C}_i^A. \quad (3.75)$$

3.3.8. Strong couplings of the resonances

Due to the lack of experimental data there is large uncertainty associated with $\mathcal{R}MB$ coupling at the $\mathcal{R} \rightarrow MB$ vertex. We have fixed $\mathcal{R}MB$ coupling using the data of branching ratio and decay width of these resonances from PDG [19] and use the expression for the decay rate which is obtained by writing the most general form of $\mathcal{R}MB$ Lagrangian given by [10]:

$$\mathcal{L}_{R\frac{1}{2}MB} = \frac{g_{R\frac{1}{2}MB}}{f_m} \bar{\Psi}_{R\frac{1}{2}} \Gamma_{\frac{1}{2}}^\mu \partial_\mu \phi^i T_i \Psi \quad (3.76)$$

$$\mathcal{L}_{R\frac{3}{2}MB} = \frac{g_{R\frac{3}{2}MB}}{f_m} \bar{\Psi}_{R\frac{3}{2}} \Gamma_{\frac{3}{2}}^\mu \partial^\mu \phi^i T_i \Psi \quad (3.77)$$

where f_m is the meson decay constant, which in the case of pion production becomes $f_m = f_\pi = 92.4$ MeV [19] and for eta and kaon production becomes $f_m = f_\eta = f_K = 105$ MeV [272]. $g_{R\frac{1}{2}MB}$ and $g_{R\frac{3}{2}MB}$ are, respectively, the $\mathcal{R}MB$ coupling strength for spin $\frac{1}{2}$ and $\frac{3}{2}$ resonances. Ψ is the nucleon field and $\Psi_{R\frac{1}{2}}$ and $\Psi_{R\frac{3}{2}}$ are the fields associated with the resonances of spin $\frac{1}{2}$ and spin $\frac{3}{2}$, respectively. ϕ^i are the mesonic field and T_i are the isospin operator which is $T = \vec{\tau}$ for isospin $\frac{1}{2}$ states and $T = T^\dagger$ for isospin $\frac{3}{2}$ states ($\vec{\tau}$ and T^\dagger are the isospin operator for doublet and quartet, respectively). The interaction vertex $\Gamma_{\frac{1}{2}}^\mu$ is $\gamma^\mu \gamma^5$ (γ^μ) for spin $\frac{1}{2}$ resonances with positive (negative) parity. Similarly, the interaction

vertex $\Gamma_{\frac{3}{2}}^\mu$, for spin $\frac{3}{2}$ resonances for positive (negative) parity state, are \mathbb{I}_4 (γ_5). Using the above Lagrangian one may obtain the expression for the decay width in the resonance rest frame as

$$\Gamma_{R_{\frac{1}{2}} \rightarrow MB} = \frac{\mathcal{C}}{4\pi} \left(\frac{g_{R_{\frac{1}{2}} MB}}{f_m} \right)^2 (M_R \pm M_B)^2 \frac{E_N \mp M_B}{M_R} |\vec{q}_{cm}|, \quad (3.78)$$

$$\Gamma_{R_{\frac{3}{2}} \rightarrow MB} = \frac{\mathcal{C}}{12\pi} \left(\frac{g_{R_{\frac{3}{2}} MB}}{f_m} \right)^2 \frac{E_N \pm M_B}{M_R} |\vec{q}_{cm}|^3, \quad (3.79)$$

where the upper(lower) sign represents the positive(negative) parity resonance state. The parameter \mathcal{C} is obtained from the isospin analysis and found out to be 3 for isospin $\frac{1}{2}$ state and 1 for isospin $\frac{3}{2}$ states. $|\vec{q}_{cm}|$ is the outgoing pion momentum measured from resonance rest frame and E_N is the nucleon energy, which are given by,

$$|\vec{q}_{cm}| = \frac{\sqrt{(W^2 - m_m^2 - M_B^2)^2 - 4m_m^2 M_B^2}}{2M_R}, \quad E_N = \frac{W^2 + M_B^2 - m_m^2}{2M_R}, \quad (3.80)$$

where W is the CM energy carried by the resonance.

In view of the above, we fix $N\Delta\pi$ coupling($g_{\pi N\Delta}$) by comparing $\Delta \rightarrow N\pi$ decay width evaluated in the rest frame of Δ resonance,

$$\Gamma_\Delta(s) = \frac{1}{6\pi} \left(\frac{g_{\pi N\Delta}}{m_\pi} \right)^2 \frac{M}{\sqrt{s}} \left[\frac{\lambda^{\frac{1}{2}}(s, m_\pi^2, M^2)}{2\sqrt{s}} \right]^3 \Theta(\sqrt{s} - M - m_\pi), \quad s = p_\Delta^2, \quad (3.81)$$

where $\lambda(x, y, z) = x^2 + y^2 + z^2 - 2xy - 2xz - 2yz$ is Källén function. To get the offshell effect of $\Delta(1232)$ resonance we have taken momentum dependent width.

3.4. Single pion production

Historically, the weak pion production induced by (anti)neutrinos has been studied for a long time starting from 1962 [273, 274, 275, 276] in the energy region of (anti)neutrinos relevant for the early experiments done at CERN, ANL and BNL. These early calculations used various approaches based on the

- (i) dynamical models with dispersion theory,
- (ii) quark models with higher symmetry like $SU(6)$, and
- (iii) phenomenological Lagrangians for describing the interaction of mesons with nucleons and excitation of higher resonances.

These calculations have been comprehensively summarized by Adler [256], Llewellyn Smith [175] and Schreiner and von Hippel [270].

In the low energy region corresponding to the threshold production of pions various theoretical models motivated by the chiral symmetry were used to study these processes. For example, the low energy theorems (LET) based on PCAC [277, 278] and/or current algebra (CA) as well as the effective Lagrangians incorporating the chiral symmetry which were formulated to study the photo and electroproduction of pions were extended to study the weak production of pions induced by (anti)neutrinos. The early work using this approach has been summarized by Adler and Dashen [279] and Treiman et al. [280]. In recent years, the advances made in the field of chiral perturbation theory have been used to study the (anti)neutrino induced pion production in the threshold region [160, 166, 281, 282, 283].

After the experimental results from the hydrogen and deuterium bubble chamber experiments from ANL [268] and BNL [271] and later experiments from CERN [284, 285, 286] and other laboratories on the nuclear targets, many new calculations were made using the phenomenological Lagrangian [270, 287, 288, 289, 290, 291, 292, 293, 294, 295], the Lagrangian based on the chiral symmetry [160, 162, 165, 166, 265, 267, 283, 296, 297, 298, 163] and the quark model [157]. In this article it is not possible to describe all the approaches mentioned above and we choose to focus on the effective Lagrangian approach to describe the single pion production induced by (anti)neutrinos from the nucleon targets. We use an effective Lagrangian obtained using the nonlinear realization of chiral symmetry to calculate the NR contribution and a phenomenological Lagrangian to calculate the resonance excitations and its decay to pions, as discussed earlier in Section 3.3.5 and for details, readers are referred to Ref. [10].

In the following, we first discuss the pion production induced by CC in Section 3.4.1 and then the pion production from NC induced processes are discussed in Section 3.4.2.

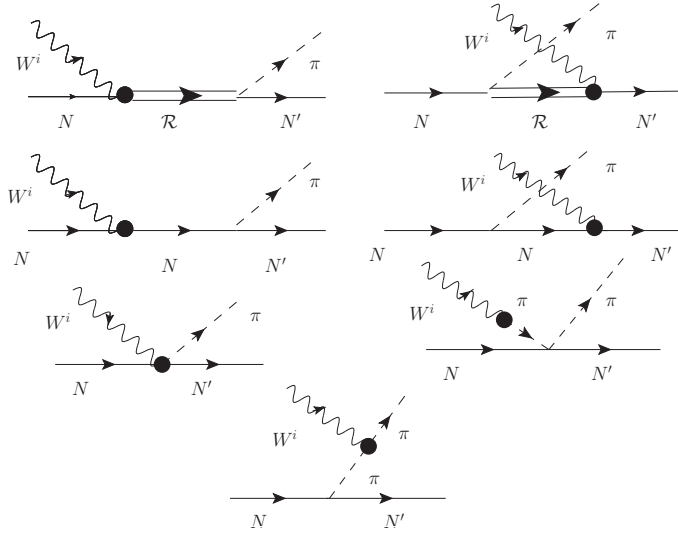


Figure 3.4: Feynman diagrams contributing to the hadronic current corresponding to $W^i N \rightarrow N' \pi^{\pm,0}$, where ($W^i \equiv W^{\pm}$; $i = \pm$) for CC processes and ($W^i \equiv Z^0$; $i = 0$) for NC processes with $N, N' = p$ or n . First row: direct and cross diagrams for resonance production where intermediate term \mathcal{R} stands for different resonances. Second row: nucleon pole (NP and CNP) terms. The contact term (CT) and pion pole (PP) term (third row left to right) and pion in flight (PF) (fourth row).

3.4.1. Charged current (anti)neutrino induced processes

The various possible reactions which may contribute to the single pion production through CC (anti)neutrino induced reaction on a nucleon target are the following:

$$\begin{aligned} \nu_l p &\rightarrow l^- p \pi^+, & \nu_l n &\rightarrow l^- n \pi^+, & \nu_l n &\rightarrow l^- p \pi^0 \\ \bar{\nu}_l n &\rightarrow l^+ n \pi^-, & \bar{\nu}_l p &\rightarrow l^+ p \pi^-, & \bar{\nu}_l p &\rightarrow l^+ n \pi^0 \end{aligned} \quad ; l = e, \mu \quad (3.82)$$

The Feynman diagrams which may contribute to the matrix element of the hadronic current are shown in Fig. 3.4. The NRB terms include five diagrams viz. direct (NP) and cross nucleon pole (CP), contact term (CT), pion pole (PP) and pion in flight (PF) terms. For the $\Delta(1232)$ resonance we have included both direct (s-channel) and cross (u-channel) diagrams. Apart from the $\Delta(1232)$ resonance, which mainly (Table 3.5) decays to $N\pi$, we have also taken contributions from $P_{11}(1440)$, $S_{11}(1535)$, $S_{31}(1620)$, and $S_{11}(1650)$ spin half resonances and $D_{13}(1520)$, $D_{33}(1700)$, and $P_{13}(1720)$ spin three-half resonances and considered both s-channel and u-channel contributions. In the following, we present the formalism in brief which has been used for the NRB terms and the resonant spin half and spin three-half contributions to the one pion production processes.

The contribution from the NRB terms in the case of CC ($W^i \equiv W^{\pm}$; $i = \pm$) and NC ($W^i \equiv Z^0$; $i = 0$) reactions $W^i N \rightarrow N' \pi$ has been obtained using nonlinear sigma model [10, 160, 166] described in Section 3.3.1. In the lowest order, the contributions to the hadronic current are written as [160]:

$$j^\mu|_{NP} = a \mathcal{A}^{NP} \bar{u}(\vec{p}') \not{p}_\pi \gamma_5 \frac{\not{p} + \not{q} + M}{(p+q)^2 - M^2} [V_N^\mu(Q^2) - A_N^\mu(Q^2)] u(\vec{p}), \quad (3.83)$$

$$j^\mu|_{CP} = a \mathcal{A}^{CP} \bar{u}(\vec{p}') [V_N^\mu(Q^2) - A_N^\mu(Q^2)] \frac{\not{p}' - \not{q} + M}{(p'-q)^2 - M^2} \not{p}_\pi \gamma_5 u(\vec{p}), \quad (3.84)$$

$$j^\mu|_{CT} = a \mathcal{A}^{CT} \bar{u}(\vec{p}') \gamma^\mu (g_A f_{CT}^V(Q^2) \gamma_5 - f_\rho ((q - p_\pi)^2)) u(\vec{p}), \quad (3.85)$$

$$j^\mu|_{PP} = a \mathcal{A}^{PP} f_\rho ((q - p_\pi)^2) \frac{q^\mu}{m_\pi^2 + Q^2} \bar{u}(\vec{p}') \not{q} u(\vec{p}), \quad (3.86)$$

$$j^\mu|_{PF} = a \mathcal{A}^{PF} f_{PF}(Q^2) \frac{(2p_\pi - q)^\mu}{(p_\pi - q)^2 - m_\pi^2} 2M \bar{u}(\vec{p}') \gamma_5 u(\vec{p}), \quad (3.87)$$

with $a = \cos \theta_C$ for CC induced process. q is the four momentum transfer ($= k - k'$), $q^2 (= -Q^2) \leq 0$ and p_π is the pion momentum and m_π is the mass of pion. The constant factor \mathcal{A}^i , $i = NP, CP, CT, PP$ and PF , and are tabulated in Table 3.5.

The vector ($V_N^\mu(Q^2)$) and axial-vector ($A_N^\mu(Q^2)$) currents for nucleon pole diagrams in the case of CC and NC interactions are calculated neglecting SCC and are given by,

$$V_N^\mu(Q^2) = f_1(Q^2) \gamma^\mu + f_2(Q^2) i \sigma^{\mu\nu} \frac{q_\nu}{2M}, \quad A_N^\mu(Q^2) = \left(g_1(Q^2) \gamma^\mu + g_3(Q^2) \frac{q^\mu}{M} \right) \gamma_5, \quad (3.88)$$

Constant term \rightarrow	$\mathcal{A}(\text{CC } \nu)$			$\mathcal{A}(\text{CC } \bar{\nu})$			$\mathcal{A}(\text{NC } \nu(\bar{\nu}))$			
Final states \rightarrow	$p\pi^+$	$n\pi^+$	$p\pi^0$	$n\pi^-$	$n\pi^0$	$p\pi^-$	$n\pi^+$	$p\pi^0$	$p\pi^-$	$n\pi^0$
NP	0	$\frac{-ig_A}{\sqrt{2}f_\pi}$	$\frac{-ig_A}{2f_\pi}$	0	$\frac{ig_A}{2f_\pi}$	$\frac{-ig_A}{\sqrt{2}f_\pi}$	$\frac{-ig_A}{\sqrt{2}f_\pi}$	$\frac{-ig_A}{2f_\pi}$	$\frac{ig_A}{\sqrt{2}f_\pi}$	$\frac{-ig_A}{2f_\pi}$
CP	$\frac{-ig_A}{\sqrt{2}f_\pi}$	0	$\frac{ig_A}{2f_\pi}$	$\frac{-ig_A}{\sqrt{2}f_\pi}$	$\frac{-ig_A}{2f_\pi}$	0	$\frac{ig_A}{\sqrt{2}f_\pi}$	$\frac{-ig_A}{2f_\pi}$	$\frac{-ig_A}{\sqrt{2}f_\pi}$	$\frac{-ig_A}{2f_\pi}$
CT	$\frac{-i}{\sqrt{2}f_\pi}$	$\frac{i}{\sqrt{2}f_\pi}$	$\frac{i}{f_\pi}$	$\frac{-i}{\sqrt{2}f_\pi}$	$\frac{-i}{f_\pi}$	$\frac{i}{\sqrt{2}f_\pi}$	$\frac{\sqrt{2}i}{f_\pi}$	0	$\frac{-\sqrt{2}i}{f_\pi}$	0
PP	$\frac{i}{\sqrt{2}f_\pi}$	$\frac{-i}{\sqrt{2}f_\pi}$	$\frac{-i}{f_\pi}$	$\frac{i}{\sqrt{2}f_\pi}$	$\frac{i}{f_\pi}$	$\frac{-i}{\sqrt{2}f_\pi}$	$\frac{\sqrt{2}i}{f_\pi}$	0	$\frac{-\sqrt{2}i}{f_\pi}$	0
PF	$\frac{-ig_A}{\sqrt{2}f_\pi}$	$\frac{ig_A}{\sqrt{2}f_\pi}$	$\frac{ig_A}{f_\pi}$	$\frac{-ig_A}{\sqrt{2}f_\pi}$	$\frac{-ig_A}{f_\pi}$	$\frac{ig_A}{\sqrt{2}f_\pi}$	$\frac{\sqrt{2}ig_A}{f_\pi}$	0	$\frac{-\sqrt{2}ig_A}{f_\pi}$	0

Table 3.5: The values of constant term(\mathcal{A}^i) appearing in Eq. (3.87), where i corresponds to the nucleon pole (NP), cross nucleon pole (CP), contact term (CT), pion pole (PP) and pion in flight (PF) terms. f_π is pion weak decay constant and g_A is axial nucleon coupling.

I (J)	$\mathcal{C}^{\mathcal{R}}(\text{CC } \nu)$			$\mathcal{C}^{\mathcal{R}}(\text{CC } \bar{\nu})$		
	$p \rightarrow p\pi^+$	$n \rightarrow n\pi^+$	$n \rightarrow p\pi^0$	$n \rightarrow n\pi^-$	$p \rightarrow n\pi^0$	$p \rightarrow p\pi^-$
$\frac{3}{2} (\frac{3}{2})$	$\frac{\sqrt{3}f^*}{m_\pi}$	$\sqrt{\frac{1}{3}} \frac{f^*}{m_\pi}$	$-\sqrt{\frac{2}{3}} \frac{f^*}{m_\pi}$	$\frac{\sqrt{3}f^*}{m_\pi}$	$\sqrt{\frac{2}{3}} \frac{f^*}{m_\pi}$	$\sqrt{\frac{1}{3}} \frac{f^*}{m_\pi}$
$\frac{3}{2} (\frac{1}{2})$	$\frac{\sqrt{3}f^*}{m_\pi}$	$\sqrt{\frac{1}{3}} \frac{f^*}{m_\pi}$	$-\sqrt{\frac{2}{3}} \frac{f^*}{m_\pi}$	$\frac{\sqrt{3}f^*}{m_\pi}$	$\sqrt{\frac{2}{3}} \frac{f^*}{m_\pi}$	$\sqrt{\frac{1}{3}} \frac{f^*}{m_\pi}$
$\frac{1}{2} (\frac{3}{2})$	0	$\sqrt{2} \frac{f^*}{m_\pi}$	$\frac{f^*}{m_\pi}$	0	$-\frac{f^*}{m_\pi}$	$\sqrt{2} \frac{f^*}{m_\pi}$
$\frac{1}{2} (\frac{1}{2})$	0	$\sqrt{2} \frac{f^*}{m_\pi}$	$\frac{f^*}{m_\pi}$	0	$-\frac{f^*}{m_\pi}$	$\sqrt{2} \frac{f^*}{m_\pi}$

Table 3.6: Coupling constant($\mathcal{C}^{\mathcal{R}}$) for spin and isospin $\frac{1}{2}$ and spin $\frac{3}{2}$ resonances for the charge current (anti)neutrino induced pion production. Here f^* stands for $\mathcal{R} \rightarrow N\pi$ coupling which for $\Delta(1232)$ resonance is $g_{\Delta N\pi}$ and $g_{R\frac{1}{2}N\pi}$ ($g_{R\frac{3}{2}N\pi}$) for spin $\frac{1}{2}$ ($\frac{3}{2}$) resonances.

where $f_{1,2}(Q^2)$ and $g_{1,3}(Q^2)$ are the vector and axial-vector form factors for the nucleons. The form factors $f_{1,2}(Q^2)$ are expressed in terms of the electromagnetic nucleon form factors ($F_{1,2}^{p,n}(Q^2)$) as:

$$f_{1,2}(Q^2) = F_{1,2}^p(Q^2) - F_{1,2}^n(Q^2), \quad (3.89)$$

where $F_i^{p,n}(Q^2)$; $i = 1, 2$ are the Dirac and Pauli form factors of the nucleons. These form factors are in turn expressed in terms of the experimentally determined Sachs' electric $G_E^{p,n}(Q^2)$ and magnetic $G_M^{p,n}(Q^2)$ form factors [185].

On the other hand, the axial-vector form factor ($g_1(Q^2)$) is generally taken to be of the dipole form and is given by

$$g_1(Q^2) = g_A(Q^2) = g_A(0) \left(1 + \frac{Q^2}{M_A^2}\right)^{-2}, \quad (3.90)$$

where $g_A(0)$ is the axial charge and is obtained from the QE neutrino and antineutrino scattering as well as from the pion electro-production data. We have used $g_A(0)=1.267$ and $M_A=1.026\text{GeV}$ [203], in the numerical calculations.

The next contribution from the axial-vector part comes from the pseudoscalar form factor $g_3(Q^2)$, the determination of which is based on PCAC and PDDAC and is related to $g_1(Q^2)$ through the relation

$$g_3(Q^2) = \frac{2M^2 g_1(Q^2)}{m_\pi^2 + Q^2}. \quad (3.91)$$

In order to conserve vector current for CC processes at the weak vertex, the two form factors viz. $f_{PF}(Q^2)$ and $f_{CT}^V(Q^2)$ are expressed in terms of the isovector nucleon form factor as [160]

$$f_{PF}(Q^2) = f_{CT}^V(Q^2) = 2f_1(Q^2). \quad (3.92)$$

The $\pi\pi NN$ vertex has the dominant ρ -meson cloud contribution and following Ref. [160], we have introduced ρ -form factor ($f_\rho(Q^2)$) at $\pi\pi NN$ vertex and taken it to be of monopole form:

$$f_\rho(Q^2) = \frac{1}{1 + Q^2/m_\rho^2}; \quad \text{with } m_\rho = 0.776 \text{ GeV}. \quad (3.93)$$

$f_\rho(Q^2)$ also has been used with axial part of the CT diagram in order to be consistent with the assumption of PCAC.

We have already discussed in Section 3.3.6, the excitation and decay of spin $\frac{1}{2}$ and $\frac{3}{2}$ resonances into a meson and a baryon in the final state. In the case of single pion production, we have taken the contribution from spin $\frac{1}{2}$ resonances like $P_{11}(1440)$, $S_{11}(1535)$, $S_{31}(1620)$, $S_{11}(1650)$, and spin $\frac{3}{2}$ resonances like $P_{33}(1232)$, $D_{13}(1520)$, $D_{33}(1700)$, $P_{13}(1720)$.

I(J)	$\mathcal{C}^{\mathcal{R}}(\text{NC } \bar{\nu}(\bar{\nu}))$			
	$p \rightarrow n\pi^+$	$p \rightarrow p\pi^0$	$n \rightarrow p\pi^-$	$n \rightarrow n\pi^0$
$\frac{3}{2} \left(\frac{3}{2}\right)$	$\frac{1}{\sqrt{3}} \frac{f^*}{m_\pi}$	$\sqrt{\frac{2}{3}} \frac{f^*}{m_\pi}$	$-\frac{1}{\sqrt{3}} \frac{f^*}{m_\pi}$	$\sqrt{\frac{2}{3}} \frac{f^*}{m_\pi}$
$\frac{3}{2} \left(\frac{1}{2}\right)$	$\frac{1}{\sqrt{3}} \frac{f^*}{m_\pi}$	$\sqrt{\frac{2}{3}} \frac{f^*}{m_\pi}$	$-\frac{1}{\sqrt{3}} \frac{f^*}{m_\pi}$	$\sqrt{\frac{2}{3}} \frac{f^*}{m_\pi}$
$\frac{1}{2} \left(\frac{3}{2}\right)$	$-\frac{1}{\sqrt{2}} \frac{f^*}{m_\pi}$	$\frac{1}{2} \frac{f^*}{m_\pi}$	$\frac{1}{\sqrt{2}} \frac{f^*}{m_\pi}$	$\frac{1}{2} \frac{f^*}{m_\pi}$
$\frac{1}{2} \left(\frac{1}{2}\right)$	$-\frac{1}{\sqrt{2}} \frac{f^*}{m_\pi}$	$\frac{1}{2} \frac{f^*}{m_\pi}$	$\frac{1}{\sqrt{2}} \frac{f^*}{m_\pi}$	$\frac{1}{2} \frac{f^*}{m_\pi}$

Table 3.7: Coupling constant($\mathcal{C}^{\mathcal{R}}$) for spin and isospin $\frac{1}{2}$ and spin $\frac{3}{2}$ resonances for the charge current (anti)neutrino induced pion production. Here f^* stands for $\mathcal{R} \rightarrow N\pi$ coupling which for $\Delta(1232)$ resonance is $g_{\Delta N\pi}$ and $g_{R\frac{1}{2}N\pi}$ ($g_{R\frac{3}{2}N\pi}$) for spin $\frac{1}{2}$ ($\frac{3}{2}$) resonances.

It should be noted that in the vector sector, the helicity amplitudes for all these resonance excitations are given by the MAID parameterization [262]. In the case of spin $\frac{1}{2}$ resonances, the s-channel and u-channel hadronic currents for the positive and negative parity resonances are given in Eqs. (3.46) and (3.47), with the explicit form of the vector and axial-vector form factors given in Eqs. (3.33) and (3.34) for the isospin $\frac{1}{2}$ resonances and in Eqs. (3.42) and (3.43) for the isospin $\frac{3}{2}$ resonances. The coefficient \mathcal{C} for CC and NC induced processes is given in Tables 3.6 and 3.7, respectively. Similarly in the case of positive and negative parity spin $\frac{3}{2}$ resonances, the general expression of the hadronic current for the s- and u-channels are given in Eqs. (3.65) and (3.66). The vector and axial-vector form factors used in the case of isospin $\frac{1}{2}$ resonances are given in Eqs. (3.52) and (3.64), respectively while for the isospin $\frac{3}{2}$ resonances, these form factors are given in Eqs. (3.53) and (3.64).

The axial-vector form factors as discussed in Eqs. (3.59) and (3.60) along with the vector form factors given in Eq. (3.58), have been used to analyze the present experimental cross sections for the weak pion production. Most of the recent theoretical calculations [267, 160, 265, 296] use a simpler modification to the dipole form viz.

$$C_5^A(Q^2) = \frac{C_5^A(0)}{(1 + Q^2/M_{A\Delta}^2)^2} \frac{1}{1 + Q^2/(3M_{A\Delta}^2)}. \quad (3.94)$$

With the nonvanishing axial-vector form factors determined in terms of $C_5^A(Q^2)$ and the vector form factors determined from the electron scattering experiments, the weak pion production cross section is described in terms of $C_5^A(Q^2)$ with the parameters $C_5^A(0)$ and axial mass $M_{A\Delta}$. Keeping $M_{A\Delta} = 1.026\text{GeV}$ and then varying $C_5^A(0)$, we obtain the best possible value to be $C_5^A(0) = 1$ to obtain a good description of reanalyzed data [299] of ANL and BNL experiments for $\nu_\mu p \rightarrow \mu^- p\pi^+$ reaction [166]. We find that while fitting the reanalyzed data for the reaction $\nu_\mu p \rightarrow \mu^- p\pi^+$, the contributions to the cross section is predominantly obtained from $\Delta(1232)$ resonant terms and the background terms give small contribution. This has been further discussed in Section 3.4.3.

3.4.2. Neutral current (anti)neutrino induced processes

In this section, we briefly discuss the single pion production induced by NC (NC1 π). The older data on NC1 π production are available from ANL [300] and Gargamelle [301] experiments. Recently, NC1 π production measurements have been performed by the MiniBooNE [302], K2K [303], SciBooNE [304], MicroBooNE [305], and other collaborations. The NC π^0 production in neutrino interactions plays an important role in the background studies of $\nu_\mu \leftrightarrow \nu_e$ or $\bar{\nu}_\mu \leftrightarrow \bar{\nu}_e$ oscillations in the appearance mode as well as in discriminating between $\nu_\mu \rightarrow \nu_\tau$ and $\nu_\mu \rightarrow \nu_s$ modes. Furthermore, in the reconstruction of neutrino energy using QE events like $\nu_e + n \rightarrow e^- + p$ or $\bar{\nu}_e + p \rightarrow e^+ + n$, a missing electron or positron produced by the photon from the π^0 decay may be mistaken as QE event. Moreover, NC induced pion production may also help to distinguish between the production of ν_τ and $\bar{\nu}_\tau$ in some oscillation scenarios at neutrino energies much below the τ production threshold but above the pion threshold [306].

The NC induced (anti)neutrino scattering processes form the free nucleon target are given by:

$$\nu_l(\bar{\nu}_l)p \rightarrow \nu_l(\bar{\nu}_l)n\pi^+, \quad \nu_l(\bar{\nu}_l)p \rightarrow \nu_l(\bar{\nu}_l)p\pi^0, \quad \nu_l(\bar{\nu}_l)n \rightarrow \nu_l(\bar{\nu}_l)n\pi^0, \quad \nu_l(\bar{\nu}_l)n \rightarrow \nu_l(\bar{\nu}_l)p\pi^-. \quad (3.95)$$

In the case of NC induced processes, the expressions for the different terms contributing to the NRB are given in Eqs. (3.83)–(3.87), with $a = 1$ and the values of \mathcal{C} for the different pion production channels given in Table 3.5. The neutral current vector form factors are expressed as:

$$f_{1,2}(Q^2) \xrightarrow{\text{for } p} \tilde{f}_{1,2}^p(Q^2) = \left(\frac{1}{2} - 2\sin^2\theta_W\right) F_{1,2}^p(Q^2) - \frac{1}{2}F_{1,2}^n(Q^2), \quad (3.96)$$

$$f_{1,2}(Q^2) \xrightarrow{\text{for } n} \tilde{f}_{1,2}^n(Q^2) = \left(\frac{1}{2} - 2\sin^2\theta_W\right) F_{1,2}^n(Q^2) - \frac{1}{2}F_{1,2}^p(Q^2), \quad (3.97)$$

where θ_W is the weak mixing angle, and the axial-vector form factor is given by

$$\tilde{g}_1^{p,n}(Q^2) = \pm \frac{1}{2} g_1(Q^2), \quad (3.98)$$

where the plus (minus) sign stands for proton (neutron) target. The contribution of the pseudoscalar form factor being proportional to the lepton mass vanishes for NC induced processes. The structure of the hadronic current for NC induced

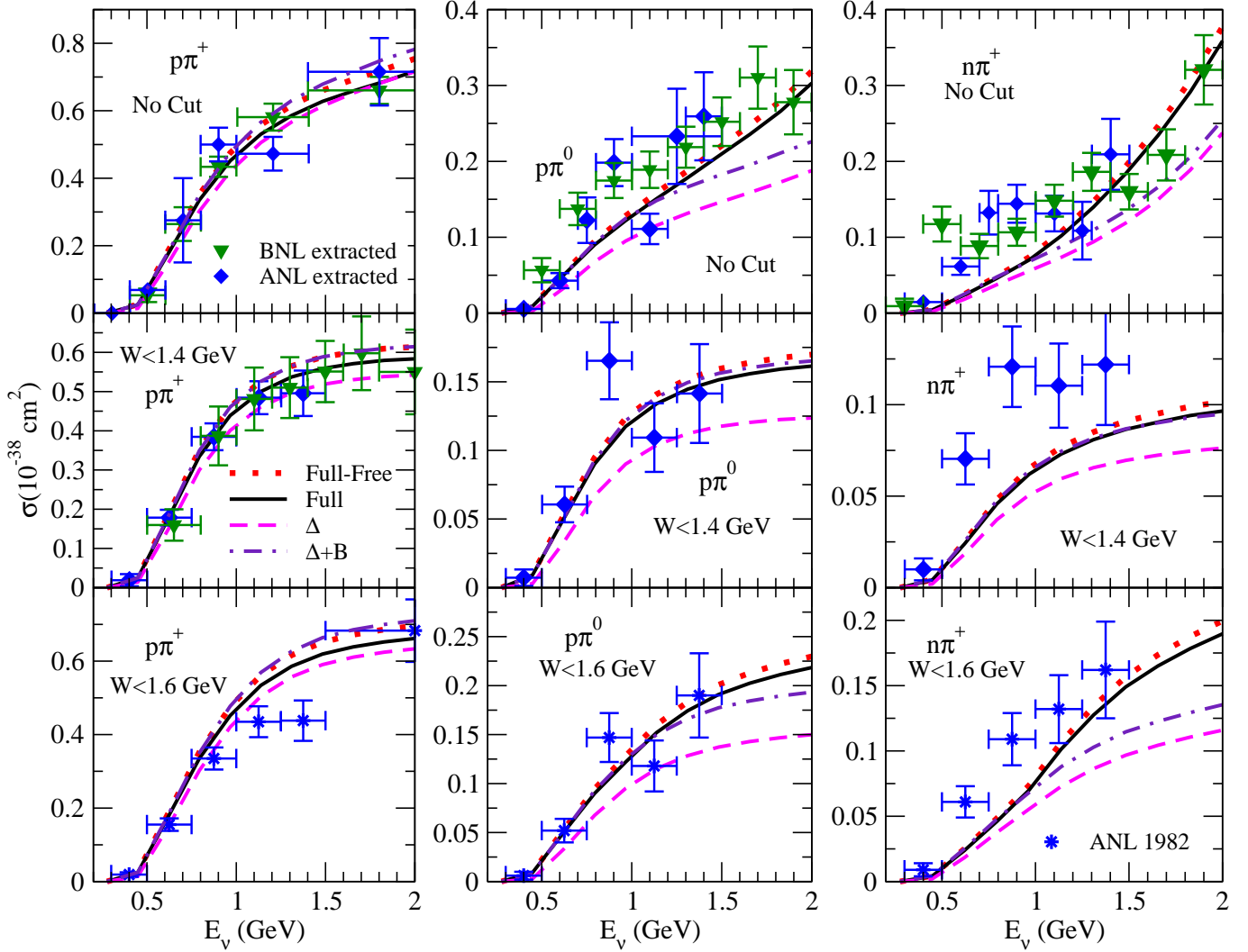


Figure 3.5: Total scattering cross section for CC neutrino induced pion production processes: $\nu_\mu p \rightarrow \mu^- p\pi^+$ (left panel), $\nu_\mu n \rightarrow \mu^- p\pi^0$ (central panel), $\nu_\mu n \rightarrow \mu^- n\pi^+$ (right panel). The dashed line is the result calculated in the $\Delta(1232)$ dominance model, dashed-dotted line is the result obtained when we include NRB terms in our calculations. The solid line is the result of our full calculation when other resonances like $P_{11}(1440)$, $D_{13}(1520)$, $S_{11}(1535)$, $S_{31}(1620)$, $S_{11}(1650)$, $D_{33}(1700)$ and $P_{13}(1720)$ are also included. All the above three cases are with deuteron effect. The dotted line is the result of the full calculation without deuteron effect. The results in the top panels are obtained when we have not included any cut on the invariant mass. The middle panel shows the results with a cut of 1.4 GeV on the W , while in the bottom panel a cut of $W < 1.6$ GeV is introduced while calculating total scattering cross section. Data points quoted as ANL extracted and BNL extracted are the reanalyzed data by Wilkinson et al. [299] and Rodrigues et al. [307]. Other data points in figures are the results from ANL [268] experiment.

s-channel and u-channel spin as well as isospin $\frac{1}{2}$ and $\frac{3}{2}$ resonances is similar to that of CC induced reactions. In the case of NC induced single pion production, only the couplings $\mathcal{C}^{\mathcal{R}}$ and the form factors corresponding to $N \rightarrow \mathcal{R}$ transitions are different as compared to CC induced processes. In Section 3.3.7, we have already discussed in detail NC vector and axial-vector form factors for spin $\frac{1}{2}$ and $\frac{3}{2}$ resonances and NC couplings $\mathcal{C}^{\mathcal{R}}$ are given in Table 3.7. For the numerical calculations, we have used NC vector and axial-vector form factors described in Section 3.3.7 with the hadronic current given in Eqs. (3.46) and (3.47) for spin $\frac{1}{2}$ resonances and Eqs. (3.65) and (3.66) for spin $\frac{3}{2}$ resonances.

3.4.3. Results and discussion

In this section, we present the results of the numerical calculations and discuss the findings. Due to the limitations on the validity of the nonlinear sigma model at higher energies [160], we have put a constraint on W as $W_{min} = M + m_\pi$

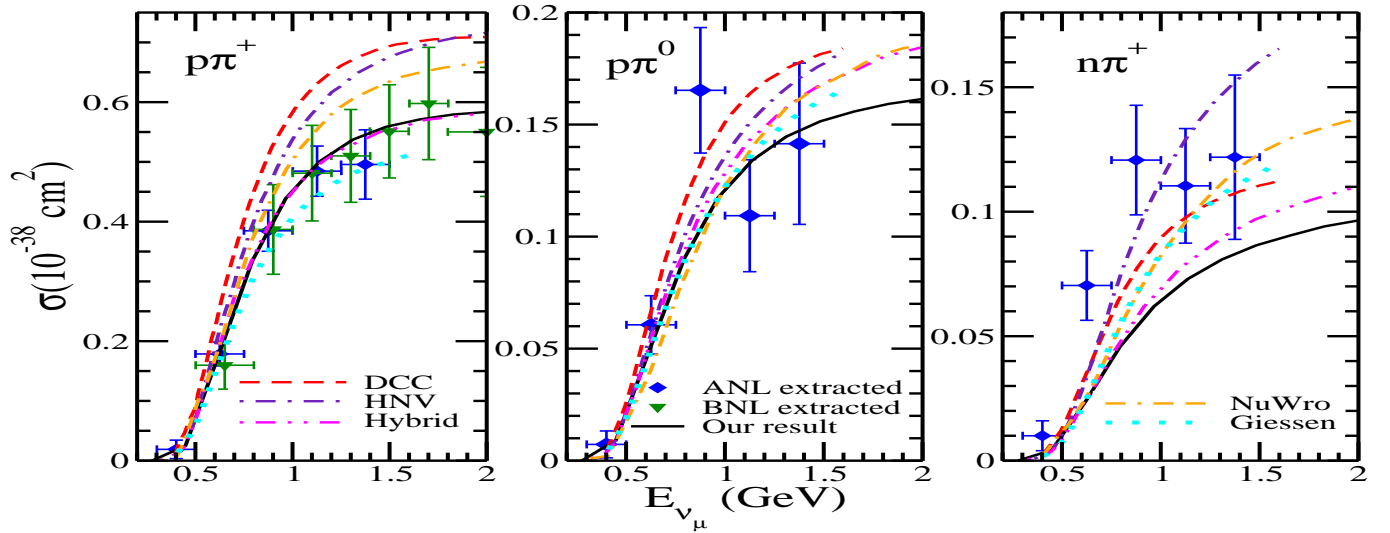


Figure 3.6: σ vs. $E_{\nu\mu}$ for the processes $\nu_{\mu}p \rightarrow \mu^{-}p\pi^{+}$ (left panel), $\nu_{\mu}n \rightarrow \mu^{-}p\pi^{0}$ (central panel), $\nu_{\mu}n \rightarrow \mu^{-}n\pi^{+}$ (right panel) with $W < 1.4$ GeV. Solid line is the result of the present model with deuteron effect; compared with other theoretical models like DCC [309] (dashed line), HNV [160] (dashed-dotted line), Hybrid [297] (double-dotted-dashed line), NuWro [297] (double-dashed-dotted line) and Giessen [296] (dotted line). Data points have the same meaning as in Fig. 3.5.

and $W_{max} = 1.2$ GeV while evaluating the NRB terms. This constraint on W (i.e. $M + m_{\pi} \leq W \leq 1.2$ GeV) has been put in all numerical evaluations while considering NRB contribution.

Since earlier experiments to measure CC neutrino induced single pion production were mainly performed using hydrogen/deuteron target like the experiments at ANL [268] and BNL [269], therefore, deuteron correction factor must be taken into account. In recent analyses by Wilkinson et al. [299] and Rodrigues et al. [307], experimental results of ANL [268] and BNL [269] have been normalized to the deuteron data. Therefore, we have taken deuteron effect by writing [166]:

$$\left(\frac{d\sigma}{dQ^2 dW} \right)_{\nu d} = \int d\vec{p}_p^d |\Psi_d(\vec{p}_p^d)|^2 \frac{M}{E_p^d} \left(\frac{d\sigma}{dQ^2 dW} \right)_{\text{off shell}}, \quad (3.99)$$

where the four momentum of the proton inside the deuteron is described by $p^{\mu} = (E_p^d, \vec{p}_p^d)$ with $E_p^d (= M_{\text{Deuteron}} - \sqrt{M^2 + |\vec{p}_p^d|^2})$ as the energy of the off shell proton inside the deuteron and M_{Deuteron} is the deuteron mass. $\left(\frac{d\sigma}{dQ^2 dW} \right)_{\text{off shell}}$ is obtained by using Eq. (3.2). In the above expression $\Psi_d(\vec{p}_d)$ is the deuteron wave function taken from the works of Lacombe et al. [308].

We have calculated the total scattering cross section for CC neutrino induced pion production processes and the results are presented in Fig. 3.5. The experimental data for $\pi^{+}p$ channel where no cut on W is applied is the reanalyzed data by Wilkinson et al. [299] of the ANL [268] and BNL [269] experiments. The experimental data for $\pi^{0}p$ and $\pi^{+}n$ channels for no cut on W are the reanalyzed data by Rodrigues et al. [307] of the ANL [268], BNL [269], and other experiments. While for all the three channels with a cut of 1.4 GeV on W , we have used the reanalyzed data by Rodrigues et al. [307] and for all the pion production channels with $W < 1.6$ GeV, the experimental data are of ANL [268] experiment.

- (i) In the case of $\nu_{\mu}p \rightarrow \mu^{-}p\pi^{+}$ induced reaction, the main contribution to the total scattering cross section comes from the $\Delta(1232)$ resonance when no cut on W is applied while when this cut is applied there is some contribution from the higher resonances and the background terms which are considered in this work. It should be noticed that in the case when no cut on W is applied or when $W < 1.4$ GeV is considered, our theoretical results are in very good agreement with the reanalyzed experimental data by Wilkinson et al. [299] and Rodrigues et al. [307]. While in the case when $W < 1.6$ GeV cut is applied, we are consistent with the experimental data obtained by the ANL [268]. Quantitatively, we find that due to the presence of the NRB terms there is an increase in the cross section which is about 14% at $E_{\nu\mu} = 1$ GeV and becomes $\sim 9\%$ at $E_{\nu\mu} = 2$ GeV, when no cut on W is applied. However, when the cuts on W are applied, then due to the presence of background contributions, this increase in the cross section further increases and become $\sim 13\%$ at 2 GeV for $W < 1.4$ GeV and 12% for $W < 1.6$ GeV.
- (ii) For $\nu_{\mu}n \rightarrow \mu^{-}p\pi^{0}$ as well as $\nu_{\mu}n \rightarrow \mu^{-}n\pi^{+}$ processes, there are significant contributions from the NRB terms as well as other higher resonant terms besides the $\Delta(1232)$ dominance. In the case of $\nu_{\mu}n \rightarrow \mu^{-}p\pi^{0}$ our results with deuteron effects are in a good agreement with the reanalyzed data as well as with the original data from ANL experiment at $W < 1.6$ GeV. Due to the presence of the background terms, without any constraint on W , the total increase is about 32% at $E_{\nu\mu} = 1$ GeV which becomes 20% at $E_{\nu\mu} = 2$ GeV. With the inclusion of higher resonances,

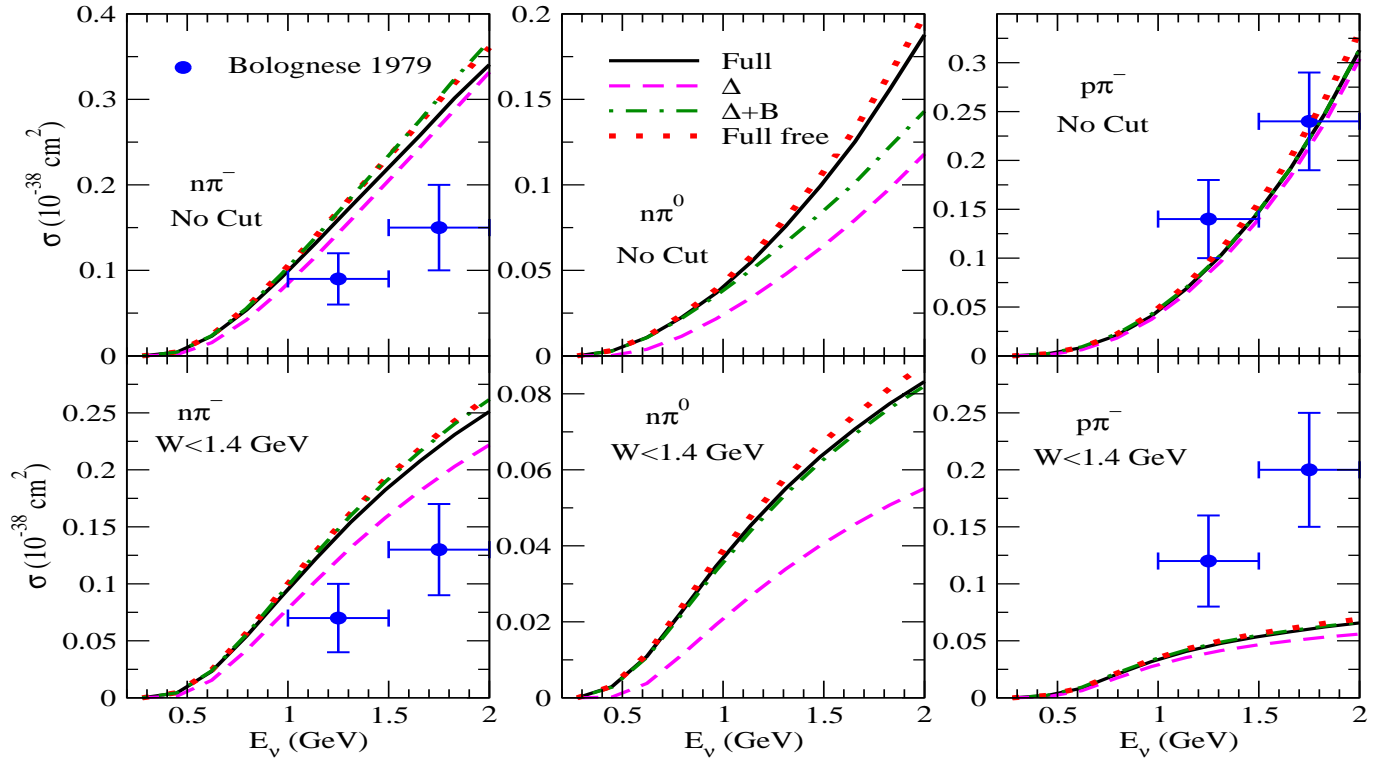


Figure 3.7: σ vs. $E_{\bar{\nu}_\mu}$ for CC induced $\bar{\nu}_\mu n \rightarrow \mu^+ n \pi^-$ (left panel), $\bar{\nu}_\mu p \rightarrow \mu^+ n \pi^0$ (central panel), and $\bar{\nu}_\mu p \rightarrow \mu^+ p \pi^-$ (right panel) processes, with deuteron effect. Data points are the experimental results from Ref. [310]. Lines have the same meaning as in Fig. 3.5.

there is a further increase of about 3% at $E_{\nu_\mu} = 1$ GeV and 40% at $E_{\nu_\mu} = 2$ GeV. It may be observed from the figure the our results for without cut on W and with a cut of $W < 1.6$ GeV are quite consistent with the experimental data for the $n\pi^+$ channel. The net contribution to the total pion production due to the presence of the NRB terms in $\nu_\mu n \rightarrow \mu^- n \pi^+$ reaction results in an increase in the cross section of about 22% at $E_{\nu_\mu} = 1$ GeV which becomes 8% at $E_{\nu_\mu} = 2$ GeV with no cut on W . When other higher resonances are also taken into account there is further increase in the cross section by about 3% at $E_{\nu_\mu} = 1$ GeV which becomes 40% at $E_{\nu_\mu} = 2$ GeV. Thus, we find that the inclusion of higher resonant terms lead to a significant increase in the cross section for $\nu_\mu n \rightarrow \mu^- n \pi^+$ and $\nu_\mu n \rightarrow \mu^- p \pi^0$ processes. Furthermore, it may also be concluded from the above observations that contribution from NRB terms decreases with the increase in neutrino energy, while the total scattering cross section increases when we include other higher resonances in our calculations. When a cut of 1.4 GeV or 1.6 GeV on the CM energy is applied, then due to the presence of background terms, the increase in the cross section is about 24% at $E_{\nu_\mu} = 1$ GeV which becomes about 20% at $E_{\nu_\mu} = 2$ GeV for $\nu_\mu n \rightarrow \mu^- n \pi^+$ reaction. When higher resonances are also taken into account there is a further increase in the cross section which is about 8% at $E_{\nu_\mu} = 1$ GeV and 2% at $E_{\nu_\mu} = 2$ GeV for $W < 1.6$ GeV. Similarly, in the case of $\nu_\mu n \rightarrow \mu^- p \pi^0$ there is a significant increase in the total cross section due to the presence of the NRB terms and higher resonances.

In Fig. 3.6, we have compared the theoretical results for the single pion production induced by neutrinos when a cut of 1.4 GeV is applied on W , obtained in the different models like the present model (Fig 3.5), the dynamical coupled channel (DCC) model by Nakamura et al. [309], the HNV model by Hernandez et al. [160], the extension of HNV model by incorporating Regge model at high energies (Hybrid) by Gonzalez-Jimenez et al. [297], the results from NuWro [297] Monte Carlo generator, and the Giessen model by Lalakulich et al. [296]. It may be observed from the figure that in the case of $p\pi^+$ channel, the results obtained in our model are quite consistent with the results obtained by the hybrid model and are in a very good agreement with the reanalyzed data of ANL [268] and BNL [269] by Wilkinson et al. [299] and Rodrigues et al. [307]. However, the results obtained in the other models like DCC, HNV, etc., are higher than the results obtained by us as well as the experimental data, but are consistent with one another. Moreover, the results obtained by the Giessen group [296] are lower than our results. In the case of $p\pi^0$ channel, our results are in a quite good agreement with the experimental data, while the results obtained in the other theoretical models are higher than our results. At energies $E_{\nu_\mu} < 0.8$ GeV, the results obtained in the various models are consistent with each other. Furthermore, in the case of $n\pi^+$ production, our results are smaller than the experimental data, while the other theoretical models give higher values of the cross section than obtained in the present model. In this case, the results obtained by HNV model as well as by the NuWro generator show a good agreement with the experimental data. It may be noticed from the figure that there is a large difference among the various theoretical models and Monte Carlo generators available in the literature.

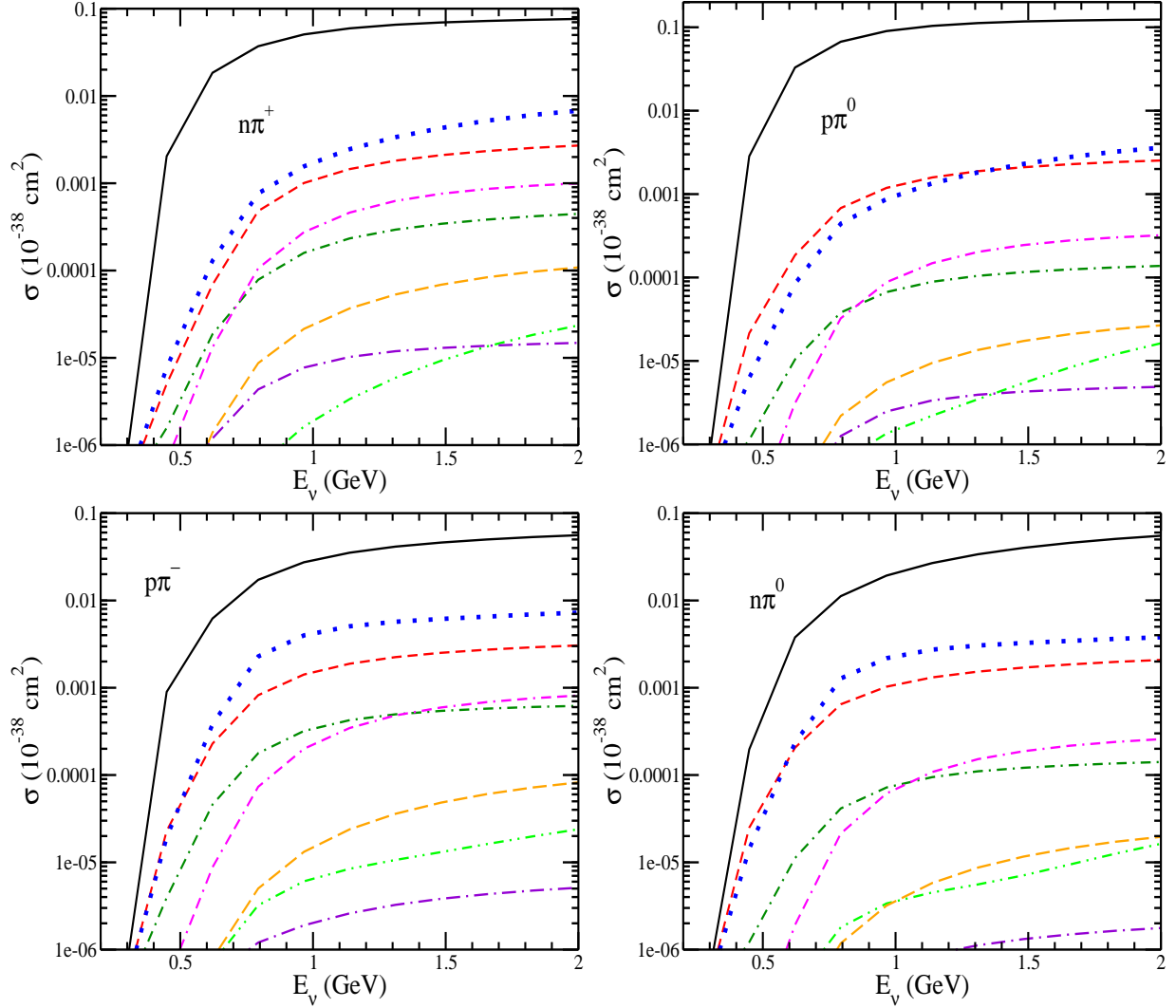


Figure 3.8: The results are presented for the total scattering cross section for $\nu_\mu n \rightarrow \mu^- n \pi^+$ (upper left panel), $\nu_\mu n \rightarrow \mu^- p \pi^0$ (upper right panel), $\bar{\nu}_\mu p \rightarrow \mu^+ p \pi^-$ (lower left panel), and $\bar{\nu}_\mu p \rightarrow \mu^+ n \pi^0$ (lower right panel) processes where the individual contribution of various resonances like $P_{33}(1232)$ (solid line), $P_{11}(1440)$ (dotted line), $D_{13}(1520)$ (short dashed line), $S_{11}(1535)$ (double-dashed-dotted line), $S_{31}(1620)$ (long dashed-dotted line), $S_{11}(1650)$ (long dashed line), $D_{33}(1700)$ (short dashed-dotted line) and $P_{13}(1720)$ (double-dotted-dashed line) have been shown.

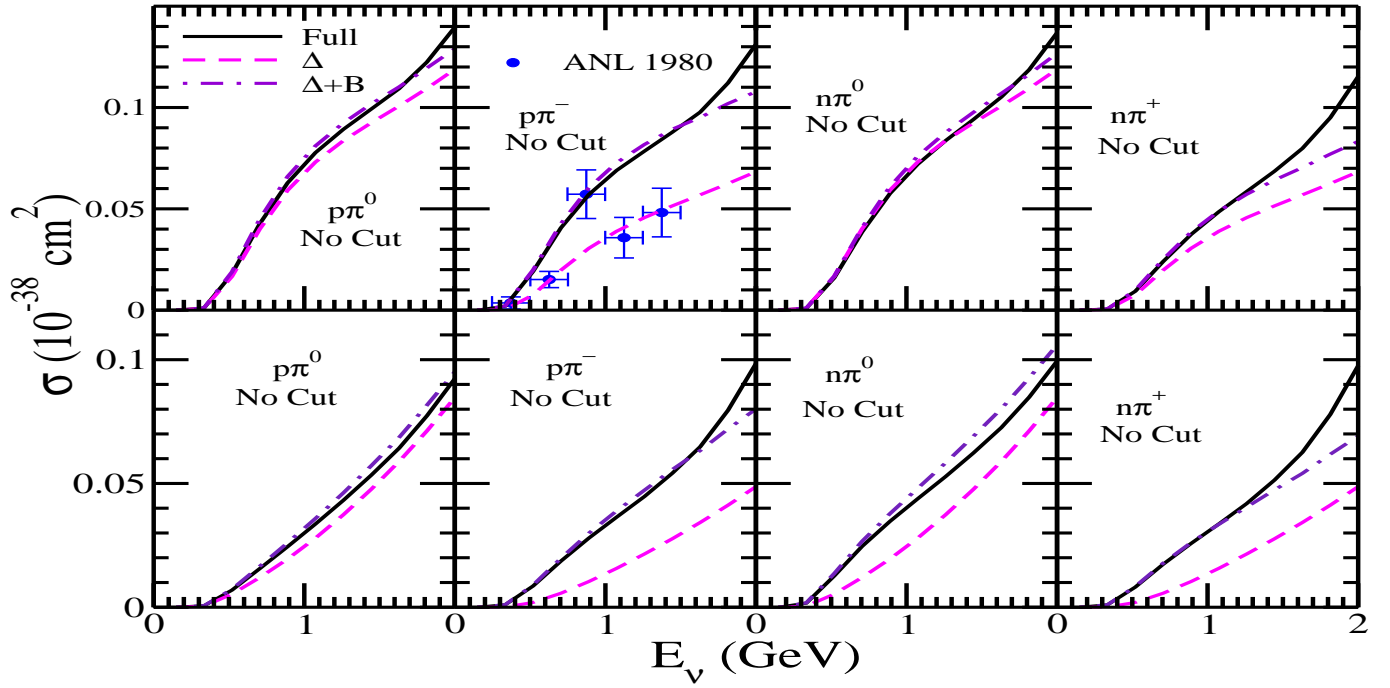


Figure 3.9: Total scattering cross section for NC neutrino (upper panel) and antineutrino (lower panel) induced pion production processes with deuteron effect. The results are presented from the left for $\nu p \rightarrow \nu p \pi^0$, $\nu n \rightarrow \nu p \pi^-$, $\nu n \rightarrow \nu n \pi^0$ and $\nu p \rightarrow \nu n \pi^+$ processes. Data points are the experimental results from Ref. [300]. The theoretical results presented here should be corrected for NME before making any comparison with the experimental data. Lines have the same meaning as in Fig. 3.5.

In order to understand the dynamics of the single pion production, which is the simplest IE process, further theoretical and experimental work is required.

In Fig. 3.7, we have shown the results for CC antineutrino induced pion production processes. These results are presented in the $\Delta(1232)$ dominance model, including NRB terms as well as with our full model.

- (i) In the case of $\bar{\nu}_\mu n \rightarrow \mu^+ n \pi^-$ reaction, there is very small contribution from the higher resonances other than $\Delta(1232)$ resonance for both cases i.e., when the results are obtained with no cut on W as well as when a cut of $W < 1.4$ GeV is applied. The inclusion of NRB terms increases the cross section by around 24% (26%) at $E_{\bar{\nu}_\mu} = 1$ (2) GeV when no cut on W is applied, which becomes around 27% (17%) at $E_{\bar{\nu}_\mu} = 1$ (2) GeV when a cut of $W < 1.4$ GeV is applied.
- (ii) In $\bar{\nu}_\mu p \rightarrow \mu^+ n \pi^0$ reaction, inclusion of NRB terms increases the cross section by around 62% (21%) at $E_{\bar{\nu}_\mu} = 1$ (2) GeV when no cut on W is applied, and becomes 76% (50%) at $E_{\bar{\nu}_\mu} = 1$ (2) GeV when a cut of $W < 1.4$ GeV is applied. When other higher resonances are included, the cross section further increases by $\sim 10\%$ (40%) at $E_{\bar{\nu}_\mu} = 1$ (2) GeV at no cut and becomes almost 10% (6%) at $E_{\bar{\nu}_\mu} = 1$ (2) GeV.
- (iii) In the case of $\bar{\nu}_\mu p \rightarrow \mu^+ p \pi^-$ reaction, when no cut on W is applied the effect of NRB terms as well as contribution from higher resonances is very small even at $E_{\bar{\nu}_\mu} = 2$ GeV. We find the theoretical results to be consistent with the experimental data. However, when $W < 1.4$ GeV cut is applied, due to the inclusion of NRB terms, the cross section increases by about 20% at $E_{\bar{\nu}_\mu} = 1$ GeV, which becomes 18% at $E_{\bar{\nu}_\mu} = 2$ GeV. While in the case of $p \pi^-$ production, there is almost negligible contribution from the higher resonances.

We have compared the present results with the experimental data of Gargamelle experiment [310] performed at CERN PS where propane was used as the nuclear target. Since propane is a composite target with more than one nuclear target, therefore, the cross sections would get modulated due to NME. Thus, the theoretical results presented in Fig. 3.7 should be corrected for NME before making any comparison with the experimental data. We would like to point out that, in our earlier works [311, 312, 313] on CC and NC pion production in the $\Delta(1232)$ dominance model, we have observed that NME reduces the cross section significantly when the calculations are performed for nuclear targets, which will be discussed later in Section 5.5.

To explicitly show the contribution of individual resonances to the total scattering cross section, in Fig. 3.8, we have presented the results for $\nu_\mu n \rightarrow \mu^- n \pi^+$, $\nu_\mu n \rightarrow \mu^- p \pi^0$, $\bar{\nu}_\mu p \rightarrow \mu^+ p \pi^-$, and $\bar{\nu}_\mu p \rightarrow \mu^+ n \pi^0$ processes as a function of incoming (anti)neutrino energy. It may be observed that the dominant contribution comes from $\Delta(1232)$ resonance, followed by $P_{11}(1440)$ and $D_{13}(1520)$ resonances. However, the contribution for the neutrino and the antineutrino induced processes are not similar, for example, larger $\Delta(1232)$ dominance may be observed in the neutrino case than in the case

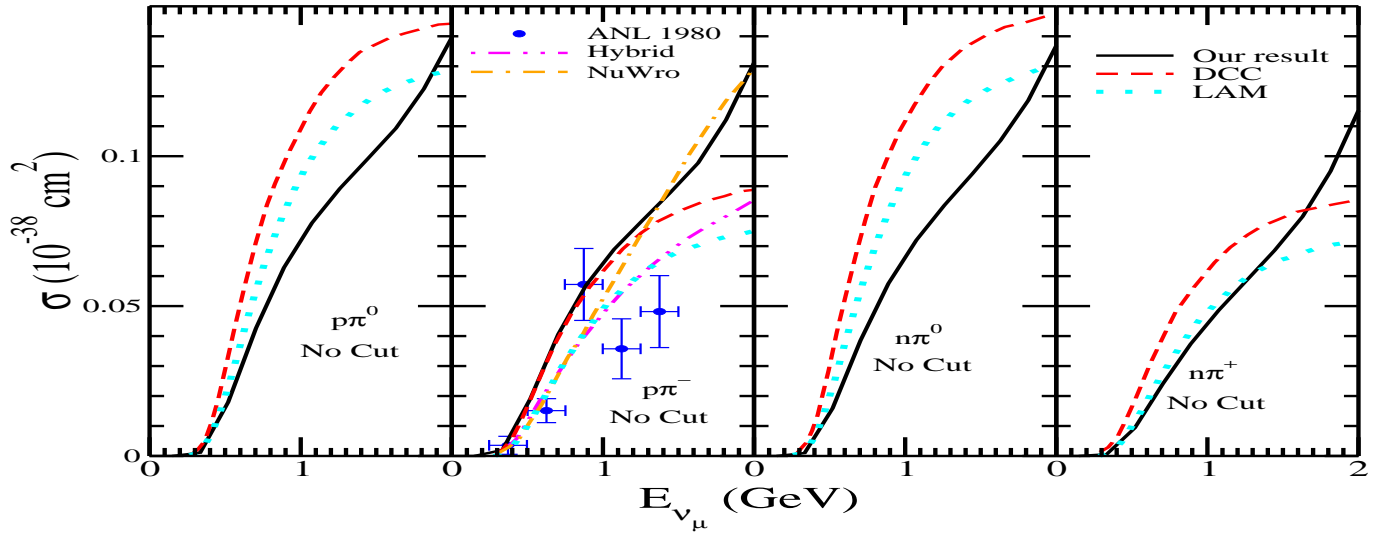


Figure 3.10: Comparison of our results for the total scattering cross section for NC neutrino induced pion production processes with deuteron effect. The results are presented from the left for $\nu_\mu p \rightarrow \nu_\mu p \pi^0$, $\nu_\mu n \rightarrow \nu_\mu p \pi^-$, $\nu_\mu n \rightarrow \nu_\mu n \pi^0$ and $\nu_\mu p \rightarrow \nu_\mu n \pi^+$ processes. Data points are the experimental results from Ref. [300]. Lines have the same meaning as in Fig. 3.6.

of antineutrino induced processes. For the case of neutrino induced $n\pi^+$ process, at $E_\nu = 1\text{ GeV}$, the contribution to the total scattering cross section from $P_{11}(1440)$ ($D_{13}(1520)$) resonances is around 3%(2%) as that of the contribution from $\Delta(1232)$ resonance, which increases and becomes around 9%(4%) at $E_\nu = 2\text{ GeV}$. However, for the case of neutrino induced $p\pi^0$ production, the contribution from $P_{11}(1440)$ and $D_{13}(1520)$ resonances are almost similar and is around 1% at $E_\nu = 1\text{ GeV}$, which becomes 3% at $E_\nu = 2\text{ GeV}$. For antineutrino induced $p\pi^-$ production, at $E_\nu = 1\text{ GeV}$, the contribution to the total scattering cross section from $P_{11}(1440)$ ($D_{13}(1520)$) resonance is around 14%(5%) at $E_\nu = 1\text{ GeV}$ which becomes around 13%(5%) at $E_\nu = 2\text{ GeV}$ as that of the contribution from $\Delta(1232)$ resonance. Similar results are obtained in the case of $n\pi^0$ production induced by antineutrinos.

In Fig. 3.9, we have plotted the total scattering cross section for NC (anti)neutrino induced pion production processes on proton and neutron targets. The experimental points are the data from ANL experiment [300]. It may be observed from the figure that in the case of $\nu(\bar{\nu})n \rightarrow \nu(\bar{\nu})p\pi^-$ and $\nu(\bar{\nu})p \rightarrow \nu(\bar{\nu})n\pi^+$ processes, besides $\Delta(1232)$ resonant term, there is significant contribution from the NRB terms which results in an increase in the total scattering cross section in these channels. However, in the case of $p\pi^0$ and $n\pi^0$ production reactions, the effect of NRB is small as compared to the other processes. We also observe that when higher resonances are included, there is no appreciable change in the cross sections in the case of (anti)neutrino induced $p\pi^0$ and $n\pi^0$ production cross sections, while in the case of $p\pi^-$ and $n\pi^+$ productions, we observe a significant contribution from the higher resonances, especially at $E_\nu > 1.5\text{ GeV}$ in the case of $p\pi^-$ production and at $E_\nu > 1.2\text{ GeV}$ in the case of $n\pi^+$ production.

In Fig. 3.10, we have compared our results for neutrino induced NC processes viz., $\nu_\mu p \rightarrow \nu_\mu p \pi^0$, $\nu_\mu n \rightarrow \nu_\mu p \pi^-$, $\nu_\mu n \rightarrow \nu_\mu n \pi^0$ and $\nu_\mu p \rightarrow \nu_\mu n \pi^+$, with other theoretical models like the DCC [309], the Hybrid [297], NuWro [297], and Giessen [314] models. It may be observed from the figure that in the case of $p\pi^-$ production, our results are in good agreement with the results of NuWro Monte Carlo generator, while the results of the other models are quite lower. However, in the case of other channels, our results are consistent with the results of DCC and Giessen models.

3.5. Eta production

η -meson is an isoscalar pseudoscalar particle ($I = 0$, $J^P = 0^-$) with mass 547.86 MeV. As the (anti)neutrino energy increases, these particles are produced at $E_{\nu_l(\bar{\nu}_l)} \geq 0.71(.88)\text{ GeV}$ for $\nu_e(\bar{\nu}_\mu)$ induced CC reactions. The (anti)neutrino induced eta production is interesting because of the several reasons. Being an isoscalar particle, the η meson is one of the important probes to search for the strange quark ($s\bar{s}$) content of the nucleons [315]. A precise determination of the η production cross section would also help in understanding the background in the proton decay searches through the $p \rightarrow \eta e^+$ decays. Therefore, the background contribution of η production due to the atmospheric neutrino interactions in search of proton decays should be well estimated. Furthermore, since the η production is expected to be dominated by $S_{11}(1535)$ resonance excitation as this state appears near the threshold of the $N\eta$ system and has large branching ratio to $N\eta$ decay modes, a precise measurement of the cross section for η production will also allow to determine the axial-vector properties of this resonance. The production of η particle in electromagnetic reactions induced by photons and electrons have been studied theoretically and experimentally and the contribution of the vector currents to these processes is fairly known.

The weak production of η mesons via CC interactions which are produced by $\nu_l(\bar{\nu}_l)$ from the nucleon targets (Fig. 3.11)

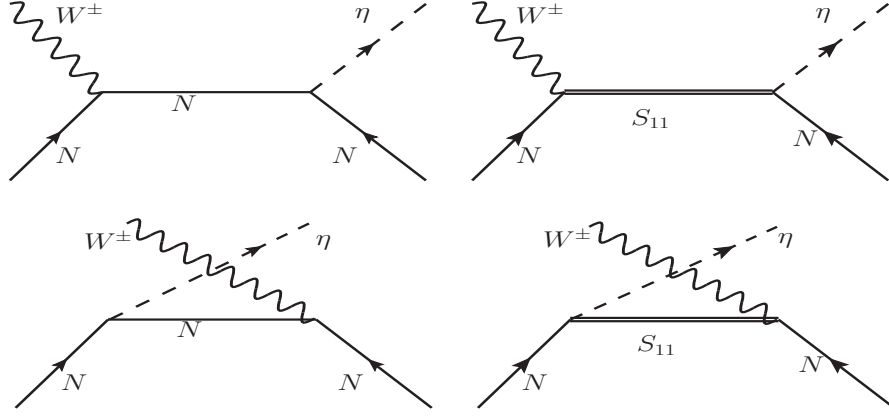


Figure 3.11: Feynman diagrams for the processes $\nu/\bar{\nu}(k) + N(p) \longrightarrow \mu^\mp(k') + \eta(p_\eta) + N'(p')$. First row from left to right: s-channel nucleon pole (SC) and S_{11} resonance (SC N^*); second row: u-channel nucleon pole (UC) and S_{11} resonance (UC N^*).

are given by

$$\nu_\ell + n \longrightarrow l^- + \eta + p, \quad \bar{\nu}_\ell + p \longrightarrow l^+ + \eta + n. \quad (3.100)$$

In the case of electromagnetic production of η meson and associated particle production, the experimental data are available from the MAMI and CLAS collaborations, respectively, for the total as well as differential scattering cross sections. Also several theoretical models are available in the literature to study these processes induced by photons and electrons. While in the case of weak interactions, these processes are almost unexplored both theoretically as well as experimentally. Due to this reason, in order to study the eta production in the weak sector, a model that would explain the experimentally available data from photon and electron induced processes has to be developed. In the case of pion production, the weak vector part of the hadronic current, in general, is related to the electromagnetic current via the CVC hypothesis. Since the electromagnetic production of pions is very well studied, therefore, in the case of weak production of pions, we have directly used those information as inputs. Keeping this in mind, we have developed a model to study eta production induced by photons to fix the strong and electromagnetic couplings by fitting our results with the experimental data available in the literature. Then we have applied the same model to study electron induced reactions where the Q^2 dependence in the form factors comes into play. With these inputs from the electromagnetic sector, we study the single η production induced by (anti)neutrinos in Section 3.5.2. For completeness, in Section 3.5.1, we discuss the single η production induced by photons.

3.5.1. η production induced by photons

The differential cross section for the photoproduction of η mesons off the free nucleon, i.e.,

$$\gamma(q) + N(p) \longrightarrow N(p') + \eta(p_\eta), \quad (3.101)$$

is written as

$$d\sigma = \frac{1}{4(q \cdot p)} (2\pi)^4 \delta^4(q + p - p_\eta - p') \frac{d\vec{p}_\eta}{(2\pi)^3 (2E_\eta)} \frac{d\vec{p}'}{(2\pi)^3 (2E')} \overline{\sum} \sum_r |\mathcal{M}^r|^2, \quad (3.102)$$

where $N = p$ or n , the quantities in the parentheses of Eq. (3.101) represent the four momenta of the corresponding particles, E_η and E' , respectively, are the energies of the outgoing eta and nucleon. $\overline{\sum} \sum |\mathcal{M}^r|^2$ is the square of the transition matrix element \mathcal{M}^r , for photon polarization state r , averaged and summed over the initial and final spin states. \mathcal{M}^r is written in terms of the real photon polarization vector ϵ_μ^r and the matrix element of the electromagnetic current taken between the hadronic states of $|N\rangle$ and $|N\eta\rangle$, i.e.

$$\mathcal{M}^r = e \epsilon_\mu^r(q) \langle N(p') \eta(p_\eta) | J^\mu | N \rangle, \quad (3.103)$$

where $e = \sqrt{4\pi\alpha}$ is the strength of the electromagnetic interaction, with $\alpha = \frac{1}{137}$ being the fine-structure constant. In the case when the photon polarization remains undetected, the summation over all the polarization states is performed which gives

$$\sum_{r=\pm 1} \epsilon_\mu^{*(r)} \epsilon_\nu^{(r)} \longrightarrow -g_{\mu\nu}. \quad (3.104)$$

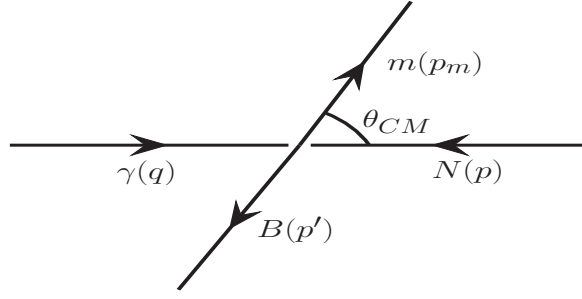


Figure 3.12: Diagrammatic representation of the process $\gamma(q) + N(p) \rightarrow m(p_m) + B(p')$ in CM frame. The quantities in the parentheses represent the four momenta of the corresponding particles. θ_{CM} is the angle between photon and meson in the CM frame.

The hadronic tensor $\mathcal{J}^{\mu\nu}$ is written in terms of the hadronic current J^μ as

$$\mathcal{J}^{\mu\nu} = \overline{\sum} \sum_{spins} J^{\mu\dagger} J^\nu = \text{Tr} \left[(\not{p} + M) \tilde{J}^\mu (\not{p}' + M') J^\nu \right], \quad \tilde{J}^\mu = \gamma_0 (J^\mu)^\dagger \gamma_0, \quad (3.105)$$

where M and M' are the masses of the incoming and outgoing nucleons, respectively. The hadronic matrix element of the electromagnetic current J^μ receives the contribution from the background terms and the terms contributing to the resonance excitations.

Using Eqs. (3.104) and (3.105), the transition matrix element squared is obtained as

$$\overline{\sum}_r \sum_{spin} |\mathcal{M}^r|^2 = -\frac{e^2}{4} g_{\mu\nu} \mathcal{J}^{\mu\nu}. \quad (3.106)$$

Following the above expressions, the differential cross section $\frac{d\sigma}{d\Omega}$ in the CM frame is written as

$$\left. \frac{d\sigma}{d\Omega} \right|_{CM} = \frac{1}{64\pi^2 s} \frac{|\vec{p}'|}{|\vec{p}|} \overline{\sum}_r \sum_{spin} |\mathcal{M}^r|^2, \quad (3.107)$$

where s is the CM energy squared obtained as

$$s = W^2 = (q + p)^2 = M^2 + 2ME_\gamma, \quad (3.108)$$

with E_γ being the energy of the incoming photon in the laboratory frame.

The hadronic currents for the various NR terms shown in Fig 3.11 are obtained using the nonlinear sigma model described in Section 3.3.1. The expressions of the hadronic currents for s -, u - channels are obtained as [160, 166]:

$$J^\mu|_{sN} = -A_s F_s(s) \bar{u}(p') \not{p}_\eta \gamma_5 \frac{\not{p} + \not{q} + M}{s - M^2} \left(\gamma^\mu e_N + i \frac{\kappa_N}{2M} \sigma^{\mu\nu} q_\nu \right) u(p), \quad (3.109)$$

$$J^\mu|_{uN} = -A_u F_u(u) \bar{u}(p') \left(\gamma^\mu e_N + i \frac{\kappa_N}{2M} \sigma^{\mu\nu} q_\nu \right) \frac{\not{p}' - \not{q} + M}{u - M^2} \not{p}_\eta \gamma_5 u(p), \quad (3.110)$$

where N stands for a proton or a neutron in the initial and final states, s is defined in Eq. (3.108) and $u = (p' - q)^2$, A_i 's; $i = s, u$ are the coupling strengths of s , and u channels, respectively, and are obtained as

$$A_s = A_u = \left(\frac{D - 3F}{2\sqrt{3}f_\eta} \right), \quad (3.111)$$

D and F are the axial-vector couplings of the baryon octet and $f_\eta = 105$ MeV is the η decay constant. The value of κ for proton, and neutron are $\kappa_p = 1.793$, and $\kappa_n = -1.91$ in units of μ_N .

In order to take into account the hadronic structure of the nucleons, the form factors $F_s(s)$, and $F_u(u)$, are introduced at the strong vertex. Various parameterizations of these form factors are available in the literature [316]. We use the most general form of the hadronic form factor which is taken to be of the dipole form [170]:

$$F_x(x) = \frac{\Lambda_B^4}{\Lambda_B^4 + (x - M_x^2)^2}, \quad x = s, u \quad (3.112)$$

where Λ_B is the cut-off parameter for the s - and u -channel NRB terms. The value of Λ_B is fitted to the experimental data for both the proton and neutron targets simultaneously and the best fitted value is $\Lambda_B = 0.78$ GeV for s - and u -channel diagrams. x represents the Mandelstam variables s , u , and $M_x = M$ corresponds to the mass of the exchanged nucleons in the s and u channels. One of the most important property of the electromagnetic current is gauge invariance which corresponds to the current conservation and is implemented in the case of η production.

In Section 3.3.5, we have already discussed the structure of hadronic current contributing to spin $\frac{1}{2}$ and $\frac{3}{2}$ resonance excitations and their subsequent decays to meson-baryon final state. In the case of photon induced resonance excitations, the hadronic current is purely vector in nature. Since η is an isoscalar meson, therefore, it couples to spin $\frac{1}{2}$ resonances only. The vertex function for positive and negative parity spin $\frac{1}{2}$ resonances are given in Eq. (3.30). In the case of real photons, which are purely transverse in nature i.e., the amplitude $S_{\frac{1}{2}} = 0$, the vector form factors are expressed only in terms of $A_{\frac{1}{2}}$ helicity amplitude.

The explicit relation between the coupling $F_2^{R^+, R^0}$ and the helicity amplitude $A_{\frac{1}{2}}^{p,n}$, in the limit $Q^2 = 0$, is given by:

$$A_{\frac{1}{2}}^{p,n} = \sqrt{\frac{2\pi\alpha}{M} \frac{(M_R \mp M)^2}{M_R^2 - M^2}} \left[\frac{M_R \pm M}{2M} F_2^{R^+, R^0} \right], \quad (3.113)$$

where the upper (lower) sign stands for the positive (negative) parity resonance. M_R is the mass of corresponding resonance. In the case of η production, we have considered three spin $\frac{1}{2}$ resonances viz. $S_{11}(1535)$, $S_{11}(1650)$, and $P_{11}(1710)$, where the dominant contribution to the total scattering cross section comes from $S_{11}(1535)$ resonance. In the present work, we have used the value of $A_{\frac{1}{2}}$ for these resonances given in PDG [19].

The most general form of the hadronic currents for the s - and u - channel processes where a resonance state $R_{\frac{1}{2}}$ is produced and decays to a η and a nucleon in the final state, are written as

$$\begin{aligned} j^\mu|_s &= \frac{g_{RN\eta}}{f_\eta} \bar{u}(p') \not{p}_\eta \Gamma_s \left(\frac{\not{p} + \not{q} + M_R}{s - M_R^2 + iM_R\Gamma_R} \right) \Gamma_{\frac{1}{2}\pm}^\mu u(p), \\ j^\mu|_u &= \frac{g_{RN\eta}}{f_\eta} \bar{u}(p') \Gamma_{\frac{1}{2}\pm}^\mu \left(\frac{\not{p}' - \not{q} + M_R}{u - M_R^2 + iM_R\Gamma_R} \right) \not{p}_\eta \Gamma_s u(p), \end{aligned} \quad (3.114)$$

where Γ_R is the decay width of the resonance, $\Gamma_s = 1(\gamma_5)$ stands for the positive (negative) parity resonances. $\Gamma_{\frac{1}{2}+}$ and $\Gamma_{\frac{1}{2}-}$ are, respectively, the vertex function for the positive and negative parity resonances, defined in Eq. (3.30). $g_{RN\eta}$ is the coupling strength for the process $R \rightarrow N\eta$, given in Table 3.4.

In analogy with the NR terms, we have considered the following form factors at the strong vertex, in order to take into account the hadronic structure:

$$F_x^*(x) = \frac{\Lambda_R^4}{\Lambda_R^4 + (x - M_x^2)^2}, \quad (3.115)$$

where Λ_R is the cut-off parameter whose value is fitted to the experimental data, x represents the Mandelstam variables s , u , and $M_x = M_R$ corresponding to the mass of the nucleon resonances exchanged in the s , and u channels. In general, Λ_R would be different from Λ_B , however, in the case of η production by photons, it happens that the same value of Λ_R as that of Λ_B i.e. $\Lambda_R = \Lambda_B = 0.78$ GeV gives the best results. The same values of Λ_R and Λ_B help us to minimize the number of free parameters used to fit the experimental data.

In Fig. 3.13, we have presented the results for the total scattering cross section σ as a function of W for $\gamma + p \rightarrow p + \eta$ and $\gamma + n \rightarrow n + \eta$ processes in the region of W from η production threshold to $K\Lambda$ production threshold. We have compared our theoretical results with the experimental data obtained by the MAMI crystal ball [168] collaboration for the proton target and the quasifree neutron data from Werthmuller et al. [169]. It may be observed from the figure that in the case of η production from the proton and neutron targets, our results are in very good agreement with the available experimental data with a very few free parameters. We have fitted the value of strong coupling constant $g_{RN\eta}$ from the photoproduction channels that would be used as an input in the weak production of η mesons, discussed in the next section.

However, in the case of electron induced eta production one has to include the structure of the hadronic current by taking into account the nucleon-nucleon and nucleon-resonance transition form factors at the electromagnetic vertex. The Q^2 dependence of the nucleon-resonance vector form factors is obtained by fitting the experimental data available for electroproduction of the eta mesons, where electromagnetic coupling fixed from the photoproduction are used as the values of these form factors at $Q^2 = 0$. The results for the electroproduction of η mesons from the nucleons will be reported elsewhere [317].

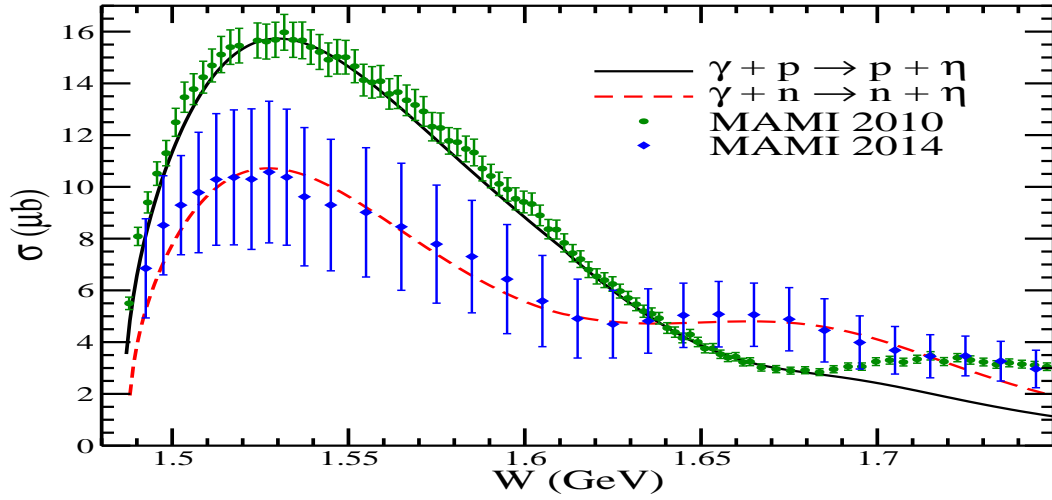


Figure 3.13: Cross section for $\gamma N \rightarrow \eta N$, $N = n, p$ process. The experimental points for proton target are obtained from MAMI crystal ball [168] and for neutron target, we have used the quasifree neutron data from Werthmüller et. al. [169], and the results are shown up to the ΛK threshold.

3.5.2. η production induced by (anti)neutrinos

(Anti)neutrino induced single η production off the nucleon target (Fig. 3.11) are given by the following reactions

$$\nu_\mu(k) + n(p) \rightarrow \mu^-(k') + \eta(p_\eta) + p(p'), \quad (3.116)$$

$$\bar{\nu}_\mu(k) + p(p) \rightarrow \mu^+(k') + \eta(p_\eta) + n(p'), \quad (3.117)$$

where the quantities in the parenthesis are the four momenta of the particles.

The general expression of the differential scattering cross section for the reactions shown in Eqs. (3.116) and (3.117) in the laboratory frame is given in Eq. (3.5), with $\vec{p}_m = \vec{p}_\eta$ as the three-momentum of the outgoing eta-meson and $E_m = E_\eta$, the energy of the eta-meson. The transition matrix element, in terms of the leptonic and the hadronic currents, is given in Eq. (3.3). The leptonic current is given in Eq. (2.10) and the hadronic current receives contribution from the NRB terms as well as from the resonance excitations and their subsequent decay to $N\eta$ final state.

The hadronic currents for the NRB terms, *i.e.*, Born diagrams (*s*- and *u*-channels) with nucleon poles, using the nonlinear sigma model discussed in Section 3.3.1, are obtained as [283, 298]:

$$J_{N(s)}^\mu = a \frac{D - 3F}{2\sqrt{3}f_\pi} \bar{u}_N(p') \not{p}_\eta \gamma^5 \frac{\not{p} + \not{q} + M}{(p + q)^2 - M^2} [V_N^\mu - A_N^\mu] u_N(p), \quad (3.118)$$

$$J_{N(u)}^\mu = a \frac{D - 3F}{2\sqrt{3}f_\pi} \bar{u}_N(p') [V_N^\mu - A_N^\mu] \frac{\not{p} - \not{p}_\eta + M}{(p - p_\eta)^2 - M^2} \not{p}_\eta \gamma^5 u_N(p), \quad (3.119)$$

where $a = \cos \theta_C$, and V_N^μ , A_N^μ , are defined in Eq. (3.88), respectively, in terms of the vector and axial-vector form factors discussed in Section 3.3.6.

In analogy with the photoproduction of η mesons, in the case of (anti)neutrino interactions we have considered only $S_{11}(1535)$, $S_{11}(1650)$, and $P_{11}(1710)$ resonances, which decay to $N\eta$ in the final state. The hadronic states for these resonance excitations and their subsequent decays in the *s*- and *u*- channels are given in Eqs. (3.46) and (3.47). The determination of the vector and axial-vector $N - R$ transition form factors are discussed in detail in Section 3.3.6, and the strong coupling $g_{RN\eta}$ is fixed by the photoproduction processes, obtained using the method discussed in Section 3.3.8 and are tabulated in Table. 3.4.

Fig. 3.14 shows the results for the total scattering cross sections for the processes $\nu_\mu + n \rightarrow \mu^- + \eta + p$ and $\bar{\nu}_\mu + p \rightarrow \mu^+ + \eta + n$. The individual contributions from $S_{11}(1535)$ resonance excitations, where both the direct and crossed diagrams are considered, as well as the full model (sum of all the diagrams) are shown. It may be observed from the figure that in the case of both neutrino and antineutrino induced reactions, $S_{11}(1535)$ has the dominant contribution. We have also compared the results for the neutrino induced η with the results of DCC model [309] and found that from threshold up to $E_{\nu_\mu} \sim 1.3$ GeV our results are consistent with the results of DCC model. While at $E_{\nu_\mu} > 1.3$ GeV, our results are higher than the results obtained using DCC model. The Q^2 -distribution, momentum-distribution, etc. will be reported elsewhere [317].

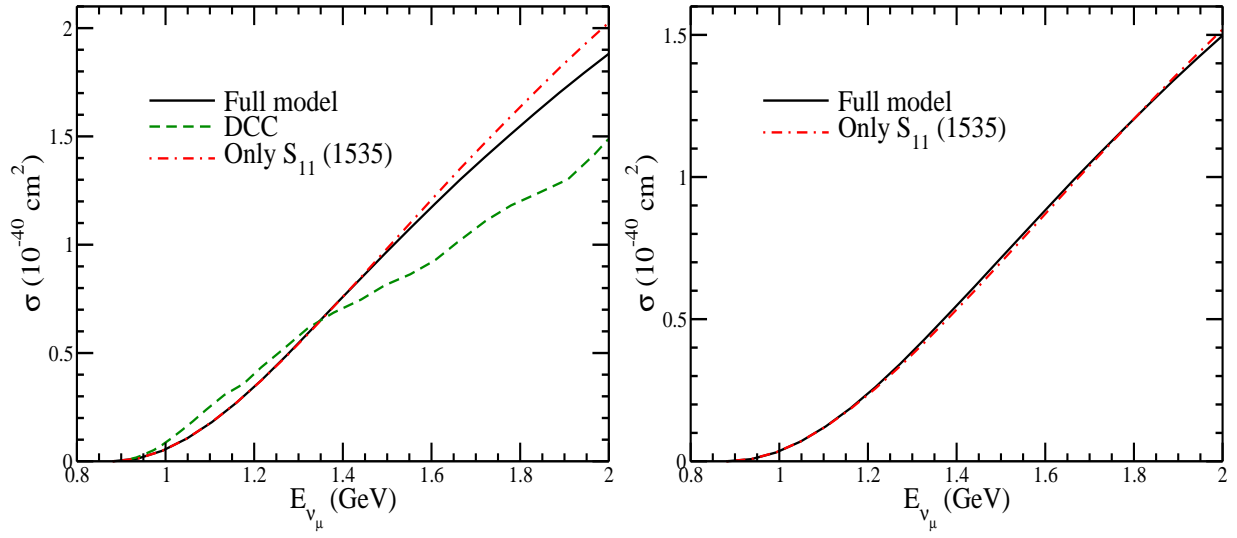


Figure 3.14: Total scattering cross section for CC induced η production i.e. $\nu_\mu + n \rightarrow \mu^- + \eta + p$ (left panel) and $\bar{\nu}_\mu + p \rightarrow \mu^+ + \eta + n$ (right panel). Full model consists of the contributions from all the diagrams including $S_{11}(1535)$, $S_{11}(1650)$, and $P_{11}(1710)$. In the case of neutrino induced η production, we have also compared our results of the full model with the results obtained in the DCC model by Nakamura et al. [309].

3.6. Strange particle production

With the increase in (anti)neutrino energy single kaon is produced for $E_{\nu_l(\bar{\nu}_l)} \geq 0.62$ (0.79) GeV for $\nu_e(\nu_\mu)$ induced reactions off the nucleon target, by the strangeness changing $|\Delta S| = 1$ CC interaction like

$$\begin{aligned} \nu_l + n &\rightarrow l^- + n + K^+, & \bar{\nu}_l + p &\rightarrow l^+ + p + K^-, \\ \nu_l + p &\rightarrow l^- + p + K^+, & \bar{\nu}_l + n &\rightarrow l^+ + n + K^-, \\ \nu_l + n &\rightarrow l^- + p + K^0, & \bar{\nu}_l + p &\rightarrow l^+ + n + \bar{K}^0, \end{aligned} \quad (3.120)$$

where $l = e, \mu$. Due to lowest threshold among the processes which give rise to a strange particle, the single kaon production becomes an important source of kaons for a wide range of energies, and thus their study is important for the lower energy accelerator experiments as well as for the atmospheric neutrino experiments.

For the antineutrinos, single hyperon (like Λ , Σ , etc.) is produced in $\bar{\nu}_e(\bar{\nu}_\mu)$ induced reactions off the nucleon target for $E_{\bar{\nu}_l} \geq 0.19$ (0.32) GeV (for Λ production), by the strangeness changing $|\Delta S| = 1$ CC interaction like

$$\bar{\nu}_\ell + p \rightarrow l^+ + \Lambda, \quad \bar{\nu}_\ell + p \rightarrow l^+ + \Sigma^0, \quad \bar{\nu}_\ell + n \rightarrow l^+ + \Sigma^-,$$

which are prohibited for neutrino induced process due to the $\Delta S = \Delta Q$ selection rule. This process is an additional source of pion production through hyperon decays, which is significant in the energy region of antineutrinos up to 1 GeV, especially in the presence of nuclear medium and final state interaction effects, which are discussed later in Section 5.4.7.

With the further increase in antineutrino energies, besides a hyperon, a pion may also be produced in the final state with a threshold of $E_{\bar{\nu}_l} \geq 0.37$ (0.52) GeV (for Λ production) in $\bar{\nu}_e(\bar{\nu}_\mu)$ induced processes, like

$$\begin{aligned} \bar{\nu}_\ell + p &\rightarrow l^+ + \Lambda + \pi^0, & \bar{\nu}_\ell + n &\rightarrow l^+ + \Lambda + \pi^-, \\ \bar{\nu}_\ell + p &\rightarrow l^+ + \Sigma^0 + \pi^0, & \bar{\nu}_\ell + n &\rightarrow l^+ + \Sigma^0 + \pi^-, \\ \bar{\nu}_\ell + p &\rightarrow l^+ + \Sigma^+ + \pi^-, & \bar{\nu}_\ell + n &\rightarrow l^+ + \Sigma^- + \pi^0. \end{aligned} \quad (3.121)$$

Then we have associated particle production accompanied by a kaon and a hyperon where strangeness quantum number is conserved while all the above processes of strange particle production ($|\Delta S| = 1$) are Cabibbo suppressed. The threshold for Λ (Σ) production for $\nu_\mu(\bar{\nu}_\mu)$ induced reactions is about $E_{\nu_\mu(\bar{\nu}_\mu)} \geq 1.05$ (1.25) GeV:

$$\begin{aligned} \nu_l + p &\rightarrow l^- + \Sigma^+ + K^+, & \bar{\nu}_l + p &\rightarrow l^+ + \Lambda + K^0, \\ \nu_l + n &\rightarrow l^- + \Lambda + K^+, & \bar{\nu}_l + p &\rightarrow l^+ + \Sigma^0 + K^0, \\ \nu_l + n &\rightarrow l^- + \Sigma^0 + K^+, & \bar{\nu}_l + p &\rightarrow l^+ + \Sigma^- + K^+, \\ \nu_l + n &\rightarrow l^- + \Sigma^+ + K^0, & \bar{\nu}_l + n &\rightarrow l^+ + \Sigma^- + K^0. \end{aligned} \quad (3.122)$$

Similarly for the antineutrinos, Ξ ($S = -2$) is produced along with a kaon for $E_{\bar{\nu}_l} \geq 1.28$ (1.5) GeV in $\bar{\nu}_e(\bar{\nu}_\mu)$ induced reactions off the nucleon target, by the strangeness changing $|\Delta S| = 1$ CC interaction, like

$$\bar{\nu}_\ell + p \rightarrow l^+ + K^+ + \Xi^-, \quad \bar{\nu}_\ell + p \rightarrow l^+ + K^0 + \Xi^0, \quad \bar{\nu}_\ell + n \rightarrow l^+ + K^0 + \Xi^-.$$

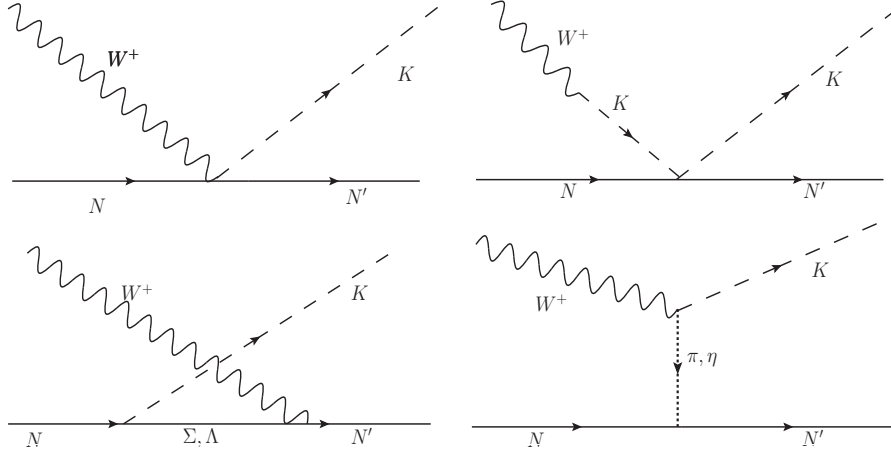


Figure 3.15: Feynman diagrams for the process $\nu N \rightarrow lN'K$. First row from left to right: contact term (CT), kaon pole term (KP); second row: u-channel diagram ($C\Sigma$, $C\Lambda$) and pion (eta) in flight (πP , (ηP)).

Process	A_{CT}	B_{CT}	$A_{C\Sigma}$	$A_{C\Lambda}$	A_{KP}	$A_{\pi P}$	$A_{\eta P}$
$\nu_l + n \rightarrow l^- + K^+ + n$	1	$D - F$	$-(D - F)$	0	1	1	1
$\nu_l + p \rightarrow l^- + K^+ + p$	2	$-F$	$-(D - F)/2$	$(D + 3F)$	2	-1	1
$\nu_l + n \rightarrow l^- + K^0 + p$	1	$-(D + F)$	$(D - F)/2$	$(D + 3F)$	1	-2	0

Table 3.8: Values of the constant parameters appearing in Eq. (3.124) for the hadronic currents.

In the following we briefly describe all the above processes of single kaon production taking up CC production induced by (anti)neutrino in the $|\Delta S| = 1$ sector in Sections 3.6.1 and 3.6.2, and the associated particle production ($\Delta S = 0$) in Sections 3.6.3 and 3.6.4.

3.6.1. Charged current ν_l induced K^+/K^0 production

The basic reaction for the neutrino induced CC kaon production is

$$\nu_l(k) + N(p) \rightarrow l^-(k') + N'(p') + K^j(p_K), \quad (3.123)$$

where $N, N' = p$ or n ; $l = e, \mu$; $j = K^+$ or K^0 .

The reaction shown in the above equation produces a K^+ or a K^0 meson on proton/neutron target, using neutrino beam, which has $S = +1$ in the final hadronic state. Since there are no resonance with $S = +1$, therefore, there is no contribution from the resonance excitation to these reactions, and only NR Born diagrams contribute.

The first calculation for these processes were done by Shrock [318], Amer [319], and Dewan [320] and the first experimental results were reported by the ANL/BNL experiments with very low statistics [285, 321]. It is expected that in future the experiments like the DUNE [322] and Hyper-Kamiokande [323] will be able to observe more events of kaon production.

We describe here the latest calculation by our group [162] using the effective Lagrangian based on the nonlinear sigma model described in Section 3.3.1, and its extension to include the description of strange particles using $SU(3)$ symmetry. The expression for the differential scattering cross section is given in Eq. (3.5), where $E_m = E_K$, is the energy of the outgoing kaon and $\vec{p}_m = \vec{p}_K$ represents the three-momentum of the kaon. The transition matrix element for these processes (Eq. (3.123)) is given in Eq. (3.3) with $a = \sin \theta_C$, where the expression for the leptonic current l_μ is given in Eq. (2.10) and the hadronic current matrix element for the different diagrams shown in Fig. 3.15, using effective

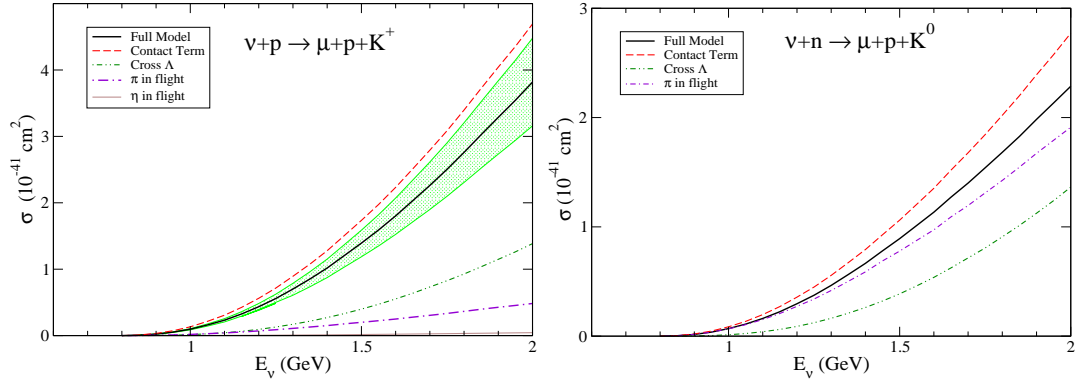


Figure 3.16: Contribution of the different terms to the total scattering cross section for the $\nu_\mu + p \rightarrow \mu^- + K^+ + p$ (left panel) and $\nu_\mu + n \rightarrow \mu^- + K^0 + p$ (right panel) processes.

Lagrangian approach discussed in Section 3.3.1 and obtained in Ref. [162], is given by:

$$\begin{aligned}
j^\mu|_{CT} &= -iA_{CT}\frac{\sqrt{2}}{2f_\pi}\bar{u}(p')(\gamma^\mu + \gamma^\mu\gamma^5 B_{CT})u(p), \\
j^\mu|_{Cr\Sigma} &= iA_{Cr\Sigma}\frac{\sqrt{2}}{2f_\pi}\bar{u}(p')\left(\gamma^\mu + i\frac{\kappa_p + 2\kappa_n}{2M}\sigma^{\mu\nu}q_\nu + (D-F)\left(\gamma^\mu + \frac{q^\mu}{Q^2 + m_K^2}\not{q}\right)\gamma^5\right)\frac{\not{p} - \not{p}_K + M_\Sigma}{(p - p_K)^2 - M_\Sigma^2}\not{p}_K\gamma^5 u(p), \\
j^\mu|_{Cr\Lambda} &= iA_{Cr\Lambda}\frac{\sqrt{2}}{4f_\pi}\bar{u}(p')\left(\gamma^\mu + i\frac{\kappa_p}{2M}\sigma^{\mu\nu}q_\nu - \frac{D+3F}{3}\left(\gamma^\mu + \frac{q^\mu}{Q^2 + m_K^2}\not{q}\right)\gamma^5\right)\frac{\not{p} - \not{p}_K + M_\Lambda}{(p - p_K)^2 - M_\Lambda^2}\not{p}_K\gamma^5 u(p), \\
j^\mu|_{KP} &= -iA_{KP}\frac{\sqrt{2}}{4f_\pi}\bar{u}(p')(\not{q} + \not{p}_K)u(p)\frac{1}{Q^2 + m_K^2}q^\mu, \\
j^\mu|_\pi &= iA_{\pi P}(D+F)\frac{\sqrt{2}}{2f_\pi}\frac{M}{(q - p_K)^2 - M_\pi^2}\bar{u}(p')\gamma^5(q^\mu - 2p_K^\mu)u(p), \\
j^\mu|_\eta &= iA_{\eta P}(D-3F)\frac{\sqrt{2}}{2f_\pi}\frac{M}{(q - p_K)^2 - M_\eta^2}\bar{u}(p')\gamma^5(q^\mu - 2p_K^\mu)u(p),
\end{aligned} \tag{3.124}$$

where, $q = k - k'$ is the four momentum transfer, κ_p and κ_n are, respectively, the proton and neutron anomalous magnetic moments. The value of the various parameters appearing in the expressions of the hadronic currents of the different channels are shown in Table-3.8.

To incorporate the hadronic structure in the matrix element, a dipole form factor

$$F(Q^2) = \frac{1}{\left(1 + \frac{Q^2}{M_F^2}\right)^2}, \tag{3.125}$$

is used with mass $M_F \simeq 1$ GeV.

Fig. 3.16 shows the results of the contributions of the different diagrams to the total scattering cross sections for the processes $\nu_\mu p \rightarrow \mu^- K^+ p$ and $\nu_\mu n \rightarrow \mu^- K^0 p$. It may be observed that the contact term has a dominant contribution to the total scattering cross section in both the processes discussed above. The curve labeled as the full model is calculated with a dipole form factor with $M_F = 1$ GeV. The band corresponds to variation of M_F by 10%. The process $\nu_\mu n \rightarrow \mu^- K^0 p$ has a cross section of a similar size and the contact term is the largest followed by the π exchange diagram and the u-channel (Λ) term. A destructive interference between the different terms has been observed and this resulted in the total cross section obtained with the full model to be smaller than that produced by the contact term. For more details and results, see Ref. [162].

3.6.2. Charged current $\bar{\nu}_l$ induced K^-/\bar{K}^0 production

In the case of antineutrino induced reactions K^- or \bar{K}^0 particle are produced off a nucleon target with $S = -1$ in the final state. Consequently there would be resonance excitation with $S = -1$ in the final state which will decay to produce K^- or \bar{K}^0 particles as shown in Fig. 3.17 where $\Sigma^*(1385)$ is a resonance with spin $J = \frac{3}{2}$ and isospin $I = 1$ along with the NR Born diagrams. In this section, we are briefly discussing antikaon production, for details see Ref. [163].

The basic reaction for the antineutrino induced CC antikaon production is

$$\bar{\nu}_l(k) + N(p) \rightarrow l^+(k') + N'(p') + K^i(p_K),$$

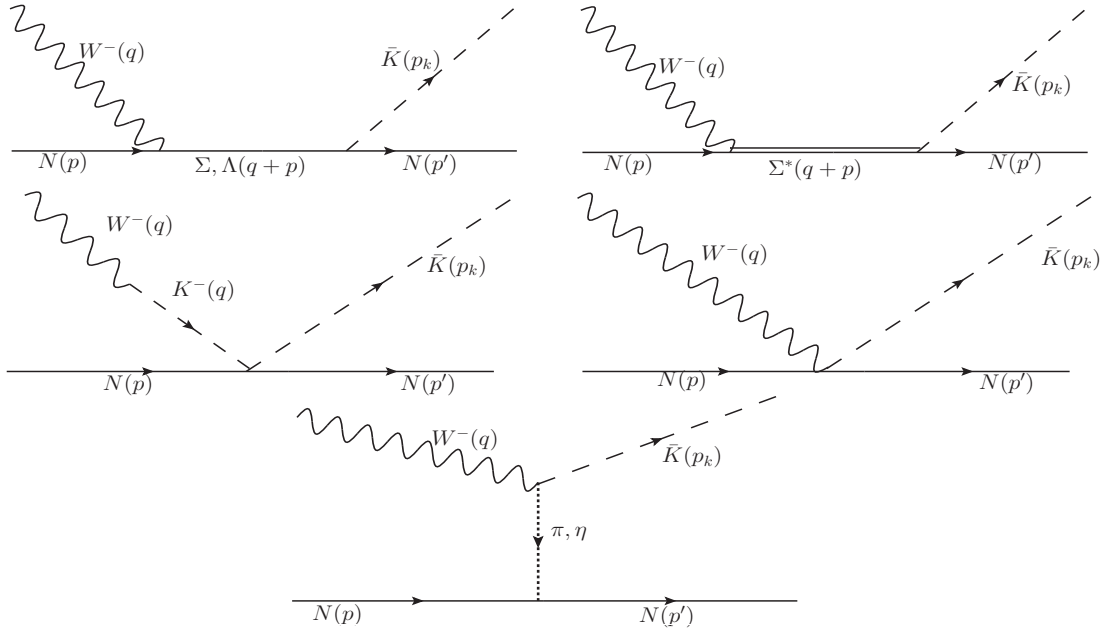


Figure 3.17: Feynman diagrams for the process $\bar{\nu}N \rightarrow lN'\bar{K}$. First row from left to right: s-channel Σ, Λ propagator (SC), s-channel Σ^* Resonance (SCR), second row: kaon pole term (KP); contact term (CT) and last row: pion (eta) in flight ($\pi P/\eta P$).

Process	B_{CT}	A_{CT}	A_{Σ}	A_{Λ}	A_{KP}	A_{π}	A_{η}	A_{Σ^*}
$\bar{\nu}_l + n \rightarrow l^+ + K^- + n$	$D - F$	1	-1	0	-1	1	1	2
$\bar{\nu}_l + p \rightarrow l^+ + K^- + p$	$-F$	2	$-\frac{1}{2}$	1	-2	-1	1	1
$\bar{\nu}_l + p \rightarrow l^+ + \bar{K}^0 + n$	$-(D + F)$	1	$\frac{1}{2}$	1	-1	-2	0	-1

Table 3.9: Values of the constant parameters appearing in Eq. (3.126) for the hadronic currents.

where $N, N' = p$ or n ; $l = e, \mu$; $i = K^-$ or \bar{K}^0 .

The expression for the differential scattering cross section is given in Eq. (3.5), where $E_m = E_K$ is the energy of the outgoing antikaon and $\vec{p}_m = \vec{p}_K$ represents the three-momentum of the antikaon. The transition matrix element is defined in Eq. (3.3) with $a = \sin \theta_C$ and the leptonic current, given in Eq. (2.10). The different channels which contribute to the hadronic currents are the s-channel with Σ, Λ (SC) and Σ^* (SCR) as the intermediate states, the kaon pole (KP) term, the contact term (CT), and the meson ($\pi P, \eta P$) exchange terms [163].

The hadronic currents for the background terms discussed in Section 3.3.1 and obtained in Ref. [163], are written as

$$\begin{aligned}
J^\mu|_{CT} &= iA_{CT} \frac{\sqrt{2}}{2f_\pi} \bar{u}(p') (\gamma^\mu + B_{CT} \gamma^\mu \gamma_5) u(p) \\
J^\mu|_{\Sigma} &= iA_{\Sigma} (D - F) \frac{\sqrt{2}}{2f_\pi} \bar{u}(p') \not{p}_K \gamma_5 \frac{\not{p} + \not{q} + M_{\Sigma}}{(p+q)^2 - M_{\Sigma}^2} \left(\gamma^\mu + i \frac{(\kappa_p + 2\kappa_n)}{2M} \sigma^{\mu\nu} q_\nu + (D - F) \left\{ \gamma^\mu + \frac{q^\mu}{Q^2 + m_K^2} \not{q} \right\} \gamma^5 \right) u(p) \\
J^\mu|_{\Lambda} &= iA_{\Lambda} (D + 3F) \frac{1}{2\sqrt{2}f_\pi} \bar{u}(p') \not{p}_K \gamma_5 \frac{\not{p} + \not{q} + M_{\Lambda}}{(p+q)^2 - M_{\Lambda}^2} \left(\gamma^\mu + i \frac{\kappa_p}{2M} \sigma^{\mu\nu} q_\nu \right. \\
&\quad \left. - \frac{(D + 3F)}{3} \left\{ \gamma^\mu + \frac{q^\mu}{Q^2 + m_K^2} \not{q} \right\} \gamma^5 \right) u(p) \\
J^\mu|_{KP} &= -iA_{KP} \frac{\sqrt{2}}{2f_\pi} \bar{u}(p') \not{q} u(p) \frac{q^\mu}{Q^2 + m_K^2} \\
J^\mu|_{\pi} &= iA_{\pi} \frac{M\sqrt{2}}{2f_\pi} (D + F) \frac{2p_K^\mu - q^\mu}{(q - p_K)^2 - m_\pi^2} \bar{u}(p') \gamma_5 u(p) \\
J^\mu|_{\eta} &= iA_{\eta} \frac{M\sqrt{2}}{2f_\pi} (D - 3F) \frac{2p_K^\mu - q^\mu}{(q - p_K)^2 - m_\eta^2} \bar{u}(p') \gamma_5 u(p)
\end{aligned} \tag{3.126}$$

The hadronic current for $\Sigma^*(1385)$ ($J = \frac{3}{2}, I = 1$) is written in analogy with the hadronic current of the Δ resonance as discussed in Section 3.3.5. The factors A_i for each diagram contributing to the hadronic current are tabulated in

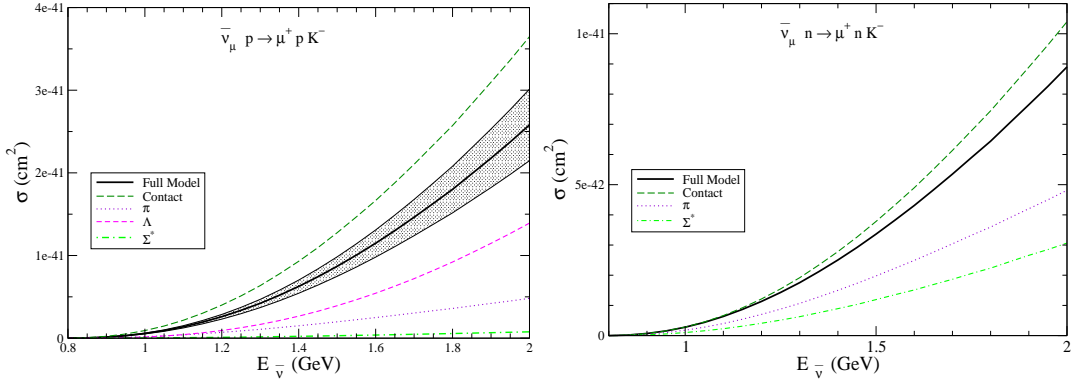


Figure 3.18: Total scattering cross section for the processes $\bar{\nu}_\mu p \rightarrow \mu^+ p K^-$ and $\bar{\nu}_\mu n \rightarrow \mu^+ n K^-$.

Table-3.9. In analogy with the single kaon production, a global dipole form factor given in Eq. (3.125) with $M_F \simeq 1$ GeV is used in the hadronic currents, except for the resonance excitation, for which the form factors are related to the Δ^+ excitation discussed in Section 3.3.5.

In Fig. 3.18, the different contributions of the hadronic current to the $\bar{\nu}_\mu p \rightarrow \mu^+ p K^-$ and $\bar{\nu}_\mu n \rightarrow \mu^+ n K^-$ reactions are presented. It may be observed that the cross section is dominated by the NR terms, where the contact term gives the largest contribution among all the NR terms. The destructive interference leads to a total scattering cross section smaller than that obtained by the contact term only. It should be noted that in the case of $\bar{\nu}_\mu p \rightarrow \mu^+ p K^-$ process, $\Sigma^*(1385)$ has negligible contribution. This can be understood because the mass of Σ^* is below the kaon production threshold. The curve labeled as full model is calculated with a dipole form factor with a mass of 1 GeV. The band corresponds to a 10% variation in M_F . For the $\bar{\nu}_\mu n \rightarrow \mu^+ n K^-$ case, the contribution of Σ^* resonance is substantial due to the larger value of the couplings (see Table-3.9).

3.6.3. Associated particle production induced by photons

As discussed in Section 3.5.1, before calculating the scattering cross section for (anti)neutrino induced associated particle production, the strong and electromagnetic couplings are fixed by calculating the total cross section of associated production induced by photons. Here, we focus only on the production of $K\Lambda$ in the final state induced by photon, where the general reaction may be written as:

$$\gamma(q) + p(p) \rightarrow \Lambda(p') + K^+(p_K). \quad (3.127)$$

The differential scattering cross section for the above reaction is calculated in the same way as presented in Section 3.5.1, with the expression of $\frac{d\sigma}{d\Omega}$ given in Eq. (3.107). The hadronic current receives contribution from both the NR and resonance excitations, as shown in Fig. 3.19. Unlike the case of η production, in this case, spin $\frac{3}{2}$ resonances with $I = \frac{1}{2}$ also contribute significantly.

The hadronic currents for the various NR terms shown in Fig. 3.19(a)–(d) are obtained using the nonlinear sigma model described in Section 3.3.1 and are obtained as [170]:

$$J^\mu|_s = -A_s F_s(s) \bar{u}(p') \not{p}_K \gamma_5 \frac{\not{p} + \not{q} + M}{s - M^2} \left(\gamma^\mu e_p + i \frac{\kappa_p}{2M} \sigma^{\mu\nu} q_\nu \right) u(p), \quad (3.128)$$

$$J^\mu|_t = -A_t F_t(t) \bar{u}(p') [(\not{p} - \not{p}') \cdot \gamma_5] u(p) \frac{(2p_K^\mu - q^\mu)}{t - m_K^2}, \quad (3.129)$$

$$J^\mu|_{u\Lambda} = -A_u^\Lambda F_u^\Lambda(u) \bar{u}(p') \left(\gamma^\mu e_\Lambda + i \frac{\kappa_\Lambda}{2M_\Lambda} \sigma^{\mu\nu} q_\nu \right) \frac{\not{p}' - \not{q} + M_\Lambda}{u - M_\Lambda^2} \not{p}_K \gamma_5 u(p), \quad (3.130)$$

$$J^\mu|_{u\Sigma^0} = -A_u^{\Sigma^0} F_u^{\Sigma^0}(u) \bar{u}(p') \left(\gamma^\mu e_{\Sigma^0} + i \frac{\kappa_{\Sigma^0}}{2M_{\Sigma^0}} \sigma^{\mu\nu} q_\nu \right) \frac{\not{p}' - \not{q} + M_{\Sigma^0}}{u - M_{\Sigma^0}^2} \not{p}_K \gamma_5 u(p), \quad (3.131)$$

$$J^\mu|_{CT} = A_{CT} F_{CT} \bar{u}(p') \gamma^\mu \gamma_5 u(p), \quad (3.132)$$

where s and u are already defined and $t = (p - p')^2$. The couplings A_i 's for the different terms, obtained in the nonlinear sigma model are:

$$A_s = A_t = A_u^\Lambda = A_{CT} = - \left(\frac{D + 3F}{2\sqrt{3}f_K} \right), \quad A_u^{\Sigma^0} = \left(\frac{D - F}{2f_K} \right). \quad (3.133)$$

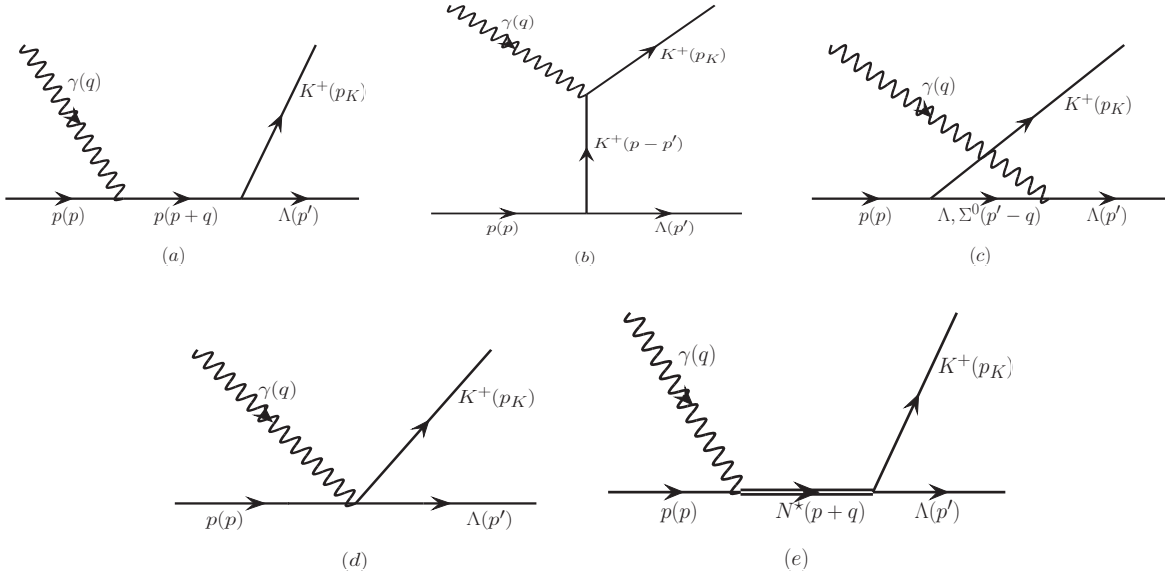


Figure 3.19: Feynman diagram for the various channels possible for the process $\gamma(q) + p(p) \rightarrow K^+(p_K) + \Lambda(p')$. (a) s channel, (b) t channel, (c) u channel and (d) contact term constitute the NR terms. (e) nucleon resonances in the s channel. The quantities in the bracket represent four momenta of the corresponding particles.

The value of κ for lambda i.e. $\kappa_\Lambda = -0.613$ and for sigma i.e. $\kappa_{\Sigma^0} = 1.61$, are in units of μ_N .

One of the most important property of the electromagnetic current is the gauge invariance that corresponds to the current conservation, which is implemented for the full current. The total hadronic current for the NR terms is given by

$$J^\mu = J^\mu|_s + J^\mu|_t + J^\mu|_{u\Lambda} + J^\mu|_{u\Sigma^0} + J^\mu|_{CT}. \quad (3.134)$$

The condition to fulfill gauge invariance is $q_\mu J^\mu = 0$, which gives

$$q_\mu J^\mu = -\frac{D+F}{2\sqrt{3}f_K} \bar{u}(p') \left[(\not{p}_K F_s + (\not{p}' - \not{p}) F_t - \not{q} F_{CT}) \gamma_5 \right] u(p). \quad (3.135)$$

From the above equation, it is evident that the hadronic current is not gauge invariant. Therefore, in order to restore gauge invariance, the following term is added to Eq. (3.135)

$$q_\mu J_{add}^\mu = -\frac{D+F}{2\sqrt{3}f_K} \bar{u}(p') \left[\not{p}_K (F_{CT} - F_s) + (\not{p}' - \not{p})(F_{CT} - F_t) \right] \gamma_5 u(p). \quad (3.136)$$

Thus, the presence of the additional terms given in Eq. (3.136) implies that the gauge invariance can be achieved if the hadronic current J^μ is supplemented by adding an additional term J_{add}^μ given by

$$J_{add}^\mu = -\frac{D+F}{2\sqrt{3}f_K} \bar{u}(p') \left[\frac{2\not{p}_K p^\mu}{s - M^2} (F_{CT} - F_s) + \frac{2p_K^\mu}{t - M_K^2} (\not{p} - \not{p}') (F_{CT} - F_t) \right] u(p). \quad (3.137)$$

In order to take into account the effect of the form factor for the contact term, there are different prescriptions available in the literature, for example that of Ohta [324], Haberzettl et al. [325], Davidson and Workman [326], etc. In the present work, we have followed the prescription of Davidson and Workman [326], where F_{CT} is given by:

$$F_{CT} = F_s(s) + F_t(t) - F_s(s) \times F_t(t). \quad (3.138)$$

In the case of associated particle production, we have considered six nucleon resonances exchanged in the s channel, out of which four are spin $\frac{1}{2}$ viz. $S_{11}(1650)$, $P_{11}(1710)$, $P_{11}(1880)$, and $S_{11}(1895)$, and two are spin $\frac{3}{2}$ resonances viz. $P_{13}(1720)$, and $P_{13}(1900)$. We have already discussed the case of spin $\frac{1}{2}$ resonances in Section 3.5.1. However, for completeness, in this section we write the general form of the hadronic currents for the s channel processes where a resonance state with spin $\frac{1}{2}$ is produced and decays to a kaon and a lambda in the final state as [170]:

$$j^\mu|_R^{\frac{1}{2}\pm} = -\bar{u}(p') \frac{g_{RK\Lambda}}{f_K} \not{p}_K \Gamma_s \frac{\not{p} + \not{q} + M_R}{s - M_R^2 + iM_R \Gamma_R} \Gamma_{\frac{1}{2}\pm}^\mu u(p), \quad (3.139)$$

Resonance	Helicity amplitude			
	$A_{\frac{1}{2}}^p (10^{-3} \text{ GeV}^{-1/2})$	$A_{\frac{3}{2}}^p (10^{-3} \text{ GeV}^{-1/2})$	$A_{\frac{1}{2}}^n (10^{-3} \text{ GeV}^{-1/2})$	$A_{\frac{3}{2}}^n (10^{-3} \text{ GeV}^{-1/2})$
$P_{11}(1880)$	21	-	-60	-
$S_{11}(1895)$	-16	-	13	-
$P_{13}(1900)$	24	-67	0.7	0.7

Table 3.10: Values of the helicity amplitudes $A_{\frac{1}{2}}^{p,n}$ and $A_{\frac{3}{2}}^{p,n}$ for $P_{11}(1880)$, $S_{11}(1895)$, and $P_{13}(100)$ resonances taken from PDG [19].

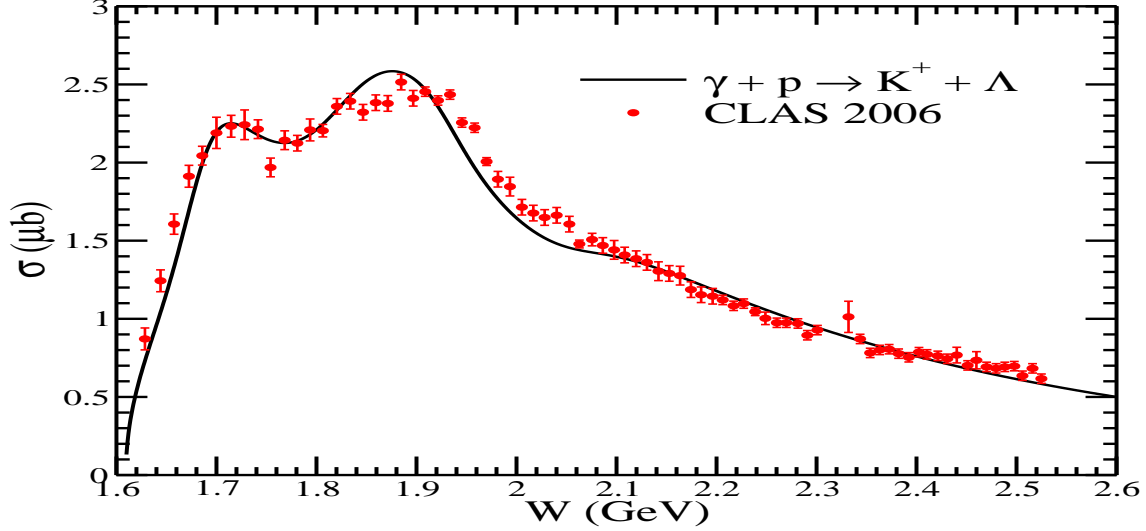


Figure 3.20: Comparison of σ vs. W for the process $\gamma + p \rightarrow K^+ + \Lambda$ (black solid line) calculated in our model with the experimental data taken from the CLAS 2006 [171] (solid circle).

where Γ_R is the decay width of the resonance, $\Gamma_s = 1(\gamma_5)$ stands for the positive (negative) parity resonances. $\Gamma_{\frac{1}{2}+}$ and $\Gamma_{\frac{1}{2}-}$ are, respectively, the vertex function for the positive and negative parity resonances, defined in Eq. (3.30). $g_{RK\Lambda}$ is the coupling strength for the process $R \rightarrow K\Lambda$, given in Table 3.4. For a more detailed discussion, see Ref. [170].

In the following, we briefly discuss spin $\frac{3}{2}$ resonance excitations. The general structure of the hadronic current for $N - R$ transition has already been discussed in Section 3.3.5. In the case of real photon scattering, the electromagnetic couplings $C_i^{p,n}$ are related to the helicity amplitudes $A_{\frac{1}{2}}$, $A_{\frac{3}{2}}$ and $S_{\frac{1}{2}}$, which are obtained using Eqs. (3.55)–(3.57) in the limit $Q^2 = 0$. In the numerical calculations, we have taken $S_{\frac{1}{2}} = 0$ as we are dealing with the real photons. The fitted values of $A_{\frac{1}{2}}$ and $A_{\frac{3}{2}}$ have been taken from PDG [19] for spin $\frac{1}{2}$ and $\frac{3}{2}$ resonances, and are quoted in Tables 3.2 and 3.10.

The most general expression of the hadronic current for the s channel spin $\frac{3}{2}$ resonance exchange may be written as [170]:

$$j^\mu \Big|_R^{\frac{3}{2}\pm} = ie \frac{g_{RK\Lambda}}{f_K} \frac{p_K^\alpha \Gamma_s}{s - M_R^2 + iM_R \Gamma_R} \bar{u}(p') P_{\alpha\beta}^{3/2}(p_R) \Gamma_{\frac{3}{2}\pm}^{\beta\mu} u(p), \quad p_R = p + q, \quad (3.140)$$

where $\Gamma_s = 1(\gamma_5)$ for positive (negative) parity resonances, f_K is defined in Section 3.3.8, $g_{RK\Lambda}$ is the coupling strength for $R \rightarrow K\Lambda$ transition, the values of which are given in Table 3.4. M_R is the mass of the resonance, Γ_R is its decay width and $P_{\alpha\beta}^{3/2}(p_R)$ is given in Eq. (3.67).

In Fig. 3.20, we have presented the results for the total scattering cross section as a function of W for the photon induced $K\Lambda$ production. The theoretical calculations are compared with the experimental data from the CLAS experiment [171]. It may be observed from the figure that there is good agreement of our results with the experimental data.

3.6.4. Associated particle production induced by (anti)neutrinos

The study of the neutrino induced $\Delta S = 0$ associated particle production processes provide an improved understanding of the basic symmetries of the SM, structure of the weak hadronic form factors, strange-quark content of the nucleon, coupling constants, etc. Moreover the kaon production through the associated production also constitutes a background in the proton decay searches i.e. $p \rightarrow K\bar{\nu}$. Therefore, an understanding and reliable estimate of the cross sections for the neutrino induced kaon production contributing as the background event is important and has been emphasized [327, 328].

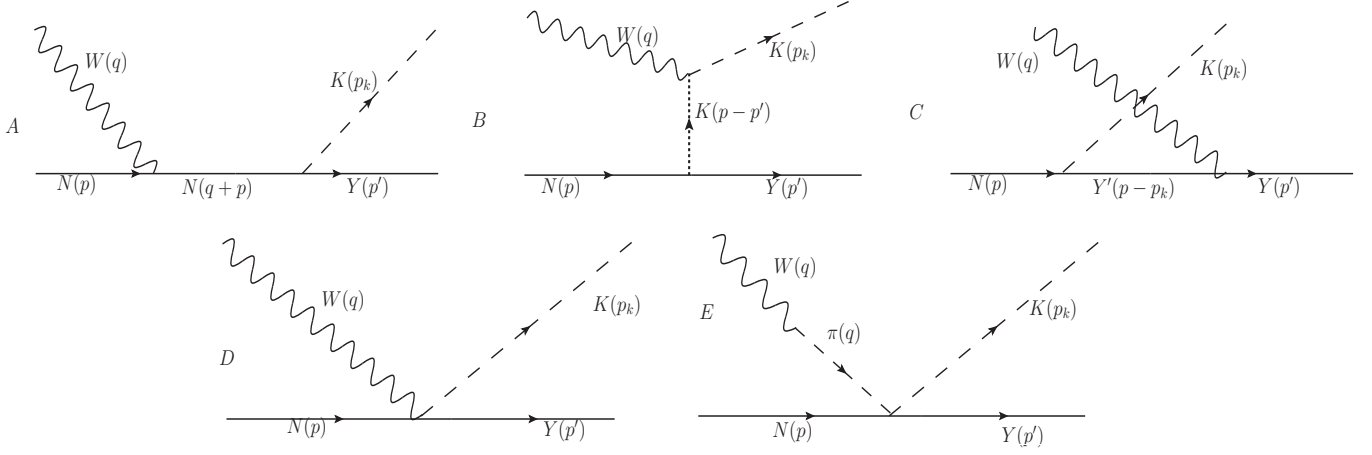


Figure 3.21: Feynman diagrams corresponding to the (anti)neutrino induced $\Delta S = 0$ associated particle production processes.

A_{CT}	B_{CT}	A_{SY}	A_{UY}	A_{TY}	A_{π}
$Y' = \Sigma$			$Y' = \Lambda$		
$-\frac{\sqrt{3}}{2f_K}$	$-\frac{1}{3}(D + 3F)$	$\frac{D+3F}{2\sqrt{3}f_K}$	$\frac{\sqrt{2}}{3f_K}(D - F)$	0	$\frac{D+3F}{2\sqrt{3}f_K}$
					$-\frac{\sqrt{3}}{4f_K}$

Table 3.11: Constant factors appearing in the hadronic current in Eq. (3.142).

The experimental observations of the neutrino induced associated particle production processes were performed earlier at BNL [329], ANL [330] and CERN [232, 233, 331]. However, these experiments have very low statistics and large systematic errors. Attempts are being made to study them in the context of the present day neutrino experiments with high intensity $\nu(\bar{\nu})$ beams.

Theoretically, the early attempts were made by Shrock [318], Amer [319], Dewan [320] and Mecklenburg [332]. The associated particle production cross sections used for example in the NUANCE Monte Carlo generator [333] consider only the resonant kaon production based on the Rein and Sehgal model for the pion production [157]. Moreover, these cross sections miss the experimental data points by almost a factor of four [334]. Therefore, a better estimation of the weak interaction induced associated particle production cross section is needed.

Here, the formalism for writing the hadronic current is the same as adopted in the case of pion and eta meson production processes discussed in Section 3.4 and 3.5.2, respectively. The CC induced $\Delta S = 0$ processes are the following

$$\nu_l(k) + N(p) \longrightarrow l^-(k') + Y(p') + K(p_K), \quad \bar{\nu}_l(k) + N(p) \longrightarrow l^+(k') + Y(p') + K(p_K), \quad \text{where } l = e, \mu. \quad (3.141)$$

For demonstrating the results, in this work we have focused only on the production of $K\Lambda$ induced by (anti)neutrinos, and the results for the other channels will be reported elsewhere [335]. We have considered the contribution of the NRB terms shown in Fig. 3.21 as well as from the isospin $\frac{1}{2}$ resonances exchanged in s -channel, as Λ being an isoscalar particle, does not couple to the isospin $\frac{3}{2}$ resonances in order to conserve isospin at the strong vertex. We have taken only those resonances in the numerical calculations, which make significant contribution to the cross section for $W < 2$ GeV.

The differential scattering cross section for the processes given in Eq. (3.141) is given in Eq. (3.5) with $E_m = E_K$ and $\vec{p}_m = \vec{p}_K$, the outgoing kaon's energy and three-momentum, respectively, and E'_p is replaced with E_Y , the energy of the outgoing hyperon. The transition matrix element for the associated particle production process is given in Eq. (3.3) with the leptonic current defined in Eq. (2.10). The contribution to the hadronic current J^μ comes from the different pieces of the Lagrangian corresponding to the Feynman diagrams shown in Fig. 3.21.

In analogy with the weak pion production discussed in Section 3.4, the hadronic currents corresponding to the diagrams

shown in Fig. 3.21 are obtained as:

$$\begin{aligned}
j^\mu|_s &= ia A_{SY} \bar{u}(p') \not{p}_K \gamma_5 \frac{\not{p} + \not{q} + M}{(p+q)^2 - M^2} [V^\mu - A^\mu] u(p) \\
j^\mu|_u &= ia A_{UY} \bar{u}(p') [V^\mu - A^\mu] \frac{\not{p} - \not{p}_K + M_\Sigma}{(p-p_K)^2 - M_\Sigma^2} \not{p}_K \gamma_5 u(p) \\
j^\mu|_{PF} &= ia A_{TY} f_{PF}(Q^2) (M + M_\Lambda) \bar{u}(p') \gamma_5 u(p) \frac{2p_K^\mu - q^\mu}{(p-p')^2 - m_K^2} \\
j^\mu|_{CT} &= ia A_{CT} \bar{u}(p') [\gamma^\mu f_\rho((q-p_K)^2) + B_{CT} f_{CT}(Q^2) \gamma^\mu \gamma_5] u(p) \\
j^\mu|_{PP} &= ia A_\pi f_\rho((q-p_K)^2) \bar{u}(p') [\not{q} + \not{p}_K] u(p) \frac{q^\mu}{q^2 - m_\pi^2}
\end{aligned} \tag{3.142}$$

where,

$$V^\mu = f_1^{YY'}(Q^2) \gamma^\mu + i \frac{f_2^{YY'}(Q^2)}{M + M'} \sigma^{\mu\nu} q_\nu \tag{3.143}$$

$$A^\mu = g_1^{YY'}(Q^2) \gamma^\mu \gamma_5 + g_3^{YY'}(Q^2) \frac{2q^\mu}{M + M'} \gamma_5 \tag{3.144}$$

are the vector (V^μ) and axial-vector (A^μ) transition currents for $Y \leftrightarrow Y'$ with $Y = Y' \equiv$ nucleon and/or hyperon. The vector and axial-vector form factors $f_{1,2}^{YY'}(Q^2)$ and $g_{1,3}^{YY'}(Q^2)$ are determined assuming the Cabibbo theory and the various symmetry properties of the weak hadronic current discussed in Section 2.2 and Appendix B. The form factors $f_{CT}(Q^2)$, $f_{PF}(Q^2)$ and $f_\rho((q-p_K)^2)$ are introduced in the contact, pion pole and pion in flight terms to taken into account the hadronic structure. It may be observed from the Feynman diagrams (Fig. 3.21) that the pion in flight term is purely vector in nature while the pion pole diagram is possible only with axial-vector current. In the case of contact term, the term associated with B_{CT} represents the vector part of the weak hadronic current while the term with γ^μ is associated with the axial-vector part. CVC hypothesis imposes the following condition on the form factors $f_{CT}(Q^2)$ and $f_{PF}(Q^2)$, i.e.,

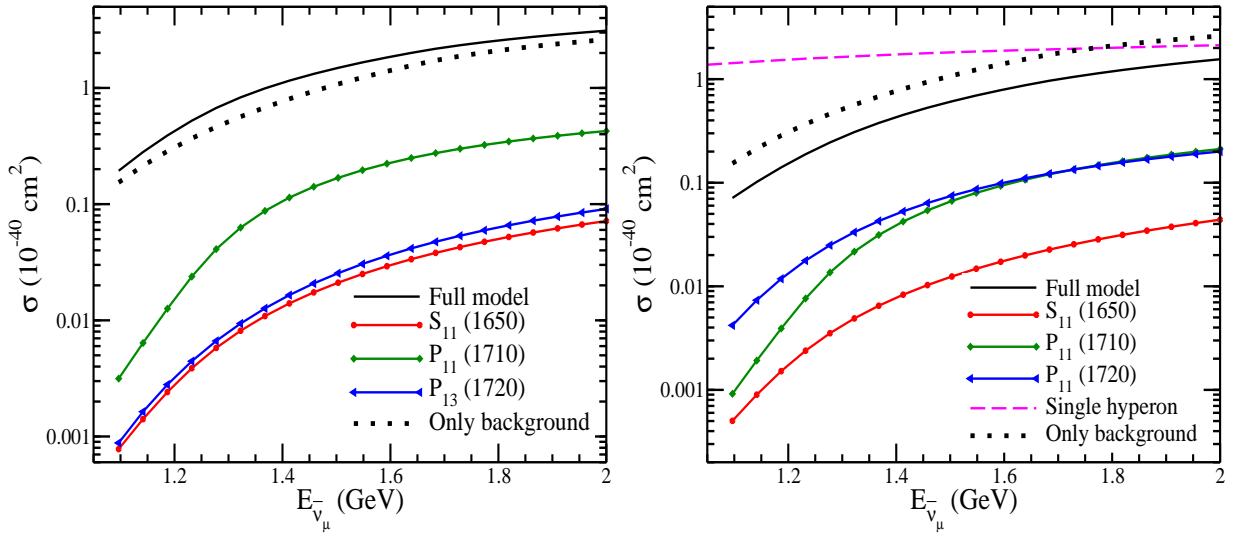
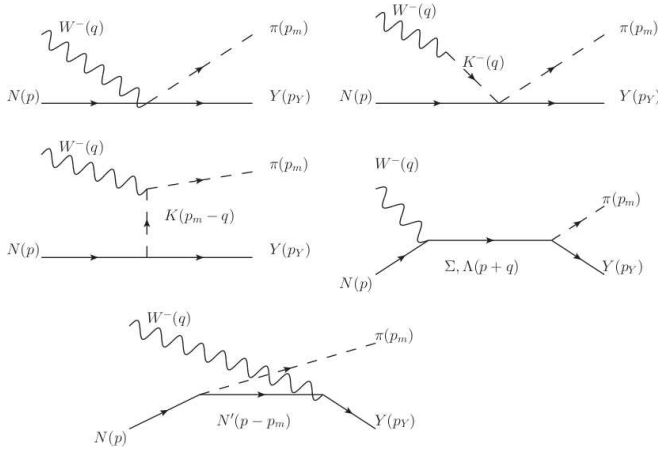


Figure 3.22: Cross section for $\nu_\mu + n \rightarrow \mu^- + \Lambda + K^+$ (left panel) and $\bar{\nu}_\mu + p \rightarrow \mu^+ + \Lambda + K^0$ (right panel) processes. Solid (dotted) line represents the results of the full model (only NRB terms), solid line with circle, diamond and left triangle, respectively, represents the individual contribution from $S_{11}(1650)$, $P_{11}(1710)$, and $P_{13}(1720)$ resonances. For comparison, in the right panel we have also shown the result of single hyperon production (dashed line) induced by the $|\Delta S| = 1$ reaction.

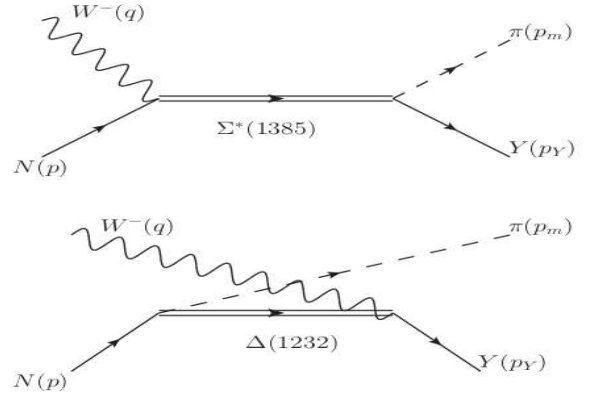
$$f_{CT}(Q^2) = f_1(Q^2) - 2F_1^n(Q^2) \left(\frac{D-F}{D+3F} \right) \left(\frac{u - M_\Sigma M_\Lambda + M M_\Sigma - M M_\Lambda}{M_\Sigma^2 - u} \right), \tag{3.145}$$

$$f_{PF}(Q^2) = 2F_1^n(Q^2) \left(\frac{D-F}{D+3F} \right) \left(\frac{(M + M_\Sigma)(u - M_\Lambda^2)}{(M + M_\Lambda)(M_\Sigma^2 - u)} \right) - f_1(Q^2), \tag{3.146}$$

where $u = (p-p_K)^2$, $f_1(Q^2) = F_1^p(Q^2) - F_1^n(Q^2)$ is the vector form factor with $F_1^p(Q^2)$ and $F_1^n(Q^2)$ being the nucleon electromagnetic form factors, discussed in Section 2.1. In analogy with the single pion production, the form factor $f_\rho(Q^2)$



(a) From top to bottom and from left to right: the contact term (CT), the kaon pole (KP), the kaon-in-flight (KF), the s-channel Σ and Λ (s- Σ and s- Λ) and the u-channel N (u- N) diagrams.



(b) Resonance diagrams included in the s-channel: $\Sigma^*(1385)$ and the u-channel: $\Delta(1232)$.

Figure 3.23: Feynman diagrams for the Cabibbo suppressed πY production process off nucleons induced by antineutrinos [172].

corresponding to the axial-vector current is given by:

$$f_\rho(Q^2) = \frac{1}{1 + Q^2/m_\rho^2}; \quad \text{with } m_\rho = 0.776 \text{ GeV.} \quad (3.147)$$

We have already discussed in Section 3.3.6, the excitation and decay of spin $\frac{1}{2}$ and $\frac{3}{2}$ resonances into a meson and a baryon in the final state. In this case of associated particle production, we have taken the contribution from both spin $\frac{1}{2}$ resonances like $S_{11}(1650)$, $P_{11}(1710)$, and spin $\frac{3}{2}$ resonances like $P_{13}(1720)$, in the numerical calculations. It should be noted that the helicity amplitudes for some of these resonances ($S_{11}(1650)$ and $P_{13}(1720)$) are given by the MAID parameterization [262]. While for $P_{11}(1710)$, we have fitted the Q^2 dependence of the helicity amplitudes to the experimental data of Ref. [264]. In the case of spin $\frac{1}{2}$ resonances, the s-channel hadronic currents for the positive ($P_{11}(1710)$) and negative ($S_{11}(1650)$) parity resonances are given in Eq. (3.46), with the explicit form of the vector and axial-vector form factors given in Eqs. (3.33) and (3.34) for the isospin $\frac{1}{2}$ resonances. Similarly in the case of positive parity spin $\frac{3}{2}$ resonances ($P_{13}(1720)$), the general expression of the hadronic current for the s-channel is given in Eq. (3.65). In this expression, the vector and axial-vector form factors used in the case of isospin $\frac{1}{2}$ resonances are given in Eqs. (3.52) and (3.64), respectively. $\mathcal{C}^{\mathcal{R}} = \frac{g_{K\Lambda R}}{f_K}$ for both spin $\frac{1}{2}$ and $\frac{3}{2}$ resonances. Using the expression for the hadronic current given in Eq. (3.142) for the background terms and Eqs. (3.46) and (3.65) for the resonance excitations, the hadronic tensor $J^{\mu\nu}$ is obtained, which contracts with the leptonic tensor $L^{\mu\nu}$ to get the expression for the matrix element squared.

In Fig. 3.22, we have presented the results for $\nu_\mu n \rightarrow \mu^- \Lambda K^+$ and $\bar{\nu}_\mu p \rightarrow \mu^+ \Lambda K^0$ processes as a function of incoming (anti)neutrino energy. The results are presented for the full model as well as for the individual contribution from $S_{11}(1650)$, $P_{11}(1710)$ and $P_{13}(1720)$ resonances. For comparison, the results for the background contribution are also presented. In the case of neutrino induced associated particle production, there is constructive interference between the background and resonance terms in the entire range of neutrino energies considered in this work. The most dominant contribution among the resonances is of $P_{11}(1710)$, which is an order of magnitude smaller than the results obtained for the full model at $E_{\nu_\mu} = 2$ GeV. While the contributions from $S_{11}(1650)$ and $P_{13}(1720)$ are almost comparable to each other and both are about 15 times smaller than the results of the full model.

However, in the case of antineutrino induced associated production, there is a destructive interference between the background and the resonance terms and the results obtained with the background terms only are almost two times the results of the full model in the entire antineutrino energy range. Among the resonances, in the low energy region ($E_{\bar{\nu}_\mu} < 1.5$ GeV), the most dominant contribution is from $P_{13}(1720)$ resonance followed by $P_{11}(1710)$ and $S_{11}(1650)$ resonances. With the increase in antineutrino energy ($E_{\bar{\nu}_\mu} > 1.6$ GeV), the results obtained from the individual contribution of $P_{13}(1720)$ and $P_{11}(1710)$ resonances overlap and are found to be an order of magnitude smaller than the results obtained using full model. As we have already discussed in Section 2.2, the hyperons are also produced in the $\Delta S = 1$ QE scattering of antineutrinos with the nucleon target, which are Cabibbo suppressed, while in the present case hyperons are produced in association with a kaon and are not Cabibbo suppressed. In view of this, we have compared the results of Λ production in the $\Delta S = 0$ associated particle production with the results of Λ production in the $\Delta S = 1$ QE process, and found that the Λ production induced by the $\Delta S = 1$ QE process dominates the associated particle production in the region of antineutrino energy $E_{\bar{\nu}_\mu} \lesssim 2$ GeV (Fig. 3.22).

Reaction	$\mathcal{A}_{\text{CT}}^{N \rightarrow Y \pi}$	$a^{N \rightarrow Y \pi}$	$\mathcal{A}_{\text{KP}}^{N \rightarrow Y \pi}$	$\mathcal{A}_{\text{KF}}^{N \rightarrow Y \pi}$	$\mathcal{A}_{\text{s-}\Sigma}^{N \rightarrow Y \pi}$	$\mathcal{A}_{\text{u-N}'}^{N \rightarrow Y \pi}$	$\mathcal{A}_{\text{s-}\Lambda}^{N \rightarrow Y \pi}$
$\bar{\nu}_l + p \rightarrow l^+ + \pi^0 + \Lambda$	$\frac{\sqrt{3}}{2\sqrt{2}f_\pi}$	$F + \frac{D}{3}$	$-\frac{\sqrt{3}}{2\sqrt{2}f_\pi}$	$-\frac{(D+3F)}{2\sqrt{6}f_\pi}$	$\frac{D}{\sqrt{3}f_\pi}$	$\frac{D+F}{2f_\pi}$	0
$\bar{\nu}_l + n \rightarrow l^+ + \pi^- + \Lambda$	$\frac{\sqrt{3}}{2f_\pi}$	$F + \frac{D}{3}$	$-\frac{\sqrt{3}}{2f_\pi}$	$-\frac{(D+3F)}{2\sqrt{3}f_\pi}$	$\frac{D}{\sqrt{3}f_\pi}$	$\frac{D+F}{\sqrt{2}f_\pi}$	0
$\bar{\nu}_l + p \rightarrow l^+ + \pi^0 + \Sigma^0$	$\frac{1}{2\sqrt{2}f_\pi}$	$F - D$	$-\frac{1}{2\sqrt{2}f_\pi}$	$\frac{(D-F)}{2\sqrt{2}f_\pi}$	0	$\frac{D+F}{2f_\pi}$	$\frac{D}{\sqrt{3}f_\pi}$
$\bar{\nu}_l + p \rightarrow l^+ + \pi^- + \Sigma^+$	$\frac{1}{\sqrt{2}f_\pi}$	$F - D$	$-\frac{1}{\sqrt{2}f_\pi}$	$\frac{(D-F)}{\sqrt{2}f_\pi}$	$-\frac{F}{f_\pi}$	0	$\frac{D}{\sqrt{3}f_\pi}$
$\bar{\nu}_l + p \rightarrow l^+ + \pi^+ + \Sigma^-$	0	0	0	0	$\frac{F}{f_\pi}$	$\frac{D+F}{\sqrt{2}f_\pi}$	$\frac{D}{\sqrt{3}f_\pi}$
$\bar{\nu}_l + n \rightarrow l^+ + \pi^- + \Sigma^0$	$-\frac{1}{2f_\pi}$	$F - D$	$\frac{1}{2f_\pi}$	$\frac{(F-D)}{2f_\pi}$	$\frac{F}{f_\pi}$	$\frac{D+F}{\sqrt{2}f_\pi}$	0
$\bar{\nu}_l + n \rightarrow l^+ + \pi^0 + \Sigma^-$	$\frac{1}{2f_\pi}$	$F - D$	$-\frac{1}{2f_\pi}$	$\frac{(D-F)}{2f_\pi}$	$-\frac{F}{f_\pi}$	$-\frac{D+F}{2f_\pi}$	0

Table 3.12: Constants $\mathcal{A}_i^{N \rightarrow Y \pi}$ and $a^{N \rightarrow Y \pi}$ (for the axial-vector piece of the CT diagram) for each reaction and diagram shown in Fig. 3.23a.

3.6.5. Single pion production with hyperon ($Y\pi$)

In antineutrino induced reactions, single pion can be produced along with a hyperon i.e.

$$\bar{\nu}_l(k) + N(p) \rightarrow l^+(k') + \pi(p_\pi) + Y(p_Y), \quad (3.148)$$

where N stands for a nucleon and Y can be a Σ or Λ hyperon. The four-momenta of particles are given in parentheses.

These processes get contribution from the NR as well as resonance channels (Fig. 3.23) specially from $\Delta(1232)$ and $\Sigma^*(1385)$ resonances (Fig. 3.23b). Recently, Benitez Galan et al. [172] have studied such processes (Eq. (3.148)) where the hadronic matrix element are calculated using effective $V - A$ strangeness-changing weak CC with vector and axial-vector form factors for the $N - Y$ and $N - Y'$ transitions. The vector and axial-vector form factors are determined in the same way as discussed in Section 3.6.4, and the values of the coefficients a and b are tabulated in Table B.1.

The matrix element of the hadronic currents for the NR Born diagrams shown in Fig 3.23a are obtained as [172]:

$$J_{\text{CT}}^\mu = i a \mathcal{A}_{\text{CT}}^{N \rightarrow Y \pi} F_D(Q^2) \bar{u}(\vec{p}_Y) [\gamma^\mu - a^{N \rightarrow Y \pi} \gamma^\mu \gamma_5] u(\vec{p}), \quad (3.149)$$

$$J_{\text{KP}}^\mu = -i a \mathcal{A}_{\text{KP}}^{N \rightarrow Y \pi} F_D(Q^2) \frac{q^\mu}{Q^2 + m_K^2} \bar{u}(\vec{p}_Y) \left[\not{q} - \frac{(M_Y - M)}{2} \right] u(\vec{p}), \quad (3.150)$$

$$J_{\text{KF}}^\mu = i a \mathcal{A}_{\text{KF}}^{N \rightarrow Y \pi} F_D(Q^2) \frac{2p_\pi^\mu - q^\mu}{(p_\pi - q)^2 - m_K^2} (M_Y + M) \bar{u}(\vec{p}_Y) \gamma_5 u(\vec{p}), \quad (3.151)$$

$$J_{\text{s-}Y'}^\mu = i a \mathcal{A}_{\text{s-}Y'}^{N \rightarrow Y \pi} \bar{u}(\vec{p}_Y) \not{p}_\pi \gamma_5 \frac{\not{p} + \not{q} + M_{Y'}}{(p + q)^2 - M_{Y'}^2} [V_{NY'}^\mu(Q^2) - A_{NY'}^\mu(Q^2)] u(\vec{p}), \quad (3.152)$$

$$J_{\text{u-N}'}^\mu = i a \mathcal{A}_{\text{u-N}'}^{N \rightarrow Y \pi} \bar{u}(\vec{p}_Y) [V_{N'Y}^\mu(Q^2) - A_{N'Y}^\mu(Q^2)] \frac{\not{p} - \not{p}_\pi + M}{(p - p_\pi)^2 - M^2} \not{p}_\pi \gamma_5 u(\vec{p}), \quad (3.153)$$

where $a = \sin \theta_C$, $Y, = \Sigma, \Lambda$; $Y' = \Sigma^*$; $N, N' = p, n$; $F_D(q^2)$ is a global dipole form factor, taken as

$$F_D(Q^2) = \frac{1}{\left(1 + \frac{Q^2}{M_D^2}\right)^2}, \quad M_D \simeq 1 \text{ GeV}. \quad (3.154)$$

for the CT, KP and KF diagrams. In Eqs. (3.149)–(3.153), the $\mathcal{A}_i^{N \rightarrow Y \pi}$ are global constants that depend on the particular reaction and are given in Table 3.12.

The vector and axial-vector weak vertices of Eqs. (3.152) and (3.153) are given by

$$V_{NY'}^\mu(Q^2) = f_1^{NY'}(Q^2) \gamma^\mu + \frac{i f_2^{NY'}(Q^2)}{M + M_{Y'}} \sigma^{\mu\nu} q_\nu, \quad A_{NY'}^\mu(Q^2) = g_1^{NY'}(Q^2) \left(\gamma^\mu + \frac{q^\mu \not{q}}{Q^2 + m_K^2} \right) \gamma_5,$$

with the vector $f_{1,2}^{NY'}(Q^2)$ and axial-vector $g_1^{NY'}(Q^2)$ form factors, discussed in Section 3.6.4.

The $Y\pi$ states in the reaction induced by the antineutrinos can also be produced by exciting the Σ^* and Δ -resonances in the s and u channels. Since $\Sigma^*(1385)$ and $\Delta(1232)$ are members of the same decuplet, therefore, under the assumption of exact $SU(3)$ flavor symmetry for the couplings, the weak transition form factors connecting an octet state to a decuplet state can be obtained. We have already discussed the coupling of baryon decuplet and octet with mesons in Section 3.3.4. The general structure of the hadronic current, the $N - R$ transition form factors, and the propagator for an intermediate baryon decuplet exchange is presented in Section 3.3.5.

The results for the total cross sections in case of the full model corresponding to all the possible $Y\pi$ channels induced by muon antineutrinos off nucleons as a function of the antineutrino energy in the laboratory frame are presented in

Reaction	$\mathcal{A}_{s-\Sigma^*}^{N \rightarrow Y \pi}$	$\mathcal{A}_{u-\Delta}^{N \rightarrow Y \pi}$
$\bar{\nu}_l + p \rightarrow l^+ + \pi^0 + \Lambda$	$\frac{C}{\sqrt{2}f_\pi}$	0
$\bar{\nu}_l + n \rightarrow l^+ + \pi^- + \Lambda$	$\frac{C}{f_\pi}$	0
$\bar{\nu}_l + p \rightarrow l^+ + \pi^0 + \Sigma^0$	0	$2\sqrt{\frac{2}{3}} \frac{C}{f_\pi}$
$\bar{\nu}_l + p \rightarrow l^+ + \pi^- + \Sigma^+$	$\frac{C}{\sqrt{6}f_\pi}$	$\frac{C\sqrt{6}}{f_\pi}$
$\bar{\nu}_l + p \rightarrow l^+ + \pi^+ + \Sigma^-$	$-\frac{C}{\sqrt{6}f_\pi}$	$\sqrt{\frac{2}{3}} \frac{C}{f_\pi}$
$\bar{\nu}_l + n \rightarrow l^+ + \pi^- + \Sigma^0$	$-\frac{C}{\sqrt{3}f_\pi}$	$-\frac{2C}{\sqrt{3}f_\pi}$
$\bar{\nu}_l + n \rightarrow l^+ + \pi^0 + \Sigma^-$	$\frac{C}{\sqrt{3}f_\pi}$	$\frac{2C}{\sqrt{3}f_\pi}$

Table 3.13: Constants $\mathcal{A}_i^{N \rightarrow Y \pi}$ for each reaction and the resonance (s- Σ^* and u- Δ) diagrams shown in Fig.3.23b.

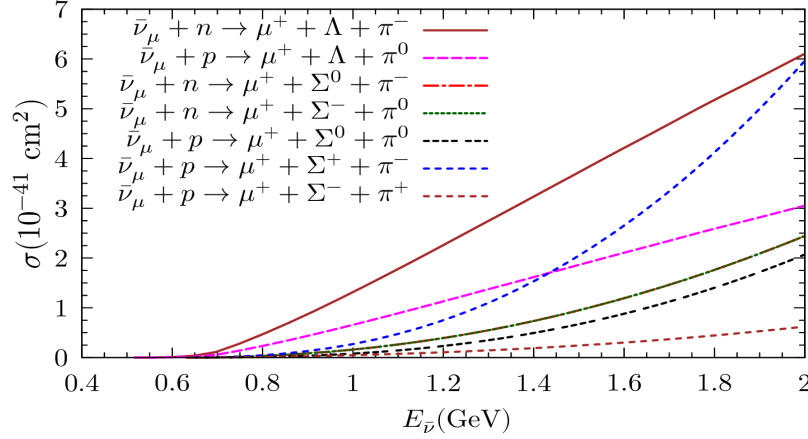


Figure 3.24: Plot of the total cross sections for $Y\pi$ production off nucleons induced by muon antineutrinos as a function of the antineutrino energy in the laboratory frame. The figure is taken from Ref. [172].

Fig. 3.24. It may be observed that the total cross sections have the same order of magnitude as those of the single K and \bar{K} production ($1K/\bar{K}$) cross sections off nucleons studied in Refs. [162, 163]. While the $1K/\bar{K}$ cross sections are smaller than the single pion cross sections because of the smallness of the Cabibbo angle; the $Y\pi$ cross section misses the strong $\Delta(1232)$ -like mechanism, apart from the threshold effect.

3.6.6. Kaon production with Ξ hyperon

The K meson can also be produced in the antineutrino reactions accompanied by a Ξ baryon through the reactions like

$$\bar{\nu}_\mu + N \rightarrow \mu^+ + K + \Xi \quad (3.155)$$

In Fig. 3.25 the Feynman diagrams that contribute to the matrix element of the hadronic current have been shown. Recently Alam et al. [173] have studied such processes, by considering NRB terms and $\Sigma^*(1385)$ resonance following the formalism discussed by us in Sections 3.3.1 and 3.3.5 for NRB and resonance contribution, respectively. The intermediate states contributing to this process are $Y = \Lambda, \Sigma$ baryons in the s and u channels as shown in Fig. 3.25.

The NRB terms have direct and cross diagrams, the corresponding matrix elements are calculated using the effective Lagrangian based on $SU(3)$ symmetry (Section 3.3.1) and are given by

$$\begin{aligned}
j_{cc}^\mu |_{sY} &= \frac{iA_s a}{f_\pi} \bar{u}(\vec{p}'_\Xi) \not{p}_K \gamma^5 \frac{\not{p} + \not{q} + M_Y}{(p+q)^2 - M_Y^2} \Gamma_{NY}^\mu u(\vec{p}), \\
j_{cc}^\mu |_{uY} &= \frac{iA_u a}{f_\pi} \bar{u}(\vec{p}'_\Xi) \Gamma_{Y\Xi}^\mu \frac{\not{p} - \not{p}_K + M_Y}{(p-p_K)^2 - M_Y^2} \not{p}_K \gamma^5 u(\vec{p}), \\
\Gamma_{B_i B_j}^\mu(Q^2) &= f_1^{B_i B_j}(Q^2) \gamma^\mu + i f_2^{B_i B_j}(Q^2) \frac{\sigma^{\mu\nu}}{M_{B_i} + M_{B_j}} q_\nu - g_1^{B_i B_j}(Q^2) \gamma^\mu \gamma^5 - g_3^{B_i B_j}(Q^2) \frac{2q^\mu}{M_{B_i} + M_{B_j}} \gamma^5, \quad (3.156)
\end{aligned}$$

where $a = \sin \theta_C$. The weak vertex function $\Gamma_{B_i B_j}^\mu(Q^2)$ denotes the weak transition from baryon B_i to B_j and it is written in terms of transition vector ($f_{1,2}^{B_i B_j}(Q^2)$) and axial-vector ($g_{1,3}^{B_i B_j}(Q^2)$) form factors. The determination of these form factors has been discussed in detail in Section 2.2 and Appendix B.

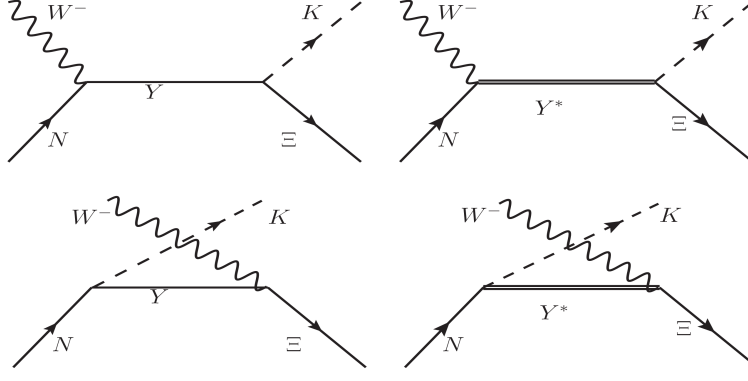


Figure 3.25: Feynman diagrams for the Ξ production. The intermediate states Y are the ($S = -1$) Λ, Σ hyperons, and Y^* is $\Sigma^*(1385)$ resonance.

Table 3.14: Constant factors (A_s, A_u) in Eq. (3.156).

Process	Direct term (A_s)			Cross term (A_u)		
	$Y = \Lambda$	$Y = \Sigma$	$Y = \Sigma^*$	$Y = \Lambda$	$Y = \Sigma$	$Y = \Sigma^*$
$\bar{\nu}_l + p \longrightarrow l^+ + K^+ + \Xi^-$	$-\frac{D-3F}{2\sqrt{3}}$	$\frac{D+F}{2}$	$\frac{1}{\sqrt{6}}$	$-\frac{D+3F}{2\sqrt{3}}$	$\frac{D-F}{2}$	$\frac{1}{\sqrt{6}}$
$\bar{\nu}_l + p \longrightarrow l^+ + K^0 + \Xi^0$	$-\frac{D-3F}{2\sqrt{3}}$	$-\frac{D+F}{2}$	$-\frac{1}{\sqrt{6}}$	0	$\frac{D-F}{\sqrt{2}}$	$\sqrt{\frac{2}{3}}$
$\bar{\nu}_l + n \longrightarrow l^+ + K^0 + \Xi^-$	0	$\frac{D+F}{\sqrt{2}}$	$\sqrt{\frac{2}{3}}$	$-\frac{D+3F}{2\sqrt{3}}$	$-\frac{D-F}{2}$	$-\frac{1}{\sqrt{6}}$

The couplings A_s and A_u in Eqs. (3.156) are obtained from the $SU(3)$ rotations at strong vertices of the diagrams given in Fig. 3.25 and are given in Table 3.14. The axial-vector couplings are used at the strong $BB'K$ vertices. As in the case of $Y\pi$ production, the contribution of $\Sigma^*(1385)$ both in the s- and u-channels is also taken into account in the case of $K\Xi$ production. The details of the Lagrangian for strong vertex of the decuplet baryons with mesons and octet baryons are given in Section 3.3.4, while for the weak vertex the details are given in Section 3.3.5.

The results are presented for $\bar{\nu}_\mu$ induced total cross section in Fig. 3.26 [173]. The full model results are shown by solid curves, while dashed lines show the results by applying a cut in the $K\Xi$ invariant mass of $W_{cut} = 2$ GeV for the corresponding processes (identified by the same color). It is found that among the three channels, $n \rightarrow K^0\Xi^-$ is the most dominant one followed by $p \rightarrow K^0\Xi^0$ and $p \rightarrow K^+\Xi^-$, and these results are compared with the results for the inclusive kaon production (Section 3.6.4) with $\Delta S = 0$ mechanisms and it has been observed that the cross section for K^0 and K^+ are about 3 and 6 percent of the corresponding $\Delta S = 0$ processes, respectively [173]. This is in agreement with Cabibbo suppression for $|\Delta S| = 1$ processes with respect to their $\Delta S = 0$ counterparts.

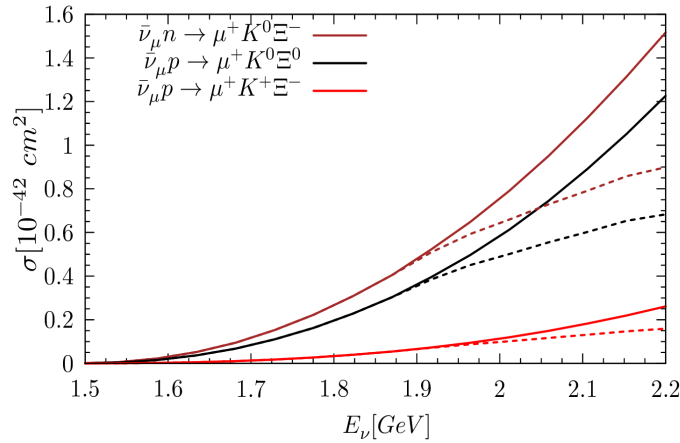


Figure 3.26: Total cross section σ vs. E_ν for the different channels of Eq. (3.155). Dashed lines show the results with $W_{cut} = 2.0$ GeV for each process (same color). The figure has been taken from Ref. [173].

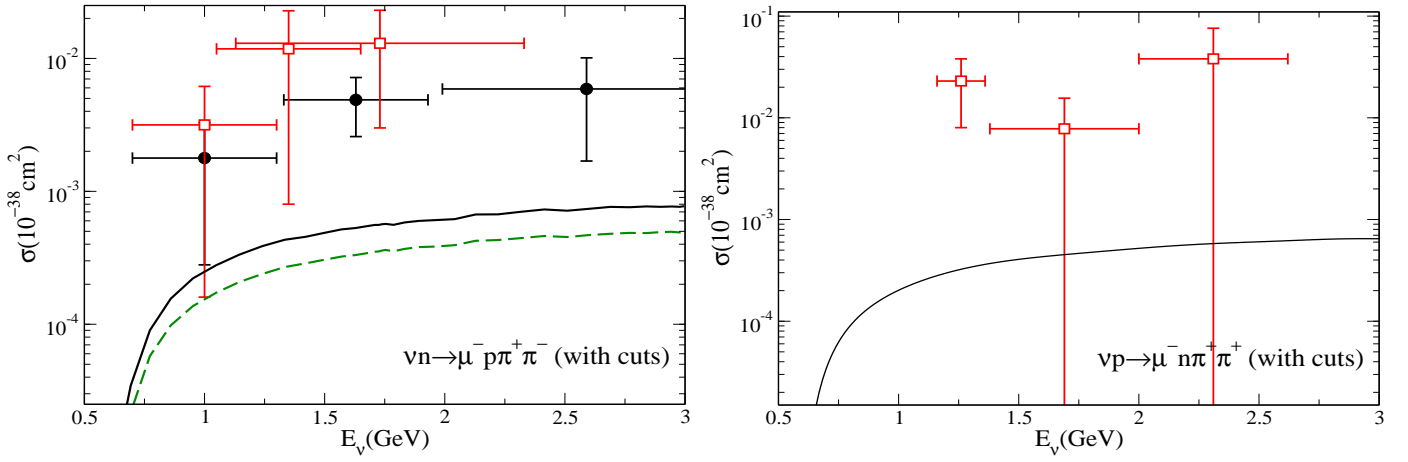


Figure 3.27: Cross section for the $\nu n \rightarrow \mu^- p \pi^+ \pi^-$ (left panel) and $\nu p \rightarrow \mu^- n \pi^+ \pi^+$ (right panel) processes with cuts as explained in Ref. [161]. Dashed line: background terms. Solid line: full model with set FF1 of nucleon-Roper transition form factors. Data from Ref. [269] (solid circles) and Ref. [336] (open squares).

3.7. Two pion production

There exists very few attempts to measure the two pion production induced by neutrinos and antineutrinos. Experiments done at ANL [321, 336] and BNL [269] investigated the two pion production processes in the threshold region, in order to test the predictions of chiral symmetry. Biswas et al. [337] used PCAC and current algebra methods to calculate the threshold production of two pions. Adjei et al. [338] made specific predictions using an effective Lagrangian incorporating the chiral symmetry. However, these models did not include any resonance production, and kept only terms up to $\mathcal{O}(1/f_\pi^2)$.

In general the reaction for neutrino induced two pion production off the nucleon target can be written as

$$\nu_l(k) + N(p) \rightarrow l^-(k') + N(p') + \pi(k_{\pi_1}) + \pi(k_{\pi_2}). \quad (3.157)$$

In recent years, Hernandez et al. [161] were the first one to study the two pion production using the effective Lagrangian given by the $SU(2)$ nonlinear σ model discussed in Section 3.3.1. This model provides expressions for the NR hadronic currents that couple with the lepton current, in terms of the first sixteen Feynman diagrams depicted in Ref. [161] and includes the contribution from the Roper resonance ($P_{11}(1440)$) to the two pion production, which has significant coupling to the 2π channel.

The results for the cross section for the $\nu n \rightarrow \mu^- p \pi^+ \pi^-$ channel in the left panel of Fig. 3.27 and for the channel $\nu p \rightarrow \mu^- n \pi^+ \pi^+$ in the right panel are presented. Recently, Nakamura et al. [309] have also studied two pion production in the DCC model in the CC induced reactions on proton and neutron targets and compared their results with ANL [321, 336] and BNL [269] data. These results show that more work both theoretically as well as experimentally are needed to understand the 2π production.

3.8. NC $\nu(\bar{\nu})$ induced single photon production off the nucleon target

The photon production can take place through the basic reactions on neutron and proton targets initiated by (anti)neutrinos through the CC and NC processes i.e.

$$\begin{aligned} \nu_l + n &\rightarrow l^- + p + \gamma, (CC) \\ \bar{\nu}_l + p &\rightarrow l^+ + n + \gamma, (CC) \\ \nu_l(\bar{\nu}_l) + N &\rightarrow \nu_l(\bar{\nu}_l) + N + \gamma, (NC) \end{aligned} \quad (3.158)$$

In the case of nuclear targets the incoherent and coherent production of photons induced by the CC and NC interactions can take place. The one photon production induced by the NC processes has been recently discussed in considerable detail due to its possible relevance in explaining the low energy excess of electron events observed in some neutrino oscillations experiments [339, 340, 341, 342, 343, 344, 164]. In the oscillation experiments for the $\nu_e(\bar{\nu}_e)$ appearance mode in $\nu_\mu(\bar{\nu}_\mu)$ beam i.e. $\nu_\mu(\bar{\nu}_\mu) \rightarrow \nu_e(\bar{\nu}_e)$, for $E_{\nu(\bar{\nu})}$ of $\sim 1\text{GeV}$, detecting $e^-(e^+)$ via Cerenkov radiation in CCQE scattering of $\nu_e(\bar{\nu}_e)$ has an important background arising due to the neutral current induced $1\pi^0$ production, where a π^0 decays into two photons ($\pi^0 \rightarrow \gamma\gamma$), and may give rise to overlapping rings or with one photon missing in the detection, resembles with an $e^-(e^+)$ event.

The process of photon production in weak processes has been discussed quite early in case of radiative muon capture, for a review see Refs. [345, 346] and neutrino reactions [347] using phenomenological effective Lagrangians. Gershtein

et al. [347] estimated the cross section for the NC reaction given in Eq. (3.158) by including the production through the exchange of virtual mesons like π^0 , ω^0 , ρ^0 and f^0 . However, in recent calculations of the one photon production in neutrino reactions the approaches based on the phenomenological effective Lagrangians as well as the effective Lagrangians based on the chiral symmetry have been used [340, 341, 344, 164], in order to understand the electron excess events in the MiniBooNE experiment [348] and also for the experiments which are being performed in the few GeV energy region like the T2K experiment. Hill et al. [340], and Zhang and Serot [341], have calculated the one photon production cross section using effective field theory, have taken into account the contribution to the transition amplitude from nucleon pole (NP and CNP), $\Delta(1232)$ pole (ΔP and $C\Delta P$), and pion, σ , ω , ρ meson exchange in the t-channel. In addition, Zhang and Serot [341] have also considered contact terms arising due to symmetry. Wang et al. [164, 349] have used the model described here in Section-3.4.1, where they considered NP and CNP, ΔP and $C\Delta P$, pion exchange term in the t-channel, as well as the contributions from the higher resonances viz. $P_{11}(1440)$, $D_{13}(1520)$ and $S_{11}(1535)$. They observed that the cross section is dominated by Δ production and its subsequent decay to $N\gamma$, similar to the observations made by earlier groups. They also find that there is significant contributions from the NP, CNP nonresonant terms in the $\sim 1\text{GeV}$ energy region, and for $E_{\nu(\bar{\nu})} > 1.5\text{GeV}$, the contribution from the $D_{13}(1520)$ resonance has been found to be significant. Furthermore, with the same values of $C_5^A(0)$ and M_A^Δ (Eq.3.64), all these results [340, 341, 342, 343, 344, 164], are consistent for $E_{\nu(\bar{\nu})} \leq 1.2\text{GeV}$. In the case of incoherent single photon production off nuclear targets, it has been found that when nuclear medium effects on the Δ properties (Section 5.5) are taken into account, there is about 30% reduction in the cross section from the free nucleon case for $E_{\nu(\bar{\nu})} \sim 1\text{GeV}$ [164]. These calculations have also been performed for the coherent NC 1γ production by these authors [164], and observed that Δ contribution alone gives about 90% contribution to the total production cross section. These results are qualitatively in agreement with the results of Zhang and Serot [343] for $E_{\nu(\bar{\nu})} < 1.5\text{GeV}$. Moreover, it was found that (anti)neutrino induced coherent NC γ cross sections are (10)15% of the incoherent NC γ cross sections.

4. Deep inelastic scattering

4.1. Introduction

It is well known that with electrons of energy in the region of few hundreds of MeV, which corresponds to the de Broglie wavelength of the virtual photons being of the order of nuclear radius, the QE electron-nucleus scattering is used to study the structure of the nucleus specially its charge and magnetic moment distributions. With the increase in energy in the region of a few GeV, when the de Broglie wavelength becomes smaller, the electron scattering takes place from the nuclear constituents like the protons and neutrons and determines the charge and magnetic moment distributions of the nucleon (nucleus) which are discussed in some detail in Section 2.1.5. These distributions are obtained in terms of the electromagnetic charge ($G_E(Q^2)$) and magnetic moment ($G_M(Q^2)$) form factors which are defined in terms of the deviation of the electron-nucleon (nucleus) scattering cross sections from the Mott scattering cross sections corresponding to the point particles. In the elastic (QE) scattering of electrons from nucleons (nuclei), the nucleon (nuclear) electromagnetic ($G_E^{N(A)}(Q^2)$ and $G_M^{N(A)}(Q^2)$) form factors depend upon only one independent kinematic variable chosen to be $Q^2 (= -q^2 \geq 0)$ due to the condition of the scattering being elastic (QE) i.e. $(q+p)^2 = p'^2$ which in the laboratory frame reduces to $Q^2 = 2M(E - E')$, where M is the mass of the target nucleon(nucleus). $G_E^{N(A)}(Q^2)$ and $G_M^{N(A)}(Q^2)$ are generally characterized by a steep fall with increase in Q^2 discussed in Section 2.1.5, and the radius of the nucleon (nucleus) charge and magnetic moment distributions are obtained using the relation

$$\langle r_{N(A)}^{2,charge} \rangle = -6 \frac{dG_E^{N(A)}}{dQ^2} \Big|_{Q^2=0}, \quad \langle r_{N(A)}^{2,mag. mom.} \rangle = -\frac{6}{\mu} \frac{dG_M^{N(A)}}{dQ^2} \Big|_{Q^2=0}. \quad (4.1)$$

With further increase in energy of the electrons, the de Broglie wavelength becomes very small which enables the electrons to probe deep into the composite structure of the nucleons. When the energy of the electrons is large enough to break the nucleons into the jet of hadrons the inelastic scattering takes place, as shown in Fig. 4.1, the process is known as DIS. In these processes the energy-momentum conservation implies $(q+p)^2 = p'^2 = W^2$, and $q^2 = (k-k')^2 \simeq -2EE'(1-\cos\theta)$, θ being the laboratory scattering angle. In case of the inclusive DIS no measurement is made on the final state hadrons X , while in the case of the exclusive IE scattering the excitation of nucleons to the definite resonance states X as discussed in Section 2 is studied. In these cases, the cross section is described in terms of the two kinematic variables i.e. energy (E') and scattering angle (θ) of the final state leptons or equivalently Q^2 and the energy transferred ν to the target, defined as

$$\nu = E - E' = \frac{M_X^2 + Q^2 - M^2}{2M}, \quad M_X^2 = W^2,$$

where $M_X = W$ is the mass of the hadronic system X . Out of these variables ν , Q^2 and W defining the kinematics of the DIS reactions, only two are linearly independent which are generally chosen to be ν and Q^2 . The first set of DIS experiments with electron beams of different energies were done at SLAC in 1968 with the 20 GeV electron accelerator

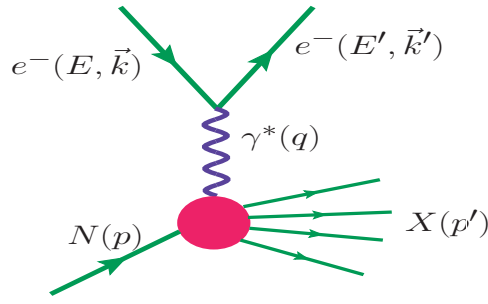


Figure 4.1: Feynman diagram representing the electron-proton DIS process.

with Q^2 in the range of $1 < Q^2 < 10 \text{ GeV}^2$ [350]. The first results on the cross sections were analyzed in terms of two functions $\nu W_2(\nu, Q^2)$ and $MW_1(\nu, Q^2)$ in analogy with the form factors in the case of elastic scattering and are called structure functions. These results were very surprising and led to a new understanding of the nucleon structure and its dynamic properties which complemented our knowledge of the nuclear structure obtained through the study of its static properties in terms of the quark model proposed by Gell-Mann [351] and Zweig [352]. Specifically the DIS experiments by Taylor, Friedman and Kendall [350, 353, 354, 355, 356] showed that:

- The DIS cross sections are an order of magnitude larger than the elastic cross sections from the proton target with a very weak Q^2 dependence as shown in Fig. 4.2 [357]. This is indicative of the electron scattering taking place not from the proton as a composite object but from its constituents which seem to be point particles without any structure.
- The structure functions $\nu W_2(\nu, Q^2)$ and $MW_1(\nu, Q^2)$ do not depend upon the two variables Q^2 and ν as expected but when studied as a function of Q^2 and $x = \frac{Q^2}{2M\nu}$, the cross sections are almost independent of Q^2 in the region of high Q^2 and depend only upon the variable x . This shows that Q^2 and ν dependence of the cross sections scale, and there is dependence on only one variable x . Such behavior of the cross sections was theoretically predicted by Bjorken assuming that the scattering takes place from the point like constituents of nucleons and the phenomenon is called Bjorken scaling with x as the Bjorken variable.

The physical interpretation of Bjorken scaling and the variable x was given by Feynman who explained the DIS results in terms of a parton model in which electrons are assumed to scatter incoherently from point like constituents of nucleon called partons. The partons were later identified with quarks as proposed by Gell-Mann [351] and Zweig [352]. Therefore the model is popularly known as the quark-parton model. In the following sections we describe briefly the formalism of DIS in the quark-parton model in the region of high Q^2 and ν , and various corrections needed to extend it to the region of lower Q^2 .

4.2. DIS of electrons from nucleons

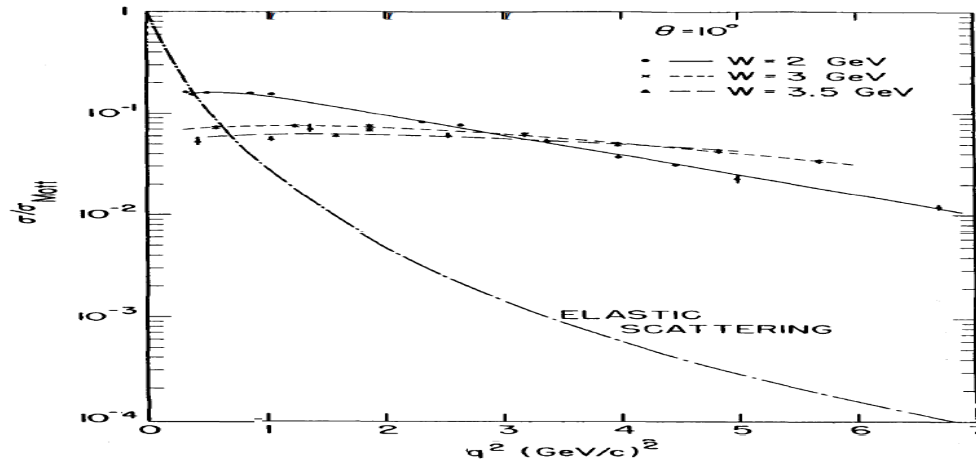


Figure 4.2: Ratio of the double differential scattering cross section (σ/σ_{Mott}) vs Q^2 for the process $e + p \rightarrow e + X$ at the different values of CM energy W and scattering angle of 10° . Figure has been taken from Ref. [357].

The matrix element for the DIS of electrons on nucleons corresponding to the Fig. 4.1, is written as

$$\mathcal{M} = - \left(\frac{e^2}{q^2} \right) l_\mu J^\mu, \quad (4.2)$$

where $l_\mu = \bar{u}(k') \gamma_\mu u(k)$, and $J^\mu(p, p') = \langle p | J_{em}^\mu | X \rangle$. The differential cross section $d\sigma$ for production of X particles, summed over all X in the laboratory frame is given by

$$d\sigma = \frac{1}{4ME} \frac{d^3 k'}{(2\pi)^3 2E'} L_{\mu\nu} J^{\mu\nu}, \quad \text{where} \quad (4.3)$$

$$L_{\mu\nu} = \frac{1}{2} \sum_{\text{spins}} l_\mu^\dagger l_\nu = 2(k_\mu k'_\nu + k_\nu k'_\mu - (k \cdot k' - m_l^2) g_{\mu\nu}), \quad (4.4)$$

$$J^{\mu\nu} = \sum_N \frac{1}{2} \sum_s \int \prod_{n=1}^N \frac{d^3 p'_n}{(2\pi)^3 (2E'_n)} \sum_{s_n} \langle ps | \tilde{J}_\mu^\dagger | X \rangle \langle X | J_\nu | ps \rangle (2\pi)^4 \delta^4(p + q - \sum_n p'_n) \quad (4.5)$$

where N number of X particles are produced. Since all the final hadronic momenta p'_n are integrated and a sum over all the final hadrons are performed in Eq. (4.5), the hadronic tensor $J^{\mu\nu}$ will depend only upon the momenta q^μ and p^ν . However, for convenience of interpretation, we redefine the second rank tensor $J^{\mu\nu}$ in terms of $W^{\mu\nu}$ as $J^{\mu\nu} = 4\pi M W^{\mu\nu}$ and construct the most general form for $W^{\mu\nu}$ using p^μ , q^ν and $g^{\mu\nu}$ as

$$\begin{aligned} W_N^{\mu\nu} = & -g^{\mu\nu} W_{1N}^{EM}(\nu, Q^2) + \frac{p^\mu p^\nu}{M^2} W_{2N}^{EM}(\nu, Q^2) - i\epsilon^{\mu\nu\lambda\sigma} \frac{p_\lambda q_\sigma}{2M^2} W_{3N}^{EM}(\nu, Q^2) + \frac{q^\mu q^\nu}{M^2} W_{4N}^{EM}(\nu, Q^2) \\ & + \frac{(p^\mu q^\nu + p^\nu q^\mu)}{M^2} W_{5N}^{EM}(\nu, Q^2) + i \frac{(p^\mu q^\nu - p^\nu q^\mu)}{M^2} W_{6N}^{EM}(\nu, Q^2), \end{aligned} \quad (4.6)$$

$W_{iN}^{EM}(\nu, Q^2)$, ($i = 1 - 6$) are the nucleon structure functions which are functions of ν and Q^2 . Since $L_{\mu\nu}$ is symmetric tensor, the terms involving $W_{3N}^{EM}(\nu, Q^2)$ and $W_{6N}^{EM}(\nu, Q^2)$ would not contribute in the electromagnetic interaction processes. The CVC at the hadronic vertex implies $q_\nu W_N^{\mu\nu} = q_\mu W_N^{\mu\nu} = 0$, which leads to the following relations

$$\left. \begin{aligned} W_{4N}^{EM}(\nu, Q^2) &= \frac{M^2}{q^2} W_{1N}^{EM}(\nu, Q^2) + \left(\frac{p \cdot q}{q^2} \right)^2 W_{2N}^{EM}(\nu, Q^2), \text{ and } \\ W_{5N}^{EM}(\nu, Q^2) &= \frac{-p \cdot q}{q^2} W_{2N}^{EM}(\nu, Q^2). \end{aligned} \right\} \quad (4.7)$$

Thus there are only two independent structure functions, which are generally chosen to be $W_{1N}^{EM}(\nu, Q^2)$ and $W_{2N}^{EM}(\nu, Q^2)$ and the expression of $W_N^{\mu\nu}$ is written in terms of these two structure functions as:

$$W_N^{\mu\nu} = \left(\frac{q^\mu q^\nu}{q^2} - g^{\mu\nu} \right) W_{1N}^{EM}(\nu, Q^2) + \left(p^\mu - \frac{p \cdot q}{q^2} q^\mu \right) \left(p^\nu - \frac{p \cdot q}{q^2} q^\nu \right) \frac{W_{2N}^{EM}(\nu, Q^2)}{M^2}. \quad (4.8)$$

Contraction of $L_{\mu\nu}$ with $W_N^{\mu\nu}$ in the limit of massless lepton results

$$L_{\mu\nu} W_N^{\mu\nu} = 4W_{1N}^{EM}(\nu, Q^2) [-q^2] + 4 \frac{W_{2N}^{EM}(\nu, Q^2)}{M^2} [2p \cdot kp \cdot k' - M^2 k \cdot k']. \quad (4.9)$$

Using the above equation in Eq. (4.3), the expression for the differential scattering cross section is obtained as [10]:

$$\frac{d^2 \sigma}{d\Omega' dE'} = \frac{4\alpha^2 E'^2}{Q^4} \left\{ 2 \sin^2 \left(\frac{\theta}{2} \right) W_{1N}^{EM}(\nu, Q^2) + \cos^2 \left(\frac{\theta}{2} \right) W_{2N}^{EM}(\nu, Q^2) \right\}. \quad (4.10)$$

This is analogous to the expression for the differential scattering cross section $\frac{d^2 \sigma}{d\Omega' dE'}$ for elastic scattering from a point particle like the $e\mu \rightarrow e\mu$ scattering [10]:

$$\left(\frac{d^2 \sigma}{dE' d\Omega'} \right)_{e\mu \rightarrow e\mu} = \left(\frac{4\alpha^2 E'^2}{Q^4} \right) \left[\cos^2 \left(\frac{\theta}{2} \right) + \frac{Q^2}{2m^2} \sin^2 \left(\frac{\theta}{2} \right) \right] \delta \left(\nu - \frac{Q^2}{2m} \right), \quad (4.11)$$

where m is the muon mass. Rewriting the expression given in Eq. (4.11) in terms of $W_{1N}^{EM}(\nu, Q^2)$ and $W_{2N}^{EM}(\nu, Q^2)$, we identify that

$$W_{2N}^{EM}(\nu, Q^2) = \delta \left(\nu - \frac{Q^2}{2m} \right) \text{ and } W_{1N}^{EM}(\nu, Q^2) = \frac{Q^2}{4m^2} \delta \left(\nu - \frac{Q^2}{2m} \right). \quad (4.12)$$

Therefore, in case of the elastic electron scattering from spin 1/2 point particles, Eq. (4.12) implies that

$$\nu W_{2N}^{EM}(\nu, Q^2) = \delta \left(1 - \frac{Q^2}{2m\nu} \right) \text{ and } m W_{1N}^{EM}(\nu, Q^2) = \frac{1}{2} \frac{Q^2}{2m\nu} \delta \left(1 - \frac{Q^2}{2m\nu} \right). \quad (4.13)$$

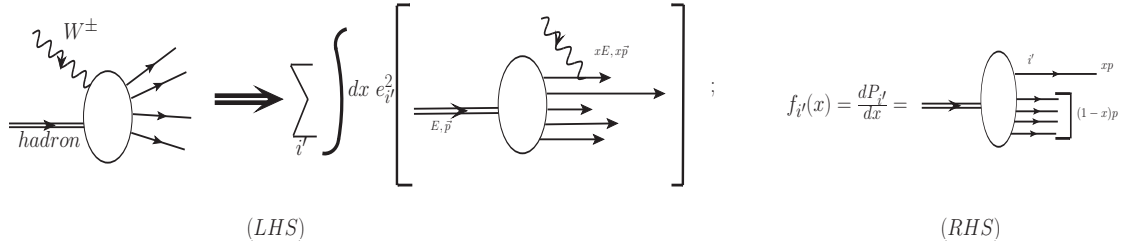


Figure 4.3: Figure on the LHS depicts incoherent sum of the contributions and on the RHS represents momentum shared by the charged partons. E , p and M are the energy, momentum and mass of the parent hadron.

It may be noticed that $\nu W_2(\nu, Q^2)$ and $mW_1(\nu, Q^2)$ which represent now point structure functions depend only upon the variable $\frac{Q^2}{2m\nu}$ and not separately on ν and Q^2 . Similar behavior of $\nu W_{2N}^{EM}(\nu, Q^2)$ and $mW_{1N}^{EM}(\nu, Q^2)$ in the case of DIS shows that the DIS of electrons from proton takes place from the point like constituents of the proton and not from the proton as a composite particle. It should be noted that this behavior of $\nu W_{2N}^{EM}(\nu, Q^2)$ and $mW_{1N}^{EM}(\nu, Q^2)$ in the case of electron muon scattering is due to the kinematics which in the case of DIS of electrons in $ep \rightarrow eX$ scattering is due to the dynamics of DIS as a result of electrons scattering from the point like constituents of the proton which leads to the phenomenon of scaling proposed by Bjorken and elaborated by Feynman as the parton model of DIS.

4.3. Parton model of DIS

Feynman proposed that it is convenient to visualize the DIS in an infinite momentum frame in which the electron scattering takes place from its constituents called partons. In this frame, parton motion is time dilated and hadron is Lorentz contracted as shown in Fig. 4.3. Moreover, the basic assumptions of the parton model are:

- i) In an infinite momentum frame, a rapidly moving nucleon appears as a jet of partons, all of which travel more or less in the same direction as that of the parent hadron such that the transverse momentum of the parton $p_T = 0$.
- ii) The basic process of electron scattering takes place from free partons to which all the energy $\nu = E - E'$ is transferred. The cross section is then summed incoherently over the contributions of partons in the nucleon (represented by the LHS of Fig. 4.3).
- iii) The momentum and energy of the nucleon is shared among the partons such that for partons transverse momentum $p_T = 0$, longitudinal momentum $p_L = xp$, energy $E' = xE$, mass $m = (x^2 E^2 - x^2 p^2)^{1/2} = xM$, where p , E and M are the momentum, energy and mass of the nucleon.
- iv) One defines the parton momentum distribution (represented on the RHS of Fig. 4.3) as $f_i(x) = \frac{dP_i}{dx}$, where $f_i(x)$ is the probability that the struck charged parton i carries a fraction x of the nucleon's four momentum p .
- v) These partons carry a fraction x of the nucleon's momentum and energy. All the fractions x add up to 1 such that

$$\sum_{i'} \int dx x f_{i'}(x) = 1,$$

where i' is sum over the charged (quarks) as well as the neutral (gluons) partons in the nucleon.

- vi) The cross sections and the structure functions $\nu W_2(\nu, Q^2)$ and $MW_1(\nu, Q^2)$ are then calculated as an incoherent sum of the cross sections from all the partons with momentum xp , energy xE and mass $m = xM$ integrated over x and weighted with the momentum distribution $f_i(x)$ for each parton i . Consequently we write

$$\nu W_2^{ep}(\nu, Q^2) = \sum_i e_i^2 \int dx f_i(x) \nu W_2^{ep_i \rightarrow ep_i}(\nu, Q^2) = \sum_i e_i^2 \int dx f_i(x) \delta\left(1 - \frac{Q^2}{2Mx\nu}\right),$$

where e_i is the charge of the parton q_i in units of $|e|$.

$$\begin{aligned} \nu W_2^{ep}(\nu, Q^2) &= \sum_i e_i^2 \int dx f_i(x) x \delta\left(x - \frac{Q^2}{2M\nu}\right) \\ \Rightarrow \nu W_2^{ep}(\nu, Q^2) \rightarrow F_2(x) &= \sum_i e_i^2 x f_i(x), \quad x = \frac{Q^2}{2M\nu}, \end{aligned}$$

where expression for νW_2 is used from Eq. (4.13), in case of electron scattering from point particles. Similarly,

$$\begin{aligned} W_1^{ep}(\nu, Q^2) &= \sum_i e_i^2 \int dx f_i(x) \frac{Q^2}{2M\nu} \frac{1}{2x} \delta\left(x - \frac{Q^2}{2M\nu}\right), \\ MW_1^{ep}(\nu, Q^2) \rightarrow F_1(x) &= \sum_i e_i^2 f_i(x) x \frac{1}{2x} = \frac{1}{2x} \nu W_2^{ep}(\nu, Q^2), \\ \text{i.e. } F_2(x) &= \sum_i e_i^2 x f_i(x), \quad F_1(x) = \frac{1}{2x} F_2(x), \end{aligned} \quad (4.14)$$

which is known as the Callan-Gross relation ($F_2(x) = 2xF_1(x)$). The application of the parton model to DIS of electrons from proton leads to the following conclusions:

- (a) The parton model reproduces the phenomenon of Bjorken scaling and the Bjorken variable $x = \frac{Q^2}{2M\nu}$ is identified as the fraction of the proton momentum carried by the partons.
- (b) It is well known that in case of the electron scattering from a spin zero point particle, there is no $W_1(\nu, Q^2)$ term implying $F_1(x) = 0$ which is not true experimentally. Therefore, partons have nonzero spin.
- (c) The separation of electron scattering from nucleons into the longitudinal (σ_L) and transverse (σ_T) components of virtual photon scattering from nucleons shows that in the limit $\nu \rightarrow \infty$, $q^2 \rightarrow \infty$, with $x = \frac{Q^2}{2M\nu}$ fixed

$$\sigma_L \rightarrow 0$$

in the case of the partons having spin 1/2. This is confirmed experimentally implying that the partons have spin 1/2, thus identifying them with the quarks.

- (d) Using Eq. (4.14), one writes

$$\frac{1}{x} F_2^{ep}(x) = \frac{4}{9} (u_p(x) + \bar{u}_p(x)) + \frac{1}{9} (d_p(x) + \bar{d}_p(x)) + \frac{1}{9} (s_p(x) + \bar{s}_p(x)), \quad (4.15)$$

$$\frac{1}{x} F_2^{en}(x) = \frac{4}{9} (u_n(x) + \bar{u}_n(x)) + \frac{1}{9} (d_n(x) + \bar{d}_n(x)) + \frac{1}{9} (s_n(x) + \bar{s}_n(x)), \quad (4.16)$$

where $u_p(x)$ and $\bar{u}_p(x)$ are the probability distributions of u quarks and antiquarks within the proton. The isospin invariance implies that $u_p(x) = d_n(x) = u(x) = u_v(x) + u_s(x)$, $d_p(x) = u_n(x) = d(x) = d_v(x) + d_s(x)$, where $q_{v,s}$ for each quark are the valence and sea quarks. Assuming a symmetric sea i.e. all the sea quark constituents have similar distribution i.e. $u_s(x) = \bar{u}_s(x) = d_s(x) = \bar{d}_s(x) = s_s(x) = \bar{s}_s(x) = S(x)$ (say), results

$$\frac{1}{x} F_2^{ep}(x) = \frac{1}{9} [4u_v(x) + d_v(x)] + \frac{4}{3} S, \quad \frac{1}{x} F_2^{en}(x) = \frac{1}{9} [u_v(x) + 4d_v(x)] + \frac{4}{3} S \quad (4.17)$$

Eqs. (4.15)–(4.17) predict the following relations:

- * Neglecting sea quark contributions

$$\frac{F_2^{en}}{F_2^{ep}} = \frac{u_v + 4d_v + \frac{4}{3}S}{4u_v + d_v + \frac{4}{3}S} \Rightarrow \frac{1}{4} \leq \frac{F_2^{en}}{F_2^{ep}} \leq 4. \quad (4.18)$$

lower (upper) limits due to the dominance of $u_v(d_v)$ independent of the value of x . If sea quarks dominates, then the ratio would be 1. These predictions have been confirmed experimentally.

- * Using Eq. (4.17) for proton and neutron

$$\frac{1}{x} (F_2^{ep}(x) - F_2^{en}(x)) = \frac{1}{3} [u_v(x) - d_v(x)], \quad (4.19)$$

leading to

$$\int \frac{dx}{x} (F_2^{ep}(x) - F_2^{en}(x)) = \frac{1}{3}, \quad (4.20)$$

when there is contribution from the valence quarks only i.e., without their sea quark partners, then the peak should occur at $x = 1/3$, if there are two valence u quarks and one d quark inside the proton and two valence d quarks and one u quark inside the neutron, which was found to be true in the experimental data from SLAC [350].

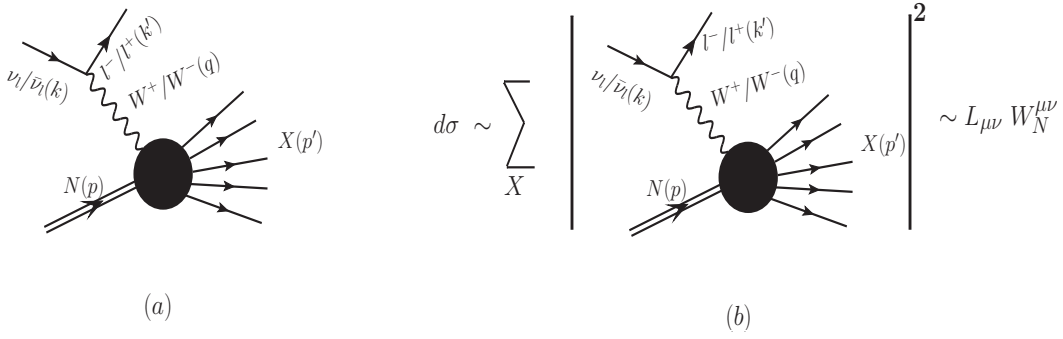


Figure 4.4: $\nu_l(\bar{\nu}_l) - N$ inclusive scattering where the summation sign represents the sum over all the hadronic states such that the cross section ($d\sigma$) for the DIS $\propto L_{\mu\nu}W_N^{\mu\nu}$. X represents the jet of hadrons in the final state.

* Defining $\epsilon_q = \int_0^1 x (q + \bar{q}) dx$, for u and d quarks and neglecting strangeness ϵ_s component, we get

$$\int dx F_2^{ep}(x) = \frac{4}{9}\epsilon_u + \frac{1}{9}\epsilon_d = 0.18, \quad \int dx F_2^{en}(x) = \frac{1}{9}\epsilon_u + \frac{4}{9}\epsilon_d = 0.12,$$

0.18 and 0.12 are the experimentally observed values [350] resulting $\epsilon_u + \epsilon_d = 0.54$, which implies that only 54% of the momentum is carried by the valence quarks. The remaining fraction of the momentum is carried by the gluons as the momentum fraction carried by the strange quarks is small. This indicates significant participation of gluons and sea quarks in the DIS specially in the low x region. This leads to the violation of Bjorken scaling. Moreover, with electron scattering from gluons, the QCD effects which describe the quark-gluon interactions also come into play to modify the predictions of QPM. These are discussed in the following sections in the context of neutrino-nucleon scattering.

4.4. ν -N scattering in the DIS region

The general expression of the double differential scattering cross section for CC induced $\nu_l(\bar{\nu}_l) - N$ scattering in the laboratory frame corresponding to the reaction:

$$\nu_l(k)/\bar{\nu}_l(k) + N(p) \rightarrow l^-(k')/l^+(k') + X(p'); \quad l = e, \mu, \tau, \quad (4.21)$$

shown in Fig. 4.4 is given by

$$\frac{d^2\sigma_N^{WI}}{d\Omega' dE'} = \frac{1}{2\pi^2} \frac{|\vec{k}'|}{|\vec{k}|} \overline{\sum} \sum |\mathcal{M}|^2. \quad (4.22)$$

For CC induced process, the matrix element square i.e. $\overline{\sum} \sum |\mathcal{M}|^2$ in Eq. (4.22), averaged over the initial spin states and summed over the final spin states, is given in terms of the leptonic ($L_{\mu\nu}$) and hadronic ($W_N^{\mu\nu}$) tensors as

$$\overline{\sum} \sum |\mathcal{M}|^2 = \frac{G_F^2}{2} \left(\frac{M_W^2}{Q^2 + M_W^2} \right)^2 L_{\mu\nu} W_N^{\mu\nu}, \quad (4.23)$$

where G_F is the Fermi coupling constant and M_W is the mass of the intermediate vector boson W^\pm . The leptonic tensor $L_{\mu\nu}$ is given in Eq. (2.15). In the case of DIS, the hadronic final state is unknown, therefore, the hadronic tensor $W_N^{\mu\nu}$ is written to parameterize our ignorance of the hadronic current. The most general form of the hadronic tensor is constructed by using the available four vectors at the disposal of hadronic vertex, i.e., the metric tensor $g^{\mu\nu}$, four momentum p^μ and the four momentum transfer q^μ . Using the expression for the leptonic tensor $L_{\mu\nu}$ from Eq. (2.15) and the hadronic tensor $W_N^{\mu\nu}$ from Eq. (4.6), the expression of the differential cross section in terms of the nucleon structure functions $W_{iN}(\nu, Q^2)$; ($i = 1 - 3$) for the case of massless lepton ($m_l \rightarrow 0$) is obtained as [10]:

$$\frac{d^2\sigma}{d\Omega' dE'} = \frac{G_F^2 E'^2 \cos^2\left(\frac{\theta}{2}\right)}{2\pi^2 \left(1 + \frac{Q^2}{M_W^2}\right)^2} \left[2 \tan^2\left(\frac{\theta}{2}\right) W_{1N}(\nu, Q^2) + W_{2N}(\nu, Q^2) \pm \left(\frac{E + E'}{M}\right) \tan^2\left(\frac{\theta}{2}\right) W_{3N}(\nu, Q^2) \right]. \quad (4.24)$$

In the case of massive lepton, all the five structure functions (as mentioned in Eq. (4.6)) would contribute $W_{iN}^{WI}(\nu, Q^2)$ ($i = 1 - 5$), while the contribution of the term with $W_{6N}(\nu, Q^2)$ vanishes when contracted with the leptonic tensor.

The scattering cross section in terms of the Bjorken scaling variable x and inelasticity $y = \frac{\nu}{E_\nu}$ is expressed as

$$\begin{aligned} \frac{d^2\sigma}{dx dy} &= \frac{G_F^2 E_\nu Q^2}{2\pi x(1 + \frac{Q^2}{M_W^2})^2} \left\{ \left[y^2 x + \frac{m_l^2 y}{2E_\nu M} \right] \frac{M}{\nu} W_{1N}(x, Q^2) + \left[\left(1 - \frac{m_l^2}{4E_\nu^2} \right) - \left(1 + \frac{Mx}{2E_\nu} \right) y \right] W_{2N}(x, Q^2) \right. \\ &\quad \left. \pm 2 \left[xy \left(1 - \frac{y}{2} \right) - \frac{m_l^2 y}{4E_\nu M} \right] W_{3N}(x, Q^2) + \frac{m_l^2 (m_l^2 + Q^2)}{4E_\nu^2 M^2} W_{4N}(x, Q^2) - \frac{m_l^2}{E_\nu M} W_{5N}(x, Q^2) \right\}. \end{aligned} \quad (4.25)$$

Following the same analogy as discussed in Section 4.3, the weak nucleon structure functions $W_{iN}^{WI}(\nu, Q^2)$ ($i = 1 - 5$) are written in terms of the dimensionless nucleon structure functions $F_{iN}^{WI}(x, Q^2)$ ($i = 1 - 5$) as:

$$\begin{aligned} MW_{1N}(\nu, Q^2) &= F_{1N}(x, Q^2), \quad \frac{Q^2}{2xM} W_{2N}(\nu, Q^2) = F_{2N}(x, Q^2), \quad \frac{Q^2}{xM} W_{3N}(\nu, Q^2) = F_{3N}(x, Q^2), \\ \frac{Q^2}{2M} W_{4N}(\nu, Q^2) &= F_{4N}(x, Q^2), \quad \frac{Q^2}{2xM} W_{5N}(\nu, Q^2) = F_{5N}(x, Q^2), \end{aligned} \quad (4.26)$$

which leads to the following expression of the differential scattering cross section [358]:

$$\begin{aligned} \frac{d^2\sigma}{dx dy} &= \frac{G_F^2 M E_\nu}{\pi(1 + \frac{Q^2}{M_W^2})^2} \left\{ \left[y^2 x + \frac{m_l^2 y}{2E_\nu M} \right] F_{1N}(x, Q^2) + \left[\left(1 - \frac{m_l^2}{4E_\nu^2} \right) - \left(1 + \frac{Mx}{2E_\nu} \right) y \right] F_{2N}(x, Q^2) \right. \\ &\quad \left. \pm \left[xy \left(1 - \frac{y}{2} \right) - \frac{m_l^2 y}{4E_\nu M} \right] F_{3N}(x, Q^2) + \frac{m_l^2 (m_l^2 + Q^2)}{4E_\nu^2 M^2 x} F_{4N}(x, Q^2) - \frac{m_l^2}{E_\nu M} F_{5N}(x, Q^2) \right\}, \end{aligned} \quad (4.27)$$

where M is the mass of the target nucleon and m_l is the mass of the final state charged lepton. x and y are the scaling variables which lie in the following ranges:

$$\frac{m_l^2}{2M(E_\nu - m_l)} \leq x \leq 1; \quad a - b \leq y \leq a + b, \quad \text{with} \quad (4.28)$$

$$a = \frac{1 - m_l^2 \left(\frac{1}{2ME_\nu x} + \frac{1}{2E_\nu^2} \right)}{2 \left(1 + \frac{Mx}{2E_\nu} \right)}, \quad b = \frac{\sqrt{\left(1 - \frac{m_l^2}{2ME_\nu x} \right)^2 - \frac{m_l^2}{E_\nu^2}}}{2 \left(1 + \frac{Mx}{2E_\nu} \right)}. \quad (4.29)$$

In general, the dimensionless nucleon structure functions are derived in the quark-parton model assuming Bjorken scaling and are functions of only one variable x . In this model, these structure functions obey Callan-Gross [359] and Albright-Jarlskog [360] relations, respectively, given by

$$F_1(x) = \frac{F_2(x)}{2x}; \quad F_5(x) = \frac{F_2(x)}{2x}.$$

At the leading order of perturbative QCD, the structure functions are derived in terms of the parton distribution functions $q_i(x)$ and $\bar{q}_i(x)$ as:

$$F_2(x) = \sum_i x[q_i(x) + \bar{q}_i(x)]; \quad xF_3(x) = \sum_i x[q_i(x) - \bar{q}_i(x)]; \quad F_4(x) = 0. \quad (4.30)$$

Generally, the proton ($F_{2,3}^p(x)$) and the neutron ($F_{2,3}^n(x)$) structure functions are obtained in the four flavor quark scheme, assuming that the heavy quark flavors (b and t) do not contribute as they are massive in comparison to the nucleon's mass ($M \ll m_b$ or m_t), as:

$$\begin{aligned} F_2^{\nu p}(x) &= 2x[d(x) + s(x) + \bar{u}(x) + \bar{c}(x)], \quad F_2^{\bar{\nu} p}(x) = 2x[u(x) + c(x) + \bar{d}(x) + \bar{s}(x)], \\ F_2^{\nu n}(x) &= 2x[u(x) + s(x) + \bar{d}(x) + \bar{c}(x)], \quad F_2^{\bar{\nu} n}(x) = 2x[d(x) + c(x) + \bar{u}(x) + \bar{s}(x)], \\ xF_3^{\nu p}(x) &= 2x[d(x) + s(x) - \bar{u}(x) - \bar{c}(x)], \quad xF_3^{\bar{\nu} p}(x) = 2x[u(x) + c(x) - \bar{d}(x) - \bar{s}(x)], \\ xF_3^{\nu n}(x) &= 2x[u(x) + s(x) - \bar{d}(x) - \bar{c}(x)], \quad xF_3^{\bar{\nu} n}(x) = 2x[d(x) + c(x) - \bar{u}(x) - \bar{s}(x)]. \end{aligned}$$

In the above expressions, $xu(x)$ represents the probability of finding an up quark with the target nucleon's momentum fraction x and similarly for other quark flavors. These probability distributions are also known as the parton distribution functions (PDFs). These PDFs for the nucleon have phenomenologically been determined by various groups and they are known in the literature by the acronyms MRST [361], GRV [362], GJR [363], MSTW [364], ABMP [365], ZEUS [366], HERAPDF [367], NNPDF [368], CTEQ [369], CTEQ-Jefferson Lab (CJ) [370], MMHT [371], etc.

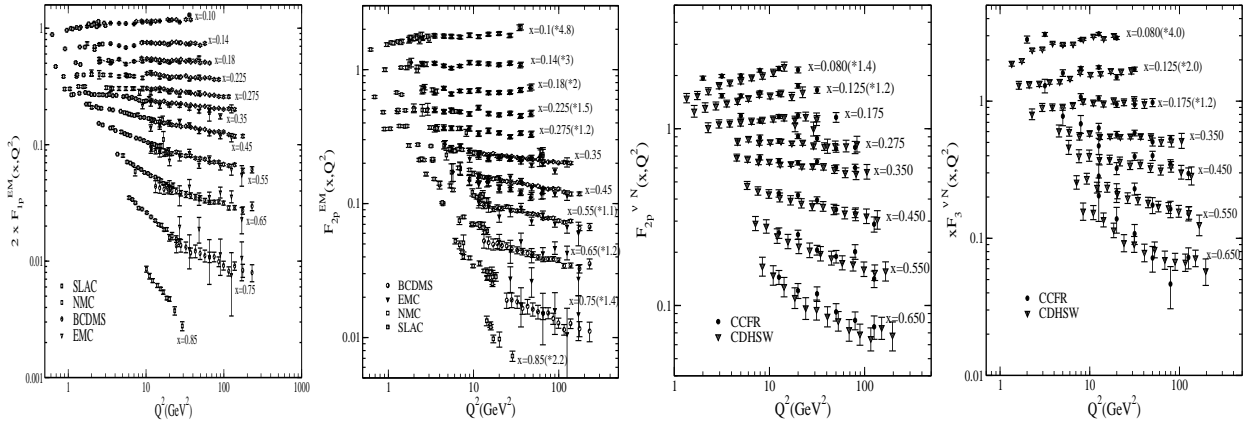


Figure 4.5: Experimental results of nucleon structure functions for electromagnetic [376, 377, 378, 379, 380] and weak [381, 382] interaction induced DIS processes.

For an isoscalar nucleon target, the structure functions are defined for nucleon F_{iN} as:

$$F_{iN} = \frac{F_{ip} + F_{in}}{2}, \quad (i = 1 - 5). \quad (4.31)$$

The neutrino scattering experiments performed at CERN using heavy liquid bubble chamber Gargamelle also provided some conclusive evidence in support of the quark-parton model [372]:

- For an isoscalar nucleon target, the ratio of the $F_2(x)$ structure functions in electron and neutrino scattering in the parton model depends only on the quark charges, i.e.,

$$\frac{\frac{1}{2} \int [F_2^{\nu p}(x) + F_2^{\nu n}(x)] dx}{\frac{1}{2} \int [F_2^{ep}(x) + F_2^{en}(x)] dx} = \frac{2}{e_u^2 + e_d^2} = \frac{18}{5}, \quad (4.32)$$

where the strange quark contribution has been neglected, and e_u and e_d are respectively the electric charges of the u and d quarks. The observed value for this ratio was 3.4 ± 0.7 [373]. This test provided the most convincing evidence that the nucleons are made up of the quarks which have fractional electric charge as real dynamical entities.

- In the quark-parton model for the point-like constituents, it was observed that the total (anti)neutrino scattering cross section is proportional to the energy in CM frame which was verified by the Gargamelle collaboration [373].
- The Gross-Llewellyn Smith sum rule [374] in the quark-parton model states that:

$$\int_0^1 F_{3N}(x) dx = \int_0^1 [u(x) - \bar{u}(x) + d(x) - \bar{d}(x)] dx = 3. \quad (4.33)$$

which was reported by the Gargamelle collaboration to be 3.2 ± 0.6 [373].

In the lowest order of perturbative QCD, the partons are treated as free, noninteracting constituents of nucleon, but the partons present inside the nucleon may interact among themselves via the gluon exchange which can be described using QCD. The incorporation of contribution from the gluon emission induces the Q^2 dependence of the nucleon structure functions, leading to the violation of Bjorken scaling. The Q^2 evolution of the structure functions is determined by the Dokshitzer-Gribov-Lipatov-Altarelli-Parisi (DGLAP) evolution equation [375]. In Fig. 4.5, the experimental results for the nucleon structure functions from several electron scattering experiments [376, 377, 378, 379, 380], and neutrino scattering experiments like CCFR [381], CDHSW [382], etc. are presented in a wide range of x and Q^2 . One may notice from the figure that with the increase in x and Q^2 , the structure functions decreases, while for lower x and Q^2 there is a rise. This behavior of structure functions show scaling breakdown. In the next section, we discuss some of the experimental results for the total cross section from various neutrino scattering experiments.

4.5. Experimental results

The total scattering cross section for CC DIS process in (anti)neutrino scattering has been experimentally measured by several experiments such as CCFRR [383], CCFR90 [384], CCFR96 [385], CDHS [386], NuTeV [387], BEBC-WBB [388], ANL [321], CHARM [389], etc., and some of them have been shown here in Fig. 4.6. These experiments have been

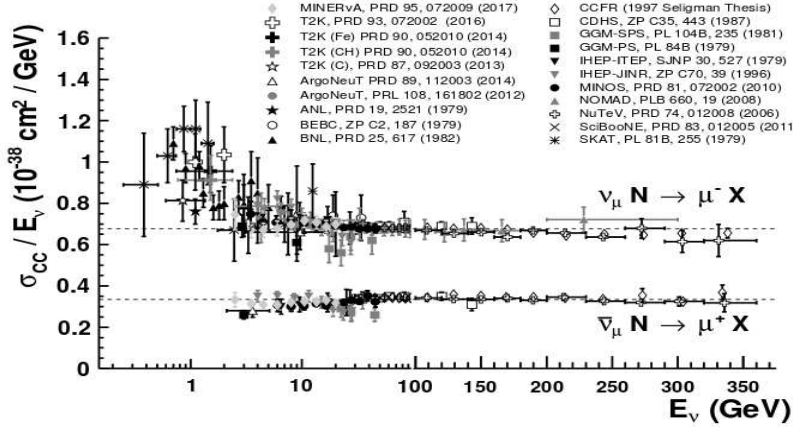


Figure 4.6: Charged current total cross section for $\nu_\mu - N$ and $\bar{\nu}_\mu - N$ processes [19].

performed on the various targets like hydrogen, deuterium, marble, iron, freon, freon-propane, etc. The world average values of the total scattering cross section for the neutrino and antineutrino interactions with nucleon/nuclear targets are [390]:

$$\sigma^{\nu N} / E_\nu = 0.677 \pm 0.014 \times 10^{-38} \text{cm}^2 \text{GeV}^{-1}, \quad \sigma^{\bar{\nu} N} / E_{\bar{\nu}} = 0.334 \pm 0.008 \times 10^{-38} \text{cm}^2 \text{GeV}^{-1}.$$

By integrating $\frac{d^2 \sigma^{\nu N}}{dx dy}$ over x and y between the limits 0 and 1, the expressions of the total scattering cross section for an isoscalar nucleon target for neutrino and antineutrino induced processes are obtained as

$$\sigma^{\nu N} = \frac{G_F^2 s}{2\pi} \sum_q \int x \left(q(x) + \frac{\bar{q}(x)}{3} \right) dx, \quad \sigma^{\bar{\nu} N} = \frac{G_F^2 s}{2\pi} \sum_q \int x \left(\frac{q(x)}{3} + \bar{q}(x) \right) dx, \quad (4.34)$$

in 3q (viz. u, d, s) or 4q (viz. u, d, s, c) model. Through the total scattering cross section, one may directly determine the total momentum carried by all the quarks and antiquarks i.e.

$$\int x(q(x) + \bar{q}(x)) dx = \frac{3\pi}{2 G_F^2 s} (\sigma^{\nu N} + \sigma^{\bar{\nu} N}) \quad (4.35)$$

and the fraction carried by the antiquarks as:

$$\frac{\int x \bar{q}(x) dx}{\int x(q(x) + \bar{q}(x)) dx} = \frac{1}{2} \left(\frac{3\sigma^{\bar{\nu} N} - \sigma^{\nu N}}{\sigma^{\nu N} + \sigma^{\bar{\nu} N}} \right), \quad (4.36)$$

which were experimentally found to be [389]:

$$\int x(q(x) + \bar{q}(x)) dx = 0.492 \pm 0.006 \pm 0.019, \quad \frac{\int x \bar{q}(x) dx}{\int x(q(x) + \bar{q}(x)) dx} = 0.154 \pm 0.005 \pm 0.011.$$

From the above equations, it may be noticed that in the limits of high Q^2 and ν , charged partons carry only 50% of the nucleon's momentum and among them antiquarks carry 15% of the charged partons momentum, and the rest of 50% of the momentum is carried by the gluons. It is therefore very important to understand the momentum distribution of gluons and the role of gluons in DIS processes.

4.6. QCD corrections

In the naive quark-parton model, a quark is treated as free fermion, while QCD tells us that quarks carry color and the color is exchanged by eight bicolored gluons. These gluons also interact among themselves. Therefore, the parton model of Feynman, Bjorken, Paschos, and others should be extended to envisage the dynamical role of gluons as the carrier of the strong force associated with the colored quarks. In the higher orders of perturbative QCD (pQCD), partons present inside the nucleon interact among themselves via the gluon exchange and the contribution from the gluons is responsible for the Q^2 dependence of the nucleon structure functions. For example, in the case of electromagnetic interactions, $\gamma^* q \rightarrow qg$ and $\gamma^* g \rightarrow q\bar{q}$ are the possible channels, which are depicted in Fig. 4.7 [391]. Generally, the Q^2 dependence of the structure functions is determined by evolving the Q^2 dependent parton densities using the DGLAP evolution equation [375]. If we

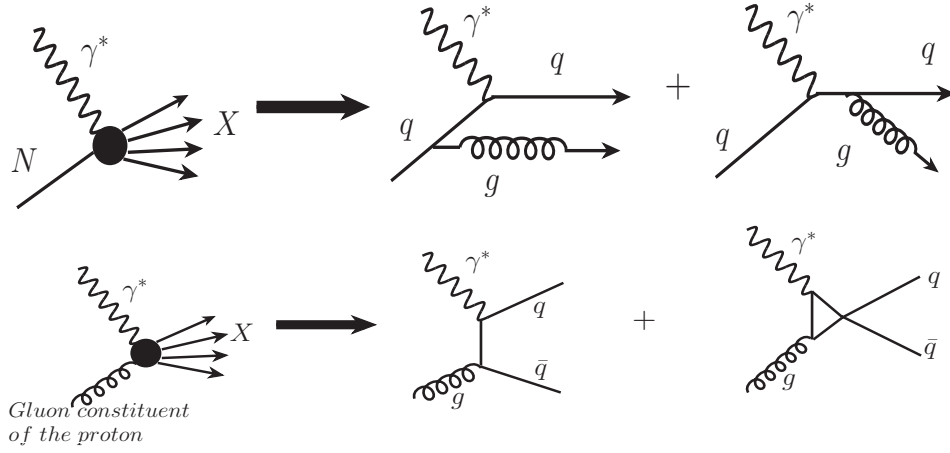


Figure 4.7: Diagrammatic representation of the processes $\gamma^* q \rightarrow qg$ (upper panel) and $\gamma^* g \rightarrow q\bar{q}$ (lower panel) [391].

know the PDFs at some initial value of four momentum transfer square say, Q_0^2 , then with the help of DGLAP evolution equation it is possible to know the value of PDFs at any other Q^2 ($> Q_0^2$) at all Bjorken x .

Since the structure functions are expressed in terms of the parton density distribution functions, therefore, it is important to understand their behavior in the entire kinematic region of x and Q^2 . For lower values of Q^2 , a few GeV^2 or less, the methods of the pQCD are not applicable due to the large value of the strong coupling $\alpha_s(Q^2)$ and the nonperturbative phenomena become important. In this region of Q^2 , the quark-quark and the quark-gluon interaction effects play important role reflecting the dynamics of the internal constituents of the nucleon. Therefore, these dynamical effects deal with the interaction of struck quark with surrounding quarks via the gluon exchange. In DIS, by using a factorization theorem the nonperturbative physics is kept into a set of well defined, gauge invariant and universal quantities, which may be expressed by the matrix element of the parton operators between the hadron states, and the matrix element is expressed in terms of an expansion in inverse power of the momentum transfer. Basically, the quantity used to expand these matrix element is the parameter λ/Q , where λ is a nonperturbative (hadronic) scale. The perturbative scale Q makes the coupling running and has to be large (at least a few GeV) in order to make perturbation theory applicable, keeping λ to be of the order of $\lambda_{QCD} \approx 200 \text{ MeV}$ such that $\lambda/Q \ll 1$ and this expansion is called the twist expansion. In the following, we discuss in brief the perturbative and nonperturbative corrections considered in this work:

(i) NLO evolution

In the naive parton model in the limit of $Q^2 \rightarrow \infty$, $\nu \rightarrow \infty$ with $x = \frac{Q^2}{2M\nu} \rightarrow \text{“a finite value”}$, nucleon structure functions are the function of x . The probability of the gluon emission due to the interaction involves the strong coupling constant $\alpha_s(Q^2)$, which depends on Q^2 . In the limit of $Q^2 \rightarrow \infty$, $\alpha_s(Q^2)$ becomes very small and, therefore, the higher order terms in a perturbative approach in which structure functions are expanded in orders of $\frac{\alpha_s(Q^2)}{2\pi}$ can be neglected. While for a moderate value of Q^2 , $\alpha_s(Q^2)$ is large and higher order terms such as next-to-leading order (NLO) give a significant contribution. The Q^2 evolution of structure functions is determined by the DGLAP evolution equation [375]. In this approach, the nucleon structure functions are expressed in terms of the convolution of coefficient function ($C_{f,i}$; ($f = q, g; i = 1 - 5$)) with the density distribution of partons ($f(x)$) inside the nucleon as [10]

$$x^{-1}F_i(x) = \sum_{f=q,g} C_{f,i}^{(n)}(x) \otimes f(x), \quad (4.37)$$

where the superscript $n = 0, 1, 2, \dots$ for $N^{(n)}\text{LO}$ evolution and the symbol \otimes is the Mellin convolution

$$C_{f,i}(x) \otimes f(x) = \int_x^1 C_{f,i}(y) f\left(\frac{x}{y}\right) \frac{dy}{y}. \quad (4.38)$$

The parton coefficient functions are generally expressed in power of $\frac{\alpha_s(Q^2)}{2\pi}$ as [392]:

$$C_{f,i}(x, Q^2) = \sum_n \left(\frac{\alpha_s(Q^2)}{2\pi} \right)^n c_{f,i}^{(n)}(x). \quad (4.39)$$

By using the above expression in Eq. (4.37), one obtains

$$\begin{aligned}
\sum_{f=q,g} C_{f,i}(x, Q^2) \otimes f(x) &= \sum_{f=q,g} \sum_n \left(\frac{\alpha_s(Q^2)}{2\pi} \right)^n c_{f,i}^{(n)}(x) \otimes f(x) \\
&= \sum_n \left(\frac{\alpha_s(Q^2)}{2\pi} \right)^n \left[c_{ns,i}^{(n)}(x) \otimes q_{ns}(x) + \langle e^2 \rangle \left\{ c_{ns,i}^{(n)}(x) \otimes q_s(x) + c_{ps,i}^{(n)}(x) \otimes q_s(x) \right. \right. \\
&\quad \left. \left. + c_{g,i}^{(n)}(x) \otimes g(x) \right\} \right],
\end{aligned}$$

where $\langle e^2 \rangle$ is the average charge of partons which is $\langle e^2 \rangle = \frac{5}{18}$ for the electromagnetic interaction and $\langle e^2 \rangle = 1$ for the weak interaction, for the four quark flavors (u, d, s, c). $q_s(x)$, $q_{ns}(x)$ are the singlet and the nonsinglet quark distributions and $g(x)$ is the gluon distribution. $c_{ns,i}^{(n)}(x)$ is the coefficient function for the nonsinglet and $c_{ps,i}^{(n)}(x)$ and $c_{g,i}^{(n)}(x)$ are the coefficient functions for the pure-singlet quark and gluon, respectively. For example, in the case of $F_2(x)$, one obtains the following expression [393]:

$$\begin{aligned}
\sum_{f=q,g} C_{f,2}(x, Q^2) \otimes f(x) &= x^{-1} F_{2N}^{EM,WI}(x) = \sum_n \left(\frac{\alpha_s(Q^2)}{2\pi} \right)^n \left[c_{ns,2}^{(n)}(x) \otimes q_{ns}(x) + \langle e^2 \rangle \left\{ c_{ns,2}^{(n)}(x) \otimes q_s(x) \right. \right. \\
&\quad \left. \left. + c_{ps,2}^{(n)}(x) \otimes q_s(x) + c_{g,2}^{(n)}(x) \otimes g(x) \right\} \right], \tag{4.40}
\end{aligned}$$

where the singlet and nonsinglet quark distributions in 4-flavor scheme are given by

$$q_s(x) = u(x) + \bar{u}(x) + d(x) + \bar{d}(x) + s(x) + \bar{s}(x) + c(x) + \bar{c}(x), \quad q_{ns}(x) = F_{2N}^{EM,WI}(x) - \langle e^2 \rangle q_s.$$

At the leading order ($n = 0$), the coefficient functions for the quarks and gluons are, respectively $c_{ns,2}^{(0)}(x) = \delta(1-x)$, $c_{ps,2}^{(0)} = 0$ and $c_{g,2}^{(0)}(x) = 0$, which lead to

$$x^{-1} F_{2N}^{EM,WI}(x) = c_{ns,2}^{(0)}(x) \otimes \{q_{ns}(x) + \langle e^2 \rangle q_s(x)\},$$

while at NLO ($n = 1$), $c_{ps,2}^{(1)} = 0$ using which in Eq. (4.40), the following expression is obtained:

$$x^{-1} F_{2N}^{EM,WI}(x) = \sum_n \left(\frac{\alpha_s(Q^2)}{2\pi} \right)^n \left[c_{ns,2}^{(1)}(x) \otimes \{q_{ns}(x) + \langle e^2 \rangle q_s(x)\} + \langle e^2 \rangle c_{g,2}^{(1)}(x) \otimes g(x) \right].$$

Similarly, one may obtain the expression for $n = 2$, which corresponds to NNLO term and so on. For the expressions of quark and gluon coefficient functions and other details, see Refs. [392, 393, 394, 395, 396].

Moreover, the expression for the weak structure function $F_{3N}^{WI}(x)$ in terms of the coefficient function and the parton density distribution function ($f(x) = q_v(x)$ as mainly valence quarks contribute in $F_{3N}(x)$) is given by [397]:

$$F_{3N}^{WI}(x) = \sum_n \left(\frac{\alpha_s(Q^2)}{2\pi} \right)^n c_{ns,3}^{(n)}(x) \otimes q_v(x),$$

where $q_v(x)$ is the valence quark distribution and $c_{ns,3}^{(n)}(x)$ is the nonsinglet coefficient function corresponding to the different perturbative terms including leading order and the other higher order terms. For detailed discussion, see Refs. [395, 397].

(ii) Target mass corrections effect

The target mass correction (TMC) is a nonperturbative effect which comes into the picture at low Q^2 , where perturbation theory fails. The TMC effect is significant at low Q^2 and high x , and has been found to be important in the determination of the distribution of valence quarks. Unfortunately, this kinematic region has not been explored much, unlike the region of high Q^2 and low x . The TMC effect is also known as “kinematic higher twist effect”. In 1976, Georgi and Politzer determined the TMC to electroweak structure functions, using operator product expansion (OPE), at the leading order of QCD [398]. Thus, these are subleading $\frac{1}{Q^2}$ corrections to the leading twist structure functions.

In the region of low Q^2 , and in the presence of heavier quarks like charm, bottom, etc., x is modified to ξ , which is known as the Nachtmann variable and is related to the Bjorken variable x as [399]:

$$\xi = \frac{2x}{1+\rho}; \quad \rho = \sqrt{1+4\mu x^2}, \quad \mu = \frac{M^2}{Q^2}, \quad x = \frac{Q^2}{2M\nu}. \tag{4.41}$$

ξ depends only on the hadronic mass and does not have corrections due to the masses of final state quarks. However, for the massive partons, the Nachtmann variable ξ gets modified to the slow rescaling variable $\bar{\xi}$. The variables ξ and $\bar{\xi}$ are related as:

$$\bar{\xi} = \xi \left(1 + \frac{m_c^2}{Q^2} \right) = \frac{\xi}{\lambda}. \quad (4.42)$$

It may be noticed from Eqs. (4.41) and (4.42) that the Nachtmann variable corrects the Bjorken variable for the effect of hadronic mass while the generalized variable $\bar{\xi}$ further corrects ξ for the effect of the partonic masses. The simplified expressions of target mass corrected structure functions for massless quarks (u , d , and s) are given in Ref. [400, 401]. TMC effect has been discussed by several authors such as Scheinbein et al. [399], Ellis et al. [402], Aivazis et al. [403], Brady et al. [404], etc. by taking into account different approaches like OPE, collinear factorization, ξ -scaling, and the approach discussed by Ellis-Furmanski-Petronzio [402]. In our numerical calculations, the nucleon structure functions ($F_{iN}(x, Q^2)$; ($i = 1 - 3$)) are evaluated by incorporating the TMC effect following the works of Scheinbein et al. [399].

(iii) **Inclusion of charm quark mass effect:**

When the mass of the charm quark is included, the dimensionless structure functions at NLO are given by [405, 406]

$$F_i^c(x, Q^2) = (1 - \delta_{i4}) \cdot s'(\bar{\xi}, \mu^2) + \frac{\alpha_s(\mu^2)}{2\pi} \left\{ \int_{\bar{\xi}}^1 \frac{dy'}{y'} \left[C_q^i(y', \frac{Q^2}{\mu^2}, \lambda) s'(\frac{\bar{\xi}}{y'}, \mu^2) + C_g^i(y', \frac{Q^2}{\mu^2}, \lambda) g'(\frac{\bar{\xi}}{y'}, \mu^2) \right] \right\}, \quad (4.43)$$

for scattering off the CKM rotated weak eigenstate [358]

$$s' = s \cdot \cos^2 \theta_C + d \cdot \sin^2 \theta_C, \quad (4.44)$$

and its QCD evolution partner g'

$$g' = g \cdot \cos^2 \theta_C + g \cdot \sin^2 \theta_C, \quad (4.45)$$

where s , d , and g are the quarks and gluon density distributions and θ_C is the Cabibbo angle. In Eq. (4.43), C_q^i and C_g^i ; ($i = 1 - 5$) are respectively the fermionic and gluonic coefficient functions at NLO which are taken from Ref. [407]. $\bar{\xi}$ is the slow rescaling variable and the variables λ and y' are defined as

$$\lambda = \frac{Q^2}{(Q^2 + m_c^2)}, \quad y' = \frac{\bar{\xi}}{y}, \quad (4.46)$$

where m_c is the charm quark mass. The terms at NLO (C_q^i and C_g^i ; ($i = 1 - 5$)) with strong coupling constant $\frac{\alpha_s(\mu^2)}{2\pi}$ give finite contribution. From the above expression, it may be noticed that though at the leading order $F_4(x) = 0$, however, when the NLO terms are taken into account, a nonzero contribution for $F_4(x)$ is obtained [358].

(iv) **Dynamical higher twist effect:**

Higher twist (HT: twist-4) is a dynamical effect arising due to the multiparton correlations [408, 409, 410]. This effect involves the interaction of the struck quark with other quarks via the exchange of gluon and it suppresses by the power of $\left(\frac{1}{Q^2}\right)^n$, where $n = 1, 2, \dots$. This effect is also pronounced in the region of low Q^2 and high x , like the TMC effect, but is negligible for high Q^2 and low x . In the formalism of OPE [408, 409], the structure functions $F_i(x, Q^2)$ are expressed in terms of powers of $1/Q^2$ (power corrections):

$$F_i(x, Q^2) = F_i^{j=2}(x, Q^2) + \frac{\mathcal{H}_i^{j=4}(x)}{Q^2} + \dots, \quad i = 1, 2, 3, \quad (4.47)$$

where the first term ($j = 2$) is known as the twist-two or leading twist (LT) term, and it corresponds to the scattering off a free quark. This term obeys the Altarelli-Parisi equation and is expressed in terms of PDFs. It is responsible for the evolution of structure functions via perturbative QCD $\alpha_s(Q^2)$ corrections. The term corresponding to $j = 4$ is known as the twist-4 or higher twist term and it reflects the multiparton correlations. It has been observed by Zaidi et al. [401] that the scattering cross section obtained with TMC and HT corrections at NLO have negligible difference from the results obtained at NNLO with the TMC effect only.

4.7. Results and discussion

In this section, we present the results for the nucleon structure functions (Fig. 4.8) and the total scattering cross sections (Figs. 4.9 and 4.10) obtained using the formalism discussed in the previous section. All the results are presented at NLO by incorporating the following considerations:

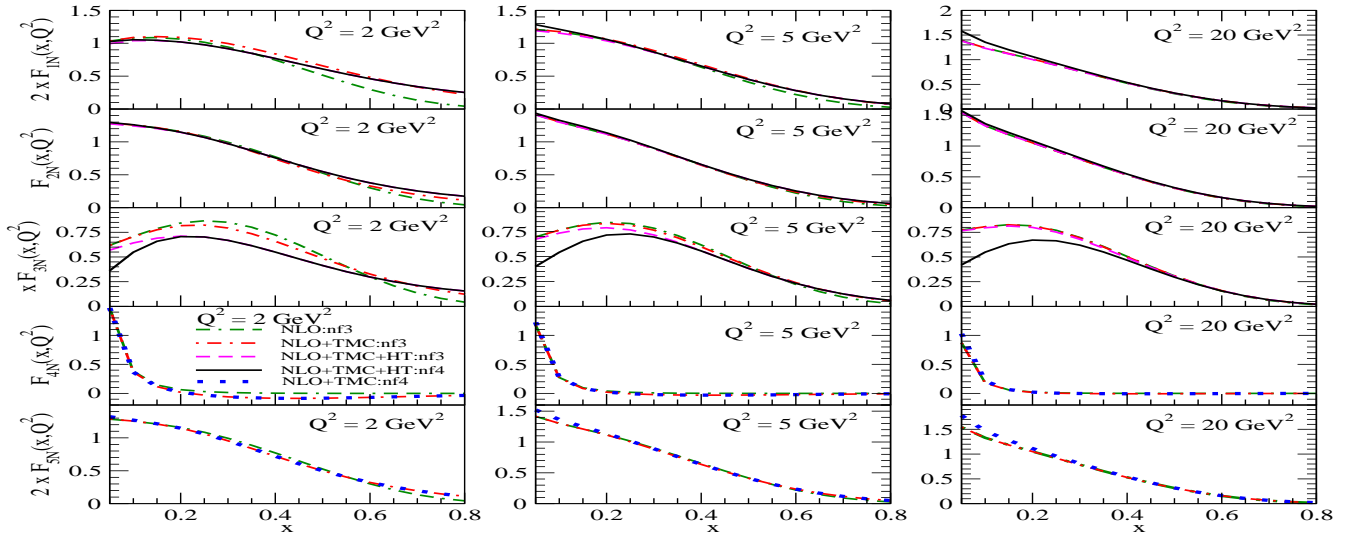


Figure 4.8: Results for the free nucleon structure functions $F_{iN}(x, Q^2)$; ($i = 1 - 5$) (top to bottom) at the different values of Q^2 viz. 2, 5 and 10 GeV^2 (left to right) are shown. These results are obtained at NLO using MMHT nucleon PDFs parameterization [371]. The results are shown without the TMC effect (double dashed-dotted line), with the TMC effect in the 3-flavor(nf3) scheme (dashed-dotted line) as well as four flavor(nf4) scheme(dotted line), with TMC and HT effects in the 3-flavor(nf3) scheme (dashed line) as well as four flavor(nf4) scheme(solid line).

- The target mass correction effect for the massive as well as massless quarks.
- The higher twist effect in terms of function $\mathcal{H}_i^{j=4}(x)$ using Eq. (4.47) in the evaluation of $F_{iN}(x, Q^2)$; $i = 1 - 3$.
- The effect of massive charm quark.

The results for the free $\nu_l(\bar{\nu}_l) - N$ scattering have been obtained in the three (nf3)- and four (nf4)- flavor schemes [401]. All the results are presented using MMHT PDFs parameterization of Harland-Lang et al. [371]. A cut in Q^2 of $Q^2 \geq 1 \text{ GeV}^2$ has been used to obtain the numerical results. The tau lepton mass has been considered in the numerical calculations for $\nu_\tau(\bar{\nu}_\tau) - N$ scattering [358].

In Fig. 4.8, the results for the free nucleon structure functions $2xF_{1N}(x, Q^2)$, $F_{2N}(x, Q^2)$, $xF_{3N}(x, Q^2)$, $F_{4N}(x, Q^2)$ and $2xF_{5N}(x, Q^2)$ are shown at the three different values of Q^2 viz. 2 GeV^2 , 5 GeV^2 and 20 GeV^2 . These results are presented at NLO without the TMC effect, with the TMC effect in 3-flavor and 4-flavor schemes, with TMC and HT effects in 3-flavor and 4-flavor schemes. It may be observed that the TMC effect is dominant in the region of high x and low Q^2 and it becomes small at low x and high Q^2 . Quantitatively, the TMC effect is found to be different in $F_{2N}(x, Q^2)$ from $F_{1N}(x, Q^2)$ while the TMC effect in $F_{5N}(x, Q^2)$ is similar to the effect in $F_{2N}(x, Q^2)$, whereas, in the case of $F_{4N}(x, Q^2)$ the whole contribution arises in the leading order due to the TMC effect. The contribution of $F_{4N}(x, Q^2)$ to the cross sections being dependent on the lepton mass (Eq. (4.27)), is important for the ν_τ scattering and in the region of $x \leq 0.2$. This contribution to the cross section becomes almost negligible for $x > 0.2$ when TMC effect is not incorporated but with the inclusion of TMC effect a nonzero though small contribution in the region of high x and low Q^2 has been found. The difference in the results of nucleon structure functions $F_{iN}(x, Q^2)$; ($i = 1 - 5$) evaluated at NLO with and without the TMC effect at $x = 0.3$ is 5%(3%) in $F_{1N}(x, Q^2)$, 2%(< 1%) in $F_{2N}(x, Q^2)$, 7%(~ 3%) in $F_{3N}(x, Q^2)$ and 4%(~ 2%) in $F_{5N}(x, Q^2)$ for $Q^2 = 2(5) \text{ GeV}^2$.

In Fig. 4.9, we compare the results for σ/E vs E with the results of Li et al. [79] (solid line with circles), Kretzer et al. [405] (solid line with right triangle without a cut on W ; dotted line with a cut of $W > 1.4 \text{ GeV}$), Jeong et al. [411] (dash-dotted line), Hagiwara et al. [412] (solid line with cross symbol), Paschos et al. [413] (dashed line with diamond), Gazizov et al. [414] (solid line with down triangle), Anelli et al. [415] (double dash-dotted line), as well as with the Monte Carlo generators GENIE [416] and NuWro [417]. These results are presented for both cases of cuts on the CM energy taken to be 1.4 GeV (dashed line) and 2 GeV (solid line) by incorporating TMC and HT effects at NLO in the four flavor scheme. Our results with a cut of $W > 1.4 \text{ GeV}$ is in good agreement with the result of Kretzer et al. [405] while there are significant differences from the result of Jeong et al. [411]. Notice that the results of the total scattering cross section with the same CM energy cut reported by Kretzer and Reno [405] and Jeong and Reno [411] are also different from each other. The difference is mainly due to the choice of lower cuts on Q^2 in the evaluation of PDFs. It is important to point out that the results given by the different models [79, 405, 411, 412, 413, 414, 415, 418] have significant differences due to their choice of different kinematic regions. Furthermore, we have observed that the effect of CM energy cut is more pronounced in the case of $\bar{\nu}_\tau - N$ DIS than in $\nu_\tau - N$ DIS process. Moreover, one may also notice that the total scattering cross section gets suppressed with the increase in the kinematic cut on the CM energy. It implies that a suitable choice

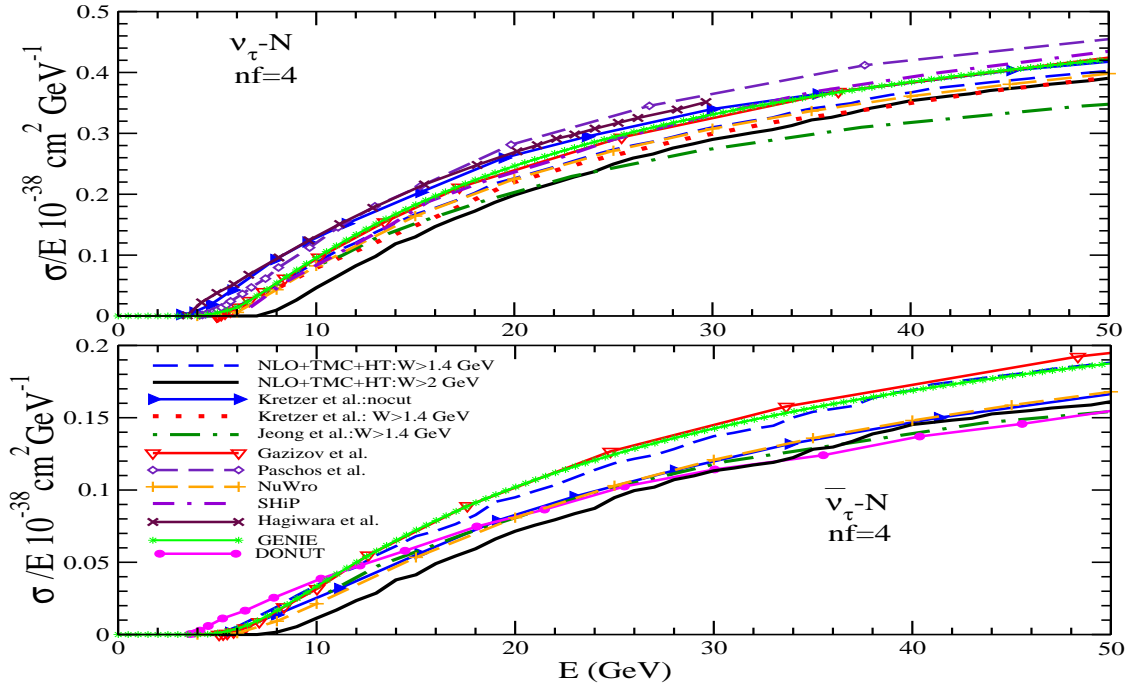


Figure 4.9: $\frac{\sigma}{E}$ vs E with a W cut of 1.4 GeV (dashed line) and 2 GeV (solid line), for tau type neutrinos (top panel) and antineutrinos (bottom panel) with the TMC [407] and HT [410] effects. These results are compared with the results of different models available in the literature [79, 405, 411, 412, 413, 414, 415] as well as with the Monte Carlo generators GENIE [416] and NuWro [417].

of W and Q^2 to define the DIS region and using them to calculate the nucleon structure functions, differential and total scattering cross sections are quite important. The constraints in the kinematic variables Q^2 and W should be kept in mind while comparing the predictions of the cross sections in various theoretical models.

To understand the effect of lepton mass on the cross section, in Fig. 4.10, the ratio of the total scattering cross sections $\frac{\sigma_{\nu_\tau - N}}{\sigma_{\nu_\mu - N}}$ vs E (dashed and solid lines) and $\frac{\sigma_{\bar{\nu}_\tau - N}}{\sigma_{\bar{\nu}_\mu - N}}$ vs E (dash-dotted and double dash-dotted lines) with cuts of $W > 1.4$ GeV and $W > 2$ GeV, are shown. These results are evaluated at NLO with TMC effect in the three flavor scheme. Notice that the lepton mass effect is important through out the energy region shown here. However, this effect becomes small with the increase in energy and therefore the ratio increases but does not reach unity even at 100 GeV. It is important to point out that for the ratio with CM energy cut of 2 GeV, the lepton mass effect is more pronounced than in the case of $W > 1.4$ GeV. One may also notice that the lepton mass effect is quantitatively different for neutrino and antineutrino induced processes, though qualitatively it shows similar behavior. For example, the ratio obtained with a cut of $W > 2$ GeV deviates from unity by 89%(36%) for neutrino and 91%(38%) for antineutrino at $E = 10(50)$ GeV.

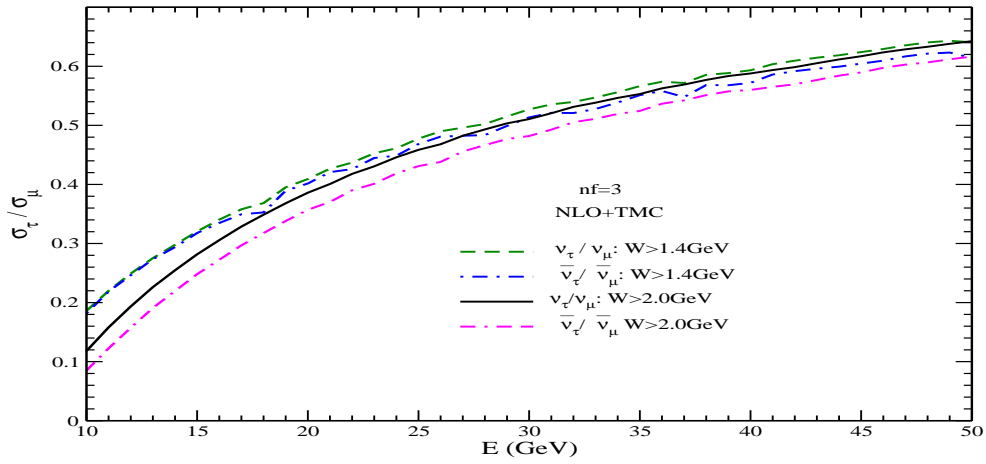


Figure 4.10: Ratio of the total scattering cross section $\frac{\sigma_{\nu_\tau}}{\sigma_{\nu_\mu}}$ vs E are shown with $W > 1.4$ GeV and $W > 2$ GeV for $\nu_\tau - N$ and $\bar{\nu}_\tau - N$ DIS. Dashed and dashed-dotted lines represent the results with $W > 1.4$ GeV while the solid and double dashed-dotted lines represent the results with $W > 2$ GeV for neutrinos and antineutrinos, respectively. The effect of TMC [407] is also included.

5. Neutrino scattering from nuclei

Most of the (anti)neutrino experiments are done with the nuclear targets in the entire energy region of $\nu_l(\bar{\nu}_l)$ starting from a few MeV to several hundreds of GeV. A theoretical description of these processes requires a knowledge of nuclear structure of the initial and final nuclei in addition to the knowledge of the neutrino interactions with nucleons within the nucleus. While the theory of the basic neutrino interactions with nucleon is described by the SM of electroweak interactions, given in Section 2.1, an appropriate knowledge of the nuclear structure of the initial and final nuclei depends upon the various energy scales used to study the (anti)neutrino-nucleus reactions. In the low energy region, neutrinos scatter elastically (quasielastically) by the weak NC (CC) interactions where the target nucleus can be in the ground state or can be excited to the higher excited states which then decays by emitting photons, electrons with neutrinos, or nucleons. As the energy increases, the IE processes occur in which leptons are produced along with the new particles like pions, kaons, or other mesons which are emitted along with the residual nucleus in the final state. In both cases, a realistic description of the nuclear wave functions in the initial and the final states corresponding to the various nuclear excitations is needed. However, in the case of inclusive reactions where only leptons are observed in the final state and a sum over all the nuclear states are performed, the nuclear wave functions of a large number of excited states in the final nucleus are needed. To obtain a reliable description of all the excited states is quite a difficult task. Alternatively, some approximation methods are used in the case of inclusive scattering like the closure approximation or the Fermi gas models, where only a reliable description of the initial state nuclear wave functions or nuclear density is needed [10]. With further increase in energy, jet of hadrons are produced in the final state along with a charged lepton, and the process is known as DIS.

In general, NME depends upon the behavior of bound nucleons in the nucleus and their response to the external probes depending upon their energy and the type of reactions induced by them. In the case of QE and IE processes, the general consideration of NME include the Fermi motion as the nucleon inside the nucleus is not at rest, Pauli blocking effect arising due to the exclusion principle when more than one nucleon is involved in the reaction, and the multinucleon correlation effects due to the strong interaction of the nucleons, and the meson exchange current effect. In most of the calculations using the impulse approximation (IA), some of these effects due to the Fermi motion, binding energy and Pauli principle on the nucleon are simulated by using a spectral function $S(\vec{p}, E)$ which is related to the imaginary part of the nucleon Green's function, and describes the energy and momentum distribution of the nucleons in the nuclear ground state. In the simplest model like the nonrelativistic Fermi gas model, it is given by theta function in the initial states i.e. $\Theta(p_F - p)$, where p_F is the Fermi momentum and has been used most frequently in early calculations. In the nuclear models using the mean field approximation, the nucleon spectral function $S(\vec{p}, E)$ has been calculated without taking into account the multinucleon correlation effects. While some recent models include the multinucleon correlation effects. For example, see the discussion in Ref. [419]. The effect of nucleon correlation helps in explaining the experimental data as observed earlier in experiments done at Saclay and NIKHEF [420, 421] and recently at JLab [422, 423] as seen in the case of $(e, e'p)$ processes in nuclei. In view of this, the phenomenologically determined values of $S(\vec{p}, E)$ from $(e, e'p)$ experiments is used in the calculations of the quasielastic and inelastic scattering of (anti)neutrinos from the nuclear targets. In the case of IE reactions, where mesons like π , K , η , etc. are produced, the most studied process is the single pion production, which is dominated by the resonance production. One considers modification of the properties of the various excited resonances especially their masses and widths in the nuclear medium. However, these modifications are well studied only in the case of Δ resonance. In addition, the pion produced in the decay of these resonances undergo final state interaction with the residual nucleus, where elastic scattering, charge exchange process (like $\pi^- p \rightarrow \pi^0 n$) or pion absorption ($\pi NN \rightarrow NN$) may take place. If the produced pion is absorbed in the nucleus, it mimics a QE-like event. With further increase in energy, the process of DIS takes place in which the (anti)neutrinos interact with the subnucleonic degrees of freedom like the mesons and quarks in the nucleons. In the case of DIS, shadowing and antishadowing corrections become important in the region of low Bjorken variable x (see Section 5.8). In the intermediate region of x , the mesonic contributions become important where the interaction of an intermediate vector boson (W , Z) takes place with the virtual mesons in the nucleus and in the region of high x , Fermi motion effects are important.

In the following, we take up the $\nu(\bar{\nu})$ -nucleus scattering in the low, intermediate, and high energy regions and discuss NME.

5.1. Coherent elastic neutrino-nucleus scattering in the low energy region

The weak NC in the $\Delta S = 0$ sector predicted in the SM allow the existence of the elastic scattering of (anti)neutrino from nucleons and nucleus without any threshold constraints and can take place even at very low energies. In the case of nuclear targets, it was pointed out by Freedman [424] and later by Kopeliovich and Frakfurt [425] that if the (anti)neutrino energy and the momentum transfer are too low to induce any excitation or particle emission in the nucleus and the nucleus remains in the ground state, then it is possible that scattering from individual nucleons can be in phase leading to coherent scattering. This coherent scattering would lead to a considerable enhancement in the cross section, which grows with the increase in the number of nucleons. The necessary condition to observe the phenomenon of coherence in ν -nucleus

scattering is that at these (anti)neutrino energies, the momentum transfer Q is low enough to satisfy the condition $Q \ll \frac{1}{R}$, where R is the radius of the nucleus.

While the condition of coherence favors the use of the medium and heavy nuclear targets with larger A , it also presents formidable problems in its detection. In coherent reactions induced by NC interactions, the only observable is the recoiling nucleus with a very small kinetic energy i.e. in the energy region of keV for (anti)neutrinos of a few MeV energy, which is very difficult to measure experimentally. However, the latest developments in the detector technology have enabled the measurement of very low energy recoils of nuclei, resulting in the observation of the coherent reactions for example by the COHERENT collaboration at ORNL at its spallation neutron source facility using the intense muon neutrino beam obtained from the pions decaying at rest [426]. The first observation of coherent elastic neutrino-nucleus scattering (CEvNS) was reported by this collaboration in CsI(Na), using the scintillating crystal detector followed by its observation in Ar with a single-phase liquid Ar detector [427] and later with the larger exposure of CsI(Na) [428]. Many new experiments are planned to be done with other nuclear targets and further substantiate the observation of CEvNS in near future [426, 429].

The elastic $\nu(\bar{\nu})$ -nucleus scattering process represented by the reaction

$$\nu(\bar{\nu}) + {}^A_ZX_N \longrightarrow \nu(\bar{\nu}) + {}^A_ZX_N \quad (5.1)$$

takes place when $\nu(\bar{\nu})$ scatters elastically from the nucleus A_ZX_N which is a composite system of A nucleons. Using the quantum mechanical principle of superposition, the scattering amplitude $F(\vec{k}', \vec{k})$ for a $\nu(\bar{\nu})$ with initial and final momentum \vec{k} and \vec{k}' respectively, is written as the sum of the scattering amplitude from each nucleon in the nucleus i.e. $f_j(\vec{k}', \vec{k})$ and is given in the lowest order as:

$$F(\vec{k}', \vec{k}) = \sum_{j=1}^A f_j(\vec{k}', \vec{k}) e^{i(\vec{k}-\vec{k}') \cdot \vec{x}_j}. \quad (5.2)$$

In the low energy region of the $\nu(\bar{\nu})$, if Q is very small as compared to the inverse of R , i.e. $QR \ll 1$, then the scattering amplitude $F(\vec{k}', \vec{k})$ becomes the coherent sum of the individual amplitudes from nucleons $f_j(\vec{k}', \vec{k})$ i.e.

$$F(\vec{k}', \vec{k}) = \sum_{j=1}^Z f_j^p(\vec{k}', \vec{k}) + \sum_{j=1}^N f_j^n(\vec{k}', \vec{k}) \quad (5.3)$$

and the scattering is called the coherent elastic $\nu(\bar{\nu})$ -nucleus scattering.

For the scattering processes induced by the electroweak probes like the electrons and (anti)neutrinos, where the contribution from the multiple scattering amplitudes are small, Eq. (5.2) gives a satisfactory description of the scattering in the lowest order. In general, the individual scattering amplitudes are different for the proton and neutron targets in nuclei, and the summations over nucleons in Eq. (5.3) runs separately over protons and neutrons. In order to calculate the scattering amplitudes $f_j(\vec{k}', \vec{k})$ from the individual nucleons in the low energy region, the interaction Lagrangian of the neutrino and the electron for their interaction with nucleon given by the SM of the electroweak interactions is used.

In the SM, the coherent scattering is driven by NC interaction Lagrangian $L^{NC}(x)$ given in Section 1.3, where l_μ^{NC} and J_μ^{NC} are the leptonic and hadronic currents whose matrix elements between the neutrino and the nucleon states is explicitly given in Section 2.1.3. In the region of low energy of the scattering processes, the nucleons are treated as nonrelativistic particles and a nonrelativistic reduction of the matrix elements [10] can be used to calculate the cross sections. The nonrelativistic reduction of the matrix elements [10] shows that in the leading order of $\mathcal{O}(\frac{q}{M})$ only the time component of the vector current with the weak charge operator and the space component of the axial-vector current with the spin operator contribute to the matrix element, which gives rise to the spin independent and the spin dependent parts of the coherent scattering. Further simplification is achieved if simple scalar and isoscalar nuclear targets with spin zero and $N = Z$ are used as considered in the early works of Freedman [424] and others, where the axial-vector currents do not contribute. In general, the contribution of the spin dependent amplitudes to the coherent process is quite small as compared to the contribution of the spin independent amplitude as the number of unpaired protons (neutrons) in the spin space is quite small as compared to the total number of protons (neutrons) in the nucleus. This has been explicitly shown recently by Hoferichter et al. [430] and many others quoted in this work. A simple calculation shows that the differential cross section $\frac{d\sigma}{dT}$, where the recoil energy of the nucleus $T \sim \frac{Q^2}{2M_A}$, with M_A being mass of the target nucleus, is given by [431]:

$$\left(\frac{d\sigma}{dT} \right)_{\nu A} = \frac{G_F^2 M_A}{2\pi} F^2(Q^2) \left[(f_1 + g_1)^2 + (f_1 - g_1)^2 \left(1 - \frac{T}{E_\nu} \right)^2 - (f_1^2 - g_1^2) \frac{M_A T}{E_\nu^2} \right], \quad (5.4)$$

and $F(Q^2)$ is the nuclear form factor. f_1 and g_1 are the vector and axial-vector couplings of the neutral vector boson in the SM to the nucleus $A(Z, N)$ given by:

$$f_1 = \tilde{f}_1^p Z + \tilde{f}_1^n N \quad \text{and} \quad g_1 = \tilde{g}_1^p Z + \tilde{g}_1^n N, \quad (5.5)$$

where $\tilde{f}_1^{p(n)}$ and $\tilde{g}_1^{p(n)}$, respectively, are the vector and axial-vector NC couplings of the (anti)neutrino to the proton (neutron). Neglecting the axial-vector contribution as compared to the contribution of the vector current, we obtain in the case of isoscalar nuclear targets with spin zero, the expression for the kinetic energy distribution as:

$$\left(\frac{d\sigma}{dT}\right)_{\nu A} \simeq \frac{G_F^2 M_A}{2\pi} F^2(Q^2) f_1^2 \left[1 + \left(1 - \frac{T}{E_\nu}\right)^2 - \frac{M_A T}{E_\nu^2} \right], \quad (5.6)$$

where f_1 is calculated using the SM values of \tilde{f}_1^p and \tilde{f}_1^n given by:

$$\tilde{f}_1^p = \frac{1}{2} - 2 \sin^2 \theta_W, \quad \tilde{f}_1^n = -\frac{1}{2} \quad (5.7)$$

leading to

$$\left(\frac{d\sigma}{dT}\right)_{\nu A} \simeq \frac{G_F^2 M_A}{2\pi} F^2(Q^2) \frac{Q_W^2}{4} \left[1 + \left(1 - \frac{T}{E_\nu}\right)^2 - \frac{M_A T}{E_\nu^2} \right], \quad (5.8)$$

where $Q_W = Q_W^n N + Q_W^p Z$ is called the weak charge of the nucleus with $Q_W^p = 1 - 4 \sin^2 \theta_W$ and $Q_W^n = -1$ being the weak charges of proton and neutron, respectively. The nuclear form factor $F(Q^2)$ is the Fourier transform of the nucleon density distribution in the nucleus and is given by

$$F(Q^2) = 4\pi \int dr r^2 \frac{\sin qr}{qr} \rho_N(r), \quad (5.9)$$

where $\rho_N(r)$ is the common density distribution for the protons and neutrons. In the case of $N \neq Z$ nuclei and neglecting the axial-vector contribution, $F(Q^2)Q_W$ is replaced by

$$F(Q^2)Q_W \rightarrow Z(1 - 4 \sin^2 \theta_W)F_p(Q^2) - NF_n(Q^2) \quad (5.10)$$

with

$$F_p(Q^2) = \frac{4\pi}{Z} \int dr r^2 \frac{\sin qr}{qr} \rho_p(r), \quad F_n(Q^2) = \frac{4\pi}{N} \int dr r^2 \frac{\sin qr}{qr} \rho_n(r). \quad (5.11)$$

The form factor $F_p(Q^2)$ obtained from the analysis of electron scattering experiments by Helm [432] and Klein-Nystrand [433] using the Gaussian or the surface diffuse density distribution are generally used. A similar density distribution for neutrons $F_n(Q^2)$ with a radius parameter larger than the proton is used. In recent years, theoretical calculations for these form factors based on the relativistic mean field, energy density functional, shell model, and coupled-clusters theory, to describe the nuclear structure have been made [431]. However it has been shown that [430] in the low energy region of relevance to the coherent scattering, the nuclear model dependence of the form factors $F_{p,n}(Q^2)$ is quite small.

The numerical values of the weak charges $Q_W^{p,n}$ of protons and neutrons including the radiative corrections are given by [431, 434]; $Q_W^{\nu_e, p} = 0.0766$, and $Q_W^{\nu_e, n} = -1.0233$ making the contributions from the protons to the CEvNS very small. Further assuming $T \ll E_\nu$ and neglecting the proton contribution, i.e., $F^2(Q^2)Q_W^2 \simeq F_n^2(Q^2)N^2$, we can write the recoil energy distribution as

$$\frac{d\sigma}{dT} \simeq \frac{G_F^2 M_A}{4\pi} N^2 F_n^2(Q^2) \left(1 - \frac{M_A T}{2E_\nu^2}\right). \quad (5.12)$$

In the above expression, radiative corrections have not been taken into account. Since the CEvNS is an elastic neutral current reaction in which the recoil nucleus is the only observable, therefore, the energy and direction of the recoiling nucleus need to be measured. While the recoil energy distribution is given in Eq. (5.12), the directional distribution is given by

$$\frac{d\sigma}{d\Omega_R} = \frac{G_F^2}{16\pi^2} Q_W^2 |F(Q^2)|^2 E_\nu (1 + \cos \theta_R), \quad (5.13)$$

showing that the CEvNS is peaked in the forward direction $\theta_R \sim 0$, where θ_R is the angle between the incoming and the outgoing neutrinos [431].

The first experimental program to measure the CEvNS cross section was started by the COHERENT collaboration at ORNL using its SNS facility using prompt monoenergetic neutrinos from $\pi^+ \rightarrow \mu^+ \nu_\mu$ decays and the delayed neutrinos from the subsequent decays of muons i.e. $\mu^+ \rightarrow e^+ \nu_e \bar{\nu}_\mu$ with continuous energy spectra. These spectra are described by $\phi_\nu(E_\nu)$ written as [429]:

$$\phi_{\nu_\mu}(E_\nu) = \frac{2m_\pi}{m_\pi^2 m_\mu^2} \delta \left(1 - \frac{2E_\nu m_\pi}{m_\pi^2 - m_\mu^2}\right), \quad (5.14)$$

$$\phi_{\nu_e}(E_\nu) = \frac{192}{m_\mu} \left(\frac{E_\nu}{m_\mu}\right)^2 \delta \left(\frac{1}{2} - \frac{E_\nu}{m_\mu}\right), \quad (5.15)$$

$$\phi_{\bar{\nu}_\mu}(E_\nu) = \frac{64}{m_\mu} \left(\frac{E_\nu}{m_\mu}\right)^2 \delta \left(\frac{3}{4} - \frac{E_\nu}{m_\mu}\right). \quad (5.16)$$

The COHERENT collaboration reported the CEvNS cross sections on CsI(Na) using a crystal detector with a 14.6 kg mass target exposed for 308 days with observation of 134 ± 22 events while the SM prediction is 173 ± 48 events [435]. A later analysis of the full CsI(Na) data with higher statistics reported the number of events to be 306 ± 20 while the SM prediction is 341 ± 11 (theory) ± 42 (expt.) events [436]. The dominant contribution to the systematic uncertainty is due to the uncertainty in the simulated flux of neutrinos which is around 10%. This corresponds to a flux averaged cross section $\langle \sigma \rangle = 165^{+30}_{-25} \times 10^{-40} \text{ cm}^2$ and $\sin^2 \theta_W = 0.22 \pm 0.028 \pm 0.026$ at $Q^2 = 50 \text{ MeV}^2$ using Helm model for the nuclear form factor.

The second result reported from the COHERENT collaboration is from COH Ar-10 experiment in which a single phase liquid argon detector was used with 24kg LAr as target and reported the observation of 159 ± 43 CEvNS events [427]. The uncertainties are due to the uncertainties in the neutrino flux as well as in the neutrino-nucleus cross sections and are about 13% [427, 437]. This corresponds to the flux averaged cross section $\langle \sigma \rangle = 2.2 \pm 0.7 \times 10^{-39} \text{ cm}^2$ consistent with the prediction of SM $1.8 \times 10^{-39} \text{ cm}^2$. Both of these cross sections measured in Cs and Ar are within 1σ of the prediction of SM.

Encouraged by these measurements, the COHERENT collaboration has already planned many CEvNS experiments to be done in future with LAr (24kg), LAr (612kg), Ge (18kg) and NaI(Tl) (3388kg), D_2O (600kg), Fe, Pb (1000kg), etc. detectors. The scintillator experiments at other laboratories around the world have been planned proposing other nuclear targets like Xe, Pb, Si, Ge, Cu, etc. However, various experiments proposed for the search of dark matter are developing detectors which can also be used to observe CEvNS using astrophysical neutrinos from supernovae, solar or atmospheric neutrinos. An excellent compilation of such future experiments is given in Ref. [431].

The physics reach of the CEvNS is very rich. A high precision determination of the CEvNS observables like the energy and angular distributions of the recoiling nucleus provides opportunity to explore various physics topics because the theoretical uncertainties in calculating these observables are quite small. This is because the value of the mixing angle θ_W in SM and the nuclear form factors in the region of very low momentum transfer are quite well known, the uncertainty arises only due to the determination of the neutrino flux, which can be improved in future. In the following, we list some physics topics in the weak interaction physics where the study of CEvNS is likely to make important contributions:

- Establishes the occurrence of coherence phenomenon in (anti)neutrino-nucleus scattering cross sections by confirming the N^2 (Eq. (5.12)) dependence of CEvNS.
- With high precision data and a knowledge of the nuclear form factors directly determine the weak mixing angle θ_W and complement its determination from the polarized electron scattering measurements, both of which directly measure the weak charge Q_W in terms of θ_W .
- CEvNS observables can help to determine the electromagnetic properties of (anti)neutrinos. The electromagnetic interactions being the charge conserving interactions can also contribute to the CEvNS observable with different type of energy and angular distributions of the recoil nucleus. A high precision determination of these observables will determine the EM properties of (anti)neutrinos like the
 - charge radius of (anti)neutrino and its flavor dependence if any using the $\nu_e(\bar{\nu}_e)$ and $\nu_\mu(\bar{\nu}_\mu)$ beams with π DAR and μ DAR neutrinos at the accelerators.
 - magnetic moment of the neutrinos by observing the recoil energy and angular distributions of the target nucleus in $\nu(\bar{\nu})$ -nucleus scattering and its flavor dependence. The differential cross section in the presence of magnetic moment of neutrino gives an additional contribution [438, 439]:

$$\left(\frac{d\sigma}{dQ^2} \right)_{\text{MagMom}} = \left(\frac{\mu_\nu}{\mu_B} \right)^2 \frac{\pi \alpha^2 Z^2}{m_e^2 Q^2} \left(1 - \frac{p \cdot q}{2M_A E_\nu} \right)^2 F_{\text{ch}}^2(Q^2), \quad (5.17)$$

where $p \cdot q = \frac{Q^2}{2} = -M_A T$, which may be written as

$$\left(\frac{d\sigma}{dT} \right)_{\text{MagMom}} = \left(\frac{\mu_\nu}{\mu_B} \right)^2 \frac{\pi \alpha^2 Z^2}{m_e^2} \left(\frac{1 - T/E_\nu}{T} + \frac{T}{4E_\nu^2} \right) F_{\text{ch}}^2(Q^2), \quad (5.18)$$

where α is the fine structure constant and $F_{\text{ch}}(Q^2)$ is the charge form factor of the nucleus, with $F_{\text{ch}}(0) = 1$, μ_ν is the magnetic moment of the neutrino and μ_B is the Bohr magneton.

- observation of a nonvanishing magnetic moment could also help to distinguish between Dirac and Majorana neutrinos.
- CEvNS can be used as strong probe to study NSI and BSM physics specially in the vector sector where the CEvNS gets the dominant contribution. Any significant deviation from the SM predictions would indicate the presence of NSI interactions. The CEvNS with $N \neq Z$ nuclei and nonzero spin can be used to explore the NSI in the axial-vector sector.

- The CEvNS with relatively higher energy beams can be used to determine the neutron distribution of nuclei as has been done using the PV observables in electron scattering. For example, the COHERENT result implies a neutron radius $R_n = 5.0 \pm 0.7$ fm and a neutron skin i.e. $R_n - R_p = 0.2 \pm 0.7$ fm for Cs, which is consistent with the theoretical calculations [440]. Such measurements can be extended to other nuclei and would compliment the studies made using PV electron scattering.

5.2. Neutrino trident production

The neutrino trident production is a process in which an (anti)neutrino scattering from nucleus “A” produces a pair of charged leptons of opposite charges along with the (anti)neutrinos in the final state. The charge lepton pair produced in the final state may be of the same flavor i.e. l^+l^- ($l = e, \mu, \tau$) or of the mixed flavor like $\mu^\pm e^\mp$, $\mu^\pm \tau^\pm$, $\tau^\pm e^\mp$, consistent with the LFN conservation for each flavor. The reactions are represented as

$$\begin{aligned} \nu_l(\bar{\nu}_l) + A &\rightarrow \nu_l(\bar{\nu}_l) + l'^-(l'^+) + l'^+(l'^-) + A && \text{(NC interaction),} \\ \nu_l(\bar{\nu}_l) + A &\rightarrow l^-(l^+) + l'^-(l'^+) + \bar{\nu}_{l'}(\nu_{l'}) + A && \text{(CC interaction).} \end{aligned} \quad (5.19)$$

Some of the reactions are induced by both the CC as well as NC, while the others by either CC or NC. The various possible reactions induced by CC and NC are shown in Table 5.1.

Scattering process	SM contribution
$\nu_\mu(\bar{\nu}_\mu)A \rightarrow \nu_\mu(\bar{\nu}_\mu)\mu^-\mu^+A$	CC + NC
$\nu_\mu(\bar{\nu}_\mu)A \rightarrow \nu_e(\bar{\nu}_e)e^\pm\mu^\mp A$	CC
$\nu_\mu(\bar{\nu}_\mu)A \rightarrow \nu_\mu(\bar{\nu}_\mu)e^-e^+A$	NC
$\nu_e(\bar{\nu}_e)A \rightarrow \nu_e(\bar{\nu}_e)e^-e^+A$	CC+NC
$\nu_e(\bar{\nu}_e)A \rightarrow \nu_\mu(\bar{\nu}_\mu)\mu^\pm e^\mp A$	CC
$\nu_e(\bar{\nu}_e)A \rightarrow \nu_e(\bar{\nu}_e)\mu^-\mu^+A$	NC

Table 5.1: Various (anti)neutrino induced trident processes from a nucleus A.

The neutrino induced trident production from the nuclear targets has been theoretically studied for more than 60 years, but the first detailed calculations were made by Czyz et al. [441] followed by many others using the effective V-A theory of weak interactions with and without using the charged intermediate vector bosons (W^\pm). A summary of the earlier

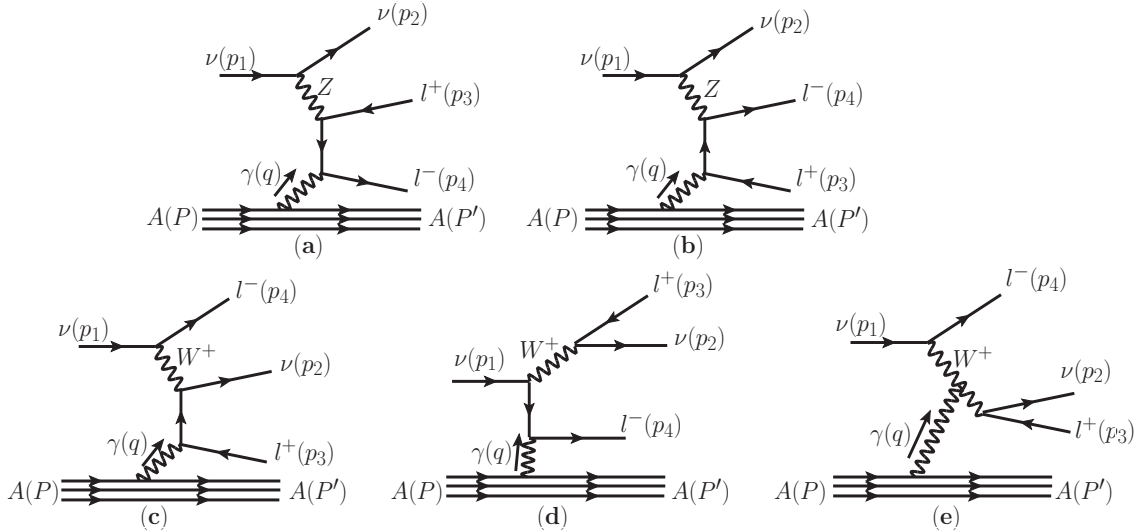


Figure 5.1: Leading hadronic contribution to the (anti)neutrino trident production in the SM.

calculations is given by Llewellyn Smith [175]. After the prediction of NC in the SM and its contribution, it was found that NC mediated by Z boson interferes destructively with the charged W boson contribution in the l^+l^- ($l = e, \mu, \tau$) channels, reducing the event rate of trident production by 40%. Experimentally the first observation of (anti)neutrino induced trident production was reported by the CHARM-II [442] and CCFR [443] collaborations followed by the NuTeV collaboration [444] in the $\nu_\mu(\bar{\nu}_\mu) + Z \rightarrow \nu_\mu(\bar{\nu}_\mu) + \mu^- + \mu^+ + Z$ channel. The ratios of these observed cross section to the

SM predicted values are [445]:

$$\frac{\sigma(\nu_\mu \rightarrow \nu_\mu \mu^+ \mu^-)_{\text{experiment}}}{\sigma(\nu_\mu \rightarrow \nu_\mu \mu^+ \mu^-)_{\text{SM}}} = \begin{cases} 1.58 \pm 0.64 & (\text{CHARM-II}) \\ 0.82 \pm 0.28 & (\text{CCFR}) \\ 0.72^{+1.73}_{-0.72} & (\text{NuTeV}) \end{cases} \quad (5.20)$$

The (anti)neutrino trident production takes place in the Coulomb field of the nucleus and the charge leptons connect the nucleus through the photon exchange as shown in Fig. 5.1. Therefore, the hadronic part of the matrix element is described by the electromagnetic form factors. The dominant contribution to the trident production is given by the diagrams 5.1a - 5.1d, there are other additional contributions which are quite small i.e.

- An additional contribution to all the diagrams in Fig. 5.1a - 5.1d, due to the Z exchange of the hadronic vertex.
- At the leptonic vertex in the case of NC contributions, there could also be an electromagnetic production through the photon exchange, if the neutrinos have magnetic moment μ_ν . The contribution of this term is very small, unless μ_ν is quite large. If sufficient number of trident events are observed, it could be used to put a limit on μ_ν . With current experimental information on the trident events, the limits obtained are $10^{-8} \mu_B$ [431] i.e two order of magnitude smaller than those obtained from the other experiments [19].
- There is an additional contribution from the diagram Fig. 5.1e, which is quite small due to two W boson propagators.
- In principle, the photon at the hadronic vertex can interact with the whole nucleus or the individual nucleons or with the quarks in the nucleus. Depending upon the energy and the momentum carried by the virtual photon which is transferred to the hadronic system leading to the coherent, diffractive or DIS production of tripletons. It has been shown that the contribution to the total trident production is dominated by the coherent production in the few GeV region of neutrino energies [446].

In view of this, we focus on the coherent production of tridents, which are contributed by the leading diagrams of Fig. 5.1a-5.1d with the photon exchange at the hadronic vertex and the W or Z exchange at the leptonic vertex of the tridents and mention the other processes only briefly. The reader is referred to the literature for the diffractive and the DIS production of trident [446].

The earlier calculations of (anti)neutrinos induced trident production are done for the coherent production using the effective photon approximation (EPA). In this approximation, the cross section for the full scattering process is calculated in two parts. In the first part, the cross section $\sigma(s)$ is obtained for the photo-trident production process i.e. $\gamma\nu \rightarrow \nu l^\pm l'^\mp$ with real photons with the CM energy (\sqrt{s}) of $\gamma\nu$ system using the effective $V - A$ theory or the SM. Quantitatively, the radiative contribution of these three processes to the trident production depends upon the specific pair of leptons produced in the final state and the energy region of the neutrinos. Typically the contribution of the diffractive scattering varies between 10% – 40% being largest in the case of $\mu^- \mu^+$ channels but Magill [447] find a larger contribution. The contribution of DIS is smaller than 10%.

In the second part, this cross section is multiplied by the probability $P(s, q^2)$ of the nucleus producing a virtual photon with virtuality q^2 given by

$$P(s, q^2) = \frac{Z^2 e^2}{4\pi^2} \frac{ds}{s} \frac{dq^2}{q^2} |F(q^2)|^2, \quad (5.21)$$

where \sqrt{s} is the CM energy of the incoming neutrino and a real photon system, Ze is the charge and $F(q^2)$ is the electromagnetic form factor of nucleus determined from the electron scattering experiments. In recent years, the applicability of EPA in the various kinematic regions of s and q^2 has been described by some authors and a full calculation in the case of spin zero nuclei has been done as outlined below [446, 447].

The full matrix element \mathcal{M} for the trident production by the (anti)neutrinos corresponding to the diagrams 5.1a-5.1d is given using the SM as

$$i\mathcal{M} = L^\mu(\{p_j\}, q) \frac{-ig_{\mu\nu}}{q^2} H_X^\nu(P, P'); \quad j = 2 - 4. \quad (5.22)$$

The total leptonic amplitude $L^\mu(\{p_j\}, q)$ is given by

$$L^\mu \equiv -\frac{ieG_F}{\sqrt{2}} [\bar{u}(p_2)\gamma^\tau(1 - \gamma_5)u(p_1)] \times \bar{u}(p_4) \left[\gamma_\tau(V_{\alpha\beta\kappa} - A_{\alpha\beta\kappa}\gamma_5) \frac{1}{(\not{q} - \not{p}_3 - m_3)} \gamma^\mu + \gamma^\mu \frac{1}{(\not{p}_4 - \not{q} - m_4)} \gamma_\tau(V_{\alpha\beta\kappa} - A_{\alpha\beta\kappa}\gamma_5) \right] v(p_3), \quad (5.23)$$

and the total hadronic $H_X^\nu(P, P')$ amplitude is given by

$$H_X^\nu \equiv \langle H(P) | J_{\text{EM}}^\nu(q^2) | H(P') \rangle, \quad (5.24)$$

ν Process	$\bar{\nu}$ Process	V_{ijk}	A_{ijk}	Mediator
$\nu_e \rightarrow \nu_e e^+ e^-$	$\bar{\nu}_e \rightarrow \bar{\nu}_e e^+ e^-$	$\frac{1}{2} + 2 \sin^2 \theta_W$	$\frac{1}{2}$	W,Z
$\nu_\mu \rightarrow \nu_\mu \mu^+ \mu^-$	$\bar{\nu}_\mu \rightarrow \bar{\nu}_\mu \mu^+ \mu^-$	$\frac{1}{2} + 2 \sin^2 \theta_W$	$\frac{1}{2}$	W,Z
$\nu_e \rightarrow \nu_\mu \mu^+ e^-$	$\bar{\nu}_e \rightarrow \bar{\nu}_\mu e^+ \mu^-$	1	1	W
$\nu_\mu \rightarrow \nu_e e^+ \mu^-$	$\bar{\nu}_\mu \rightarrow \bar{\nu}_e \mu^+ e^-$	1	1	W
$\nu_e \rightarrow \nu_e \mu^+ \mu^-$	$\bar{\nu}_e \rightarrow \bar{\nu}_e \mu^+ \mu^-$	$-\frac{1}{2} + 2 \sin^2 \theta_W$	$-\frac{1}{2}$	Z
$\nu_\mu \rightarrow \nu_\mu e^+ e^-$	$\bar{\nu}_\mu \rightarrow \bar{\nu}_\mu e^+ e^-$	$-\frac{1}{2} + 2 \sin^2 \theta_W$	$-\frac{1}{2}$	Z
$\nu_\mu \rightarrow \nu_\mu \tau^+ \tau^-$	$\bar{\nu}_\mu \rightarrow \bar{\nu}_\mu \tau^+ \tau^-$	$-\frac{1}{2} + 2 \sin^2 \theta_W$	$-\frac{1}{2}$	Z
$\nu_\mu \rightarrow \nu_\tau \mu^- \tau^+$	$\bar{\nu}_\mu \rightarrow \bar{\nu}_\tau \mu^+ \tau^-$	1	1	W
$\nu_\tau \rightarrow \nu_\tau \mu^- \mu^+$	$\bar{\nu}_\tau \rightarrow \bar{\nu}_\tau \mu^+ \mu^-$	1	1	W
$\nu_\tau \rightarrow \nu_\tau \mu^+ \mu^-$	$\bar{\nu}_\tau \rightarrow \bar{\nu}_\tau \mu^- \mu^+$	$-\frac{1}{2} + 2 \sin^2 \theta_W$	$-\frac{1}{2}$	Z
$\nu_\tau \rightarrow \nu_\tau e^+ e^-$	$\bar{\nu}_\tau \rightarrow \bar{\nu}_\tau e^- e^+$	$-\frac{1}{2} + 2 \sin^2 \theta_W$	$-\frac{1}{2}$	Z

Table 5.2: Modified vector and axial coupling constants for the different combinations of incident neutrino flavors and final states

where $q \equiv P - P'$ is the four momentum transfer, m_3 (m_4) the positively (negatively) charged lepton mass, $V_{\alpha\beta\kappa}$ ($A_{\alpha\beta\kappa}$) $\equiv g_V^\beta (g_A^\beta) \delta_{\beta\kappa} + \delta_{\alpha\beta}$ ($\beta = \alpha$ or κ) the vector (axial-vector) couplings, depending on the channel. $J_{EM}^\nu(q^2)$ is the electromagnetic current for the hadronic system A (a nucleus or a nucleon). $V_{\alpha\beta k}$ and $A_{\alpha\beta k}$ for various processes are given in the Table 5.2. Using this matrix element, the differential cross section is given by

$$\frac{d^2\sigma_{\nu X}}{dQ^2 d\hat{s}} = \frac{1}{32\pi^2(s - M_A^2)^2} \frac{H_X^{\mu\nu} L_{\mu\nu}}{Q^4}, \quad (5.25)$$

where

$$L_{\mu\nu} = \frac{1}{2s+1} \overline{\sum} \sum_{spins} L_\mu^\dagger L_\nu, \quad H^{\mu\nu} = \frac{1}{2J+1} \overline{\sum} \sum_{spins} H^{\mu\dagger} H^\nu. \quad (5.26)$$

In the case of coherent scattering, the hadronic matrix element is taken as the matrix element of electromagnetic current between nuclear states of initial and final momentum P^μ and P'^μ , respectively, and for a spin zero nucleus “ A ”, it is given by

$$H = \langle A(P') | J_{EM}^\mu | A(P) \rangle F(Q^2) (P + P')^\mu, \quad (5.27)$$

where $F(Q^2)$ is the nuclear form factor.

In the case of nucleons, the hadronic matrix element for the protons and neutrons is given as [10]:

$$\langle N(P) | J_{EM}^\mu | N(P') \rangle = e \bar{u}(P') \left[F_1^N(Q^2) \gamma^\mu + i \sigma^{\mu\nu} F_2^N(Q^2) \frac{q_\nu}{2M} \right] u(p) \quad (5.28)$$

for $N = p, n$ and

$$H_N^{\mu\nu} = Z H_p^{\mu\nu}(P, P') + (A - Z) H_n^{\mu\nu}(P, P'). \quad (5.29)$$

However, the nucleons are not free but bound with a momentum and energy distribution which is described by the spectral function $S(\vec{p}, E)$. Such spectral functions for the nucleon have been determined experimentally from the electron-nucleus scattering from many nuclei and have been used extensively in the calculations of QE $\nu - A$ scattering. The simplest form of $S(\vec{p}, E)$ is given by a theta function $\Theta(P_F - P)$ in the case of Fermi gas model in which the free nucleon cross section is multiplied by a quenching factor $R(\vec{q})$ to obtain the cross section from the bound nucleons [175, 448], i.e.

$$\frac{d^2\sigma_{\nu-N}}{dQ^2 ds} \rightarrow R(|\vec{q}|) \frac{d^2\sigma_{\nu-N}}{dQ^2 ds}, \quad (5.30)$$

where

$$\begin{aligned} R(|\vec{q}|) &= \frac{3}{2} \frac{|\vec{q}|}{2p_F} - \frac{1}{2} \left(\frac{|\vec{q}|}{2p_F} \right)^3 & \text{if } |\vec{q}| < 2p_F \\ &= 1, & \text{if } |\vec{q}| > 2p_F, \end{aligned} \quad (5.31)$$

and p_F is the Fermi momentum of the nucleons in the nucleus, generally taken to be different for proton and neutron in case of $N \neq Z$ nuclei. Taking the values of the hadronic current given in Eqs. (5.28) and (5.29), the cross section is calculated with help of Eq. (5.30). Generally, the cross section for the trident production is calculated in terms of the photon flux for the longitudinal and transverse photons following the standard procedure. In the region of very low

$Q^2, Q^2 \sim 0$ the contribution from the transverse photons dominates corresponding to the real photon, justifying the use of EPA in the coherent production.

In the case of DIS, the cross section for the (anti)neutrino nucleon scattering $\frac{d\sigma_{\nu N}}{dQ}$ is obtained by convoluting the (anti)neutrino parton (q) cross section $\frac{d\sigma_{\nu q}}{dQ}$ with the nucleon ($N = p, n$) parton distribution functions $f_q^N(\xi, Q)$, with Q being the four momentum transfer and is given by [447]:

$$\sigma_{\nu N} = \sum_q \int_{\xi_{min}}^1 d\xi \int_{Q_{min}}^{Q_{max}} dQ \frac{d\sigma_{\nu q}(\xi, q)}{dQ} f_q^N(\xi, Q), \quad (5.32)$$

where ξ is the fractional momentum of the partons (q) with $\xi_{min} \geq 0$ to enable the creation of lepton pair. With $\sigma_{\nu N}$ calculated from Eq. (5.32), the DIS contribution to the nuclear cross section is obtained using

$$\sigma_{\nu A} = Z\sigma_{\nu p} + (A - Z)\sigma_{\nu n}. \quad (5.33)$$

The details for calculating $\frac{d\sigma_{\nu q}}{dQ}$ can be found in Ref. [447]. Fig. 5.2 shows some representative results (reactions given in Table 5.1) for coherent trident cross section of (anti)neutrino scattering on ^{40}Ar and ^{208}Pb [446].

In recent years, the rare process of the neutrino trident production has been studied in some detail as a probe of new physics proposed in many theoretical models of BSM physics, which propose the existence of new vector bosons (Z') and new scalar boson (S'), which couple to the leptons and the quarks [447, 449]. The effect of coupling of these new bosons to the leptons at the leptonic vertex has been studied for the different values of mass and coupling of these bosons and varying them in the reasonable limits, which are constrained by the limits obtained mainly from the recent experiment in muon ($g - 2$) measurements and the limits obtained from the search of such bosons in the BaBar and Belle experiments [450]. In view of the importance of such theoretical studies, many experiments to measure the neutrino trident production with accelerator and atmospheric neutrinos have been proposed.

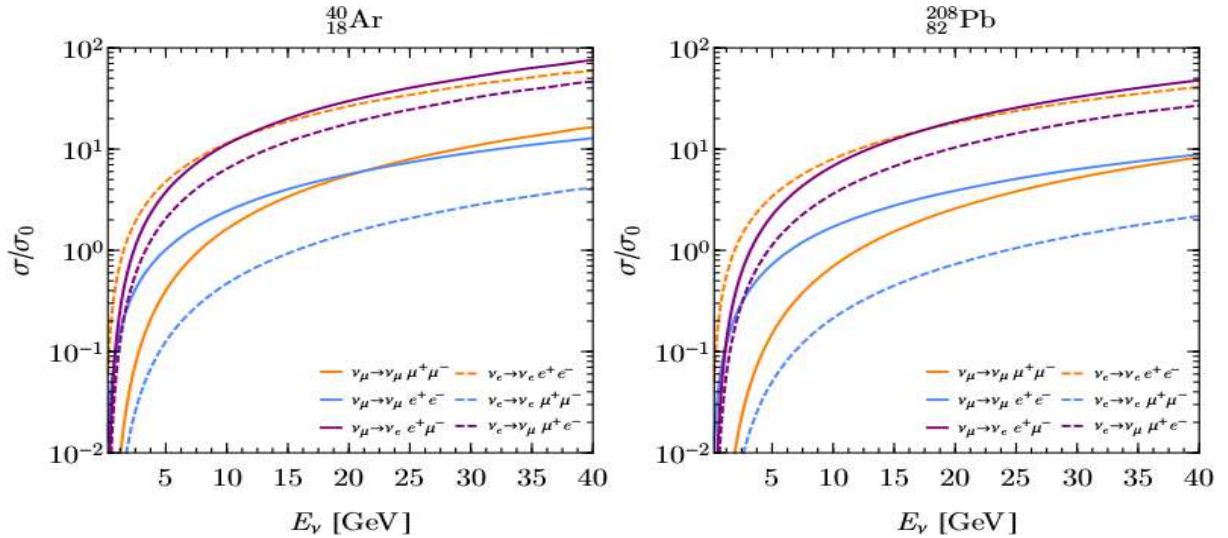


Figure 5.2: Coherent trident cross section for (anti)neutrino scattering on ^{40}Ar and ^{208}Pb . The figures are taken from Ref. [446].

A summary of the feasibility of seeing neutrino trident production events in these experiments using accelerator neutrinos has been given by Ballett et al. [446]. On the other hand, the use of atmospheric neutrinos to see the neutrino trident production in IceCube, ARCA and DeepCore has been discussed by Ge et al. [449].

5.3. Exclusive reactions in ν -nucleus scattering in the low energy region

With the increase in (anti)neutrino energies, corresponding to the de Broglie wavelength of the (anti)neutrinos being smaller than the nuclear radius, the interaction takes place with the individual nucleons in the nucleus, leading the target nucleus to be in any one of its excited states defined by a definite spin (\vec{S}), parity (P), and angular momentum (\vec{J}) or its breaking leading to a residual nucleus which can be in its ground state or in an excited state. These are called exclusive reactions. In both cases particles like photons, electrons, nucleons or alpha particles can be emitted as a decay product of the excited nuclear states through α, β and γ decays or as the direct emission of these particles in the knock out reactions in case of the emission of the nucleons and alpha particles. With further increase in energy, new particles like mesons ($\pi, 2\pi, K, \eta, \rho$, etc.) or associated production of strange particles ($K\Lambda, K\Sigma$, etc.) can take place. These reactions can be induced by the CC as well as NC in the ν -nucleus reactions using ν_e, ν_μ and ν_τ beams. However,

in the low energy region (below τ production threshold), the CC reactions are induced only by the $\nu_e(\bar{\nu}_e)$ and $\nu_\mu(\bar{\nu}_\mu)$, while NC reactions can be induced by (anti)neutrinos of all flavors. In this section, we discuss the low energy exclusive neutrino-nucleus reactions in which the final nucleus is either in the ground state or in an excited state, for example

$$\begin{aligned}\nu_{e(\mu)} + {}^A_Z X_N &\rightarrow e^-(\mu^-) + {}^A_{Z+1} Y_{N-1} ({}^A_{Z+1} Y_{N-1}^*) \\ \bar{\nu}_{e(\mu)} + {}^A_Z X_N &\rightarrow e^+(\mu^+) + {}^A_{Z-1} Y_{N+1} ({}^A_{Z-1} Y_{N+1}^*) \\ \nu_{e,\mu,\tau} + {}^A_Z X_N &\rightarrow \nu_{e,\mu,\tau} + {}^A_Z X_N ({}^A_Z X_N^*)\end{aligned}\quad (5.34)$$

Historically, the first study of the exclusive $\bar{\nu}$ -nucleus scattering was done by Cowan et al. [9] with the reactor antineutrinos with $E_{\bar{\nu}_e} \leq 10$ MeV on Cl target leading to the detection of antineutrino. In the very low energy region, the “superallowed” Fermi and Gamow-Teller transitions to the ground state of final nucleus take place. The theoretical calculations of the neutrino-nucleus cross section of these reactions have minimal uncertainties arising due to the theoretical inputs. This is because most of the nuclei are theoretically well described in their ground state and the Q^2 dependence of the nuclear form factor is almost constant in this low energy region. Moreover, the parameters describing the nuclear transitions involved in these reactions, are also well determined from either the β decays of these nuclei or the low energy (p, n) reactions. As the (anti)neutrino energy increases relevant to the $\nu_e(\bar{\nu}_e)$ and $\nu_\mu(\bar{\nu}_\mu)$ beams from the pion and muon decays at rest (as well as decays in flight) available at the particle accelerators, many nuclear states are excited needing information about the nuclear wave functions of various nuclei in their ground state as well as in the excited states, which are reachable by both the allowed and forbidden Fermi and Gamow-Teller transitions. In the simplest description of neutrino-nucleus reactions, the impulse approximation with the shell model wave functions calculated using different types of nucleon-nucleon potentials has been used in literature to study the exclusive neutrino reactions from nuclear targets. The effect of nucleon-nucleon correlations in the nuclear wave functions have also been included in a few calculations using various theoretical tools like the RPA, CRPA, QRPA etc. Moreover, the contribution of the meson exchange current (MEC) and other subnuclear degrees of freedom have also been included in some calculations [151].

We present in the following, the basics of the general formalism for describing the exclusive (anti)neutrino-nucleus reactions applicable at low and intermediate energies. The basic CC and NC reactions on nuclear targets take place on nucleon $N = n, p$ and are written as:

$$\begin{aligned}\nu_l + n &\longrightarrow l^- + p, & \bar{\nu}_l + p &\longrightarrow l^+ + n, & l = e, \mu, \tau & \Delta S = 0 \text{ (CC)} \\ \nu_l(\bar{\nu}_l) + n(p) &\longrightarrow \nu_l(\bar{\nu}_l) + n(p), & & & & \Delta S = 0 \text{ (NC)} \\ \bar{\nu}_l + n(p) &\longrightarrow l^+ + \Sigma^- (\Lambda, \Sigma^0), & & & & |\Delta S| = 1 \text{ (CC)}\end{aligned}\quad (5.35)$$

for which the matrix elements of the weak leptonic l^μ and hadronic J^μ currents are given in Eqs. (2.10) and (2.11).

In case of the nucleons bound in the nucleus, these matrix elements are to be taken between the initial ($|i\rangle$) and final ($|f\rangle$) nuclear states i.e.

$$\begin{aligned}\mathcal{M}_{fi}^{CC(NC)} &= \langle f | \mathcal{H}_W^{CC(NC)} | i \rangle, \\ \text{where } \mathcal{H} &= -\frac{G_F a}{\sqrt{2}} \int d\vec{x} l_{CC(NC)}^\mu J_\mu^{CC(NC)}(x),\end{aligned}\quad (5.36)$$

$l_{CC(NC)}^\mu$ is the leptonic current, $J_\mu^{CC(NC)}$ is the hadronic current operator in the nucleus, which are given in Eqs. (2.11) and (2.18), and $a = \cos \theta_C(1)$ for CC (NC) induced processes.

Since the leptons in Eq. (5.35) are free point particles, therefore, we can describe them by plane waves (neglecting the Coulomb effect of the charged lepton in final state) to write

$$l_\mu(x) = l_\mu e^{-i\vec{q}\cdot\vec{x}}, \quad q = k' - k = p - p', \quad (5.37)$$

such that the matrix element \mathcal{M}_{fi} between the initial ($|i\rangle$) and final ($|f\rangle$) states, using the notation l^μ for $l_{CC(NC)}^\mu$ and J^μ for $J_\mu^{CC(NC)}$ for simplicity, is written as

$$\mathcal{M}_{fi} = -\frac{G_F a}{\sqrt{2}} \langle f | \int e^{-i\vec{q}\cdot\vec{x}} l^\mu J_\mu(x) d\vec{x} | i \rangle = -\frac{G_F a}{\sqrt{2}} \langle f | \int e^{-i\vec{q}\cdot\vec{x}} (l^0 J_0 - \vec{l} \cdot \vec{J}) d\vec{x} | i \rangle. \quad (5.38)$$

The matrix element \mathcal{M}_{fi} is calculated using the multipole expansion of the $e^{-i\vec{q}\cdot\vec{x}}$ and $\vec{l} e^{-i\vec{q}\cdot\vec{x}}$. For that, we write

$$\vec{l} = \sum_{\lambda=0,\pm 1} l_\lambda \hat{e}_\lambda, \quad (5.39)$$

where $\hat{e}_\lambda (\lambda = \pm 1, 0)$ are the components of the unit vector ($\hat{e}_x, \hat{e}_y, \hat{e}_z$) in the spherical basis defined as

$$e_{\pm 1} = \pm \frac{\hat{e}_x \pm i\hat{e}_y}{\sqrt{2}}, \quad \hat{e}_0 = \hat{e}_z, \quad \vec{e}_\lambda \cdot \vec{e}_{\lambda'} = \delta_{\lambda\lambda'}, \quad \text{such that} \quad l_\lambda = \sum \vec{l} \cdot \hat{e}_\lambda \quad (5.40)$$

and write

$$e^{i\vec{q}\cdot\vec{x}} = \sum_{J=0}^{\infty} \sqrt{4\pi(2J+1)} i^J j_J(qx) Y_{J0}(\Omega_x), \quad (5.41)$$

where $Y_{J0}(\Omega_x)$ are the spherical harmonics and $j_J(qx)$ are the spherical Bessel's function.

Using the definition of the vector spherical harmonics $\vec{\mathcal{Y}}_{J1}^M$ defined as

$$\vec{\mathcal{Y}}_{J1}^M = \sum_{m\lambda} \langle lm1\lambda | l1JM \rangle Y_{lm}(\theta, \phi) \vec{e}_\lambda, \quad (5.42)$$

where $\langle lm1\lambda | l1JM \rangle$ is the Clebsch-Gordan (CG) coefficients and choosing $\hat{q} \parallel \hat{e}_Z$ i.e. unit vector along the Z axis, we can write

$$\vec{e}_\lambda e^{i\vec{q}\cdot\vec{x}} = \sum_l \sum_{J=0}^{\infty} \sqrt{4\pi(2l+1)} i^J j_l(qx) \langle l01\lambda | l1J\lambda \rangle \vec{\mathcal{Y}}_{J1}^\lambda, \quad x = |\vec{x}|, \quad q = |\vec{q}|. \quad (5.43)$$

In Eq. (5.43), we perform the expansion over l , using the values of the CG coefficients for $\lambda = \pm 1$ and $\lambda = 0$ explicitly. There would be, in general, three terms for each $\lambda (= \pm 1, 0)$, corresponding to $l = J+1, J, J-1$. Using the nonvanishing values of CG coefficients in each case and the following properties of the vector spherical harmonics $\vec{\mathcal{Y}}_{J1}^M$ i.e. [451]:

$$\vec{\nabla}_r \times j_J(r) \vec{\mathcal{Y}}_{J1}^M = -i \left(\frac{J}{2J+1} \right)^{\frac{1}{2}} j_{J+1}(r) \vec{\mathcal{Y}}_{J,J+1}^M + i \left(\frac{J+1}{2J+1} \right)^{\frac{1}{2}} j_{J-1}(r) \vec{\mathcal{Y}}_{J,J-1}^M, \quad (5.44)$$

$$\vec{\nabla}_r j_J(r) Y_{JM} = \left(\frac{J+1}{2J+1} \right)^{\frac{1}{2}} j_{J+1}(r) \vec{\mathcal{Y}}_{J,J+1}^M - \left(\frac{J}{2J+1} \right)^{\frac{1}{2}} j_{J-1}(r) \vec{\mathcal{Y}}_{J,J-1}^M, \quad (5.45)$$

the expression for $\vec{e}_\lambda e^{i\vec{q}\cdot\vec{x}}$ given in Eq. (5.43) is evaluated.

After performing some basic algebraic manipulations, the following expressions are obtained [10]:

$$\begin{aligned} \vec{e}_{\vec{q}\lambda} e^{i\vec{q}\cdot\vec{x}} &= -\frac{i}{q} \sum_{J=0}^{\infty} [4\pi(2J+1)]^{\frac{1}{2}} i^J \vec{\nabla} (j_J(qx) Y_{J0}(\Omega_x)), & \text{for } \lambda = 0 \\ &= -\sum_{J \geq 1}^{\infty} [2\pi(2J+1)]^{\frac{1}{2}} i^J \left[\lambda_{j_J}(qx) \vec{\mathcal{Y}}_{J1}^\lambda + \frac{1}{q} \vec{\nabla} \times (j_J(qx) \vec{\mathcal{Y}}_{J1}^\lambda) \right], & \text{for } \lambda = \pm 1. \end{aligned} \quad (5.46)$$

Therefore, the matrix element in Eq. (5.38) is written using Eq. (5.46) as [10]

$$\begin{aligned} \langle f | \hat{H}_W | i \rangle &= +\frac{G_F a}{\sqrt{2}} \langle f | \left(\sum_{J=0}^{\infty} [4\pi(2J+1)]^{\frac{1}{2}} (-i)^J [l_3 \hat{L}_{J0}(q) - l_0 \hat{C}_{J0}(q)] \right. \\ &\quad \left. - \sum_{\lambda=\pm 1} l_\lambda \sum_{J \geq 1}^{\infty} [2\pi(2J+1)]^{\frac{1}{2}} (-i)^J \times [\lambda \hat{T}_{J-\lambda}^{mag}(q) + \hat{T}_{J-\lambda}^{el}(q)] \right) | i \rangle, \end{aligned} \quad (5.47)$$

where

$$\hat{C}_{JM}(q) \equiv \int d\vec{x} [j_J(qx) Y_{JM}(\Omega_x)] \cdot \hat{J}_0(\vec{x}); \quad \hat{L}_{JM}(q) \equiv \frac{i}{q} \int d\vec{x} [\vec{\nabla} (j_J(qx) Y_{JM}(\Omega_x))] \cdot \hat{J}(\vec{x}), \quad (5.48)$$

$$\hat{T}_{JM}^{el}(q) \equiv \frac{i}{q} \int d\vec{x} [\vec{\nabla} \times j_J(qx) \vec{\mathcal{Y}}_{J1}^M] \cdot \hat{J}(\vec{x}); \quad \hat{T}_{JM}^{mag}(q) \equiv \int d\vec{x} [j_J(qx) \vec{\mathcal{Y}}_{J1}^M] \cdot \hat{J}(\vec{x}), \quad (5.49)$$

and are called multipoles.

In the following, we enumerate some features of the above multipoles:

- (i) The $C_{JM}(q)$, $L_{JM}(q)$, $T_{JM}^{el}(q)$ and $T_{JM}^{mag}(q)$ are called, respectively, the Coulomb, longitudinal, transverse electric, and transverse magnetic multipoles of the current.
- (ii) The weak current operator $J^\mu(J^0, \vec{J})$ appearing in the definition of multipoles contains vector (V^μ) and axial-vector (A^μ) currents in both cases of CC and NC reactions. Therefore, each multipole ($M_{JM} = C_{JM}, L_{JM}, T_{JM}^{el}, T_{JM}^{mag}$) consists of the vector and axial-vector multipoles and is generally written as:

$$M_{JM} \longrightarrow M_{JM}^V(q) + M_{JM}^A(q),$$

where $M_{JM}^V(q)$ and $M_{JM}^A(q)$ are the multipoles corresponding to vector and axial-vector currents.

Multipole	C_{JM}^V	L_{JM}^V	$T_{JM}^{el,V}$	$T_{JM}^{mag,V}$	C_{JM}^A	L_{JM}^A	$T_{JM}^{el,A}$	$T_{JM}^{mag,A}$
Parity	$(-1)^J$	$(-1)^J$	$(-1)^J$	$(-1)^{J+1}$	$(-1)^{J+1}$	$(-1)^{J+1}$	$(-1)^{J+1}$	$(-1)^J$

Table 5.3: Parity of vector and axial-vector multipoles.

- (iii) The parity of M_{JM}^V is defined in the conventional way with reference to the electromagnetic vector current. The parity of the vector ($M_{JM}^V(q)$) and axial-vector ($M_{JM}^A(q)$) multipoles is opposite to each other, which are shown in Table-5.3.
- (iv) In general, there are 8 multipoles to be considered, four corresponding to the vector currents and four corresponding to the axial-vector currents. However, since the vector current is conserved i.e.

$$q_\mu J^\mu = 0 \quad \Rightarrow \quad q_0 J^0 = \vec{q} \cdot \vec{J}. \quad (5.50)$$

Taking $\vec{q} \parallel \hat{e}_z$, we get a relation between the Coulomb and longitudinal multipoles i.e.

$$q_0 \langle J_f | C_{JM}^V | J_i \rangle - q_z \langle J_f | L_{JM}^V | J_i \rangle = 0. \quad (5.51)$$

Therefore, the $\nu(\bar{\nu})$ cross sections are given in terms of seven multipoles while the electron scattering is described in terms of three multipoles.

- (v) The single nucleon current operators (J_0, \vec{J}) to be used with the nuclear wave functions in the impulse approximation are derived from the definition of the vector and axial-vector current operators for the free nucleon given in Section 2.1. In the case of a nucleus, the nucleons are treated nonrelativistically, therefore, the nonrelativistic reduction of the current operators can be used. In the case of CC reactions, we obtain J_{CC}^μ in the lowest order of momenta, neglecting the term $O\left(\frac{\vec{q}^2}{M^2}\right)$, $O\left(\frac{\vec{p}^2}{M^2}\right)$ as [10]

$$J_{CC}^0 = \left(f_1(q^2) + g_1(q^2) \vec{\sigma} \cdot \frac{2\vec{p} - \vec{q}}{2M} \right) \tau^\pm, \quad (5.52)$$

$$\vec{J}_{CC} = \left(g_1(q^2) \vec{\sigma} - i(f_1(q^2) + f_2(q^2)) \frac{\vec{\sigma} \times \vec{q}}{2M} \right) \tau^\pm + f_1(q^2) \frac{2\vec{p} - \vec{q}}{2M} \tau^\pm. \quad (5.53)$$

The operator $\tau^{+(-)}$ corresponds to the $\nu(\bar{\nu})$ scattering processes. Similar expressions are obtained for the NC interactions with $f_1(q^2)$, $f_2(q^2)$ and $g_1(q^2)$ replaced by NC form factors $\tilde{f}_1(q^2)$, $\tilde{f}_2(q^2)$ and $\tilde{g}_1(q^2)$ and $\tau^{+(-)}$ replaced by the isoscalar (\mathbb{I}_4) and isovector operators (τ_3) depending upon the isospin structure of J_{NC}^μ .

It should be noted that the terms involving $\frac{q_0}{2M}$ are of the order of $O\left(\frac{q^2}{4M^2}\right)$ as $q_0 = -\frac{q^2}{2M}$ for the elastic scattering and are, therefore, neglected in the case of nuclear transitions at low energies. The nuclear operators corresponding to the nucleon operators given in Eqs. (5.52) and (5.53) are, therefore, written in the impulse approximation as

$$J^{0s}(\vec{x}) = \sum_{j=1}^A \left[f_1(q^2) + g_1(q^2) \left(\frac{p(j)}{M} \delta(x - x_0) \right)_{sym} \right] \tau^\pm \delta(\vec{x} - \vec{x}_j), \quad (5.54)$$

$$\vec{J}^s(\vec{x}) = \sum_{j=1}^A \left[g_1(q^2) \vec{\sigma} + f_1(q^2) \frac{2\vec{p} \cdot \vec{q}}{2M} - i \frac{f_1(q^2) + 2M(q^2)}{2M} \vec{\sigma}(j) \times \vec{q} \right] \tau^\pm \delta(\vec{x} - \vec{x}_j), \quad (5.55)$$

where \vec{x}_j is the position coordinate of the interacting nucleon. This shows that various operators in the nuclear space which enter in the current $J^0(x)$ and $\vec{J}(x)$ operators are the type $\tau^\pm(j)$, $\tau^\pm(j)\sigma(j)$ and $\tau^\pm(j)\vec{p}(j)(= -i\tau^\pm(j)\vec{\nabla}(j))$ multiplied by the spherical harmonics (Y_{JM}), vector spherical harmonics (\vec{Y}_{JML}), the gradient ($\vec{\nabla} \cdot \vec{Y}$), and the curl ($\vec{\nabla} \times \vec{Y}$) operators of the vector spherical harmonics as shown in the definition of the multipoles in Eqs. (5.48) and (5.49).

Using the matrix element in Eq. (5.38), the cross section is calculated for the transition between the initial state $|i\rangle$ and the final state $|f\rangle$ of the nucleus, which are defined by the definite angular momenta and parity as $|J_i M_i\rangle$ and $|J_f M_f\rangle$ and is given by

$$\frac{d\sigma}{d\Omega} = \frac{k'E'}{4\pi^2} \sum_{\text{lepton spins}} \frac{1}{2J_i + 1} \sum_{\mathcal{M}_i} \sum_{\mathcal{M}_f} |\langle J_f \mathcal{M}_f | \mathcal{H} | J_i \mathcal{M}_i \rangle|^2. \quad (5.56)$$

Since the matrix element of \mathcal{H} is written in terms of the various multipoles with definite angular momentum and parity, $|J\lambda\rangle$ (see Eqs. (5.48) and (5.49)), the standard angular momentum algebra can be used to calculate the cross section given in Eq. (5.56). The general expression for the cross section is obtained as [10]:

$$\begin{aligned} \left(\frac{d\sigma}{d\Omega}\right)_{\nu\bar{\nu}} &= \left(\frac{q}{\epsilon}\right) \frac{G^2 \epsilon^2}{4\pi^2} \frac{4\pi}{2J_i+1} \left[\sum_{J=0}^{\infty} \{ (1 + \hat{\nu} \cdot \vec{\beta}) |\langle J_f || \hat{M}_J || J_i \rangle|^2 \right. \\ &+ [1 - \hat{\nu} \cdot \vec{\beta} + 2(\hat{\nu} \cdot \vec{\beta})(\hat{q} \cdot \vec{\beta})] |\langle J_f || \hat{L}_J || J_i \rangle|^2 \\ &- [\hat{q} \cdot (\hat{\nu} + \vec{\beta})] 2 \operatorname{Re} \langle J_f || \hat{L}_J || J_i \rangle \langle J_f || \hat{M}_J || J_i \rangle^* \} \\ &+ \sum_{J \geq 1} \{ [1 - (\hat{\nu} \cdot \hat{q})(\hat{q} \cdot \vec{\beta})] |\langle J_f || \hat{T}_J^{mag} || J_i \rangle|^2 + |\langle J_f || \hat{T}_J^{el} || J_i \rangle|^2 \\ &\pm [\hat{q} \cdot (\hat{\nu} - \vec{\beta})] 2 \operatorname{Re} \langle J_f || \hat{T}_J^{mag} || J_i \rangle \langle J_f || \hat{T}_J^{el} || J_i \rangle^* \} \Big], \end{aligned} \quad (5.57)$$

where $\hat{\nu} \equiv \frac{\vec{\nu}}{|\vec{\nu}|}$, $\hat{q} \equiv \frac{\vec{q}}{|\vec{q}|}$, $\langle J_f || \hat{J} || J_i \rangle$ is the reduced matrix element of the multipole M_J^M with angular momentum \vec{J} . In the relativistic limit, β which depends upon the lepton velocity becomes $\beta \rightarrow 1$.

In order to calculate the nuclear matrix elements, we need the nuclear wave functions for $|i\rangle$ and $|f\rangle$ states which are essentially the nonrelativistic wave functions of the nucleons bound in a nucleus by a nucleon-nucleon potential.

The nuclear states $|i\rangle$ and $|f\rangle$ characterized by the angular momentum (and parity) $|J_i M_i\rangle$ and $|J_f M_f\rangle$ are generally expressed as:

$$|i\rangle \equiv |J_i M_i\rangle \equiv \psi_{n l \frac{1}{2} J_i M_i}(\vec{x}) = N R_{nl}(r) [Y_{lm_l}(\theta, \phi) \otimes Y_{\frac{1}{2} m_s}]_{J_i M_i}, \quad (5.58)$$

$$\text{and } |f\rangle \equiv |J_f M_f\rangle \equiv \psi_{n' l' \frac{1}{2} J_f M_f}(\vec{x}) = N' R_{n'l'}(r) [Y_{l' m_{l'}}(\theta, \phi) \otimes Y_{\frac{1}{2} m_{s'}}]_{J_f M_f}, \quad (5.59)$$

where $R_{nl}(r)$ and $R_{n'l'}(r)$ are the radial wave functions of the initial and final nucleus obtained by solving the Schrödinger equation for nucleons moving in a central potential like the harmonic oscillator potential. In a more sophisticated description of the nuclear wave functions, various forms of the nucleon-nucleon potentials are included to describe the residual interactions to take into account the effect of pairing and other nucleon-nucleon correlation effects [10]. Using these wave functions and the transition current operators written in Eqs. (5.54) and (5.55), and the multipoles defined in Eqs. (5.48) and (5.49), the matrix element defined in Eq. (5.38) is calculated. The expressions for the matrix elements for various multipoles using the harmonic oscillator wave functions have been given by Haxton [452].

Eq. (5.57) is the general result, which is used to calculate the nuclear cross section for QE ν and $\bar{\nu}$ reactions leading to discrete nuclear states in various nuclei from the deuteron to medium and heavy nuclei. Once the initial and final states are fixed, only the multipoles which are compatible with the change in angular momentum and parity would contribute. It should be noted that for an exclusive reaction leading to a specific transition, very few multipoles carrying spin and parity corresponding to ΔJ and parity change in the transitions would contribute.

Moreover, in case of light nuclei like H, D, ^3He , ^4He and ^{12}C , these cross sections have also been calculated treating these nuclei as elementary particles. This method known as the elementary particle treatment (EPT) was introduced by Fuji and Yamaguchi [453], and Kim and Primakoff [454] almost 60 years ago, and has been used later by Mintz et al. [455], specially for ^2D , ^3He and ^{12}C nuclei. In the case of deuteron target, many calculations have been made using EPT as well as the relativistic wave functions of the deuteron, with the parameters of these wave functions determined from extensive experimental efforts in the study of electrodisintegration of the deuteron i.e. $e + d \rightarrow e + n + p$. Very recently, an alternative approach based on the effective field theory (EFT) has been used to calculate the low energy CC and NC weak processes on the deuteron like the $\nu_e + d \rightarrow e^- + p + p$ and $\nu_\mu + d \rightarrow \nu_\mu + n + p$ in the context of solar neutrino experiments at SNO and applied to antineutrino induced reactions relevant for reactor experiments. The deuteron target is also very useful for studying the effect of meson exchange currents in weak interactions, which were shown to play very important role in case of the electrodisintegration of deuteron. In the case of the low energy weak reactions from deuteron for energies up to 20 MeV relevant for the solar neutrinos and lower energies relevant for the reactor antineutrinos, all the above methods predict cross sections in agreement with each other within 1–2 % [456, 457].

Most of the exclusive (anti)neutrino-nucleus reactions in the low energy region have been done in hydrogen and deuteron targets while some experiments have been done with nuclear targets like ^{12}C , ^{37}Cl , ^{56}Fe , ^{71}Ga and ^{127}I . The experimental and theoretical results have been summarized by Formaggio and Zeller [226], and by Fukugita and Yamagida [458]. However, we show some low energy (anti)neutrino-nucleus cross sections for ^2D , ^{12}C , ^{37}Cl and ^{71}Ga calculated with the above formalism.

Fig. 5.3 shows the total scattering cross section σ vs E_ν for the (anti)neutrino NC and CC reactions on deuteron. These results are taken from Nakamura et al. [457]. Table-5.4 shows the total cross section folded over the reactor spectrum for the CC and NC induced processes on the deuteron target [459]. The theoretical results are from Kubodera et al. [460] while the experimental results are from Riley et al. [461] and Willis et al. [462].

Fig. 5.4 shows the results of σ vs E_ν for the exclusive reaction $\nu_e + {}^{12}\text{C} \rightarrow e^- + {}^{12}\text{N}_{gs}$ from the muon decay at rest neutrinos. The figure has been taken from Ref. [226]. The experimental results are from the KARMEN [463] and LSND [464] measurements. The theoretical curve is from the works of Fukugita et al. [465] obtained in a model independent way with a direct evaluation of the nuclear matrix element from β decays. In Fig. 5.4, we also present the results of the cross section for CC ν_e induced process on heavier nuclei like ${}^{37}\text{Cl}$ and ${}^{71}\text{Ga}$ from Ortiz et al. [466] and by Bahcall et al. [467].

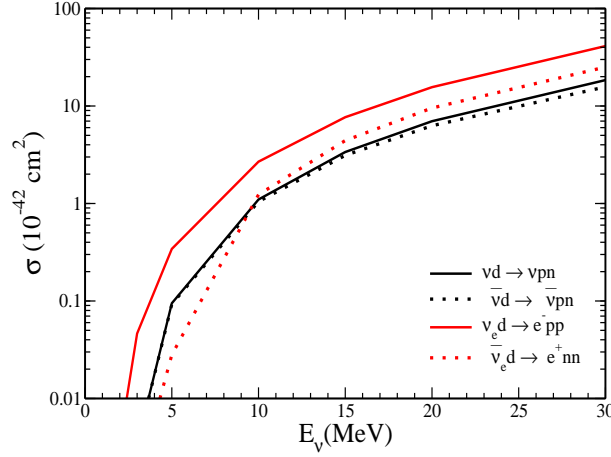


Figure 5.3: The total scattering cross section σ (in 10^{-42}cm^2) vs E_ν for the (anti)neutrino NC and CC reactions on deuteron target $\nu + D \rightarrow \nu + n + p$, $\bar{\nu} + D \rightarrow \bar{\nu} + n + p$, $\nu_e + D \rightarrow e^- + p + p$ and $\bar{\nu}_e + D \rightarrow e^+ + n + n$ [456, 457].

5.4. Inclusive quasielastic scattering in the low and intermediate energy regions

Experimentally, the inclusive QE scattering has been studied by the accelerator as well as the atmospheric neutrinos. In the case of accelerator neutrinos, the first experiments were done following the suggestions from Markov, Pontecorvo, and Schwartz, using the particle accelerators with energy of neutrinos in the few GeV region at BNL, ANL, and CERN using spark chambers with aluminum and iron nuclear targets and with the bubble chamber filled with freon and propane as targets. The theoretical interpretation of these experiments were initially done using the Fermi gas model to account for NME. Subsequently various versions of the shell model for describing the nuclear structure were used to study the NME in (anti)neutrino scattering from the nuclear targets following the theoretical techniques for describing the electron-nucleus scattering in this energy region. This approach is useful in calculating the inclusive as well as the exclusive reactions to specific nuclear states in the final nucleus in studying the low energy (anti)neutrino reactions induced by the solar and reactor (anti)neutrinos.

The second generation of the accelerator (anti)neutrino experiments were done with the hydrogen and deuteron filled bubble chambers at ANL and BNL followed by the experiments at FNAL, CERN, BNL and Serpukhov bubble chambers filled with heavier nuclear targets. These experiments with reasonably good statistics played very important role in determining the weak form factors of the nucleon and led to the study of the axial-vector response of the nucleons in the region of large energy ($\nu = E_\nu - E_l$) transfer and the four momentum transfer squared (Q^2) to the nuclear systems.

In recent times, most of the experiments in QE inclusive scattering were done with the accelerator neutrinos obtained by the pion decay at rest in the case of ν_e with $E_{\nu_e} < 52.8$ MeV and pion decay in flight in the case of ν_μ with $E_{\nu_\mu} < 286$ MeV. Although the first experiments were done at BNL in ${}^{12}\text{C}$ which had very low statistics but later experiments done by the LSND and KARMEN collaborations at LANL and RAL in ${}^{12}\text{C}$ produced results with better statistics. The LSND results reported in the $\bar{\nu}_e \rightarrow e^+$ QE inclusive reactions supported the existence of neutrino oscillations proposed in the context of explaining the solar neutrino anomaly. Furthermore, the evidence of the existence of neutrino oscillations reported by the IMB and Kamiokande experiments with the atmospheric neutrinos in $\nu_\mu \rightarrow \mu^-$ QE reactions, motivated the neutrino physics community to study the QE inclusive reactions like $\nu_e \rightarrow e^-$ and $\nu_\mu \rightarrow \mu^-$ with accelerator neutrinos in the intermediate energy region of around $E_{\nu(\bar{\nu})} \sim 1$ GeV. Consequently, many experiments like the K2K and T2K at JPARC, MiniBooNE, MINOS, NOvA, MicroBooNE, ArgoNEUT, and MINERvA at the Fermilab in the few GeV energy region and NOMAD at CERN at relatively higher energies have been done. For a general discussion on the historical development of the accelerator neutrino beams and detectors, see Refs. [95, 96].

In the case of atmospheric neutrinos, the experiments on inclusive QE (anti)neutrino-nucleus scattering were done first by the underground experiments in the deep mines of India and South Africa in the context of cosmic ray studies [10]. In 1970's when the grand unified theory (GUT) predicted proton decays, many experiments were designed to search for the proton decay events in which the atmospheric (anti)neutrino interactions producing the charged leptons are serious

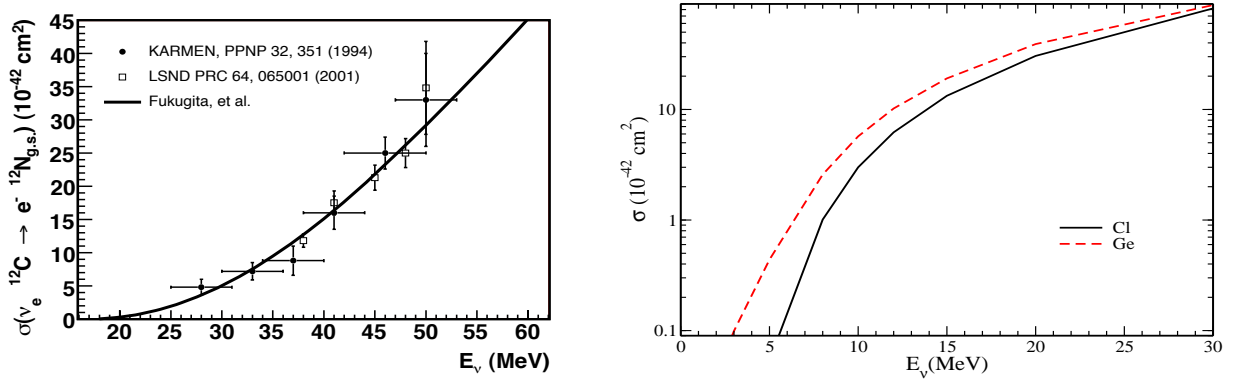


Figure 5.4: (Left panel) The total scattering cross section σ vs E_ν for the exclusive reaction $\nu_e + {}^{12}\text{C} \rightarrow e^- + {}^{12}\text{N}_{gs}$ from the muon decay at rest. The figure has been taken from Ref [226]. The data points are from the KARMEN [463] and LSND [464] experimental measurements. The theoretical curve is from the works of Fukugita et al. [465]. (Right panel) The total scattering cross section σ (in 10^{-42}cm^2) vs E_{ν_e} for the reactions $\nu_e + {}^{37}\text{Cl} \rightarrow e^- + {}^{37}\text{Ar}$ and $\nu_e + {}^{71}\text{Ga} \rightarrow e^- + {}^{71}\text{Ge}$ [466, 467].

	$\sigma(\bar{\nu} + d \rightarrow e^+ + n + n)$ ($\times 10^{-45}\text{cm}^2$)	$\sigma(\bar{\nu} + d \rightarrow \bar{\nu} + p + n)$ ($\times 10^{-45}\text{cm}^2$)
Theory [460]	10.02	6.02
Experiment [461]	9.83 ± 2.04	6.08 ± 0.77

Table 5.4: CC and NC reactor averaged cross section $\langle \sigma \rangle$ (10^{-45}cm^2) in deuteron.

background. Though no proton decay event was observed, but the efforts started a comprehensive study of the atmospheric neutrinos with an energy spectrum, which is theoretically predicted to have peak around 500 MeV and have large tail extending up to few GeV.

Theoretically, the SM is used to describe the basic reactions of (anti)neutrinos on nucleons moving in a nucleus, with the NME taken into consideration using an appropriate nuclear model for describing the nuclear structure. In general, the appropriate nuclear model to describe NME depends upon the energy region and the type of reaction under consideration.

Generally, the following nuclear effects play important role in the case of inclusive QE reactions:

(i) Fermi motion and nuclear binding

The nucleons are bound in a nucleus due to the strong nucleon-nucleon forces represented by a potential $V(\vec{r})$, in which they are moving with a momentum \vec{p} . The momentum distribution of the nucleons bound in a nucleus is described by the wave function $\Psi(\vec{r})$, which is obtained by solving the Schrödinger equation in the nuclear potential $V(\vec{r})$ with a Hamiltonian H given by

$$H = -\frac{\vec{\nabla}^2}{2M} + V(\vec{r}). \quad (5.60)$$

Depending upon the potential $V(\vec{r})$, there are various approaches to obtain the wave function $\Psi(\vec{r})$. In the simplest approach of the shell model, $V(\vec{r})$ is taken to be a central potential but more sophisticated approaches also include the residual interactions in addition to the central potential $V(\vec{r})$ for describing the short and long range nucleon-nucleon correlations and pairing of the nucleons in nuclei. The parameters of the central potential and the residual interactions are fitted to reproduce the static properties of the nuclei like the binding energy, nuclear moments, nuclear deformations, etc. The effect of the Fermi motion, \vec{p}_F and the binding energy is taken into account through

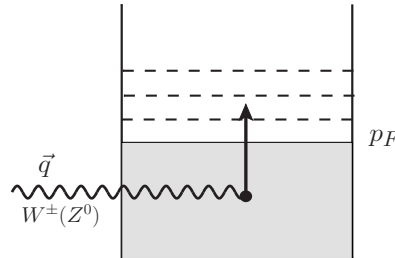


Figure 5.5: Diagrammatic representation of Pauli blocking.

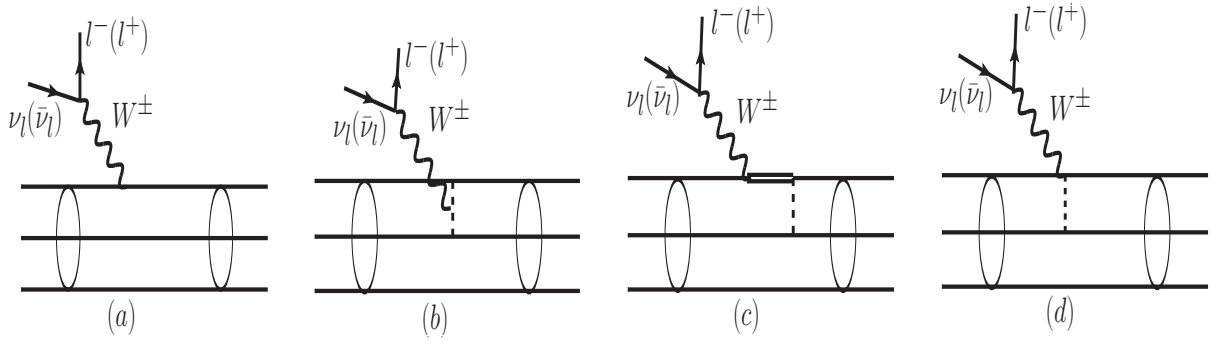


Figure 5.6: Neutrino-nucleus scattering with MEC. Diagrams (b), (c) and (d) also have exchange diagrams.

these wave functions and through the kinematics of the reaction.

In other approach of the Fermi gas model, the nucleon momentum \vec{p} is constrained such that $|\vec{p}| \leq p_F$, the Fermi momentum which is given by

$$p_F = [3\pi^2 \rho]^{1/3}, \quad (5.61)$$

where ρ is the density of the nucleon in the nucleus. In such models, the momentum distribution of the initial nucleon is essentially given by a step function $\Theta(p_F - p)$ and the energy of the nucleon $E \neq \sqrt{|\vec{p}|^2 + M^2}$ but is modified by the binding energy. This momentum and energy distribution is called the spectral function of the nucleon $S(\vec{p}, E)$ and is given, in the Fermi gas model, by

$$S(\vec{p}, E) \propto \Theta(p_F - p) \delta(E - \sqrt{|\vec{p}|^2 + M^2} + \epsilon), \quad (5.62)$$

where ϵ is the separation energy, which depends upon the binding energy (B.E.). In the modern Fermi gas models, the spectral function $S(\vec{p}, E)$, obtained phenomenologically from the electron-nucleus scattering experiments is used.

(ii) Pauli's principle

The Pauli principle guides the occupancy of the nucleons in various shell model states, which are predicted for a given central potential $V(\vec{r})$, and thus describes the nuclear states occupied by the valence nucleons and the structure of the core consisting of the closed shells. This is very important in theoretical calculations of various reactions in the shell model, where the interaction with the valence nucleons and the effect of core polarizations are considered. In the context of Fermi gas model, all the nuclear states in the Fermi sea up to the momentum p_F are filled, thus constraining the final nucleon to have momentum $p' > p_F$. Due to the interaction with a W^\pm/Z^0 boson, a nucleon may occupy a state above the Fermi sea with the momentum $p' > p_F$ and creates a particle-hole (1p - 1h) pair in the nucleus as shown in Fig. 5.5.

In the simplest versions of the Fermi gas model, the results of the free nucleon cross section are modified due to the above considerations on the momentum distribution of the initial and final nucleons by multiplying them with the spectral function $S(\vec{p}, E) \Theta(p' - p_F)$ with the corresponding modification on the energy of the final nucleon.

(iii) Meson exchange currents

The QE reactions are generally calculated in the impulse approximation where the (anti)neutrino interacts with a single nucleon. The nuclear cross section is calculated as an incoherent or coherent sum of the transition amplitudes depending upon the kinematics and dynamics of the reactions (Fig. 5.6(a)). However, it has been shown in the electromagnetic reactions with photons and electrons from nuclei that the interaction of the external probes like γ or e can also take place with the nonnucleonic degrees of freedom of the nucleus like the meson or Δ degrees of freedom.

These are called meson exchange currents (MEC). The effect of MEC are important in some kinematic regions as shown in the case of photon and electron scattering from the nuclei as well as in the β decays of nuclei leading to the quenching of axial-vector coupling. It could also play important role in the QE (anti)neutrino-nucleus scattering in which W^\pm and Z^0 bosons interact with nonnucleonic degrees of freedom in nuclei like mesons and Δ resonances as shown in Fig. 5.6 (b) and (c) or via the contact interaction term as shown in Fig. 5.6 (d).

(iv) Nucleon-nucleon correlations

The nucleons which interact with (anti)neutrinos are highly correlated due to the pion exchange as well as the rho and omega exchanges leading to the long range and the short range correlations. Most of the calculations in the

shell model are done using the nuclear wave functions with a central potential $V(\vec{r})$. These wave functions need to be calculated with potentials describing the short range as well as the long range correlations. Various attempts have been made to include them to calculate the QE inclusive reactions but most of them have been confined to the low energy region. For a general discussion, see Ref. [10]. In the case of Fermi gas model calculations, the long range correlation has been taken into account using the method of random phase approximation (RPA) along with a realistic spectral function $S(\vec{p}, E)$ to describe the energy and momentum distribution of the nucleons in the initial nucleus, which is obtained phenomenologically from the electron-nucleus scattering experiments [422, 423].

(v) Final state interaction (FSI)

This is one of the most important effects of nuclear medium in the IE reactions but is also important in the QE reactions, when a meson produced in the IE reaction is reabsorbed in the nucleus mimicking a QE-like reaction. In the case when only nucleons are produced in the final hadronic state inside the nucleus, the FSI of the nucleon is taken into account by calculating the final nuclear wave function with a nucleon-nucleon potential, which includes the nucleon-nucleon correlations as described in (iv) above. The QE-like process in which a pion produced in an IE reaction is reabsorbed in the nucleus leads to an enhancement in the genuine QE cross section, which needs to be understood and corrected. Moreover, in the case of (anti)neutrino reactions, this phenomenon of QE-like events also affects the neutrino energy reconstruction where the initial neutrino energy is constructed using the QE kinematics of the reactions. These QE-like events contributing to the QE cross section do not come from the genuine QE reactions but from the reactions where an additional pion is produced corresponding to the IE pion production, which do not obey the QE kinematics. Therefore, a knowledge of FSI is very important both for the determination of the genuine QE cross sections as well as for the energy reconstruction of (anti)neutrinos.

These nuclear effects have been taken into account with various degrees of sophistication in several calculations done within the shell model as well as in the Fermi gas model, and other models. In the low energy region corresponding to the supernova neutrinos and the neutrinos from the pion and muon decays at rest (and also in flight in some cases), a small number of states are excited in the final nucleus, one sums over the cross section from each excited state. The theoretical calculation of the total cross section and the other observables in such cases requires a knowledge of the ground state of the initial nucleus as well as the wave function of the ground state and all the other excited states of the final nucleus. The NME described in (i)–(iv) above are taken into account in the shell model approach by calculating the nuclear wave functions in the initial and final states with various versions of the residual interaction describing the nucleon-nucleon potentials, using different approaches like the RPA [468, 469, 470, 471, 472, 473], continuous RPA (CRPA) [474, 475, 476, 477, 478], quasi particle RPA (QRPA) [479, 480, 481, 482, 483], projected QRPA [484], relativistic RPA [485] and relativistic nuclear energy density functional (RNEDF) [486], RPA with Hartree-Fock (HF-RPA) wave functions [468], etc. The results obtained in these approaches have been reviewed by Kolbe et al. [487], and recently by Balasi et al. [488], and Jachowicz and Nikolakopoulos [489]. Alternate approaches, using the relativistic distorted wave impulse approximation methods using relativistic mean fields as well as the Green’s function approaches using the nucleon-nucleon optical model to describe the final state interactions of the nucleons have been used by the Spanish-Italian groups [490, 491, 492, 493]. In recent years, the methods of SuperScaling Approach (SuSA) based on the scaling behavior of the nuclear response functions observed in the electron-nucleus scattering have been applied to study the QE (anti)neutrino-nucleus scattering by the MIT-Spanish-Italian groups [494, 495].

In the case of light nuclei like ^4He , ^6Li , and ^{12}C , the ab initio calculations of the nuclear response functions based on the Green’s function Monte Carlo methods have been used by the Argonne-Rome group [496, 497]. In these approaches, some authors have also calculated the effect of MEC. These microscopic methods were used to calculate the cross sections for transitions to all the accessible states (ground and excited states) in the final nucleus and sum over them to obtain the total cross section. These methods become quite intractable when (anti)neutrino energies approach the GeV region in which case some approximation methods are used.

Historically, the approximation methods based on the Fermi gas model [498, 499, 500] and the closure approximation with the shell model wave functions [175, 501] have been used to analyze the early (anti)neutrino-nucleus experiments from CERN, ANL, and BNL laboratories. In view of the recent experiments in the few GeV region done at Fermilab, JPARC, and CERN, various improved versions of the Fermi gas model have been used. It is not possible to summarize in this report, all the microscopic approaches, which consider NME and we focus in the following only on the latest work done using the Fermi gas model to describe NME in (anti)neutrino-nucleus QE scattering. For details, see Ref. [10].

5.4.1. (Anti)neutrino-nucleus quasielastic scattering in Fermi gas models

The first application of the Fermi gas model to the (anti)neutrino-nucleus scattering results from CERN was done by Berman et al. [500] using the works of Gatto [498, 499], where the free nucleon differential cross section $\frac{d\sigma}{dQ^2}$ is multiplied

by a factor $(1 - \frac{D}{N})$ and D is given by [175, 448, 500]:

$$\begin{aligned} D &= Z \text{ for } x < u - v \\ &= \frac{1}{2}A \left\{ 1 - \frac{3x}{4}(u^2 + v^2) + \frac{x^3}{2} - \frac{3}{32x}(u^2 - v^2)^2 \right\} \quad \text{for } u - v < x < u + v \\ &= 0 \text{ for } x > u + v \end{aligned} \quad (5.63)$$

with $x = \frac{|\vec{q}|}{2p_F}$, $u = (\frac{2N}{A})^{1/3}$, $v = (\frac{2Z}{A})^{1/3}$ and $N (= A - Z)$, Z , A are neutron, proton and mass numbers of the initial nucleus, respectively. p_F is the Fermi momentum and the three momentum transfer $|\vec{q}| = \sqrt{q_0^2 + Q^2}$, $Q^2 = -q^2 \geq 0$.

Smith and Moniz [502] improved the Fermi gas model calculations and used the following expression for the double differential cross section:

$$\begin{aligned} \frac{d^2\sigma}{dk'd\Omega_l} &= \frac{G_F^2 k'^2 \cos^2(\frac{1}{2}\chi)}{2\pi^2 M} \left\{ W_2 + [2W_1 + \frac{m_l^2}{M^2} W_\alpha] \tan^2(\frac{1}{2}\chi) + (W_\beta + W_8) m_l^2 / (ME_l \cos^2(\frac{1}{2}\chi)) \right. \\ &\quad \left. - 2W_8/M \tan(\frac{1}{2}\chi) \sec(\frac{1}{2}\chi) [-Q^2 \cos^2(\frac{1}{2}\chi) + |\vec{q}|^2 \sin^2(\frac{1}{2}\chi) + m_l^2]^{\frac{1}{2}} \right\}, \end{aligned} \quad (5.64)$$

where $\cos \chi = \frac{k'}{E_l} \cos \theta$. The form of W_i 's and other details are given in Ref. [502].

Gaissner and O'Connell [503] have used the relativistic response function $R(\vec{q}, q_0)$, in a Fermi gas model to take into account NME. The expression for the double differential scattering cross section is given by

$$\begin{aligned} \frac{d^2\sigma}{d\Omega_l dE_l} &= C \frac{d\sigma_{free}}{d\Omega_l} R(\vec{q}, q_0), \\ R(\vec{q}, q_0) &= \frac{1}{\frac{4}{3}\pi p_{F_N}^3} \int \frac{d^3 p_N M^2}{E_N E_{N'}} \delta(E_N + q_0 - E_B - E_{N'}) \theta(p_{F_N} - |\vec{p}_N|) \theta(|\vec{p}_N + \vec{q}| - p_{F_{N'}}), \end{aligned} \quad (5.65)$$

where p_{F_N} ($p_{F_{N'}}$) is the Fermi momentum for the initial (final) nucleon, $N, N' = n$ or p and $C = A - Z$ for neutrino induced process and $C = Z$ for the antineutrino induced process. $\frac{d\sigma_{free}}{d\Omega_l}$ is the differential scattering cross section for the (anti)neutrino reaction on free (proton) neutron target.

In 1990's, the local Fermi gas model (LFGM) was used to study the (anti)neutrino-nucleus scattering in the low as well as in the intermediate energy regions to study NME on the cross section and possible modification of M_A due to NME [469, 471, 504]. In recent years, LFGM has been improved by taking into account the relativistic effects, the effects of long range nucleon-nucleon correlations and the use of a realistic spectral function $S(\vec{p}, E)$ to describe the nucleon energy and momentum distribution instead of a step function in momentum space used in the earlier calculations [505, 506]. The effect of $2p-2h$ excitations as well as MEC have also been taken into account in this approach by using different formalisms given by Martini et al. [507, 508, 509, 510], and Nieves et al. [511, 512], which have demonstrated the importance of NME in the determination of the cross section and the effective M_A in the nuclear medium. In the following we describe very briefly, the (anti)neutrino-nucleus QE scattering in the LFGM.

In the local density approximation, the cross section is evaluated as a function of local Fermi momentum $p_F(r)$ and integrated over the whole nucleus. In this approach, the incoming neutrino scatters from a neutron moving in a finite nucleus of neutron density $\rho_n(r)$, such that the differential cross section is given by

$$\left(\frac{d^2\sigma}{dE_l d\Omega_l} \right)_{\nu A} = 2 \int d\vec{r} \rho_n(r) \left(\frac{d^2\sigma}{dE_l d\Omega_l} \right)_{\nu n}, \quad (5.66)$$

where r is the radius of the nucleus and the factor of 2 is to take into account the spin degrees of freedom.

It is assured that the nucleons in a nucleus (or nuclear matter) occupy one nucleon per unit cell in phase space so that the total number of nucleons N is given by

$$N = 2V \int_0^{p_F} \frac{d^3 p}{(2\pi)^3} \implies \rho = \frac{N}{V} = 2 \int_0^{p_F} \frac{d^3 p}{(2\pi)^3}, \quad (5.67)$$

where the factor of 2 is to take into account isospin degrees of freedom of the nucleon. All the states up to a maximum momentum p_F ($p < p_F$) are filled. The momentum states higher than $|\vec{p}| > |\vec{p}_F|$ are unoccupied such that the occupation number $n(\vec{p}, \vec{r})$ is defined as:

$$n(\vec{p}, \vec{r}) = \begin{cases} 1, & p < p_F \\ 0, & p > p_F \end{cases}. \quad (5.68)$$

In this model, the Fermi momentum is a function of r and is not a constant, protons and neutrons are supposed to have different Fermi sphere such that

$$p_{F_p}(r) = (3\pi^2 \rho_p(r))^{\frac{1}{3}}; \quad p_{F_n}(r) = (3\pi^2 \rho_n(r))^{\frac{1}{3}},$$

Nucleus	c_1		c_2		Q -value	
	c_1^n	c_1^p	c_2^n	c_2^p	ν	$\bar{\nu}$
^{12}C	1.692	1.692	1.082*	1.082*	16.8	13.9
^{16}O	1.833	1.833	1.544*	1.544*	14.9	10.9
^{40}Ar	3.64	3.47	0.569	0.569	2.5	8.0
^{56}Fe	4.05	3.971	0.5935	0.5935	6.8	4.8
^{208}Pb	6.89	6.624	0.549	0.549	2.4	5.5

Table 5.5: Different parameters used for the numerical calculations of the nuclear density for the various nuclei. c_1 and c_2 are the density parameters (in Fermi units) defined for modified harmonic oscillator as $\rho(r) = \rho_0(1 + c_2(\frac{r}{c_1})^2)\exp(-(\frac{r}{c_1})^2)$ and for 2-parameter Fermi density as $\rho(r) = \rho_0/(1 + \exp(\frac{r-c_1}{c_2}))$. For ^{12}C and ^{16}O we have used modified harmonic oscillator density(* c_2 is dimensionless) and for ^{40}Ar , ^{56}Fe and ^{208}Pb nuclei, 2-parameter Fermi density have been used, where superscript n and p in density parameters ($c_i^{n,p}$; $i=1,2$) stand for neutron and proton, respectively. The Q -value of the reaction for different nuclei are given in MeV.

where, $\rho_p(r)$ and $\rho_n(r)$ are, respectively, the proton and the neutron densities inside the nucleus and are, in turn, expressed in terms of the nuclear density $\rho(r)$ as

$$\rho_p(r) \rightarrow \frac{Z}{A}\rho(r); \quad \rho_n(r) \rightarrow \frac{A-Z}{A}\rho(r), \quad (5.69)$$

where $\rho(r)$ is generally parameterized in terms of harmonic oscillator density, two parameter Fermi density, Gaussian density, etc. and the density parameters are determined in the electron scattering experiments. For our numerical calculations, we have taken the density parameters from Refs. [513, 514, 515], which are summarized in Table-5.5. For the antineutrino induced reaction on the free nucleon or nucleons bound in a nucleus, the role of neutron and proton gets interchanged.

The expression of the differential scattering cross section for say neutrino-nucleus scattering is written as

$$\sigma_{\nu A}(E_l, \Omega_l) = \left(\frac{d^2\sigma}{dE_l d\Omega_l} \right)_{\nu A} = 2 \int d\vec{r} d\vec{p} \frac{1}{(2\pi)^3} n_n(\vec{p}, \vec{r}) \left(\frac{d^2\sigma}{dE_l d\Omega_l} \right)_{\nu n}, \quad (5.70)$$

where the expression of $\left(\frac{d^2\sigma}{dE_l d\Omega_l} \right)_{\nu n}$ is given in Eq. (2.8).

Now in Eq. (2.8), the neutron energy E_n and the proton energy E_p are replaced by $E_n(|\vec{p}|)$ and $E_p(|\vec{p} + \vec{q}|)$, where \vec{p} is the momentum of the target nucleon inside the nucleus. This is because inside the nucleus the nucleons are not free and their momenta are constrained to satisfy the Pauli principle as discussed above, i.e., $p < p_{F_n}$ and $p' (= |\vec{p} + \vec{q}|) > p_{F_p}$.

Moreover, in the finite nucleus, there is a threshold energy for the reaction to proceed known also as the Q -value of the reaction, which we have taken to be the value corresponding to the lowest allowed Fermi or Gamow-Teller transition. In Table-5.5, we have also tabulated Q -value of the reaction for the nuclear targets for which the numerical results have been presented.

These considerations lead to a modification in the δ function used in Eq. (2.8) i.e. $\delta[q_0 + E_n - E_p]$ is modified to $\delta[q_0 + E_n(\vec{p}) - E_p(\vec{p} + \vec{q}) - Q]$ and the factor

$$\int \frac{d\vec{p}}{(2\pi)^3} n_n(\vec{p}, \vec{r}) \frac{M_n M_p}{E_n E_p} \delta[q_0 + E_n - E_p] \quad (5.71)$$

occurring in Eq. (5.70) is replaced by $-(1/\pi)\text{Im}U_N(q_0, \vec{q})$, where $U_N(q_0, \vec{q})$ is the Lindhard function corresponding to the 1particle-1hole (ph) excitation shown in Fig. 5.7, and is given by [469]:

$$U_N(q_0, \vec{q}) = \int \frac{d\vec{p}}{(2\pi)^3} \frac{M_n M_p}{E_n E_p} \frac{n_n(p) [1 - n_p(\vec{p} + \vec{q})]}{q_0 + E_n(p) - E_p(\vec{p} + \vec{q}) + i\epsilon} \quad (5.72)$$

where $q_0 = E_\nu - E_l - Q$. For the antineutrino reaction the suffix n and p will get interchanged.

The imaginary part of the Lindhard function (Eq. (5.72)) corresponds to the intermediate particles in Fig. 5.7 to be on shell, thereby describing the process $\nu_l + n \rightarrow l^- + p$. If we consider the initial nucleon at rest (the static limit) i.e. $E_n = M_n$ and neglect any Pauli blocking for the proton, then the expression for the free neutrino-neutron cross section will be obtained. Therefore, the role of the Lindhard function is to take into account Pauli blocking as well as the Fermi motion of the nucleon in the nucleus when the neutrino interaction takes place.

The imaginary part of the Lindhard function is obtained to be [469]:

$$\text{Im}U_N(q_0, \vec{q}) = -\frac{1}{2\pi} \frac{M_n M_p}{|\vec{q}|} [E_{F_1} - A] \quad (5.73)$$

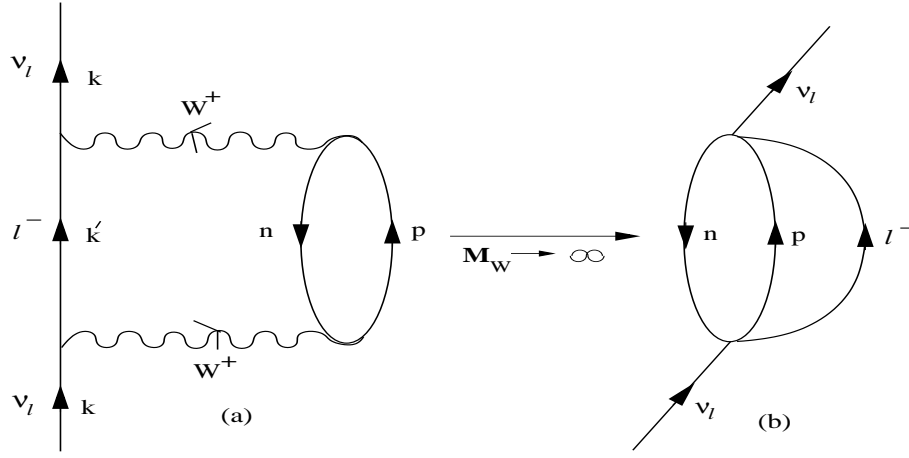


Figure 5.7: Diagrammatic representation of the neutrino self-energy corresponding to the ph -excitation leading to $\nu_l + n \rightarrow l^- + p$ in nuclei. In the large mass limit of the intermediate vector boson (i.e. $M_W \rightarrow \infty$) the diagram (a) is reduced to (b) which is used to calculate $|\mathcal{M}|^2$ in Eq. (2.14).

with $Q^2 \geq 0$, $E_{F_2} - q_0 < E_{F_1}$ and $\frac{-q_0 + |\vec{q}| \sqrt{1 + \frac{4M^2}{Q^2}}}{2} < E_{F_1}$, where $E_{F_1} = \sqrt{p_{F_n}^2 + M_n^2}$, $E_{F_2} = \sqrt{p_{F_p}^2 + M_p^2}$ and

$$A = \text{Max} \left[M_n, E_{F_2} - q_0, \frac{-q_0 + |\vec{q}| \sqrt{1 + \frac{4M^2}{Q^2}}}{2} \right].$$

With the inclusion of these nuclear effects, the total cross section $\sigma(E_\nu)$ is written as

$$\sigma(E_\nu) = -2G_F^2 \cos^2 \theta_C \int_{r_{min}}^{r_{max}} r^2 dr \int_{k'_{min}}^{k'_{max}} k' dk' \int_{Q_{min}^2}^{Q_{max}^2} dQ^2 \frac{1}{E_\nu^2 E_l} L_{\mu\nu} J^{\mu\nu} \text{Im} U_N[E_\nu - E_l - Q, \vec{q}]. \quad (5.74)$$

In the above expression r_{min} and r_{max} are the minimum and maximum limits of nuclear size. k'_{min} and k'_{max} are minimum and maximum values of outgoing lepton momenta. The energy and momentum of the outgoing lepton get modified due to the Coulomb interaction, which is taken into account in a modified effective momentum approximation (MEMA) [469].

In the local density approximation, the effective energy of the lepton in the Coulomb field of the final nucleus is given by [469, 516]:

$$E_{eff} = E_l + V_c(r), \quad \text{where} \quad V_c(r) = 4\pi\alpha Z_f \left(\frac{1}{r} \int_0^r \frac{\rho_p(r')}{Z_f} r'^2 dr' + \int_r^\infty \frac{\rho_p(r')}{Z_f} r' dr' \right) \quad (5.75)$$

with α as fine structure constant and Z_f as the charge of outgoing lepton, taken as -1 for neutrino and $+1$ for antineutrino. This leads to a change in the imaginary part of the Lindhard function occurring in Eq. (5.74)

$$\text{Im} U_N[E_\nu - E_l - Q, \vec{q}] \rightarrow \text{Im} U_N(E_\nu - E_l - Q - V_c(r), \vec{q}).$$

When the electroweak interactions take place in nuclei, the strength of the electroweak couplings may change from their free nucleon values due to the presence of strongly interacting nucleons. Though CVC forbids any change in the charge coupling, other couplings like the magnetic, axial charge and pseudoscalar are likely to change from their free nucleon values. There exists considerable work in understanding the quenching of the magnetic moment and the axial charge in nuclei due to the nucleon-nucleon correlations. In our approach, the nucleon-nucleon correlation effects are reflected in the modification of nuclear response in the longitudinal and transverse channels. Due to PCAC, the axial current is strongly coupled to the pion field in the nuclear medium and therefore axial couplings are more likely to change due to the pionic effects modifying the nuclear response functions. To demonstrate an idea of these effects, we perform nonrelativistic reduction of the hadronic current (J_μ in Eq. (2.11)) [10], and see the occurrence of $g_1 \vec{\sigma} \vec{\tau}$, $f_2 \vec{\sigma} \times \vec{q} \vec{\tau}$ and $g_3 \vec{\sigma} \cdot \vec{q} \vec{\tau}$ terms in the weak current, which are linked to the spin-isospin excitations in nuclei, while f_2 and g_3 are coupled to the transverse and longitudinal channels, respectively, g_1 is coupled to both [10]. In a nuclear target, the coupling of these terms to the mesonic channels can be described through the diagram shown in Fig. 5.8.

The $ph-ph$ interaction is shown by the dashed line in Fig. 5.8 and is described by the π and ρ exchanges modulated by the effect of short range correlations. For the $ph-ph$ potential, we use $V_N(q) = V_\pi(q) + V_\rho(q)$ in terms of the longitudinal and transverse components expressed as

$$V_N(q) = \frac{f^2}{m_\pi^2} [V_t(q)(\delta_{ij} - \hat{q}_i \hat{q}_j) + V_l(q) \hat{q}_i \hat{q}_j] (\sigma_i \sigma_j) (\vec{\tau} \cdot \vec{\tau}) \quad (5.76)$$

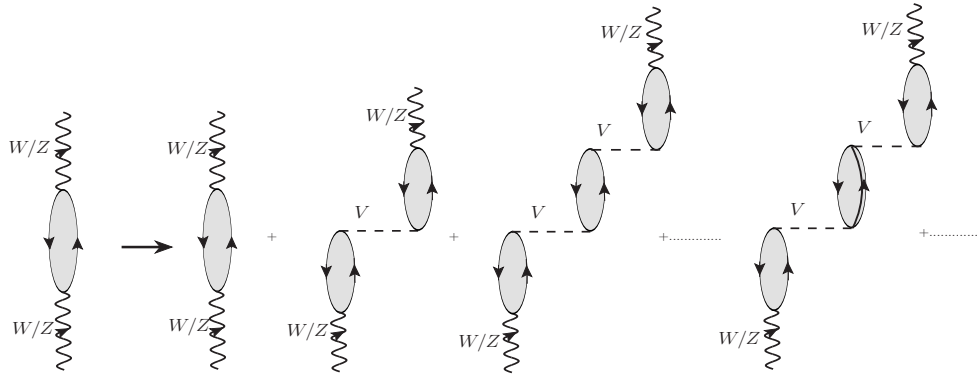


Figure 5.8: RPA effects in the ph contribution to the W/Z self-energy, where particle-hole, Δ -hole, Δ - Δ , etc. excitations contribute.

for the ph case, $\vec{\sigma}$ and $\vec{\tau}$ are Pauli matrices acting on the nucleon spin and isospin spaces, respectively. A similar potential V_Δ in the case of $ph - \Delta h$ interaction is obtained by substituting $\vec{\sigma} \rightarrow \vec{S}$, $\vec{\tau} \rightarrow \vec{T}$ and $f \rightarrow f^* = 2.15f$. V_l is the strength of the potential in the longitudinal channel and V_t is the strength of the potential in the transverse channel. Thus, we calculate this reduction in the vector-axial-vector (VA) and the axial-vector-axial-vector (AA) response functions due to the long range nucleon-nucleon correlations treated in the RPA. The representation into the longitudinal and the transverse channels is useful when one tries to sum the geometric series in Fig. 5.8, where the longitudinal and the transverse channels decouple and can be summed independently.

The potential $V(q)$ is explicitly written as:

$$V_l(q) = \frac{f^2}{m_\pi^2} \left[\frac{q^2}{-q^2 + m_\pi^2} \left(\frac{\Lambda_\pi^2 - m_\pi^2}{\Lambda_\pi^2 - q^2} \right)^2 + g' \right], \quad V_t(q) = \frac{f^2}{m_\pi^2} \left[\frac{q^2}{-q^2 + m_\rho^2} C_\rho \left(\frac{\Lambda_\rho^2 - m_\rho^2}{\Lambda_\rho^2 - q^2} \right)^2 + g' \right], \quad (5.77)$$

$\frac{f^2}{4\pi} = 0.8$, $\Lambda_\pi = 1.3$ GeV, $C_\rho = 2$, $\Lambda_\rho = 2.5$ GeV, m_π and m_ρ are the pion and rho meson masses, and g' is the Landau-Migdal spin-isospin parameter taken to be 0.7, which has been used quite successfully to explain many electromagnetic and weak processes in nuclei [471, 517, 518].

Using the matrix elements at the weak WNN vertex and the $ph - ph$ potential, the contribution of Fig. 5.8 is written as

$$U(q) = U(q) + U(q)V_N(q)U(q) + U(q)V_N(q)U(q)V_N(q)U(q) + \dots \quad (5.78)$$

Writing the potential $V_N(q)$ in terms of V_l and V_t , the above series can be separated in the longitudinal and the transverse components. The longitudinal component is then written as [10]:

$$U_L(q) = \left[\frac{U(q)}{1 - U(q)V_l} \right] \hat{q}_i \hat{q}_j \sigma_i \sigma_j \vec{\tau}_1 \cdot \vec{\tau}_2. \quad (5.79)$$

Similarly, the transverse component is given by [10]:

$$U_T(q) = \left[\frac{U(q)}{1 - U(q)V_t} \right] (\delta_{ij} - \hat{q}_i \hat{q}_j) \sigma_i \sigma_j \vec{\tau}_1 \cdot \vec{\tau}_2. \quad (5.80)$$

Therefore, we can write Eq. (5.78) as:

$$U(q) \rightarrow \tilde{U}(q) = \left[\left(\frac{U(q)}{1 - U(q)V_t} \right) (\delta_{ij} - \hat{q}_i \hat{q}_j) + \left(\frac{U(q)}{1 - U(q)V_l} \right) \hat{q}_i \hat{q}_j \right] \sigma_i \sigma_j \vec{\tau}_1 \cdot \vec{\tau}_2, \quad (5.81)$$

where $U = U_N + U_\Delta$, with U_N and U_Δ as the Lindhard functions for ph and Δh excitations, respectively, in the medium and the expressions for U_N and U_Δ are taken from Ref. [519, 520]. The different couplings of N and Δ are incorporated in U_N and U_Δ and then the same interaction strengths $V_l(q)$ and $V_t(q)$ are used to calculate the RPA response. These effects have been discussed by Nieves et al. [521] as well as by Athar et al. [522].

By using the above method of renormalization, we consider the different components of the hadronic tensor $J_{\mu\nu}$ (Eq. (2.16)) and sum up the RPA series shown in Fig. 5.8. For convenience we take \vec{q} to be along the z direction and neglect all the corrections of order $O\left(\frac{p_F \vec{p}}{M^2}, \frac{p_F \vec{p}'}{M^2}, \frac{p_F q_0}{M^2}\right)$, and the different components of $J_{\mu\nu}$ like J_{00} , J_{0z} , J_{zz} , etc. with renormalization

effect are obtained as [521, 522]:

$$\begin{aligned} \frac{J_{00}^{RPA}}{M^2} &= (f_1(Q^2))^2 \left[\left(\frac{E(\vec{p})}{M} \right)^2 + \left(\frac{q_0 E(\vec{p}) - Q^2/4}{M^2} \right) \right] + \frac{Q^2}{M^2} \left(\frac{f_2(Q^2)}{2} \right)^2 \left[\frac{\vec{p}^2 + q_0 E(\vec{p}) + q_0^2/4}{M^2} - \frac{q_0^2}{Q^2} \right] \\ &- \frac{1}{2} (f_1(Q^2) f_2(Q^2)) \left(\frac{|\vec{q}|}{M} \right)^2 + g_1^2(Q^2) \left[\frac{\vec{p}^2 + q_0 E(\vec{p}) - Q^2/4}{M^2} + U_L \left(\frac{q_0^2}{m_\pi^2 + Q^2} \right) \left(\frac{Q^2}{m_\pi^2 + Q^2} \right) \right] \end{aligned} \quad (5.82)$$

$$\begin{aligned} \frac{J_{0z}^{RPA}}{M^2} &= \frac{1}{2} (f_1(Q^2))^2 \left[\frac{E(\vec{p})}{M} \left(\frac{2p_z + |\vec{q}|}{M} \right) + \frac{q_0 p_z}{M^2} \right] + \frac{1}{2} \frac{Q^2}{M^2} \left(\frac{f_2(Q^2)}{2} \right)^2 \left[\frac{E(\vec{p})}{M} \left(\frac{2p_z + |\vec{q}|}{M} \right) \right. \\ &- \frac{2q_0 |\vec{q}|}{Q^2} + \frac{q_0 (2p_z + |\vec{q}|)}{2M^2} \left. \right] - \frac{1}{2} (f_1(Q^2) f_2(Q^2)) \left[\frac{q_0 |\vec{q}|}{M^2} \right] + g_1^2(Q^2) \left[U_L \frac{E(\vec{p})}{M} \left(\frac{2p_z + |\vec{q}|}{2M} \right) \right. \\ &+ \left. \frac{q_0 p_z}{2M^2} + U_L \left(\frac{q_0 |\vec{q}|}{m_\pi^2 + Q^2} \right) \left(\frac{Q^2}{m_\pi^2 + Q^2} \right) \right] \end{aligned} \quad (5.83)$$

$$\begin{aligned} \frac{J_{zz}^{RPA}}{M^2} &= (f_1(Q^2))^2 \left[\frac{p_z^2 + |\vec{q}| p_z + Q^2/4}{M^2} \right] + \frac{1}{4} \frac{Q^2}{M^2} \left(\frac{f_2(Q^2)}{2} \right)^2 \left[\left(\frac{2p_z + |\vec{q}|}{M} \right)^2 - \frac{q_0^2}{Q^2} \right] \\ &- \frac{1}{2} (f_1(Q^2) f_2(Q^2)) \left(\frac{q_0}{M} \right)^2 + g_1^2(Q^2) \left[U_L + \frac{p_z^2 + |\vec{q}| p_z + Q^2/4}{M^2} + U_L \left(\frac{|\vec{q}|}{m_\pi^2 + Q^2} \right) \left(\frac{Q^2}{m_\pi^2 + Q^2} \right) \right] \end{aligned} \quad (5.84)$$

$$\begin{aligned} \frac{J_{xx}^{RPA}}{M^2} &= (f_1(Q^2))^2 \left[\frac{p_x^2 + Q^2/4}{M^2} \right] + \frac{Q^2}{M^2} \left(\frac{f_2(Q^2)}{2} \right)^2 \left[U_T + \frac{p_x^2}{M^2} \right] \\ &+ \frac{1}{2} (f_1(Q^2) f_2(Q^2)) U_T \left(\frac{Q^2}{M^2} \right) + g_1^2(Q^2) \left[U_L + \frac{p_x^2 + Q^2/4}{M^2} \right] \end{aligned} \quad (5.85)$$

$$\frac{J_{xy}^{RPA}}{M^2} = i g_1(Q^2) [f_1(Q^2) + f_2(Q^2)] \left[\frac{q_0 p_z}{M^2} - U_T \frac{|\vec{q}| E(\vec{p})}{M^2} \right]. \quad (5.86)$$

Thus, in a local density approximation in the presence of NME including the RPA effect, the total cross section $\sigma(E_\nu)$, is written as

$$\sigma(E_\nu) = -2G_F^2 \cos^2 \theta_C \int_{r_{min}}^{r_{max}} r^2 dr \int_{k'_{min}}^{k'_{max}} k' dk' \int_{Q_{min}^2}^{Q_{max}^2} dQ^2 \frac{1}{E_\nu E_l} L_{\mu\nu} J_{RPA}^{\mu\nu} \text{Im} U_N [E_\nu - E_l - Q - V_c(r), \vec{q}] \quad (5.87)$$

where $J_{RPA}^{\mu\nu}$ is the modified hadronic tensor when RPA effect is incorporated and the energy transferred to the hadronic tensor also gets modified from $q_0 = E_\nu - E_l$ to $q_0 = E_\nu - E_l - Q - V_c$.

5.4.2. Inclusive quasielastic scattering at low energy

5.4.2.1 Theoretical results and comparison with experimental data

We summarize in this section, the experimental and theoretical results [468, 469, 470, 471, 472, 475, 487, 521, 522, 523, 524, 525, 526, 527, 528, 529, 530, 531, 532, 533, 534, 535, 536, 537] for the low energy inclusive (ν_e, e^-) , (ν_μ, μ^-) scattering cross sections from the KARMEN and LSND collaborations in ^{12}C , presented in Table-5.6 along with the theoretical predictions for these processes in various nuclear models. Most of the theoretical methods used to obtain these results were earlier developed to study the related process of the inclusive muon capture for which the results are also included in Table 5.6. We have included theoretical results only from those calculations, which quote results for the relevant physical observable for all the three processes i.e. the total cross section for the (ν_e, e^-) and (ν_μ, μ^-) inclusive scattering as well as the total rate for muon capture in ^{12}C using the same nuclear model.

The various microscopic nuclear models referred in the column 3 of Table-5.6, in general use the shell model with varying model spaces including states from 1 $\hbar\omega$ to 4 $\hbar\omega$ excitations to calculate the ground state of the initial as well as the ground state and excited states of the final nuclei and transitions between them. The various models use different forms of the phenomenological nucleon-nucleon potentials like the Bonn potential, Landau-Migdal potential or the Skymre model potential to calculate the nuclear states. Moreover, the residual interaction between the nucleons which leads to the pairing and also to the quasi-particle excitations of nucleons in the nuclei are also included in some nuclear models to calculate the nuclear wave functions of the higher excited states and the continuum state in the final nucleus. Depending upon the various assumptions and approximations, many nuclear models have been used to calculate the total cross sections for (ν_e, e^-) and (ν_μ, μ^-) inclusive reactions as well as the muon capture rate. The results for the inclusive cross sections, and muon capture rates from these calculations are shown in Table-5.6, column-3. In column-4, we show the results for these observables obtained in various versions of the Fermi gas model. It should be noted that the different entries for the total cross sections or the capture rate

Process	Experiments	Microscopic theories	Fermi gas model
$\sigma(\nu_\mu)$ ($\times 10^{-40}$) cm^2 $\nu_\mu(^{12}C, X)\mu^-$	$11.2 \pm 0.3 \pm 1.8$ [524] $10.6 \pm 0.3 \pm 1.8$ [526]	28.8, 22.4, 14.5, 15.2 [468] 27.0, 21.1, 13.5, 14.3 [468] 19.25 [475], 19.59 [523] 18.18, 17.80 [527], 30.0, 19.2 [528] 15.6, 13.2, 17.0, 31.3, 19.1 [531] 15.18, 19.23, 20.29, 21.08 [472]	16.65 ± 1.37 [471] 19 [470] 13.2 ± 0.7 , 9.7 ± 0.3 , 12.2 [525] $22.7-24.1$ [529, 530] 25 [469], 11.9 [521]
$\sigma(\nu_e)$ ($\times 10^{-42}$) cm^2 $\nu_e(^{12}C, X)e^-$	$14.8 \pm 0.7 \pm 1.4$ [535]	15.2, 15.6 [532], 14.6 [533, 534] 16.42, 16.70, 55.1, 52.0 [472] 19.28, 18.15 [527] 6.9, 3.5, 4.1, 5.4, 3.1 [531] 23.7, 15.1 [528], 15 [487], 12.14 [523] 114.4, 76.3, 16.5, 22.7 [468] 90.6, 63.2, 12.9, 17.6 [468]	14 [521], 15.48 ± 1.13 [471] 14 [470] 13.8 ± 0.4 , 14.3 ± 0.6 , 8.6 [525] 15.3 [469] 13.6 [522]
$\Gamma(\mu^-)$ ($\times 10^4$) sec^{-1} $\mu^-(^{12}C, X)\nu_\mu$	3.88 ± 0.05 [536]	4.82, 4.26, 4.07, 4.47 [537] 5.24, 3.35 [528], 3.56, 4.53 [531] 2.98, 2.99, 3.17, 3.40 [531] 8.0, 6.87, 3.09, 3.48 [468] 8.4, 7.22, 3.23, 3.64 [468] 3.32, 4.06, 5.12 [472], 5.79 [527]	3.3 [469] 3.37 ± 0.16 , 3.22 , 3.19 ± 0.06 [525] 3.60 ± 0.22 [471], 3.21 [521]

Table 5.6: Latest experimental results and various theoretical results in different nuclear models for inclusive cross section for ν_e and ν_μ scattering and muon capture rates in ^{12}C .

quoted under the same reference in column-3 and 4 of Table-5.6 corresponds to the various versions of the nuclear models and the parameters used in that model.

The following general observations about the theoretical results and their comparisons with the experimental results shown here in Table 5.6, can be made:

- (i) There is no microscopic nuclear model, which is able to explain all the three weak processes involving ν_e , ν_μ and muon capture. Even in a given model by changing the parameters of the model i.e. the various versions of the model, it is possible to explain either the cross section for the inclusive QE reactions or the inclusive muon capture but not both of them simultaneously [468, 472, 475, 487, 523, 527, 528, 531, 532, 533, 534, 537].
- (ii) In the case of LFGM also the earlier nonrelativistic calculations by Singh and Oset [469, 471], Umno et al. [529, 530], Kosmas and Oset [470], Nieves et al. [521], and Athar et al. [522] including RPA, reproduce (ν_e, e^-) but overestimate the (ν_μ, μ^-) reaction cross section and underestimate (μ^-, ν_μ) capture rate. The LFGM has been considerably improved in the latest calculations by Nieves and Sobczyk [525], where relativistic transition operators and the spectral function of nucleons are used to calculate all the three processes. These models reproduce (ν_e, e^-) and (ν_μ, μ^-) inclusive cross sections quite well but underestimate the inclusive (μ^-, ν_μ) capture rate.

In summary, a satisfactory understanding of the nuclear reactions with ν_μ , ν_e scattering, and μ capture in nuclear targets in the energy region of $E < 230$ MeV is desirable.

5.4.2.2 Inclusive cross sections with monoenergetic KDAR neutrinos with $E_{\nu_\mu} = 236$ MeV

The monoenergetic muon neutrinos from KDAR are identified as an ideal probe to study the neutrino-nucleus cross sections in the low energy region in order to benchmark NME in the exclusive as well as in the inclusive reactions in this energy region. An experiment for measuring neutrino cross section $\sigma(E_{\nu_\mu})$ with monoenergetic neutrinos would be free from the uncertainties arising from the reconstruction procedure of the initial neutrino energy present in most of the experiments using beams of continuous energy of the muon neutrinos from accelerators. Some new experiments have been planned to measure inclusive cross sections in ^{12}C and ^{40}Ar using the monoenergetic neutrinos from kaons decaying at rest. The monoenergetic neutrinos from kaons decaying at rest $K^+ \rightarrow \mu^+ \nu_\mu$ are copiously produced with an energy $E_{\nu_\mu} = 236$ MeV, along with a continuous energy spectrum of ν_e and ν_μ from Kl_3 decays like $K^+ \rightarrow \pi^0 e^+ \nu_e$ and $K^+ \rightarrow \pi^0 \mu^+ \nu_\mu$.

The first measurement of the inclusive cross section in ^{12}C nucleus with the monoenergetic KDAR muon neutrinos has been recently reported by the MiniBooNE collaboration to be $\sigma = (2.7 \pm 1.2) \times 10^{-39} cm^2$ [538]. Theoretically, this reaction in ^{12}C in the energy region of few hundreds of MeV, has been studied by many authors, but specific calculations and discussions of the inclusive cross section for $E_{\nu_\mu} = 236$ MeV have been done recently by Akbar et al. [539] in the relativistic Fermi gas model with RPA to include the effect of correlations and Nikolakopoulos et

Experimental and Theoretical Models	Cross section
MiniBooNE Exp. [538]	2.7 ± 1.2
Akbar et al. [539]	0.91
Martini et al. [509, 464]	$1.3 \pm 0.2(\text{np-nh})$
GENIE [541]	1.75
NuWro [542, 543]	$1.3 \pm 0.4(\text{np-nh})$
NUANCE [333]	1.4
CRPA [493]	1.58
RMF [493]	1.56
RFG [540]	1.66
RFG 34 [540]	1.38

Table 5.7: Experimental and theoretical results for the inclusive cross section for KDAR neutrinos. The cross sections are in units of 10^{-39}cm^2 .

al. [540] in a microscopic model using CRPA to include the effect of nucleon-nucleon correlations. Nikolakopoulos et al. [540] have also extrapolated the results of some earlier calculations to predict the inclusive neutrino cross sections at $E_{\nu_\mu} = 236 \text{ MeV}$ and presented a comparative study of the theoretical and experimental results. In Table 5.7, we present a list of the theoretical results for the inclusive cross sections at $E_{\nu_\mu} = 236 \text{ MeV}$ in the process $\nu_\mu + {}^{12}\text{C} \rightarrow \mu^- + X$ obtained in various theoretical calculations along with the Monte Carlo predictions [541, 542, 543] and the experimental result from the MiniBooNE experiment [538] for comparison.

We see that all the theoretical predictions for the cross section lie in the wide range of $(0.91 \text{ to } 1.66) \times 10^{-39} \text{cm}^2/\text{neutron}$ and underestimate the experimental results for the inclusive cross sections at $E_{\nu_\mu} = 236 \text{ MeV}$. A comparison of the theoretical results of the inclusive neutrino cross sections in ${}^{12}\text{C}$ in the case of monoenergetic neutrinos at $E_{\nu_\mu} = 236 \text{ MeV}$ and the earlier theoretical results in the energy region of the LSND experiment i.e. $E_{\nu_\mu} < 280 \text{ MeV}$ with the experimental data show that:

- (i) The theoretical predictions using various nuclear models for the inclusive cross sections for the reaction $\nu_\mu + {}^{12}\text{C} \rightarrow \mu^- + X$ with monoenergetic neutrinos have a large range of variation. This is surprising in the case of ${}^{12}\text{C}$ which is one of the theoretically better studied nucleus.
- (ii) Most of the theoretical predictions for the inclusive cross section for this reaction overestimate the experimental results for the LSND experiment with neutrino energy E_{ν_μ} in the range of $120 \text{ MeV} < E_{\nu_\mu} < 280 \text{ MeV}$, while the theoretical predictions in the case of the KDAR neutrino with $E_{\nu_\mu} = 236 \text{ MeV}$ underestimate the experimental result.
- (iii) The latest experimental as well as theoretical results for the inclusive cross sections using the monoenergetic KDAR muon neutrinos together with the results obtained in the case of LSND and KARMEN experiments with electron and muon neutrinos along with the capture rate of (μ^-, ν_μ) process in ${}^{12}\text{C}$ show that the theoretical calculations done in the impulse approximation for all the weak nuclear processes of (μ^-, ν_μ) , (ν_e, e^-) and (ν_μ, μ^-) in the low energy region are not theoretically understood satisfactorily, with a given nuclear model used to describe the structure of ${}^{12}\text{C}$ nucleus.

5.4.3. Quasielastic (anti)neutrino scattering at intermediate energy with $\nu_e(\bar{\nu}_e)$ and $\nu_\mu(\bar{\nu}_\mu)$

(i) Nuclear model dependence

In this section, the results obtained using Eq. (5.87) with and without RPA effects are presented and the findings are discussed. In Fig. 5.9, the results are presented for the ratio of scattering cross section per interacting nucleon obtained using LFG model (Eq. (5.74)) and LFG model with RPA effect (LFG + RPA) (Eq. (5.87)) for (anti)neutrino induced processes in ${}^{12}\text{C}$, ${}^{40}\text{Ar}$, ${}^{56}\text{Fe}$ and ${}^{208}\text{Pb}$ to the scattering cross section on free nucleon target in the energy region from threshold to 0.8 GeV . Performing calculations using LFG, we find that in ${}^{12}\text{C}$ NME like Fermi motion, Pauli blocking, binding energy, result in the reduction of cross section by $\sim 30(42)\%$ at $E_\nu = 0.3 \text{ GeV}$ and around $20(30)\%$ at $E_\nu = 0.6 \text{ GeV}$ from free nucleon case for $\nu_e(\bar{\nu}_e)$ induced processes. Inclusion of RPA correlation in LFG, reduces the cross section for $\nu_e(\bar{\nu}_e)$ scattering from free nucleon by $\sim 55(56)\%$ at $E_\nu = 0.3 \text{ GeV}$ and $35(45)\%$ at $E_\nu = 0.6 \text{ GeV}$. Similar results may be observed for ${}^{40}\text{Ar}$, ${}^{56}\text{Fe}$ and ${}^{208}\text{Pb}$ nuclear targets. In general, the reduction in the cross section increases with the increase in mass number. For ν_μ and $\bar{\nu}_\mu$ induced processes at lower energies the reduction is larger and for $E_\nu > 0.4 \text{ GeV}$, the reduction in $\nu_e(\bar{\nu}_e)$ and $\nu_\mu(\bar{\nu}_\mu)$ cross sections is almost the same.

To compare our results with other variants of the Fermi gas model, we have obtained total scattering cross section in ${}^{40}\text{Ar}$ using Fermi gas model of Smith and Moniz [502], Llewellyn Smith [175] and Gaisser and O'Connell [503] and calculated fractional difference $\delta\sigma_{\text{Model}} (= \frac{\sigma_{\text{free}} - \sigma_{\text{Model}}}{\sigma_{\text{free}}})$, the results for which are shown in Fig. 5.10. Here

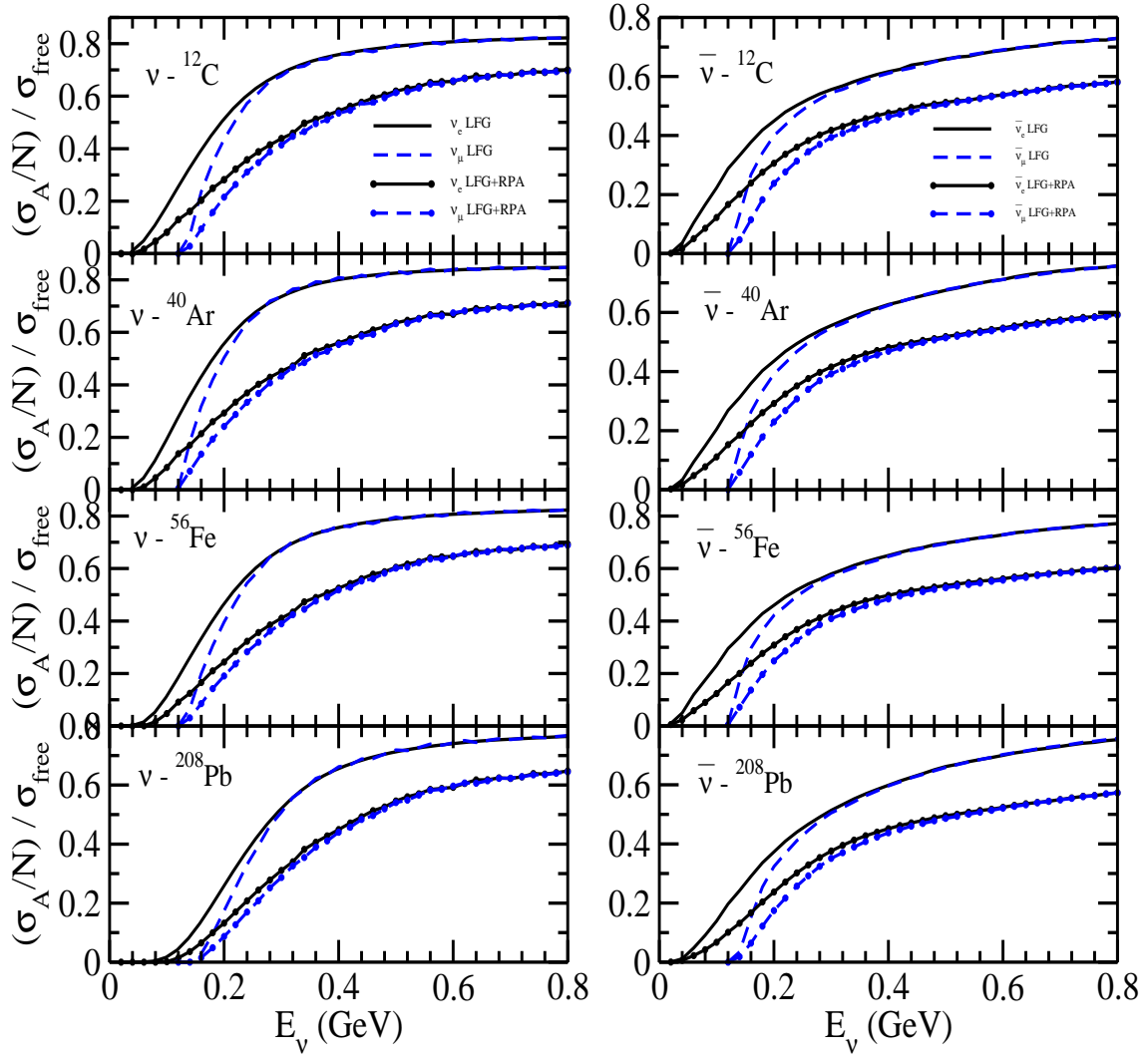


Figure 5.9: Ratio $\frac{\sigma_A/N}{\sigma_{free}}$ vs E_ν , for neutrino (left panel) and antineutrino (right panel) induced processes in ^{12}C , ^{40}Ar , ^{56}Fe , and ^{208}Pb . The solid (dashed) line represents cross section obtained from electron (muon) type neutrino and antineutrino. For neutrino induced process $N = A - Z$, is neutron number and for antineutrino induced process $N = Z$, is proton number. σ_A is cross section in nuclear target and has been evaluated using LFGM and LFG with RPA effect (LFG+RPA) and σ_{free} is the cross section for the free nucleon case.

σ_{free} stands for the (anti)neutrino induced interaction cross section on free nucleon target and σ_{Model} stands for the (anti)neutrino induced interaction cross section for the nucleons bound inside the nucleus. The results for neutrino (ν_e , ν_μ) is different from antineutrino ($\bar{\nu}_e$, $\bar{\nu}_\mu$) and is mainly due to the interference terms with g_1 which come with an opposite sign. In the case of LFG with RPA effects, the effect of renormalization is large and this suppresses the terms with f_2 and g_1 , which results in a large change in neutrino vs antineutrino results. We find appreciable difference in the results when various nuclear models are used, and that may be observed from Fig. 5.10.

(ii) Effect of lepton mass and its kinematic implications

There are two types of corrections which appear when lepton mass m_l ($l = e, \mu$) is taken into account in the cross section calculations for the reaction $\nu_l(\bar{\nu}_l) + N \rightarrow l^-(l^+) + N'$, ($N, N' = n, p$) which can be classified as kinematical and dynamical in origin. The kinematical effects arise due to $E_l \neq |\vec{k}'|$ in presence of m_l and the minimum and maximum values of four momentum transfer square ($Q^2 = -q^2 \geq 0$) i.e. Q_{min}^2 and Q_{max}^2 are modified, affecting the calculations of total cross sections. These effects are negligible for highly relativistic leptons but could become important at low energies near threshold specially for muons. On the other hand, the dynamical corrections arise as additional term proportional to $\frac{m_l^2}{M^2}$ in the existing contribution of vector and axial-vector form factors as well as new contributions due to induced pseudoscalar and other form factors associated with the SCC come into play. In fact all the contributions from the pseudoscalar form factor $g_3(Q^2)$ are proportional to $\frac{m_l^2}{M^2}$ while the contribution from the second class axial-vector form factor $g_2(Q^2)$ is proportional either to $\frac{m_l^2}{M^2}$ or $\frac{Q^2}{M^2}$ or both.

To study the lepton mass dependence on $\nu_e(\bar{\nu}_e)$ and $\nu_\mu(\bar{\nu}_\mu)$ induced scattering cross sections in the free nucleon

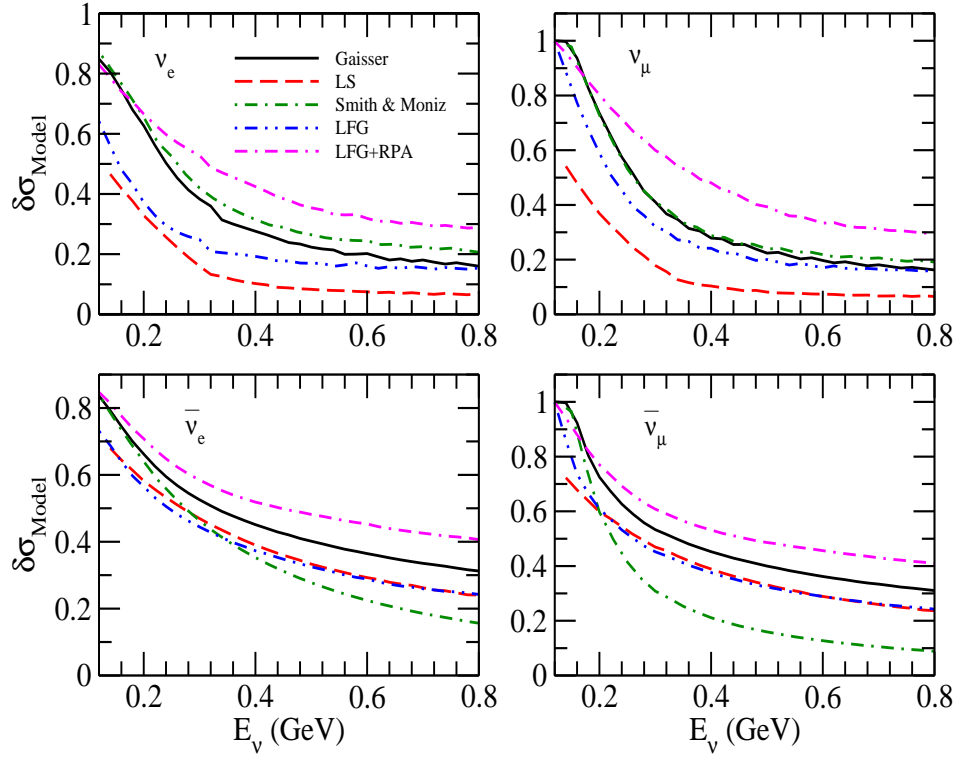


Figure 5.10: The fractional suppression in cross section $\delta\sigma_{Model} \left(= \frac{\sigma_{free} - \sigma_{Model}}{\sigma_{free}} \right)$ vs E_ν , where σ_{free} is the cross section obtained for the free nucleon and σ_{Model} is per interacting nucleon cross section in ^{40}Ar obtained using the different nuclear models. The results are presented for the cross sections obtained from the different models of Fermi gas (σ_{Model}) viz. Smith and Moniz [502] (dashed dotted line), Llewellyn Smith [175] (dashed line), Gaisser O'Connell [503] (solid line), and with (double dashed dotted line) & without RPA (dashed double dotted line) effect using LFGM. The top panel is for neutrino and bottom panel is for antineutrino induced processes.

as well as in the nuclear targets, we define $\Delta_I = \frac{\sigma_{\nu_e(\bar{\nu}_e)} - \sigma_{\nu_\mu(\bar{\nu}_\mu)}}{\sigma_{\nu_e(\bar{\nu}_e)}}$ for (anti)neutrino induced reaction in ^{12}C and ^{40}Ar nuclear targets, where $I = i, ii, iii$, which respectively stands for the cross sections obtained in (i) free (anti)neutrino case, (ii) the LFG model and (iii) the LFG + RPA model. The results are presented in Fig. 5.11, which show that the differences in the electron and muon production cross sections for $\nu_l(\bar{\nu}_l)$ induced reactions on ^{12}C target are appreciable at low energies $E_\nu < 0.4 \text{ GeV}$.

(iii) Vector form factors

The various parameterizations of the vector form factors have been discussed in Section 2.1.5, and we find the dependence on the choice of the different parameterizations of the vector form factors on the (anti)neutrino-nucleus cross sections to be negligible.

(iv) Axial vector form factor

It is believed that NME due to 2p-2h excitations, MEC and multinucleon correlations are taken into account then the recent experimental results can also be considered to be consistent with a smaller value of M_A [509, 511, 544, 545, 546]. However, it may be observed from Table-2.2 that even with the same nuclear target, different values of M_A have been obtained from the neutrino experiments done in different energy regions highlighting the energy region in which NME play significant role.

To study the explicit dependence of the cross section on the value of M_A , we define δ_{M_A} as

$$\delta_{M_A} = \frac{\sigma_{\nu_l}(M_A^{modified}) - \sigma_{\nu_l}(M_A = W_A)}{\sigma_{\nu_l}(M_A = W_A)}, \quad \text{WA} = \text{world average} = 1.026 \text{ GeV} \quad (5.88)$$

where $l = e$ or μ . We observe from Fig. 5.12 that for the free nucleon, when a modified value of M_A i.e. $M_A^{modified} = 0.9(1.2) \text{ GeV}$ is used instead of world average value of 1.026 GeV then a decrease(increase) of 5–15% is obtained for ν_e/ν_μ reactions in the energy range of 0.2–0.8 GeV. In the case of $\bar{\nu}_e/\bar{\nu}_\mu$ -nucleon reactions this decrease(increase) is about 5–10% in the same energy range. When NME are taken into account, for example, in the case of ^{40}Ar nucleus this decrease(increase) remains almost the same. Therefore, the uncertainty in the (anti)neutrino-nucleus cross sections is the same as in the case of free (anti)neutrino-nucleon scattering processes.

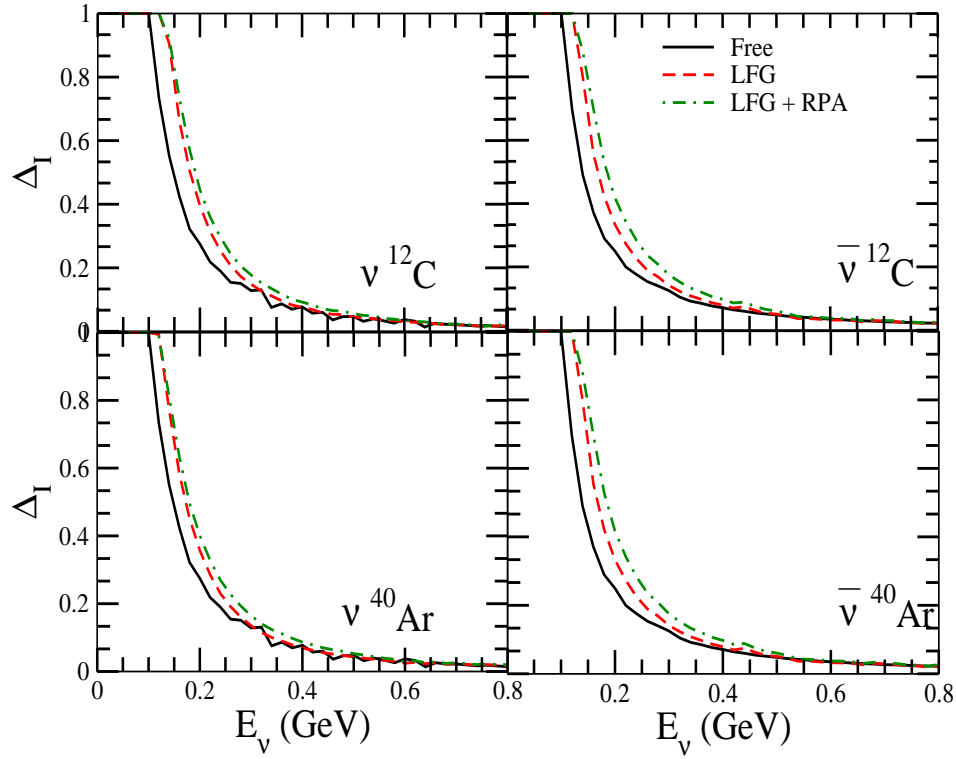


Figure 5.11: $\Delta_I = \frac{\sigma_{\nu e}(\bar{\nu}_e) - \sigma_{\nu \mu}(\bar{\nu}_\mu)}{\sigma_{\nu e}(\bar{\nu}_e)}$ for neutrino (left panel) and antineutrino (right panel) induced processes in ^{12}C and ^{40}Ar targets. Here I stands for the results of the cross sections obtained (i) for the free nucleon case (solid line) (ii) in the LFG (dashed line) and (iii) for LFG with RPA effect (dash-dotted line).

(v) **Pseudoscalar form factor**

To study the effect of the pseudoscalar form factor $g_3(Q^2)$ on muon production cross section, we define

$$\delta_{g_3}(E_\nu) = \frac{\sigma_{\nu\mu}(g_3 \neq 0) - \sigma_{\nu\mu}(g_3 = 0)}{\sigma_{\nu\mu}(g_3 = 0)}, \quad (5.89)$$

and similar expression for antineutrino is used. For the numerical calculations, the expression of $g_3(Q^2)$ given in Eq. (2.47) has been used. The results are presented in the left panel of Fig. 5.13. We find that δ_{g_3} is more sensitive in the case of $\bar{\nu}_\mu$ induced CCQE process than ν_μ induced process for the free nucleon case as well as for ^{40}Ar nuclear target. This sensitivity decreases with the increase in $\nu_\mu/\bar{\nu}_\mu$ energy and almost vanishes beyond 0.6 GeV.

We also study the sensitivity of pseudoscalar form factor $g_3(Q^2)$ to find out the difference in the electron vs muon production cross sections that are obtained using Eq. (2.47). For this purpose we define

$$\Delta_1(E_\nu) = \frac{\sigma_{\nu\mu}(g_3 \neq 0) - \sigma_{\nu e}(g_3 \neq 0)}{\sigma_{\nu e}(g_3 \neq 0)}; \quad \Delta_2(E_\nu) = \frac{\sigma_{\nu\mu}(g_3 = 0) - \sigma_{\nu e}(g_3 = 0)}{\sigma_{\nu e}(g_3 = 0)}; \quad \Delta_{g_3} = \Delta_1(E_\nu) - \Delta_2(E_\nu). \quad (5.90)$$

and the results for Δ_{g_3} are shown in the right panel of Fig. 5.13.

We have calculated the fractional difference Δ_{g_3} as given in Eq. (5.90) for the free nucleon case as well as for the nucleon bound in ^{40}Ar nuclear target using the LFG with RPA effect. We observe that the inclusion of pseudoscalar form factor decreases the fractional change (Δ_{g_3}) by about 3(8)% at $E_{\nu(\bar{\nu})} \sim 0.2\text{GeV}$ and becomes smaller with the increase in energy. When NME (LFG+RPA) are taken into account in the evaluation of cross sections in ^{40}Ar then this difference increases to 4(15)% at the same energy for neutrino(antineutrino) induced processes.

(vi) **Second class axial-vector form factor**

In the case of QE (anti)neutrino scattering from nuclear targets, the effect of the axial-vector form factor associated with SCC on the total scattering cross section is similar to that observed in the case of (anti)neutrino-nucleon QE scattering, and the effect is found to be less than a percent.

(viii) **Radiative corrections**

Radiative corrections are potential source of difference between electron and muon production cross sections in (anti)neutrino reactions due to their logarithmic dependence on the lepton mass through terms like $\log(\frac{E_\nu^*}{m_l})$, where

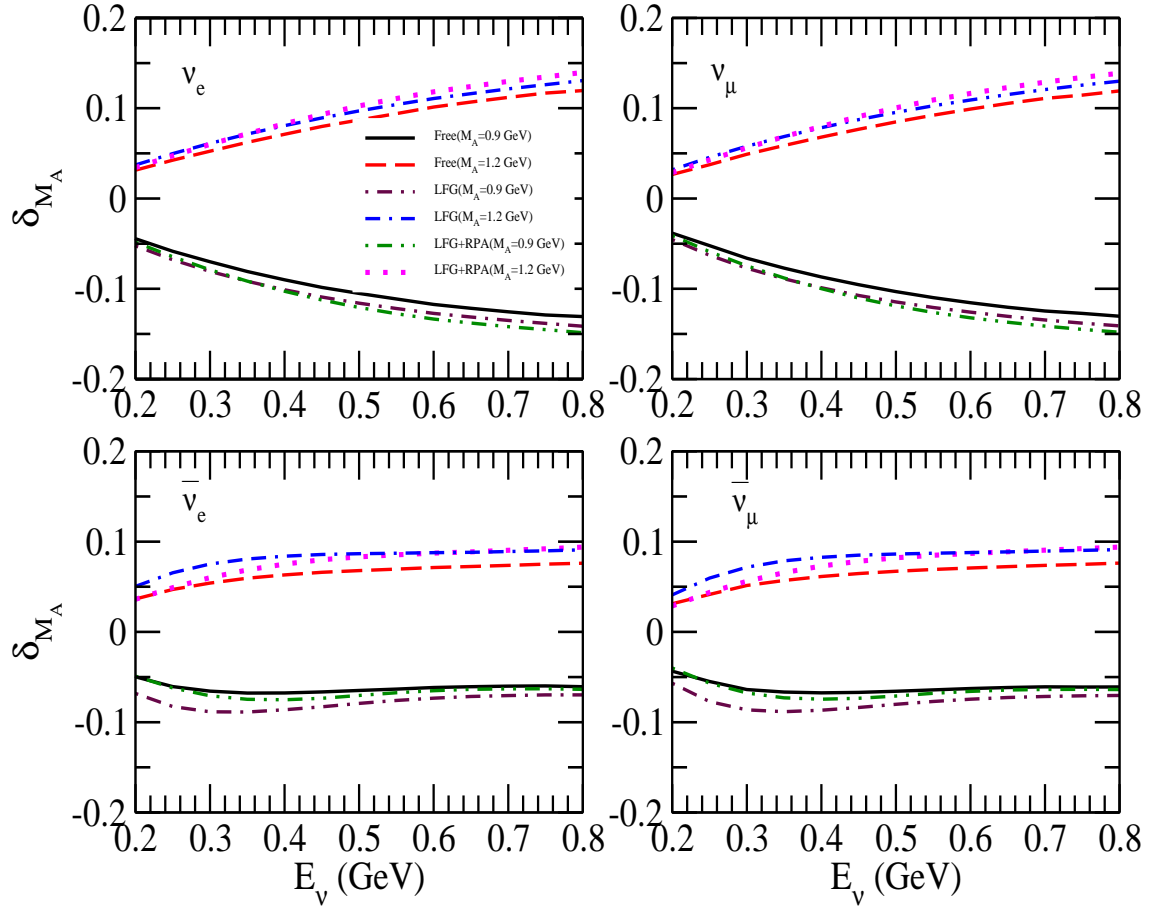


Figure 5.12: The dependence of cross section on M_A obtained using Eq. (5.88). The results are shown for $\nu_e(\bar{\nu}_e)$ and $\nu_\mu(\bar{\nu}_\mu)$ induced processes on free nucleon as well as on ^{40}Ar target using LFG with and without RPA effect. Solid (dashed) line denotes results for the free nucleon case with $M_A = 0.9 \text{ GeV}$ (1.2 GeV), results obtained using LFG are shown by dash-dotted (double dash-dotted) line with $M_A = 0.9 \text{ GeV}$ (1.2 GeV) and results for LFG with RPA effect are shown by dash-double dotted (dotted) line with $M_A = 0.9 \text{ GeV}$ (1.2 GeV).

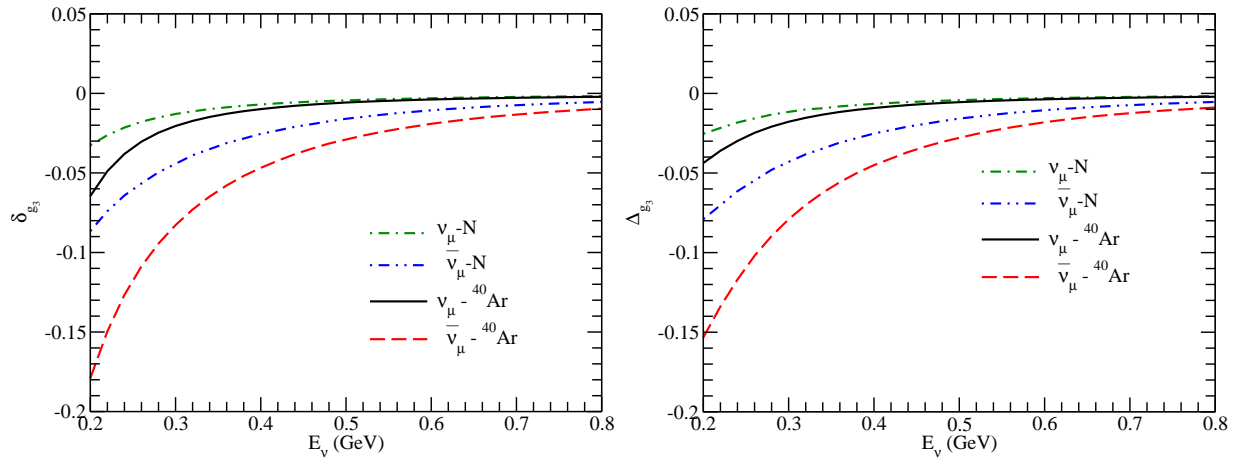


Figure 5.13: (Left panel) Results of the fractional change δ_{g_3} defined in Eq. (5.89) as a function of (anti)neutrino energy. (Right panel) Results of the fractional change Δ_{g_3} defined in Eq. (5.89) as a function of (anti)neutrino energy. The results are shown for the ν_μ induced cross section for the free nucleon case (dashed dotted line), as well as for the nucleons bound in ^{40}Ar (solid line) nuclear target obtained using LFG with RPA effect. The results corresponding to $\bar{\nu}_\mu$ induced CCQE process are shown by dashed double dotted line (free nucleon case) and dashed line (^{40}Ar target).

E_l^* is some energy scale in the reaction. The radiative corrections in CC QE neutrino-nucleon reactions relevant for the present oscillation experiments in the energy region of few GeV have been recently calculated by Bodek [547], Day and McFarland [548], Graczyk [549], and Tomalak et al. [550]. Bodek [547], and Day and McFarland [548] make use of leading log approximation given by De Rujula et al. [551] to calculate the contribution of soft photon emission by the lepton leg bremsstrahlung diagram which gives major contribution to the radiative corrections depending on the lepton mass m_l . On the other hand, Graczyk [549] includes the contribution of other diagrams like two boson exchange involving W and γ , propagator correction in addition to the soft photon bremsstrahlung. These effects have also been discussed by us in Ref. [552].

5.4.4. MiniBooNE axial dipole mass anomaly and nuclear medium effects

In the axial vector sector, the dipole mass M_A is generally taken to be the world average value, determined from the QE scattering or $M_A = 1.014 \pm 0.016$ GeV determined from the threshold pion electroproduction from proton/deuteron [203, 202]. However, using these values of M_A , the inclusive total and differential cross sections, obtained from the high statistics experiment in ^{12}C , performed by the MiniBooNE collaboration, were underestimated [209, 553, 554]. The MiniBooNE results were analyzed using the relativistic Fermi gas model and the microscopic nuclear models, which failed to explain the observed cross sections using the world average value of M_A [555]. It was also reported that a higher value of $M_A = 1.35 \pm 0.17$ [556, 557] can explain both the total and differential cross sections. This value of M_A is considerably larger than the world average value of M_A determined from earlier experiments. The higher value of M_A is also in disagreement with the results of another high statistics experiment performed by the NOMAD collaboration in ^{56}Fe , which reported a value of $M_A = 1.05 \pm 0.02 \pm 0.06$ GeV [204], consistent with the world average value. This is known as the MiniBooNE axial dipole mass anomaly.

Assuming that the uncertainties in the neutrino flux at the MiniBooNE detector were well estimated and are reflected in the uncertainties quoted in the cross section measurements, there was a general consensus that NME are not adequately taken into account. This may be because:

1. The effects of nuclear medium beyond the impulse approximation like MEC, $np - nh$, and $ph - \Delta h$ excitations are not included adequately in the impulse approximation, despite indications that they are quite important in the region of the low and intermediate energy neutrino-nucleus reactions.
2. In the intermediate energy region of the MiniBooNE experiment, where the ν_μ spectrum peaks around 750 MeV, the real pions would be produced which could be reabsorbed in the nuclear medium mimicking the genuine QE inclusive events leading to an enhancement in the observed inclusive cross section for QE reactions. The effect of these events called the QE-like events were not included adequately in the theoretical calculations.
3. In most of the neutrino reactions, the energy of the initial neutrinos is reconstructed using free particle QE kinematics of neutrino-nucleon reactions in the nuclear medium. This kinematics is affected by the entanglement of the kinematics of the QE-like events due to the IE processes i.e. $\nu_\mu NN \rightarrow \mu \Delta N \rightarrow \mu NN$ or scattering from the correlated pair $\nu_\mu NN \rightarrow \mu NN$ in the nucleus with the genuine lepton events produced in the real QE $\nu_\mu N \rightarrow \mu N$ scattering. The effect of this entanglement was not included in reconstructing the neutrino energy leading to underestimate the flux averaged cross sections.

A careful investigation of the above NME beyond impulse approximation was undertaken in view of the MiniBooNE axial dipole mass anomaly. The earlier calculations of Singh and Oset [469], Marteau et al. [558], and Nieves et al. [521, 559] were, respectively, improved by Martini et al. [508, 509] and Nieves et al. [560] in which the $2p - 2h$, $ph - \Delta h$, MEC effects as well as the pion reabsorption effects were taken into account. It was shown that the contribution of these effects is quite substantial in the energy region of MiniBooNE experiment and the observed cross section is reproduced quite well when the above mentioned NME are taken into account using the world average value of M_A and can explain the axial dipole mass anomaly. These results were further improved by the calculations of Rocco et al. [561] and Ivanov et al. [562] using the nucleon spectral functions to describe the energy and momentum distribution of the nucleons in the nucleus.

5.4.5. Nuclear medium effects due to two particle-two hole excitations

The MiniBooNE puzzle initiated an extensive debate on NME in (anti)neutrino-nucleus scattering. Since the ^{12}C nucleus used in many neutrino oscillation experiments is one of the better understood nucleus theoretically as well as experimentally from the study of electron nucleus scattering regarding its wave function, the discrepancy in the measurement of neutrino cross section at MiniBooNE was very difficult to be explained. It was attributed to other nuclear effects beyond the impulse approximation due to MEC and nucleon-nucleon correlations or FSI effects leading to QE like events. In earlier treatments of including such effects, the diagrams corresponding to Fig. 5.14 were taken into consideration while the diagrams corresponding to Fig. 5.15, where W and Z bosons interacting directly with the nonnucleonic degrees of freedom in the nucleus were not fully incorporated.

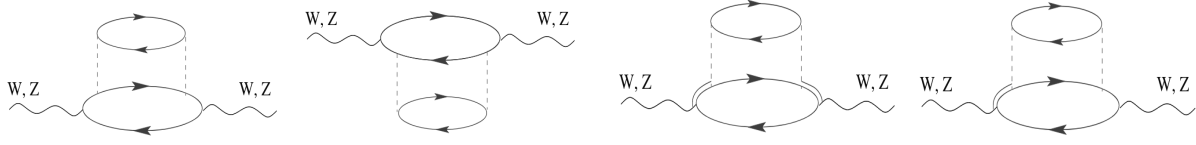


Figure 5.14: Diagrams showing some typical 2p-2h contributions arising due to the $N - N$ and $N - \Delta$ correlations. Solid (dashed) lines denote nucleon (pion) propagators. Double lines represent $\Delta(1232)$ propagators. Arrows pointing to the right (left) denote particle (hole) states.

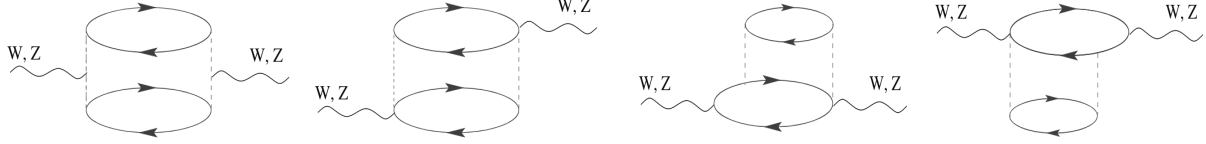


Figure 5.15: Diagrams showing some typical 2p-2h contributions arising due to the meson exchange. Solid (dashed) lines denote nucleon (pion) propagators. Double lines represent $\Delta(1232)$ propagators. Arrows pointing to the right (left) denote particle (hole) states.

It was suggested by the Lyon group [507, 508, 509] for the first time that the processes like 2p-2h, or in general n particle-n hole (np-nh), which are multi-nucleon correlation effects could be important. Fig. 5.16 shows the results of QE-like ν_μ - ^{12}C cross sections measured by the MiniBooNE collaboration [209, 348] and the theoretical curves are the results with and without 2p-2h excitations using the model of Martini et al. [507]. This was followed by the works of Valencia group [511, 560], which were in agreement with the theoretical observations made by the Lyon group [507]. This was in addition to the long range nuclear correlations discussed in Section 5.4.1 using RPA. Both these groups use microscopic approach. This led to lots of interest among the scientific community to understand the multinucleon correlation effects. Presently these studies may be broadly divided into three categories:

- In the first approach, one starts from an independent particle model (IPM). For example, LFGM has been used by the Lyon [507, 508, 509, 510, 563, 564, 565] and the Valencia [505, 511, 512, 560, 566, 567] groups and their umbrella collaborations. The Ghent [568, 569, 570] and the La Plata [571] groups use nonrelativistic and relativistic mean field approaches. In addition to that they took into account 2p-2h contributions to the neutrino-nucleus cross section.
- In the second approach, one starts from a correlated wave function and the 2p-2h excitations self evolve due to the short range correlations. In addition to that, the contribution from MEC in some of the works have also been included. For example, the works of group using Green's function Monte Carlo method [496, 497, 572, 573] or the group using spectral function approach [561, 574, 575, 576, 577] are based on this approach.
- The third approach is more phenomenological as these methods are constrained by the electron scattering phenomenology, for example, the SuSA [494, 578], and the model developed by Geissen group (GiBUU) [579]. Amaro et al. [580, 581] and Megias et al. [495] calculated the MEC effect in the SuSA model. In the works of Refs. [582, 583, 584, 585, 586, 587, 588, 589], the multinucleon excitations are included via a microscopic fully relativistic calculation of the 2p-2h excitations. While the GiBUU includes 2p-2h excitations via an empirical spin-isospin response deduced from the electron scattering data [579].

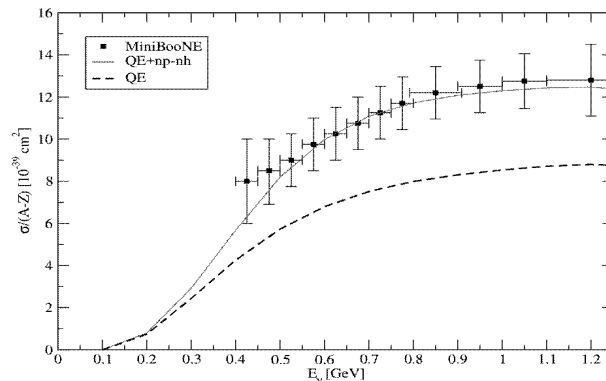


Figure 5.16: “QE-like” ν_μ - ^{12}C cross sections measured by the MiniBooNE collaboration [209, 348] compared to Martini *et al.* [507] calculations.

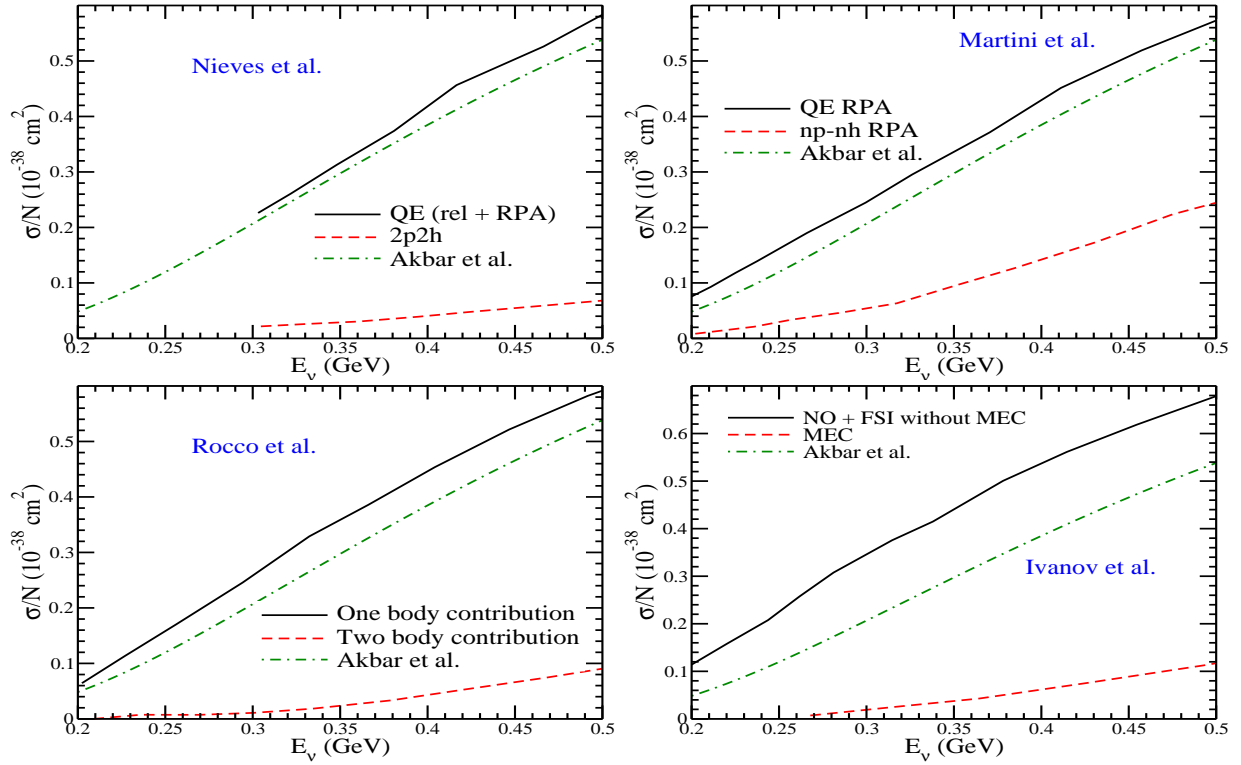


Figure 5.17: ν_μ scattering cross section in ^{12}C per neutron target. Clockwise from the top left: (1) Nieves et al. [560] in the relativistic Fermi gas model with RPA effect and without 2p-2h contribution (solid line) and only the 2p-2h contribution (dashed line); (2) Martini et al. [508, 509] relativistic Fermi gas model with RPA effect and without np-nh contribution (solid line) and only the np-nh contribution (dashed line); (3) Ivanov et al. [562] using realistic spectral function with nucleon-nucleon correlations and without MEC contribution (solid line) and only the MEC contribution (dashed line), and (4) Rocco et al. [561] using impulse approximation with spectral function and without 2p-2h contribution (solid line), and only the 2p-2h contribution (dashed line). The results of Akbar et al. [539] has been shown by dash-dotted line using the relativistic Fermi gas model with RPA effect.

5.4.6. Nuclear medium effects beyond the impulse approximation

We have discussed the importance of NME like the 2p-2h, ph- Δ h and MEC beyond the impulse approximation in the case of inclusive neutrino scattering in ^{12}C in the intermediate energy region of several hundreds of MeV. These effects were also shown earlier to be important in the very low energy region of the nuclear beta decays [511, 590, 591, 592, 593, 594, 595], solar neutrino reaction and muon capture [536, 596].

In the case of π -DIF neutrinos corresponding to the low energy neutrinos of $E_\nu < 236$ MeV, the calculations of Hayes and Towner [531] were performed in a microscopic nuclear model using a multiparticle shell model with large basis space, while the calculations of Umino et al. [529, 530] were done using the relativistic Fermi gas model. Both the calculations find a reduction of about 20% in the inclusive cross sections while in the case of KDAR neutrinos, the work of Nikolakopoulos et al. [540] finds an increase of about 20-25% obtained from extrapolating the works of NuWro [542, 543] and Martini et al. [508, 509].

Recently an ab initio calculation of the inclusive ν_μ cross section in ^{12}C has been done by Rocco et al. [561] including the contribution of some two body effects. Moreover, Ivanov et al. [562] have made an improvement over the calculations of Nieves et al. [560] by using an spectral function $S(\vec{p}, E)$ for the nucleon energy and momentum distribution to calculate the inclusive cross sections in the relativistic Fermi gas model. We show in Fig. 5.17, the results for the inclusive cross section $\sigma(E_{\nu_\mu})$ as a function of the neutrino energy E_{ν_μ} in the energy range $0 < E_{\nu_\mu} < 500$ MeV in various models. It is clear from Fig. 5.17 that the calculations by Rocco et al. [561] and Ivanov et al. [562] show an enhancement in the inclusive cross section at $E_{\nu_\mu} = 236$ MeV which are quantitatively small as compared to the results quoted by Nikolakopoulos et al. [540].

We observe from the results shown in Table 5.7, that:

- (i) The contribution of NME beyond the impulse approximation is to increase the inclusive cross sections but the increase is not sufficient enough to explain the results of the KDAR neutrinos.
- (ii) Such an increase in the inclusive cross section in the theoretical predictions due to NME, in the similar energy region of the π -DIF neutrinos would further enhance the disagreement between the theoretical and the experimental results in the case of LSND experiment.

- (iii) Moreover, this would also be in contradiction with earlier results of such effects calculated in the work of Hayes and Towner [531] in a microscopic model and Umino et al. [529, 530] in the case of Fermi gas model.

It is clear that present status of the theoretical calculations for the inclusive cross section in the process $\nu_\mu + {}^{12}\text{C} \rightarrow \mu^- + X$ in the low energy region of few hundreds of MeV is not satisfactory even with the inclusion of NME beyond the impulse approximation calculated in various models available in the literature.

5.4.7. $|\Delta S| = 1$ quasielastic scattering in nuclei

We have discussed in Section 2.2 single hyperon production in the antineutrino induced CC interaction from the free nucleon target. When the reactions shown in Eqs. (2.55) and (2.56) take place on nucleons which are bound in the nucleus, Fermi motion and Pauli blocking effects of initial nucleons play important role, which have been recently discussed in the literature [223, 252, 597]. In the work of Ref. [597], the Fermi motion effects are calculated in LFGM which has been discussed in detail in Section 5.4.1. For example, for Λ or Σ^0 production in an antineutrino interaction with the nucleus, the differential scattering cross section is expressed in terms of the differential scattering cross section for an antineutrino scattering from a free nucleon i.e. $\frac{d\sigma}{dQ^2}|_{\bar{\nu}N}$ (Eq. (3.107)) and integrated over the whole nucleus, which for example in the case of an antineutrino interaction on a proton target is given by

$$\frac{d\sigma}{dQ^2}|_{\bar{\nu}A} = 2 \int d^3r \rho_p(r) \frac{d\sigma}{dQ^2}|_{\bar{\nu}N}, \quad (5.91)$$

where a factor of 2 is to account for the spin degrees of freedom and the expression for $\rho_p(r)$ is given in Eq. (5.69). Similarly for a Σ^- production from an antineutrino interaction from a neutron target $\rho_p(r)$ is replaced by $\rho_n(r)$.

Following Eqs. (5.67) and (5.70), we may write Eq. (5.91) as

$$\frac{d\sigma}{dQ^2}|_{\bar{\nu}A} = 2 \int d^3r \int \frac{d^3p}{(2\pi)^3} n_p(p, r) \left[\frac{d\sigma}{dQ^2} \right]_{\bar{\nu}N}, \quad (5.92)$$

where $n_p(p, r)$ is the occupation number of the nucleon. $n_p(p, r) = 1$ for $p \leq p_{F_p}$ and is equal to zero for $p > p_{F_p}$, where p_{F_p} is the Fermi momentum of the proton.

5.4.8. Final state interaction

The produced hyperons are affected by the final state interaction (FSI) within the nucleus through the hyperon-nucleon elastic processes like $\Lambda N \rightarrow \Lambda N$, $\Sigma N \rightarrow \Sigma N$, etc. and the charge exchange scattering processes like $\Lambda n \rightarrow \Sigma^- p$, $\Lambda n \rightarrow \Sigma^0 n$, $\Sigma^- p \rightarrow \Lambda n$, $\Sigma^- p \rightarrow \Sigma^0 n$, etc. Because of these interactions in the nucleus, the probability of Λ or Σ production changes. This has been taken into account by using the prescription given in Ref. [597]. In this prescription, an initial hyperon produced at a position r within the nucleus, interacts with a nucleon to produce a new hyperon state within a short distance dl with a probability $P = P_Y dl$, where P_Y is the probability per unit length given by [597]:

$$P_Y = \sigma_{Y+n \rightarrow f}(E) \rho_n(r) + \sigma_{Y+p \rightarrow f}(E) \rho_p(r),$$

f denotes a possible final hyperon-nucleon [$Y_f(\Sigma \text{ or } \Lambda) + N(n \text{ or } p)$] state with energy E in the hyperon-nucleon CM system, $\rho_n(r)$ ($\rho_p(r)$) is the local density of the neutron (proton) in the nucleus, and σ is the total scattering cross section for CC channel like $Y(\Sigma \text{ or } \Lambda) + N(n \text{ or } p) \rightarrow f$ [597]. Now a particular channel is selected, which gives rise to a hyperon Y_f in the final state with probability P . For the selected channel, the Pauli blocking effect is taken into account by first randomly selecting a nucleon in the local Fermi sea, then a random scattering angle is generated in the hyperon-nucleon CM system assuming the cross sections to be isotropic. By using this information, hyperon and nucleon momenta are calculated and Lorentz boosted to the lab frame. If the nucleon in the final state has momentum above the Fermi momentum, we have a new hyperon type (Y_f) and/or a new direction and energy of the initial hyperon (Y_i). This process is continued until the hyperon gets out of the nucleus.

The results for the total cross section $\sigma(E_{\bar{\nu}_\mu})$ vs $E_{\bar{\nu}_\mu}$ for Λ and Σ^- production are obtained by integrating Eq. (5.92) over Q^2 , for various nuclei of interest like ${}^{12}\text{C}$, ${}^{16}\text{O}$, ${}^{40}\text{Ar}$ and ${}^{208}\text{Pb}$ relevant to ongoing or proposed antineutrino experiments. It is found that NME due to Pauli blocking are very small (not shown here) [223, 252, 597]. However, the final state interactions due to $\Sigma - N$ and $\Lambda - N$ interactions in various channels tend to increase the Λ production and decrease the Σ^- production. The quantitative increase (decrease) in Λ (Σ) yield due to FSI increases with the increase in nucleon number. Due to the FSI effect of the hyperon with the nucleon in the nucleus, the enhancement in the Λ production cross section is 22–25% in ${}^{12}\text{C}$ and ${}^{16}\text{O}$ for $E_{\bar{\nu}_\mu} = 0.6 - 1$ GeV, which increases to 34–38% in ${}^{40}\text{Ar}$ and 52–62% in ${}^{208}\text{Pb}$. While the decrease in Σ^- production cross section is about 40–46% in ${}^{12}\text{C}$ and ${}^{16}\text{O}$ for $E_{\bar{\nu}_\mu} = 0.6 - 1$ GeV, which becomes 50–56% in ${}^{40}\text{Ar}$ and 68–70% in ${}^{208}\text{Pb}$. Σ^0 production cross section is separately affected and the relation $\sigma(\bar{\nu}_\mu + p \rightarrow \mu^+ + \Sigma^0) = \frac{1}{2} \sigma(\bar{\nu}_\mu + n \rightarrow \mu^+ + \Sigma^-)$ is modified in the nucleus due to the presence of other nucleons. For

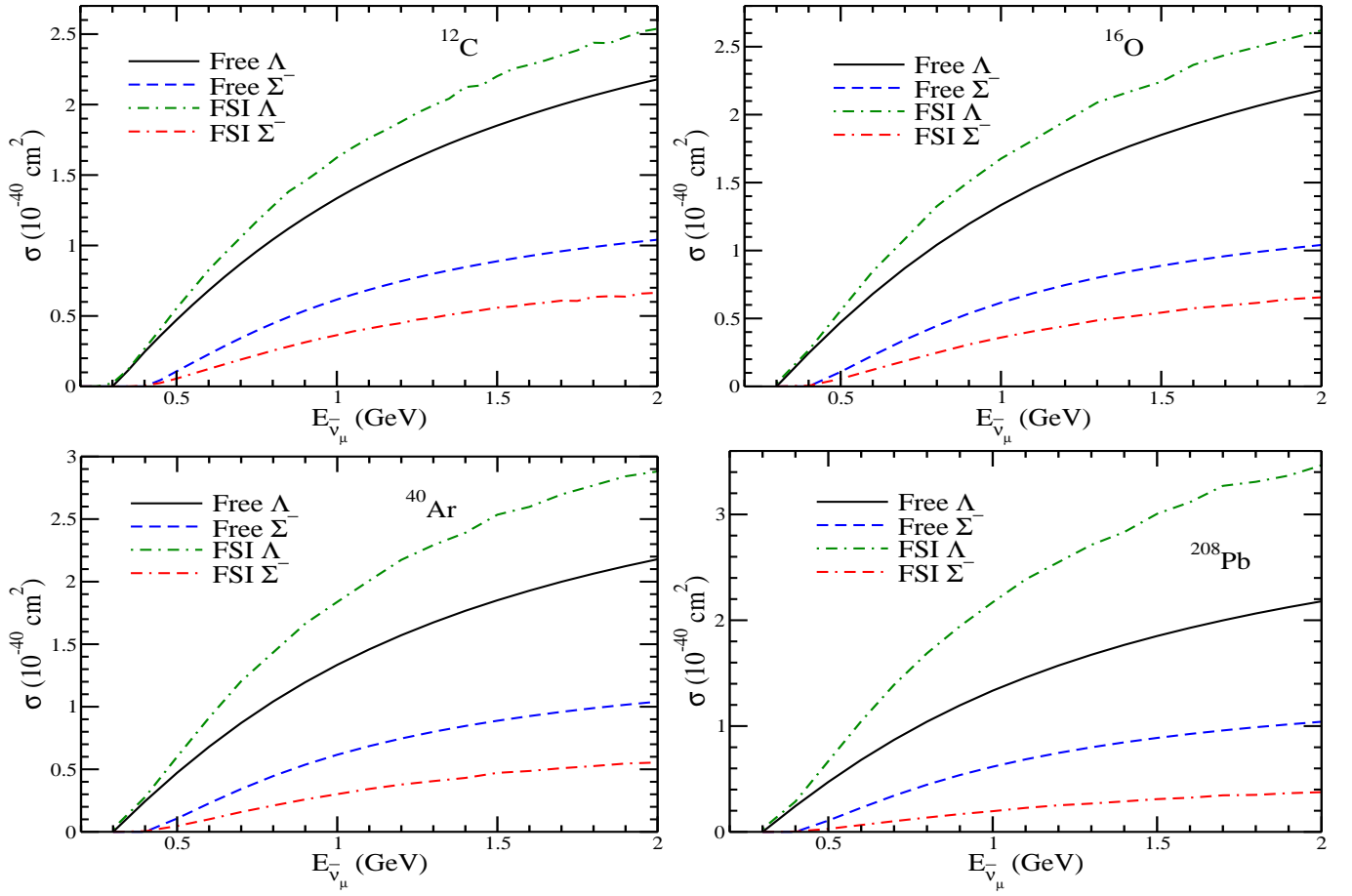


Figure 5.18: σ (per active nucleon) vs $E_{\bar{\nu}_\mu}$ in ^{12}C (top-left panel), ^{16}O (top-right panel), ^{40}Ar (bottom-left panel) and ^{208}Pb (bottom-right panel) nuclear targets, for the QE hyperon production. The results for Λ production (per proton) are shown without (solid line) and with FSI (dash-dotted line). Corresponding results are shown for Σ^- production (per neutron) without (dashed line) and with FSI (double dash-dotted line) [223, 252].

example, the decrease (not shown here) in Σ^0 production cross section is 28–32% in ^{12}C and ^{16}O for $E_{\bar{\nu}_\mu} = 0.6 - 1$ GeV, which becomes 45–52% in ^{40}Ar and 64–70% in ^{208}Pb .

We also see that though Σ^+ is not produced in the basic reactions, it can appear due to the final state interaction processes like $\Lambda p \rightarrow \Sigma^+ n$ and $\Sigma^0 p \rightarrow \Sigma^+ n$. In Fig. 5.19, the results for the Σ^+ production cross section are presented as a function of antineutrino energy in various nuclei. The total scattering cross section for Σ^+ production increases with the increase in nucleon number though per nucleon target it decreases, for example a suppression is observed in ^{208}Pb than ^{40}Ar . This may be due to considerably higher Fermi energy of neutrons than protons in ^{208}Pb which inhibits the production of Σ^+ through $\Lambda p \rightarrow \Sigma^+ n$ and $\Sigma^0 p \rightarrow \Sigma^+ n$ reactions in ^{208}Pb due to threshold considerations. It will be interesting to test these predictions whenever the experimental results are available in future.

5.5. Inelastic scattering and pion production in the Δ dominance model

We have discussed in Section 3.4, single pion production in (anti)neutrino induced reactions on the nucleon targets. In the case of free nucleon, it is observed that the single pion production in the sub-GeV region is dominated by the Δ resonance excitation which decays subsequently to a pion and a nucleon. The NR terms and the higher resonances also play important role especially in the $p\pi^0$ and $n\pi^+$ channels in the neutrino modes (Fig. 3.5) and $n\pi^0$ and $p\pi^-$ channels in the antineutrino modes (Fig. 3.7). These results for σ vs. E_{ν_μ} are obtained with $C_3^A = 0$, $C_5^A(0) = 1$, $C_4^A(Q^2) = -\frac{1}{4}C_5^A(Q^2)$ and $M_A = 1.03$ GeV for the $N - \Delta$ transition form factor in the axial-vector sector. When the processes shown in Eqs. (3.82) and (3.95) take place inside the nucleus, there are two possibilities of the pion production i.e. the target nucleus remains in the ground state leading to coherent production of pions or is excited and/or broken up leading to incoherent production of pions. As these processes take place inside the nucleus, NME come into play, which modifies the resonance properties like its mass and width. In literature, the nuclear medium modifications have been studied in the weak sector only in the case of Δ excitation, therefore, for the pion production in (anti)neutrino scattering from the nucleus, the calculations have been done in the Δ dominance model. Both the production processes in the Δ dominance model using the local density approximation have been considered to calculate single pion production from

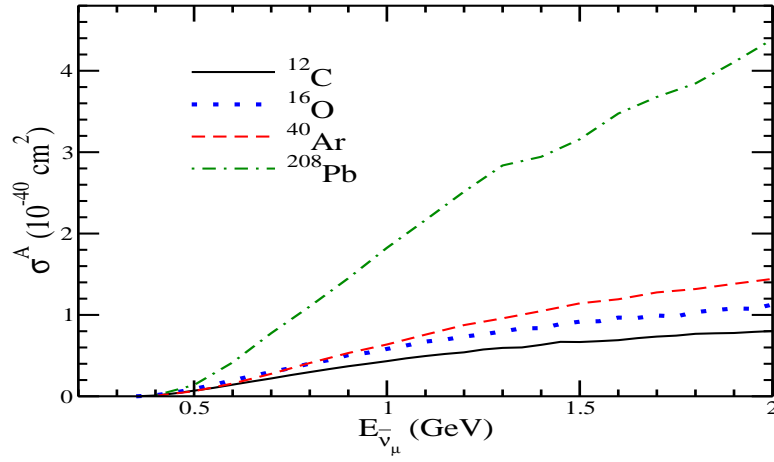


Figure 5.19: σ vs $E_{\bar{\nu}_\mu}$, for Σ^+ production arising due to final state interaction effect of Λ and Σ^0 hyperons in nuclei. Solid line is the result in ^{12}C , dotted is the result in ^{16}O , dashed line is the result in ^{40}Ar and dash-dotted line is the result in ^{208}Pb [223, 252].

the several nuclear targets like ^{12}C , ^{16}O , ^{40}Ar and ^{208}Pb . In the delta dominance model, if one take $C_5^A(0) = 1.2$ and $M_A = 1.05$ GeV, then the results obtained with these parameters for the single pion production from free nucleons almost resemble the pion production from the free nucleons when the contribution from the higher resonances and NRB as well as their interferences are taken with $C_5^A(0) = 1$ and $M_A = 1.03$ GeV (Fig. 3.5). In this section, we are discussing incoherent pion production. The effect of nuclear medium on the production of Δ is treated by including the modification of Δ properties in the medium. Once the pions are produced, they undergo final state interactions with the residual nucleus, which has been taken into account.

In the local density approximation (Section 5.4.1), the cross section for the reaction say $\nu_l(k) + N(p) \rightarrow l^-(k') + N'(p') + \pi^i(p_\pi)$, where $i = \pm, 0$ and $N, N' = p$ or n inside a nuclear target is evaluated as a function of local Fermi momentum ($p_F(r)$) and integrated over the size of whole nucleus i.e.

$$\left(\frac{d\sigma}{dE_\pi d\Omega_\pi} \right)_{\nu A} = \int d\vec{r} \rho_N(r) \left(\frac{d\sigma}{dE_\pi d\Omega_\pi} \right)_{\nu N},$$

where the expression for $\left(\frac{d\sigma}{dE_\pi d\Omega_\pi} \right)_{\nu N}$ is given in Eq. (3.4) for the free nucleon target. While for the scattering of (anti)neutrino with a nucleon inside the nucleus, the interacting nucleon is not as rest i.e. $E_N = \sqrt{|\vec{p}_N|^2 + M^2}$ and $E'_N = \sqrt{|\vec{p}'_N|^2 + M^2} = \sqrt{|\vec{q} - \vec{p}_\pi + \vec{p}_N|^2 + M^2}$, and therefore

$$\left(\frac{d\sigma}{dE_\pi d\Omega_\pi} \right)_{\nu N} = \frac{1}{32(2\pi)^5} \int d\Omega' dE' \delta^0(E_N(\vec{p}) + q_0 - E_{N'}(\vec{p}') - E_\pi(\vec{p}_\pi)) \frac{|\vec{k}'||\vec{p}_\pi|}{EE_N E_{N'}} \left(\frac{G_F^2}{2} \cos^2 \theta_c L_{\mu\nu} J^{\mu\nu} \right), \quad (5.93)$$

where $L_{\mu\nu}$ is the leptonic tensor, the expression for which is given in Eq. (2.15) and the hadronic tensor $J^{\mu\nu} = \frac{1}{2} \sum j^\mu j^{\nu\dagger}$ where the hadronic current

$$j^\mu = \mathcal{I} \bar{u}(\vec{p}') \frac{f_{\pi N \Delta}}{m_\pi} p_\pi^\sigma \mathcal{P}_{\sigma\lambda} \mathcal{O}^{\lambda\mu} u(\vec{p}). \quad (5.94)$$

$\mathcal{I} = \sqrt{3}$ for Δ^{++} and Δ^- excitations, otherwise $\mathcal{I} = 1$. In the above expression $\mathcal{O}^{\lambda\mu}$ is the $N - \Delta$ transition operator, the expression for which is given in Eq. (3.49) and $\mathcal{P}_{\sigma\lambda}$ is the Δ propagator in the momentum space, is given in Eq. (3.67).

Following Eqs. (5.67) and (5.70), we may write Eq. (5.93) as

$$\left(\frac{d\sigma}{dE_\pi d\Omega_\pi} \right)_{\nu A} = 2 \int d\vec{r} \sum_{N=n,p} \frac{d\vec{p}_N}{(2\pi)^3} \Theta_1(E_F^N(r) - E_N) \Theta_2(E_N + q_0 - E_\pi - E_F^N(r)) \times \left(\frac{d\sigma}{dE_\pi d\Omega_\pi} \right)_{\nu N}.$$

Thus, in the local density approximation the expression for the total cross section for the neutrino induced CC $1\pi^+$ production from the nuclear target is written as

$$\begin{aligned} \sigma_A(E) &= \frac{1}{(4\pi)^5} \int_{r_{min}}^{r_{max}} \left(\rho_p(r) + \frac{1}{9} \rho_n(r) \right) d\vec{r} \int_{Q_{min}^2}^{Q_{max}^2} dQ^2 \times \int_{k'_{min}}^{k'_{max}} dk' \int_{-1}^{+1} d\cos\theta_\pi \\ &\times \int_0^{2\pi} d\phi_\pi \frac{\pi |\vec{k}'||\vec{k}_\pi|}{M E_\nu^2 E_l} \frac{1}{E'_p + E_\pi \left(1 - \frac{|\vec{q}|}{|\vec{k}_\pi|} \cos\theta_\pi \right)} \left(\frac{G_F^2}{4} \cos^2 \theta_c L_{\mu\nu} J^{\mu\nu} \right). \end{aligned} \quad (5.95)$$

For $1\pi^-$ production ($\rho_p(r) + \frac{1}{9}\rho_n(r)$) in the above expression, is replaced by ($\rho_n(r) + \frac{1}{9}\rho_p(r)$) and for the π^0 production, it is replaced by $\frac{2}{3}(\rho_p(r) + \rho_n(r))$, where $\rho_p(r)$ and $\rho_n(r)$ are already defined in Section 5.4.1.

The nuclear medium modification on the Δ properties like the modification in its mass and width arises from the following sources:

- (a) The intermediate nucleon state is partly blocked for the Δ decay because some of these states are occupied (Pauli blocking). The decayed nucleon must be in an unoccupied state. The Pauli correction is taken into account by assuming a local Fermi sea at each point of the nucleus of density $\rho(r)$, and forcing the nucleon to be above the Fermi sea. This leads to an energy dependent modification in the Δ decay width given as [598]:

$$\Gamma \rightarrow \tilde{\Gamma} - 2\text{Im}\Sigma_\Delta, \quad (5.96)$$

where $\tilde{\Gamma}$ is the Pauli blocked width of Δ in the nuclear medium and its relativistic form is [598, 599]:

$$\tilde{\Gamma} = \frac{1}{6\pi} \left(\frac{f_{\pi N\Delta}}{m_\pi} \right)^2 \frac{M}{\sqrt{s}} |\vec{p}'_{cm}|^3 F(p_F, E_\Delta, p_\Delta), \quad \text{where} \quad |\vec{p}'_{cm}| = \frac{\sqrt{(s - M^2 - m_\pi^2)^2 - 4M^2 m_\pi^2}}{2\sqrt{s}}, \quad (5.97)$$

and $F(p_F, E_\Delta, p_\Delta)$, the Pauli correction factor is written as [598, 599]:

$$F(p_F, E_\Delta, p_\Delta) = \frac{p_\Delta |\vec{p}'_{cm}| + E_\Delta E'_{p_{cm}} - E_F \sqrt{s}}{2p_\Delta |\vec{p}'_{cm}|}, \quad (5.98)$$

with p_F as the Fermi momentum, $E_F = \sqrt{M^2 + p_F^2}$ and \vec{p}'_{cm} , $E'_{p_{cm}}$ the nucleon momentum and the relativistic nucleon energy in the final πN CM frame. If $F(p_F, E_\Delta, p_\Delta) > 1$ it is replaced by 1 in Eq. (5.97), and similarly, if $F(p_F, E_\Delta, p_\Delta) < 0$ then it is replaced by 0 in Eq. (5.97).

In the above expression \sqrt{s} is CM energy in the Δ rest frame averaged over the Fermi sea, \bar{s} and is given as [598, 599]

$$\bar{s} = M^2 + m_\pi^2 + 2E_\pi \left(M + \frac{3}{5} \frac{p_F^2}{2M} \right). \quad (5.99)$$

- (b) The produced nucleon in the Δ decay inside the nuclear medium feels a single particle potential due to all the other nucleons in the nucleus, known as the binding effect, which is taken care by the real part of the Δ self energy. This effect modifies the mass of Δ in the medium as [598, 599]:

$$M_\Delta \rightarrow \tilde{M}_\Delta = M_\Delta + \text{Re}\Sigma_\Delta. \quad (5.100)$$

The Δ self energy plays a very important role in the different pion nuclear reactions. For a thorough study of the Δ self energy, readers are referred to the model developed by Oset and Salcedo [598]. For the scalar part of the Δ self energy, the numerical results are parameterized in the approximate analytical form (excluding the Pauli corrected width), and are given as [598, 599]:

$$-\text{Im}\Sigma_\Delta = C_Q \left(\frac{\rho}{\rho_0} \right)^\alpha + C_{A2} \left(\frac{\rho}{\rho_0} \right)^\beta + C_{A3} \left(\frac{\rho}{\rho_0} \right)^\gamma, \quad (5.101)$$

which is determined mainly by the one pion interaction in the nuclear medium. This includes the two body, three body and the QE absorption contributions for the produced pions in the nucleus. The coefficients C_Q accounts for the QE part, the term with C_{A2} for two body absorption and the one with C_{A3} for three body absorption, and are parameterized in the range of energies $80 \text{ MeV} < T_\pi < 320 \text{ MeV}$, where T_π is the pion kinetic energy, as [598, 599]:

$$C(x) = ax^2 + bx + c, \quad x = \frac{T_\pi}{m_\pi}, \quad (5.102)$$

where C stands for all the coefficients i.e. C_Q , C_{A2} , C_{A3} , α and $\beta(\gamma = 2\beta)$. The different coefficients used have been taken from Ref. [598, 599].

The real part of the Δ self energy has been approximately taken as [598, 599]

$$\text{Re}\Sigma_\Delta \simeq 40.0 \left(\frac{\rho}{\rho_0} \right) \text{ MeV}. \quad (5.103)$$

- (c) It should be noted that $\tilde{\Gamma}$ describes the Δ decaying into nucleon and pion. The various terms in the $\text{Im}\Sigma_\Delta$ correspond to the different responses of Δ in the nuclear medium as explained earlier. C_Q term in $\text{Im}\Sigma_\Delta$ gives

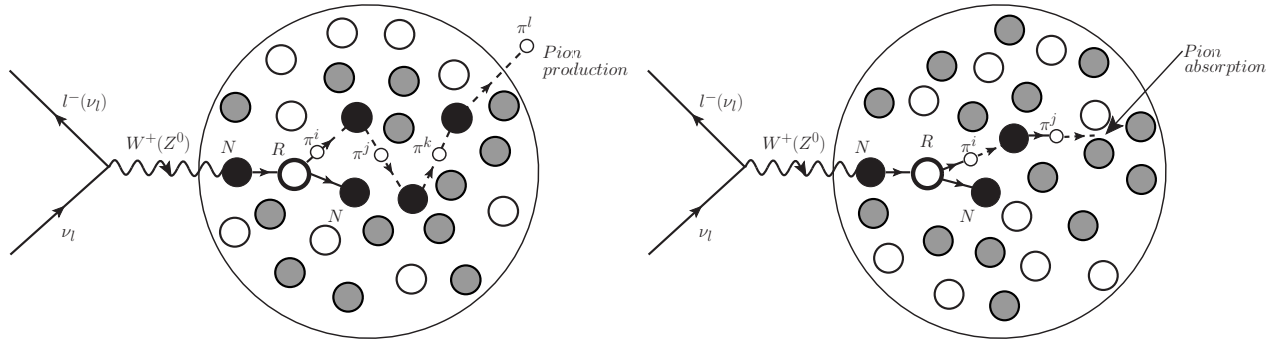


Figure 5.20: Pion production inside a nuclear target and its interaction with the nucleons in the nucleus while coming out. The pions may undergo elastic scattering, charge exchange (for example $\pi^+ + n \rightarrow \pi^0 + p$) reaction, etc. and therefore the charge of pion may change on way before it comes out of the nucleus (left panel). In a neutrino induced reaction on a nucleon target when a pion is absorbed in the nuclear medium while coming out and constitutes the QE like process (right panel). The open (shaded) circles represent protons (neutrons) inside a nucleus and the dark shaded circle represents a nucleon (p or n) with which a neutrino interacts through a CC (NC) reaction and a nonresonant (NR) or a resonant (R) state is formed, which gives rise to a proton or a neutron and a pion (π^i), where i represents the charge state.

additional contribution to the pion production which arises solely due to NME. Some of the Δ s are absorbed through two body and three body absorption processes and do not lead to pion production. These are described by C_{A2} and C_{A3} terms in the expression for $Im\Sigma_\Delta$ given in Eq. (5.101) and do not contribute to the lepton production accompanied by pions. These constitute QE-like events besides the pions which are physically produced but reabsorbed in the nucleus due to FSI, which shall be discussed later in the text. Only the C_Q term in the expression for $Im\Sigma_\Delta$ (Eq. (5.101)) contributes to the lepton production accompanied by a pion. These have been discussed by us in Refs. [312, 313].

5.5.1. Final state interaction effect

The effective pions which are produced after considering the Δ renormalization effect undergo final state interaction with the residual nucleus. Due to strong interactions with the nucleons, some of these pions can change direction, energy, charge, or even produce more pions through $\pi N \rightarrow \pi\pi N$ like reactions or may be lost through the $\pi NN \rightarrow NN$ reaction. These effects need to be taken into account [600]. Therefore, the production cross sections for the pions from the nuclear targets are affected by the presence of strong interactions of final state pions in the nuclear medium (Fig. 5.20). For example, a pion produced in the nuclear medium may get absorbed by the nucleons and thus mimicking a QE-like event (see Fig. 5.20) or can suffer elastic, and charge exchange scattering with the nucleons. There are generally two approaches to treat these final state interactions of pions. In one approach, the distortion of pion wave functions is calculated in an optical potential by solving the Schrodinger or Klein-Gordon equation of motion or approximation methods using Glauber model is used. In another approach, a microscopic method is used in which the motion of the pion inside the nucleus is followed step by step in which the pion suffers interaction with the nucleon. This approach has been discussed by Vicente Vacas et al. [600] and is used by us in many calculations of treating the FSI of pions [311, 313, 601, 602].

In the second approach, the final state interaction of pions is treated using Monte Carlo simulations by generating pion of given momentum and charge at point \vec{r} in the nucleus. Assuming the real part of the pion nuclear potential to be weak as compared to their kinetic energies they are propagated in straight lines till they are out of the nucleus. At the beginning they are placed at (\vec{b}, z_{in}) , with a random impact parameter \vec{b} , with $|\vec{b}| < R$, where R is the nuclear radius which is taken to be a point where nuclear density $\rho(R)$ falls to $10^{-3}\rho_0$, where ρ_0 is the central density, and $z_{in} = -\sqrt{R^2 - |\vec{b}|^2}$. Then it is moved in small steps δl along the z -direction until it comes out of the nucleus or interact. If $P(p_\pi, r, \lambda)$ is the probability per unit length at the point r of a pion of momentum \vec{p}_π and charge λ , then $P\delta l \ll 1$. A random number x is generated such that $x \in [0, 1]$ and if $x > P\delta l$, then it is assumed that pion has not interacted while traveling a distance δl , however, if $x < P\delta l$ then the pion has interacted and depending upon the weight factor of each channel given by its cross section it is decided whether the interaction was QE, charge exchange reaction, pion production or pion absorption [600]. For example, for the QE scattering

$$P_{N(\pi^\lambda, \pi^{\lambda'})N'} = \sigma_{N(\pi^\lambda, \pi^{\lambda'})N'} \times \rho_N,$$

where N is a nucleon, ρ_N is its density and σ is the elementary cross section for the reaction $\pi^\lambda + N \rightarrow \pi^{\lambda'} + N'$ obtained from the phase shift analysis. For a pion to be absorbed, P is expressed in terms of the imaginary part of the pion self energy Π i.e. $P_{abs} = -\frac{Im\Pi_{abs}(p_\pi)}{p_\pi}$, where the self energy Π is related to the pion optical potential $V(\vec{r})$ [600].

In Fig. 5.21, results for the Q^2 distribution $\frac{d\sigma}{dQ^2}$ and the pion momentum distribution $\frac{d\sigma}{dp_\pi}$ are shown for CC $\nu_\mu(\bar{\nu}_\mu)$ induced incoherent one π^+ (π^-) production cross section. These results are presented for the differential scattering cross

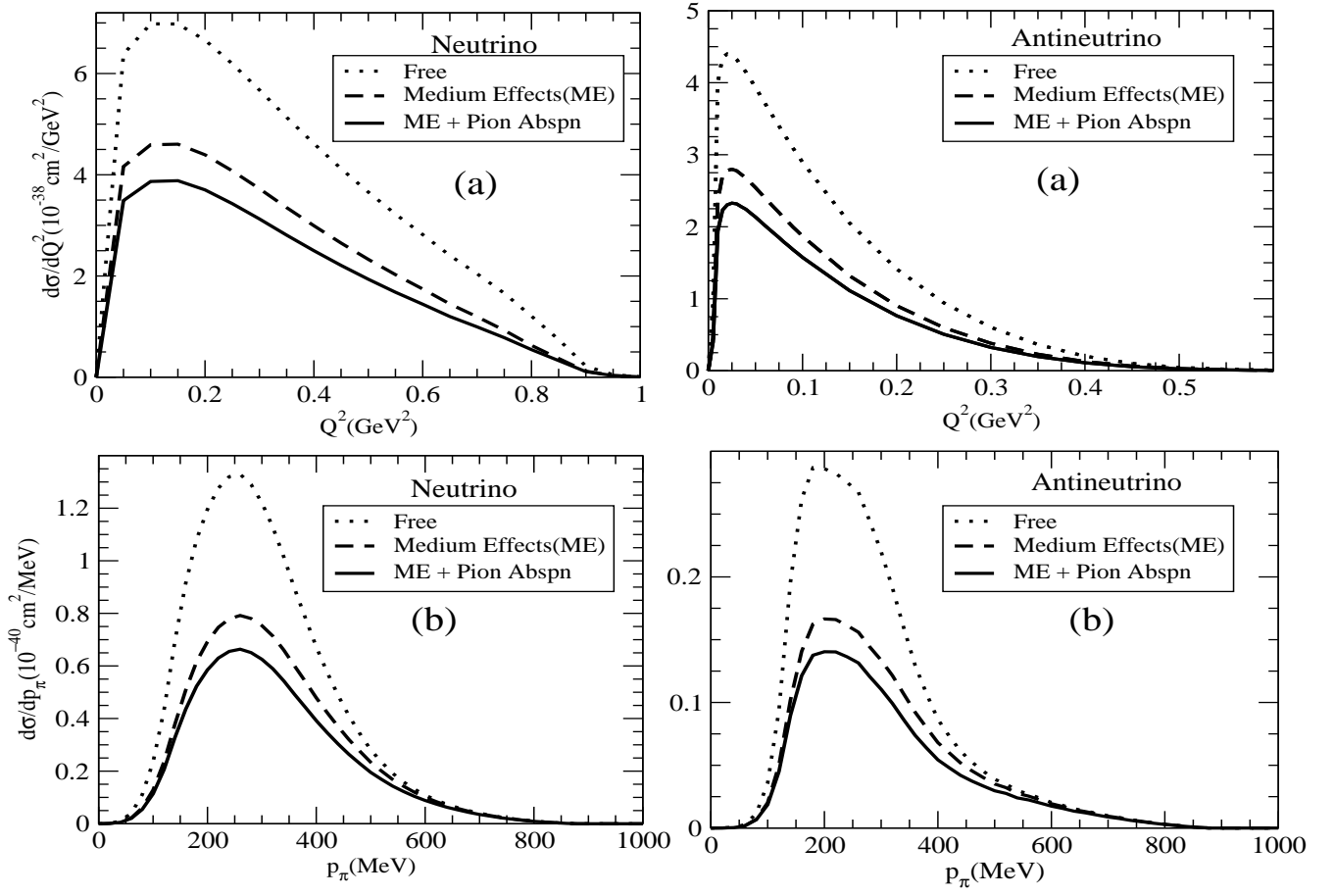


Figure 5.21: $\frac{d\sigma}{dQ^2}$ and $\frac{d\sigma}{dp_\pi}$ for the $\nu_\mu(\bar{\nu}_\mu)$ induced CC one $\pi^+(\pi^-)$ process on ^{12}C target at $E_\nu = 1\text{GeV}$ [311, 313, 602].

section calculated with and without NME, and with NME including the pion absorption effects. For the Q^2 -distribution shown in Fig. 5.21, it may be seen that the reduction in the cross section as compared to the cross section calculated without NME is around 35% in the peak region. When pion absorption effects are also taken into account there is a further reduction of around 15%. The results for the antineutrino induced one π^- production cross section are qualitatively similar in nature but quantitatively we find that the peak shifts towards a slightly lower value of Q^2 . Also in this figure, the results for the pion momentum distribution have been shown. In this case, the reduction in the cross section in the peak region is around 40% when NME are taken into account, which further reduces by about 15% when pion absorption effects are also taken into account.

In Fig. 5.22, the results for the total scattering cross section σ for CC ν_μ ($\bar{\nu}_\mu$) induced one π^+ (π^-) production cross section are shown. With the inclusion of NME the reduction in the cross section from the cross section calculated without NME for the neutrino energies between 1-2 GeV is 30-35% which further reduces by about 15% when pion absorption effects are also taken into account. The results with antineutrinos are qualitatively similar to the results obtained in the case of neutrino scattering. For more details, see Refs. [311, 602].

5.6. A comparative discussion of results for quasielastic hyperon and delta production from nuclei leading to pions

We have seen in Section 5.4.7 that in the case of antineutrinos, the QE hyperon (Λ , Σ^0 and Σ^-) production also contributes to the total scattering cross section. The produced hyperons then decay into a nucleon and a pion, thus, giving additional contribution to the single pion production i.e.

$$\begin{aligned}
 \bar{\nu}_l + p &\rightarrow l^+ + \Lambda; & \Lambda &\rightarrow n + \pi^0 & [35.8\%], & p + \pi^- & [63.9\%] \\
 \bar{\nu}_l + p &\rightarrow l^+ + \Sigma^0; & \Sigma^0 &\rightarrow \gamma + \Lambda & [100\%], & \Lambda &\rightarrow n + \pi^0, p + \pi^- \\
 \bar{\nu}_l + n &\rightarrow l^+ + \Sigma^-; & \Sigma^- &\rightarrow n + \pi^-, & [99.85\%]
 \end{aligned} \tag{5.104}$$

where the quantities in the square brackets represent the branching ratios of the respective decay modes. The pions are produced as a result of hyperon decays as shown in Eq. (5.104). However, when the hyperons are produced in a

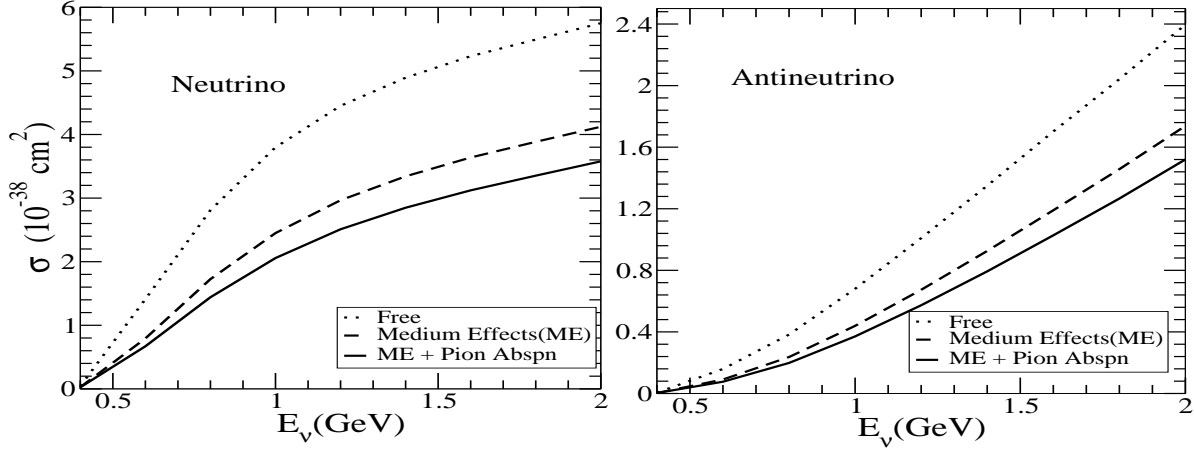


Figure 5.22: σ for ν_μ ($\bar{\nu}_\mu$) induced CC incoherent $\pi^+(\pi^-)$ production on ^{12}C target [311, 313, 602].

nuclear medium, some of them disappear through the hyperon-nucleon interaction processes like $YN \rightarrow NN$, though it is suppressed due to the nuclear effects. The pionic modes of hyperons are Pauli blocked as the momentum of the nucleons available in these decays is considerably below the Fermi level of energy for most nuclei leading to a long lifetime for the hyperons in the nuclear medium. Therefore, the hyperons which survive the $YN \rightarrow NN$ decay in the nuclear medium live long enough to travel and decay outside the nucleus. In view of this, no final state interaction of the produced pions with the nucleons inside the nuclear medium in the case of these pion producing reactions is considered.

This mode of pion production is important in the low energy region ($E_{\bar{\nu}_\mu} < 1$ GeV), even though, the dominant contribution to the single pion production comes from the Δ excitations in the few GeV energy region as discussed in Section 5.5. The cumulative effects of the lower threshold energy for the hyperon production compared to the delta production, and the near absence of the FSI for the pions coming from the hyperon decay compensate for the Cabibbo suppression as compared to the pions coming from the Δ excitations in the low energy region. This makes the study of hyperon production processes important in the context of oscillation experiments with antineutrinos in the sub-GeV energy region.

To quantify our statement, in Fig. 5.23 and Figs. 5.24 the results for π^- and π^0 productions in nuclei like ^{12}C , ^{16}O , ^{40}Ar and ^{208}Pb are presented. These results are shown for the cross sections obtained without and with NME+FSI effect, for the pion production arising due to the Λ production, total hyperon (Y) production and the Δ production. For the hyperon production, NMEs in the production process as well as the FSI due to hyperon-nucleon interactions have been taken into account. Similarly, for the pions arising from Δ , the nuclear medium modification on Δ properties and the pion FSI effect have been considered, which results in large reduction in the pion production cross section.

Using the results of σ , the results for the ratio of hyperon to delta production cross sections are obtained, with and without NME+FSI, for π^- as well as π^0 productions for all the nuclear targets considered here by defining

$$R_N = \frac{\sigma(Y \rightarrow N\pi)}{\sigma(\Delta \rightarrow N\pi)} \Big|_{\text{without NME+FSI effects}}, \quad R_A = \frac{\sigma(Y \rightarrow N\pi)}{\sigma(\Delta \rightarrow N\pi)} \Big|_{\text{with NME+FSI effects}}. \quad (5.105)$$

This ratio directly tells us the enhancement of the ratio R_A due to NME+FSI with the increase in the mass number of the nuclear targets as the pions getting produced through the Δ -resonant channel undergo a suppression due to NME+FSI effect, while the pions getting produced from the hyperons (all the interactions taken together i.e. Λ as well as Σ contributions) have comparatively smaller NME+FSI effect.

In Fig. 5.23, the results for the total scattering cross section σ vs $E_{\bar{\nu}_\mu}$, for $\bar{\nu}_\mu$ scattering off the nucleon in ^{12}C , ^{16}O , ^{40}Ar and ^{208}Pb nuclear targets giving rise to π^- through the Δ , Λ and Y productions with and without NME and FSI are presented. In the case of hyperon production for ^{12}C , the effect of FSI due to $Y - N$ interaction leads to increase in the cross section of Λ production from the free case, which is about 23 – 24% for $E_{\bar{\nu}_\mu} = 0.6 - 1$ GeV, while the change in the total hyperon production cross section results in a decrease in the cross section due to the FSI effect which is about 3 – 5% at these energies. In the case of pions produced through Δ excitations, NME+FSI lead to an overall reduction of around 50% in the π^- production for the antineutrino energies $0.6 < E_{\bar{\nu}_\mu} < 1$ GeV. This results in the change in the ratio of R_N (Eq. (5.105)) from 0.28 and 0.14 respectively at $E_{\bar{\nu}_\mu} = 0.6$ and 1 GeV to R_A (Eq. (5.105)) $\rightarrow 0.58$ and 0.25 at these energies. In the case of ^{16}O nuclear target, the observations are similar to what has been discussed in the case of ^{12}C nuclear target. For $\bar{\nu}_\mu$ scattering off ^{40}Ar , in the case of Λ production, the effect of FSI leads to increase in the cross section which is about 34 – 38% for $E_{\bar{\nu}_\mu} = 0.6 - 1$ GeV, however, the overall change in the π^- production from the hyperons results in a net reduction in the cross section from the free case, which is about 6 – 8% at these energies. In the

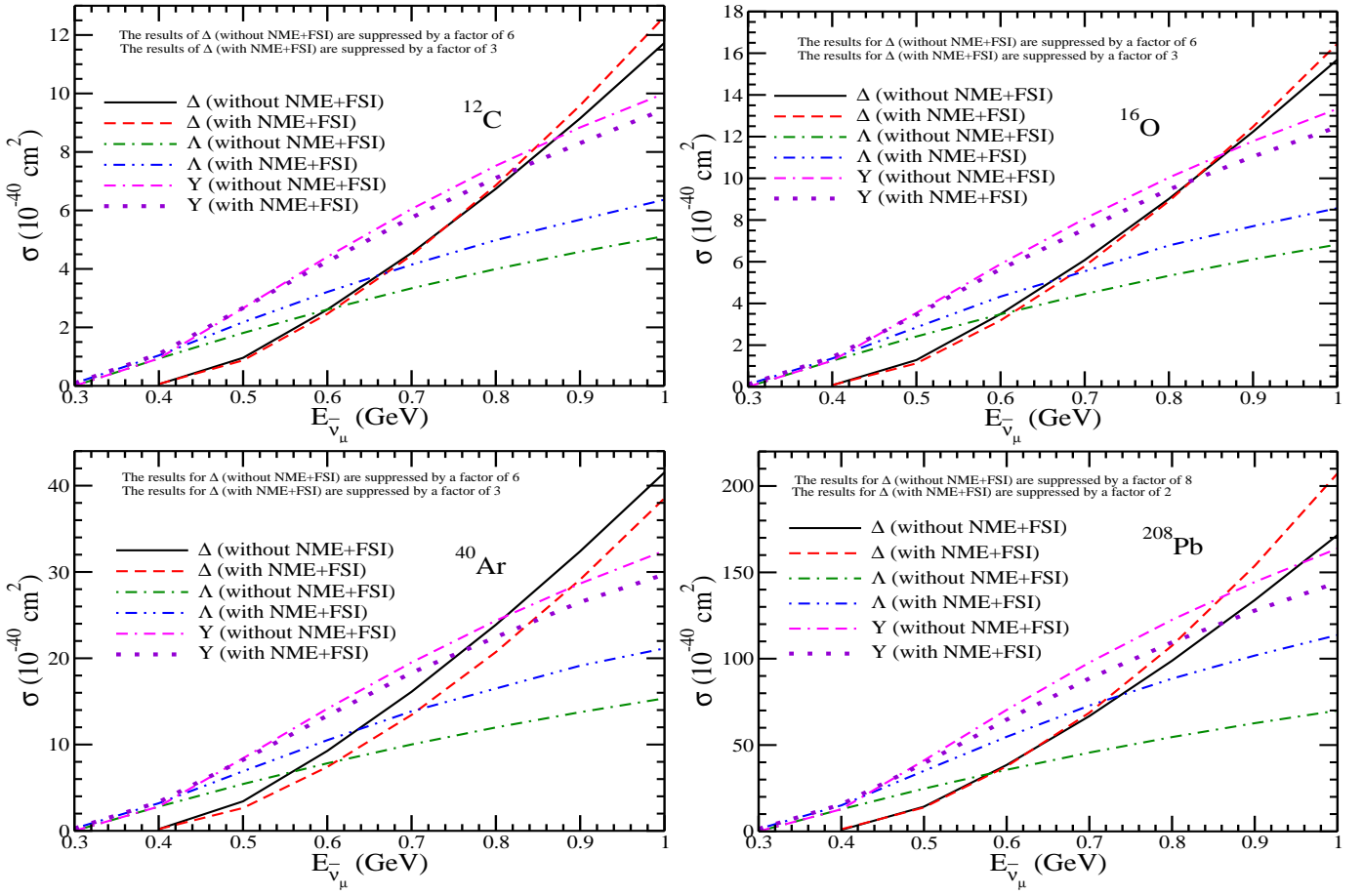


Figure 5.23: Results for CC π^- production in ^{12}C (upper left panel), ^{16}O (upper right panel), ^{40}Ar (lower left panel) and ^{208}Pb (lower right panel) with and without NME+FSI. The results are presented for the pion production from the Δ , Λ and total hyperon $Y(=\Lambda+\Sigma)$. Notice that in the case of ^{12}C , ^{16}O and ^{40}Ar , the results of Δ without NME+FSI are suppressed by a factor of 6 and the results with NME+FSI are suppressed by a factor of 3, while in the case of ^{208}Pb , the results of Δ without NME+FSI are suppressed by a factor of 8 and the results with NME+FSI are suppressed by a factor of 2 to bring them on the same scale [223].

case of pions produced through Δ excitations, NME+FSI leads to a reduction of around 55 – 60% in the π^- production for the antineutrino energies $0.6 \leq E_{\bar{\nu}_\mu} \leq 1$ GeV, and the reduction is less at higher energies. This results in the change in the ratio of R_N from 0.25 and 0.13 respectively at $E_{\bar{\nu}_\mu} = 0.6$ and 1 GeV to R_A , 0.6 and 0.26 at the corresponding energies. For a heavy nuclear target like ^{208}Pb , the change in the cross section due to NME+FSI is quite large. For example, the reduction in the cross section due to NME+FSI when a Δ is produced as the resonant state, is about 75% at $E_{\bar{\nu}_\mu} = 0.6$ GeV and 70% at $E_{\bar{\nu}_\mu} = 1$ GeV from the cross sections calculated without the medium effect. The enhancement in the Λ production cross section is about 55 – 60% at these energies. While the overall change in the π^- production from the hyperons results in a net reduction which is about 8 – 12%. This results in the change in the ratio of R_N from 0.23 and 0.12 respectively at $E_{\bar{\nu}_\mu} = 0.6$ and 1 GeV to $R_A \rightarrow 0.86$ and 0.35.

In Fig. 5.24, the results for the total scattering cross section σ vs $E_{\bar{\nu}_\mu}$, for $\bar{\nu}_\mu$ scattering off nucleon in ^{12}C , ^{16}O , ^{40}Ar and ^{208}Pb nuclear targets giving rise to π^0 through the Δ , Λ and Y productions with and without NME+FSI are presented. In the case of π^0 arising due to hyperon decay, the contribution comes from the Λ and Σ^0 decay, while there is no contribution from Σ^- . Due to the FSI effect in $Y - N$ ($Y = \Lambda, \Sigma^{-,0}$), there is substantial increase in the Λ production cross section and reduction in the Σ^0 production cross section from the free case, which leads to an overall increase in the π^0 production. Therefore, unlike the π^- production where there is an overall reduction, in the case of π^0 production, there is a net increase in the cross section which is about 13 – 14% in ^{12}C and ^{16}O , 22 – 23% in ^{40}Ar and 26 – 38% in ^{208}Pb for $E_{\bar{\nu}_\mu} = 0.6$ to 1 GeV. The different Clebsch-Gordan coefficients for Δ and the branching ratios for the hyperons give a different value of R_N and R_A . The ratio R_N from 0.58 and 0.26 at $E_{\bar{\nu}_\mu} = 0.6$ and 1 GeV, respectively, changes in nucleus to $R_A \rightarrow \sim 1.3$ and ~ 0.5 , in ^{12}C and ^{16}O , from 0.55 and 0.25 respectively at $E_{\bar{\nu}_\mu} = 0.6$ and 1 GeV to 1.68 and 0.66 in ^{40}Ar , and from 0.56 and 0.26 respectively at $E_{\bar{\nu}_\mu} = 0.6$ and 1 GeV to 3 and 1.2 in ^{208}Pb . Thus, in the case of π^0 production, there is significant increase in $Y \rightarrow N\pi$ to $\Delta \rightarrow N\pi$ ratio when NME+FSI are taken into account specially in the case of heavier nuclear targets. Therefore, these pions arising due to hyperon production and its subsequent decay must be taken into account while doing the analysis for CC antineutrino induced single pion production from nuclear

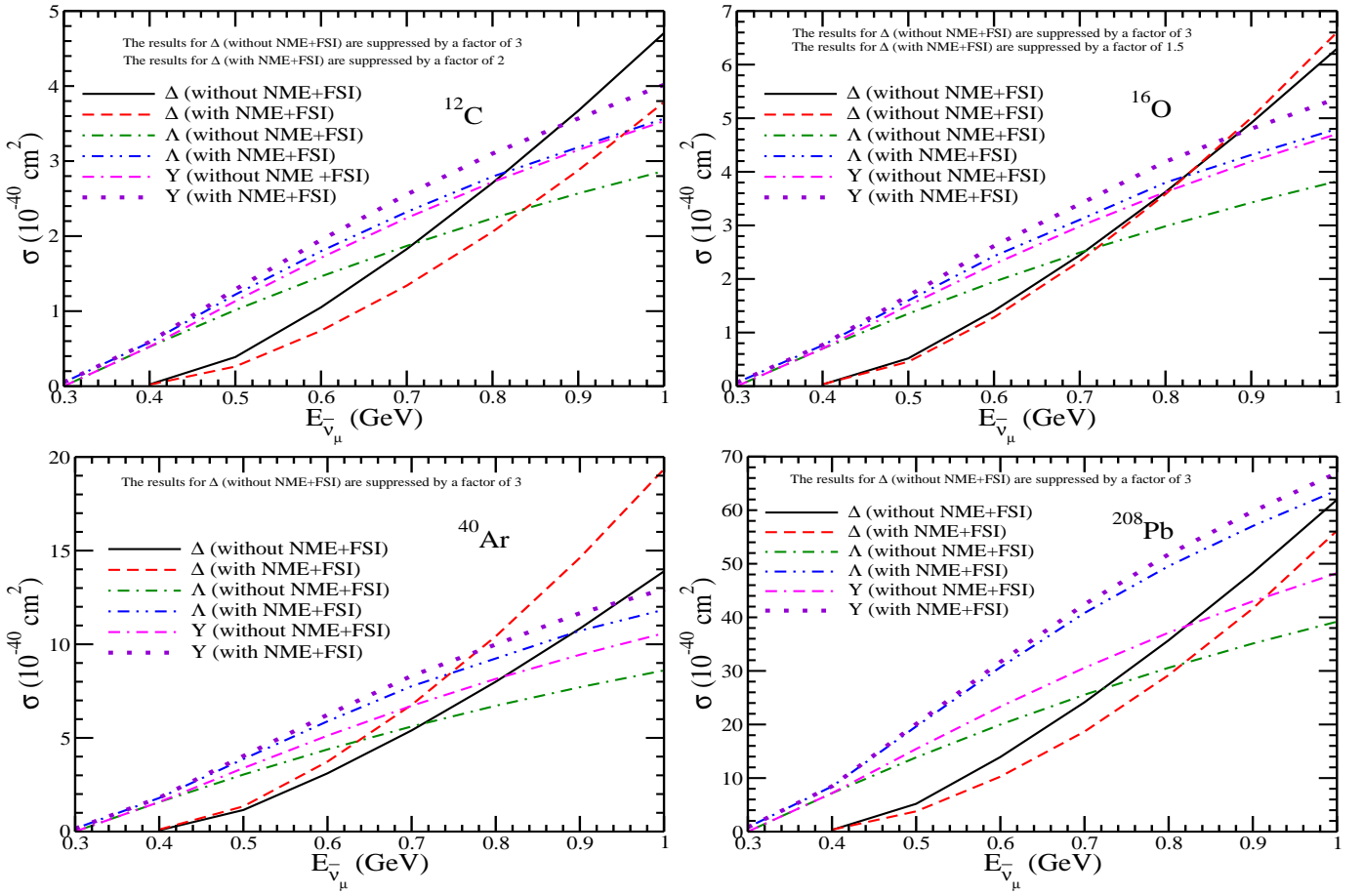


Figure 5.24: Results for CC π^0 production in ^{12}C (upper left panel), ^{16}O (upper right panel), ^{40}Ar (lower left panel) and ^{208}Pb (lower right panel) with and without NME+FSI. The results are presented for the pion production from Δ , Λ and total hyperon $Y = \Lambda + \Sigma$. Notice that in the case of ^{12}C , the results of Δ without NME+FSI are suppressed by a factor of 3 and the results with NME+FSI are suppressed by a factor of 2 while in the case of ^{16}O , the results of Δ without NME+FSI are suppressed by a factor of 3 and the results with NME+FSI are suppressed by a factor of 1.5. Moreover, in the case of ^{40}Ar and ^{208}Pb , the results of Δ without NME+FSI are suppressed by a factor of 3 [223].

targets. For more details, see Refs. [252, 223].

5.7. Coherent production of mesons

Coherent meson production is the process in which (anti)neutrino scatters from the nucleus producing mesons but the nucleus stays in the ground state and such processes can take place via CC as well as NC induced reactions like

$$\nu_l(\bar{\nu}_l)(k) + A(p_A) \rightarrow l^-(l^+)(k') + m^+(m^-)(k_m) + A(p_A'), \quad (\text{CC}) \quad (5.106)$$

$$\nu_l(\bar{\nu}_l)(k) + A(p_A) \rightarrow \nu_l(\bar{\nu}_l)(k') + m^0(k_m) + A(p_A'), \quad (\text{NC}) \quad (5.107)$$

where $m = \pi, K$, etc., $q = k - k'$, and the quantities in the bracket represent the respective momenta of the particles. The momentum transferred to the nuclear target is very small.

In a coherent meson production, almost all the energy transferred (q_0) from the leptonic vertex (Fig. 5.25) is taken by the outgoing meson (E_m) i.e. $q_0 \approx E_m$. The momentum transfer squared to the nucleus is given by $t = (q - k_m)^2 = (p_A' - p_A)^2 \simeq -2M_A T_A$, for $M_A \gg T_A$, with M_A and T_A being, respectively, the mass of the target nucleus and kinetic energy of the recoiling nucleus in the laboratory frame. In these reactions, the momentum transfer to the nucleus is so small that the coherence condition $Q \ll \frac{1}{R}$ (Section 5.1) is satisfied and the individual amplitudes for the pion production from each nucleon in the nucleus add coherently. In view of the smallness of the momentum and energy transfer, most of the energy-momentum from the lepton system is transferred to the meson making t very small. Since the nuclear form factor falls very rapidly with t , the coherent meson production is dominant in the forward direction i.e. $t \approx 0$.

The importance of studying coherent pion production has been realized in the context of neutrino oscillation experiments. In the analysis of neutrino oscillation experiments, it is important to reconstruct the initial neutrino energy spectrum from the observed charged lepton energy spectrum using the kinematics of the QE reactions from the nuclear

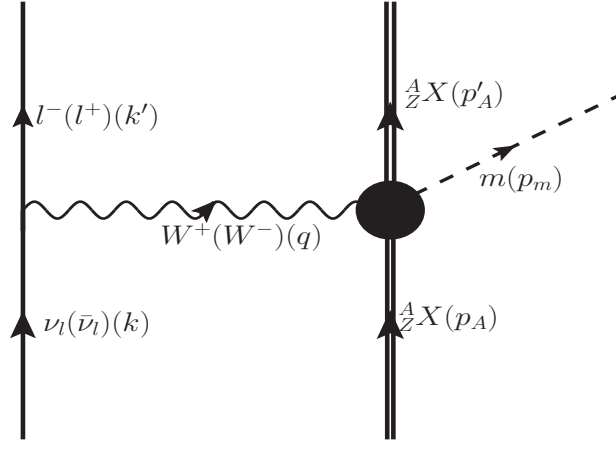


Figure 5.25: Feynman diagram depicting coherent production of mesons in CC (anti)neutrino scattering from nuclear target.

targets in which most of the leptons (e and μ) are produced in the forward direction. Most of the π^\pm , π^0 (through the electromagnetic shower as their decay products) produced in the forward direction through the coherent reactions mimic the real μ^+ , μ^- and e^- , which introduce uncertainty in the QE cross section for lepton production and the reconstruction of the neutrino energy. For example, around 1 GeV this uncertainty in the (anti)neutrino estimated energy could be in the range 150-200 MeV. A knowledge of these uncertainties is crucial in interpreting the results for ν_μ ($\bar{\nu}_\mu$) disappearance or ν_e ($\bar{\nu}_e$) appearance in the context of neutrino oscillation studies making the study of coherent pion production very important in the neutrino-nucleus reactions.

5.7.1. Coherent pion production

Experimentally, the coherent pion production in the high energy region was first reported by the Aachen-Padova collaboration [603] in 1983 while studying isolated π^0 s produced in the ν_μ and $\bar{\nu}_\mu$ induced processes. This was followed by a study performed by the Aachen-Gargamelle group [604] where coherent NC π^0 events in the Gargamelle heavy freon exposure were isolated. Later there were several ν_μ and $\bar{\nu}_\mu$ experiments like CHARM [605, 606], SKAT [607, 608], where NC induced coherent pions were observed over a wide range of neutrino energies using different nuclear targets. In the recent accelerator experiments being performed to study neutrino oscillations like the K2K [609], SciBooNE [610], MiniBooNE [611], NOvA [612], T2K [613], etc., as well as the dedicated $\nu_l - A$ cross section experiments MINERvA [614] and NOMAD [615] have put either a limit on coherent pion cross section or have provided cross sections at some energies. For example:

- The K2K experiment [609] at a neutrino energy of 1.3 GeV, has put an upper limit of 0.6×10^{-2} on the cross section ratio of coherent pion production to the total CC interaction cross section at 90%CL.
- The SciBooNE experiment [610] at neutrino energy of 1.1 GeV, has put an upper limit of 0.67×10^{-2} on the cross section ratio of coherent pion production to the total CC interaction cross section at 90%CL.
- The MiniBooNE collaboration [611] has studied the coherent fraction $\frac{\sigma_{\text{coh}}}{\sigma_{\text{coh}} + \sigma_{\text{incoh}}} = 19.5 \pm 1.1(\text{stat}) \pm 2.5(\text{sys})\%$ for the π^0 production at $E_\nu < 2$ GeV.
- The NOMAD experiment [615] at the CERN SPS has reported NC induced coherent π^0 production cross section to be $72.6 \pm 8.1(\text{stat}) \pm 6.9(\text{sys}) \times 10^{-40} \frac{\text{cm}^2}{\text{nucleus}}$ for $< E_\nu > \simeq 25$ GeV.
- The T2K experiment [613] has reported a value of $1.03 \pm 0.25(\text{stat}) \pm 0.70(\text{sys}) \times 10^{-39} \frac{\text{cm}^2}{\text{nucleus}}$ for $< E_\nu > \simeq 1.5$ GeV.
- MINERvA collaboration [614] has reported the flux-averaged cross sections for the coherent π^+ (π^-) production induced by ν_μ ($\bar{\nu}_\mu$) on the carbon target to be $[3.49 \pm 0.11(\text{stat}) \pm 0.37(\text{flux}) \pm 0.20(\text{other-sys})][2.65 \pm 0.15(\text{stat}) \pm 0.31(\text{flux}) \pm 0.30(\text{other-sys})] \times 10^{-39} \frac{\text{cm}^2}{12C}$, respectively, for E_ν in the range of 1.5 to 20 GeV.
- Recently the NOvA collaboration [612] has reported the result of the flux averaged cross section for the neutrino induced NC coherent π^0 production corresponding to an average energy $< E_{\nu_\mu} > = 2.7$ GeV to be $13.8 \pm 0.9(\text{stat}) \pm 2.3(\text{syst}) \times 10^{-40} \text{cm}^2/\text{nucleus}$.

Theoretically there are two different approaches which have been used to study the coherent pion production. The first approach is based on the Adler's PCAC model [256] which relates the coherent pion scattering cross section at $Q^2 = 0$

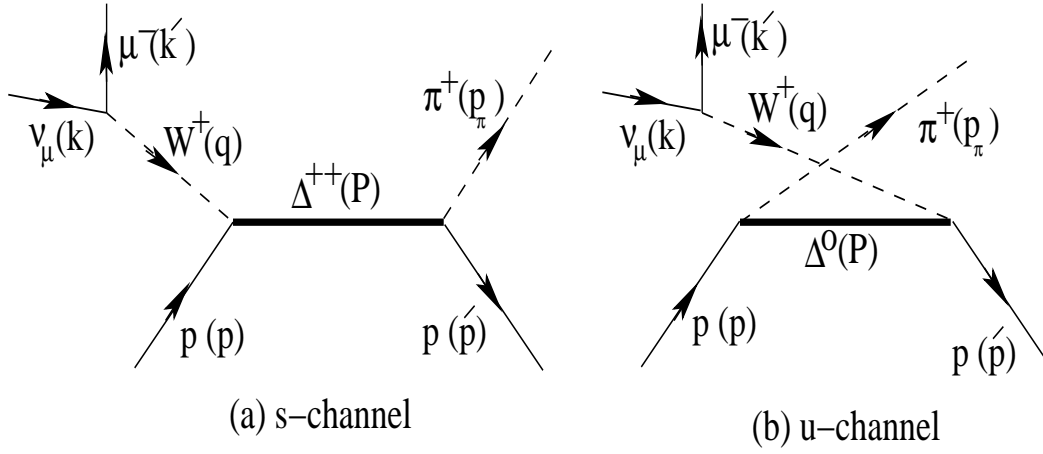


Figure 5.26: Feynman diagram depicting coherent production of mesons in CC (anti)neutrino scattering from nuclear target.

with the pion-nucleus elastic scattering cross section. This approach takes NME into account only through the final state interaction of the outgoing pions with the nucleus. The first calculation based on this approach was done by Rein and Sehgal [157] followed by many others in later years [616, 617, 618, 619, 620].

In this approach, the triple differential cross section for π^0 production is given by [157]:

$$\frac{d\sigma^{\pi^0}}{dx dy d|t|} = \frac{G_F^2 M f_\pi^2 A^2}{2\pi^2} E(1-y) \frac{1}{16\pi} (\sigma_{tot}^{\pi N})^2 (1+r^2) \left(\frac{m_A^2}{m_A^2 + Q^2} \right)^2 e^{-b|t|} F_{abs}, \quad (5.108)$$

where $x = Q^2/2M\nu$, $y = \nu/E$, $\sigma^{\pi N}$ is the pion-nucleon cross section, f_π is the pion decay constant, m_A is 1GeV, M denotes the nucleon mass, A is the number of nucleons within the nucleus, $r (= \text{Re}f_{\pi N}(0)/\text{Im}f_{\pi N}(0))$ is defined as the ratio of the real to imaginary part of the forward pion-nucleon scattering amplitude, $b = 1/3R^2$, with $R(R = R_0 A^{1/3})$ as the nuclear radius, and F_{abs} describes the effects of pion absorption in the nucleus, and is given by

$$F_{abs} = \exp \left\{ -\frac{9A^{1/3}}{16\pi R_0^2} \sigma_{inel}^{\pi N} \right\}, \quad (5.109)$$

where the experimental results for the average pion-nucleon cross section were used.

The above expression was obtained for the massless leptons even for the CC process. In a later work, Rein and Sehgal [617] took into account the lepton mass by introducing a multiplicative correction factor.

Later, Berger and Sehgal [619] used experimental data for pion-carbon scattering in the low energy region relevant for the contemporary cross section measurements of the coherent pion production in this energy region to describe the pion absorption effect in the nucleus and obtained the results for the coherent pion production. In another model, Kartavtsev et al. [621], Paschos and Schalla [620], and Higuera and Paschos [622] have included the lepton mass in all their kinematical calculations for the CC coherent pion production and used pion-nucleus cross section in neutrino scattering. These authors have compared their results for the charged and NC neutrino induced coherent pion production cross section with the results from the experimental collaborations of MiniBooNE [623, 624], K2K [609], Aachen-Padova [603] and Gargamelle [604] experiments.

The second approach is the use of microscopic models for pion production that have been developed by various groups [625, 626, 627, 628, 629, 630, 631, 342, 390], which are based on the single nucleon process $\nu_l(\bar{\nu}_l) + N \rightarrow l^-(l^+) + N + \pi^+(\pi^-)$, dominated by Δ production in the nucleus as shown in Fig. 5.26. The total cross section is then obtained by coherently summing the contribution of the pion production amplitudes from all the nucleons in the nucleus. The nuclear medium modification of the Δ properties in the nucleus (Section 5.5) and the FSI of the outgoing pion with the nuclear target are taken into account. Different treatments for the FSI of pion with the nucleus have been taken. For example the work of [625, 629, 627] uses Klein-Gordon equation, while Refs. [626, 342] use semiclassical eikonal approximation and Nakamura et al [390] uses Lippmann-Schwinger equation.

In this approach, the first calculation was done by the Aligarh group [626] using relativistic formalism in the Δ -dominance model. They performed the calculations for CC and NC (anti)neutrino induced coherent pion productions for several nuclear targets in the intermediate neutrino energy region of a few GeV. The NME are taken into account in the weak production process as well as in the final state interaction of the outgoing pions with the nucleus. The calculation uses the local density approximation to the delta hole model which was initially developed for photo and electro production of pions from nuclei [518]. The final state interaction of pions has been treated in eikonal approximation with the pion optical potential described in terms of the self energy of a pion in a nuclear medium calculated in this model [598, 599].

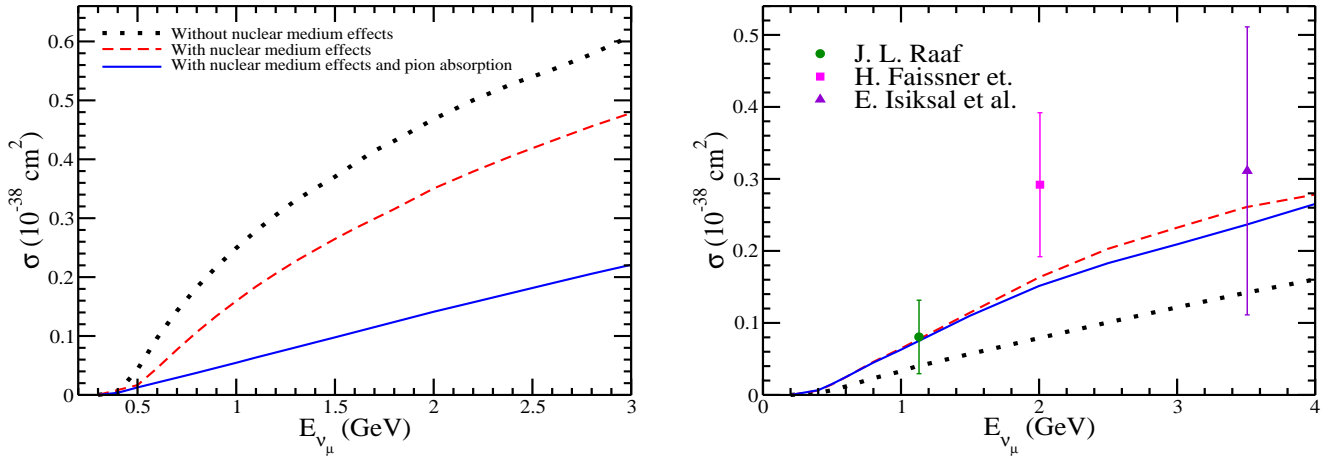


Figure 5.27: σ vs E_{ν_μ} for CC coherent $1\pi^+$ production in ^{12}C (left panel). The results are shown without NME (dotted line) and with NME (dashed line). When both the pion absorption and NME are taken into account, the results are shown by the solid line. In the right panel, the results are shown for the total cross section σ vs E_ν for the coherent π^0 production in ^{12}C (solid), ^{27}Al (dashed) and freon (dotted) with nuclear medium and pion absorption effects, along with the experimental results of Refs. [603, 604, 623, 624].

The amplitude for CC $1\pi^+$ production from the proton is written using the Feynman diagram shown in Fig. 5.26 and is given by [626]:

$$\mathcal{M} = \mathcal{I} \frac{G_F}{\sqrt{2}} \cos \theta_C l^\mu \mathcal{J}_\mu \mathcal{F}_p(\vec{q} - \vec{k}_\pi), \quad (5.110)$$

where $\mathcal{I} = \sqrt{3}$ (1) for s (u) channel, l^μ is the leptonic current given in Eq. (2.10) and the hadronic current \mathcal{J}_μ is given by

$$\mathcal{J}_\mu = \frac{f_{\pi N\Delta}}{m_\pi} \sum_s \bar{\Psi}^s(p') \left[k_{\pi\sigma} \Lambda^{\sigma\lambda} \Gamma_{\lambda\mu}^{\frac{3}{2}} \right] \Psi^s(p), \quad (5.111)$$

where $\Lambda^{\sigma\lambda}$ is the relativistic Δ propagator given by

$$\Lambda^{\sigma\lambda} = \frac{\not{P} + M_\Delta}{P^2 - M_\Delta^2 + i\Gamma M_\Delta} \left[g^{\sigma\lambda} - \frac{1}{3} \gamma^\sigma \gamma^\lambda - \frac{2}{3M_\Delta^2} P^\sigma P^\lambda + \frac{(P^\sigma \gamma^\lambda - \gamma^\sigma P^\lambda)}{3M_\Delta} \right], \quad (5.112)$$

and $\Gamma_{\lambda\mu}^{\frac{3}{2}}$ is the weak N- Δ transition vertex given as the sum of vector and axial part using Eq. (3.49) (Section 3.3.5). The nuclear form factor $\mathcal{F}_p(\vec{q} - \vec{k}_\pi)$ in Eq. (5.110) is given as [626]:

$$\mathcal{F}_p(\vec{q} - \vec{k}_\pi) = \int d\vec{r} \rho_p(r) e^{-i(\vec{q} - \vec{k}_\pi) \cdot \vec{r}}, \quad (5.113)$$

with $\rho_p(r)$ is the proton density in the nucleus. For production from nuclear targets, the contributions from the protons and neutrons are considered. Incorporating the isospin factors for charged pion production from proton and neutron targets corresponding to W^+ exchange diagram, the nuclear form factor is obtained as

$$\mathcal{F}(\vec{q} - \vec{k}_\pi) = \int d\vec{r} \left[\rho_p(r) + \frac{1}{3} \rho_n(r) \right] e^{-i(\vec{q} - \vec{k}_\pi) \cdot \vec{r}}. \quad (5.114)$$

Using these expressions, the differential cross section is given as:

$$\frac{d^5\sigma}{d\Omega_\pi d\Omega_{\bar{\nu}_\mu} dE_\mu} = \frac{1}{8} \frac{1}{(2\pi)^5} \frac{|\vec{k}'| |\vec{k}_\pi|}{E_{\bar{\nu}}} \mathcal{R} \sum \sum |\mathcal{M}|^2, \quad \text{where} \quad (5.115)$$

$$\mathcal{R} = \left[\frac{M |\vec{k}_\pi|}{E_{p'} |\vec{k}_\pi| + E_\pi (|\vec{k}_\pi| - |\vec{q}| \cos \theta_\pi)} \right], \quad (5.116)$$

is a kinematical factor incorporating the recoil effects, which is very close to unity for low Q^2 , relevant for the coherent reactions. In this model, the results of the cross sections for the antineutrino processes are obtained by replacing $[\rho_p(r) + \frac{1}{3}\rho_n(r)]$ by $[\rho_n(r) + \frac{1}{3}\rho_p(r)]$. For NC coherent pion production, it is replaced by $\frac{2}{3} [\rho_p(r) + \rho_n(r)]$. The NME due to renormalization of Δ properties in the nuclear medium have been treated in the same manner as discussed in Section 5.5. Accordingly the Δ propagator $\Lambda^{\sigma\lambda}$ in \mathcal{J}_μ given by Eq. (5.112) is modified due to the modifications in mass

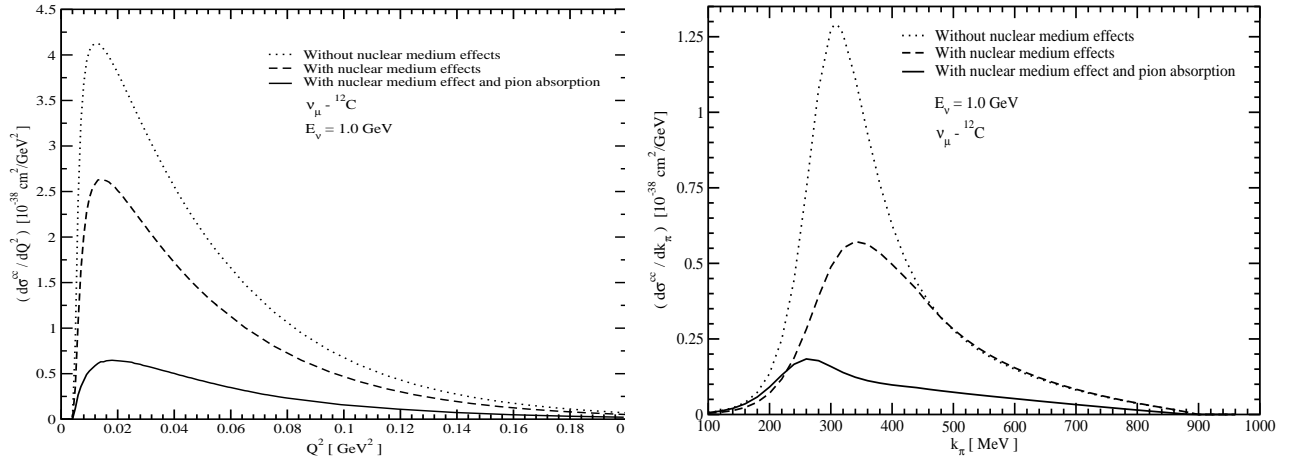


Figure 5.28: $\frac{d\sigma}{dQ^2}$ vs Q^2 for CC coherent $1\pi^+$ production in ^{12}C (left panel). $\frac{d\sigma}{dk_\pi}$ vs k_π for CC coherent $1\pi^+$ production in ^{12}C (right panel). Line and points have the same meaning as in Fig. 5.27 [602, 626].

and width of the Δ in the nuclear medium discussed in Section 5.5. However, the final state interaction of the pions with the residual nucleus has been treated in a different way. The final state interaction in coherent production of pions is taken into account by replacing the plane wave pion by a distorted wave pion. The distortion of the pion is calculated in the eikonal approximation in which the distorted pion wave function is written as [626]:

$$e^{i(\vec{q}-\vec{k}_\pi)\cdot\vec{r}} \rightarrow \exp \left[i(\vec{q}-\vec{k}_\pi) \cdot \vec{r} - \frac{i}{v} \int_{-\infty}^z V_{opt}(\vec{b}, z') dz' \right], \quad (5.117)$$

where $\vec{r} = (\vec{b}, z)$, \vec{q} and \vec{k}_π are the momentum transfer and the pion momentum, respectively. The pion optical potential V_{opt} is related with the pion self-energy Π as $\Pi = 2\omega V_{opt}$, with ω as the energy of the pion and $|\vec{v}| = |\vec{k}_\pi|/\omega$. The pion self-energy is calculated in local density approximation of the Δ -hole model and is given as [600]:

$$\Pi(\rho(\vec{b}, z')) = \frac{4}{9} \left(\frac{f_{\pi N \Delta}}{m_\pi} \right)^2 \frac{M^2}{\bar{s}} |\vec{k}_\pi|^2 \rho(\vec{b}, z') G_{\Delta h}(\bar{s}, \rho), \quad (5.118)$$

where \bar{s} is the CM energy in the Δ decay averaged over the Fermi sea and $G_{\Delta h}(\bar{s}, \rho)$ is the Δ -hole propagator given by:

$$G_{\Delta h}(s, \rho(\vec{b}, z')) = \frac{1}{\sqrt{\bar{s}} - M_\Delta + \frac{1}{2}i\tilde{\Gamma}(\bar{s}, \rho) - i\text{Im}\Sigma_\Delta(\bar{s}, \rho) - \text{Re}\Sigma_\Delta(\bar{s}, \rho)}. \quad (5.119)$$

When the pion absorption effect is taken into account the nuclear form factor $\mathcal{F}(\vec{q}-\vec{k}_\pi)$ modifies to $\tilde{\mathcal{F}}(\vec{q}-\vec{k}_\pi)$ and is given as [626]:

$$\tilde{\mathcal{F}}(\vec{q}-\vec{k}_\pi) = 2\pi \int_0^\infty b db \int_{-\infty}^\infty dz \rho(\vec{b}, z) \left[J_0(k_\pi^t b) e^{i(|\vec{q}|-k_\pi^l)z} e^{-if(\vec{b}, z)} \right], \quad (5.120)$$

where

$$f(\vec{b}, z) = \int_z^\infty \frac{1}{2|\vec{k}_\pi|} \Pi(\rho(\vec{b}, z')) dz', \quad (5.121)$$

and the pion self-energy Π is defined in Eq. (5.118).

These modifications lead to the following expression for the total scattering cross section

$$\sigma = \frac{1}{8} \frac{1}{(2\pi)^5} \int d\Omega_\pi \int d\Omega_{\bar{\nu}\mu} \int dE_\mu \frac{|\vec{k}'| |\vec{k}_\pi|}{E_{\bar{\nu}}} \mathcal{R} \sum \sum |\tilde{\mathcal{M}}|^2, \quad (5.122)$$

where

$$\tilde{\mathcal{M}} = \mathcal{I} \frac{G_F}{\sqrt{2}} \cos \theta_C l^\mu \tilde{\mathcal{J}}_\mu \tilde{\mathcal{F}}(\vec{q}-\vec{k}_\pi), \quad \tilde{\mathcal{J}}_\mu = \frac{f_{\pi N \Delta}}{m_\pi} \sum_s \bar{\Psi}^s(p) \left[k_{\pi\sigma} \tilde{\Lambda}^{\sigma\lambda} \mathcal{O}_{\lambda\mu} \right] \Psi^s(p), \quad (5.123)$$

where $\tilde{\Lambda}^{\sigma\lambda}$ is the modified Δ propagator inside the nuclear medium.

In Fig. 5.27, the results are presented for the total scattering cross section σ for the coherent CC reaction induced by ν_μ in ^{12}C . These results are shown without NME, with NME and when the pion absorption effect is taken into account. It is found that the NME lead to a reduction of around 45% for $E_\nu=0.7$ GeV, 25-35% around $E_\nu=1.0 - 2.0$ GeV and it is about 20% at $E_\nu=3.0$ GeV while the reduction due to final state interaction is quite large. This suppression in the cross section due to the nuclear medium and the pion absorption effects is about 80% for $E_\nu \sim 1.0$ GeV, 70% for $E_\nu \sim 2.0$ GeV and 65% for $E_\nu \sim 3.0$ GeV. We show in the right panel of Fig. 5.27, the total cross section $\sigma^{\text{NC}}(E_\nu)$ for NC induced π^0 production from ^{12}C , ^{27}Al and CF_3Br (freon), along with the experimental results from the MiniBooNE collaboration for ^{12}C [623, 624], from the Aachen collaboration for ^{27}Al [603] and from the Gargamelle collaboration for freon [604]. It may be seen that the theoretical results for NC induced coherent π^0 production are in reasonable agreement with presently available experimental results in the intermediate energy region. The recently reported result by the NOvA collaboration for NC induced coherent $1\pi^0$ production cross section with mass number $A = 13.8$ at $\langle E_{\nu_\mu} \rangle = 2.7$ GeV is $13.8 \pm 0.9(\text{stat}) \pm 2.3(\text{syst}) \times 10^{-40} \text{cm}^2/\text{nucleus}$ [612], and is found to be in very good agreement with the results of Ref. [626].

In Fig. 5.28, the results are presented for the Q^2 -distribution i.e. $\left(\frac{d\sigma^{\text{CC}}}{dQ^2}\right)$ for the coherent CC reaction induced by ν_μ in ^{12}C (left panel) at neutrino energy $E_{\nu_\mu}=1.0$ GeV where NME, and NME+FSI effects are shown explicitly. It may be observed that the reduction in the cross section in the peak region is around 35%, and decreases further uniformly. The total reduction in the cross section is around 85% in the peak region when pion absorption effect is also taken into account, and decreases further uniformly. In the right panel of this figure, we present the results for the momentum distribution of pion $\left(\frac{d\sigma^{\text{CC}}}{dk_\pi}\right)$ for the coherent CC reaction induced by ν_μ in ^{12}C at neutrino energy $E_{\nu_\mu}=1$ GeV where NME and NME+FSI effects are shown explicitly. We find that the reduction in the cross section due to the NME increases with the pion momentum k_π and just before the peak region it starts decreasing, in the peak region it is about 60% and decreases further, for example, it is about 45%, 20% and 5% at $k_\pi=350$ MeV, 400 MeV and 450 MeV, respectively, after which both are approximately the same. The effect of the pion absorption show the further strong reduction in the cross section, and in the peak region ($k_\pi=320 - 360$ MeV of nuclear effects) it is about 75-80%, accompanied by the shift in the peak towards the lower value of the pion momentum \vec{k}_π , and then decreases further. Similar trend is observed in case of ^{16}O . For a detailed discussion, see Refs. [626, 602, 311].

Alvarez-Ruso et al. [628] and Amaro et al. [629] have also included NR contributions (Section 3.3.1) besides the delta resonance and found the contribution of NR terms to be very small. For the FSI of pion with the nucleus, they solved the Klein-Gordon equation. To see the difference in the results obtained by our group [626, 602, 311] and by solving Klein-Gordon equation for the treatment of pion FSI [628], a comparison was done by Alvarez-Ruso et al. [632] and found the difference to be very small. Therefore, while comparing the experimental data for the coherent pion production, Monte Carlo generators generally use the prescription of Ref. [626] for its simplicity.

Nakamura et al. [390] have used dynamical model in coupled channels using the prescription of Ref. [288] where the bare $N - \Delta$ transition from a constituent quark model is renormalized by meson clouds. Then the medium modification of the Δ properties and pion FSI have been taken into account. They have fitted the free parameters of the scattering potential and pion-nucleus optical potential to the pion-nucleus elastic scattering data. For CC process the flux averaged cross section corresponding to K2K experiment was found to be $\sigma_{\text{CC}}^{\text{avg}} = 6.3 \times 10^{-40} \text{cm}^2$ corresponding to the K2K observed result of $\sigma_{K2K} < 7.7 \times 10^{-40} \text{cm}^2$ [609]. For NC reaction, the flux averaged cross section for the π^0 production calculated in this model gives $\sigma_{\text{NC}}^{\text{avg}} = 2.8 \times 10^{-40} \text{cm}^2$ while the experimentally observed number from the MiniBooNE collaboration is $\sigma_{\text{MiniBooNE}} = 7.7 \pm 1.6 \pm 3.6 \times 10^{-40} \text{cm}^2$ [623, 624].

5.7.2. Coherent kaon production

The coherent kaon production has been studied by Alvarez-Ruso et al. [633] using the formalism discussed here in Sections 3.6.1 and 3.6.2 for the kaon and antikaon productions off the nucleon target, respectively. The differential cross section for reaction (3.126) in the laboratory frame has been taken as:

$$\frac{d^5\sigma}{d\Omega_i dk'_0 d\Omega_K} = \frac{1}{4(2\pi)^5} \frac{|\vec{k}'||\vec{p}_K|}{|\vec{k}|M^2} \frac{G^2}{2} L_{\mu\nu} \mathcal{M}_{K^+}^\mu(q, p_K) (\mathcal{M}_{K^+}^\nu(q, p_K))^*, \quad (5.124)$$

where the nuclear current $\mathcal{M}_{K^+}^\mu$ is obtained as the coherent sum over all nucleons, leading to the nuclear densities

$$\mathcal{M}_{K^+}^\mu(q, p_K) = \int d^3\vec{r} e^{i\vec{q}\cdot\vec{r}} \left\{ \rho_p(\vec{r}) \mathcal{J}_{pK^+}^\mu(q, \hat{p}_K) + \rho_n(\vec{r}) \mathcal{J}_{nK^+}^\mu(q, \hat{p}_K) \right\} \phi_{>}^*(\vec{p}_K, \vec{r}). \quad (5.125)$$

In the above expression

$$\mathcal{J}_{NK^+}^\mu(q, \hat{p}_K) = \frac{1}{2} \sum_i \text{Tr} \left[(\not{p} + M) \gamma^0 \Gamma_{i,NK^+}^\mu(q, \hat{p}_K) \right] \frac{M}{p_0}, \quad (5.126)$$

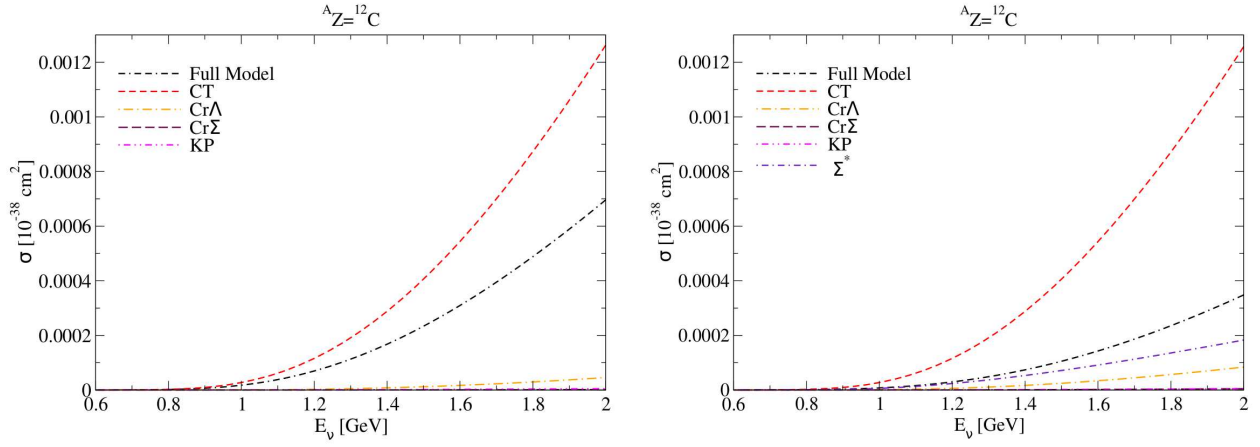


Figure 5.29: Total cross section as a function of the neutrino energy to the coherent K^+ (left panel) and K^- (right panel) reaction on ^{12}C , when kaon distortion effect is taken into account. Figure has been taken from Ref. [633].

where the index i refers to all the possible mechanisms in Figs. 3.15 and 3.17; $\Gamma_{i;NK^+}^\mu$ is given in Eq. (3.124) with $j_i^\mu = \bar{N}(p')\Gamma_{i;NK^+}^\mu N(p)$. The initial and final nucleons in the nucleus, are assumed to be on shell with $\vec{p} = (\vec{p}_K - \vec{q})/2$ and $\vec{p}' = -\vec{p}$.

$\phi_{>}^*(\vec{p}_K, \vec{r})$ in Eq. (5.124) denotes the outgoing kaon wave function obtained by solving the Klein-Gordon equation for the kaons moving in an optical potential V_{opt} :

$$\left(-\vec{\nabla}^2 - \vec{p}_K^2 + 2p_K^0 V_{\text{opt}}\right) \phi_{>}^*(\vec{p}_K, \vec{r}) = 0. \quad (5.127)$$

Fig. 5.29 shows the results for the coherent K^+ and K^- production cross sections vs neutrino energy, respectively for ν_μ (left panel) and $\bar{\nu}_\mu$ (right panel) reaction on ^{12}C nuclear target. Like the ν_μ induced single kaon production off nucleon target discussed here in Section 3.6.1, here also the dominant contribution is from the contact term and due to the destructive interference there is reduction in the total cross sections when all the contributions (Figs 3.15 and 3.17) are taken into account. It has been observed by these authors [633] that at $E_{\nu_\mu}=2\text{GeV}$, the cross section per nucleon for carbon nucleus is a factor of about forty smaller than the one obtained for the free nucleon case. Recently MINERvA collaboration [634] has reported at 3σ C.L., the evidence for coherent kaon production in the neutrino induced scattering on carbon nuclear target but no real events were reported to be observed.

5.8. Deep inelastic $\nu_l/\bar{\nu}_l - A$ scattering

5.8.1. Introduction

When a (anti)neutrino interacts with a bound nucleon inside a nucleus, the scattering cross sections and the nucleon structure functions get modified due to NME. The reaction for this interaction process via CC DIS channel is represented as

$$\nu_l/\bar{\nu}_l(k) + A(p) \longrightarrow l^-/l^+(k') + X(p'), \quad (5.128)$$

where A is the target nucleus, X is jet of hadrons in the final state, $l = e, \mu, \tau$, and the quantities in the parentheses are the four momenta of the corresponding particles, and is shown in Fig. 5.30.

The experimental evidence of NME in DIS channel was first reported by the European Muon Collaboration (EMC) in 1983 when it measured the scattering cross sections by using the very high energy muon beams off ^{56}Fe and ^2D targets and found that the ratio of the cross sections per nucleon in ^{56}Fe and ^2D to be considerably different from unity [635]. As the DIS cross sections are generally expressed in terms of the nucleon structure functions, the EMC observation implied that the structure functions for a nucleon bound inside a nucleus are different from the structure functions of a free nucleon. This effect is famously known as the EMC effect. The spectacular discovery of EMC effect motivated physicists to perform similar DIS experiments with (anti)neutrino beams using different nuclear targets. The first experiment using neutrino beam were done at CERN on ^{20}Ne and ^{56}Fe targets by the BEBC and CDHS collaborations followed by the CDHSW and NOMAD collaborations using ^{208}Pb and ^{12}C targets, respectively. Similar experiments at FNAL were done first by the CCFR, NuTeV, followed by MINOS and MINERvA, collaborations using ^{56}Fe . Several other experiments using charged lepton beam were performed by the different collaborations like SLAC [636], HERMES [637], BCDMS [638, 639], NMC [640, 641], JLab [642], etc. using nuclear targets, both moderate and heavy, for a wide range of Bjorken variable

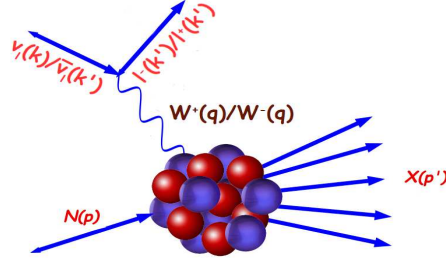


Figure 5.30: The Feynman diagram showing the charged (anti)neutrino induced DIS process with bound nucleons.

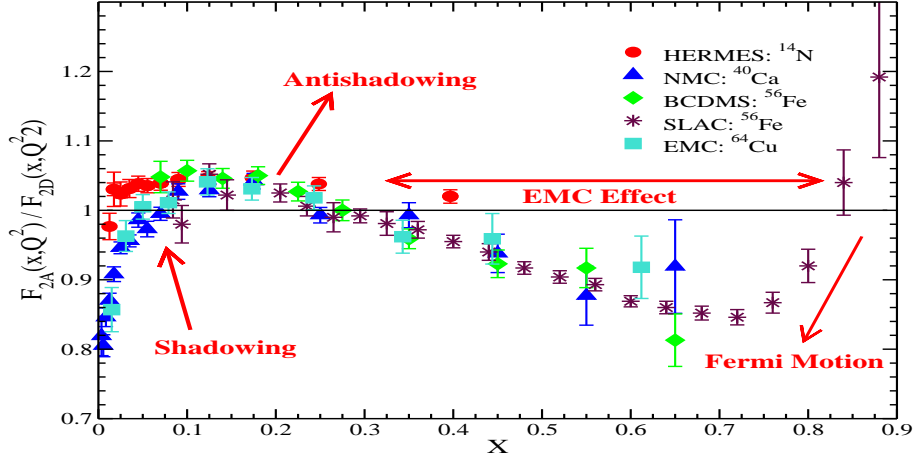


Figure 5.31: Ratio $R(x, Q^2) = \frac{F_{2A}(x, Q^2)}{F_{2D}(x, Q^2)}$; (A = target nucleus) vs x shows NME in structure function. Experimental data are taken from Refs. [636, 637, 639, 641, 643].

$x(0 < x < 1)$ and Q^2 . From the experimental observations, some general features of the ratio $R(x, Q^2) = \frac{F_{2A}(x, Q^2)}{F_{2D}(x, Q^2)}$ may be inferred:

- The x dependence of $R(x, Q^2)$ has considerable structure, i.e., it is different in the different regions of x .
- The shape of the effect is almost independent of A .
- The strength of the NME increases with the increase in mass number A .
- The functional form of $R(x, Q^2)$ has a very weak dependence on Q^2 .

Generally, NME manifested through the ratio $R(x, Q^2)$ are broadly divided into four regions of x as shown in Fig. 5.31 [636, 637, 639, 641, 643] in which the x dependence is attributed to different physical effects. These are:

1. **Shadowing Effect:** In the region of low $x(< 0.1)$, a suppression is found in the ratio $R(x, Q^2)$ which is known as the shadowing effect. This suppression becomes more pronounced with the increase in the mass number A .
2. **Antishadowing Effect:** This is the region of $0.1 \leq x \leq 0.2$, where there is an enhancement in the ratio of structure functions ($R(x, Q^2)$) and has been found to have almost no nuclear mass dependence.
3. **EMC Effect:** The ratio $R(x, Q^2)$ shows a dip in the region of $0.2 < x < 0.7$ and this is known as EMC effect, named after the first experimental observation by the EMC collaboration [635].
4. **Fermi Motion:** The nucleons bound inside the nuclear target are moving with some Fermi momentum which increases with the increase in the mass number. This is responsible for the abrupt rise in the ratio of structure functions in the region of $x \geq 0.7$.

It was observed that the results for NME on mass dependence A were consistent with $\log(A)$ and average nuclear density $\bar{\rho}_A = \frac{\rho_A}{A}$, where ρ_A is the nuclear density [644]. In recent years the MINERvA collaboration has measured the (anti)neutrino-nucleus cross sections using several targets like carbon, water, iron and lead in a wide energy spectrum, where the contribution to the cross section comes from different reaction channels. MINERvA has explicitly studied DIS channel [645, 646, 647, 648] as it aims to perform EMC kind of measurements in the weak sector covering a wide

range of x and Q^2 . For this purpose, MINERvA performed the analysis of (anti)neutrino-nucleus DIS data and reported the results for the ratio of scattering cross sections $\frac{d\sigma_A/dx}{d\sigma_{CH}/dx}$; ($A = {}^{12}\text{C}$, ${}^{56}\text{Fe}$, ${}^{208}\text{Pb}$) vs x . It has been observed that MINERvA's experimental results on $R(x, Q^2)$ are not satisfactorily explained by either the phenomenological models or theoretical models in the entire range of Bjorken x [647, 648]. Hence, it is crucial to develop a better understanding of NME both theoretically, where dynamics of the nucleons in the nuclear medium is taken into consideration, as well as phenomenologically, which involve the determination of the effective parton distribution of nucleons within a nucleus. In the following, we first discuss the theoretical approach.

Theoretically several attempts have been made to understand these effects and many models have been proposed. These models are based on the basis of nuclear binding, nuclear medium modification including short range correlations in nuclei [644, 649], pion excess in nuclei [650, 651, 652, 653, 654, 655], multi-quark clusters [656, 657, 658], dynamical rescaling [659, 660], nuclear shadowing [661, 662], etc. However, no comprehensive theoretical or phenomenological understanding of the nuclear modifications of the bound nucleon properties across the complete range of x and Q^2 consistent with the presently available experimental data exists [663, 664, 665, 666]. Furthermore, initially it was thought that NME in electromagnetic and weak structure functions should be similar in $F_{1A}(x, Q^2)$ and $F_{2A}(x, Q^2)$ despite the additional contribution from the axial current in the weak sector. Recently in a phenomenological study Kalantarians et al. [667] have made a comparison of electromagnetic vs weak nuclear structure functions ($F_{2A}^{EM}(x, Q^2)$ vs $F_{2A}^{WI}(x, Q^2)$) and found out that at low x these two structure functions are different. Theoretically there have been very few calculations to study NME in the weak structure functions, where explicitly a comparative study of electromagnetic and weak nuclear structure functions have been made [401, 668]. Our group [401, 668] has explicitly studied the difference in the electromagnetic and weak nuclear structure functions, both for $F_{2A}^{EM}(x, Q^2)$ and $F_{2A}^{WI}(x, Q^2)$, $F_{1A}^{EM}(x, Q^2)$ and $F_{1A}^{WI}(x, Q^2)$. More theoretical as well experimental studies are needed in the weak sector to understand NME for a wide range of x and Q^2 for moderate as well as heavy nuclear targets.

In the weak sector, there are only two groups who have theoretically studied NME in the weak nuclear structure functions, one is Kulagin and Petti [669] and the other is Athar et al. (Aligarh-Valencia group) [358, 401, 670, 671, 672, 673, 674, 675, 676, 677, 678]. Kulagin and Petti in their model of nuclear DIS took into account nuclear effects like the nuclear shadowing, Fermi motion, binding energy, nuclear pion excess and off-shell corrections to bound structure functions. While the Aligarh-Valencia group [358, 401, 670, 671, 672, 673, 674, 675, 676, 677, 678] have used a microscopic model which uses relativistic nucleon spectral function to describe target nucleon momentum distribution incorporating the effects of Fermi motion, binding energy and nucleon correlations in a field theoretical model. The spectral function that describes the energy and momentum distribution of the nucleons in nuclei is obtained by using the Lehmann's representation for the relativistic nucleon propagator and nuclear many body theory is used to calculate it for an interacting Fermi sea in the nuclear matter [679]. A local density approximation is then applied to translate these results to a finite nucleus. Furthermore, the contributions of the pion and rho meson clouds in a many body field theoretical approach have also been considered. In Section 5.8.2, we discuss in brief the theoretical approach of the Aligarh-Valencia group to understand NME in $\nu_l(\bar{\nu}_l)$ -nucleus scattering.

5.8.2. Formalism

The general expression of the differential scattering cross section for (anti)neutrino-nucleus DIS process

$$\nu_l(k) + A(p_A) \rightarrow l^-(k') + X(p'_A); \quad l = e \text{ or } \mu \text{ or } \tau, \quad (5.129)$$

is written in analogy with CC $\nu_l(\bar{\nu}_l) - N$ scattering discussed in Section 4 by replacing the nucleon hadronic tensor $W_N^{\mu\nu}$ with the nuclear hadronic tensor $W_A^{\mu\nu}$ and is given by:

$$\frac{d^2\sigma_A}{dQ^2 d\nu} = \frac{G_F^2}{4\pi E_\nu E_l} \left(\frac{M_W^2}{Q^2 + M_W^2} \right)^2 \frac{|\vec{k}'|}{|\vec{k}|} L_{\mu\nu} W_A^{\mu\nu}, \quad (5.130)$$

or it may be expressed in terms of the scaling variables as

$$\frac{d^2\sigma_A}{dx dy} = \left(\frac{G_F^2 y M E_l}{2\pi E_\nu} \right) \left(\frac{M_W^2}{M_W^2 + Q^2} \right)^2 \frac{|\vec{k}'|}{|\vec{k}|} L_{\mu\nu} W_A^{\mu\nu}, \quad (5.131)$$

$W_A^{\mu\nu}$ is written in terms of the weak nuclear structure functions $W_{iA}^{WI}(\nu, Q^2)$ ($i = 1, 2, 3$) as

$$\begin{aligned} W_A^{\mu\nu} = & \left(\frac{q^\mu q^\nu}{q^2} - g^{\mu\nu} \right) W_{1A}(\nu_A, Q^2) + \frac{W_{2A}(\nu_A, Q^2)}{M_A^2} \left(p_A^\mu - \frac{p_A \cdot q}{q^2} q^\mu \right) \left(p_A^\nu - \frac{p_A \cdot q}{q^2} q^\nu \right) \pm \frac{i}{2M_A^2} \epsilon^{\mu\nu\rho\sigma} p_{A\rho} q_\sigma W_{3A}(\nu_A, Q^2) \\ & + \frac{W_{4A}(\nu_A, Q^2)}{M_A^2} q^\mu q^\nu + \frac{W_{5A}(\nu_A, Q^2)}{M_A^2} (p_A^\mu q^\nu + q^\mu p_A^\nu) + \frac{i}{M_A^2} (p_A^\mu q^\nu - q^\mu p_A^\nu) W_{6A}(\nu_A, Q^2). \end{aligned} \quad (5.132)$$

In the above expression M_A is the mass and p_A is the four momentum of the initial nuclear target and the positive/negative sign is for the $\nu_l/\bar{\nu}_l$. The leptonic tensor in Eq. (5.131) has the same form as given in Eq. (2.15). $W_{6A}(\nu_A, Q^2)$ does not contribute to the cross section as it vanishes when contracted with the leptonic tensor $L_{\mu\nu}$. The nuclear structure functions $W_{iA}(\nu_A, Q^2)$ ($i = 1-5$) are written in terms of the dimensionless nuclear structure functions $F_{iA}(x_A)$; ($i = 1-5$) as [401, 407]:

$$F_{1A}(x_A) = W_{1A}(\nu_A, Q^2); \quad F_{2A}(x_A) = \frac{Q^2}{2xM_A^2}W_{2A}(\nu_A, Q^2); \quad F_{3A}(x_A) = \frac{Q^2}{xM_A^2}W_{3A}(\nu_A, Q^2); \quad (5.133)$$

$$F_{4A}(x_A) = \frac{Q^2}{2M_A^2}W_{4A}(\nu_A, Q^2); \quad F_{5A}(x_A) = \frac{Q^2}{2xM_A^2}W_{5A}(\nu_A, Q^2), \quad (5.134)$$

where $\nu_A (= \frac{p_A \cdot q}{M_A} = q^0)$ is the energy transferred to the nuclear target in the rest frame of the nucleus i.e. $p_A = (p_A^0, \vec{p}_A = 0)$ and $x_A (= \frac{Q^2}{2p_A \cdot q} = \frac{Q^2}{2p_A^0 q^0} = \frac{Q^2}{2A M q^0} = \frac{x}{A})$ is the Bjorken scaling variable corresponding to the nucleus.

The expression for the differential cross section for the $\nu_l/\bar{\nu}_l - A$ scattering is then written as [677]:

$$\begin{aligned} \frac{d^2\sigma_A}{dx dy} &= \frac{G_F^2 M E_\nu}{\pi(1 + \frac{Q^2}{M_W^2})^2} \left\{ \left[y^2 x + \frac{m_l^2 y}{2E_\nu M} \right] F_{1A}(x, Q^2) + \left[\left(1 - \frac{m_l^2}{4E_\nu^2}\right) - \left(1 + \frac{Mx}{2E_\nu}\right) y \right] F_{2A}(x, Q^2) \right. \\ &\quad \left. \pm \left[xy \left(1 - \frac{y}{2}\right) - \frac{m_l^2 y}{4E_\nu M} \right] F_{3A}(x, Q^2) + \frac{m_l^2 (m_l^2 + Q^2)}{4E_\nu^2 M^2 x} F_{4A}(x, Q^2) - \frac{m_l^2}{E_\nu M} F_{5A}(x, Q^2) \right\}, \end{aligned} \quad (5.135)$$

where the kinematic variables have the same meaning as defined in Section 4. For $\nu_e/\bar{\nu}_e$ and $\nu_\mu/\bar{\nu}_\mu$ interactions with a nuclear target (i.e. in the limit $m_l \rightarrow 0$), only the first three terms of Eq. (5.135), i.e. the terms with $F_{1A}(x, Q^2)$, $F_{2A}(x, Q^2)$ and $F_{3A}(x, Q^2)$ would contribute. However, for the $\nu_\tau/\bar{\nu}_\tau$ induced processes, all the five structure functions ($F_{iA}(x, Q^2)$; ($i = 1-5$)) contribute and this has been discussed recently by Zaidi et al. [677]. Here the discussions are made only for the massless lepton case.

The nucleons bound inside the nucleus are moving continuously with a finite momentum, i.e. \vec{p}_N is nonzero and the motion of such nucleons corresponds to the Fermi motion. Therefore, these nucleons are off shell. If the momentum transfer is taken to be along the Z -axis then $q^\mu = (q^0, 0, 0, q^z)$ and the Bjorken variable x_N corresponding to the nucleon bound inside a nucleus is written as:

$$x_N = \frac{Q^2}{2p_N \cdot q} = \frac{Q^2}{2(p_N^0 q^0 - \vec{p}_N^z q^z)}. \quad (5.136)$$

The momentum ($p_N \neq 0$) of the initial nucleon is constrained by the Fermi momentum (p_{F_N}) of the nucleon in the nucleus, i.e., $p_N \leq p_{F_N}$. These bound nucleons interact among themselves via the strong interaction and thus various NME come into play which are effective in the different regions of the Bjorken variable x .

5.8.3. Fermi motion, binding and nucleon correlation effects

In the local density approximation, using many body field theoretical approach, the scattering cross section for a (anti)neutrino interacting with a bound nucleon ($\nu_l + N \rightarrow l^- + X$) is obtained by considering a flux of neutrinos hitting a collection of target nucleons over a given length of time. Now a majority will simply pass through the target without interacting while a certain fraction will interact with the target nucleons leaving the pass-through fraction and entering the fraction of neutrinos yielding final state leptons and hadrons. Then the concept of "neutrino self energy" is used which has a real and imaginary part. The real part modifies the lepton mass while the imaginary part is related to this fraction of interacting neutrinos and gives the total number of neutrinos that have participated in the interactions that give rise to the charged leptons and hadrons.

The neutrino self energy is evaluated corresponding to the diagram shown in Fig. 5.32 (left panel). The cross section for an element of volume dV in the rest frame of the nucleus is related to the probability per unit time (Γ) of the ν_l interacting with a nucleon bound inside a nucleus. $\Gamma dt dS$ provides probability times a differential of area (dS) which is nothing but the cross section ($d\sigma$) [652], i.e.

$$d\sigma = \Gamma dt dS = \Gamma \frac{dt}{dl} ds dl = \Gamma \frac{1}{v} dV = \Gamma \frac{E_l}{|\vec{k}|} d^3r, \quad (5.137)$$

where $v (= \frac{|\vec{k}|}{E_l})$ is the velocity of the incoming ν_l . The probability per unit time of the interaction of ν_l with the nucleons in the nuclear medium to give the final state is related to the imaginary part of the ν_l self energy $\Sigma(k)$, as [652]:

$$-\frac{\Gamma}{2} = \frac{m_\nu}{E_\nu(\vec{k})} \text{Im}\Sigma(k), \quad (5.138)$$

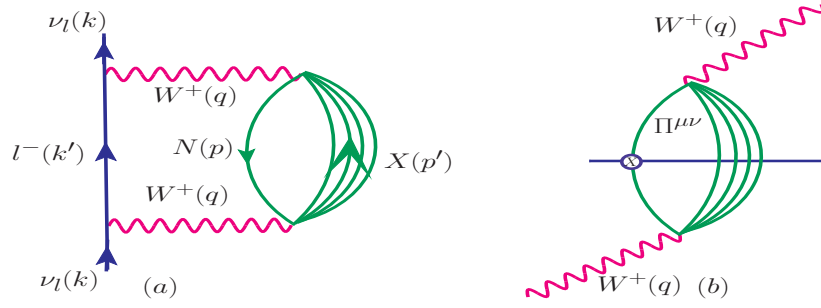


Figure 5.32: Diagrammatic representation of **(a)** the neutrino self-energy and **(b)** the intermediate vector boson W^+ self-energy.

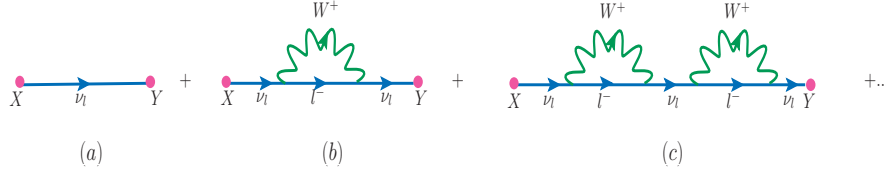


Figure 5.33: Fermion two point function and its modification.

where $Im(\Sigma(k))$ is the imaginary part of the neutrino self energy (shown in Fig. 5.32 (left panel)). By using Eq. (5.138) in Eq. (5.137), we obtain

$$d\sigma = \frac{-2m_\nu}{|\vec{k}|} Im\Sigma(k) d^3r. \quad (5.139)$$

In many body field theory the interaction of neutrino with a potential provided by a nucleus can be explained as the modification to the fermion two point function as depicted in Fig. 5.33. Figure 5.33(a) corresponds to the free field fermion propagator while Figure 5.33(b,c) constitutes to the neutrino self-energy. Thus to get $d\sigma$, we are required to evaluate the imaginary part of the neutrino self energy $Im\Sigma(k)$ which is obtained by following the Feynman rules [10]:

$$Im\Sigma(k) = \frac{G_F}{\sqrt{2}} \frac{4}{m_\nu} \int \frac{d^3k'}{(2\pi)^4} \frac{\pi}{E(\vec{k}')} \theta(q^0) \left(\frac{M_W}{Q^2 + M_W^2} \right)^2 Im[L_{\mu\nu}^{WI} \Pi^{\mu\nu}(q)]. \quad (5.140)$$

In the above expression, $\Pi^{\mu\nu}(q)$ is the W boson self-energy, which is written in terms of the nucleon (G_l) and meson (D_j) propagators (depicted in Fig. 5.32 (right panel)) following the Feynman rules and is given by

$$\begin{aligned} \Pi^{\mu\nu}(q) &= \left(\frac{G_F M_W^2}{\sqrt{2}} \right) \times \int \frac{d^4p}{(2\pi)^4} G(p) \sum_X \sum_{s_p, s_l} \prod_{i=1}^N \int \frac{d^4p'_i}{(2\pi)^4} \prod_l G_l(p'_l) \\ &\times \prod_j D_j(p'_j) < X | J^\mu | N > < X | J^\nu | N >^* (2\pi)^4 \times \delta^4(k + p - k' - \sum_{i=1}^N p'_i), \end{aligned} \quad (5.141)$$

where s_p is the spin of the nucleon, s_l is the spin of the fermions in X , $< X | J^\mu | N >$ is the hadronic current for the initial state nucleon to the final state hadrons, index l , j are respectively, stands for the fermions and bosons in the final hadronic state X , and $\delta^4(k + p - k' - \sum_{i=1}^N p'_i)$ ensures the conservation of four momentum at the vertex. $G(p^0, \vec{p})$ is the nucleon propagator which inside the nuclear medium provides information about the propagation of the nucleon from the initial state to the final state or vice versa.

The relativistic nucleon propagator $G(p^0, \vec{p})$ in a nuclear medium is obtained by starting with the relativistic free nucleon Dirac propagator $G^0(p^0, \vec{p})$, which is written in terms of the contribution from the positive and negative energy components of the nucleon described by the Dirac spinors $u(\vec{p})$ and $v(\vec{p})$ [652, 679]. Only the positive energy contributions are retained as the negative energy contributions are suppressed. In the interacting Fermi sea, the relativistic nucleon propagator is then written in terms of the nucleon self energy $\Sigma^N(p^0, \vec{p})$ which is shown in Fig. 5.34. In nuclear many body technique, the quantity that contains all the information on the single nucleon properties is the nucleon self energy $\Sigma^N(p^0, \vec{p})$. For an interacting Fermi sea the relativistic nucleon propagator is written in terms of the nucleon self energy and in nuclear matter the interaction is taken into account through Dyson series expansion which is the quantum field theoretical analogue of the Lippmann-Schwinger equation for the dressed nucleons, and in principle an infinite series in

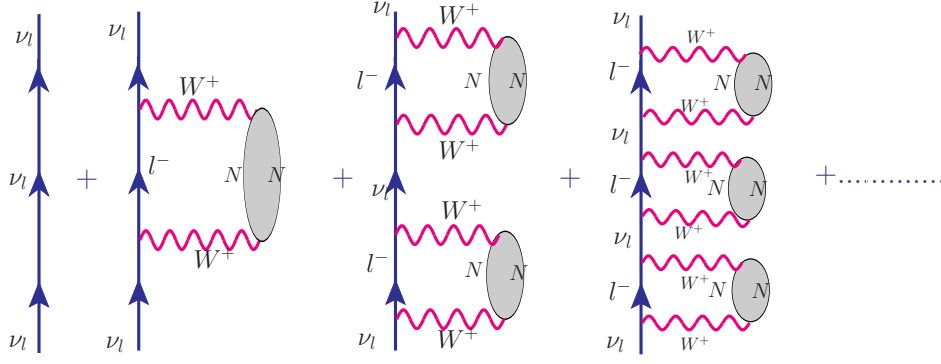


Figure 5.34: Diagrammatic representation of neutrino self-energy in the nuclear medium.

perturbation theory. This perturbative expansion is summed in a ladder approximation as

$$\begin{aligned}
 G(p^0, \vec{p}) &= \frac{M}{E(\vec{p})} \frac{\sum_r u_r(\vec{p}) \bar{u}_r(\vec{p})}{p^0 - E(\vec{p})} + \frac{M}{E(\vec{p})} \frac{\sum_r u_r(\vec{p}) \bar{u}_r(\vec{p})}{p^0 - E(\vec{p})} \Sigma^N(p^0, \vec{p}) \times \frac{M}{E(\vec{p})} \frac{\sum_s u_s(\vec{p}) \bar{u}_s(\vec{p})}{p^0 - E(\vec{p})} + \dots \\
 &= \frac{M}{E(\vec{p})} \frac{\sum_r u_r(\vec{p}) \bar{u}_r(\vec{p})}{p^0 - E(\vec{p}) - \sum_r \bar{u}_r(\vec{p}) \Sigma^N(p^0, \vec{p}) u_r(\vec{p}) \frac{M}{E(\vec{p})}},
 \end{aligned} \tag{5.142}$$

where $\Sigma^N(p^0, \vec{p})$ is the nucleon self energy which is obtained following the techniques of many body theory. This has been taken from Ref. [679, 680] which uses the nucleon-nucleon scattering cross section and the spin-isospin effective interaction with random phase approximation(RPA) correlation as inputs. In this approach, the real part of the self energy of nucleon is obtained by means of the dispersion relations using the expressions for the imaginary part. The Fock term, which does not have imaginary part, does not contribute either to $Im\Sigma^N(p^0, \vec{p})$ or to $Re\Sigma^N(p^0, \vec{p})$ through the dispersion relation and its contribution to $\Sigma^N(p^0, \vec{p})$ is explicitly calculated and added to $Re\Sigma^N(p^0, \vec{p})$ [679]. The model however misses some contributions from similar terms of Hartree type which are independent of nucleon momentum p . This semi-phenomenological model of nucleon self energy is found to be in reasonable agreement with those obtained in sophisticated many body calculations and has been successfully used in the past to study NME in many processes induced by photons, pions and leptons [517, 681]. The expression for the nucleon self energy in the nuclear matter i.e. $\Sigma^N(p^0, \vec{p})$ is taken from Ref. [679], and the dressed nucleon propagator is expressed as [652]:

$$G(p^0, \vec{p}) = \frac{M}{E(\vec{p})} \sum_r u_r(\vec{p}) \bar{u}_r(\vec{p}) \left[\int_{-\infty}^{\mu} d\omega \frac{S_h(\omega, \vec{p})}{p^0 - \omega - i\eta} + \int_{\mu}^{\infty} d\omega \frac{S_p(\omega, \vec{p})}{p^0 - \omega + i\eta} \right], \tag{5.143}$$

where $S_h(\omega, \vec{p})$ and $S_p(\omega, \vec{p})$ are the hole and particle spectral functions, respectively. $\mu = \epsilon_F + M$ is the chemical potential, $\omega = p^0 - M$ is the removal energy and η is the infinitesimal small quantity, i.e. $\eta \rightarrow 0$. The hole and particle spectral functions are given by [652, 679]:

$$S_h(p^0, \vec{p}) = \frac{1}{\pi} \frac{\frac{M}{E_N(\vec{p})} \text{Im}\Sigma^N(p^0, \vec{p})}{\left(p^0 - E_N(\vec{p}) - \frac{M}{E_N(\vec{p})} \text{Re}\Sigma^N(p^0, \vec{p})\right)^2 + \left(\frac{M}{E_N(\vec{p})} \text{Im}\Sigma^N(p^0, \vec{p})\right)^2}; \text{ for } p^0 \leq \mu \tag{5.144}$$

$$S_p(p_0, \vec{p}) = -\frac{1}{\pi} \frac{\frac{M}{E(\vec{p})} \text{Im}\Sigma^N(p_0, \vec{p})}{\left(p_0 - E(\vec{p}) - \frac{M}{E(\vec{p})} \text{Re}\Sigma^N(p_0, \vec{p})\right)^2 + \left(\frac{M}{E(\vec{p})} \text{Im}\Sigma^N(p_0, \vec{p})\right)^2}; \text{ for } p_0 > \mu \tag{5.145}$$

which obey the following relations

$$\int_{-\infty}^{\mu} dp_0 S_h(p_0, \vec{p}) = n(\vec{p}); \quad \int_{\mu}^{\infty} dp_0 S_p(p_0, \vec{p}) = 1 - n(\vec{p}), \tag{5.146}$$

where $n(\vec{p})$ is the Fermi occupation number.

Hence, one may obtain the spectral function sum rule which is given by

$$\int_{-\infty}^{\mu} S_h(\omega, \vec{p}) d\omega + \int_{\mu}^{+\infty} S_p(\omega, \vec{p}) d\omega = 1 \tag{5.147}$$

with the removal energy $\omega (= p^0 - M)$. For the numerical calculations, the expression of chemical potential, i.e.

$$\mu = \frac{p_{FN}^2}{2M} + \text{Re}\Sigma^N\left[\frac{p_{FN}^2}{2M}, p_{FN}\right] \tag{5.148}$$

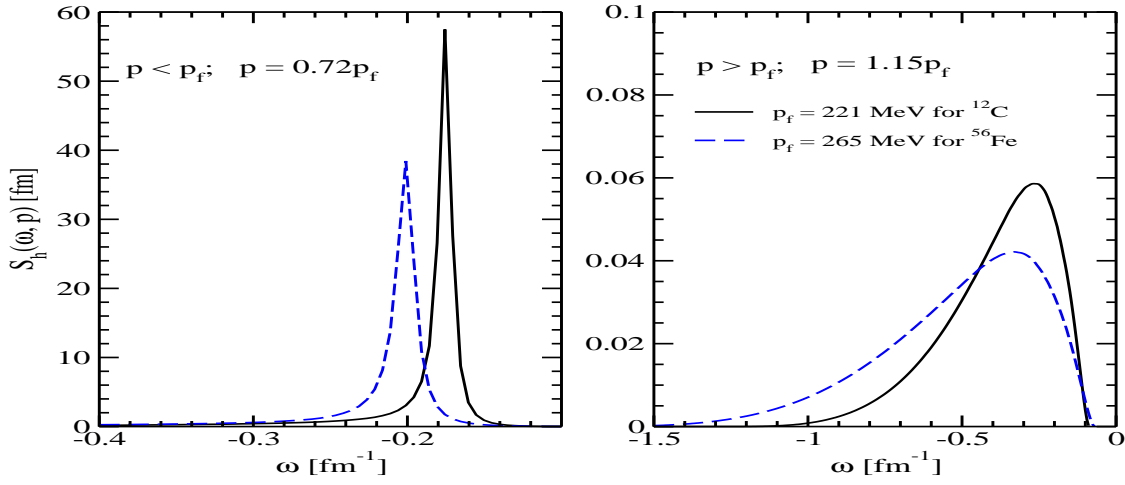


Figure 5.35: $S_h(\omega, \vec{p})$ vs ω for $p < p_F$ (Left panel) and $p > p_F$ (Right panel) in ^{12}C (solid line) and ^{56}Fe (dashed line).

has been taken from Ref. [679] which is defined in terms of Fermi momentum (p_{F_N}) and the nucleon self energy (Σ^N) [679].

For an inclusive process, only the hole spectral function contributes. In Fig. 5.35, following Ref. [652], we have plotted $S_h(\omega, \vec{p})$ vs ω (where $\omega = p_0 - M$), for $p < p_F$ and $p > p_F$ in ^{12}C and ^{56}Fe nuclei. It may be observed that for $p < p_F$ the hole spectral function S_h almost mimics a delta function as it corresponds to a Lorentzian distribution with a very narrow width. While for $p > p_F$, S_h is not exactly zero, although very small in magnitude but has a longer range. This behavior is different from independent particle model, where it is exactly zero and this difference arises due to nucleon correlation [682]. The details are given in Ref. [401, 683].

The cross section is then obtained by using Eqs. (5.139) and (5.140) as:

$$\frac{d^2\sigma_A}{dx dy} = -\frac{G_F^2 M y}{2\pi} \frac{E_l}{E_\nu} \frac{|\vec{k}'|}{|\vec{k}|} \left(\frac{M_W^2}{Q^2 + M_W^2} \right)^2 L_{\mu\nu} \int \text{Im} \Pi^{\mu\nu}(q) d^3r. \quad (5.149)$$

Comparing Eq. (5.149) with Eqs. (5.131), and using Eqs. (5.141) and (5.143), the expression of the nuclear hadronic tensor for an isospin symmetric nucleus in terms of the nucleonic hadronic tensor and spectral function, is obtained as [683]

$$W_A^{\mu\nu} = 4 \int d^3r \int \frac{d^3p}{(2\pi)^3} \frac{M}{E(\vec{p})} \int_{-\infty}^{\mu} dp^0 S_h(p^0, \vec{p}, \rho(r)) W_N^{\mu\nu}(p, q), \quad (5.150)$$

where the factor of 4 is for the spin-isospin of nucleon and $\rho(r)$ is the charge density of the nucleon in the nucleus which is given in Appendix C. S_h incorporates the effects like Fermi motion, binding energy and nucleon correlations and is physically interpreted as equal to the joint probability of (i) removing a nucleon with momentum \vec{p} from the correlated ground state, and (ii) finding the resulting system of (A-1) nucleons with energy in the interval p_0 and $p_0 + dp_0$.

Moreover, we have ensured that the spectral function is properly normalized and checked it by obtaining the correct baryon number (A) for a given nucleus [683]:

$$4 \int \frac{d^3p}{(2\pi)^3} \int_{-\infty}^{\mu} S_h(\omega, p, p_{F_N}(\vec{r})) d\omega = \rho(\vec{r}), \quad (5.151)$$

that leads to the following normalization condition

$$4 \int d^3r \int \frac{d^3p}{(2\pi)^3} \int_{-\infty}^{\mu} S_h(\omega, \vec{p}, \rho(r)) d\omega = A. \quad (5.152)$$

The binding energy per nucleon for a nucleus is given by [683]:

$$|E_A| = -\frac{1}{2} \left(\langle E_N - M \rangle + \frac{A-2}{A-1} \langle T \rangle \right), \quad (5.153)$$

with $\langle T \rangle$ as the average kinetic energy, $\langle E_N \rangle$ as the total nucleon energy and have been tabulated in Appendix C for the nuclei for which numerical calculations have been made. Thus, by normalizing the spectral function to a given number of nucleons in the nucleus and getting a binding energy very close to the experimental value, no free parameter is left. Details are given in Ref. [679, 683].

For a nonisoscalar nuclear target $W_A^{\mu\nu}$ is written in terms of the proton/neutron hole spectral function (S_h^j ; $j = p, n$) and the corresponding hadronic tensor ($W_j^{\mu\nu}$; $j = p, n$) is expressed as

$$W_A^{\mu\nu} = 2 \sum_{j=p,n} \int d^3r \int \frac{d^3p}{(2\pi)^3} \frac{M}{E_N(\vec{p})} \int_{-\infty}^{\mu_j} dp^0 S_h^j(p^0, \vec{p}, \rho(r)) W_j^{\mu\nu}(p, q), \quad (5.154)$$

where the factor of 2 is due to the two possible projections of nucleon spin and μ_j ; ($j = p, n$) is the chemical potential for the proton/neutron. In the local density approximation, the hole spectral functions of protons and neutrons are the function of local Fermi momentum and the equivalent normalization is written as

$$2 \int \frac{d^3p}{(2\pi)^3} \int_{-\infty}^{\mu} S_h^{p,n}(\omega, p, p_{F_{p,n}}(\vec{r})) d\omega = \rho_{p,n}(\vec{r}), \quad (5.155)$$

$p_{F_{p(n)}}$ is the Fermi momentum of proton/neutron inside the nucleus which is expressed in terms of the proton/neutron density as discussed above. The hole spectral functions are normalized separately to the respective proton and neutron numbers in a nuclear target as [401, 683]:

$$2 \int d^3r \int \frac{d^3p}{(2\pi)^3} \int_{-\infty}^{\mu_p} S_h^p(\omega, \vec{p}, \rho_p(r)) d\omega = Z, \quad (5.156)$$

$$2 \int d^3r \int \frac{d^3p}{(2\pi)^3} \int_{-\infty}^{\mu_n} S_h^n(\omega, \vec{p}, \rho_n(r)) d\omega = N. \quad (5.157)$$

The hadronic tensor ($W_j^{\mu\nu}$) is then written in terms of the dimensionless proton and neutron structure functions ($F_{ij}(x, Q^2)$; $i = 1 - 5$; $j = p, n$). By using Eq. (5.154) and the general form of hadronic tensor with an appropriate choice of x, y, z components, we obtain the following expressions of the dimensionless nuclear structure functions for a nonisoscalar nuclear target [400, 401, 683]:

$$F_{iA,N}(x_A, Q^2) = 4 \int d^3r \int \frac{d^3p}{(2\pi)^3} \frac{M}{E_N(\vec{p})} \int_{-\infty}^{\mu} dp^0 S_h(p^0, \vec{p}, \rho(r)) \times f_{iN}(x, Q^2), \quad (5.158)$$

where $i = 1 - 5$ and

$$f_{1N}(x, Q^2) = AM \left[\frac{F_{1N}(x_N, Q^2)}{M} + \left(\frac{p^x}{M} \right)^2 \frac{F_{2N}(x_N, Q^2)}{\nu_N} \right], \quad (5.159)$$

$$f_{2N}(x, Q^2) = \left(\frac{F_{2N}(x_N, Q^2)}{M^2 \nu_N} \right) \left[\frac{Q^4}{q^0 (q^z)^2} \left(p^z + \frac{q^0 (p^0 - \gamma p^z)}{Q^2} q^z \right)^2 + \frac{q^0 Q^2 (p^x)^2}{(q^z)^2} \right], \quad (5.160)$$

$$f_{3N}(x, Q^2) = A \frac{q^0}{q^z} \times \left(\frac{p^0 q^z - p^z q^0}{p \cdot q} \right) F_{3N}(x_N, Q^2), \quad (5.161)$$

$$f_{4N}(x, Q^2) = A \left[F_{4N}(x_N, Q^2) + \frac{p^z Q^2}{q^z} \frac{F_{5N}(x, Q^2)}{M \nu_N} \right], \quad (5.162)$$

$$f_{5N}(x, Q^2) = A \frac{F_{5N}(x_N, Q^2)}{M \nu_N} \times \left[q^0 (p^0 - \gamma p^z) + Q^2 \frac{p^z}{q^z} \right], \quad (5.163)$$

where $\nu_N = \frac{p \cdot q}{M} = \frac{p^0 q^0 - p^z q^z}{M}$, $\gamma = \frac{q^0}{q^z}$. Using these expressions, the effect of Fermi motion, binding energy and nucleon correlations have been included through the use of hole spectral function. Furthermore, bound nucleons may interact with each other via meson exchange such as π , ρ , etc., and the interaction of the intermediate vector boson with the mesons play an important role in the evaluation of nuclear structure functions [401, 674]. Hence, we have incorporated these effects in the numerical calculations and discussed the mesonic contributions in the following Section 5.8.4.

5.8.4. Mesonic contribution

There are virtual mesons (mainly π and ρ mesons) associated with each nucleon bound inside the nucleus. This mesonic cloud gets strengthened by the strong attractive nature of the nucleon-nucleon interaction, which leads to a reasonably good probability of interaction of virtual bosons(IVB) with a meson instead of a nucleon [652, 653, 684, 685]. It has been observed by us that the mesonic contribution, which is mainly dominated by the pion cloud, becomes more pronounced in the heavier nuclear targets and significant in the intermediate region of x ($0.2 < x < 0.6$). It may be pointed out that calculations performed with only the spectral function, result in a reduction in the nuclear structure function from the

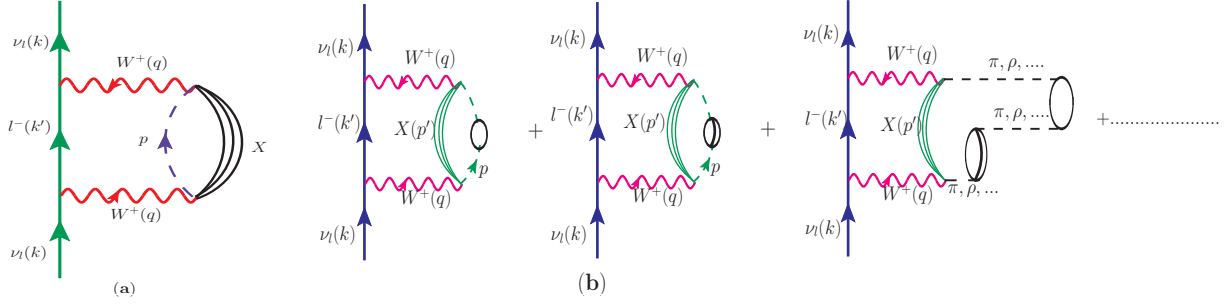


Figure 5.36: Neutrino self-energy diagram accounting for lepton-meson DIS (a) the bound nucleon propagator is substituted with a meson(π or ρ) propagator with momentum p represented here by dashed line (b) by including particle-hole ($1p^{-1}h$), delta-hole ($1\Delta^{-1}h$), $1p1h - 1\Delta1h$, etc. interactions.

free nucleon structure function, while the inclusion of mesonic cloud contribution leads to an enhancement of the nuclear structure function.

To obtain the contribution from the virtual mesons, the neutrino self energy is again evaluated using many body techniques [652], and to take into account mesonic effects a diagram similar to the one shown in Fig. 5.32 is drawn, except that instead of a nucleon now there is a meson which results in the change of a nucleon propagator by a meson propagator.

The meson propagator does not corresponds to the free mesons but it corresponds to the mesons which arise due to NME [679]. In the nuclear medium these mesons arise through ph , Δh , $ph - \Delta h$, $2p - 2h$, etc. interactions as shown in Fig. 5.36. The mesonic structure functions $F_{iA,a}(x_a, Q^2)$, ($i = 1, 2, 5; a = \pi, \rho$) are obtained as [652, 677]:

$$F_{iA,a}(x_a, Q^2) = -6\kappa \int d^3r \int \frac{d^4p}{(2\pi)^4} \theta(p^0) \delta Im D_a(p) 2m_a f_{ia}(x_a), \quad \text{where} \quad (5.164)$$

$$f_{1a}(x_a) = Am_a \left[\frac{F_{1a}(x_a)}{m_a} + \frac{|\vec{p}|^2 - (p^z)^2}{2(p^z q^z - p^0 q^0)} \frac{F_{2a}(x_a)}{m_a} \right], \quad (5.165)$$

$$f_{2a}(x_a) = \left(\frac{F_{2a}(x_a)}{m_a^2 \nu} \right) \left[\frac{Q^4}{q^0 (q^z)^2} \left(p^z + \frac{q^0 (\gamma p^z - p^0)}{Q^2} q^z \right)^2 + \frac{q^0 Q^2 (|\vec{p}|^2 - (p^z)^2)}{2(q^z)^2} \right], \quad (5.166)$$

$$f_{5a}(x_a) = A \frac{F_{5a}(x_a)}{m_a \nu} \times \left[q^0 (\gamma p^z - p^0) + Q^2 \frac{p^z}{q^z} \right]. \quad (5.167)$$

In Eqs. (5.164), (5.165) and (5.166) $\kappa = 1(2)$ for pion (rho meson), $\nu = \frac{q^0 (\gamma p^z - p^0)}{m_a}$, $x_a = -\frac{Q^2}{2p \cdot q}$, m_a is the mass of the meson (π or ρ). $D_a(p)$ is the meson(π or ρ) propagator in the nuclear medium and is written as

$$D_a(p) = [p_0^2 - \vec{p}^2 - m_a^2 - \Pi_a(p_0, \vec{p})]^{-1}, \quad \text{with} \quad \Pi_a(p_0, \vec{p}) = \frac{f^2}{m_\pi^2} \frac{C_\rho F_a^2(p) \vec{p}^2 \Pi^*}{1 - \frac{f^2}{m_\pi^2} V_j' \Pi^*}. \quad (5.168)$$

In the above expression, $f = 1.01$, $C_\rho = 1$ for the pion and $C_\rho = 3.94$ for the rho meson. $F_a(p) = \frac{(\Lambda_a^2 - M_a^2)}{(\Lambda_a^2 - p^2)}$ is the πNN or ρNN form factor, $p^2 = p_0^2 - \vec{p}^2$, $\Lambda_a = 1 \text{ GeV}$ (this was fixed by Aligarh-Valencia group to describe NME in electromagnetic nuclear structure functions to explain experimental data from JLab and other experiments for a wide range of nuclear targets [671]). For pion (rho meson), V_j' is the longitudinal (transverse) part of the spin-isospin interaction and Π^* is the irreducible meson self energy that contains the contribution of particle-hole and delta-hole excitations. Various quark and antiquark PDFs parameterizations for pions are available in the literature such as given by Conway et al. [686], Martin et al. [361], Sutton et al. [687], Wijesooriya et al. [688], Gluck et al. [689], etc. Aligarh-Valencia group has observed [400] that the choice of pionic PDF parameterizations would not make any significant difference in the event rates. In this work, the parameterization given by Gluck et al. [689] has been taken into account for pions and for the rho mesons same PDFs as for the pions have been used. It is important to mention that mesonic contribution does not play any role to $F_{3A}(x, Q^2)$. The reason is that $F_{3A}(x, Q^2)$ depends mainly on the valence quark distribution and not on the sea quarks distribution. In the evaluation of $F_{4A}(x, Q^2)$, the mesonic contribution has not been incorporated because the mesonic PDFs for $F_{4A}(x, Q^2)$ are not available in the literature and for $F_{5A}(x, Q^2)$ mesonic effect is included by using the Albright-Jarlskog relation [360] at the leading order as the parameterization for mesonic PDFs for $F_{2A}(x, Q^2)$ is available in the literature.

5.8.5. Shadowing and antishadowing effects

The (anti)shadowing effect in the nuclear structure functions is a leading twist effect which arises due to the (constructive) destructive interference of amplitudes in the multiple parton scattering processes. It is a coherent effect as it results from coherent scattering of hadronic fluctuations from at least two nucleons in the target nucleus. There are two broad approaches to understand it, one is known as Glauber-Gribov formalism [690, 691, 692], and the other is known as Regge-Gribov framework [693, 694, 695]. For shadowing the initial works used generalized vector dominance(GVD) model [691, 692, 696, 697, 698] in the Glauber-Gribov formalism, while recently color dipole model has also been used [699, 700]. These coherent corrections are found to be different in the electromagnetic and weak interaction channels because the hadronization process of the corresponding intermediate vector bosons are different. In the literature, different approaches are available to incorporate these coherent corrections and discussed by Nikoleav and Zakharov [699], Armesto et al. [701, 702], Kopeliovich et al. [703], Kulagin and Petti [669, 684], etc. We have followed the prescription of Kulagin and Petti [669, 684] who have used the formalism developed by Glauber and Gribov, and considers the multiple scattering of the hadronic components of the virtual photon(in electromagnetic interaction induced processes) or W/Z (in weak interaction induced processes) with the target nucleus. Then it considers the structure functions at small x as a superposition of contributions from different hadronic states. In the case of (anti)neutrino induced DIS processes, they have treated (anti)shadowing differently from the prescription applied in the case of electromagnetic structure functions [669, 684], due to the presence of the axial-vector current in the neutrino interactions. The interference between the vector and the axial-vector currents introduces C-odd terms in the neutrino cross sections, which are described by structure function $F_{3A}(x, Q^2)$. In their calculation of nuclear corrections, separate contributions to different structure functions according to their C-parity have been taken into account. This results in a different dependence of medium effects on the nuclear structure functions depending upon their C-parity specially in the nuclear (anti)shadowing region [672]. For example, to determine the nuclear structure function $F_{iA}(x, Q^2)$; ($i = 1 - 3, 5$) with the shadowing effect:

$$F_{iA}^S(x, Q^2) = \delta R(x, Q^2) \times F_{iN}(x, Q^2), \quad (5.169)$$

where $F_{iA}^S(x, Q^2)$; ($i = 1 - 3, 5$) is the nuclear structure function with shadowing effect and the factor $\delta R(x, Q^2)$ is given in Ref. [684].

The expression for $F_{iA}(x, Q^2)$, ($i = 1, 2, 5$) in the full theoretical model is given by

$$F_{iA}(x, Q^2) = F_{iA,N}(x, Q^2) + F_{iA,\pi}(x, Q^2) + F_{iA,\rho}(x, Q^2) + F_{iA}^S(x, Q^2), \quad (5.170)$$

where $F_{iA,N}(x, Q^2)$ is the structure function with only the hole spectral function which takes care of Fermi motion, binding energy and nucleon correlations. Through $F_{iA,\pi(\rho)}(x, Q^2)$ pion(rho) meson cloud contributions have been included and the shadowing effect is incorporated by using $F_{iA}^{WI,S}(x, Q^2)$. The final expression for $F_{3A}(x, Q^2)$ is given by

$$F_{3A}(x, Q^2) = F_{3A,N}(x, Q^2) + F_{3A,shd}(x, Q^2). \quad (5.171)$$

In view of $F_{4N}(x, Q^2)$ being very small as it vanishes in the leading order and contributes only due to higher order corrections we have evaluated $F_{4A}(x, Q^2)$ using only the spectral function and therefore write

$$F_{4A}(x, Q^2) = F_{4A,N}(x, Q^2). \quad (5.172)$$

For $F_{5A}(x, Q^2)$, the Albright-Jarlskog relation is used.

5.8.6. Phenomenological approach to understand NME in DIS

The phenomenological studies of nuclear parton distribution functions (nPDFs) are broadly based on the analysis of experimental data on charged lepton-nucleus DIS, Drell-Yan processes with π and p and neutrino-nucleus DIS, etc. Several studies have been made to understand nPDFs [704, 705, 706, 707, 708, 709, 710, 711, 712, 713, 714, 715, 716, 717, 718, 719, 720, 721, 722, 723, 724]. In these studies, the approaches which have been used are the following:

- In the first approach used by Eskola et al. [704, 705, 711], Hirai et al. [707] and de Florian and Sassot [708] mainly the charged lepton-nucleus and Drell-Yan proton-nucleus scattering data (for detail see Table 5.8) have been used. In this approach a set of free nucleon PDFs given by any standard parameterization available in literature is taken to calculate the free proton ($f_i^p(x, Q_0)$) and free neutron ($f_i^n(x, Q_0)$) structure functions. Then using some global fitting techniques the nuclear correction factors are found and that is multiplied with the free nucleon PDFs to provide agreement with the nuclear experimental data. The free nucleon PDFs multiplied with this nuclear correction factor $R_i^A(x_i, Q_0)$ give nuclear PDFs F_2^A and F_3^A , i.e.,

$$F_{2,3}^A(x, Q) = R_i(x, Q, A) F_{2,3}^N(x, Q).$$

In an analysis de Florian et al. [716] also included ν -A DIS data in their analysis along with l -A, p -A, d -A data and reported that there is no conflict between the nuclear modification of the l^\pm -A DIS and ν -A DIS data.

Phenomenological group	data type used
EKS98 [704, 705]	$l+A$ DIS, $p+A$ DY
HKM [706]	$l+A$ DIS
HKN04 [707]	$l+A$ DIS, $p+A$ DY
nDS [708]	$l+A$ DIS, $p+A$ DY
EKPS [709]	$l+A$ DIS, $p+A$ DY
HKN07 [710]	$l+A$ DIS, $p+A$ DY
EPS08 [709]	$l+A$ DIS, $p+A$ DY, h^\pm, π^0, π^\pm in $d+Au$
EPS09 [711]	$l+A$ DIS, $p+A$ DY, π^0 in $d+Au$
EPPS16 [712]	$l+A$ and $\nu+A$ DIS, $p+A$ and $\pi - A$ DY, $d - A$, and LHC proton-lead collisions data
nCTEQ [713, 714]	$l+A$ DIS, $p+A$ DY
nCTEQ [715]	$l+A$ and $\nu+A$ DIS, $p+A$ DY
DSSZ [716]	$l+A$ and $\nu+A$ DIS, $p+A$ DY, π^0, π^\pm in $d+Au$, computed with nFFs
TUJU21 [717]	$l+A$ and $\nu+A$ DIS, data for W^\pm and Z^0 boson production in $p + Pb$
KSASG20 [718]	$l+A$ and $\nu+A$ DIS, $p+A$ DY
nNNPDF2.0 [719]	NC DIS and CC $\nu_l - A$ DIS, data for W^\pm and Z^0 boson production in $p + Pb$

Table 5.8: The developments in the global DGLAP analysis of nPDFs since 1998. DY = Drell-Yan dilepton production; nFFS = nuclear fragmentation functions [720].

- In the second approach the nCTEQ group [715] have obtained F_2^A and F_3^A by analyzing charged lepton-A DIS data and DY $p-A$ data sets, and $\nu(\bar{\nu})-A$ DIS data sets separately. In the nCTEQ framework [721], the parton distributions of the nucleus are constructed as:

$$F_i^{(A,Z)}(x, Q) = \frac{Z}{A} F_i^{p/A}(x, Q) + \frac{A-Z}{A} F_i^{n/A}(x, Q), \quad (5.173)$$

Isospin symmetry is used to construct the PDFs of a neutron in the nucleus, $F_i^{n/A}(x, Q)$, by exchanging up- and down-quark distributions from those of the proton. The observation of nCTEQ group from this analysis is that F_2^A in electromagnetic interaction is different in nature than F_2^A in weak interaction in some regions of Bjorken x . Thus the results in these two approaches are not in complete agreement with each other [716, 715].

In Fig. 5.37, taken from Ref. [713], the results for the nuclear correction factors for $F_2^{\nu A}$ and $F_2^{\bar{\nu} A}$ are shown at $Q^2 = 5$ and 20 GeV^2 obtained from the various groups, such as Hirai et al. [707, 710] who have used phenomenological analysis of experimental data from lepton-nucleus and Drell-Yan experiments, the results of Kulagin and Petti [684, 669, 725] obtained in a theoretical model using spectral function, the SLAC/NMC [703] curve obtained from an A and Q^2 independent parameterization of calcium and iron charged lepton DIS data [703], and the phenomenological analysis of CTEQ group [715]. From the figure, it may be noticed that the nuclear correction factor has large variation and the present phenomenological results do differ among themselves and particularly from the analysis of CTEQ group [715]. It may be noticed that the results of CTEQ analysis do not show shadowing at low Q^2 , while the correction factor shows the antishadowing shifts towards lower values of x . Furthermore, CTEQ results of the nuclear correction factor has also been found to be smaller than those obtained from charged lepton nucleus scattering data as well as obtained in the theoretical study of Kulagin and Petti [669, 684]. Recently, using the nCTEQ framework, this group has included more neutrino data and made a comparative analysis of $l^\pm - A$ and $\nu_l/\bar{\nu}_l - A$ DIS cross sections and obtained the nuclear correction factor [726]. In their work [726], the global analysis used to extract the nuclear PDFs is based on the nCTEQ15WZSIH analysis which incorporates the charged lepton DIS data, LHC W and Z boson production data and single inclusive hadron production data from RHIC and LHC. Furthermore, nCTEQ collaboration [726] has also incorporated the deuteron corrections by using the CJ15 analysis while determining the fitted nPDFs which are labeled as nCTEQ15WZSIHdeut. In order to study the compatibility between the $l^\pm - A$ and $\nu_l/\bar{\nu}_l - A$ data they have compared the results of nuclear structure function ratios obtained by using the nCTEQ15WZSIHdeut analysis to the results obtained by using the

- DimuNeu analysis, based on inclusive and semi-inclusive neutrino data only from CDHSW, CCFR, NuTeV and CHORUS experiments.
- BaseDimuNeu analysis, based on inclusive neutrino and charged lepton data along with the other data sets incorporated in nCTEQ15WZSIHdeut analysis.

In Fig. 5.38, the ratios are presented for $\frac{F_2^{l^\pm A}}{F_2^D}$ (top panel), $R[F_2] = \frac{F_2^{(\nu A + \bar{\nu} A)}}{f_2^p + f_2^n}$ (middle panel) and $R[F_3] = \frac{F_3^{(\nu A + \bar{\nu} A)}}{f_3^p + f_3^n}$ (bottom panel) at $Q^2 = 8 \text{ GeV}^2$, where $A = {}^{56}\text{Fe}$ is the nuclear target and $f_i^{p/n}$; ($i = 2, 3$) are the free proton/neutron structure functions. These authors [726] included the deuteron corrections in F_2^D , while obtaining the ratio for $\frac{F_2^{l^\pm A}}{F_2^D}$, however,

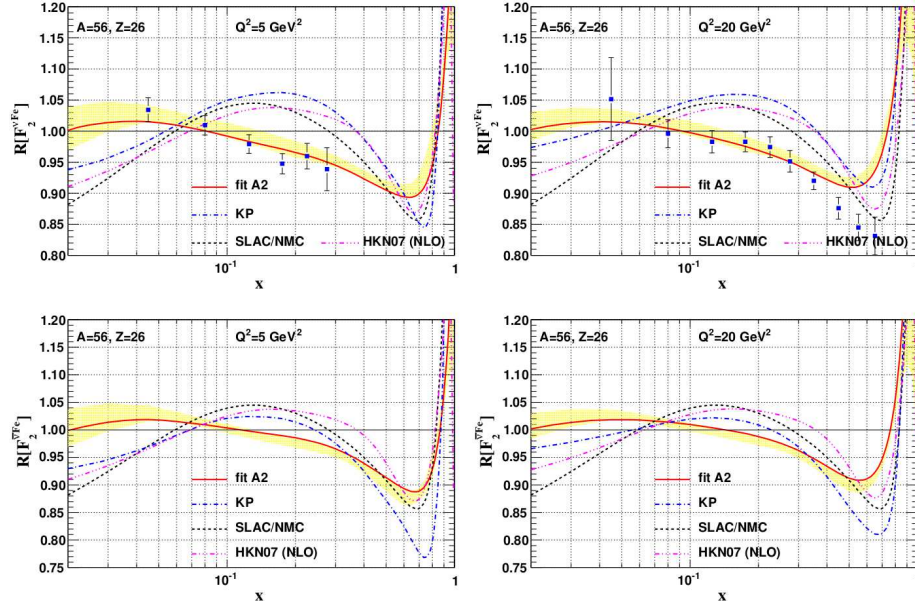


Figure 5.37: Nuclear correction factor R for the structure function F_2 in CC νFe scattering at a) $Q^2 = 5 \text{ GeV}^2$ and b) $Q^2 = 20 \text{ GeV}^2$. The solid curve shows the result of the nCTEQ analysis of NuTeV differential cross sections (labeled fit A2), divided by the results obtained with the reference fit (free-proton) PDFs; the uncertainty from the A2 fit is represented by the yellow band. Plotted also are NuTeV data points of the average F_2 to illustrate the consistency of the fit with the input points. For comparison the correction factor from the Kulagin–Petti (KP) model [725] (dashed-dotted line), Hirai et al. fit [710] (double-dashed-dotted line), and the SLAC/NMC parameterization (dashed line) of the charged-lepton nuclear correction factor are also shown. We compute this for $\{A = 56, Z = 26\}$. Figure has been taken from [713].

these corrections are absent in the case of $R[F_2]$ and $R[F_3]$. It may be observed from the figure that the predictions of the nCTEQ15WZSIHdeut and the DimuNeu analyses are incompatible with each other. The predictions from BaseDimuNeu for $l^\pm - A$ are compatible up to 1σ level with the results from nCTEQ15WZSIHdeut, however it is incompatible for $\nu_l/\bar{\nu}_l - A$ at $x = 0.025$. It is important to notice that the tension in the case of (anti)neutrino observables is larger as compared to the charged lepton case. One may notice similar observations while comparing the predictions from the BaseDimuNeu and DimuNeu analyses. These results are also compared with the corresponding experimental data from SLAC, NuTeV and CDHSW. The tension between $l^\pm - A$ and $\nu_l/\bar{\nu}_l - A$ data sets observed from Fig. 5.38 requires more study to understand NME in neutrino and antineutrino reactions on nuclear targets.

5.8.7. Isoscalarity correction

For heavy nuclear targets, where the number of neutrons is greater than the number of protons $N > Z$, the isoscalarity corrections become important. Hence, it is required to study the effect of the corrections arising due to neutron excess on nuclear structure functions for a given nuclear target by treating it to be isoscalar ($N = Z$) as well as nonisoscalar ($N \neq Z$). These corrections are phenomenologically taken into account by multiplying the results by a correction factor R_A^{Iso} defined as

$$R_A^{Iso} = \frac{[\sigma^{\nu/\bar{\nu}p} + \sigma^{\nu/\bar{\nu}n}]/2}{[Z\sigma^{\nu/\bar{\nu}p} + (A-Z)\sigma^{\nu/\bar{\nu}n}]/A} = \frac{[F_2^{\nu/\bar{\nu}p} + F_2^{\nu/\bar{\nu}n}]/2}{[ZF_2^{\nu/\bar{\nu}p} + (A-Z)F_2^{\nu/\bar{\nu}n}]/A}, \quad (5.174)$$

where $F_2^{\nu/\bar{\nu}p,n}$ and $\sigma^{\nu/\bar{\nu}p,n}$ are, respectively, the weak structure functions and scattering cross sections for proton and neutron.

While in the Aligarh-Valencia model isoscalarity corrections have been taken in an entirely different way by separately normalizing the hole spectral function for the proton (Eq. (5.156)) and neutron (Eq. (5.157)) numbers for a nonisoscalar nuclear target, and to the nucleon numbers for an isoscalar nuclear target (Eq. (5.152)) as discussed in Sec. 5.8.2 and it has been observed that these two different prescriptions (Eq. (5.174), and using Eqs. (5.156) and (5.157)) give different isoscalarity correction effect, which has been discussed in Ref [10].

5.8.8. Results and discussion

Before applying the formalism to understand NME in weak interaction induced processes, Aligarh-Valencia group applied their formalism to the electromagnetic interaction induced processes [400, 675, 683].

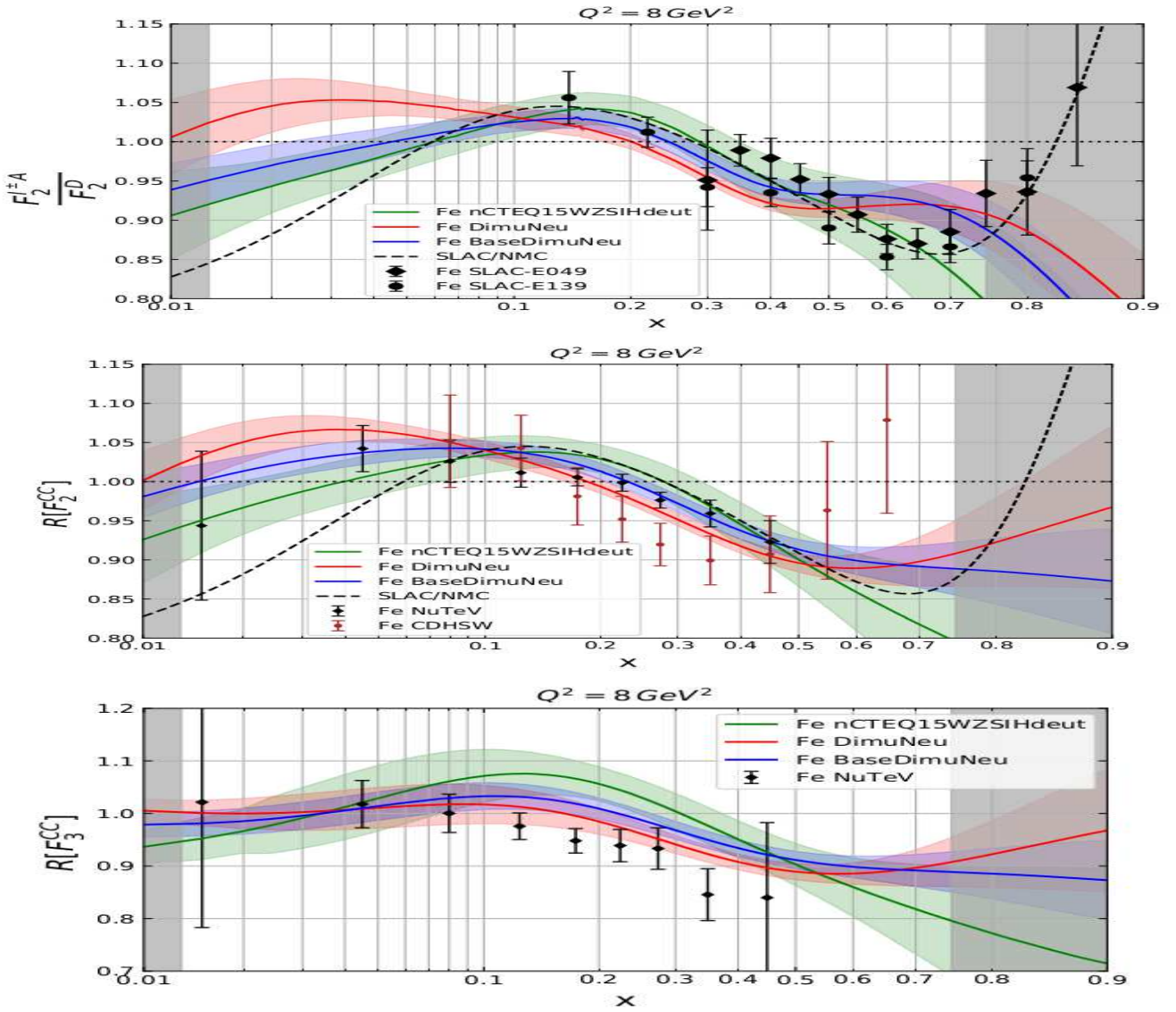


Figure 5.38: $R^{\pm A} = \frac{F_2^{\pm A}}{F_2^D}$ and $R(\nu A + \bar{\nu} A) = \frac{F_i^{\nu A + \bar{\nu} A}}{f_i^p + f_i^n}$; ($i = 2, 3$) using the fitted nuclear PDFs, i.e., nCTEQ15WZSIHdeut [726]. F_2^D includes the deuteron correction factor and f_i^p and f_i^n are the free proton and neutron structure functions. This figure is taken from Ref. [726] (courtesy Jorge G. Morfin).

The numerical results are presented for the nuclear structure functions $F_{2A}^{EM}(x, Q^2)$, $F_{2A}^{WI}(x, Q^2)$ and $F_{3A}^{WI}(x, Q^2)$ calculated in the Aligarh-Valencia model and compared with the experimental results. In case of $F_{2A}^{EM}(x, Q^2)$ where ample data are available in several nuclear targets for a wide range of x and Q^2 , the results are presented in Fig. 5.39 for some of the nuclear targets like ^{12}C , ^{27}Al , ^{56}Fe and ^{63}Cu which are obtained using the MMHT nucleonic PDFs at NNLO by incorporating the target mass corrections as discussed in Section 4. These results for $F_{2A}^{EM}(x, Q^2)$ vs x , at the different values of Q^2 ($\approx 2 - 4 \text{ GeV}^2$) are compared with the experimental observations of JLab [727]. The theoretical results are presented for the spectral function only (SF) and for the full model (total) which includes the shadowing and mesonic cloud contributions. The results obtained in the full model get enhanced due to mesonic effect which is significant in the region of low and intermediate x . For example, at $Q^2 \simeq 3 \text{ GeV}^2$ this enhancement in carbon is found to be 23% at $x = 0.1$, 21% at $x = 0.2$ and 10% at $x = 0.4$ while in copper it becomes 32% at $x = 0.1$, $\sim 29\%$ at $x = 0.2$ and 13% at $x = 0.4$. It may be noticed that the mesonic cloud contributions decreases with the increase in x . However, it becomes more pronounced for the heavier nuclear targets. It may be noticed from the figure that our theoretical results show a good agreement with the experimental data [727] in the region of intermediate x , however, for $x > 0.6$ and $Q^2 \approx 2 \text{ GeV}^2$ they slightly underestimate the experimental results. One should remember that the region of high x and low Q^2 is the transition region of nucleon resonance excitations and DIS, therefore, the theoretical results are expected to underestimate the experimental data as the theoretical results do not include the resonance contribution. However, with the increase in Q^2 , theoretical results show better agreement with the experimental observations of JLab [727] in the entire range of x .

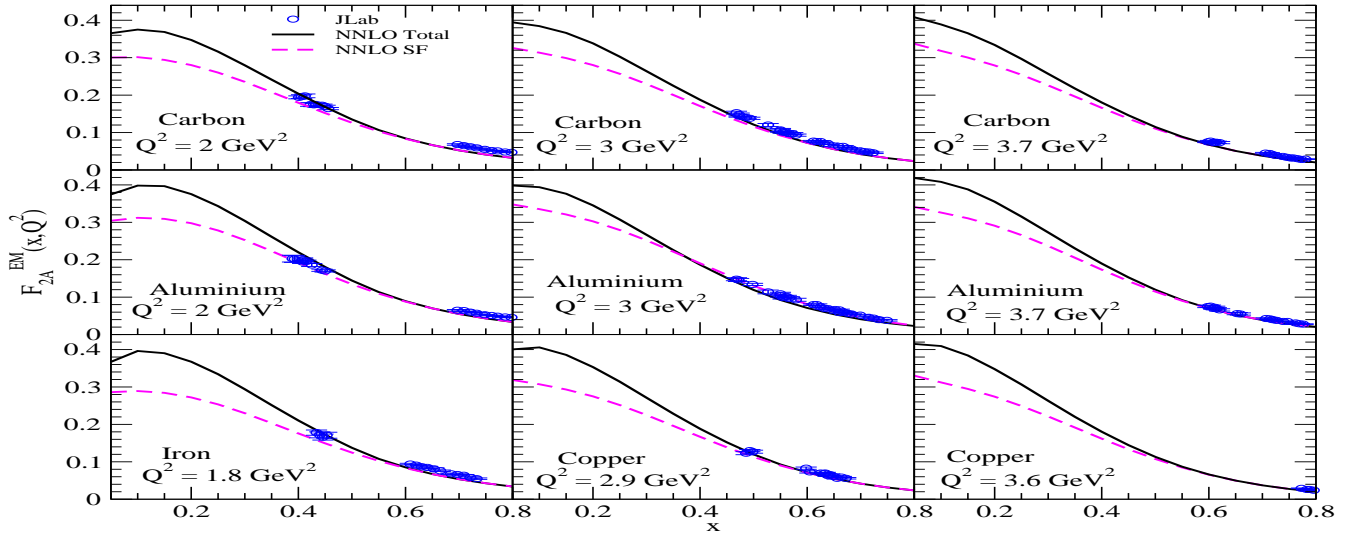


Figure 5.39: $F_{2A}^{EM}(x, Q^2)$ ($A = {}^{12}\text{C}$, ${}^{27}\text{Al}$, ${}^{56}\text{Fe}$ and ${}^{63}\text{Cu}$) vs x are shown at different Q^2 . The results are obtained for the spectral function only (dashed line) and for the full model (solid line) with TMC effect using MMHT nucleonic PDFs at NNLO. The results are compared with the experimental data of JLab [727] (empty circles). For the numerical calculations MMHT PDFs parameterization [371] has been used.

In Fig. 5.40, the results are presented for $F_{2A}^{WI}(x, Q^2)$ vs x for ${}^{12}\text{C}$, ${}^{56}\text{Fe}$ and ${}^{208}\text{Pb}$, for the isoscalar nuclear targets, at the different values of Q^2 relevant for the current neutrino experiments. From the figure, it may be observed that the mesonic contributions result in an enhancement in the nuclear structure functions and is significant in the low and intermediate region of x . Moreover, the effect is more pronounced at low Q^2 , which becomes larger with the increase in mass number A . For example, in comparison to the total contributions (solid line) in carbon, the mesonic contribution at $x = 0.1$ is found to be 24% in iron which increases to 33% in lead. With the increase in x (say $x = 0.4$), the enhancement due to the mesonic contributions reduces to 13% and 18% respectively and becomes almost negligible for $x \geq 0.6$ at $Q^2 = 2 \text{ GeV}^2$. To depict the coherent nuclear effects (shadowing) which results in suppression of the structure functions at low x , the results without shadowing are shown with the double-dash-dotted line, and with the increase in mass number of the nuclear target (${}^{56}\text{Fe}$ vs ${}^{208}\text{Pb}$), the strength of suppression becomes larger in the region of low x .

In Fig. 5.41, we present a comparison of the results for the electromagnetic ($F_{2A}^{EM}(x, Q^2)$) and weak ($(F_{2A}^{Weak}(x, Q^2))$) nuclear structure functions vs x in iron nucleus for a wide range of Q^2 viz. $1.5 < Q^2 < 55 \text{ GeV}^2$ using the full model at NLO. The numerical calculations are performed using the CTEQ6.6 nucleonic PDFs parameterization [369]. The theoretical results for weak nuclear structure functions (dashed line) are scaled by a factor of $\frac{5}{18}$ (see Eq. (4.32)) in order to make it comparable with the results from the electromagnetic interaction channel (solid line). These results are also compared with the available charged lepton-nucleus scattering data from the JLab [727], EMC [728] and SLAC [636, 665, 729, 730] experiments as well as with the (anti)neutrino-nucleus data from CDHSW [382], CCFR [381] and NuTeV [387] collaborations. The theoretical results of nuclear structure functions in Fig. 5.41 are shown by the band for the above mentioned range of Q^2 . We have observed that the present results are consistent with the CCFR [381], JLab [727], NuTeV [387] data at medium and high values of Q^2 but not in good agreement at low Q^2 with the older experiments like CDHSW [382] and EMC [728]. In the inset of the figure, we have shown the curves for the two different values of Q^2 viz. $Q^2 = 1.5 \text{ GeV}^2$ and $Q^2 = 50 \text{ GeV}^2$ up to $x \leq 0.1$. One may observe that at low x , EM nuclear structure function is slightly lower than the weak nuclear structure function which is about $\sim 4\%$ in iron at $x = 0.1$, and the difference decreases with the increase in x and almost becomes negligible for $x > 0.3$. We find that (not shown here) with the increase in mass number this difference increases. For example, in ${}^{208}\text{Pb}$ it becomes $\sim 7\%$ while for low mass nuclei like carbon this difference decreases to $\sim 1 - 2\%$ at $x = 0.1$.

In Figs. 5.42, the theoretical predictions for ν -Fe and ν -Pb deep inelastic differential scattering cross sections of the Aligarh-Valencia group as well as the predictions using the phenomenological approach of nCTEQnu nuclear PDFs are presented at $E_\nu = 35 \text{ GeV}$ relevant for the MINERvA experiment. The results of Aligarh-Valencia group are shown using only the spectral function as well as using the full model (Eqs. (5.170) and (5.171)). It can be observed that the mesonic contributions play important role in the region of $x \leq 0.5$. Comparing the two approaches for ν_l scattering, the nCTEQnu-based results are somewhat lower than the theoretical prediction from Aligarh-Valencia group at the low x , while the results of the two approaches are in reasonable agreement with each other in the region of higher x . Similar observations have been made for antineutrino induced scattering on these nuclear targets which have been discussed in Ref. [152].

The MINERvA experiment at the Fermilab is studying NME in several nuclear targets like carbon, hydrocarbon, water, iron and lead for a wide range of Bjorken x and Q^2 , and have recently presented the results for the ratio of

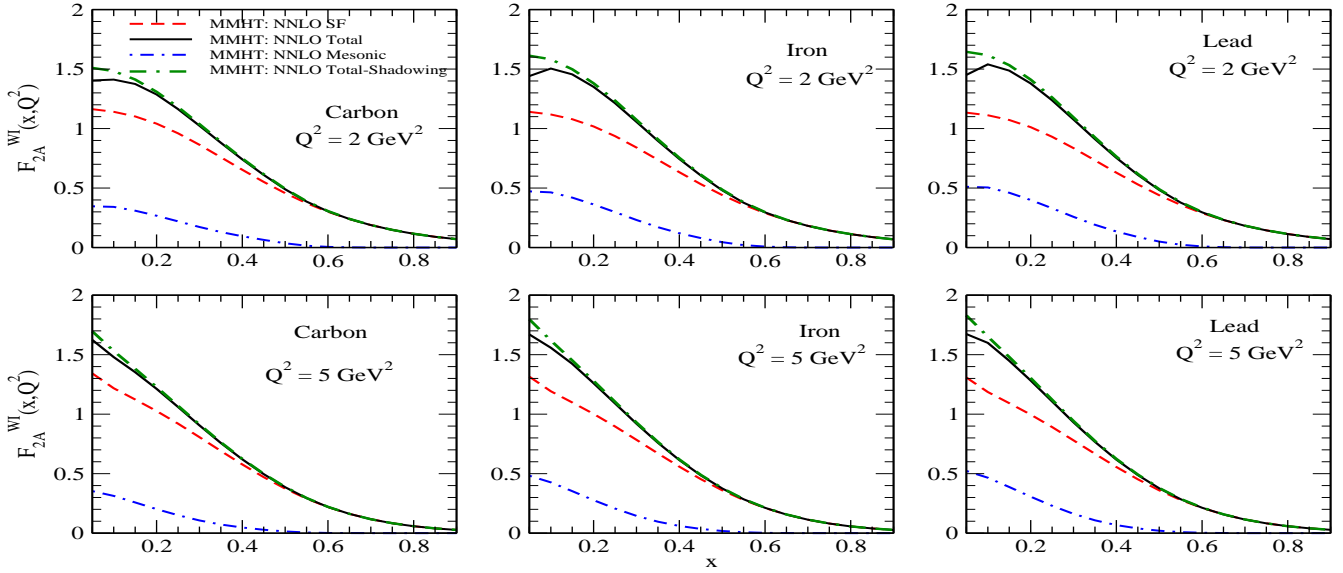


Figure 5.40: Results are shown for the weak nuclear structure function $F_{2A}^{WI}(x, Q^2)$ vs x at $Q^2 = 2, 5 \text{ GeV}^2$, in ^{12}C , ^{56}Fe and ^{208}Pb for (i) only the spectral function (dashed line), (ii) only the mesonic contribution (dash-dotted line) using Eq. (5.164), (iii) the full calculation (solid line) using Eq. (5.170) and (iv) the double dash-dotted line is the result without the shadowing and antishadowing effects. The numerical calculations have been performed at NNLO using the MMHT [371] nucleon PDFs parameterizations.

differential cross section in several nuclear targets [647]. In Fig. 5.43, we show the results for the ratio $(\frac{d\sigma_{Fe}^{WI}/dx}{d\sigma_{CH}^{WI}/dx})$ vs x in the case of $\nu_l(\bar{\nu}_l) - A$ DIS scattering for ^{56}Fe and ^{208}Pb which are summarized below:

- The deviation of the ratio from unity is significant in iron as well as in lead although it is comparatively smaller in $\frac{d\sigma_{Fe}^{WI}/dx}{d\sigma_{CH}^{WI}/dx}$ than in $\frac{d\sigma_{Pb}^{WI}/dx}{d\sigma_{CH}^{WI}/dx}$. This reflects the A dependence of NME in which the contribution of mesons increases with A at low and intermediate x . For example, at $E = 25 \text{ GeV}$ the contribution of mesons is found to be 9%(~ 7%) at $x = 0.1$ and 1%(1%) at $x = 0.3$ in lead(iron). It is important to notice that even for high energy neutrino beams the effect of nuclear medium on the differential scattering cross section are significant.
- To quantify the mass dependence, the difference between the results of $\frac{d\sigma_{Fe}^{WI}/dx}{d\sigma_{CH}^{WI}/dx}$ and $\frac{d\sigma_{Pb}^{WI}/dx}{d\sigma_{CH}^{WI}/dx}$ obtained by using the full model at $E = 25 \text{ GeV}$ (solid line) has been found to be $\simeq 5\%$ at $x = 0.05$, 4% at $x = 0.1$ and $\sim 7\%$ at $x = 0.6$.

- The isoscalarity correction is found to be significant. For example, it has been found that at $E = 25 \text{ GeV}$, this effect is 2%(5%), and 5%(13%) at $x = 0.3$ and 0.7, respectively, in iron(lead) when no kinematical cut is applied on W .

In a recent MINERvA analyses for ν_μ induced CC inclusive scattering process off hydrocarbon target, the results for the differential cross sections as a function of lepton kinematics like the longitudinal and transverse momenta of muons have been reported by Filkins et al. [645] at $\langle E_\nu \rangle = 3.5 \text{ GeV}$ and by Ruterbories et al. [646] at $\langle E_\nu \rangle \sim 6 \text{ GeV}$, where they have compared the results from MINERvA experiment with the results from the theoretical model developed by Aligarh-Valencia group (labeled as AMU DIS) [677, 401, 675] and also with the phenomenological results of nCTEQ15 [721], Cloet et al. [731] and nCTEQnu [732]. Here we will only discuss the results of Ref. [646] for the ratio of DIS cross sections from different DIS models employing the kinematic constrain $W \geq 2.0 \text{ GeV}/c^2$ and $Q^2 \geq 1.0 \text{ GeV}^2/c^4$ to the MINERvA's simulated results (labeled as MINERvA tune v1) [646] which are shown in Fig. 5.44. From the figure, it may be noticed that although the theoretical predictions [675] and the phenomenological results [721, 732] show reasonable agreement among themselves but none of them are able to completely explain the MINERvA's experimental data in the entire range of the charged lepton momentum.

- The energy dependence of the scattering cross section has also been shown by comparing the numerical results which are obtained by using the full model with $Q^2 > 1 \text{ GeV}^2$ and $W > 2 \text{ GeV}$ at $E = 25 \text{ GeV}$ (solid line with star) with the corresponding results obtained at $E = 7 \text{ GeV}$ (double dash-dotted line). It may be observed that in the region of low and intermediate x the results for the ratio of $\frac{d\sigma_{Fe}^{WI}/dx}{d\sigma_{CH}^{WI}/dx}$ at $E = 7 \text{ GeV}$ are smaller in magnitude from the results at $E = 25 \text{ GeV}$, however, with the increase in x the ratio $\frac{d\sigma_{Fe}^{WI}/dx}{d\sigma_{CH}^{WI}/dx}$ obtained for $E = 7 \text{ GeV}$ increases. While moving towards $E = 25 \text{ GeV}$ from $E = 7 \text{ GeV}$, we have observed that there is a difference of about 3%(~ 5%), ~ 2%(2%) and 10%(16%) at $x = 0.1$, $x = 0.3$ and $x = 0.75$, respectively in iron(lead).

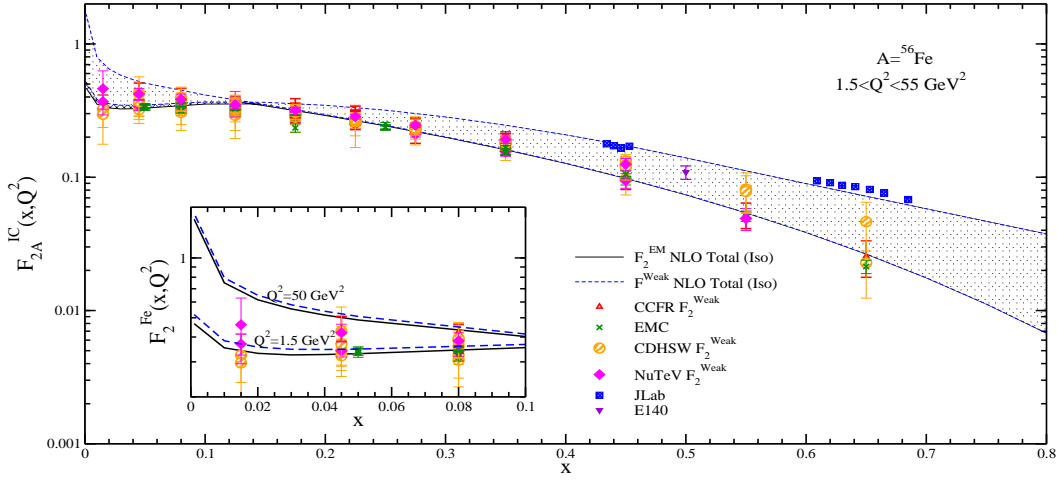


Figure 5.41: Results of EM and Weak nuclear structure functions in ^{56}Fe obtained with the full theoretical model at NLO are shown. The results of F_2^{Weak} are scaled by a factor of $\frac{5}{18}$. The results are also compared with the experimental data of Refs. [381, 382, 387, 727, 728]. For the numerical calculations CTEQ6.6 PDFs parameterization [369] has been used.

- It may be noticed that MINERvA's experimental data have large error bars which is due to the statistical uncertainties and the wide band around the simulation results is due to the systematic errors which shows an uncertainty up to $\sim 20\%$ [647]. The present numerical results have been compared with the MINERvA's experimental data, simulated results as well as with the results of Cloet et al. [731] (solid line with circle), Bodek et al. [156] (solid line with square) and the GENIE MC generator [541] (solid line with triangle). It may be observed that neither the theoretical predictions nor the phenomenological results are able to satisfactorily describe the observed ratios of the differential cross sections in the entire region of Bjorken x .
- The NME in $\frac{d\sigma_A^{WI}}{dx}$ for $\bar{\nu}_l - A$ scattering (Fig. 5.43, bottom panel) are found to be qualitatively similar to $\nu_l - A$ scattering when no cut on CM energy is applied, however, quantitatively they are different specially at low and mid values of x . For example, at $E = 7$ GeV the enhancement in the cross section when full calculation is applied vs. using the cross section results with spectral function only is about 24% at $x = 0.25$ in $\nu_l - ^{208}\text{Pb}$ scattering, while it is 65% in $\bar{\nu}_l - ^{208}\text{Pb}$ scattering, and the difference in the two results (full calculation vs. SF only) decreases with the increase in x . At $E = 25$ GeV the enhancement in the cross section is about 20% at $x = 0.25$ in $\nu_l - ^{208}\text{Pb}$ scattering, while it is $\sim 45\%$ in $\bar{\nu}_l - ^{208}\text{Pb}$ scattering.
- When a cut of 2 GeV is applied on the CM energy W , then a suppression in the region of low and mid x is observed in the $\bar{\nu}_l - A$ differential cross section, resulting in a lesser enhancement due to mesonic effects. For example, at $E = 25$ GeV, the enhancement due to the mesonic contributions becomes $\sim 18\%$ (vs 20% without cut) in $\nu_l - ^{208}\text{Pb}$ scattering while $\sim 28\%$ (vs 45% without cut) in $\bar{\nu}_l - ^{208}\text{Pb}$ scattering at $x = 0.25$. At $E = 7$ GeV, with a cut of 2 GeV on W , the enhancement is about 2% at $x = 0.25$ in $\nu_l - ^{208}\text{Pb}$ scattering, while there is reduction in $\bar{\nu}_l - A$ scattering, implying small contribution from the mesonic part. This reduction in $\frac{d\sigma_A^{WI}}{dx}$ for $\bar{\nu}_l - A$ scattering is about 15% in a wide region of $x(\leq 0.6)$.

6. Quark-hadron duality in ν_l scattering

QCD is the theory which describes strong interactions in terms of quarks and gluons with remarkable features of asymptotic freedom at high energies (E) and Q^2 and confinement at low energies and Q^2 . At low E and Q^2 , the effective degrees of freedom to describe strong interactions are the mesons and nucleons using effective Lagrangian motivated by the symmetry properties of QCD while at high E and Q^2 , the quark and gluon degrees of freedom are used to describe the strong interactions using perturbative QCD. In the case of lepton scattering processes induced by charged leptons and (anti)neutrinos on nucleons and nuclei, the inclusive cross sections at low energy are dominated by the QE (CC induced) and elastic (NC induced) scattering processes but as the energy increases beyond 1 GeV, the inclusive cross sections are expressed in terms of the structure functions corresponding to the excitation of various resonances like Δ , N^* , etc., lying in the first or higher resonance regions depending on W of the final hadrons. On the other hand, at high energy and Q^2 , the inclusive cross sections are expressed in terms of the structure functions corresponding to DIS processes. In the intermediate energy region corresponding to the transition between resonance excitations and DIS, we are yet to find a method best suited to describe the inclusive lepton scattering.

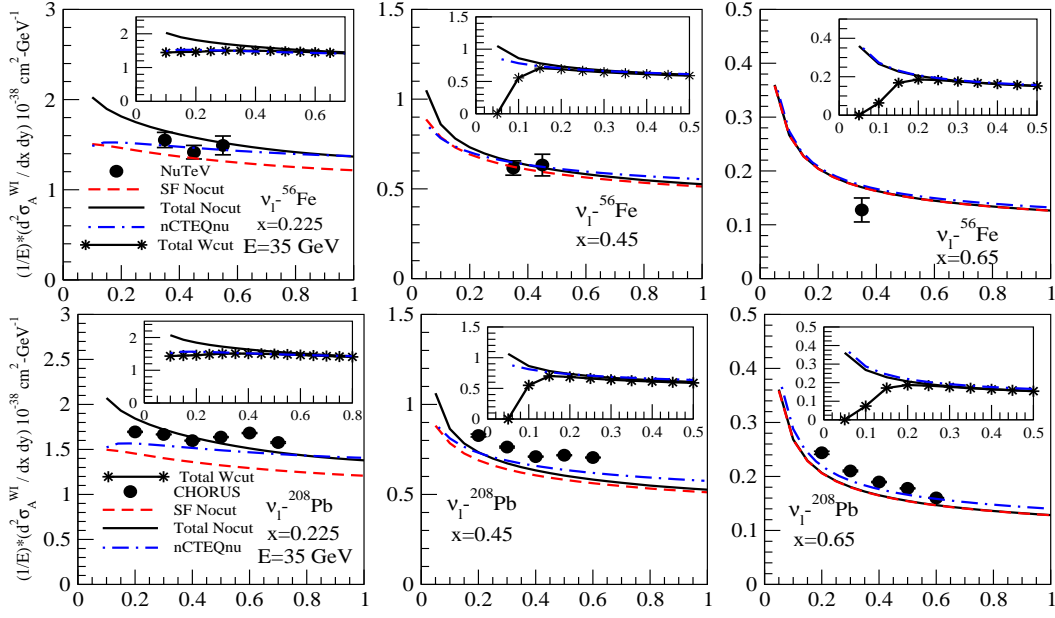


Figure 5.42: Differential cross section vs y , for the different values of x for $\nu_\mu - Fe$ (top row) and $\nu_\mu - Pb$ (bottom row) DIS. Theoretical predictions are shown with the spectral function only (dashed line) and with the full model (solid line) at NNLO. In the inset are effects of an additional kinematical cut of $W \geq 2$ GeV (solid line with star) for the full theoretical model are shown. The blue dash-dotted line in the top row is the result from nCTEQnu nPDFs with $Q^2 \geq 1.0$ GeV². Solid circles with error bars are the limited experimental data points of NuTeV at this lower energy.

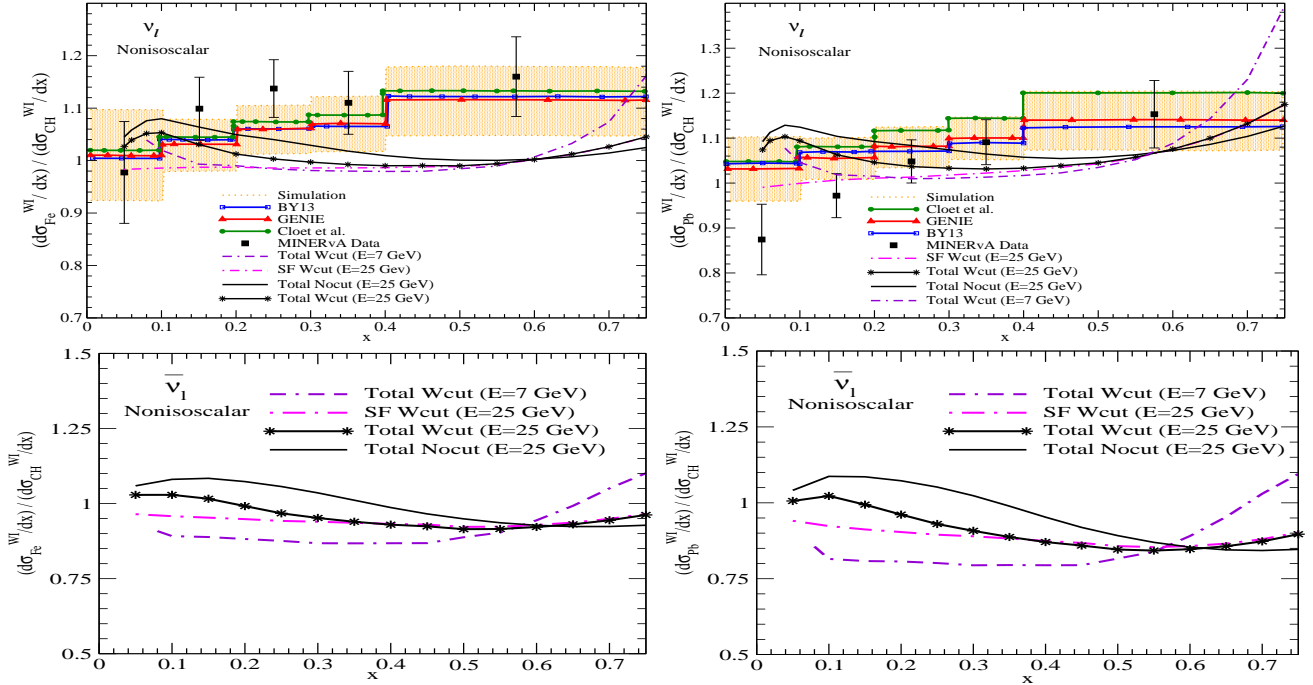


Figure 5.43: $\frac{d\sigma_A^I}{d\sigma_{CH}^I} (A = {}^{56}\text{Fe}, {}^{208}\text{Pb})$ vs x for incoming neutrino (top panel) and antineutrino (bottom panel) beam of energies $E = 7$ GeV and 25 GeV. The numerical results are obtained with the spectral function only (dash-dotted line: $E = 25$ GeV) as well as with the full model (solid line: $E = 25$ GeV, solid line with star: $E = 25$ GeV and double dash-dotted line: $E = 7$ GeV) at NNLO and are compared with the phenomenological results of Cloet et al. [731], Bodek-Yang [156], GENIE Monte Carlo [541] and with the simulated results [647]. The solid squares are the experimental points of MINERvA [647]. The results are shown for the nonisoscalar nuclear targets.

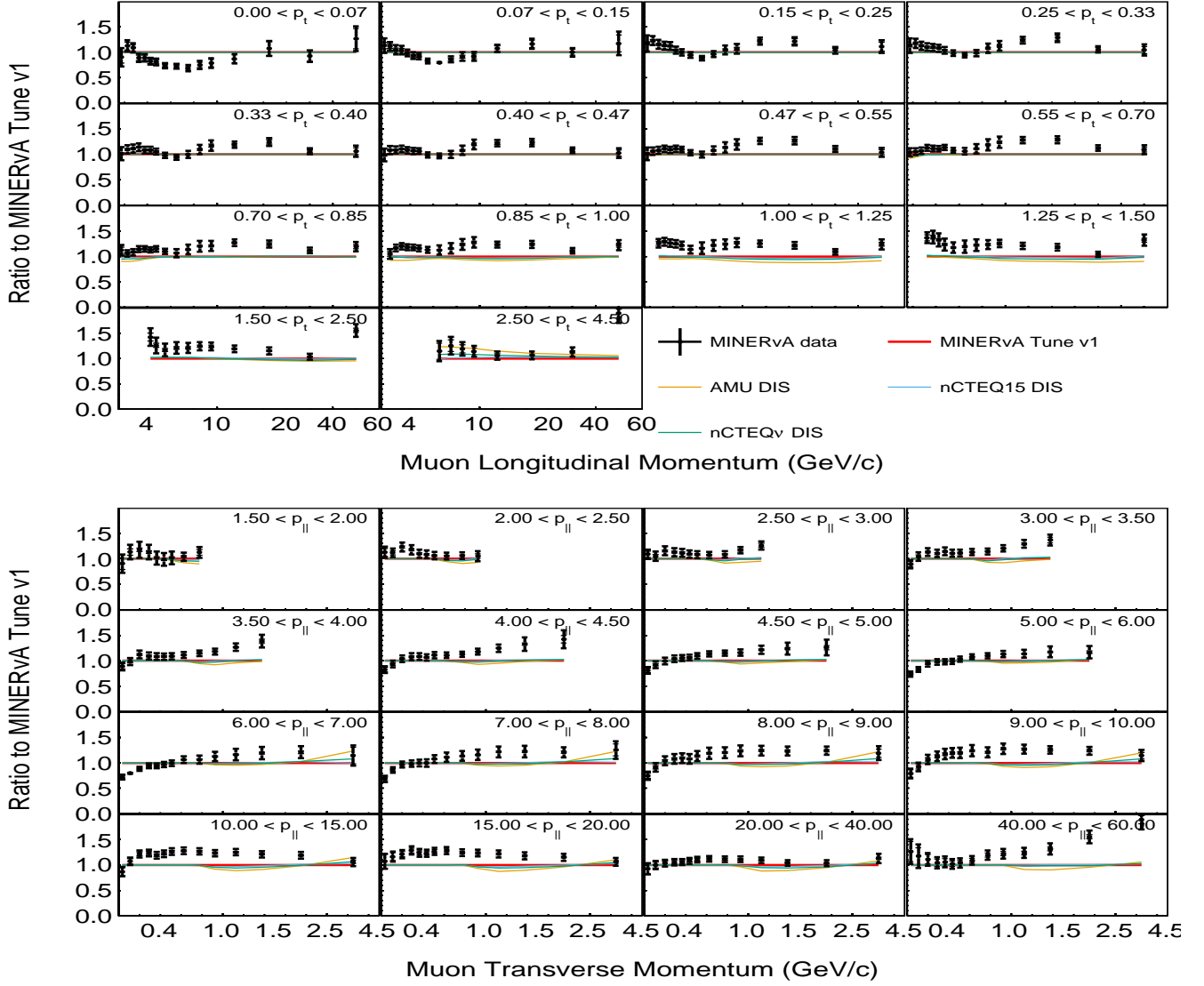


Figure 5.44: The scattering cross section ratio from different DIS models to MINERvA's simulated results [646].

The phenomenon of Quark-Hadron (QH) duality in electron scattering from proton was first observed at SLAC by Bloom and Gilman [733, 734] more than fifty years ago, and provides a connection between the low energy and the high energy description of electron-proton scattering. They found a connection between the structure function $\nu W_2(\nu, Q^2)$ in the nucleon resonance region and that in the deep inelastic continuum. QH duality states that the structure functions in low Q^2 region of resonance excitation suitably averaged over an energy interval is the same as the structure function at high Q^2 region corresponding to the DIS in the same energy interval. At the basic level it may be understood as the equality between two integrals

$$\int_{\xi_{min}}^{\xi_{max}} d\xi F^{\text{Res}}(\xi, Q_{\text{Res}}^2) \approx \int_{\xi_{min}}^{\xi_{max}} d\xi F^{\text{DIS}}(\xi, Q_{\text{DIS}}^2), \quad (6.1)$$

where F^{Res} and F^{DIS} represent the structure functions in the resonance and the DIS regions, respectively, and ξ is the Nachtmann variable and its minimum and maximum values depend upon the choice of W . Generally the minimum value of W is taken to be pion production threshold i.e. $W_{min} = M + m_\pi$, while the maximum value of W may vary from 1.6 GeV to 2.2 GeV.

Therefore, the QH-duality implies that the average over resonance structure functions produced in the inclusive eN scattering has a close resemblance with the scaling structure functions measured in the DIS region and with the increase in Q^2 the average over resonance structure functions approaches the asymptotic scaling structure functions. In other words, it establishes a connection between the quark-gluon description of $e - p$ scattering at high Q^2 in the region of DIS with the hadronic description of the same phenomenon at low Q^2 in the region of resonance excitations. This seems to be valid in each resonance region individually as well as in the entire resonance region when the structure functions are summed over higher resonances. This is termed as local duality. When the phenomenon of the local QH duality is also observed in

the case of higher moments of structure functions in electron-nucleus scattering, it is termed as the global duality, which was observed in early Jefferson Lab measurement (E94-110) [735] for $Q^2 \geq 0.5 \text{ GeV}^2$, as can be seen in Fig. 6.1, with resonances following the extrapolated DIS curve i.e. the DIS scaling curve extrapolated down into the resonance region passes through the average of the peaks and valleys of the resonance structure. This implies a connection between the behavior of the resonance excitations and DIS which ultimately signals that there is perhaps a common origin in terms of a point-like structure for both resonance and DIS interactions.

It is also observed that the ratio of resonance peak to background remains almost constant as Q^2 is varied from low to high Q^2 . It is conjectured that there may exist two component duality where the resonance contribution and the background contribution to the structure functions in the resonance excitation region corresponds respectively to the valence quarks and sea quarks contribution in structure functions in the DIS region. This has been tested at JLab [736] for $e - N$ interaction where it has been found that F_2 structure function averaged over resonances at low values of ξ behaves like the valence quark contribution obtained from the DIS with scaling. However, these observations are to be verified by model calculations as well as by the further experimental data when they become available with higher precision. The phenomenon of local duality and global duality has been observed in JLab, NMC and other experiments on electron nucleon and electron nucleus scattering [737].

Melnitchouk et al. [737] have compiled and analyzed the experimental data of the structure function $F_2(x)$ above $W^2 = 1.2 \text{ GeV}^2$ for hydrogen, deuterium and iron targets for $0.5 \leq Q^2 \leq 7 \text{ GeV}^2$ which are shown in Fig. 6.2. The solid line is the curves obtained by them, which represents $F_2(x)$ scaling curve for the nucleon that is corrected for the known nuclear medium modifications to the structure function and have been obtained using the GRV PDFs parameterization [362]. They observed that in the case of proton, the resonance structure is clearly visible and $F_2(x)$ is seen to oscillate around the scaling curve, however, for the deuterium, the resonances become less pronounced, and in iron further diminishing. In the middle panel of the figure, the prominent peak for the deuterium data is identified as the contribution from the Δ resonance and follows the scaling curve similar to those observed for the proton. However, the other resonance peaks are smeared (deuteron vs proton) so much as to be indistinguishable from the scaling structure function. Moreover, in iron it has been observed that even the QE peak is washed out by the smearing at higher Q^2 , and scaling is seen at all values of ξ and the resonance region becomes indistinguishable from the scaling regime.

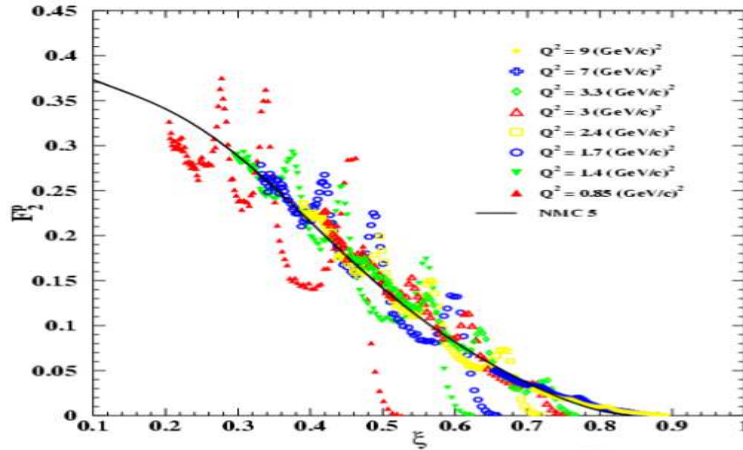


Figure 6.1: Comparison of F_2^p from the series of resonances measured by E94-110 [735] vs the Nachtmann variable ξ at the indicated Q^2 compared to the extrapolated DIS measurement from the NMC collaboration at 5 GeV^2 . Figure has been taken from Ref. [736].

Presently the different experimental observations obtained from the charged-lepton scattering results in the following features of the QH duality [737, 738]:

- the resonance excitation structure functions data oscillate around the scaling DIS structure functions data
- the resonance excitation structure functions data are on an average equivalent to the DIS structure functions data
- the resonance excitation structure functions data move towards the DIS structure functions data with the increase in Q^2 .

More experimental data with high precision are needed even for the inclusive electron-nucleon and electron-nucleus scattering, for a wide range of ξ and Q^2 and using the different nuclear targets, before the validity of QH-duality can be established conclusively in $e - N$ scattering. For sure with its verification, the description of lepton-nucleon and lepton-nucleus scattering over the entire SIS region will become much easier.

The (anti)neutrino-nucleus scattering in the energy region of SIS is currently an important topic to be explored both theoretically and experimentally as the accelerator and atmospheric neutrino experiments have significant contribution

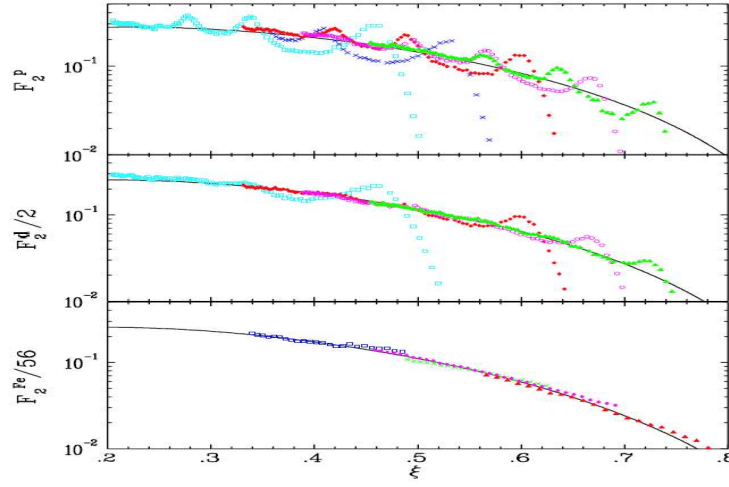


Figure 6.2: Comparison of F_2 structure function per nucleon for proton, deuteron and iron targets. The curves are GRV parameterization [362] at $Q^2 = 1 \text{ GeV}^2$, corrected for the nuclear EMC effect. Figure has been taken from Ref. [737].

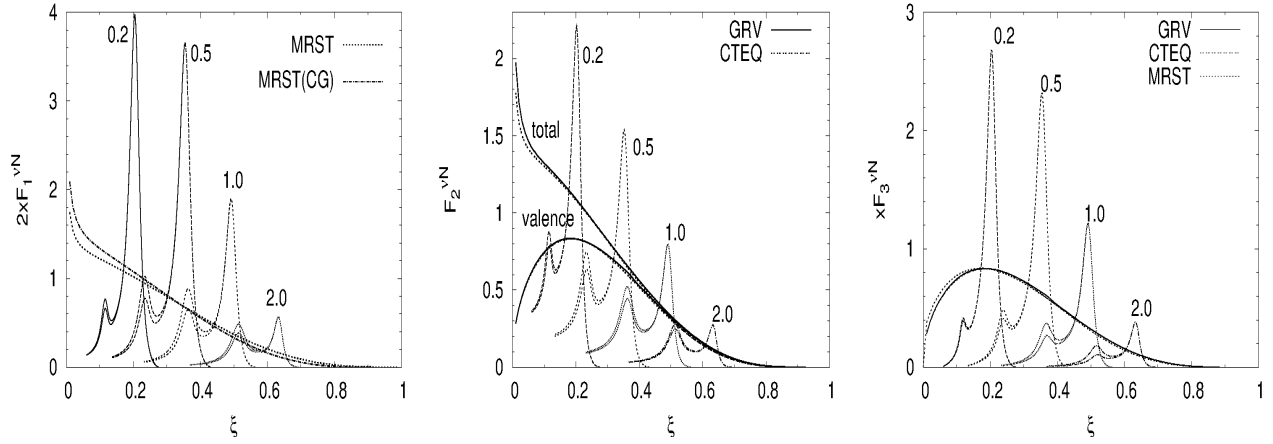


Figure 6.3: Duality for the neutrino-nucleon $F_1^{\nu-N}$, $2xF_2^{\nu-N}$ and $xF_3^{\nu-N}$ structure functions as a function of ξ at different Q^2 . Figure has been taken from Ref. [740].

from the few GeV energy region corresponding to the kinematic region of resonance excitations and DIS. The validity of QH duality in CC and NC sectors of weak interaction may provide a way to obtain (anti)neutrino-nucleon and (anti)neutrino-nucleus scattering cross sections in the transition region where either the use of effective Lagrangian or the quark-parton description is not adequate. More importantly, if duality does hold for neutrino-nucleon interactions then it would be possible to extrapolate the better-known neutrino DIS structure into the SIS region and give an indication of how well current event simulators are modeling the (anti)neutrino-nucleus cross sections in the SIS region.

Since the experimental data available from the hydrogen and deuterium bubble chamber experiments from the 70's and 80's for the resonance production in ν -N scattering lack the level of precision of the electron-nucleus scattering, the experimental study of duality in neutrino-nucleon scattering is not conclusive. Moreover, due to dearth of experimental data on ν -A scattering above the Δ resonance in the SIS region, the study of QH duality in the transition region is also very limited. Recently, the phenomenon of QH duality has been experimentally observed in the NC sector through the observation of parity violating asymmetry in the scattering of polarized electron from proton and deuteron targets at JLab [739]. Theoretically not much progress has been made except the early works of Lalakulich et al. [738, 740], Sato et al. [288] and Gross et al. [741]. This has also limited the development of the neutrino event generators as the modern ν interaction simulation efforts are not able to compare their results with the duality predictions for ν -N and ν -A interaction events in the transition region.

It has been argued by Close and Melnitchouk [742] that the isospin symmetry constraints the QH duality not to hold locally for protons and neutrons separately even if one includes several resonances with both even and odd parities as the neutrino interaction on the proton target and the antineutrino interaction on the neutron target in the few GeV energy region is dominated by the different charged states of $\Delta(1232)$ resonance which has been discussed here in detail in Section 3.4. For example, neutrino-proton structure functions are three times larger than the neutrino-neutron

structure functions and therefore resonance structure functions are significantly larger than the leading twist functions i.e. $F_i^{\nu p(\text{Res})} > F_i^{\nu p(\text{LT})}$. This clearly indicates the violation of QH-duality for neutrino interaction on a proton target. Similarly for a neutrino-neutron scattering besides the contribution from the isospin $\frac{3}{2}$ resonances, there is also significant contribution from the isospin $\frac{1}{2}$ resonances, but the total contribution from isospin $\frac{1}{2}$ resonances is smaller than that from isospin $\frac{3}{2}$ resonances due to $\Delta(1232)$ dominance which results $F_i^{\nu n(\text{Res})} < F_i^{\nu n(\text{LT})}$. Thus QH-duality is also not valid for $\nu - n$ scattering.

Therefore, one considers duality for the average of proton and neutron structure functions. This has been studied by Lalakulich et al. [740] in neutrino-nucleon scattering as well as in neutrino-nucleus interactions [738] and they find that for an isoscalar nucleon target duality holds, which has been shown in Fig. 6.3 for the neutrino-nucleon $F_1^{\nu N}$, $2xF_2^{\nu N}$ and $xF_3^{\nu N}$ structure functions at several values of Q^2 . It may be observed that for νN scattering duality holds good for F_2 and F_3 and not so well for F_1 .

Geissen-Ghent collaboration [738] have studied Bloom-Gilman duality, in electron and neutrino scattering on nuclei, and found that the ratio

$$I(Q_{\text{Res}}^2, Q_{\text{DIS}}^2) = \frac{\int_{\xi_{\min}}^{\xi_{\max}} d\xi F_j^{\text{Res}}(\xi, Q_{\text{Res}}^2)}{\int_{\xi_{\min}}^{\xi_{\max}} d\xi F_j^{\text{DIS}}(\xi, Q_{\text{DIS}}^2)} < 1, \quad (6.2)$$

where F_j represents $2xF_1$, F_2 , and xF_3 , and Res (DIS) represent resonance (DIS) structure functions at the same ξ . This collaboration [738] has emphasized the importance of including NR as well as resonance contributions while evaluating the numerator in Eq. (6.2).

To conclude, the study of QH duality needs serious attention especially by the neutrino physics community as a substantial contribution to the events is expected to come from the transition region for all the next generation planned accelerator and atmospheric neutrino experiments.

7. Monte Carlo event generators and some of the recent results from the accelerator experiments

Monte Carlo event generators are scientific programs/libraries to simulate events for the neutrino interactions with matter (electrons, nucleons and nuclei). In the neutrino sector, the early event generators were NEUGEN [743], NUANCE [333], NUX [744], NEUT [745, 746] and Geneve [747]. These were initially developed by the experimenters to simulate events for a particular experiment. For example, the earliest version of the NEUGEN event generator was written for the Soudan 2 experiment, in the mid-1980's, to simulate the neutrino backgrounds in the proton decay searches. In the earlier version of NUANCE and NEUGEN, to simulate neutrino interactions with the nuclear targets, Smith and Moniz model was used for the QE scattering from nuclei, Rein and Sehgal model was used for the resonance excitation, and for the DIS, the NME like the shadowing, anti-shadowing, Fermi motion and EMC were not considered. Later with the need of more sophisticated and robust event generators, several collaborative projects were started which led to the amalgamation of theorists, phenomenologists as well as experimenters in the development of the neutrino event generators. The recent Monte Carlo generators widely used in the accelerator and atmospheric neutrino experiments are GENIE [541, 416], NEUT [745, 746], NuWro [543], GiBUU [579], FLUKA [748], etc., which are updated regularly by the respective developers.

There are now provisions of alternative nuclear models for the QE scattering like the Smith and Moniz Fermi gas model, LFGM of the Valencia group, Superscaling model of the Donnelly group, more sophisticated models to take into account many body nucleon correlation effects like the inclusion of 2p-2h effect using either the formalism of Martini et al. [507, 508, 509, 510] or Nieves et al. [511, 749], and the final state interaction effects, etc.

Most of these modern generators (GENIE, NEUT, NuWro) have common inputs. However, the differences in their implementation, the value of the parameters used, and the approaches to avoid double counting yield different predictions. For example, in the earlier version of GENIE, the QE scattering is modeled using the relativistic Fermi gas model of Llewellyn Smith, for the baryon resonance excitations in NC and CC channels Rein and Sehgal model is used in which 16 resonances were considered and DIS is calculated using Bodek and Yang prescription. Recent version of GENIE 3 uses different models of NME for the QE neutrino induced processes like LFGM of the Valencia group with 1p-1h and 2p-2h excitations [511, 749], Superscaling approach ($1p-1h+2p-2h$) of Donnelly et al. [750], etc., GENIE is widely being used by experimenters involved in the Fermilab neutrino program like MINERvA, NOvA, MicroBooNE collaborations. These MC generators have now become essential in analyzing the neutrino events as they make use of the latest developments in nuclear theory to the description of $\nu - A$ interaction cross sections.

NEUT was developed initially by the Kamiokande collaborators to simulate atmospheric neutrino events, it is now being used by the Super-Kamiokande as well as the T2K collaborations and is continuously being updated. One among the many revised versions, NEUT version 5.3.2 describes CCQE neutrino-nucleon interactions using the spectral function (SF) approach of Benhar et al. [751] with $M_A = 1.21\text{GeV}$. The resonant pion production process is described by the Rein-Sehgal model [157] with updated nucleon-resonance transition form factors [752] and $M_A^{\text{Res}} = 0.95\text{GeV}$. For the 2p-2h interactions,

they have used the microscopic model developed by Nieves et al. [511]. DIS is modeled using GRV98 PDFs [362] with the corrections by Bodek and Yang [753]. The final state interactions describing the transport of the hadrons produced in the elementary neutrino interaction through the nucleus, are simulated using a semi-classical intranuclear cascade model.

GiBUU [754] has been developed by Mosel and his collaborators at Giessen, and uses local Thomas-Fermi gas in a mean field potential for the QE scattering, for the resonances it uses MAID analysis of electron-nucleon pion production as input for the vector part of both the resonant and NR amplitudes. It is a transport model where FSI is implemented by solving Giessen Boltzmann-Uehling-Uhlenbeck (GiBUU) equation. It encompasses a unified framework for hadron, lepton and neutrino interactions with nuclei from a few hundreds of MeV to a few tens of GeV. In recent years, tuned generators like MINERvA tune [755], MicroBooNE tune [756, 757], etc. have been used, where modifications are made in the GENIE or other versions of the generators. For example, it was found by the MINERvA collaboration [755], that the model of Nieves et al. [511], underestimates the 2p-2h strength in the dip region and therefore they increased the flux-folded strength by a significant amount. For a general discussion, see Ref. [758].

Recently the T2K collaboration [759] plotted the ratio of the double differential cross section per nucleon for ν_μ induced CC reaction for oxygen to carbon nuclear targets i.e. $R_{\mathcal{O}}$ (which has been shown in Fig. 7.1 for the two muon angle bins), and compared their data with the simulated results from the MC generators like NEUT 5.4.1 LFG, GENIE v3- SuSAv2, NuWro SF, GiBUU, NEUT 5.4.0 SF, GENIE v3 LFG, NuWro LFG and RMF (1p-1h) + SuSAv2 (2p-2h). They have also presented the results for the integrated cross sections per nucleon and compared them with the MC predictions [759].

ArgoNeuT collaboration [760] has reported the CC $\nu_\mu(\bar{\nu}_\mu)$ induced $1\pi^+(\pi^-)$ differential cross sections on ^{40}Ar and compared their results with the MC generators, which are presented in Fig. 7.2. The data for the pion angular distribution and the muon angular distribution obtained by the ArgoNeuT collaboration has been shown, where the comparisons with the different MCs like GENIE v2_12_2, NuWro 17.01.1, GiBUU and NEUT5.3.7 have also been made [760].

To highlight the difference among the predictions of the various MCs as well as their comparison with the data, in Fig. 7.3, we present an analysis of the MINERvA collaboration where they have shown absolute normalized ratios of data, and the comparison with the GENIE 2.8.4, NuWro, and GiBUU to MnvGENIEv1 for muon transverse (p_T) and longitudinal (p_L) momenta. It may be observed from Fig. 7.3 that the transverse momentum projection shows tension among all models and data in the $0.55 < p_T < 1.5$ GeV range. While in the case of longitudinal momentum, all models underpredict the cross section.

In Fig. 7.4, we show the recent results of the MicroBooNE collaboration [756], for the total cross section divided by the bin-center neutrino energy vs neutrino energy i.e. $\frac{\sigma(E_{\nu\mu})}{\langle E_{\nu\mu} \rangle}$ vs $E_{\nu\mu}$. These results are compared with the MicroBooNE MC [757], predictions from GENIE v3.0.6 [541, 416], NuWro 19.02.01 [761], NEUT 5.4.0.1 [746], and GiBUU 2019.08 [754].

It may be observed from the above results that there is agreement among the different MC generators with the data nevertheless more work is needed to understand medium effects in the nuclear targets. It needs more collaborative efforts.

8. Summary and outlook

The physics of neutrino interactions with matter has many aspects both in theory and experiment. This is because the neutrinos play very significant role in various areas of physics i.e. astrophysics, cosmology, nuclear physics, particle physics and geophysics. The neutrino physics originated with the attempts to understand the nuclear β decays which led to the discovery of weak interactions and its role in astrophysical processes of energy generation in stars, synthesis of elements, supernova explosions, and the formation of neutron stars and white dwarfs, etc. With the discovery of new particles and their weak decays, the neutrino physics became an important component of particle physics both theoretically and experimentally. The advent of high energy particle accelerators which produced unstable mesons like pions and kaons leading to the neutrino beams of $\nu_\mu(\bar{\nu}_\mu)$ and $\nu_e(\bar{\nu}_e)$ as their decay products, started the era of $\nu_l(\bar{\nu}_l)$ scattering from the nucleons and nuclei in various energy regions starting from MeV to GeV which was earlier restricted to the very low energy region of (anti)neutrinos in the region of a few tens of MeV corresponding to the reactor antineutrinos. The processes of (anti)neutrino-nucleon scattering being a weak process has small cross section and therefore requires intense (anti)neutrino beams and large volume target-detectors to enhance the (anti)neutrino induced production of charged leptons, mesons and photon events to make them statistically significant for physical interpretations. The requirement of large volume target-detectors necessitated the use of medium or heavy nuclear material as targets to perform the (anti)neutrino scattering. This led to various neutrino-nucleus experiments being done at CERN, ANL, BNL, Fermilab, and SKAT using high energy neutrino beams. The confirmation of the phenomenon of neutrino flavor oscillations with the solar neutrinos and reactor antineutrinos in the low energy region and with the accelerator and atmospheric neutrinos in the intermediate and high energy regions has started great interest in studying the (anti)neutrino-nucleus scattering in the entire energy region of (anti)neutrino spectrum. Moreover, the study of these processes in the very low energy region is of immense interest in various astrophysical processes, while in the very high energy region, they are relevant for studying the origin of cosmic rays.

In view of this, we have presented a review of the (anti)neutrino reactions with nucleons and nuclei in this work.

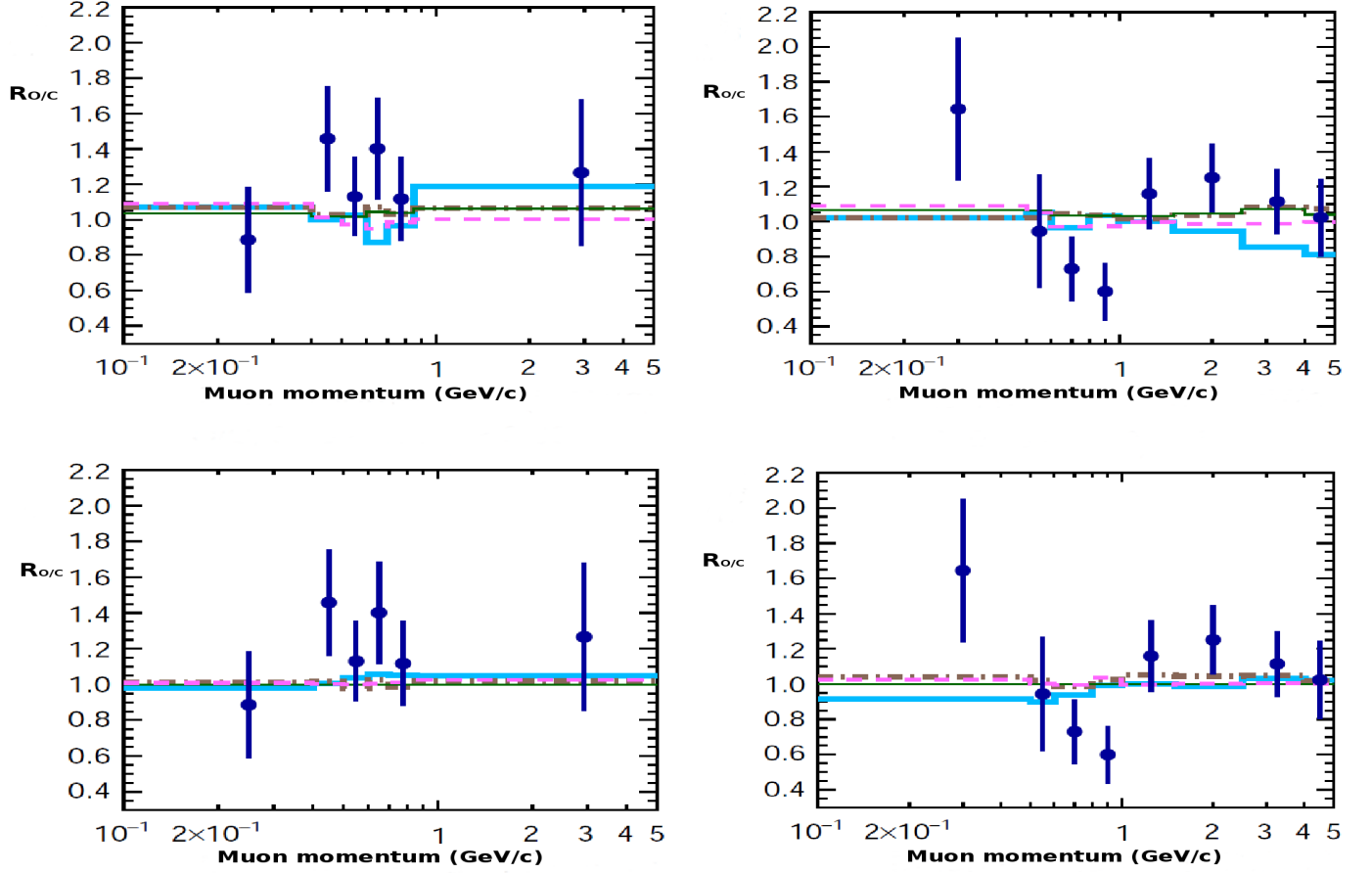


Figure 7.1: Ratio of the double differential cross section per nucleon for ν_μ induced CC reaction in oxygen and carbon i.e. $R_{O/C}$. T2K collaboration [759] has compared their data with (upper panel) NEUT 5.4.1 LFG (brown), GENIE v3- SuSAv2 (green), NuWro SF (magenta) and GiBUU (light blue) MC predictions. The left panel is for the muon angle bin $0.75 < \cos \theta_\mu < 0.86$ and the right panel is for $0.93 < \cos \theta_\mu < 1$. The lower panel is the same comparison with other MC generators like NEUT 5.4.0 SF (brown), GENIE v3 LFG (green), NuWro LFG (magenta) and RMF (1p1h) + SuSAv2 (2p2h) (light blue). This figure has been taken from Ref. [759].

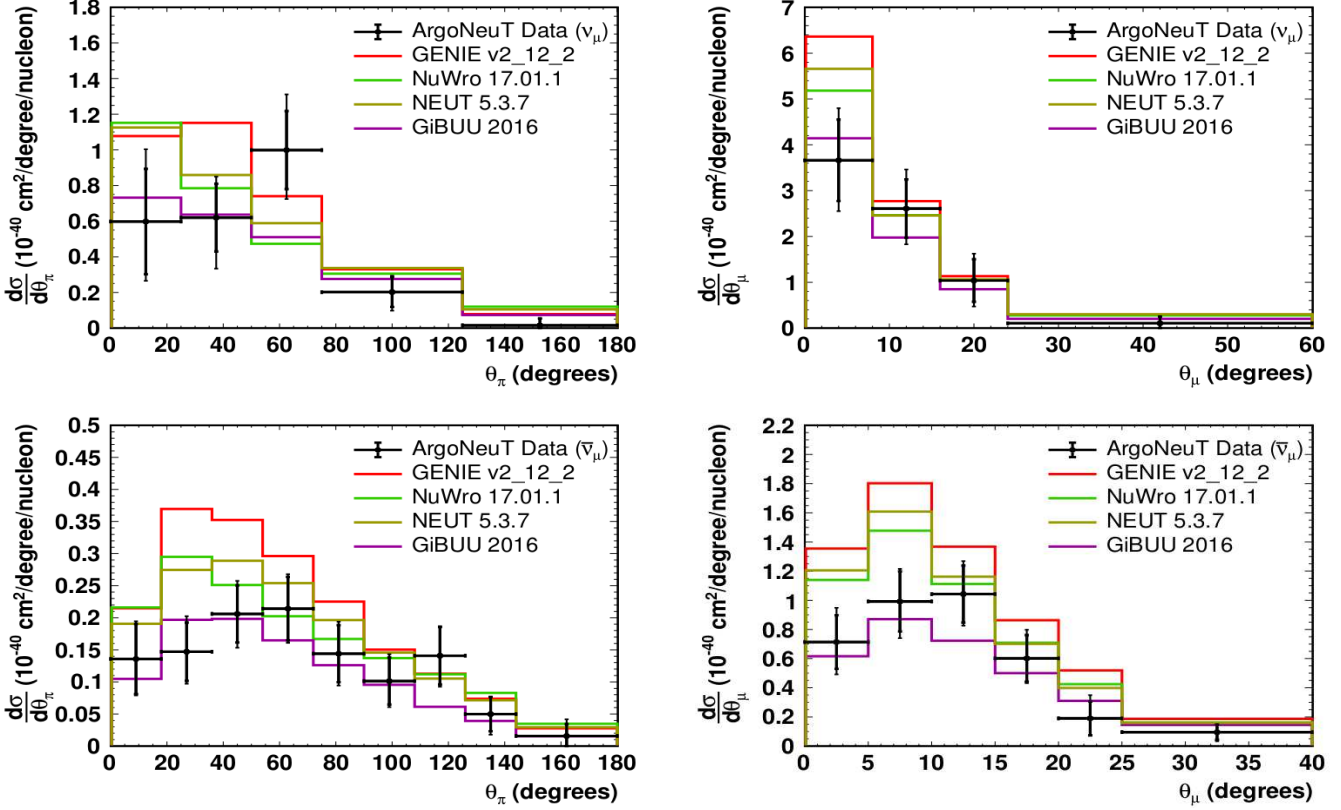


Figure 7.2: ArgoNeuT CC $\nu_\mu(\bar{\nu}_\mu)$ induced $1\pi^+$ (upper panel) and $1\pi^-$ (lower panel) differential cross sections on ^{40}Ar . Left panel is for pion angular distribution i.e. the outgoing pion angle (θ_π) w.r.t. the initial neutrino direction and the right panel is for muon angular distribution i.e. the outgoing muon angle (θ_μ) w.r.t. the initial neutrino direction. Comparisons are with the different MCs like GENIE v2_12_2 [541], NuWro 17.01.1 [543], GiBUU 2016 [579] and NEUT 5.3.7 [746]. This figure has been taken from Ref. [760].

After presenting an updated summary of the neutrino properties and its sources from natural and man made origin in Section 1, we describe briefly the SM of neutrino interactions and apply it to study the (anti)neutrino scattering from point particles like leptons and quarks in this section. In this context, the resonance scattering of neutrinos from electrons and the observation of Glashow resonance in very high energy region is discussed. In Section 2, we apply the SM to study the various (anti)neutrino reactions on nucleons like QE (elastic) scattering induced by CC (NC) weak interactions, IE production of mesons like π, K, η and hyperons like $\Lambda, \Sigma^0, \Sigma^-, \Xi^-, \Xi^0$ followed by the DIS in the region of very high energy and Q^2 corresponding to Bjorken scaling. In this region, QPM is used in the leading order of perturbative QCD to obtain results for the nucleon structure functions and the scattering cross sections. The effect of the evolution of structure functions to lower Q^2 in NLO and other corrections like TMC and HT are also discussed.

In the case of QE scattering induced by charged weak currents, the matrix element is described in terms of three vector $f_i(Q^2)$ and three axial-vector $g_i(Q^2)$ ($i = 1, 2, 3$) form factors, which are all real due to T-invariance. Using the isotriplet and CVC hypotheses, the vector form factors $f_1(Q^2)$ and $f_2(Q^2)$ are related with the Sachs' electric ($G_E^{p,n}(Q^2)$) and magnetic ($G_M^{p,n}(Q^2)$) form factors of the nucleon, and $f_3(Q^2) = 0$. The axial vector form factor $g_1(Q^2)$ at $Q^2 = 0$ is derived in terms of $g_{NN\pi}$, the pion nucleon coupling constant and f_π , the pion decay constant using PCAC and GT relation. The pseudoscalar form factor $g_3(Q^2)$ is related to $g_1(Q^2)$ with the help of the PPDAC. The principle of $G(= Ce^{i\pi I_2})$ invariance has been used to set $g_2(Q^2) = f_3(Q^2) = 0$. The Q^2 dependence of both the vector (axial-vector) form factors is parameterized by a dipole form using the dipole mass M_V (M_A) where the phenomenological values of M_V and M_A obtained from the analysis of electron and neutrino scattering experiments have been used. In the case of vector form factors, some recent parameterizations used in the analysis of electron scattering have also been used. With these inputs, the theoretical formulation of various QE reactions are studied in the strangeness conserving $\Delta S = 0$ sector for ν_l and $\bar{\nu}_l$ scattering, and in the strangeness changing $\Delta S = 1$ sector for $\bar{\nu}_l$ scattering. In the $\Delta S = 1$ sector where the hyperons $Y = \Lambda, \Sigma^{0(-)}$ are produced, $SU(3)$ symmetry has been used to obtain the $N - Y$ transition form factors. The numerical results are presented for:

- (i) The differential scattering cross section $\frac{d\sigma}{dQ^2}$, total scattering cross section $\sigma(E)$ and various components of the hadron polarizations P_L^h, P_T^h, P_P^h and the lepton polarizations P_L^l, P_T^l, P_P^l , where the subscripts L, T and P refer to the longitudinal, transverse and perpendicular components of the polarization vector and $h = N, Y(= \Lambda, \Sigma^{0(-)})$ and $l = \mu$ and τ .

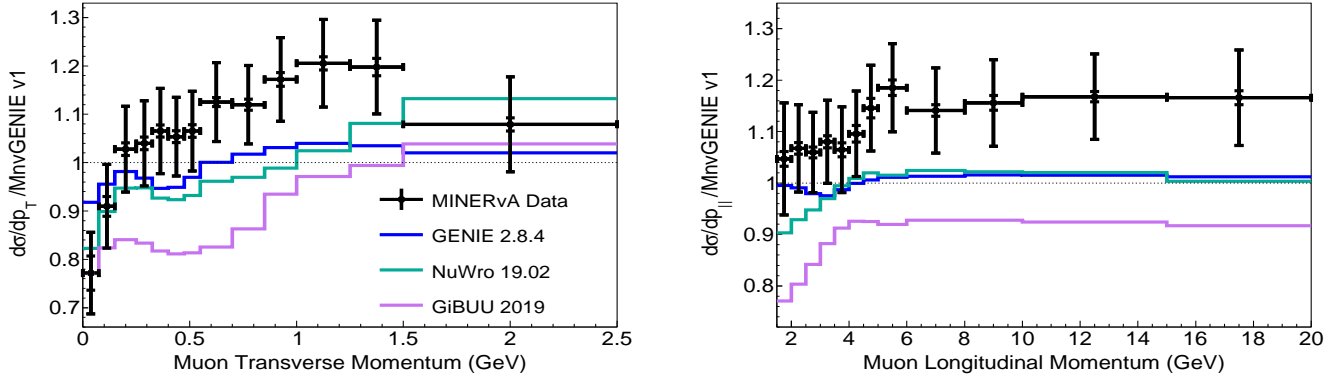


Figure 7.3: MINERvA inclusive CC differential cross sections for muon neutrinos on hydrocarbon in terms of the transverse and longitudinal muon momentum distributions [645]. The ratio is for absolutely normalized ratios of data, GENIE 2.8.4 [541], NuWro [543], and GiBUU [754] to MnvGENIEv1 [645] for p_T and p_L .

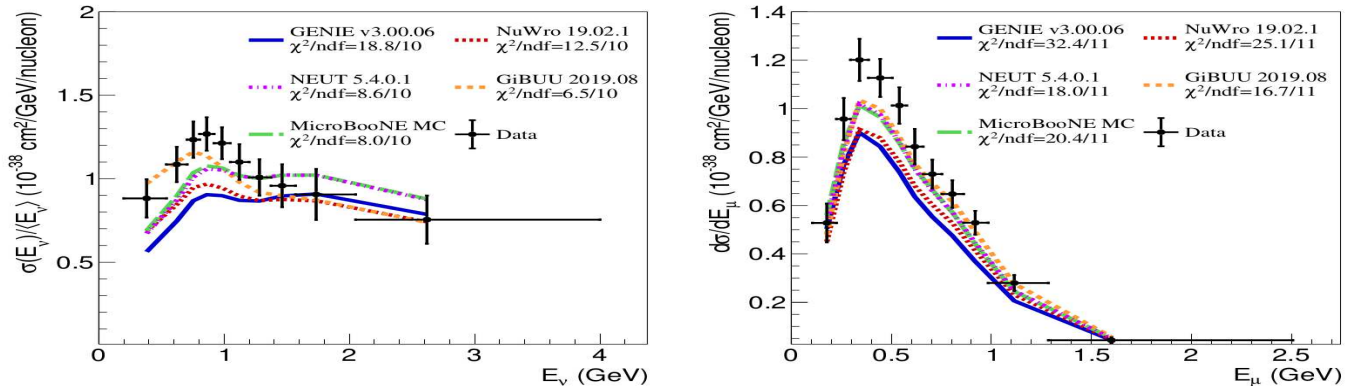


Figure 7.4: Results obtained by the MicroBooNE collaboration [756] using LArTPC located in the Fermilab Booster Neutrino Beam with a mean neutrino energy of approximately 0.8 GeV. (Left panel) The extracted ν_μ CC inclusive scattering cross section per nucleon divided by the bin-center neutrino energy i.e. $\frac{\sigma(E_{\nu_\mu})}{\langle E_{\nu_\mu} \rangle}$ vs E_{ν_μ} . (Right panel) The measured ν_μ CC differential cross section per nucleon as a function of muon energy i.e. $d\sigma/dE_\mu$ vs E_μ . These results are compared with the MicroBooNE MC [757], predictions from GENIE v3.0.6 [541, 416], NuWro 19.02.01 [761], NEUT 5.4.0.1 [746], and GiBUU 2019.08 [754].

- (ii) The sensitivity of these observables to the use of various parameterizations of the vector form factors $f_1(Q^2)$ and $f_2(Q^2)$.
- (iii) The dependence of these observables on numerical values of M_A by varying it within 10% of the world average value.
- (iv) The dependence of these observables on the pseudoscalar form factor, which is important in the case of the final state lepton becoming massive like the τ lepton.
- (v) The effect of G-noninvariance by taking $g_2(Q^2) \neq 0$ and parameterizing it in a dipole form with some representative values of $g_2(0)$ taken in the range of -3 to 3 .
- (vi) The effect of T-noninvariance by making $g_2(Q^2)$ imaginary with same representative numerical values taken for $Re\ g_2(0)$.

From the results presented in Section 2, it may be concluded that

- (i) The total and differential cross sections as well as the polarization observables of the final hadrons in the $\Delta S = 0$ QE scattering are almost insensitive to the different parameterizations of the weak vector form factors.
- (ii) There is a significant dependence of M_A on the total and differential cross sections while the polarization observables show a little effect on the variation in M_A , especially in the case of antineutrino induced QE scattering.
- (iii) The presence of SCC shows a strong dependence on the total cross section as well as on the polarization observables, irrespective of the nature of the form factor $g_2(Q^2)$ (real or imaginary) for both neutrino and antineutrino induced reactions.

- (iv) In the case of $\Delta S = 0$ reactions, the effect of pseudoscalar form factor is almost negligible for the ν_μ ($\bar{\nu}_\mu$) induced processes due to the small mass of muon. However, in the case of ν_τ ($\bar{\nu}_\tau$) induced processes, there is some dependence of $g_3(Q^2)$ on the polarization observables, especially in the threshold region.
- (v) In the case of polarization observables, it is possible to study T violation by taking the imaginary values of the form factor associated with the SCC. The transverse component of polarization of the final lepton or hadron, perpendicular to the reaction plane, arises due to the imaginary values of $g_2(0)$. Therefore, the finite value of $P_T(Q^2)$ gives evidence of T violation in the QE reactions. We have found a strong dependence of g_2^I on the transverse polarization.

In the case of QE induced $1Y$ production, with the increase in M_A , σ for $\bar{\nu}_\mu + p \rightarrow \mu^+ + \Lambda$ increase by about 10% with $M_A = 1.1$ GeV and $\sim 20\%$ with $M_A = 1.2$ GeV at $E_{\bar{\nu}_\mu} = 1$ GeV when compared with the cross section obtained using $M_A = 1.026$ GeV. We observe that in the case of Q^2 -distribution, the longitudinal $P_L(Q^2)$ and the perpendicular $P_P(Q^2)$ components of polarizations show large variations as we change $|g_2^R(0)|$ from 0 to 3, which is about 50% in the peak region of Q^2 distribution. With an imaginary $g_2(Q^2)$, there is contribution to the transverse polarization also. We find that for the process $\bar{\nu}_\mu + p \rightarrow \mu^+ + \Lambda$, $P_L(Q^2)$ the results for $P_L(Q^2)$ are less sensitive to $g_2^I(0)$ at low antineutrino energies, $P_P(Q^2)$ is sensitive to $g_2^I(0)$ at $E_{\bar{\nu}_\mu} = 1$ GeV. Moreover, $P_T(Q^2)$ shows 40% variation at $Q^2 = 0.4$ GeV², $E_{\bar{\nu}_\mu} = 1$ GeV, when $g_2^I(0)$ is varied from 0 to 3.

In Sections 3 and 4, IE and DIS processes on nucleons have been discussed. In the case of IE reactions, the production of mesons like π, η and K , and the production of hyperons like Λ, Σ , etc. have been taken up. The production of hyperons along with pions like $\Sigma\pi, \Lambda\pi$ are also discussed briefly. These IE processes take place through the NR as well as the resonance excitation mechanisms. In the case of NR mechanism, an interaction Lagrangian based on the nonlinear realization of chiral $SU(3)$ symmetry has been used to describe the interaction of nucleons and hyperons with nonstrange and strange mesons like pion, eta and kaon. The meson decay constants f_π, f_K, f_η , and meson masses are treated as parameters and their experimental values have been used. The strong couplings like $g_{NN\pi}, g_{NKY}$, etc. are expressed in terms of the meson decay constants and the symmetric and antisymmetric axial-vector couplings D and F , the values of these constants have been taken from the PDG [19] for numerical evaluations.

In the case of resonance excitation mechanisms all the resonance R with $J^P = \frac{1}{2}^\pm$ and $J = \frac{3}{2}^\pm$ with $I = \frac{1}{2}$ and $\frac{3}{2}$ up to $W = 2$ GeV have been included. Specifically we have considered $P_{33}(1232), P_{11}(1440), D_{13}(1520), S_{11}(1535), S_{31}(1620), S_{11}(1650), D_{33}(1700), P_{11}(1710), P_{13}(1720), P_{11}(1880), S_{11}(1895)$, and $P_{13}(1900)$ resonances. We have considered the contribution of individual resonances and emphasize the role of each resonance in the case of pion, η and associated particle productions. The $N \rightarrow R$ transition form factors in the vector sector have been calculated from the experimental values of the helicity amplitudes taken from the PDG [19]. The Q^2 dependence of the vector form factors has been taken from the earlier works on electroproduction. In the axial-vector sector, the leading axial-vector form factor is obtained in terms of the $R \rightarrow N\pi$ decay width and $\pi \rightarrow \mu\nu$ decay constant f_π . The pseudoscalar form factor is obtained in terms of the leading axial-vector form factor using PCAC and PDDAC as obtained in the case of $N - N$ transition. In case of spin $\frac{3}{2}^\pm$ resonances, there are additional form factors whose contributions are neglected. The Q^2 dependence of the vector and axial-vector form factors for $N - R_{\frac{3}{2}^\pm}$ resonances are treated in analogy with Δ resonance which has been extensively discussed in the literature, while the Q^2 dependence of $J = \frac{1}{2}^\pm$ resonances are treated in analogy with the nucleon case using a dipole parameterization. All the strong couplings like the $g_{RN\pi}, g_{RKY}$ etc. are taken from the experiments as reported in PDG [19]. The results have been presented for the total scattering cross sections for the following processes:

- $\nu_l(\bar{\nu}_l)N \rightarrow l^\mp N' \pi^i, \quad \bar{\nu}_l N \rightarrow l^+ Y \pi^i, i = \pm, 0 \text{ and } N, N' = p \text{ or } n.$
- $\nu_l(\bar{\nu}_l)N \rightarrow l^\mp N' K^j, \quad \bar{\nu}_l N \rightarrow l^+ \Xi K^j, j = +, 0.$
- $\nu_l(\bar{\nu}_l)N \rightarrow l^\mp N' \eta, \quad \nu_l(\bar{\nu}_\mu)N \rightarrow l^\mp \Lambda K^j.$

We find that in the case of $1\pi^+$ production in $\nu_\mu p \rightarrow \mu^- p \pi^+$ reaction, $\Delta(1232)$ resonance has the most dominant contribution. In the case when no cut on the hadronic CM energy W is applied, the presence of the NRB terms increase the cross section by about 14% at $E_{\nu_\mu} = 1$ GeV which decreases with the increase in energy and becomes $\sim 9\%$ at $E_{\nu_\mu} = 2$ GeV. However, when the cuts on W are applied, then due to the presence of background contributions, this increase in the cross section further increases and becomes $\sim 13\%$ at 2 GeV for $W < 1.4$ GeV and 12% for $W < 1.6$ GeV. While for $1\pi^0$ production in the reaction $\nu_\mu n \rightarrow \mu^- n \pi^0$ and $1\pi^+$ production in $\nu_\mu n \rightarrow \mu^- n \pi^+$ we observe significant contributions from the NRB terms as well as from other higher resonance excitations besides the $\Delta(1232)$ dominance. We find that the inclusion of the background terms, increases σ by about 32% at $E_{\nu_\mu} = 1$ GeV which becomes 20% at $E_{\nu_\mu} = 2$ GeV. When higher resonances are included then there is a further increase of about 3% at $E_{\nu_\mu} = 1$ GeV and 40% at $E_{\nu_\mu} = 2$ GeV. Similar observations have been made for the antineutrino induced processes leading to one pion production.

For η production in $\nu_\mu n \rightarrow \mu^- n \eta$ and $\bar{\nu}_\mu p \rightarrow \mu^+ n \eta$ reactions, we find that $S_{11}(1535)$ resonance excitation gives the most dominant contribution and the contribution from the NRB terms and from the $S_{11}(1650)$ and $P_{11}(1710)$ resonance excitations are almost negligible. For the single kaon production in $\nu_\mu p \rightarrow \mu^- K^+ p$ and $\nu_\mu n \rightarrow \mu^- K^0 p$ reactions, the

contact term has the dominant contribution to the total scattering cross section. Similar observation is made for the antineutrino induced process where an antikaon is produced.

For the associated particle production in the reactions $\nu_\mu n \rightarrow \mu^- \Lambda K^+$ and $\bar{\nu}_\mu p \rightarrow \mu^+ \Lambda K^0$, the background terms give the largest contribution and the contributions from the resonances like $S_{11}(1650)$, $P_{11}(1710)$ and $P_{13}(1720)$ considered in this work are small. In the case of neutrino induced $K\Lambda$ production, $P_{11}(1710)$ has the largest contribution among the resonances. While in the case of antineutrino induced associated particle production process, a destructive interference between the background and the resonance terms occurs and the results obtained with background terms only are almost two times the results of full model in the entire energy range. Among the resonances, the most dominant contribution is from $P_{13}(1720)$ followed by $P_{11}(1710)$ and $S_{11}(1650)$ in the low energy region ($E_{\bar{\nu}_\mu} < 1.5$ GeV). We would like to emphasize that the results of single hyperon production cross section are larger at low antineutrino energies in the region of 1.2 GeV and are comparable even at $E_{\bar{\nu}_\mu} = 2$ GeV with the cross section for the associated particle production of hyperons obtained in the present model.

In the case of DIS, the cross sections are calculated in the leading order of the perturbative QCD using the QPM in terms of the nucleon structure functions $F_i^N(x, Q^2)$; $i = 1 - 5$, using the Callan-Gross relation between $F_2(x, Q^2)$ and $F_1(x, Q^2)$, and Albright-Jarlskog relation between $F_5(x, Q^2)$ and $F_2(x, Q^2)$. The evaluation of the structure functions $F_i(x, Q^2)$ ($i = 1, 2, 3, 5$) at NLO and NNLO has been obtained using DGLAP equation for which results have been quoted. The corrections to the nucleon structure functions due to TMC and HT effects have been described qualitatively so that they can be applied to lower Q^2 connecting to SIS or the transition region. We find these corrections to be substantial in some regions of x and Q^2 .

Finally in Section 5, we study the NME in the QE, IE and DIS. In the case of QE scattering, NME are described in the low energy as well as in the intermediate energy regions. In the low energy region relevant to the solar, reactor and accelerator neutrinos (for (anti)neutrinos obtained from pions and kaons decaying at rest), the exclusive reactions have been studied in some nuclei like ^{12}C and ^{56}Fe , using the method based on multipole expansion. The NME are included by using the nuclear wave functions calculated with realistic nucleon-nucleon potentials which include the effect of nucleon correlations and pairing, etc. and reproduce the binding energy and other static properties of the nuclei.

In the region of intermediate and higher energies, the method based on LFGM has been used in which the long range correlations are included in a RPA approach to augment the results obtained by calculating the cross sections and angular as well as the energy distributions of the final state leptons based on the 1p-1h excitation. Further modifications of the cross sections and energy/angular distributions due to the 2p-2h and MEC have been discussed and the results are compared with the experimental results obtained by the MiniBooNE, T2K, MINERvA, etc. collaborations.

The effects due to Fermi motion, Pauli blocking, binding energy, etc. for CCQE processes reduce the cross section by $\sim 30(42)\%$ at $E_\nu = 0.3$ GeV which becomes $20(30)\%$ at $E_\nu = 0.6$ GeV, compared to the free nucleon case. When RPA correlation effects are included a further reduction of $\sim 55(56)\%$ at $E_\nu = 0.3$ GeV and $35(45)\%$ at $E_\nu = 0.6$ GeV is obtained. This reduction further gets enhanced when A is increased in the case of heavier nuclei like ^{40}Ar , ^{56}Fe and ^{208}Pb . Due to threshold effect, the reduction is larger for ν_μ and $\bar{\nu}_\mu$ induced CCQE processes at lower energies, which has been discussed quantitatively in Section 5.4.3.

For the single hyperon production in $\bar{\nu}_\mu$ induced CCQE process, the effects of Fermi motion and Pauli blocking are found to be negligible, while the effect of FSI is substantial, for example, the enhancement in the Λ production cross section is 22–25% in ^{12}C and ^{16}O for $E_{\bar{\nu}_\mu} = 0.6 - 1$ GeV, which increases to 34–38% in ^{40}Ar and 52–62% in ^{208}Pb . While the decrease in Σ^- production cross section is about 40–46% in ^{12}C and ^{16}O for $E_{\bar{\nu}_\mu} = 0.6 - 1$ GeV, which becomes 50–56% in ^{40}Ar and 68–70% in ^{208}Pb . The FSI effect also results in the production of Σ^+ , which is forbidden in the free nucleon case due to the $\Delta S = \Delta Q$ rule. These hyperons decay to pions in the nucleus and these pions contribute significantly to the total 1π production for $E_{\bar{\nu}_\mu} < 1.2\text{GeV}$, which is generally assumed to be dominated by the Δ resonance.

In the case of IE processes, NME are discussed only in the case of pion production which are dominated by the Δ -excitation. The nuclear medium modifications of the properties of Δ , specially in their mass and decay width have been included in calculating the Δ excitation and its decays. After pions are produced in the nuclear medium, the final state interaction of pions with nucleons in the medium is included in a Monte Carlo approach in which the pions go through the process of elastic scattering, charge exchange scattering and absorption as they travel through the medium. We find that NME and FSI effects together results in a net reduction of about 40% to the total pion production for neutrinos of 1 GeV energy range.

In the case of DIS, NME are included by calculating the nucleon spectral function $S(\vec{p}, E)$ for the initial nucleon in a relativistic field theoretical approach to describe the energy and momentum distribution of the nucleons in the nucleus which includes the effect of nuclear binding, Fermi motion and nucleon-nucleon correlations specially the long range correlation. The nucleon structure functions $F_i^N(x, Q^2)$ ($i = 1 - 5$) are then convoluted with the spectral function to include NME and the nuclear structure functions $F_i^A(x, Q^2)$ ($i = 1 - 5$) are calculated. The effect of TMC and HT are calculated at the nucleon level before convoluting it with the nucleon spectral function $S(\vec{p}, E)$ in the nuclei. At the nuclear level, the effect of shadowing and antishadowing is also included in a multiple scattering model used by Kulagin and Petti. These nuclear structure functions are then used to calculate the differential and total scattering cross sections. We find that the inclusion of NME are also important in the DIS region.

In addition to these considerations of NME, some new processes also become relevant in the case of (anti)neutrino scattering with nuclear targets like

- (i) Coherent elastic neutrino-nucleus scattering,
- (ii) Coherent production of π and K mesons,
- (iii) Trident production and its enhancement in the case of nuclear targets,

which are also discussed in view of their importance in contemporary studies of neutrino interactions with nuclei.

The review article attempts to present an overall picture of the properties of neutrinos and their interactions with nucleons and nuclear targets and provides experimenters, phenomenologists as well as theorists the current understanding of neutrino interactions with matter in the few GeV energy region.

Acknowledgements

It is a great pleasure to thank Prof. Amanda Faessler, the then Editor-in-Chief of Progress in Particle and Nuclear Physics, who invited MSA to write the review article. We want to thank the present Editor-in-Chief, Prof. Christian Fischer for being considerate in granting us time. We would like to thank our collaborators Eulogio Oset, Manuel J. Vicente Vacas, and Luis Alvarez Ruso from the University of Valencia, Spain; Ignacio Ruiz Simo, University of Granada, Spain, Takaaki Kajita and (Late)Morihiro Honda at the University of Tokyo, Japan, Zubair Ahmad Dar at William and Mary, US, Faiza Akbar at the University of Rochester, US, and Farhana Zaidi, Huma Haider, M. Rafi Alam, Shakeb Ahmad and Shikha Chauhan at the Aligarh Muslim University, India. Farhana Zaidi, Vaniya Ansari, Sayeed Akhter and Prameet Gaur are acknowledged for their help in the preparation of the present manuscript. MSA and AF are thankful to the Department of Science and Technology (DST), Government of India for providing financial assistance under Grant No. SR/MF/PS-01/2016-AMU.

A. Expression of the hadronic current $J_{\mu\nu}$

$$\begin{aligned}
J_{\mu\nu} = & \frac{1}{2}a^2 \left[4f_1^2(Q^2) (p'_\mu p_\nu + p'_\nu p_\mu - (p \cdot p' - MM')g_{\mu\nu}) \right. \\
& + 4 \frac{f_2^2(Q^2)}{(M+M')^2} (-MM'Q^2g_{\mu\nu} + q_\mu (-q_\nu(MM' + p \cdot p') + p'_\nu(p \cdot q) + p_\nu(p' \cdot q)) \\
& - 2g_{\mu\nu}(p \cdot q)(p' \cdot q) - Q^2g_{\mu\nu}(p \cdot p') + Q^2p_\mu p'_\nu + p_\mu q_\nu(p' \cdot q) + p'_\mu(q_\nu(p \cdot q) + Q^2p_\nu)) \\
& + \frac{16f_3^2(Q^2)}{(M+M')^2} (q_\mu q_\nu(MM' + p \cdot p')) + 4g_1^2(Q^2) ((p'_\mu p_\nu + p_\mu p'_\nu) - (p \cdot p' + MM')g_{\mu\nu}) \\
& + \frac{4g_2^2(Q^2)}{(M+M')^2} (MM'Q^2g_{\mu\nu} + q_\mu(q_\nu(MM' - p \cdot p') + p'_\nu(p \cdot q) + p_\nu(p' \cdot q)) \\
& - 2g_{\mu\nu}(p \cdot q)(p' \cdot q) - Q^2g_{\mu\nu}(p \cdot p') + Q^2p_\mu p'_\nu + p_\mu q_\nu(p' \cdot q) + p'_\mu(q_\nu(p \cdot q) + Q^2p_\nu)) \\
& + \frac{16g_3^2(Q^2)}{(M+M')^2} (q_\mu q_\nu(p' \cdot p - MM')) \\
& + \frac{4f_1(Q^2)f_2(Q^2)}{(M+M')} (q_\mu(M'p_\nu - Mp'_\nu) + 2Mg_{\mu\nu}(p' \cdot q) - Mp'_\mu q_\nu - 2M'g_{\mu\nu}(p \cdot q) + M'p_\mu q_\nu) \\
& + \frac{8f_1(Q^2)f_3(Q^2)}{(M+M')} (q_\mu(Mp'_\nu + M'p_\nu) + q_\nu(Mp'_\mu + M'p_\mu)) + 8if_1(Q^2)g_1(Q^2) (\epsilon_{\mu\nu\alpha\beta} p^\alpha p'^\beta) \\
& + \frac{8if_1(Q^2)g_2(Q^2)}{(M+M')} (M'\epsilon_{\mu\nu\alpha\beta} p^\alpha q^\beta - M\epsilon_{\mu\nu\alpha\beta} p'^\alpha q^\beta) + \frac{8f_2(Q^2)f_3(Q^2)}{(M+M')^2} (q_\nu(p_\mu(p' \cdot q) - p'_\mu(p \cdot q)) \\
& + q_\mu(p_\nu(p' \cdot q) - p'_\nu(p \cdot q))) + 8i \left(\frac{f_2(Q^2)g_1(Q^2)}{(M+M')} \right) (M\epsilon_{\mu\nu\alpha\beta} p'^\alpha q^\beta + M'\epsilon_{\mu\nu\alpha\beta} p^\alpha q^\beta) \\
& + \frac{8if_2(Q^2)g_2(Q^2)}{(M+M')^2} (q_\mu\epsilon_{\nu\alpha\beta\delta} p^\alpha p'^\beta q^\delta - q_\nu\epsilon_{\mu\alpha\beta\delta} p^\alpha p'^\beta q^\delta - Q^2\epsilon^{\mu\nu\alpha\beta} p^\alpha p'^\beta + 2(p \cdot q)\epsilon^{\mu\nu\alpha\beta} p'^\alpha q^\beta) \\
& + \frac{8if_2(Q^2)g_3(Q^2)}{(M+M')^2} (q_\mu\epsilon_{\nu\alpha\beta\delta} p^\alpha p'^\beta q^\delta - q_\nu\epsilon_{\mu\alpha\beta\delta} p^\alpha p'^\beta q^\delta) \\
& + \frac{8if_3(Q^2)g_2(Q^2)}{(M+M')^2} (q_\mu\epsilon_{\nu\alpha\beta\delta} p^\alpha p'^\beta q^\delta - q_\nu\epsilon_{\mu\alpha\beta\delta} p^\alpha p'^\beta q^\delta) \\
& + \frac{4g_1(Q^2)g_2(Q^2)}{(M+M')} (q_\mu(Mp'_\nu + M'p_\nu) - 2Mg_{\mu\nu}(p' \cdot q) + Mp'_\mu q_\nu - 2M'g_{\mu\nu}(p \cdot q) + M'p_\mu q_\nu) \\
& + \frac{8g_1(Q^2)g_3(Q^2)}{(M+M')} (q^\mu(M'p_\nu - Mp'_\nu) + q_\nu(M'p_\mu - Mp'_\mu)) \\
& \left. + \frac{8g_2(Q^2)g_3(Q^2)}{(M+M')^2} (q_\nu(p_\mu(p' \cdot q) - p'_\mu(p \cdot q)) + q_\mu(p_\nu(p' \cdot q) - p'_\nu(p \cdot q))) \right], \tag{A.1}
\end{aligned}$$

where $a = \cos\theta_C(\sin\theta_C)$ for $\Delta S = 0(1)$ CC induced processes and $a = 1$ for NC induced processes.

A.1. Expressions of $N(Q^2)$, $A^h(Q^2)$, $B^h(Q^2)$, and $C^h(Q^2)$

The expressions $N(Q^2)$, $A^h(Q^2)$, $B^h(Q^2)$, and $C^h(Q^2)$ are expressed in terms of the Mandelstam variables and the form factors as:

$$\begin{aligned}
N(Q^2) = & a^2 \left\{ f_1^2(Q^2) \left(\frac{1}{2} \left(2(M^2 - s)(M'^2 - s) - t(\Delta^2 - 2s) + t^2 + m_l^2(\Delta^2 - 2s - t) \right) \right) \right. \\
& + \frac{f_2^2(Q^2)}{(M+M')^2} \left(\frac{1}{4} \left(-2t(M^4 - 2s(M^2 + M'^2) + M'^4 + 2s^2) + 2t^2((M+M')^2 - 2s) \right) \right. \\
& \left. \left. + m_l^2(2\Delta(M+M')(M^2 + M'^2 - 2s) + t((M-3M')(M+M') + 4s) + t^2) \right) \right\}
\end{aligned}$$

$$\begin{aligned}
& + m_l^4(-((3M - M')(M + M') + t))) \\
& + g_1^2(Q^2) \left(\frac{1}{2} \left(2(M^2 - s) (M'^2 - s) - t((M + M')^2 - 2s) + t^2 + m_l^2((M + M')^2 - 2s - t) \right) \right) \\
& + \frac{|g_2(Q^2)|^2}{(M + M')^2} \left(\frac{1}{4} \left(4(\Delta^2 - t) ((M^2 - s) (M'^2 - s) + st) + m_l^2(4\Delta(M^3 + M^2M' - M(3s + t) + M's) \right. \right. \\
& + 2\Delta^2((M + M')^2 - 2s - t) - (4s + t)(\Delta^2 - t)) + 2\Delta^2(-2(M^2 - s)(M'^2 - s) - t((M + M')^2 + 2s) + t^2) \\
& + m_l^4(\Delta^2 + 4M\Delta - t)) \Big) + \frac{g_3^2(Q^2)}{(M + M')^2} (m_l^2(m_l^2 - t)(\Delta^2 - t)) \\
& + \frac{f_1(Q^2)f_2(Q^2)}{(M + M')} \left(- \left(t(M + M')(\Delta^2 - t) + m_l^2(-\Delta(M'^2 - s) + M't) + m_l^4M \right) \right) \\
& \pm f_1(Q^2)g_1(Q^2) \left(- \left(t(M^2 + M'^2 - 2s - t) + m_l^2(M^2 - M'^2 + t) \right) \right) \\
& \pm \frac{Re[f_1(Q^2)g_2(Q^2)]}{(M + M')} \left(-\Delta \left(t(M^2 + M'^2 - 2s - t) + m_l^2(M^2 - M'^2 + t) \right) \right) \\
& \pm \frac{f_2(Q^2)g_1(Q^2)}{(M + M')} \left(-(M + M') \left(t(M^2 + M'^2 - 2s - t) + m_l^2(M^2 - M'^2 + t) \right) \right) \\
& \pm \frac{Re[f_2(Q^2)g_2(Q^2)]}{(M + M')^2} \left(\Delta(-(M + M')) \left(t(M^2 + M'^2 - 2s - t) + m_l^2(M^2 - M'^2 + t) \right) \right) \\
& + \frac{Re[g_1(Q^2)g_2(Q^2)]}{(M + M')} \left((\Delta(-t(M + M')^2 + t^2) + m_l^2(M^3 + M^2M' + \Delta((M + M')^2 - 2s - t) \right. \\
& - 3Ms - Mt + M's) + m_l^4M) + \frac{g_1(Q^2)g_3(Q^2)}{(M + M')} (-2m_l^2(m_l^2M + M^3 - M^2M' - M(s + t) + M's)) \\
& + \left. \frac{Re[g_2(Q^2)g_3(Q^2)]}{(M + M')^2} (m_l^2(-2\Delta(m_l^2M + M^3 - M^2M' - M(s + t) + M's) - (\Delta^2 - t)(m_l^2 + 2M^2 - 2s - t))) \right) \Big\} \quad (A.2)
\end{aligned}$$

where (+)− sign represents the (anti)neutrino induced scattering and the Mandelstam variables are defined as,

$$s = M^2 + 2ME, \quad t = M^2 + M'^2 - 2ME', \quad (A.3)$$

with $\Delta = M' - M$.

$$\begin{aligned}
A^h(Q^2) &= -2a^2 \left[f_1^2(Q^2) \left(\pm \frac{1}{2}(M + M')(\Delta^2 - t) \right) \pm \frac{f_2^2(Q^2)}{(M + M')^2} \left(\frac{1}{2}t(M + M')(\Delta^2 - t) \right) \right. \\
&\pm g_1^2(Q^2) \left(\frac{1}{2}\Delta((M + M')^2 - t) \right) \pm \frac{|g_2(Q^2)|^2}{(M + M')^2} \left(\frac{1}{2}t\Delta((M + M')^2 - t) \right) \\
&\pm \frac{f_1(Q^2)f_2(Q^2)}{(M + M')} \left(\frac{1}{2} \left(4MM't + t^2 - \Delta^2(M + M')^2 \right) \right) + f_1(Q^2)g_1(Q^2) \left(-M' \left(M^2 + M'^2 - 2s - t \right) \right) \\
&+ \frac{Re[f_1(Q^2)g_2(Q^2)]}{(M + M')} \left(\frac{1}{2} \left((M^2 + M'^2 - 2s - t) (-t - 2M'\Delta + \Delta^2) + m_l^2(\Delta^2 - t) \right) \right) \\
&+ \frac{f_1(Q^2)g_3(Q^2)}{(M + M')} (-m_l^2(\Delta^2 - t)) + \frac{f_2(Q^2)g_1(Q^2)}{(M + M')} \left(\frac{1}{2} \left((M^2 - M'^2 - t) (M^2 + M'^2 - 2s - t) \right. \right. \\
&+ m_l^2((M + M')^2 - t)) + \frac{Re[f_2(Q^2)g_2(Q^2)]}{(M + M')^2} \left(\frac{1}{2} \left((M + M')(\Delta^2 - t) (m_l^2 + M^2 + M'^2 - 2s - t) \right. \right. \\
&+ \Delta(m_l^2((M + M')^2 - t) + (M^2 - M'^2 - t)(M^2 + M'^2 - 2s - t)) \Big) \\
&+ \left. \frac{f_2(Q^2)g_3(Q^2)}{(M + M')^2} (-m_l^2(M + M')(\Delta^2 - t)) \pm \frac{Re[g_1(Q^2)g_2(Q^2)]}{(M + M')} \left(\frac{1}{2}((M + M')^2 - t)(-\Delta^2 - t) \right) \right] \quad (A.4) \\
B^h(Q^2) &= a^2 \frac{2}{M'} \left[f_1^2(Q^2) \left(\pm \frac{1}{4} \left(t(\Delta^2 - 2s) - t^2 - 2M'\Delta(M^2 - s) + m_l^2(M^2 + 2MM' - M'^2 + t) \right) \right) \right. \\
&\pm \frac{f_2^2(Q^2)}{(M + M')^2} \left(\frac{1}{4} \left(t(M + M') \left(M^3 + M^2M' - M(M'^2 + 2s + t) + M'^3 - M't \right) \right. \right.
\end{aligned}$$

$$\begin{aligned}
& + m_l^2 \left(M^4 + t(M + M')^2 - M'^4 \right) \Big) \pm g_1^2(Q^2) \left(\frac{1}{4}((-2M'(M + M')(M^2 - s) + t((M + M')^2 - 2s) \right. \\
& - t^2 + m_l^2(M^2 - 2MM' - M'^2 + t)) \Big) \pm \frac{|g_2(Q^2)|^2}{(M + M')^2} \left(\frac{1}{4}\Delta \left(2M' \left(-2m_l^2 M^2 - M^4 + M^2(M'^2 + s + t) \right. \right. \right. \\
& + s(t - M'^2) \Big) + \Delta(-2M'(M + M')(M^2 - s) + t((M + M')^2 - 2s) - t^2) + m_l^2(M^2 - 2MM' - M'^2 + t) \Big) \\
& \pm \frac{f_1(Q^2)f_2(Q^2)}{(M + M')} \left(\frac{1}{2} \left(M^4 M' + M^3 t - M^2 M' (M'^2 + s) - Mt(M'^2 + 2s + t) + M' (M'^2 - t)(s + t) \right. \right. \\
& + m_l^2(M^3 + M^2 M' + M(M'^2 + t) - M'^3 + M't) \Big) \Big) + f_1(Q^2)g_1(Q^2) \left(\frac{1}{2} \left(t(M^2 + M'^2 - 2s) - 2s(s - M^2) - t^2 \right. \right. \\
& - m_l^2(M^2 + M'^2 - 2s - t) \Big) \Big) + \frac{Re[f_1(Q^2)g_2(Q^2)]}{(M + M')} \left(-\frac{1}{2} \left(M^4 M' - 2M^3 s + M^2(M'^3 - M'(s + t) - \Delta(2s + t)) \right. \right. \\
& + 2Ms(s + t) - M'^3 s - M'^2 \Delta t + M'st + 2\Delta s^2 + 2\Delta st + \Delta t^2 + m_l^2(M^3 + M^2 \Delta - M(3s + t) + \Delta(M'^2 - 2s - t)) \\
& + m_l^4 M) \Big) + \frac{f_1(Q^2)g_3(Q^2)}{(M + M')} (m_l^2 M(m_l^2 + M^2 - s - t)) + \frac{f_2(Q^2)g_1(Q^2)}{(M + M')} \left(\frac{1}{2} \left(-M'(M^2 - s)(M^2 + M'^2 - 2s) \right. \right. \\
& + t(M^3 + 2M^2 M' + MM'^2 + M'^3 - 3M's) - t^2(M + M') - m_l^2(M^2 M' + M(M'^2 + s) + M'(M'^2 - 2s - t)) \\
& + m_l^4 M) \Big) + \frac{Re[f_2(Q^2)g_2(Q^2)]}{(M + M')^2} \left(\frac{1}{4} \left(2 \left(M^3(-M'^3 + M'(3s + t) + \Delta t) + M^2(M'^4 - M'^3 \Delta - M'^2(3s + t) \right. \right. \right. \\
& + M'\Delta(3s + 2t) + 2st) + MM's(M'^2 - 2s - 3t) + s(M'^2 - t)(2(s + t) - M'^2) + M\Delta t(M'^2 - t) \\
& + M'\Delta(s + t)(M'^2 - 2s - t) \Big) + m_l^2(-2M^4 - 2M^3 M' + M^2(-2M'\Delta + 2s + t) - 2M\Delta(M'^2 + s) + 2MM'(3s + t) \\
& + 2M'\Delta(-M'^2 + 2s + t) - (M'^2 - t)(4s + t) - m_l^4(3M^2 - M'^2 + t) \Big) \Big) \\
& + \frac{f_2(Q^2)g_3(Q^2)}{(M + M')^2} \left(\frac{1}{2} m_l^2 \left(m_l^2(M^2 + 2MM' - M'^2 + t) - 2M'\Delta(M^2 - s) + t(\Delta^2 - 2s) - t^2 \right) \right) \\
& \pm \frac{Re[g_1(Q^2)g_2(Q^2)]}{(M + M')} \left(\frac{1}{2} \left(M'(-2m_l^2 M^2 - M^4 + M^2(M'^2 + s + t) + s(t - M'^2)) \right. \right. \\
& + \Delta \left(m_l^2(M^2 - 2MM' - M'^2 + t) - 2M'(M + M')(M^2 - s) + t((M + M')^2 - 2s) - t^2 \right) \Big) \Big] \quad (A.5)
\end{aligned}$$

$$\begin{aligned}
C^h(Q^2) &= 2a^2 \left[\pm \frac{Im[f_1(Q^2)g_2(Q^2)]}{(M + M')} (-t + 2M\Delta + \Delta^2) \pm \frac{Im[f_2(Q^2)g_2(Q^2)]}{(M + M')} \left(-t + \frac{\Delta(M^2 - M'^2 + t)}{M + M'} + \Delta^2 \right) \right. \\
&+ \left. \frac{Im[g_1(Q^2)g_2(Q^2)]}{(M + M')} (M^2 + M'^2 - 2s - t + m_l^2) + \frac{Im[g_3(Q^2)g_2(Q^2)]}{(M + M')^2} (2m_l^2 \Delta) \right] \quad (A.6)
\end{aligned}$$

A.2. Expressions of $A^l(Q^2)$, $B^l(Q^2)$ and $C^l(Q^2)$

The expressions $A^l(Q^2)$, $B^l(Q^2)$ and $C^l(Q^2)$ are expressed in terms of the Mandelstam variables and the form factors as:

$$\begin{aligned}
A^l(Q^2) &= 2a^2 \left[f_1^2(Q^2) \left(\frac{1}{2} m_l (M^2 + 2MM' - s) \right) \right. \\
&+ \frac{f_2^2(Q^2)}{(M + M')^2} \left(\frac{1}{4} m_l \left(-m_l^2((3M - M')(M + M') + t) - 2M^4 + 2M^2(M'^2 + s) + 4MM't \right. \right. \\
&- 2(M'^2 - t)(s + t) \Big) + g_1^2(Q^2) \left(\frac{1}{2} m_l (M^2 - 2MM' - s) \right) \\
&+ \frac{|g_2(Q^2)|^2}{(M + M')^2} \left(\frac{1}{4} m_l \left((\Delta^2 - t)(m_l^2 + 4M^2 + 2M'^2 - 2s - 2t) + 2\Delta(2m_l^2 M - 4M^2 \Delta \right. \right. \\
&+ 3M(M'^2 - s - t) + M'(-M'^2 + s + t) \Big) + 2\Delta^2(M^2 - 2MM' - s) \Big) \Big]
\end{aligned}$$

$$\begin{aligned}
& + \frac{g_3^2(Q^2)}{(M+M')^2} (m_l^3 (\Delta^2 - t)) + \frac{f_1(Q^2)f_2(Q^2)}{(M+M')} \left(-\frac{1}{2}m_l (2m_l^2 M - \Delta (2M^2 - M'^2 - s) - t(3M + M')) \right) \\
& + f_1(Q^2)g_1(Q^2) (-m_l (M^2 - s)) + \frac{Re[f_1(Q^2)g_2(Q^2)]}{(M+M')} (-m_l \Delta (M^2 - s)) \\
& + \frac{f_2(Q^2)g_1(Q^2)}{(M+M')} (-m_l (M+M') (M^2 - s)) + \frac{Re[f_2(Q^2)g_2(Q^2)]}{(M+M')^2} (-m_l \Delta (M+M') (M^2 - s)) \\
& + \frac{Re[g_1(Q^2)g_2(Q^2)]}{(M+M')} \left(\frac{1}{2}m_l (2m_l^2 M + 4M^3 + 2M^2(\Delta - 2M') + MM'(3M' - 4\Delta) \right. \\
& - 3M(s+t) - M'^3 + M'(s+t) - 2\Delta s) \left. \right) + \frac{g_1(Q^2)g_3(Q^2)}{(M+M')} \left(- (2m_l^3 M - m_l \Delta (M'^2 - s - t)) \right) \\
& + \frac{Re[g_3(Q^2)g_2(Q^2)]}{(M+M')^2} \left(-m_l (m_l^2 (\Delta^2 + 2M\Delta - t) - t(M'^2 - s - t)) \right) \Big] \tag{A.7}
\end{aligned}$$

$$\begin{aligned}
B^l(Q^2) & = a^2 \frac{2}{M'} \left[f_1^2(Q^2) \left(\frac{1}{4m_l} M' (m_l^2 (- (M^2 + 2MM' - M'^2 + t)) + 2 (M^2 - s) (M'^2 - s) - t\Delta^2 + 2st + t^2) \right) \right. \\
& + \frac{f_2^2(Q^2)}{(M+M')^2} \left(\frac{1}{8m_l} M' (m_l^4 ((3M - M')(M+M') + t) + m_l^2 (\Delta^2 - t) (2(M+M')^2 + t) \right. \\
& - 2t (M^4 - 2s (M^2 + M'^2) + M'^4 + 2s^2) + 2t^2 ((M+M')^2 - 2s) \left. \right) \\
& + g_1^2(Q^2) \left(\frac{1}{4m_l} M' (m_l^2 (- (M^2 - 2MM' - M'^2 + t)) + 2 (M^2 - s) (M'^2 - s) - t(M+M')^2 + 2st + t^2) \right) \\
& + \frac{|g_2(Q^2)|^2}{(M+M')^2} \left(\frac{1}{8m_l} M' (m_l^4 (- (\Delta^2 + 4M\Delta - t)) + m_l^2 (-2\Delta^2 (M^2 - 2MM' - M'^2 + t) \right. \\
& - (4M^2 - t) (\Delta^2 - t) + 4M\Delta(2M\Delta + t)) + 2\Delta^2 (2 (M^2 - s) (M'^2 - s) - t(M+M')^2 + 2st + t^2) \\
& - 8\Delta^2 ((M^2 - s) (M'^2 - s) + st) + 4 (\Delta^2 - t) ((M^2 - s) (M'^2 - s) + st) \left. \right) \\
& + \frac{g_3^2(Q^2)}{(M+M')^2} \left(-\frac{1}{2}m_l M' (m_l^2 - t) (\Delta^2 - t) \right) \\
& + \frac{f_1(Q^2)f_2(Q^2)}{(M+M')} \left(\frac{1}{2m_l} M' (m_l^2 - t) (m_l^2 M + (M+M') ((M-M')^2 - t)) \right) \\
& + f_1(Q^2)g_1(Q^2) \left(\frac{1}{2m_l} M' (m_l^2 - t) (M^2 + M'^2 - 2s - t) \right) \\
& + \frac{Re[f_1(Q^2)g_2(Q^2)]}{(M+M')} \left(\frac{1}{2m_l} M' \Delta (m_l^2 - t) (M^2 + M'^2 - 2s - t) \right) \\
& + \frac{f_2(Q^2)g_1(Q^2)}{(M+M')} \left(\frac{1}{2m_l} M' (m_l^2 - t) (M+M') (M^2 + M'^2 - 2s - t) \right) \\
& + \frac{Re[f_2(Q^2)g_2(Q^2)]}{(M+M')^2} \left(\frac{1}{2m_l} M' \Delta (m_l^2 - t) (M+M') (M^2 + M'^2 - 2s - t) \right) \\
& + \frac{Re[g_1(Q^2)g_2(Q^2)]}{(M+M')} \left(\frac{1}{2m_l} M' (-m_l^4 M + m_l^2 (-2M^3 + M^2(2M' - \Delta) + M(2M'\Delta + t) + \Delta (M'^2 - t)) \right. \\
& + \Delta (2 (M^2 - s) (M'^2 - s) - t ((M+M')^2 - 2s) + t^2) - 2\Delta ((M^2 - s) (M'^2 - s) + st) \left. \right) \\
& + \left. \frac{g_1(Q^2)g_3(Q^2)}{(M+M')} (m_l MM' (m_l^2 - t)) + \frac{Re[g_2(Q^2)g_3(Q^2)]}{(M+M')^2} \left(\frac{1}{2}m_l M' (m_l^2 - t) (\Delta^2 + 2M\Delta - t) \right) \right] \tag{A.8}
\end{aligned}$$

$$C^l(Q^2) = a^2 2 \left[\frac{Im[g_1(Q^2)g_2(Q^2)]}{(M+M')} (m_l (M+M')) + \frac{Im[g_3(Q^2)g_2(Q^2)]}{(M+M')^2} (2m_l t) \right] \tag{A.9}$$

B. Cabibbo theory, $SU(3)$ symmetry and weak $N - Y$ transition form factors

In the Cabibbo theory, the weak vector and the axial-vector currents corresponding to the $\Delta S = 0$ and $\Delta S = 1$ hadronic currents whose matrix elements are defined between the states $|N\rangle$ and $|N'\rangle$ are assumed to belong to the octet

representation of $SU(3)$. Accordingly, they are defined as:

$$V_i^\mu = \bar{q} F_i \gamma^\mu q, \quad A_i^\mu = \bar{q} F_i \gamma^\mu \gamma^5 q, \quad (\text{B.1})$$

where $F_i = \frac{\lambda_i}{2}$ ($i = 1 - 8$) are the generators of flavor $SU(3)$ and λ_i s are the well known Gell-Mann matrices.

From the property of $SU(3)$ group, it follows that there are three corresponding $SU(2)$ subgroups of $SU(3)$ which must be invariant under the interchange of quark pairs ud , ds and us respectively, if the group is invariant under the interchange of u , d and s quarks. Each of these $SU(2)$ subgroups has raising and lowering operators. One of them is $SU(2)_I$, generated by the generators $(\lambda_1, \lambda_2, \lambda_3)$ to be identified with the isospin operators (I_1, I_2, I_3) in the isospin space. For example, I_\pm of isospin is given by

$$I_\pm = I_1 \pm iI_2 = F_1 \pm iF_2 = \frac{1}{2}(\lambda_1 \pm i\lambda_2). \quad (\text{B.2})$$

The other two are defined as $SU(2)_U$ and $SU(2)_V$ generated by the generators $(\lambda_6, \lambda_7, \frac{1}{2}(\sqrt{3}\lambda_8 - \lambda_3))$ and $(\lambda_4, \lambda_5, \frac{1}{2}(\sqrt{3}\lambda_8 + \lambda_3))$, respectively, in U-spin and V-spin space with $(d \ s)$ and $(u \ s)$ forming the basic doublet representation of $SU(2)_U$ and $SU(2)_V$. For more details, see Ref. [10].

From the Gell-Mann matrices λ_i , one may obtain the raising and lowering operators with U-spin and V-spin in analogy with I-spin as:

$$U_\pm = U_1 \pm iU_2 = F_6 \pm iF_7, \quad V_\pm = V_1 \pm iV_2 = F_4 \pm iF_5.$$

In neutron β -decay, the vector and the axial-vector currents for this transition can be written as

$$\bar{\psi}_u \gamma_\mu \psi_d = \bar{q} \gamma_\mu \left(\frac{\lambda_1 + i\lambda_2}{2} \right) q = V_\mu^{1+i2}, \quad \bar{\psi}_u \gamma_\mu \gamma_5 \psi_d = \bar{q} \gamma_\mu \gamma_5 \left(\frac{\lambda_1 + i\lambda_2}{2} \right) q = A_\mu^{1+i2}.$$

Similarly, $s \rightarrow u$ and $u \rightarrow s$ transformations are written as

$$\bar{\psi}_u \gamma_\mu \psi_s = \bar{q} \gamma_\mu \left(\frac{\lambda_4 + i\lambda_5}{2} \right) q = V_\mu^{4+i5}, \quad \bar{\psi}_s \gamma_\mu \psi_u = \bar{q} \gamma_\mu \left(\frac{\lambda_4 - i\lambda_5}{2} \right) q = V_\mu^{4-i5}, \quad (\text{B.3})$$

$$\bar{\psi}_u \gamma_\mu \gamma_5 \psi_s = \bar{q} \gamma_\mu \gamma_5 \left(\frac{\lambda_4 + i\lambda_5}{2} \right) q = A_\mu^{4+i5}, \quad \bar{\psi}_s \gamma_\mu \gamma_5 \psi_u = \bar{q} \gamma_\mu \gamma_5 \left(\frac{\lambda_4 - i\lambda_5}{2} \right) q = A_\mu^{4-i5}. \quad (\text{B.4})$$

The electromagnetic current which is vector current is written using the $SU(3)$ content of the charge operator $e = I_3 + \frac{Y}{2} = \lambda_3 + \frac{1}{2\sqrt{3}}\lambda_8$ as:

$$J_\mu^{em} = V_\mu^3 + \frac{1}{\sqrt{3}}V_\mu^8. \quad (\text{B.5})$$

Therefore, the charge changing weak vector and axial-vector currents are written, in Cabibbo theory, as:

$$\begin{aligned} V_\mu^\pm &= [V_\mu^1 \pm iV_\mu^2] \cos \theta_c + [V_\mu^4 \pm iV_\mu^5] \sin \theta_c, \\ A_\mu^\pm &= [A_\mu^1 \pm iA_\mu^2] \cos \theta_c + [A_\mu^4 \pm iA_\mu^5] \sin \theta_c. \end{aligned} \quad (\text{B.6})$$

In the Cabibbo theory, the isovector part of the electromagnetic current J_{em}^μ i.e. V_μ^3 along with the weak vector currents V_μ^\pm are assumed to transform as an octet of vector currents under $SU(3)$. Similarly, the axial vector currents are also assumed to transform as an octet under $SU(3)$. The weak transition form factors $f_i(q^2)$ and $g_i(q^2)$; $i = 1 - 3$ are determined using Cabibbo theory of $V - A$ interaction extended to the strange sector.

In general, the expression for the matrix element of the transition between the two states of baryons (say B_i and B_k), through the $SU(3)$ octet (V_j or A_j) of currents can be written as:

$$\langle B_i | V_j | B_k \rangle = if_{ijk} F^V + d_{ijk} D^V, \quad \langle B_i | A_j | B_k \rangle = if_{ijk} F^A + d_{ijk} D^A. \quad (\text{B.7})$$

F^V and D^V are determined from the experimental data on the electromagnetic form factors, and F^A and D^A are determined from the experimental data on the semileptonic decays of neutron and hyperons. The physical baryon octet states are written in terms of their octet state B_i as discussed in Section 3.3.1. The matrix element of electromagnetic currents between proton, and neutron states are obtained as

$$\langle p | J_{em}^\mu | p \rangle = \frac{D^V}{3} + F^V, \quad \langle n | J_{em}^\mu | n \rangle = \frac{1}{2} \left[-\frac{2}{3} D^V - \frac{2}{3} D^V \right] = -\frac{2D^V}{3}. \quad (\text{B.8})$$

The nucleon electromagnetic form factors can be written in terms of their $SU(3)$ coupling constants as

Interaction	Transition	a	b
Electromagnetic interaction	$p \rightarrow p$	1	$\frac{1}{3}$
	$n \rightarrow n$	0	$-\frac{2}{3}$
Weak vector and axial-vector	$n \rightarrow p$	1	1
	$\Lambda \rightarrow p$	$-\sqrt{\frac{3}{2}}$	$-\frac{1}{\sqrt{6}}$
	$\Sigma^0 \rightarrow p$	$-\frac{1}{\sqrt{2}}$	$\frac{1}{\sqrt{2}}$
	$\Sigma^- \rightarrow n$	-1	1
	$\Sigma^\pm \rightarrow \Lambda$	0	$\sqrt{\frac{2}{3}}$
	$\Sigma^- \rightarrow \Sigma^0$	$\sqrt{2}$	0
	$\Xi^- \rightarrow \Lambda$	$\sqrt{\frac{3}{2}}$	$-\frac{1}{\sqrt{6}}$
	$\Xi^- \rightarrow \Sigma^0$	$\frac{1}{\sqrt{2}}$	$\frac{1}{\sqrt{2}}$
	$\Xi^0 \rightarrow \Sigma^+$	1	1
	$\Xi^- \rightarrow \Xi^0$	1	-1

Table B.1: Values of the coefficients a and b given in Eq. (B.9).

Nucleus	Nonisoscalar				Isoscalar		B.E./A	T/A
	c_1^n	c_1^p	c_2^n	c_2^p	c_1	c_2		
^{12}C	-	-	-	-	1.692	1.082*	7.6	20.0
^{27}Al	-	-	-	-	3.07	0.519	7.6	20.2
^{40}Ar	3.64	3.47	0.569	0.569	3.53	0.542	8.6	29.0
^{56}Fe	4.050	3.971	0.5935	0.5935	4.106	0.519	8.8	30.0
^{63}Cu	4.31	4.214	0.586	0.586	4.163	0.606	8.7	29.3
^{118}Sn	5.55	5.40	0.543	0.543	5.442	0.543	8.5	31.2
^{197}Au	6.79	6.55	0.522	0.522	6.38	0.535	7.9	33.8
^{208}Pb	6.890	6.624	0.549	0.549	6.624	0.549	7.8	32.6

Table C.1: Different parameters used for the numerical calculations for various nuclei. For ^{12}C we have used modified harmonic oscillator density(* c_2 is dimensionless) and for ^{40}Ar , ^{56}Fe and ^{208}Pb nuclei, 2-parameter Fermi density have been used, where superscript n and p in density parameters($c_i^{n,p}$; $i = 1, 2$) stand for the neutron and proton, respectively. Density parameters for isoscalar and nonisoscalar nuclear targets are given separately in units of fm. The kinetic energy per nucleon(T/A) and the binding energy per nucleon ($B.E./A$) obtained using Eq. (5.153) for the different nuclei are given in MeV.

$$f_i(Q^2) = aF_i^V(Q^2) + bD_i^V(Q^2), \quad g_i(Q^2) = aF_i^A(Q^2) + bD_i^A(Q^2), \quad i = 1, 2, 3. \quad (\text{B.9})$$

We obtain the Clebsch-Gordan coefficients for the electromagnetic $p \rightarrow p$ and $n \rightarrow n$ transitions, which are tabulated in Table-B.1, which leads to

$$F_i^V(Q^2) = F_i^p(Q^2) - F_i^n(Q^2), \quad D_i^V(Q^2) = -\frac{3}{2}F_i^n(Q^2). \quad (\text{B.10})$$

$F_i^V(Q^2)$ and $D_i^V(Q^2)$ determined in terms of the electromagnetic form factors of the nucleon, are used to determine all the form factors in the case of the matrix element of the weak vector current for the various $\Delta S = 0, 1$ transitions. The coefficients a and b for the various transitions are listed in Table-B.1.

C. Density parameters

The modified harmonic oscillator (MHO) density for carbon while two-parameter Fermi (2pF) density for aluminium, argon, iron, lead, etc. are given by:

$$\text{MHO density: } \rho_N(r) = \rho_0 \left[1 + c_2 \left(\frac{r}{c_1} \right)^2 \right], \quad \text{2pF density: } \rho_N(r) = \frac{\rho_0}{1 + e^{(r-c_1)/c_2}}$$

with c_1 and c_2 as the density parameters and ρ_0 as the central density [513, 514, 515]. These parameters are individually tabulated in Table C.1 for the proton and neutron in the case of nonisoscalar nuclear target as well as for the nucleon in the case of isoscalar nuclear target.

References

- [1] W. Pauli, Phys. Today 31N9 (1978) 27.
- [2] E. Fermi, Ric. Sci. 4 (1933) 491.
- [3] E. Fermi, Nuovo Cim. 11 (1934) 1. [doi:10.1007/BF02959820](https://doi.org/10.1007/BF02959820).
- [4] E. Fermi, Z. Phys. 88 (1934) 161. [doi:10.1007/BF01351864](https://doi.org/10.1007/BF01351864).
- [5] F. Perrin, Compt. Rendus 197 (1933) 1625.
- [6] W. J. Henderson, Proc. Roy. Soc. A 147 (1934) 572.
- [7] H. Bethe, R. Peierls, Nature 133 (1934) 532. [doi:10.1038/133532a0](https://doi.org/10.1038/133532a0).
- [8] F. Reines, C. L. Cowan, Nature 178 (1956) 446. [doi:10.1038/178446a0](https://doi.org/10.1038/178446a0).
- [9] C. L. Cowan, et al., Science 124 (1956) 103. [doi:10.1126/science.124.3212.103](https://doi.org/10.1126/science.124.3212.103).
- [10] M. Sajjad Athar, S. K. Singh, The Physics of Neutrino Interactions, Cambridge University Press, 2020.
- [11] E. C. G. Sudarshan, R. e. Marshak, Phys. Rev. 109 (1958) 1860. [doi:10.1103/PhysRev.109.1860.2](https://doi.org/10.1103/PhysRev.109.1860.2).
- [12] R. P. Feynman, M. Gell-Mann, Phys. Rev. 109 (1958) 193. [doi:10.1103/PhysRev.109.193](https://doi.org/10.1103/PhysRev.109.193).
- [13] J. J. Sakurai, Nuovo Cim. 7 (1958) 649. [doi:10.1007/BF02781569](https://doi.org/10.1007/BF02781569).
- [14] T. D. Lee, C. N. Yang, Phys. Rev. 102 (1956) 290. [doi:10.1103/PhysRev.102.290](https://doi.org/10.1103/PhysRev.102.290).
- [15] T. D. Lee, C.-N. Yang, Phys. Rev. 104 (1956) 254. [doi:10.1103/PhysRev.104.254](https://doi.org/10.1103/PhysRev.104.254).
- [16] C. S. Wu, et al., Phys. Rev. 105 (1957) 1413. [doi:10.1103/PhysRev.105.1413](https://doi.org/10.1103/PhysRev.105.1413).
- [17] N. Cabibbo, Phys. Rev. Lett. 10 (1963) 531. [doi:10.1103/PhysRevLett.10.531](https://doi.org/10.1103/PhysRevLett.10.531).
- [18] M. Kobayashi, T. Maskawa, Prog. Theor. Phys. 49 (1973) 652. [doi:10.1143/PTP.49.652](https://doi.org/10.1143/PTP.49.652).
- [19] P. A. Zyla, et al., PTEP 2020 (2020) 083C01. [doi:10.1093/ptep/ptaa104](https://doi.org/10.1093/ptep/ptaa104).
- [20] S. Weinberg, Phys. Rev. Lett. 19 (1967) 1264. [doi:10.1103/PhysRevLett.19.1264](https://doi.org/10.1103/PhysRevLett.19.1264).
- [21] A. Salam, Conf. Proc. C 680519 (1968) 367. [doi:10.1142/9789812795915_0034](https://doi.org/10.1142/9789812795915_0034).
- [22] S. L. Glashow, J. Iliopoulos, L. Maiani, Phys. Rev. D 2 (1970) 1285. [doi:10.1103/PhysRevD.2.1285](https://doi.org/10.1103/PhysRevD.2.1285).
- [23] C.-N. Yang, R. L. Mills, Phys. Rev. 96 (1954) 191. [doi:10.1103/PhysRev.96.191](https://doi.org/10.1103/PhysRev.96.191).
- [24] F. Englert, R. Brout, Phys. Rev. Lett. 13 (1964) 321. [doi:10.1103/PhysRevLett.13.321](https://doi.org/10.1103/PhysRevLett.13.321).
- [25] P. W. Higgs, Phys. Rev. Lett. 13 (1964) 508. [doi:10.1103/PhysRevLett.13.508](https://doi.org/10.1103/PhysRevLett.13.508).
- [26] G. 't Hooft, M. J. G. Veltman, Nucl. Phys. B 44 (1972) 189. [doi:10.1016/0550-3213\(72\)90279-9](https://doi.org/10.1016/0550-3213(72)90279-9).
- [27] B. W. Lee, J. Zinn-Justin, Phys. Rev. D 5 (1972) 3121. [doi:10.1103/PhysRevD.5.3121](https://doi.org/10.1103/PhysRevD.5.3121).
- [28] F. J. Hasert, et al., Nucl. Phys. B 73 (1974) 1. [doi:10.1016/0550-3213\(74\)90038-8](https://doi.org/10.1016/0550-3213(74)90038-8).
- [29] A. M. Cnops, et al., Phys. Rev. Lett. 41 (1978) 357. [doi:10.1103/PhysRevLett.41.357](https://doi.org/10.1103/PhysRevLett.41.357).
- [30] R. H. Heisterberg, et al., Phys. Rev. Lett. 44 (1980) 635. [doi:10.1103/PhysRevLett.44.635](https://doi.org/10.1103/PhysRevLett.44.635).
- [31] H. Faissner, et al., Phys. Rev. Lett. 41 (1978) 213, [Erratum: Phys.Rev.Lett. 41, 1083 (1978)]. [doi:10.1103/PhysRevLett.41.213](https://doi.org/10.1103/PhysRevLett.41.213).
- [32] C. Y. Prescott, et al., Phys. Lett. B 77 (1978) 347. [doi:10.1016/0370-2693\(78\)90722-0](https://doi.org/10.1016/0370-2693(78)90722-0).
- [33] G. Arnison, et al., Phys. Lett. B 122 (1983) 103. [doi:10.1016/0370-2693\(83\)91177-2](https://doi.org/10.1016/0370-2693(83)91177-2).
- [34] M. Banner, et al., Phys. Lett. B 122 (1983) 476. [doi:10.1016/0370-2693\(83\)91605-2](https://doi.org/10.1016/0370-2693(83)91605-2).

- [35] S. Chatrchyan, et al., Phys. Lett. B 716 (2012) 30. [doi:10.1016/j.physletb.2012.08.021](#).
- [36] G. Aad, et al., Phys. Lett. B 716 (2012) 1. [doi:10.1016/j.physletb.2012.08.020](#).
- [37] V. Cirigliano, G. Ecker, H. Neufeld, A. Pich, J. Portoles, Rev. Mod. Phys. 84 (2012) 399. [doi:10.1103/RevModPhys.84.399](#).
- [38] C. Lin, Rare Kaon Decays, in: 20th Conference on Flavor Physics and CP Violation , 2022. [arXiv:2208.01144](#).
- [39] S. Bifani, S. Descotes-Genon, A. Romero Vidal, M.-H. Schune, J. Phys. G 46 (2019) 023001. [doi:10.1088/1361-6471/aaf5de](#).
- [40] J. Albrecht, D. van Dyk, C. Langenbruch, Prog. Part. Nucl. Phys. 120 (2021) 103885. [doi:10.1016/j.pnpnp.2021.103885](#).
- [41] R. Aaij, et al., Nature Phys. 18 (2022) 277. [doi:10.1038/s41567-021-01478-8](#).
- [42] P. de Simone, EPJ Web Conf. 234 (2020) 01004. [doi:10.1051/epjconf/202023401004](#).
- [43] G. Caria, et al., Phys. Rev. Lett. 124 (2020) 161803. [doi:10.1103/PhysRevLett.124.161803](#).
- [44] S. Celani, Lepton Flavour Universality tests and Lepton Flavour Violation searches at LHCb. [arXiv:2111.11105](#).
- [45] C. A. Argüelles, et al., Snowmass White Paper: Beyond the Standard Model effects on Neutrino Flavor. [arXiv:2203.10811](#).
- [46] T. Katori, M. Martini, J. Phys. G 45 (1) (2018) 013001. [doi:10.1088/1361-6471/aa8bf7](#).
- [47] L. Alvarez-Ruso, Y. Hayato, J. Nieves, New J. Phys. 16 (2014) 075015. [doi:10.1088/1367-2630/16/7/075015](#).
- [48] J. G. Morfin, J. Nieves, J. T. Sobczyk, Adv. High Energy Phys. 2012 (2012) 934597. [doi:10.1155/2012/934597](#).
- [49] H. Gallagher, G. Garvey, G. P. Zeller, Ann. Rev. Nucl. Part. Sci. 61 (2011) 355. [doi:10.1146/annurev-nucl-102010-130255](#).
- [50] M. Sajjad Athar, et al., Prog. Part. Nucl. Phys. 124 (2022) 103947. [doi:10.1016/j.pnpnp.2022.103947](#).
- [51] M. Sajjad Athar, S. K. Singh, Neutrinos and their interactions [arXiv:2111.12328](#), [doi:10.1140/epjs/s11734-021-00302-x](#).
- [52] L. Alvarez-Ruso, et al., Prog. Part. Nucl. Phys. 100 (2018) 1. [doi:10.1016/j.pnpnp.2018.01.006](#).
- [53] M. E. Nahmias, Math. Proc. Cambridge Phil. Soc. 31 (1935) 99. [doi:10.1017/S0305004100012986](#).
- [54] G. W. Rodeback, J. S. Allen, Phys. Rev. 86 (1952) 446. [doi:10.1103/PhysRev.86.446](#).
- [55] A. I. Leipunski, Proe. Cam. Phil. Soc 32 (1936) 301.
- [56] A. H. Snell, F. Pleasonton, Phys. Rev. 97 (1955) 246. [doi:10.1103/PhysRev.97.246](#).
- [57] O. K.-H. J. C. Jacobsen, Det. Kgl. Danske Viedensk. Selskab. Mat . Fys. Medd. 23 (1945) 1.
- [58] C. W. Sherwin, Phys. Rev. 73 (1948) 216. [doi:10.1103/PhysRev.73.216](#).
- [59] H. R. Crane, J. Halpern, Phys. Rev. 53 (1938) 789. [doi:10.1103/PhysRev.53.789](#).
- [60] F. Reines, C. L. Cowan, Phys. Rev. 113 (1959) 273. [doi:10.1103/PhysRev.113.273](#).
- [61] B. Pontecorvo, Chalk River Laboratory report PD-205 (1946).
- [62] L. W. Alvarez, UCRL report 328 (1949).
- [63] R. Davis, Phys. Rev. Lett. 12 (1964) 303. [doi:10.1103/PhysRevLett.12.303](#).
- [64] R. Davis, Jr., D. S. Harmer, K. C. Hoffman, Phys. Rev. Lett. 20 (1968) 1205. [doi:10.1103/PhysRevLett.20.1205](#).
- [65] M. A. Markov, Neutrino preprint JINR-D577 (1960), Nauka, Moscow, Russia (1964).
- [66] B. Pontecorvo, Zh. Eksp. Teor. Fiz. 37 (1959) 1751.
- [67] M. Schwartz, Phys. Rev. Lett. 4 (1960) 306. [doi:10.1103/PhysRevLett.4.306](#).

- [68] T. D. Lee, C.-N. Yang, Phys. Rev. Lett. 4 (1960) 307. [doi:10.1103/PhysRevLett.4.307](#).
- [69] N. Cabibbo, R. Gatto, Nuovo Cim. 21 (1961) 872. [doi:10.1007/BF02785616](#).
- [70] Y. Yamaguchi CERN-61-02 (1961). [doi:10.5170/CERN-1961-002](#).
- [71] G. Danby, et al., Phys. Rev. Lett. 9 (1962) 36. [doi:10.1103/PhysRevLett.9.36](#).
- [72] J. K. Bienlein, et al., Phys. Lett. 13 (1964) 80. [doi:10.1016/0031-9163\(64\)90316-6](#).
- [73] M. L. Perl, et al., Phys. Rev. Lett. 35 (1975) 1489. [doi:10.1103/PhysRevLett.35.1489](#).
- [74] K. Kodama, et al., Phys. Rev. D 78 (2008) 052002. [doi:10.1103/PhysRevD.78.052002](#).
- [75] K. Kodama, et al., Phys. Lett. B 504 (2001) 218. [doi:10.1016/S0370-2693\(01\)00307-0](#).
- [76] N. Agafonova, et al., Phys. Lett. B 691 (2010) 138. [doi:10.1016/j.physletb.2010.06.022](#).
- [77] N. Agafonova, et al., Phys. Rev. D 89 (2014) 051102. [doi:10.1103/PhysRevD.89.051102](#).
- [78] N. Agafonova, et al., Phys. Rev. Lett. 115 (2015) 121802. [doi:10.1103/PhysRevLett.115.121802](#).
- [79] Z. Li, et al., Phys. Rev. D 98 (2018) 052006. [doi:10.1103/PhysRevD.98.052006](#).
- [80] M. G. Aartsen, et al., Phys. Rev. D 99 (2019) 032007. [doi:10.1103/PhysRevD.99.032007](#).
- [81] S. Aoki, et al., JHEP 01 (2020) 033. [doi:10.1007/JHEP01\(2020\)033](#).
- [82] C. Ahdida, et al., SND@LHC (2020). [arXiv:2002.08722](#).
- [83] A. Di Crescenzo, PoS HQL2016 (2017) 076. [doi:10.22323/1.274.0076](#).
- [84] P. Machado, H. Schulz, J. Turner, Phys. Rev. D 102 (2020) 053010. [doi:10.1103/PhysRevD.102.053010](#).
- [85] J. Strait, et al., Long-Baseline Neutrino Facility (LBNF) and Deep Underground Neutrino Experiment (DUNE): Conceptual Design Report, Volume 3: Long-Baseline Neutrino Facility for DUNE June 24, 2015 [arXiv:1601.05823](#).
- [86] B. Abi, et al., The DUNE Far Detector Interim Design Report, Volume 3: Dual-Phase Module [arXiv:1807.10340](#).
- [87] U. F. Katz, C. Spiering, Prog. Part. Nucl. Phys. 67 (2012) 651. [doi:10.1016/j.ppnp.2011.12.001](#).
- [88] E. Vitagliano, I. Tamborra, G. Raffelt, Rev. Mod. Phys. 92 (2020) 45006. [doi:10.1103/RevModPhys.92.045006](#).
- [89] K. Abe, et al., Phys. Rev. Lett. 110 (2013) 181802. [doi:10.1103/PhysRevLett.110.181802](#).
- [90] J. N. Bahcall, AAPPS Bull. 12 (4) (2002) 12. [doi:10.1016/S0920-5632\(03\)01306-9](#).
- [91] T. K. Gaisser, M. Honda, Ann. Rev. Nucl. Part. Sci. 52 (2002) 153. [doi:10.1146/annurev.nucl.52.050102.090645](#).
- [92] H. A. Bethe, J. R. Wilson, Astrophys. J. 295 (1985) 14. [doi:10.1086/163343](#).
- [93] F. Halzen, Adv. Ser. Direct. High Energy Phys. 28 (2018) 325–390. [doi:10.1142/9789813226098_0009](#).
- [94] G. Fiorentini, M. Lissia, F. Mantovani, Phys. Rept. 453 (2007) 117. [doi:10.1016/j.physrep.2007.09.001](#).
- [95] U. Dore, P. Loverre, L. Ludovici, Eur. Phys. J. H 44 (2019) 271. [doi:10.1140/epjh/e2019-90032-x](#).
- [96] K. Mahn, C. Marshall, C. Wilkinson, Ann. Rev. Nucl. Part. Sci. 68 (2018) 105. [doi:10.1146/annurev-nucl-101917-020930](#).
- [97] G. C. Hanna, B. Pontecorvo, Phys. Rev. 75 (1949) 983. [doi:10.1103/PhysRev.75.983.3](#).
- [98] K. E. Bergkvist, Nucl. Phys. B 39 (1972) 317. [doi:10.1016/0550-3213\(72\)90376-8](#).
- [99] B. Pontecorvo, Zh. Eksp. Teor. Fiz. 34 (1957) 247.
- [100] M. Gell-Mann, A. Pais, Phys. Rev. 97 (1955) 1387. [doi:10.1103/PhysRev.97.1387](#).
- [101] Z. Maki, M. Nakagawa, S. Sakata, Prog. Theor. Phys. 28 (1962) 870. [doi:10.1143/PTP.28.870](#).

- [102] B. Pontecorvo, Sov. Phys. JETP 6 (1957) 429.
- [103] Y.-L. Chan, M. C. Chu, K. M. Tsui, C. F. Wong, J. Xu, Eur. Phys. J. C 76 (6) (2016) 310. [doi:10.1140/epjc/s10052-016-4143-4](https://doi.org/10.1140/epjc/s10052-016-4143-4).
- [104] B. J. P. Jones, E. Marzec, J. Spitz, The Width of a Beta-decay-induced Antineutrino Wavepacket (2022). [arXiv:2211.00026](https://arxiv.org/abs/2211.00026).
- [105] F. Reines, et al., Phys. Rev. 117 (1960) 159. [doi:10.1103/PhysRev.117.159](https://doi.org/10.1103/PhysRev.117.159).
- [106] J. Bernstein, T. D. Lee, Phys. Rev. Lett. 11 (1963) 512. [doi:10.1103/PhysRevLett.11.512](https://doi.org/10.1103/PhysRevLett.11.512).
- [107] K. S. Babu, S. Jana, M. Lindner, JHEP 10 (2020) 040. [doi:10.1007/JHEP10\(2020\)040](https://doi.org/10.1007/JHEP10(2020)040).
- [108] B. C. Canas, O. G. Miranda, A. Parada, M. Tortola, J. W. F. Valle, Phys. Lett. B 753 (2016) 191–198, [Addendum: Phys.Lett.B 757, 568–568 (2016)]. [doi:10.1016/j.physletb.2015.12.011](https://doi.org/10.1016/j.physletb.2015.12.011).
- [109] H. F. Dylla, J. G. King, Phys. Rev. A 7 (1973) 1224. [doi:10.1103/PhysRevA.7.1224](https://doi.org/10.1103/PhysRevA.7.1224).
- [110] J. C. Zorn, G. E. Chamberlain, V. W. Hughes, Phys. Rev. 129 (1963) 2566. [doi:10.1103/PhysRev.129.2566](https://doi.org/10.1103/PhysRev.129.2566).
- [111] G. Barbiellini, G. Cocconi, Nature 329 (1987) 21. [doi:10.1038/329021b0](https://doi.org/10.1038/329021b0).
- [112] G. Degrossi, A. Sirlin, W. J. Marciano, Phys. Rev. D 39 (1989) 287. [doi:10.1103/PhysRevD.39.287](https://doi.org/10.1103/PhysRevD.39.287).
- [113] L. B. Auerbach, et al., Phys. Rev. D 63 (2001) 112001. [doi:10.1103/PhysRevD.63.112001](https://doi.org/10.1103/PhysRevD.63.112001).
- [114] M. Deniz, et al., Phys. Rev. D 81 (2010) 072001. [doi:10.1103/PhysRevD.81.072001](https://doi.org/10.1103/PhysRevD.81.072001).
- [115] M. Hirsch, E. Nardi, D. Restrepo, Phys. Rev. D 67 (2003) 033005. [doi:10.1103/PhysRevD.67.033005](https://doi.org/10.1103/PhysRevD.67.033005).
- [116] J. Bernstein, M. Ruderman, G. Feinberg, Phys. Rev. 132 (1963) 1227. [doi:10.1103/PhysRev.132.1227](https://doi.org/10.1103/PhysRev.132.1227).
- [117] J. Dorenbosch, et al., Z. Phys. C 41 (1989) 567, [Erratum: Z.Phys.C 51, 142 (1991)]. [doi:10.1007/BF01564701](https://doi.org/10.1007/BF01564701).
- [118] L. A. Ahrens, et al., Phys. Rev. D 41 (1990) 3297. [doi:10.1103/PhysRevD.41.3297](https://doi.org/10.1103/PhysRevD.41.3297).
- [119] P. A. M. Dirac, Proc. Roy. Soc. Lond. A 117 (1928) 610. [doi:10.1098/rspa.1928.0023](https://doi.org/10.1098/rspa.1928.0023).
- [120] H. Weyl, Z. Phys. 56 (1929) 330. [doi:10.1007/BF01339504](https://doi.org/10.1007/BF01339504).
- [121] T. D. Lee, C.-N. Yang, Phys. Rev. 105 (1957) 1671. [doi:10.1103/PhysRev.105.1671](https://doi.org/10.1103/PhysRev.105.1671).
- [122] L. D. Landau, Nucl. Phys. 3 (1957) 127. [doi:10.1016/0029-5582\(57\)90061-5](https://doi.org/10.1016/0029-5582(57)90061-5).
- [123] A. Salam, Nuovo Cim. 5 (1957) 299. [doi:10.1007/BF02812841](https://doi.org/10.1007/BF02812841).
- [124] E. Majorana, Nuovo Cim. 14 (1937) 171. [doi:10.1007/BF02961314](https://doi.org/10.1007/BF02961314).
- [125] R. N. Mohapatra, P. B. Pal, Massive neutrinos in physics and astrophysics, World Scientific, 1991.
- [126] M. Blasone, J. Palmer, Phys. Rev. D 69 (2004) 057301. [doi:10.1103/PhysRevD.69.057301](https://doi.org/10.1103/PhysRevD.69.057301).
- [127] K. Fujikawa, Phys. Rev. D 102 (10) (2020) 105001. [doi:10.1103/PhysRevD.102.105001](https://doi.org/10.1103/PhysRevD.102.105001).
- [128] V. Cirigliano, et al., Neutrinoless Double-Beta Decay: A Roadmap for Matching Theory to Experiment [arXiv:2203.12169](https://arxiv.org/abs/2203.12169).
- [129] A. B. Balantekin, A. de Gouvêa, B. Kayser, Phys. Lett. B 789 (2019) 488. [doi:10.1016/j.physletb.2018.11.068](https://doi.org/10.1016/j.physletb.2018.11.068).
- [130] G. Racah, Nuovo Cim. 14 (1937) 322. [doi:10.1007/BF02961321](https://doi.org/10.1007/BF02961321).
- [131] W. H. Furry, Phys. Rev. 54 (1938) 56. [doi:10.1103/PhysRev.54.56](https://doi.org/10.1103/PhysRev.54.56).
- [132] W. H. Furry, Phys. Rev. 56 (1939) 1184. [doi:10.1103/PhysRev.56.1184](https://doi.org/10.1103/PhysRev.56.1184).
- [133] M. J. Dolinski, A. W. P. Poon, W. Rodejohann, Ann. Rev. Nucl. Part. Sci. 69 (2019) 219. [doi:10.1146/annurev-nucl-101918-023407](https://doi.org/10.1146/annurev-nucl-101918-023407).
- [134] C. Quigg, Gauge theories of the strong, weak and electromagnetic interactions, Princeton University Press, 1983.

- [135] W. M. Alberico, S. M. Bilenky, C. Maieron, Phys. Rept. 358 (2002) 227. [doi:10.1016/S0370-1573\(01\)00058-8](#).
- [136] J. Erler, M. Schott, Prog. Part. Nucl. Phys. 106 (2019) 68. [doi:10.1016/j.ppnp.2019.02.007](#).
- [137] I. Dubovyk, A. Freitas, J. Gluza, T. Riemann, J. Usovitsch, JHEP 08 (2019) 113. [doi:10.1007/JHEP08\(2019\)113](#).
- [138] A. Freitas, JHEP 04 (2014) 070. [doi:10.1007/JHEP04\(2014\)070](#).
- [139] A. Pich, The Standard Model of Electroweak Interactions, in: 2010 European School of High Energy Physics, 2012, p. 1.
- [140] S. L. Glashow, Phys. Rev. 118 (1960) 316. [doi:10.1103/PhysRev.118.316](#).
- [141] V. Barger, et al., Phys. Rev. D 90 (2014) 121301. [doi:10.1103/PhysRevD.90.121301](#).
- [142] D. Biele, et al., JCAP 01 (2017) 033. [doi:10.1088/1475-7516/2017/01/033](#).
- [143] A. Loewy, S. Nussinov, S. L. Glashow, The Effect of Doppler Broadening on the 6.3 PeV W^- Resonance in $\bar{\nu}_e e^-$ Collisions [arXiv:1407.4415](#).
- [144] A. Bhattacharya, R. Gandhi, W. Rodejohann, A. Watanabe, JCAP 10 (2011) 017. [doi:10.1088/1475-7516/2011/10/017](#).
- [145] M. G. Aartsen, et al., Nature 591 (2021) 220, [Erratum: Nature 592, E11 (2021)]. [doi:10.1038/s41586-021-03256-1](#).
- [146] M. G. Aartsen, et al., J. Phys. G 48 (2021) 060501. [doi:10.1088/1361-6471/abbd48](#).
- [147] L. Alvarez-Ruso, et al., Neutrino Scattering Measurements on Hydrogen and Deuterium: A Snowmass White Paper (2022). [arXiv:2203.11298](#).
- [148] M. Bustamante, A. Connolly, Phys. Rev. Lett 122 (2019) 041101. [doi:10.1103/PhysRevLett.122.041101](#).
- [149] V. B. Valera, M. Bustamante, C. Glaser, JHEP 06 (2022) 105. [doi:10.1007/JHEP06\(2022\)105](#).
- [150] R. Abbasi, et al., Phys. Rev. D 104 (2021) 022001. [doi:10.1103/PhysRevD.104.022001](#).
- [151] L. A. Ruso, et al., Theoretical tools for neutrino scattering: interplay between lattice QCD, EFTs, nuclear physics, phenomenology, and neutrino event generators (2022). [arXiv:2203.09030](#).
- [152] M. Sajjad Athar, J. G. Morfin, J. Phys. G 48 (2021) 034001. [doi:10.1088/1361-6471/abbb11](#).
- [153] C. Andreopoulos, et al., Summary of the NuSTEC Workshop on Shallow- and Deep-Inelastic Scattering. [arXiv:1907.13252](#).
- [154] A. Bodek, U. Yang, J. Phys. G 29 (2003) 1899. [doi:10.1088/0954-3899/29/8/369](#).
- [155] A. Bodek, I. Park, U.-k. Yang, Nucl. Phys. B Proc. Suppl. 139 (2005) 113. [doi:10.1016/j.nuclphysbps.2004.11.208](#).
- [156] A. Bodek, U.-k. Yang, Axial and Vector Structure Functions for Electron- and Neutrino- Nucleon Scattering Cross Sections at all Q^2 using Effective Leading order Parton Distribution Functions [arXiv:1011.6592](#).
- [157] D. Rein, L. M. Sehgal, Annals Phys. 133 (1981) 79. [doi:10.1016/0003-4916\(81\)90242-6](#).
- [158] M. Kabirnezhad, Phys. Rev. D 97 (2018) 013002. [doi:10.1103/PhysRevD.97.013002](#).
- [159] M. Kabirnezhad, MK single pion production model (2020). [arXiv:2006.13765](#).
- [160] E. Hernandez, J. Nieves, M. Valverde, Phys. Rev. D 76 (2007) 033005. [doi:10.1103/PhysRevD.76.033005](#).
- [161] E. Hernandez, et al., Phys. Rev. D 77 (2008) 053009. [doi:10.1103/PhysRevD.77.053009](#).
- [162] M. Rafi Alam, I. Ruiz Simo, M. Sajjad Athar, M. J. Vicente Vacas, Phys. Rev. D 82 (2010) 033001. [doi:10.1103/PhysRevD.82.033001](#).
- [163] M. Rafi Alam, I. Ruiz Simo, M. Sajjad Athar, M. J. Vicente Vacas, Phys. Rev. D 85 (2012) 013014. [doi:10.1103/PhysRevD.85.013014](#).

- [164] E. Wang, L. Alvarez-Ruso, J. Nieves, Phys. Rev. C 89 (2014) 015503. [doi:10.1103/PhysRevC.89.015503](https://doi.org/10.1103/PhysRevC.89.015503).
- [165] T. Leitner, O. Buss, L. Alvarez-Ruso, U. Mosel, Phys. Rev. C 79 (2009) 034601. [doi:10.1103/PhysRevC.79.034601](https://doi.org/10.1103/PhysRevC.79.034601).
- [166] M. Rafi Alam, M. Sajjad Athar, S. Chauhan, S. K. Singh, Int. J. Mod. Phys. E 25 (2016) 1650010. [doi:10.1142/S0218301316500105](https://doi.org/10.1142/S0218301316500105).
- [167] M. Rafi Alam, I. Ruiz Simo, M. Sajjad Athar, M. J. Vicente Vacas, Phys. Rev. D 87 (2013) 053008. [doi:10.1103/PhysRevD.87.053008](https://doi.org/10.1103/PhysRevD.87.053008).
- [168] E. F. McNicoll, et al., Phys. Rev. C 82 (2010) 035208, [Erratum: Phys.Rev.C 84, 029901 (2011)]. [doi:10.1103/PhysRevC.84.029901](https://doi.org/10.1103/PhysRevC.84.029901).
- [169] D. Werthmüller, et al., Phys. Rev. C 90 (2014) 015205. [doi:10.1103/PhysRevC.90.015205](https://doi.org/10.1103/PhysRevC.90.015205).
- [170] A. Fatima, Z. Ahmad Dar, M. Sajjad Athar, S. K. Singh, Int. J. Mod. Phys. E 29 (2020) 2050051. [doi:10.1142/S0218301320500512](https://doi.org/10.1142/S0218301320500512).
- [171] R. Bradford, et al., Phys. Rev. C 73 (2006) 035202. [doi:10.1103/PhysRevC.73.035202](https://doi.org/10.1103/PhysRevC.73.035202).
- [172] M. Benitez Galan, M. R. Alam, I. Ruiz Simo, Phys. Rev. D 104 (2021) 073005. [doi:10.1103/PhysRevD.104.073005](https://doi.org/10.1103/PhysRevD.104.073005).
- [173] M. Rafi Alam, I. Ruiz Simo, Phys. Rev. D 100 (2019) 033001. [doi:10.1103/PhysRevD.100.033001](https://doi.org/10.1103/PhysRevD.100.033001).
- [174] M. Valverde, J. Nieves, E. Hernandez, S. K. Singh, M. J. Vicente Vacas, Mod. Phys. Lett. A 23 (2008) 2309. [doi:10.1142/S0217732308029265](https://doi.org/10.1142/S0217732308029265).
- [175] C. H. Llewellyn Smith, Phys. Rept. 3 (1972) 261. [doi:10.1016/0370-1573\(72\)90010-5](https://doi.org/10.1016/0370-1573(72)90010-5).
- [176] A. Fatima, M. Sajjad Athar, S. K. Singh, Phys. Rev. D 98 (2018) 033005. [doi:10.1103/PhysRevD.98.033005](https://doi.org/10.1103/PhysRevD.98.033005).
- [177] S. S. Gershtein, Y. B. Zeldovich, Zh. Eksp. Teor. Fiz. 29 (1955) 698.
- [178] S. Treiman, Comments Nucl. Part. Phys. 1 (1967) 13.
- [179] R. Jackiw, K. Johnson, Phys. Rev. 182 (1969) 1459. [doi:10.1103/PhysRev.182.1459](https://doi.org/10.1103/PhysRev.182.1459).
- [180] H. Fukuda, Y. Miyamoto, Progress of Theoretical Physics 4 (1949) 389. [doi:10.1143/ptp/4.3.389](https://doi.org/10.1143/ptp/4.3.389).
- [181] C. B. van Wyk, Phys. Rev. 80 (1950) 487.
- [182] A. Pais, R. Jost, Phys. Rev. 87 (1952) 871–875. [doi:10.1103/PhysRev.87.871](https://doi.org/10.1103/PhysRev.87.871).
- [183] C. Goebel, Phys. Rev. 103 (1956) 258. [doi:10.1103/PhysRev.103.258](https://doi.org/10.1103/PhysRev.103.258).
- [184] S. Weinberg, Phys. Rev. 112 (1958) 1375. [doi:10.1103/PhysRev.112.1375](https://doi.org/10.1103/PhysRev.112.1375).
- [185] S. Galster, et al., Nucl. Phys. B 32 (1971) 221. [doi:10.1016/0550-3213\(71\)90068-X](https://doi.org/10.1016/0550-3213(71)90068-X).
- [186] R. Bradford, A. Bodek, H. S. Budd, J. Arrington, Nucl. Phys. B Proc. Suppl. 159 (2006) 127. [doi:10.1016/j.nuclphysbps.2006.08.028](https://doi.org/10.1016/j.nuclphysbps.2006.08.028).
- [187] H. S. Budd, A. Bodek, J. Arrington, Nucl. Phys. B Proc. Suppl. 139 (2005) 90. [doi:10.1016/j.nuclphysbps.2004.11.181](https://doi.org/10.1016/j.nuclphysbps.2004.11.181).
- [188] W. M. Alberico, S. M. Bilenky, C. Giunti, K. M. Graczyk, Phys. Rev. C 79 (2009) 065204. [doi:10.1103/PhysRevC.79.065204](https://doi.org/10.1103/PhysRevC.79.065204).
- [189] P. E. Bosted, Phys. Rev. C 51 (1995) 409. [doi:10.1103/PhysRevC.51.409](https://doi.org/10.1103/PhysRevC.51.409).
- [190] S. Platchkov, et al., Nucl. Phys. A 510 (1990) 740. [doi:10.1016/0375-9474\(90\)90358-S](https://doi.org/10.1016/0375-9474(90)90358-S).
- [191] J. J. Kelly, Phys. Rev. C 70 (2004) 068202. [doi:10.1103/PhysRevC.70.068202](https://doi.org/10.1103/PhysRevC.70.068202).
- [192] V. Punjabi, et al., Eur. Phys. J. A 51 (2015) 79. [doi:10.1140/epja/i2015-15079-x](https://doi.org/10.1140/epja/i2015-15079-x).
- [193] R. Gupta, et al., Phys. Rev. D 96 (2017) 114503. [doi:10.1103/PhysRevD.96.114503](https://doi.org/10.1103/PhysRevD.96.114503).
- [194] A. S. Meyer, M. Betancourt, R. Gran, R. J. Hill, Phys. Rev. D 93 (2016) 113015. [doi:10.1103/PhysRevD.93.113015](https://doi.org/10.1103/PhysRevD.93.113015).

- [195] J. Green, et al., Phys. Rev. D 95 (2017) 114502. [doi:10.1103/PhysRevD.95.114502](https://doi.org/10.1103/PhysRevD.95.114502).
- [196] C. Alexandrou, et al., Phys. Rev. D 96 (2017) 054507. [doi:10.1103/PhysRevD.96.054507](https://doi.org/10.1103/PhysRevD.96.054507).
- [197] D.-L. Yao, L. Alvarez-Ruso, M. J. Vicente-Vacas, Phys. Rev. D 96 (2017) 116022. [doi:10.1103/PhysRevD.96.116022](https://doi.org/10.1103/PhysRevD.96.116022).
- [198] S. Capitani, et al., Int. J. Mod. Phys. A 34 (2019) 1950009. [doi:10.1142/S0217751X1950009X](https://doi.org/10.1142/S0217751X1950009X).
- [199] K. L. Miller, et al., Phys. Rev. D 26 (1982) 537. [doi:10.1103/PhysRevD.26.537](https://doi.org/10.1103/PhysRevD.26.537).
- [200] N. J. Baker, et al., Phys. Rev. D 23 (1981) 2499. [doi:10.1103/PhysRevD.23.2499](https://doi.org/10.1103/PhysRevD.23.2499).
- [201] T. Kitagaki, et al., Phys. Rev. D 28 (1983) 436. [doi:10.1103/PhysRevD.28.436](https://doi.org/10.1103/PhysRevD.28.436).
- [202] A. Bodek, S. Avvakumov, R. Bradford, H. S. Budd, Eur. Phys. J. C 53 (2008) 349. [doi:10.1140/epjc/s10052-007-0491-4](https://doi.org/10.1140/epjc/s10052-007-0491-4).
- [203] V. Bernard, L. Elouadrhiri, U.-G. Meissner, J. Phys. G 28 (2002) R1. [doi:10.1088/0954-3899/28/1/201](https://doi.org/10.1088/0954-3899/28/1/201).
- [204] V. Lyubushkin, et al., Eur. Phys. J. C 63 (2009) 355. [doi:10.1140/epjc/s10052-009-1113-0](https://doi.org/10.1140/epjc/s10052-009-1113-0).
- [205] L. Fields, et al., Phys. Rev. Lett. 111 (2013) 022501. [doi:10.1103/PhysRevLett.111.022501](https://doi.org/10.1103/PhysRevLett.111.022501).
- [206] G. A. Fiorentini, et al., Phys. Rev. Lett. 111 (2013) 022502. [doi:10.1103/PhysRevLett.111.022502](https://doi.org/10.1103/PhysRevLett.111.022502).
- [207] A. A. Aguilar-Arevalo, et al., Phys. Rev. Lett. 100 (2008) 032301. [doi:10.1103/PhysRevLett.100.032301](https://doi.org/10.1103/PhysRevLett.100.032301).
- [208] A. A. Aguilar-Arevalo, et al., Phys. Rev. D 82 (2010) 092005. [doi:10.1103/PhysRevD.82.092005](https://doi.org/10.1103/PhysRevD.82.092005).
- [209] A. A. Aguilar-Arevalo, et al., Phys. Rev. D 81 (2010) 092005. [doi:10.1103/PhysRevD.81.092005](https://doi.org/10.1103/PhysRevD.81.092005).
- [210] M. Dorman, AIP Conf. Proc. 1189 (2009) 133. [doi:10.1063/1.3274143](https://doi.org/10.1063/1.3274143).
- [211] P. Adamson, et al., Phys. Rev. D 91 (2015) 012005. [doi:10.1103/PhysRevD.91.012005](https://doi.org/10.1103/PhysRevD.91.012005).
- [212] R. Gran, et al., Phys. Rev. D 74 (2006) 052002. [doi:10.1103/PhysRevD.74.052002](https://doi.org/10.1103/PhysRevD.74.052002).
- [213] K. Abe, et al., Phys. Rev. Lett. 116 (2016) 181801. [doi:10.1103/PhysRevLett.116.181801](https://doi.org/10.1103/PhysRevLett.116.181801).
- [214] Y. Nakajima, et al., Phys. Rev. D 83 (2011) 012005. [doi:10.1103/PhysRevD.83.012005](https://doi.org/10.1103/PhysRevD.83.012005).
- [215] G. Cheng, et al., Phys. Rev. D 86 (2012) 052009. [doi:10.1103/PhysRevD.86.052009](https://doi.org/10.1103/PhysRevD.86.052009).
- [216] K. S. Kuzmin, V. V. Lyubushkin, V. A. Naumov, Eur. Phys. J. C 54 (2008) 517. [doi:10.1140/epjc/s10052-008-0582-x](https://doi.org/10.1140/epjc/s10052-008-0582-x).
- [217] I. D. Kakorin, K. S. Kuzmin, V. A. Naumov, Eur. Phys. J. C 81 (2021) 1142. [doi:10.1140/epjc/s10052-021-09945-5](https://doi.org/10.1140/epjc/s10052-021-09945-5).
- [218] M. L. Goldberger, S. B. Treiman, Phys. Rev. 111 (1958) 354. [doi:10.1103/PhysRev.111.354](https://doi.org/10.1103/PhysRev.111.354).
- [219] M. R. Schindler, T. Fuchs, J. Gegelia, S. Scherer, Phys. Rev. C 75 (2007) 025202. [doi:10.1103/PhysRevC.75.025202](https://doi.org/10.1103/PhysRevC.75.025202).
- [220] A. Tsapalis, eConf C070910 (2007) 168.
- [221] H. W. Fearing, P. C. McNamee, R. J. Oakes, Nuovo Cim. A 60 (1969) 10. [doi:10.1007/BF02823293](https://doi.org/10.1007/BF02823293).
- [222] S. Berman, M. Veltman, Physics Letters 12 (1964) 275. [doi:https://doi.org/10.1016/0031-9163\(64\)91102-3](https://doi.org/https://doi.org/10.1016/0031-9163(64)91102-3).
- [223] A. Fatima, M. Sajjad Athar, S. K. Singh, Front. in Phys. 7 (2019) 13. [doi:10.3389/fphy.2019.00013](https://doi.org/10.3389/fphy.2019.00013).
- [224] V. Cirigliano, S. Gardner, B. Holstein, Prog. Part. Nucl. Phys. 71 (2013) 93. [doi:10.1016/j.ppnp.2013.03.005](https://doi.org/10.1016/j.ppnp.2013.03.005).
- [225] S. F. Pate, J. P. Schaub, J. Phys. Conf. Ser. 295 (2011) 012037. [doi:10.1088/1742-6596/295/1/012037](https://doi.org/10.1088/1742-6596/295/1/012037).
- [226] J. A. Formaggio, G. P. Zeller, Rev. Mod. Phys. 84 (2012) 1307. [doi:10.1103/RevModPhys.84.1307](https://doi.org/10.1103/RevModPhys.84.1307).
- [227] A. Fatima, M. Sajjad Athar, S. K. Singh, Phys. Rev. D 102 (2020) 113009. [doi:10.1103/PhysRevD.102.113009](https://doi.org/10.1103/PhysRevD.102.113009).

- [228] A. Fujii, Y. Yamaguchi, Progress of Theoretical Physics 33 (1965) 552. [doi:10.1143/PTP.33.552](#).
- [229] Y. Nambu, Phys. Rev. Lett. 4 (1960) 380. [doi:10.1103/PhysRevLett.4.380](#).
- [230] R. E. Marshak, Riazuddin, C. P. Ryan, Theory of Weak Interactions in Particle Physics, Wiley, New York, 1969.
- [231] T. Eichten, et al., Phys. Lett. B 40 (1972) 593. [doi:10.1016/0370-2693\(72\)90490-X](#).
- [232] O. Erriquez, et al., Phys. Lett. B 70 (1977) 383. [doi:10.1016/0370-2693\(77\)90683-9](#).
- [233] O. Erriquez, et al., Nucl. Phys. B 140 (1978) 123. [doi:10.1016/0550-3213\(78\)90316-4](#).
- [234] G. Fanourakis, et al., Phys. Rev. D 21 (1980) 562. [doi:10.1103/PhysRevD.21.562](#).
- [235] V. V. Ammosov, et al., Z. Phys. C 36 (1987) 377. [doi:10.1007/BF01573931](#).
- [236] V. V. Ammosov, et al., JETP Lett. 43 (1986) 716.
- [237] J. Brunner, et al., Z. Phys. C 45 (1990) 551. [doi:10.1007/BF01556267](#).
- [238] J.-J. Wu, B.-S. Zou, Few Body Syst. 56 (2015) 165. [doi:10.1007/s00601-015-0973-0](#).
- [239] J. Finjord, F. Ravndal, Nucl. Phys. B 106 (1976) 228. [doi:10.1016/0550-3213\(76\)90379-5](#).
- [240] K. S. Kuzmin, V. A. Naumov, Phys. Atom. Nucl. 72 (2009) 1501. [doi:10.1134/S1063778809090105](#).
- [241] M. M. Block, Symmetries in Elementary Particle Physics, edited by A. Zichichi, Academic Press, New York, 1965.
- [242] M. Block, NAL Summer Study, 1, 215, 1968.
- [243] S. M. Bilenky, E. Christova, J. Phys. G 40 (2013) 075004. [doi:10.1088/0954-3899/40/7/075004](#).
- [244] S. M. Bilenky, E. Christova, Phys. Part. Nucl. Lett. 10 (2013) 651. [doi:10.1134/S154747711307011X](#).
- [245] K. M. Graczyk, B. E. Kowal, Phys. Rev. D 104 (2021) 033005. [doi:10.1103/PhysRevD.104.033005](#).
- [246] K. M. Graczyk, B. E. Kowal, Phys. Rev. D 101 (2020) 073002. [doi:10.1103/PhysRevD.101.073002](#).
- [247] K. M. Graczyk, B. E. Kowal, Phys. Rev. D 99 (2019) 053002. [doi:10.1103/PhysRevD.99.053002](#).
- [248] O. Tomalak, Phys. Rev. D 103 (2021) 013006. [doi:10.1103/PhysRevD.103.013006](#).
- [249] C. Thorpe, et al., Phys. Rev. C 104 (2021) 035502. [doi:10.1103/PhysRevC.104.035502](#).
- [250] A. Fatima, M. Sajjad Athar, S. K. Singh, Eur. Phys. J. A 54 (2018) 95. [doi:10.1140/epja/i2018-12534-2](#).
- [251] F. Akbar, M. Rafi Alam, M. Sajjad Athar, S. K. Singh, Phys. Rev. D 94 (2016) 114031. [doi:10.1103/PhysRevD.94.114031](#).
- [252] A. Fatima, M. Sajjad Athar, S. K. Singh, Eur. Phys. J. ST 230 (2021) 4391. [doi:10.1140/epjs/s11734-021-00272-0](#).
- [253] A. Fatima, M. Sajjad Athar, S. K. Singh, Phys. Rev. D 105 (2022) 073004. [doi:10.1103/PhysRevD.105.073004](#).
- [254] F. Akbar, M. Sajjad Athar, A. Fatima, S. K. Singh, Eur. Phys. J. A 53 (2017) 154. [doi:10.1140/epja/i2017-12340-4](#).
- [255] S. M. Bilenky, Basics of Introduction to Feynman Diagrams and Electroweak Interactions Physics, Editions Frontières, 1994.
- [256] S. L. Adler, Annals Phys. 50 (1968) 189. [doi:10.1016/0003-4916\(68\)90278-9](#).
- [257] S. Scherer, Adv. Nucl. Phys. 27 (2003) 277.
- [258] S. Scherer, M. R. Schindler, A Primer for Chiral Perturbation Theory, Vol. 830, 2012. [doi:10.1007/978-3-642-19254-8](#).
- [259] B. Kubis, An Introduction to chiral perturbation theory, 2007. [arXiv:hep-ph/0703274](#).
- [260] M. N. Butler, M. J. Savage, R. P. Springer, Nucl. Phys. B 399 (1993) 69. [doi:10.1016/0550-3213\(93\)90617-X](#).

- [261] M. Doring, E. Oset, S. Sarkar, Phys. Rev. C 74 (2006) 065204. [doi:10.1103/PhysRevC.74.065204](#).
- [262] L. Tiator, D. Drechsel, S. S. Kamalov, M. Vanderhaeghen, Eur. Phys. J. ST 198 (2011) 141. [doi:10.1140/epjst/e2011-01488-9](#).
- [263] A. Shafi, et al., Phys. Rev. C 70 (2004) 035204. [doi:10.1103/PhysRevC.70.035204](#).
- [264] K. Park, et al., Phys. Rev. C 91 (2015) 045203. [doi:10.1103/PhysRevC.91.045203](#).
- [265] T. Leitner, L. Alvarez-Ruso, U. Mosel, Phys. Rev. C 73 (2006) 065502. [doi:10.1103/PhysRevC.73.065502](#).
- [266] D. Drechsel, S. Kamalov, L. Tiator, Eur. Phys. J. A 34 (2007) 69. [doi:10.1140/epja/i2007-10490-6](#).
- [267] O. Lalakulich, E. A. Paschos, G. Piranishvili, Phys. Rev. D 74 (2006) 014009. [doi:10.1103/PhysRevD.74.014009](#).
- [268] G. M. Radecky, et al., Phys. Rev. D 25 (1982) 1161, [Erratum: Phys.Rev.D 26, 3297 (1982)]. [doi:10.1103/PhysRevD.25.1161](#).
- [269] T. Kitagaki, et al., Phys. Rev. D 34 (1986) 2554. [doi:10.1103/PhysRevD.34.2554](#).
- [270] P. A. Schreiner, F. Von Hippel, Nucl. Phys. B 58 (1973) 333. [doi:10.1016/0550-3213\(73\)90588-9](#).
- [271] T. Kitagaki, et al., Phys. Rev. D 42 (1990) 1331. [doi:10.1103/PhysRevD.42.1331](#).
- [272] A. Faessler, et al., Phys. Rev. D 78 (2008) 094005. [doi:10.1103/PhysRevD.78.094005](#).
- [273] P. Denner, Phys. Rev. 127 (1962) 664. [doi:10.1103/PhysRev.127.664](#).
- [274] N. Dombey, Phys. Rev. 127 (1962) 653. [doi:10.1103/PhysRev.127.653](#).
- [275] J. S. Bell, S. M. Berman, Nuovo Cim. C 25 (1962) 404.
- [276] J. S. Bell, C. H. Llewellyn Smith, Nucl. Phys. B 24 (1970) 285. [doi:10.1016/0550-3213\(70\)90238-5](#).
- [277] S. S. Gershtein, Y. Y. Komachenko, M. Y. Khlopov, Sov. J. Nucl. Phys. 32 (1980) 861.
- [278] Y. Y. Komachenko, M. Y. Khlopov, Yad. Fiz. 45 (1987) 467.
- [279] S. L. Adler, R. F. Dashen, Current Algebras and applications to particle physics, W. A. Benjamin, 1968.
- [280] S. Treiman, R. Jackiw, D. J. Gross, Lectures on Current Algebra and Its Applications, Princeton Series in Physics, 1972.
- [281] A. Nikolakopoulos, et al., Phys. Rev. D 97 (2018) 093008. [doi:10.1103/PhysRevD.97.093008](#).
- [282] R. González-Jiménez, K. Niewczas, N. Jachowicz, Phys. Rev. D 97 (2018) 013004. [doi:10.1103/PhysRevD.97.013004](#).
- [283] M. Rafi Alam, et al., AIP Conf. Proc. 1680 (2015) 020001. [doi:10.1063/1.4931860](#).
- [284] W.-Y. Lee, et al., Phys. Rev. Lett. 38 (1977) 202. [doi:10.1103/PhysRevLett.38.202](#).
- [285] J. Bell, et al., Phys. Rev. Lett. 41 (1978) 1008. [doi:10.1103/PhysRevLett.41.1008](#).
- [286] P. Allen, et al., Nucl. Phys. B 176 (1980) 269. [doi:10.1016/0550-3213\(80\)90450-2](#).
- [287] G. L. Fogli, G. Nardulli, Nucl. Phys. B 160 (1979) 116. [doi:10.1016/0550-3213\(79\)90233-5](#).
- [288] T. Sato, D. Uno, T. S. H. Lee, Phys. Rev. C 67 (2003) 065201. [doi:10.1103/PhysRevC.67.065201](#).
- [289] G. L. Fogli, G. Nardulli, Nucl. Phys. B 165 (1980) 162. [doi:10.1016/0550-3213\(80\)90312-0](#).
- [290] H. Kamano, S. X. Nakamura, T. S. H. Lee, T. Sato, Phys. Rev. D 86 (2012) 097503. [doi:10.1103/PhysRevD.86.097503](#).
- [291] S. X. Nakamura, H. Kamano, T. S. H. Lee, T. Sato, AIP Conf. Proc. 1663 (2015) 070005. [doi:10.1063/1.4919486](#).
- [292] E. A. Paschos, J.-Y. Yu, M. Sakuda, Phys. Rev. D 69 (2004) 014013. [doi:10.1103/PhysRevD.69.014013](#).
- [293] O. Lalakulich, E. A. Paschos, Phys. Rev. D 71 (2005) 074003. [doi:10.1103/PhysRevD.71.074003](#).

- [294] C. Barbero, G. Lopez Castro, A. Mariano, Phys. Lett. B 664 (2008) 70. [doi:10.1016/j.physletb.2008.05.011](#).
- [295] C. Barbero, G. López Castro, A. Mariano, Phys. Lett. B 728 (2014) 282. [doi:10.1016/j.physletb.2013.12.006](#).
- [296] O. Lalakulich, T. Leitner, O. Buss, U. Mosel, Phys. Rev. D 82 (2010) 093001. [doi:10.1103/PhysRevD.82.093001](#).
- [297] R. González-Jiménez, et al., Phys. Rev. D 95 (2017) 113007. [doi:10.1103/PhysRevD.95.113007](#).
- [298] M. Rafi Alam, L. Alvarez-Ruso, M. Sajjad Athar, M. J. Vicente Vacas, AIP Conf. Proc. 1663 (2015) 120014. [doi:10.1063/1.4919520](#).
- [299] C. Wilkinson, et al., Phys. Rev. D 90 (2014) 112017. [doi:10.1103/PhysRevD.90.112017](#).
- [300] M. Derrick, et al., Phys. Lett. B 92 (1980) 363, [Erratum: Phys.Lett.B 95, 461 (1980)]. [doi:10.1016/0370-2693\(80\)90283-X](#).
- [301] M. Pohl, et al., Phys. Lett. B 79 (1978) 501. [doi:10.1016/0370-2693\(78\)90415-X](#).
- [302] C. E. Anderson, AIP Conf. Proc. 1189 (2009) 195. [doi:10.1063/1.3274154](#).
- [303] S. Nakayama, et al., Phys. Lett. B 619 (2005) 255. [doi:10.1016/j.physletb.2005.05.044](#).
- [304] Y. Kurimoto, et al., Phys. Rev. D 81 (2010) 033004. [doi:10.1103/PhysRevD.81.033004](#).
- [305] P. Abratenko, et al., Measurement of neutral current single π^0 production on argon with the MicroBooNE detector [arXiv:2205.07943](#).
- [306] E. Hernandez, J. Nieves, M. Valverde, Phys. Lett. B 647 (2007) 452. [doi:10.1016/j.physletb.2007.02.051](#).
- [307] P. Rodrigues, C. Wilkinson, K. McFarland, Eur. Phys. J. C 76 (2016) 474. [doi:10.1140/epjc/s10052-016-4314-3](#).
- [308] M. Lacombe, et al., Phys. Lett. B 101 (1981) 139. [doi:10.1016/0370-2693\(81\)90659-6](#).
- [309] S. Nakamura, H. Kamano, T. Sato, Phys. Rev. D 92 (2015) 074024. [doi:10.1103/PhysRevD.92.074024](#).
- [310] T. Bolognese, J. P. Engel, J. L. Guyonnet, J. L. Riester, Phys. Lett. B 81 (1979) 393. [doi:10.1016/0370-2693\(79\)90361-7](#).
- [311] S. Ahmad, M. Sajjad Athar, S. K. Singh, Phys. Rev. D 74 (2006) 073008. [doi:10.1103/PhysRevD.74.073008](#).
- [312] M. Sajjad Athar, S. Chauhan, S. K. Singh, J. Phys. G 37 (2010) 015005. [doi:10.1088/0954-3899/37/1/015005](#).
- [313] M. Sajjad Athar, S. Chauhan, S. K. Singh, Eur. Phys. J. A 43 (2010) 209. [doi:10.1140/epja/i2010-10908-0](#).
- [314] T. Leitner, L. Alvarez-Ruso, U. Mosel, Phys. Rev. C 74 (2006) 065502. [doi:10.1103/PhysRevC.74.065502](#).
- [315] C. B. Dover, P. M. Fishbane, Phys. Rev. Lett. 64 (1990) 3115. [doi:10.1103/PhysRevLett.64.3115](#).
- [316] D. Skoupil, P. Bydžovský, Phys. Rev. C 93 (2016) 025204. [doi:10.1103/PhysRevC.93.025204](#).
- [317] A. Fatima, M. Sajjad Athar, S. K. Singh, Weak interaction induced η production in $\nu_\mu(\bar{\nu}_\mu)$ scattering off the nucleon, Paper in preparation (2022).
- [318] R. E. Shrock, Phys. Rev. D 12 (1975) 2049. [doi:10.1103/PhysRevD.12.2049](#).
- [319] A. A. Amer, Phys. Rev. D 18 (1978) 2290. [doi:10.1103/PhysRevD.18.2290](#).
- [320] H. K. Dewan, Phys. Rev. D 24 (1981) 2369. [doi:10.1103/PhysRevD.24.2369](#).
- [321] S. J. Barish, et al., Phys. Rev. D 19 (1979) 2521. [doi:10.1103/PhysRevD.19.2521](#).
- [322] A. A. Abud, et al., Snowmass Neutrino Frontier: DUNE Physics Summary, 2022. [arXiv:2203.06100](#).
- [323] J. Bian, et al., Hyper-Kamiokande Experiment: A Snowmass White Paper, 2022. [arXiv:2203.02029](#).
- [324] K. Ohta, Phys. Rev. C 40 (1989) 1335. [doi:10.1103/PhysRevC.40.1335](#).
- [325] H. Habermehl, C. Bennhold, T. Mart, T. Feuster, Phys. Rev. C 58 (1998) R40. [doi:10.1103/PhysRevC.58.R40](#).
- [326] R. M. Davidson, R. Workman, Phys. Rev. C 63 (2001) 025210. [doi:10.1103/PhysRevC.63.025210](#).

- [327] N. Solomey, Nucl. Phys. B Proc. Suppl. 142 (2005) 74. [doi:10.1016/j.nuclphysbps.2005.01.014](#).
- [328] W. A. Mann, et al., Phys. Rev. D 34 (1986) 2545. [doi:10.1103/PhysRevD.34.2545](#).
- [329] N. J. Baker, et al., Phys. Rev. D 24 (1981) 2779. [doi:10.1103/PhysRevD.24.2779](#).
- [330] S. J. Barish, et al., Phys. Rev. Lett. 33 (1974) 1446. [doi:10.1103/PhysRevLett.33.1446](#).
- [331] H. Deden, et al., Phys. Lett. B 58 (1975) 361. [doi:10.1016/0370-2693\(75\)90674-7](#).
- [332] W. Mecklenburg, Acta Phys. Austriaca 48 (1978) 293.
- [333] D. Casper, Nucl. Phys. B Proc. Suppl. 112 (2002) 161. [doi:10.1016/S0920-5632\(02\)01756-5](#).
- [334] K. Datchev, APS Meeting Abstracts 1037P (2002).
- [335] A. Fatima, M. Sajjad Athar, S. K. Singh, Weak interaction induced associated particle production in $\nu_\mu(\bar{\nu}_\mu)$ scattering off the nucleon, Paper in preparation (2022).
- [336] D. Day, et al., Phys. Rev. D 28 (1983) 2714. [doi:10.1103/PhysRevD.28.2714](#).
- [337] S. N. Biswas, S. R. Choudhury, A. K. Goyal, J. N. Passi, Phys. Rev. D 18 (1978) 3187. [doi:10.1103/PhysRevD.18.3187](#).
- [338] S. A. Adjei, D. A. Dicus, V. L. Teplitz, Phys. Rev. D 23 (1981) 672. [doi:10.1103/PhysRevD.23.672](#).
- [339] V. P. Efrosinin, Y. G. Kudenko, A. N. Khotjantsev, Phys. Atom. Nucl. 72 (2009) 459. [doi:10.1134/S1063778809030089](#).
- [340] R. J. Hill, Phys. Rev. D 81 (2010) 013008. [doi:10.1103/PhysRevD.81.013008](#).
- [341] X. Zhang, B. D. Serot, Phys. Rev. C 86 (2012) 035502. [doi:10.1103/PhysRevC.86.035502](#).
- [342] X. Zhang, B. D. Serot, Phys. Rev. C 86 (2012) 035504. [doi:10.1103/PhysRevC.86.035504](#).
- [343] X. Zhang, B. D. Serot, Phys. Lett. B 719 (2013) 409. [doi:10.1016/j.physletb.2013.01.057](#).
- [344] C. Barbero, A. Mariano, AIP Conf. Proc. 1529 (2013) 244. [doi:10.1063/1.4804127](#).
- [345] P. C. Bergbusch, et al., Phys. Rev. C 59 (1999) 2853. [doi:10.1103/PhysRevC.59.2853](#).
- [346] M. K. Cheoun, K. S. Kim, T. K. Choi, J. Phys. G 29 (2003) 2099. [doi:10.1088/0954-3899/29/9/305](#).
- [347] S. S. Gershtein, Y. Y. Komachenko, M. Y. Khlopov, Sov. J. Nucl. Phys. 33 (1981) 860.
- [348] A. A. Aguilar-Arevalo, et al., Phys. Rev. Lett. 102 (2009) 101802. [doi:10.1103/PhysRevLett.102.101802](#).
- [349] E. Wang, L. Alvarez-Ruso, Y. Hayato, K. Mahn, J. Nieves, Phys. Rev. D 92 (2015) 053005. [doi:10.1103/PhysRevD.92.053005](#).
- [350] J. I. Friedman, H. W. Kendall, Ann. Rev. Nucl. Part. Sci. 22 (1972) 203. [doi:10.1146/annurev.ns.22.120172.001223](#).
- [351] M. Gell-Mann, Phys. Lett. 8 (1964) 214. [doi:10.1016/S0031-9163\(64\)92001-3](#).
- [352] G. Zweig (1964) 22CERN-8182/Th.401(Jan. 1964) and CERN-8419/Th.412.
- [353] J. I. Friedman, H. W. Kendall, R. E. Taylor, Nobel lectures in physics 1990 (1990).
- [354] R. E. Taylor, Rev. Mod. Phys. 63 (1991) 573. [doi:10.1103/RevModPhys.63.573](#).
- [355] H. W. Kendall, Rev. Mod. Phys. 63 (1991) 597. [doi:10.1103/RevModPhys.63.597](#).
- [356] J. I. Friedman, Rev. Mod. Phys. 63 (1991) 615. [doi:10.1103/RevModPhys.63.615](#).
- [357] J. I. Friedman, Deep inelastic scattering: Comparisons with the quark model (1990).
- [358] V. Ansari, et al., Phys. Rev. D 102 (2020) 113007. [doi:10.1103/PhysRevD.102.113007](#).
- [359] C. G. Callan, Jr., D. J. Gross, Phys. Rev. Lett. 22 (1969) 156. [doi:10.1103/PhysRevLett.22.156](#).

- [360] C. H. Albright, C. Jarlskog, Nucl. Phys. B 84 (1975) 467. [doi:10.1016/0550-3213\(75\)90318-1](#).
- [361] A. D. Martin, R. G. Roberts, W. J. Stirling, R. S. Thorne, Eur. Phys. J. C 4 (1998) 463. [doi:10.1007/s100520050220](#).
- [362] M. Glück, E. Reya, A. Vogt, Eur. Phys. J. C 5 (1998) 461. [doi:10.1007/s100520050289](#).
- [363] M. Gluck, P. Jimenez-Delgado, E. Reya, Eur. Phys. J. C 53 (2008) 355. [doi:10.1140/epjc/s10052-007-0462-9](#).
- [364] A. D. Martin, W. J. Stirling, R. S. Thorne, G. Watt, Eur. Phys. J. C 63 (2009) 189. [doi:10.1140/epjc/s10052-009-1072-5](#).
- [365] S. Alekhin, J. Bluemlein, S.-O. Moch, R. Placakyte, PoS DIS2016 (2016) 016. [doi:10.22323/1.265.0016](#).
- [366] S. Chekanov, et al., Phys. Rev. D 67 (2003) 012007. [doi:10.1103/PhysRevD.67.012007](#).
- [367] Z. Zhang, Acta Phys. Polon. Supp. 8 (2015) 957. [doi:10.5506/APhysPolBSupp.8.957](#).
- [368] L. Del Debbio, et al., JHEP 03 (2007) 039. [doi:10.1088/1126-6708/2007/03/039](#).
- [369] P. M. Nadolsky, et al., Phys. Rev. D 78 (2008) 013004. [doi:10.1103/PhysRevD.78.013004](#).
- [370] A. Accardi, et al., Phys. Rev. D 81 (2010) 034016. [doi:10.1103/PhysRevD.81.034016](#).
- [371] L. A. Harland-Lang, A. D. Martin, P. Motylinski, R. S. Thorne, Eur. Phys. J. C 75 (2015) 204. [doi:10.1140/epjc/s10052-015-3397-6](#).
- [372] J. G. Morfin, Eur. Phys. J. ST 230 (2021) 4221. [doi:10.1140/epjs/s11734-021-00298-4](#).
- [373] H. Deden, et al., Nucl. Phys. B 85 (1975) 269. [doi:10.1016/0550-3213\(75\)90008-5](#).
- [374] K. A. Milton, I. L. Solovtsov, O. P. Solovtsova, Phys. Rev. D 60 (1999) 016001. [doi:10.1103/PhysRevD.60.016001](#).
- [375] G. Altarelli, G. Parisi, Nucl. Phys. B 126 (1977) 298. [doi:10.1016/0550-3213\(77\)90384-4](#).
- [376] L. W. Whitlow, et al., Phys. Lett. B 282 (1992) 475. [doi:10.1016/0370-2693\(92\)90672-Q](#).
- [377] A. C. Benvenuti, et al., Phys. Lett. B 223 (1989) 485. [doi:10.1016/0370-2693\(89\)91637-7](#).
- [378] M. Arneodo, et al., Nucl. Phys. B 481 (1996) 3. [doi:10.1016/S0550-3213\(96\)90117-0](#).
- [379] J. J. Aubert, et al., Nucl. Phys. B 259 (1985) 189. [doi:10.1016/0550-3213\(85\)90635-2](#).
- [380] M. Arneodo, et al., Phys. Lett. B 364 (1995) 107. [doi:10.1016/0370-2693\(95\)01318-9](#).
- [381] E. Oltman, et al., Z. Phys. C 53 (1992) 51. [doi:10.1007/BF01483872](#).
- [382] J. P. Berge, et al., Z. Phys. C 49 (1991) 187. [doi:10.1007/BF01555493](#).
- [383] D. MacFarlane, et al., Z. Phys. C 26 (1984) 1. [doi:10.1007/BF01572534](#).
- [384] P. S. Auchincloss, et al., Z. Phys. C 48 (1990) 411. [doi:10.1007/BF01572022](#).
- [385] W. G. Seligman, A Next-to-Leading Order QCD Analysis of Neutrino - Iron Structure Functions at the Tevatron, Ph.D. thesis, Columbia U. (1997). [doi:10.2172/1421736](#).
- [386] J. P. Berge, et al., Z. Phys. C 35 (1987) 443. [doi:10.1007/BF01596895](#).
- [387] M. Tzanov, et al., Phys. Rev. D 74 (2006) 012008. [doi:10.1103/PhysRevD.74.012008](#).
- [388] D. C. Colley, et al., Z. Phys. C 2 (1979) 187. [doi:10.1007/BF01474659](#).
- [389] J. V. Allaby, et al., Z. Phys. C 38 (1988) 403. [doi:10.1007/BF01584388](#).
- [390] S. X. Nakamura, et al., Phys. Rev. C 81 (2010) 035502. [doi:10.1103/PhysRevC.81.035502](#).
- [391] F. Halzen, A. D. Martin, Quarks and leptons: An introductory course in modern particle physics, John Wiley & Sons, 1984.
- [392] W. L. van Neerven, A. Vogt, Nucl. Phys. B 588 (2000) 345. [doi:10.1016/S0550-3213\(00\)00480-6](#).

- [393] J. A. M. Vermaseren, A. Vogt, S. Moch, Nucl. Phys. B 724 (2005) 3. [doi:10.1016/j.nuclphysb.2005.06.020](#).
- [394] S. Moch, J. A. M. Vermaseren, Nucl. Phys. B 573 (2000) 853. [doi:10.1016/S0550-3213\(00\)00045-6](#).
- [395] S. Moch, J. A. M. Vermaseren, A. Vogt, Nucl. Phys. B 688 (2004) 101. [doi:10.1016/j.nuclphysb.2004.03.030](#).
- [396] S. Moch, J. A. M. Vermaseren, A. Vogt, Phys. Lett. B 606 (2005) 123. [doi:10.1016/j.physletb.2004.11.063](#).
- [397] S. Moch, J. A. M. Vermaseren, A. Vogt, Nucl. Phys. B 813 (2009) 220. [doi:10.1016/j.nuclphysb.2009.01.001](#).
- [398] H. Georgi, H. D. Politzer, Phys. Rev. D 14 (1976) 1829. [doi:10.1103/PhysRevD.14.1829](#).
- [399] I. Schienbein, et al., J. Phys. G 35 (2008) 053101. [doi:10.1088/0954-3899/35/5/053101](#).
- [400] F. Zaidi, et al., Phys. Rev. D 99 (2019) 093011. [doi:10.1103/PhysRevD.99.093011](#).
- [401] F. Zaidi, et al., Phys. Rev. D 101 (2020) 033001. [doi:10.1103/PhysRevD.101.033001](#).
- [402] R. K. Ellis, W. Furmanski, R. Petronzio, Nucl. Phys. B 212 (1983) 29. [doi:10.1016/0550-3213\(83\)90597-7](#).
- [403] M. A. G. Aivazis, F. I. Olness, W.-K. Tung, Phys. Rev. D 50 (1994) 3085. [doi:10.1103/PhysRevD.50.3085](#).
- [404] L. T. Brady, A. Accardi, T. J. Hobbs, W. Melnitchouk, Phys. Rev. D 84 (2011) 074008, [Erratum: Phys.Rev.D 85, 039902 (2012)]. [doi:10.1103/PhysRevD.84.074008](#).
- [405] S. Kretzer, M. H. Reno, Phys. Rev. D 66 (2002) 113007. [doi:10.1103/PhysRevD.66.113007](#).
- [406] S. Kretzer, D. Mason, F. Olness, Phys. Rev. D 65 (2002) 074010. [doi:10.1103/PhysRevD.65.074010](#).
- [407] S. Kretzer, M. H. Reno, Phys. Rev. D 69 (2004) 034002. [doi:10.1103/PhysRevD.69.034002](#).
- [408] K. G. Wilson, Phys. Rev. 179 (1969) 1499. [doi:10.1103/PhysRev.179.1499](#).
- [409] E. V. Shuryak, A. I. Vainshtein, Nucl. Phys. B 199 (1982) 451. [doi:10.1016/0550-3213\(82\)90355-8](#).
- [410] M. Dasgupta, B. Webber, Phys. Lett. B 382 (1996) 273. [doi:10.1016/0370-2693\(96\)00674-0](#).
- [411] Y. S. Jeong, M. H. Reno, Phys. Rev. D 82 (2010) 033010. [doi:10.1103/PhysRevD.82.033010](#).
- [412] K. Hagiwara, K. Mawatari, H. Yokoya, Nucl. Phys. B 668 (2003) 364, [Erratum: Nucl.Phys.B 701, 405 (2004)]. [doi:10.1016/S0550-3213\(03\)00575-3](#).
- [413] E. A. Paschos, J. Y. Yu, Phys. Rev. D 65 (2002) 033002. [doi:10.1103/PhysRevD.65.033002](#).
- [414] A. Gazizov, et al., EPJ Web Conf. 116 (2016) 08003. [doi:10.1051/epjconf/201611608003](#).
- [415] M. Anelli, et al., A facility to Search for Hidden Particles (SHiP) at the CERN SPS (2015). [arXiv:1504.04956](#).
- [416] L. Alvarez-Ruso, et al., Eur. Phys. J. ST 230 (2021) 4449. [doi:10.1140/epjs/s11734-021-00295-7](#).
- [417] C. Juszczak, J. A. Nowak, J. T. Sobczyk, Nucl. Phys. B Proc. Suppl. 159 (2006) 211. [doi:10.1016/j.nuclphysbps.2006.08.069](#).
- [418] J. Conrad, A. de Gouvea, S. Shalgar, J. Spitz, Phys. Rev. D 82 (2010) 093012. [doi:10.1103/PhysRevD.82.093012](#).
- [419] O. Benhar, P. Huber, C. Mariani, D. Meloni, Phys. Rept. 700 (2017) 1. [doi:10.1016/j.physrep.2017.07.004](#).
- [420] G. J. Kramer, et al., Phys. Lett. B 227 (1989) 199–203. [doi:10.1016/S0370-2693\(89\)80022-X](#).
- [421] S. Frullani, J. Mougey, Adv. Nucl. Phys. 14 (1984) 1.
- [422] L. Jiang, et al., Phys. Rev. D 105 (11) (2022) 112002. [doi:10.1103/PhysRevD.105.112002](#).
- [423] L. Gu, et al., Phys. Rev. C 103 (3) (2021) 034604. [doi:10.1103/PhysRevC.103.034604](#).
- [424] D. Z. Freedman, Phys. Rev. D 9 (1974) 1389. [doi:10.1103/PhysRevD.9.1389](#).
- [425] V. B. Kopeliovich, L. L. Frankfurt, JETP Lett. 19 (1974) 145.
- [426] P. S. Barbeau, Y. Efremenko, K. Scholberg, COHERENT at the Spallation Neutron Source [arXiv:2111.07033](#).

- [427] D. Akimov, et al., Phys. Rev. Lett. 126 (2021) 012002. [doi:10.1103/PhysRevLett.126.012002](https://doi.org/10.1103/PhysRevLett.126.012002).
- [428] J. I. Collar, et al., Nucl. Instrum. Meth. A 773 (2015) 56. [doi:10.1016/j.nima.2014.11.037](https://doi.org/10.1016/j.nima.2014.11.037).
- [429] D. Akimov, et al., The COHERENT Experimental Program, 2022. [arXiv:2204.04575](https://arxiv.org/abs/2204.04575).
- [430] M. Hoferichter, J. Menéndez, A. Schwenk, Phys. Rev. D 102 (2020) 074018. [doi:10.1103/PhysRevD.102.074018](https://doi.org/10.1103/PhysRevD.102.074018).
- [431] M. Abdullah, et al., Coherent elastic neutrino-nucleus scattering: Terrestrial and astrophysical applications. [arXiv:2203.07361](https://arxiv.org/abs/2203.07361).
- [432] R. H. Helm, Phys. Rev. 104 (1956) 1466. [doi:10.1103/PhysRev.104.1466](https://doi.org/10.1103/PhysRev.104.1466).
- [433] S. Klein, J. Nystrand, Phys. Rev. C 60 (1999) 014903. [doi:10.1103/PhysRevC.60.014903](https://doi.org/10.1103/PhysRevC.60.014903).
- [434] J. Erler, S. Su, Prog. Part. Nucl. Phys. 71 (2013) 119. [doi:10.1016/j.ppnp.2013.03.004](https://doi.org/10.1016/j.ppnp.2013.03.004).
- [435] D. Akimov, et al., Science 357 (6356) (2017) 1123. [doi:10.1126/science.aao0990](https://doi.org/10.1126/science.aao0990).
- [436] D. Akimov, et al., Measurement of the Coherent Elastic Neutrino-Nucleus Scattering Cross Section on CsI by COHERENT [arXiv:2110.07730](https://arxiv.org/abs/2110.07730).
- [437] D. Akimov, et al., COHERENT Collaboration data release from the first detection of coherent elastic neutrino-nucleus scattering on argon [arXiv:2006.12659](https://arxiv.org/abs/2006.12659), [doi:10.5281/zenodo.3903810](https://doi.org/10.5281/zenodo.3903810).
- [438] C. Giunti, et al., Annalen Phys. 528 (2016) 198. [doi:10.1002/andp.201500211](https://doi.org/10.1002/andp.201500211).
- [439] S. K. Singh, M. Sajjad Athar, Phys. Rev. C 52 (1995) 2203. [doi:10.1103/PhysRevC.52.2203](https://doi.org/10.1103/PhysRevC.52.2203).
- [440] P. Coloma, I. Esteban, M. C. Gonzalez-Garcia, J. Menendez, JHEP 08 (2020) 030. [doi:10.1007/JHEP08\(2020\)030](https://doi.org/10.1007/JHEP08(2020)030).
- [441] W. Czyz, G. C. Sheppey, J. D. Walecka, Nuovo Cim. 34 (1964) 404. [doi:10.1007/BF02734586](https://doi.org/10.1007/BF02734586).
- [442] D. Geiregat, et al., Phys. Lett. B 245 (1990) 271. [doi:10.1016/0370-2693\(90\)90146-W](https://doi.org/10.1016/0370-2693(90)90146-W).
- [443] S. R. Mishra, et al., Phys. Rev. Lett. 66 (1991) 3117. [doi:10.1103/PhysRevLett.66.3117](https://doi.org/10.1103/PhysRevLett.66.3117).
- [444] T. Adams, et al., Phys. Rev. D 61 (2000) 092001. [doi:10.1103/PhysRevD.61.092001](https://doi.org/10.1103/PhysRevD.61.092001).
- [445] W. Altmannshofer, et al., Phys. Rev. D 100 (2019) 115029. [doi:10.1103/PhysRevD.100.115029](https://doi.org/10.1103/PhysRevD.100.115029).
- [446] P. Ballett, et al., JHEP 01 (2019) 119. [doi:10.1007/JHEP01\(2019\)119](https://doi.org/10.1007/JHEP01(2019)119).
- [447] G. Magill, R. Plestid, Phys. Rev. D 95 (2017) 073004. [doi:10.1103/PhysRevD.95.073004](https://doi.org/10.1103/PhysRevD.95.073004).
- [448] A. Bodek, Pauli Blocking for a Relativistic Fermi Gas in Quasielastic Lepton Nucleus Scattering [arXiv:2111.03631](https://arxiv.org/abs/2111.03631).
- [449] S.-F. Ge, M. Lindner, W. Rodejohann, Phys. Lett. B 772 (2017) 164. [doi:10.1016/j.physletb.2017.06.020](https://doi.org/10.1016/j.physletb.2017.06.020).
- [450] W. Altmannshofer, S. Gori, M. Pospelov, I. Yavin, Phys. Rev. Lett. 113 (2014) 091801. [doi:10.1103/PhysRevLett.113.091801](https://doi.org/10.1103/PhysRevLett.113.091801).
- [451] J. D. Walecka, Muon Physics, edited by V. M. Hughes and C. S. Wu, Academic, New York, 1975.
- [452] W. Haxton, C. Lunardini, Comput. Phys. Commun. 179 (2008) 345. [doi:10.1016/j.cpc.2008.02.018](https://doi.org/10.1016/j.cpc.2008.02.018).
- [453] A. Fujii, Y. Yamaguchi, Progress of Theoretical Physics 31 (1964) 107. [doi:10.1143/PTP.31.107](https://doi.org/10.1143/PTP.31.107).
- [454] C. W. Kim, H. Primakoff, Phys. Rev. 140 (1965) B566. [doi:10.1103/PhysRev.140.B566](https://doi.org/10.1103/PhysRev.140.B566).
- [455] S. L. Mintz, Phys. Rev. C 23 (1981) 421. [doi:10.1103/PhysRevC.23.421](https://doi.org/10.1103/PhysRevC.23.421).
- [456] S. Nozawa, Y. Kohyama, T. Kaneta, K. Kubodera, J. Phys. Soc. Jap. 55 (1986) 2636. [doi:10.1143/JPSJ.55.2636](https://doi.org/10.1143/JPSJ.55.2636).
- [457] S. Nakamura, T. Sato, V. P. Gudkov, K. Kubodera, Phys. Rev. C 63 (2001) 034617, [Erratum: Phys.Rev.C 73, 049904 (2006)]. [doi:10.1103/PhysRevC.73.049904](https://doi.org/10.1103/PhysRevC.73.049904).
- [458] M. Fukugita, T. Yanagida, Physics of neutrinos and applications to astrophysics, Springer-Verlag, Berlin, Germany, 2003. [doi:10.1007/978-3-662-05119-1](https://doi.org/10.1007/978-3-662-05119-1).
- [459] M. Butler, J.-W. Chen, X. Kong, Phys. Rev. C 63 (2001) 035501. [doi:10.1103/PhysRevC.63.035501](https://doi.org/10.1103/PhysRevC.63.035501).

- [460] K. Kubodera, S. Nozawa, Int. J. Mod. Phys. E 3 (1994) 101. [doi:10.1142/S0218301394000048](https://doi.org/10.1142/S0218301394000048).
- [461] S. P. Riley, et al., Phys. Rev. C 59 (1999) 1780. [doi:10.1103/PhysRevC.59.1780](https://doi.org/10.1103/PhysRevC.59.1780).
- [462] S. E. Willis, et al., Phys. Rev. Lett. 44 (1980) 522, [Erratum: Phys.Rev.Lett. 44, 903 (1980), Erratum: Phys.Rev.Lett. 45, 1370 (1980)]. [doi:10.1103/PhysRevLett.44.522](https://doi.org/10.1103/PhysRevLett.44.522).
- [463] B. Zeitnitz, Prog. Part. Nucl. Phys. 32 (1994) 351. [doi:10.1016/0146-6410\(94\)90034-5](https://doi.org/10.1016/0146-6410(94)90034-5).
- [464] L. B. Auerbach, et al., Phys. Rev. C 64 (2001) 065501. [doi:10.1103/PhysRevC.64.065501](https://doi.org/10.1103/PhysRevC.64.065501).
- [465] M. Fukugita, Y. Kohyama, K. Kubodera, Phys. Lett. B 212 (1988) 139. [doi:10.1016/0370-2693\(88\)90513-8](https://doi.org/10.1016/0370-2693(88)90513-8).
- [466] C. E. Ortiz, et al., Phys. Rev. Lett. 85 (2000) 2909. [doi:10.1103/PhysRevLett.85.2909](https://doi.org/10.1103/PhysRevLett.85.2909).
- [467] J. N. Bahcall, Phys. Rev. C 56 (1997) 3391. [doi:10.1103/PhysRevC.56.3391](https://doi.org/10.1103/PhysRevC.56.3391).
- [468] N. Auerbach, N. Van Giai, O. K. Vorov, Phys. Rev. C 56 (1997) R2368. [doi:10.1103/PhysRevC.56.R2368](https://doi.org/10.1103/PhysRevC.56.R2368).
- [469] S. K. Singh, E. Oset, Phys. Rev. C 48 (1993) 1246. [doi:10.1103/PhysRevC.48.1246](https://doi.org/10.1103/PhysRevC.48.1246).
- [470] T. S. Kosmas, E. Oset, Phys. Rev. C 53 (1996) 1409. [doi:10.1103/PhysRevC.53.1409](https://doi.org/10.1103/PhysRevC.53.1409).
- [471] S. K. Singh, N. C. Mukhopadhyay, E. Oset, Phys. Rev. C 57 (1998) 2687. [doi:10.1103/PhysRevC.57.2687](https://doi.org/10.1103/PhysRevC.57.2687).
- [472] C. Volpe, et al., Phys. Rev. C 62 (2000) 015501. [doi:10.1103/PhysRevC.62.015501](https://doi.org/10.1103/PhysRevC.62.015501).
- [473] C. Volpe, N. Auerbach, G. Colo, N. Van Giai, Phys. Rev. C 65 (2002) 044603. [doi:10.1103/PhysRevC.65.044603](https://doi.org/10.1103/PhysRevC.65.044603).
- [474] E. Kolbe, K. Langanke, S. Krewald, F. K. Thielemann, Nucl. Phys. A 540 (1992) 599. [doi:10.1016/0375-9474\(92\)90175-J](https://doi.org/10.1016/0375-9474(92)90175-J).
- [475] E. Kolbe, F. K. Thielemann, K. Langanke, P. Vogel, Phys. Rev. C 52 (1995) 3437. [doi:10.1103/PhysRevC.52.3437](https://doi.org/10.1103/PhysRevC.52.3437).
- [476] N. Jachowicz, S. Rombouts, K. Heyde, J. Ryckebusch, Phys. Rev. C 59 (1999) 3246. [doi:10.1103/PhysRevC.59.3246](https://doi.org/10.1103/PhysRevC.59.3246).
- [477] N. Jachowicz, K. Heyde, J. Ryckebusch, S. Rombouts, Phys. Rev. C 65 (2002) 025501. [doi:10.1103/PhysRevC.65.025501](https://doi.org/10.1103/PhysRevC.65.025501).
- [478] A. Botrugno, G. Co, Nucl. Phys. A 761 (2005) 200. [doi:10.1016/j.nuclphysa.2005.07.010](https://doi.org/10.1016/j.nuclphysa.2005.07.010).
- [479] R. Lazauskas, C. Volpe, Nucl. Phys. A 792 (2007) 219. [doi:10.1016/j.nuclphysa.2007.06.005](https://doi.org/10.1016/j.nuclphysa.2007.06.005).
- [480] M.-K. Cheoun, E. Ha, K. S. Kim, T. Kajino, J. Phys. G 37 (2010) 055101. [doi:10.1088/0954-3899/37/5/055101](https://doi.org/10.1088/0954-3899/37/5/055101).
- [481] V. C. Chasioti, T. S. Kosmas, Nucl. Phys. A 829 (2009) 234. [doi:10.1016/j.nuclphysa.2009.08.009](https://doi.org/10.1016/j.nuclphysa.2009.08.009).
- [482] V. Tsakstara, T. S. Kosmas, Phys. Rev. C 84 (2011) 064620. [doi:10.1103/PhysRevC.84.064620](https://doi.org/10.1103/PhysRevC.84.064620).
- [483] V. Tsakstara, T. S. Kosmas, Phys. Rev. C 86 (2012) 044618. [doi:10.1103/PhysRevC.86.044618](https://doi.org/10.1103/PhysRevC.86.044618).
- [484] A. R. Samana, F. Krmpotic, N. Paar, C. A. Bertulani, Phys. Rev. C 83 (2011) 024303. [doi:10.1103/PhysRevC.83.024303](https://doi.org/10.1103/PhysRevC.83.024303).
- [485] N. Paar, D. Vretenar, T. Marketin, P. Ring, Phys. Rev. C 77 (2008) 024608. [doi:10.1103/PhysRevC.77.024608](https://doi.org/10.1103/PhysRevC.77.024608).
- [486] N. Paar, H. Tutman, T. Marketin, T. Fischer, Phys. Rev. C 87 (2013) 025801. [doi:10.1103/PhysRevC.87.025801](https://doi.org/10.1103/PhysRevC.87.025801).
- [487] E. Kolbe, K. Langanke, G. Martínez-Pinedo, P. Vogel, J. Phys. G 29 (2003) 2569. [doi:10.1088/0954-3899/29/11/010](https://doi.org/10.1088/0954-3899/29/11/010).
- [488] K. G. Balasi, K. Langanke, G. Martínez-Pinedo, Prog. Part. Nucl. Phys. 85 (2015) 33. [doi:10.1016/j.pnpnp.2015.08.001](https://doi.org/10.1016/j.pnpnp.2015.08.001).
- [489] N. Jachowicz, A. Nikolakopoulos, Eur. Phys. J. ST 230 (2021) 4339. [doi:10.1140/epjs/s11734-021-00286-8](https://doi.org/10.1140/epjs/s11734-021-00286-8).
- [490] I. Ruiz Simo, V. L. Martínez-Consentino, J. E. Amaro, E. Ruiz Arriola, Phys. Rev. D 97 (2018) 116006. [doi:10.1103/PhysRevD.97.116006](https://doi.org/10.1103/PhysRevD.97.116006).

- [491] A. Meucci, C. Giusti, Phys. Rev. D 85 (2012) 093002. [doi:10.1103/PhysRevD.85.093002](https://doi.org/10.1103/PhysRevD.85.093002).
- [492] R. González-Jiménez, et al., Phys. Rev. C 88 (2013) 025502. [doi:10.1103/PhysRevC.88.025502](https://doi.org/10.1103/PhysRevC.88.025502).
- [493] R. González-Jiménez, A. Nikolakopoulos, N. Jachowicz, J. M. Udías, Phys. Rev. C 100 (2019) 045501. [doi:10.1103/PhysRevC.100.045501](https://doi.org/10.1103/PhysRevC.100.045501).
- [494] R. González-Jiménez, et al., Phys. Rev. C 90 (2014) 035501. [doi:10.1103/PhysRevC.90.035501](https://doi.org/10.1103/PhysRevC.90.035501).
- [495] G. D. Megias, et al., Phys. Rev. D 91 (2015) 073004. [doi:10.1103/PhysRevD.91.073004](https://doi.org/10.1103/PhysRevD.91.073004).
- [496] A. Lovato, et al., Phys. Rev. X 10 (2020) 031068. [doi:10.1103/PhysRevX.10.031068](https://doi.org/10.1103/PhysRevX.10.031068).
- [497] A. Lovato, et al., Phys. Rev. C 91 (2015) 062501. [doi:10.1103/PhysRevC.91.062501](https://doi.org/10.1103/PhysRevC.91.062501).
- [498] R. Gatto, Nuovo Cim. 10 (1953) 1559.
- [499] R. Gatto, Nuovo Cim. 2 (1955) 670.
- [500] S. M. Berman, Lectures on weak interactions, CERN-62-20 (1962).
- [501] J. S. Bell, C. H. Llewellyn Smith, Nucl. Phys. B 28 (1971) 317. [doi:10.1016/0550-3213\(71\)90001-0](https://doi.org/10.1016/0550-3213(71)90001-0).
- [502] R. A. Smith, E. J. Moniz, Nucl. Phys. B 43 (1972) 605, [Erratum: Nucl.Phys.B 101, 547 (1975)]. [doi:10.1016/0550-3213\(75\)90612-4](https://doi.org/10.1016/0550-3213(75)90612-4).
- [503] T. K. Gaisser, J. S. O'Connell, Phys. Rev. D 34 (1986) 822. [doi:10.1103/PhysRevD.34.822](https://doi.org/10.1103/PhysRevD.34.822).
- [504] M. Sajjad Athar, S. K. Singh, Phys. Rev. C 61 (2000) 028501. [doi:10.1103/PhysRevC.61.028501](https://doi.org/10.1103/PhysRevC.61.028501).
- [505] J. E. Sobczyk, J. Nieves, F. Sánchez, Phys. Rev. C 102 (2020) 024601. [doi:10.1103/PhysRevC.102.024601](https://doi.org/10.1103/PhysRevC.102.024601).
- [506] E. Vagnoni, O. Benhar, D. Meloni, Phys. Rev. Lett. 118 (2017) 142502. [doi:10.1103/PhysRevLett.118.142502](https://doi.org/10.1103/PhysRevLett.118.142502).
- [507] M. Martini, M. Ericson, G. Chanfray, J. Marteau, Phys. Rev. C 80 (2009) 065501. [doi:10.1103/PhysRevC.80.065501](https://doi.org/10.1103/PhysRevC.80.065501).
- [508] M. Martini, M. Ericson, G. Chanfray, J. Marteau, Phys. Rev. C 81 (2010) 045502. [doi:10.1103/PhysRevC.81.045502](https://doi.org/10.1103/PhysRevC.81.045502).
- [509] M. Martini, M. Ericson, G. Chanfray, Phys. Rev. C 84 (2011) 055502. [doi:10.1103/PhysRevC.84.055502](https://doi.org/10.1103/PhysRevC.84.055502).
- [510] M. Martini, M. Ericson, Phys. Rev. C 87 (2013) 065501. [doi:10.1103/PhysRevC.87.065501](https://doi.org/10.1103/PhysRevC.87.065501).
- [511] J. Nieves, I. Ruiz Simo, M. J. Vicente Vacas, Phys. Lett. B 707 (2012) 72. [doi:10.1016/j.physletb.2011.11.061](https://doi.org/10.1016/j.physletb.2011.11.061).
- [512] J. Nieves, I. Ruiz Simo, M. J. Vicente Vacas, Phys. Lett. B 721 (2013) 90. [doi:10.1016/j.physletb.2013.03.002](https://doi.org/10.1016/j.physletb.2013.03.002).
- [513] H. De Vries, C. W. De Jager, C. De Vries, Atom. Data Nucl. Data Tabl. 36 (1987) 495. [doi:10.1016/0092-640X\(87\)90013-1](https://doi.org/10.1016/0092-640X(87)90013-1).
- [514] C. W. De Jager, H. De Vries, C. De Vries, Atom. Data Nucl. Data Tabl. 14 (1974) 479, [Erratum: Atom.Data Nucl.Data Tabl. 16, 580–580 (1975)]. [doi:10.1016/S0092-640X\(74\)80002-1](https://doi.org/10.1016/S0092-640X(74)80002-1).
- [515] C. Garcia-Recio, J. Nieves, E. Oset, Nucl. Phys. A 547 (1992) 473. [doi:10.1016/0375-9474\(92\)90034-H](https://doi.org/10.1016/0375-9474(92)90034-H).
- [516] J. Engel, Phys. Rev. C 57 (1998) 2004. [doi:10.1103/PhysRevC.57.2004](https://doi.org/10.1103/PhysRevC.57.2004).
- [517] A. Gil, J. Nieves, E. Oset, Nucl. Phys. A 627 (1997) 543. [doi:10.1016/S0375-9474\(97\)00513-7](https://doi.org/10.1016/S0375-9474(97)00513-7).
- [518] R. C. Carrasco, E. Oset, Nucl. Phys. A 536 (1992) 445. [doi:10.1016/0375-9474\(92\)90109-W](https://doi.org/10.1016/0375-9474(92)90109-W).
- [519] E. Oset, D. Strottman, H. Toki, J. Navarro, Phys. Rev. C 48 (1993) 2395. [doi:10.1103/PhysRevC.48.2395](https://doi.org/10.1103/PhysRevC.48.2395).
- [520] E. Oset, P. Fernandez de Cordoba, L. L. Salcedo, R. Brockmann, Phys. Rept. 188 (1990) 79. [doi:10.1016/0370-1573\(90\)90091-F](https://doi.org/10.1016/0370-1573(90)90091-F).
- [521] J. Nieves, J. E. Amaro, M. Valverde, Phys. Rev. C 70 (2004) 055503, [Erratum: Phys.Rev.C 72, 019902 (2005)]. [doi:10.1103/PhysRevC.70.055503](https://doi.org/10.1103/PhysRevC.70.055503).

- [522] M. Sajjad Athar, S. Ahmad, S. K. Singh, Nucl. Phys. A 764 (2006) 551. [doi:10.1016/j.nuclphysa.2005.09.017](#).
- [523] N. Paar, D. Vretenar, P. Ring, J. Phys. G 35 (2008) 014058. [doi:10.1088/0954-3899/35/1/014058](#).
- [524] C. Athanassopoulos, et al., Phys. Rev. C 56 (1997) 2806. [doi:10.1103/PhysRevC.56.2806](#).
- [525] J. Nieves, J. E. Sobczyk, Annals Phys. 383 (2017) 455. [doi:10.1016/j.aop.2017.06.002](#).
- [526] L. B. Auerbach, et al., Phys. Rev. C 66 (2002) 015501. [doi:10.1103/PhysRevC.66.015501](#).
- [527] E. Kolbe, K. Langanke, P. Vogel, Nucl. Phys. A 652 (1999) 91. [doi:10.1016/S0375-9474\(99\)00152-9](#).
- [528] N. Auerbach, B. A. Brown, Phys. Rev. C 65 (2002) 024322. [doi:10.1103/PhysRevC.65.024322](#).
- [529] Y. Umino, J. M. Udias, Phys. Rev. C 52 (1995) 3399. [doi:10.1103/PhysRevC.52.3399](#).
- [530] Y. Umino, J. M. Udias, P. J. Mulders, Phys. Rev. Lett. 74 (1995) 4993. [doi:10.1103/PhysRevLett.74.4993](#).
- [531] A. C. Hayes, I. S. Towner, Phys. Rev. C 61 (2000) 044603. [doi:10.1103/PhysRevC.61.044603](#).
- [532] E. Kolbe, K. Langanke, S. Krewald, Phys. Rev. C 49 (1994) 1122. [doi:10.1103/PhysRevC.49.1122](#).
- [533] T. W. Donnelly, R. D. Peccei, Phys. Rept. 50 (1979) 1. [doi:10.1016/0370-1573\(79\)90010-3](#).
- [534] T. W. Donnelly, Phys. Lett. B 43 (1973) 93. [doi:10.1016/0370-2693\(73\)90417-6](#).
- [535] C. Athanassopoulos, et al., Phys. Rev. C 55 (1997) 2078. [doi:10.1103/PhysRevC.55.2078](#).
- [536] T. Suzuki, D. F. Measday, J. P. Roalsvig, Phys. Rev. C 35 (1987) 2212. [doi:10.1103/PhysRevC.35.2212](#).
- [537] F. Krmpotic, A. Samana, A. Mariano, Phys. Rev. C 71 (2005) 044319. [doi:10.1103/PhysRevC.71.044319](#).
- [538] A. A. Aguilar-Arevalo, et al., Phys. Rev. Lett. 120 (2018) 141802. [doi:10.1103/PhysRevLett.120.141802](#).
- [539] F. Akbar, M. Sajjad Athar, S. K. Singh, J. Phys. G 44 (2017) 125108. [doi:10.1088/1361-6471/aa9125](#).
- [540] A. Nikolakopoulos, V. Pandey, J. Spitz, N. Jachowicz, Phys. Rev. C 103 (2021) 064603. [doi:10.1103/PhysRevC.103.064603](#).
- [541] C. Andreopoulos, et al., Nucl. Instrum. Meth. A 614 (2010) 87. [doi:10.1016/j.nima.2009.12.009](#).
- [542] C. Juszczak, Acta Phys. Polon. B 40 (2009) 2507.
- [543] T. Golan, C. Juszczak, J. T. Sobczyk, Phys. Rev. C 86 (2012) 015505. [doi:10.1103/PhysRevC.86.015505](#).
- [544] M. Martini, M. Ericson, G. Chanfray, Phys. Rev. D 87 (2013) 013009. [doi:10.1103/PhysRevD.87.013009](#).
- [545] A. M. Ankowski, O. Benhar, M. Sakuda, Phys. Rev. D 91 (2015) 033005. [doi:10.1103/PhysRevD.91.033005](#).
- [546] O. Lalakulich, U. Mosel, K. Gallmeister, Phys. Rev. C 86 (2012) 054606. [doi:10.1103/PhysRevC.86.054606](#).
- [547] A. Bodek, Muon internal bremsstrahlung: A Conventional explanation for the excess nu(e) events in Mini-Boone [arXiv:0709.4004](#).
- [548] M. Day, K. S. McFarland, Phys. Rev. D 86 (2012) 053003. [doi:10.1103/PhysRevD.86.053003](#).
- [549] K. M. Graczyk, Phys. Lett. B 732 (2014) 315. [doi:10.1016/j.physletb.2014.03.065](#).
- [550] O. Tomalak, et al., Theory of QED radiative corrections to neutrino scattering at accelerator energies [arXiv:2204.11379](#).
- [551] A. De Rujula, R. Petronzio, A. Savoy-Navarro, Nucl. Phys. B 154 (1979) 394. [doi:10.1016/0550-3213\(79\)90039-7](#).
- [552] F. Akbar, et al., Int. J. Mod. Phys. E 24 (2015) 1550079. [doi:10.1142/S0218301315500792](#).
- [553] T. Katori, AIP Conf. Proc. 1189 (2009) 139. [doi:10.1063/1.3274144](#).
- [554] F. Sanchez, M. Sorel, L. Alvarez-Ruso (Eds.), Proceedings, 6th International Workshop on Neutrino-nucleus interactions in the few GeV region (NUINT 09): Sitges, Spain, May 18-22, 2009, Vol. 1189, 2009.

- [555] Proceedings, 7th International Workshop on Neutrino-nucleus interactions in the few GeV region (NUINT 11): Dehradun, India, March 7-11, 2011, AIP Conf. Proc. 1405 (2011) 1.
- [556] O. Benhar, D. Meloni, Nucl. Phys. A 789 (2007) 379. [doi:10.1016/j.nuclphysa.2007.02.015](#).
- [557] O. Benhar, N. Rocco, Adv. High Energy Phys. 2013 (2013) 912702. [doi:10.1155/2013/912702](#).
- [558] J. Marteau, Eur. Phys. J. A 5 (1999) 183. [doi:10.1007/s100500050274](#).
- [559] M. Valverde, J. E. Amaro, J. Nieves, Phys. Lett. B 638 (2006) 325. [doi:10.1016/j.physletb.2006.05.053](#).
- [560] J. Nieves, I. Ruiz Simo, M. J. Vicente Vacas, Phys. Rev. C 83 (2011) 045501. [doi:10.1103/PhysRevC.83.045501](#).
- [561] N. Rocco, et al., Phys. Rev. C 99 (2019) 025502. [doi:10.1103/PhysRevC.99.025502](#).
- [562] M. V. Ivanov, et al., Phys. Rev. C 99 (2019) 014610. [doi:10.1103/PhysRevC.99.014610](#).
- [563] M. Martini, M. Ericson, Phys. Rev. C 90 (2014) 025501. [doi:10.1103/PhysRevC.90.025501](#).
- [564] M. Ericson, M. Martini, Phys. Rev. C 91 (2015) 035501. [doi:10.1103/PhysRevC.91.035501](#).
- [565] M. Martini, et al., Phys. Rev. C 94 (2016) 015501. [doi:10.1103/PhysRevC.94.015501](#).
- [566] R. Gran, J. Nieves, F. Sanchez, M. J. Vicente Vacas, Phys. Rev. D 88 (2013) 113007. [doi:10.1103/PhysRevD.88.113007](#).
- [567] B. Bourguille, J. Nieves, F. Sánchez, JHEP 04 (2021) 004. [doi:10.1007/JHEP04\(2021\)004](#).
- [568] V. Pandey, et al., Phys. Rev. C 92 (2015) 024606. [doi:10.1103/PhysRevC.92.024606](#).
- [569] T. Van Cuyck, et al., Phys. Rev. C 94 (2016) 024611. [doi:10.1103/PhysRevC.94.024611](#).
- [570] T. Van Cuyck, et al., Phys. Rev. C 95 (2017) 054611. [doi:10.1103/PhysRevC.95.054611](#).
- [571] E. Berrueta Martinez, A. Mariano, C. Barbero, Phys. Rev. C 103 (2021) 015503. [doi:10.1103/PhysRevC.103.015503](#).
- [572] A. Lovato, et al., Phys. Rev. Lett. 112 (2014) 182502. [doi:10.1103/PhysRevLett.112.182502](#).
- [573] A. Lovato, et al., Phys. Rev. C 97 (2018) 022502. [doi:10.1103/PhysRevC.97.022502](#).
- [574] O. Benhar, et al., Phys. Rev. D 72 (2005) 053005. [doi:10.1103/PhysRevD.72.053005](#).
- [575] O. Benhar, A. Lovato, N. Rocco, Phys. Rev. C 92 (2015) 024602. [doi:10.1103/PhysRevC.92.024602](#).
- [576] N. Rocco, A. Lovato, O. Benhar, Phys. Rev. Lett. 116 (2016) 192501. [doi:10.1103/PhysRevLett.116.192501](#).
- [577] C. Barbieri, N. Rocco, V. Somà, Phys. Rev. C 100 (2019) 062501. [doi:10.1103/PhysRevC.100.062501](#).
- [578] J. E. Amaro, et al., Phys. Rev. C 71 (2005) 015501. [doi:10.1103/PhysRevC.71.015501](#).
- [579] K. Gallmeister, U. Mosel, J. Weil, Phys. Rev. C 94 (2016) 035502. [doi:10.1103/PhysRevC.94.035502](#).
- [580] J. E. Amaro, M. B. Barbaro, J. A. Caballero, T. W. Donnelly, Phys. Rev. Lett. 108 (2012) 152501. [doi:10.1103/PhysRevLett.108.152501](#).
- [581] V. L. Martinez-Consentino, I. R. Simo, J. E. Amaro, Phys. Rev. C 104 (2021) 025501. [doi:10.1103/PhysRevC.104.025501](#).
- [582] I. Ruiz Simo, et al., Phys. Rev. D 90 (2014) 033012. [doi:10.1103/PhysRevD.90.033012](#).
- [583] I. Ruiz Simo, et al., J. Phys. G 44 (2017) 065105. [doi:10.1088/1361-6471/aa6a06](#).
- [584] G. D. Megias, et al., Phys. Rev. D 94 (2016) 093004. [doi:10.1103/PhysRevD.94.093004](#).
- [585] I. Ruiz Simo, et al., Phys. Lett. B 762 (2016) 124. [doi:10.1016/j.physletb.2016.09.021](#).
- [586] I. Ruiz Simo, et al., Phys. Lett. B 770 (2017) 193. [doi:10.1016/j.physletb.2017.04.063](#).
- [587] J. E. Amaro, et al., Phys. Rev. C 95 (2017) 065502. [doi:10.1103/PhysRevC.95.065502](#).

- [588] I. Ruiz Simo, et al., *Annals Phys.* 388 (2018) 323. [doi:10.1016/j.aop.2017.11.029](#).
- [589] G. D. Megias, et al., *J. Phys. G* 46 (2019) 015104. [doi:10.1088/1361-6471/aaf3ae](#).
- [590] F. Dautry, M. Rho, D. O. Riska, *Nucl. Phys. A* 264 (1976) 507. [doi:10.1016/0375-9474\(76\)90420-6](#).
- [591] K. Ohta, M. Wakamatsu, *Phys. Lett. B* 51 (1974) 325. [doi:10.1016/0370-2693\(74\)90218-4](#).
- [592] M. Ericson, A. Figureau, C. Thevenet, *Phys. Lett. B* 45 (1973) 19. [doi:10.1016/0370-2693\(73\)90242-6](#).
- [593] D. O. Riska, G. E. Brown, *Phys. Lett. B* 32 (1970) 662. [doi:10.1016/0370-2693\(70\)90437-5](#).
- [594] J. Delorme, M. Ericson, *Phys. Lett. B* 156 (1985) 263. [doi:10.1016/0370-2693\(85\)91521-7](#).
- [595] W. Muller, M. Gari, *Phys. Lett. B* 102 (1981) 389. [doi:10.1016/0370-2693\(81\)91238-7](#).
- [596] N. C. Mukhopadhyay, H. C. Chiang, S. K. Singh, E. Oset, *Phys. Lett. B* 434 (1998) 7. [doi:10.1016/S0370-2693\(98\)00790-4](#).
- [597] S. K. Singh, M. J. Vicente Vacas, *Phys. Rev. D* 74 (2006) 053009. [doi:10.1103/PhysRevD.74.053009](#).
- [598] E. Oset, L. L. Salcedo, *Nucl. Phys. A* 468 (1987) 631. [doi:10.1016/0375-9474\(87\)90185-0](#).
- [599] C. Garcia-Recio, et al., *Nucl. Phys. A* 526 (1991) 685. [doi:10.1016/0375-9474\(91\)90438-C](#).
- [600] M. J. Vicente Vacas, M. K. Khankhasaev, S. G. Mashnik, Inclusive pion double charge exchange above .5-GeV (1994). [arXiv:nucl-th/9412023](#).
- [601] S. K. Singh, M. J. Vicente-Vacas, E. Oset, *Phys. Lett. B* 416 (1998) 23, [Erratum: *Phys.Lett.B* 423, 428 (1998)]. [doi:10.1016/S0370-2693\(97\)01325-7](#).
- [602] M. Sajjad Athar, S. Ahmad, S. K. Singh, *Phys. Rev. D* 75 (2007) 093003. [doi:10.1103/PhysRevD.75.093003](#).
- [603] H. Faissner, et al., *Phys. Lett. B* 125 (1983) 230. [doi:10.1016/0370-2693\(83\)91274-1](#).
- [604] E. Isiksal, D. Rein, J. G. Morfin, *Phys. Rev. Lett.* 52 (1984) 1096. [doi:10.1103/PhysRevLett.52.1096](#).
- [605] F. Bergsma, et al., *Phys. Lett. B* 157 (1985) 469. [doi:10.1016/0370-2693\(85\)90402-2](#).
- [606] P. Vilain, et al., *Phys. Lett. B* 313 (1993) 267. [doi:10.1016/0370-2693\(93\)91223-A](#).
- [607] H. J. Grabosch, et al., *Z. Phys. C* 31 (1986) 203. [doi:10.1007/BF01479528](#).
- [608] R. Nahnauer, Recent results on coherent and incoherent particle production in neutrino nucleus interactions below 30 GeV, 1986, p. 335.
- [609] M. Hasegawa, et al., *Phys. Rev. Lett.* 95 (2005) 252301. [doi:10.1103/PhysRevLett.95.252301](#).
- [610] K. Hiraide, et al., *Phys. Rev. D* 78 (2008) 112004. [doi:10.1103/PhysRevD.78.112004](#).
- [611] A. A. Aguilar-Arevalo, et al., *Phys. Lett. B* 664 (2008) 41. [doi:10.1016/j.physletb.2008.05.006](#).
- [612] M. A. Acero, et al., *Phys. Rev. D* 102 (2020) 012004. [doi:10.1103/PhysRevD.102.012004](#).
- [613] K. Abe, et al., *Phys. Rev. Lett.* 117 (2016) 192501. [doi:10.1103/PhysRevLett.117.192501](#).
- [614] A. Higuera, et al., *Phys. Rev. Lett.* 113 (2014) 261802. [doi:10.1103/PhysRevLett.113.261802](#).
- [615] C. T. Kullenberg, et al., *Phys. Lett. B* 682 (2009) 177. [doi:10.1016/j.physletb.2009.10.083](#).
- [616] D. Rein, L. M. Sehgal, *Nucl. Phys. B* 223 (1983) 29. [doi:10.1016/0550-3213\(83\)90090-1](#).
- [617] D. Rein, L. M. Sehgal, *Phys. Lett. B* 657 (2007) 207. [doi:10.1016/j.physletb.2007.10.025](#).
- [618] A. A. Belkov, B. Z. Kopeliovich, *Sov. J. Nucl. Phys.* 46 (1987) 499.
- [619] C. Berger, L. M. Sehgal, *Phys. Rev. D* 79 (2009) 053003. [doi:10.1103/PhysRevD.79.053003](#).
- [620] E. A. Paschos, D. Schalla, *Phys. Rev. D* 80 (2009) 033005. [doi:10.1103/PhysRevD.80.033005](#).
- [621] E. A. Paschos, A. Kartavtsev, G. J. Gounaris, *Phys. Rev. D* 74 (2006) 054007. [doi:10.1103/PhysRevD.74.054007](#).

- [622] A. Higuera, E. A. Paschos, Eur. Phys. J. Plus 129 (2014) 43. [doi:10.1140/epjp/i2014-14043-1](#).
- [623] J. L. Raaf, Nucl. Phys. B Proc. Suppl. 139 (2005) 47. [doi:10.1016/j.nuclphysbps.2004.11.240](#).
- [624] J. L. Raaf, A Measurement of the Neutrino Neutral Current π^0 Cross Section at MiniBooNE, Ph.D. thesis, Cincinnati U. (2005). [doi:10.2172/15020150](#).
- [625] N. G. Kelkar, E. Oset, P. Fernandez de Cordoba, Phys. Rev. C 55 (1997) 1964. [doi:10.1103/PhysRevC.55.1964](#).
- [626] S. K. Singh, M. Sajjad Athar, S. Ahmad, Phys. Rev. Lett. 96 (2006) 241801. [doi:10.1103/PhysRevLett.96.241801](#).
- [627] L. Alvarez-Ruso, L. S. Geng, S. Hirenzaki, M. J. Vicente Vacas, Phys. Rev. C 75 (2007) 055501, [Erratum: Phys.Rev.C 80, 019906 (2009)]. [doi:10.1103/PhysRevC.75.055501](#).
- [628] L. Alvarez-Ruso, L. S. Geng, M. J. Vicente Vacas, Phys. Rev. C 76 (2007) 068501, [Erratum: Phys.Rev.C 80, 029904 (2009)]. [doi:10.1103/PhysRevC.76.068501](#).
- [629] J. E. Amaro, E. Hernandez, J. Nieves, M. Valverde, Phys. Rev. D 79 (2009) 013002. [doi:10.1103/PhysRevD.79.013002](#).
- [630] T. Leitner, U. Mosel, S. Winkelmann, Phys. Rev. C 79 (2009) 057601. [doi:10.1103/PhysRevC.79.057601](#).
- [631] E. Hernandez, J. Nieves, M. J. Vicente-Vacas, Phys. Rev. D 80 (2009) 013003. [doi:10.1103/PhysRevD.80.013003](#).
- [632] L. Alvarez-Ruso, AIP Conf. Proc. 1405 (2011) 140. [doi:10.1063/1.3661574](#).
- [633] L. Alvarez-Ruso, et al., Phys. Rev. C 87 (2013) 015503. [doi:10.1103/PhysRevC.87.015503](#).
- [634] Z. Wang, et al., Phys. Rev. Lett. 117 (2016) 061802. [doi:10.1103/PhysRevLett.117.061802](#).
- [635] J. J. Aubert, et al., Phys. Lett. B 123 (1983) 275. [doi:10.1016/0370-2693\(83\)90437-9](#).
- [636] J. Gomez, et al., Phys. Rev. D 49 (1994) 4348. [doi:10.1103/PhysRevD.49.4348](#).
- [637] K. Ackerstaff, et al., Phys. Lett. B 475 (2000) 386, [Erratum: Phys.Lett.B 567, 339–346 (2003)]. [doi:10.1016/S0370-2693\(99\)01493-8](#).
- [638] G. Bari, et al., Phys. Lett. B 163 (1985) 282. [doi:10.1016/0370-2693\(85\)90238-2](#).
- [639] A. C. Benvenuti, et al., Phys. Lett. B 189 (1987) 483. [doi:10.1016/0370-2693\(87\)90664-2](#).
- [640] M. Arneodo, et al., Nucl. Phys. B 441 (1995) 12. [doi:10.1016/0550-3213\(95\)00023-2](#).
- [641] P. Amaudruz, et al., Nucl. Phys. B 441 (1995) 3. [doi:10.1016/0550-3213\(94\)00023-9](#).
- [642] J. Seely, et al., Phys. Rev. Lett. 103 (2009) 202301. [doi:10.1103/PhysRevLett.103.202301](#).
- [643] J. Ashman, et al., Z. Phys. C 57 (1993) 211. [doi:10.1007/BF01565050](#).
- [644] S. Malace, D. Gaskell, D. W. Higinbotham, I. Cloet, Int. J. Mod. Phys. E 23 (2014) 1430013. [doi:10.1142/S0218301314300136](#).
- [645] A. Filkins, et al., Phys. Rev. D 101 (2020) 112007. [doi:10.1103/PhysRevD.101.112007](#).
- [646] D. Ruterbories, et al., Phys. Rev. D 104 (2021) 092007. [doi:10.1103/PhysRevD.104.092007](#).
- [647] J. Mousseau, et al., Phys. Rev. D 93 (2016) 071101. [doi:10.1103/PhysRevD.93.071101](#).
- [648] B. Tice, et al., Phys. Rev. Lett. 112 (2014) 231801. [doi:10.1103/PhysRevLett.112.231801](#).
- [649] S. V. Akulinichev, G. M. Vagradov, S. A. Kulagin, JETP Lett. 42 (1985) 127.
- [650] R. P. Bickerstaff, A. W. Thomas, J. Phys. G 15 (1989) 1523. [doi:10.1088/0954-3899/15/10/006](#).
- [651] S. A. Kulagin, Nucl. Phys. A 500 (1989) 653. [doi:10.1016/0375-9474\(89\)90233-9](#).
- [652] E. Marco, E. Oset, P. Fernandez de Cordoba, Nucl. Phys. A 611 (1996) 484. [doi:10.1016/S0375-9474\(96\)00289-8](#).
- [653] M. Ericson, A. W. Thomas, Phys. Lett. B 128 (1983) 112. [doi:10.1016/0370-2693\(83\)90085-0](#).

- [654] R. P. Bickerstaff, G. A. Miller, Phys. Lett. B 168 (1986) 409. [doi:10.1016/0370-2693\(86\)91654-0](#).
- [655] E. L. Berger, F. Coester, Ann. Rev. Nucl. Part. Sci. 37 (1987) 463. [doi:10.1146/annurev.ns.37.120187.002335](#).
- [656] R. L. Jaffe, Phys. Rev. Lett. 50 (1983) 228. [doi:10.1103/PhysRevLett.50.228](#).
- [657] H. Mineo, et al., Nucl. Phys. A 735 (2004) 482. [doi:10.1016/j.nuclphysa.2004.02.011](#).
- [658] I. C. Cloet, W. Bentz, A. W. Thomas, Phys. Rev. Lett. 95 (2005) 052302. [doi:10.1103/PhysRevLett.95.052302](#).
- [659] O. Nachtmann, H. J. Pirner, Z. Phys. C 21 (1984) 277. [doi:10.1007/BF01577042](#).
- [660] F. E. Close, R. G. Roberts, G. G. Ross, Phys. Lett. B 129 (1983) 346. [doi:10.1016/0370-2693\(83\)90679-2](#).
- [661] L. L. Frankfurt, M. I. Strikman, Phys. Rept. 160 (1988) 235. [doi:10.1016/0370-1573\(88\)90179-2](#).
- [662] N. Armesto, J. Phys. G 32 (2006) R367. [doi:10.1088/0954-3899/32/11/R01](#).
- [663] M. Arneodo, Phys. Rept. 240 (1994) 301. [doi:10.1016/0370-1573\(94\)90048-5](#).
- [664] D. F. Geesaman, K. Saito, A. W. Thomas, Ann. Rev. Nucl. Part. Sci. 45 (1995) 337. [doi:10.1146/annurev.ns.45.120195.002005](#).
- [665] O. Hen, et al., Int. J. Mod. Phys. E 22 (2013) 1330017. [doi:10.1142/S0218301313300178](#).
- [666] G. Piller, W. Weise, Phys. Rept. 330 (2000) 1. [doi:10.1016/S0370-1573\(99\)00107-6](#).
- [667] N. Kalantarians, C. Keppel, M. E. Christy, Phys. Rev. C 96 (2017) 032201. [doi:10.1103/PhysRevC.96.032201](#).
- [668] H. Haider, M. Sajjad Athar, S. K. Singh, I. R. Simo, J. Phys. G 44 (2017) 045111. [doi:10.1088/1361-6471/aa60ea](#).
- [669] S. A. Kulagin, R. Petti, Phys. Rev. D 76 (2007) 094023. [doi:10.1103/PhysRevD.76.094023](#).
- [670] M. Sajjad Athar, S. K. Singh, M. J. Vicente Vacas, Phys. Lett. B 668 (2008) 133. [doi:10.1016/j.physletb.2008.08.019](#).
- [671] M. Sajjad Athar, I. Ruiz Simo, M. J. Vicente Vacas, Nucl. Phys. A 857 (2011) 29. [doi:10.1016/j.nuclphysa.2011.03.008](#).
- [672] H. Haider, I. R. Simo, M. Sajjad Athar, M. J. V. Vacas, Phys. Rev. C 84 (2011) 054610. [doi:10.1103/PhysRevC.84.054610](#).
- [673] H. Haider, I. R. Simo, M. Sajjad Athar, Phys. Rev. C 87 (2013) 035502. [doi:10.1103/PhysRevC.87.035502](#).
- [674] H. Haider, I. Ruiz Simo, M. Sajjad Athar, Phys. Rev. C 85 (2012) 055201. [doi:10.1103/PhysRevC.85.055201](#).
- [675] H. Haider, et al., Nucl. Phys. A 955 (2016) 58. [doi:10.1016/j.nuclphysa.2016.06.006](#).
- [676] V. Ansari, et al., Eur. Phys. J Special Topics 230. [doi:10.1140/epjs/s11734-021-00277-9](#).
- [677] F. Zaidi, et al., Phys. Rev. D 105 (2022) 033010. [doi:10.1103/PhysRevD.105.033010](#).
- [678] M. Sajjad Athar, S. K. Singh, F. Zaidi, Phys. Rev. D 105 (2022) 093002. [doi:10.1103/PhysRevD.105.093002](#).
- [679] P. Fernandez de Cordoba, E. Oset, Phys. Rev. C 46 (1992) 1697. [doi:10.1103/PhysRevC.46.1697](#).
- [680] E. Oset, A. Palanques-Mestre, Nucl. Phys. A 359 (1981) 289. [doi:10.1016/0375-9474\(81\)90238-4](#).
- [681] A. Gil, J. Nieves, E. Oset, Nucl. Phys. A 627 (1997) 599. [doi:10.1016/S0375-9474\(97\)00515-0](#).
- [682] C. Mahaux, P. F. Bortignon, R. A. Broglia, C. H. Dasso, Phys. Rept. 120 (1985) 1. [doi:10.1016/0370-1573\(85\)90100-0](#).
- [683] H. Haider, et al., Nucl. Phys. A 943 (2015) 58. [doi:10.1016/j.nuclphysa.2015.08.008](#).
- [684] S. A. Kulagin, R. Petti, Nucl. Phys. A 765 (2006) 126. [doi:10.1016/j.nuclphysa.2005.10.011](#).
- [685] C. H. Llewellyn Smith, Phys. Lett. B 128 (1983) 107. [doi:10.1016/0370-2693\(83\)90084-9](#).
- [686] J. S. Conway, et al., Phys. Rev. D 39 (1989) 92. [doi:10.1103/PhysRevD.39.92](#).

- [687] P. J. Sutton, A. D. Martin, R. G. Roberts, W. J. Stirling, Phys. Rev. D 45 (1992) 2349. [doi:10.1103/PhysRevD.45.2349](#).
- [688] K. Wijesooriya, P. E. Reimer, R. J. Holt, Phys. Rev. C 72 (2005) 065203. [doi:10.1103/PhysRevC.72.065203](#).
- [689] M. Gluck, E. Reya, A. Vogt, Z. Phys. C 53 (1992) 651. [doi:10.1007/BF01559743](#).
- [690] R. J. Glauber, ed. by W.E. Brittin and L.G. Dunham Interscience, New York.
- [691] V. N. Gribov, Sov. Phys. JETP 29 (1969) 483.
- [692] V. N. Gribov, Zh. Eksp. Teor. Fiz. 57 (1969) 1306.
- [693] V. N. Gribov, Zh. Eksp. Teor. Fiz. 53 (1967) 654.
- [694] V. A. Abramovsky, V. N. Gribov, O. V. Kancheli, Yad. Fiz. 18 (1973) 595.
- [695] V. A. Karmanov, L. A. Kondratyuk, Pisma Zh. Eksp. Teor. Fiz. 18 (1973) 451.
- [696] J. J. Sakurai, D. Schildknecht, Phys. Lett. B 40 (1972) 121. [doi:10.1016/0370-2693\(72\)90300-0](#).
- [697] J. D. Bjorken, Proc of the Int. Symp. on Electron and Photon Interactions at High energies, Cornell University (1971).
- [698] A. Bramon, E. Etim, M. Greco, Phys. Lett. B 41 (1972) 609. [doi:10.1016/0370-2693\(72\)90646-6](#).
- [699] N. N. Nikolaev, B. G. Zakharov, Z. Phys. C 49 (1991) 607. [doi:10.1007/BF01483577](#).
- [700] A. H. Mueller, Nucl. Phys. B 415 (1994) 373. [doi:10.1016/0550-3213\(94\)90116-3](#).
- [701] N. Armesto, Eur. Phys. J. C 26 (2002) 35. [doi:10.1007/s10052-002-1021-z](#).
- [702] S. J. Brodsky, Acta Phys. Polon. B 36 (2005) 635.
- [703] B. Z. Kopeliovich, J. G. Morfin, I. Schmidt, Prog. Part. Nucl. Phys. 68 (2013) 314. [doi:10.1016/j.ppnp.2012.09.004](#).
- [704] K. J. Eskola, V. J. Kolhinen, C. A. Salgado, Eur. Phys. J. C 9 (1999) 61. [doi:10.1007/s100520050513](#).
- [705] K. J. Eskola, V. J. Kolhinen, P. V. Ruuskanen, Nucl. Phys. B 535 (1998) 351. [doi:10.1016/S0550-3213\(98\)00589-6](#).
- [706] M. Hirai, S. Kumano, M. Miyama, Phys. Rev. D 64 (2001) 034003. [doi:10.1103/PhysRevD.64.034003](#).
- [707] M. Hirai, S. Kumano, T. H. Nagai, Phys. Rev. C 70 (2004) 044905. [doi:10.1103/PhysRevC.70.044905](#).
- [708] D. de Florian, R. Sassot, Phys. Rev. D 69 (2004) 074028. [doi:10.1103/PhysRevD.69.074028](#).
- [709] K. J. Eskola, V. J. Kolhinen, H. Paukkunen, C. A. Salgado, JHEP 05 (2007) 002. [doi:10.1088/1126-6708/2007/05/002](#).
- [710] M. Hirai, S. Kumano, T. H. Nagai, Phys. Rev. C 76 (2007) 065207. [doi:10.1103/PhysRevC.76.065207](#).
- [711] K. J. Eskola, H. Paukkunen, C. A. Salgado, JHEP 04 (2009) 065. [doi:10.1088/1126-6708/2009/04/065](#).
- [712] K. J. Eskola, P. Paakkinen, H. Paukkunen, C. A. Salgado, Eur. Phys. J. C 77 (2017) 163. [doi:10.1140/epjc/s10052-017-4725-9](#).
- [713] I. Schienbein, et al., Phys. Rev. D 80 (2009) 094004. [doi:10.1103/PhysRevD.80.094004](#).
- [714] T. Stavreva, et al., JHEP 01 (2011) 152. [doi:10.1007/JHEP01\(2011\)152](#).
- [715] K. Kovarik, et al., Phys. Rev. Lett. 106 (2011) 122301. [doi:10.1103/PhysRevLett.106.122301](#).
- [716] D. de Florian, R. Sassot, P. Zurita, M. Stratmann, Phys. Rev. D 85 (2012) 074028. [doi:10.1103/PhysRevD.85.074028](#).
- [717] I. Helenius, M. Walt, W. Vogelsang, TUJU21: NNLO nuclear parton distribution functions with electroweak-boson production data from the LHC (2021). [arXiv:2112.11904](#).

- [718] H. Khanpour, et al., Phys. Rev. D 104 (2021) 034010. [doi:10.1103/PhysRevD.104.034010](#).
- [719] R. Abdul Khalek, J. J. Ethier, J. Rojo, G. van Weelden, JHEP 09 (2020) 183. [doi:10.1007/JHEP09\(2020\)183](#).
- [720] K. J. Eskola, Nucl. Phys. A 910-911 (2013) 163. [doi:10.1016/j.nuclphysa.2012.12.029](#).
- [721] K. Kovarik, et al., Phys. Rev. D 93 (2016) 085037. [doi:10.1103/PhysRevD.93.085037](#).
- [722] J. F. Owens, et al., Phys. Rev. D 75 (2007) 054030. [doi:10.1103/PhysRevD.75.054030](#).
- [723] J. Pumplin, et al., JHEP 07 (2002) 012. [doi:10.1088/1126-6708/2002/07/012](#).
- [724] D. Stump, et al., JHEP 10 (2003) 046. [doi:10.1088/1126-6708/2003/10/046](#).
- [725] S. A. Kulagin, R. Petti, Nucl. Phys. B Proc. Suppl. 159 (2006) 180. [doi:10.1016/j.nuclphysbps.2006.08.036](#).
- [726] K. F. Muzakka, et al., Compatibility of Neutrino DIS Data and Its Impact on Nuclear Parton Distribution Functions (2022). [arXiv:2204.13157](#).
- [727] V. Mamyan, Measurements of F_2 and $R=\sigma_L/\sigma_T$ on Nuclear Targets in the Nucleon Resonance Region [arXiv:1202.1457](#).
- [728] J. J. Aubert, et al., Nucl. Phys. B 272 (1986) 158. [doi:10.1016/0550-3213\(86\)90346-9](#).
- [729] L. W. Whitlow, Deep Inelastic Structure Functions From Electron Scattering on Hydrogen, Deuterium, and Iron at $0.6\text{-GeV}^2 \leq Q^2 \leq 30\text{-GeV}^2$, Master's thesis (1990).
- [730] S. Dasu, et al., Phys. Rev. D 49 (1994) 5641. [doi:10.1103/PhysRevD.49.5641](#).
- [731] I. C. Cloet, W. Bentz, A. W. Thomas, Phys. Lett. B 642 (2006) 210. [doi:10.1016/j.physletb.2006.08.076](#).
- [732] I. Schienbein, et al., Phys. Rev. D 77 (2008) 054013. [doi:10.1103/PhysRevD.77.054013](#).
- [733] E. D. Bloom, F. J. Gilman, Phys. Rev. Lett. 25 (1970) 1140. [doi:10.1103/PhysRevLett.25.1140](#).
- [734] E. D. Bloom, F. J. Gilman, Phys. Rev. D 4 (1971) 2901. [doi:10.1103/PhysRevD.4.2901](#).
- [735] S. P. Malace, et al., Phys. Rev. C 80 (2009) 035207. [doi:10.1103/PhysRevC.80.035207](#).
- [736] I. Niculescu, et al., Phys. Rev. Lett. 85 (2000) 1186. [doi:10.1103/PhysRevLett.85.1186](#).
- [737] W. Melnitchouk, R. Ent, C. Keppel, Phys. Rept. 406 (2005) 127. [doi:10.1016/j.physrep.2004.10.004](#).
- [738] O. Lalakulich, et al., AIP Conf. Proc. 1189 (2009) 276. [doi:10.1063/1.3274170](#).
- [739] D. Wang, et al., Phys. Rev. Lett. 111 (2013) 082501. [doi:10.1103/PhysRevLett.111.082501](#).
- [740] O. Lalakulich, W. Melnitchouk, E. A. Paschos, Phys. Rev. C 75 (2007) 015202. [doi:10.1103/PhysRevC.75.015202](#).
- [741] F. Gross, S. Liuti, Phys. Rev. C 45 (1992) 1374. [doi:10.1103/PhysRevC.45.1374](#).
- [742] F. E. Close, W. Melnitchouk, Phys. Rev. C 68 (2003) 035210. [doi:10.1103/PhysRevC.68.035210](#).
- [743] H. Gallagher, Nucl. Phys. B Proc. Suppl. 112 (2002) 188. [doi:10.1016/S0920-5632\(02\)01775-9](#).
- [744] A. Rubbia, 1st workshop on neutrino- nucleus interactions in few gev region (nuint01) (2001).
- [745] Y. Hayato, L. Pickering, Eur. Phys. J. ST 230 (2021) 4469. [doi:10.1140/epjs/s11734-021-00287-7](#).
- [746] Y. Hayato, Acta Phys. Polon. B 40 (2009) 2477.
- [747] F. Cavanna, O. Palamara, Nucl. Phys. B Proc. Suppl. 112 (2002) 183. [doi:10.1016/S0920-5632\(02\)01767-X](#).
- [748] G. Battistoni, et al., A neutrino-nucleon interaction generator for the FLUKA Monte Carlo code, 2009.
- [749] J. Nieves, F. Sanchez, I. Ruiz Simo, M. J. Vicente Vacas, Phys. Rev. D 85 (2012) 113008. [doi:10.1103/PhysRevD.85.113008](#).
- [750] J. E. Amaro, et al., Eur. Phys. J. ST 230 (2021) 4321. [doi:10.1140/epjs/s11734-021-00289-5](#).
- [751] O. Benhar, A. Fabrocini, S. Fantoni, I. Sick, Nucl. Phys. A 579 (1994) 493. [doi:10.1016/0375-9474\(94\)90920-2](#).

- [752] K. M. Graczyk, J. T. Sobczyk, Phys. Rev. D 77 (2008) 053001, [Erratum: Phys.Rev.D 79, 079903 (2009)].
[doi:10.1103/PhysRevD.79.079903](https://doi.org/10.1103/PhysRevD.79.079903).
- [753] A. Bodek, U. K. Yang, AIP Conf. Proc. 670 (1) (2003) 110. [doi:10.1063/1.1594324](https://doi.org/10.1063/1.1594324).
- [754] O. Buss, et al., Phys. Rept. 512 (2012) 1. [doi:10.1016/j.physrep.2011.12.001](https://doi.org/10.1016/j.physrep.2011.12.001).
- [755] P. A. Rodrigues, et al., Phys. Rev. Lett. 116 (2016) 071802, [Addendum: Phys.Rev.Lett. 121, 209902 (2018)].
[doi:10.1103/PhysRevLett.116.071802](https://doi.org/10.1103/PhysRevLett.116.071802).
- [756] P. Abratenko, et al., Phys. Rev. Lett. 128 (2022) 151801. [doi:10.1103/PhysRevLett.128.151801](https://doi.org/10.1103/PhysRevLett.128.151801).
- [757] P. Abratenko, et al., Phys. Rev. D 105 (2022) 072001. [doi:10.1103/PhysRevD.105.072001](https://doi.org/10.1103/PhysRevD.105.072001).
- [758] U. Mosel, J. Phys. G 46 (2019) 113001. [doi:10.1088/1361-6471/ab3830](https://doi.org/10.1088/1361-6471/ab3830).
- [759] K. Abe, et al., Phys. Rev. D 101 (2020) 112004. [doi:10.1103/PhysRevD.101.112004](https://doi.org/10.1103/PhysRevD.101.112004).
- [760] R. Acciarri, et al., Phys. Rev. D 98 (2018) 052002. [doi:10.1103/PhysRevD.98.052002](https://doi.org/10.1103/PhysRevD.98.052002).
- [761] T. Golan, J. T. Sobczyk, J. Zmuda, Nucl. Phys. B Proc. Suppl. 229 (2012) 499.
[doi:10.1016/j.nuclphysbps.2012.09.136](https://doi.org/10.1016/j.nuclphysbps.2012.09.136).